

Politecnico di Torino
Università degli Studi di Torino
Ph.D. in Bioengineering and Surgical and Medical Sciences
XXXIII Cycle



**Politecnico
di Torino**



**UNIVERSITÀ
DEGLI STUDI
DI TORINO**

Designing bioartificial polyurethane-based supramolecular hydrogels for tissue engineering and drug delivery applications

Supervisors:

Prof Gianluca Ciardelli

Dr Monica Boffito

Candidate:

Alessandro Torchio

Doctoral Examination Committee:

Prof Mirosława El Fray, Referee, West Pomeranian University of Technology, Szczecin, Poland

Prof Nicola Tirelli, Referee, Istituto Italiano di Tecnologia, Genova, Italy

Dr Piergiorgio Gentile, Newcastle University, Newcastle upon Tyne, United Kingdom

Politecnico di Torino

May 4, 2021

*A tutta la mia famiglia,
a tutti coloro che mi vogliono bene e che mi hanno aiutato in questo percorso.*

Index of the Thesis

<i>Index</i>	I
<i>Acknowledgements</i>	VIII
<i>Brief Curriculum Vitae</i>	X
<i>List of Publications</i>	XI
<i>Abstract of the Thesis</i>	XIII

Section 1 - General Introduction and Aim of the Thesis 1

Outline	1
---------	---

Chapter 1.1 - Drug delivery and Tissue Engineering: general concepts, pros and cons of available approaches 2

1. Abstract	2
2. Preface on Tissue Engineering and Regenerative Medicine	3
3. The basic concepts of traditional drug discovery and development	5
4. Regenerative pharmacology: a new answer to clinical needs	6
4.1 Biomaterials for regenerative pharmacology and tissue engineering	7
5. Particulate platforms based on nanotechnologies for drug release: general principles and considerations	7
5.1 Physical and chemical principles for the development of drug delivery platforms	8
5.2 Drug encapsulation strategies	9
5.3 Typologies of polymeric nanostructures for drug encapsulation and release	9
5.4 Nanostructures for regenerative pharmacology as products into the market	14
6. Scaffold and injectable matrices as devices for regenerative medicine and pharmacology: general principles and considerations	15
6.1 Drug delivery and tissue engineering applications of injectable systems	16
6.2 Hydrogels	17
6.2.1 Physical hydrogels	18
6.2.2 Chemical hydrogels	21
6.2.3 3D printing: the importance of hydrogel architecture	26
6.2.4 Injectable hydrogels for the clinics	31
6.3 Solid scaffold in tissue engineering	32
6.3.1 Conventional methods for scaffold production	32
6.3.2 Non-conventional methods – 3D printing	34
6.3.3 Translation of solid scaffolds to the clinics	36
7. References	38

Chapter 1.2 – Aim of the Work 51

Section 2 – Supramolecular hydrogels based on properly synthesized poly(ether urethane)s for smart applications in drug delivery **54**

Outline 54

Chapter 2.1 – Physical hydrogels as suitable tools for regenerative pharmacology and tissue engineering **56**

1. Abstract	56
2. Physical hydrogels for biomedical applications: the importance of self-assembly	57
3. Polymer-based supramolecular complexes for thermo-sensitive hydrogel formation	57
3.1 General aspects on polymer-based thermo-sensitive supramolecular constructs	57
4. Development of self-assembling polyurethanes for hydrogel design	60
4.1 Polyurethanes: properties and potentiality in the biomedical field	60
4.2 Thermo-sensitive poly(urethane)s as self-assembling molecules for drug delivery and tissue engineering	63
5. Supramolecular hydrogels based on inclusion complexes	66
5.1 Cyclodextrins: a fundamental family of macro-cycles	66
5.2 Cyclodextrins as building blocks of hydrogels through poly(pseudo)rotaxane formation and crystallization	71
5.3 Supramolecular hydrogels based on copolymers containing hydrophobic blocks and their applications in drug delivery: the state of the art	74
6. General discussion and conclusions	79
7. References	80

Chapter 2.2 – Combining Poloxamer® 407-based poly(ether urethane)s and cyclodextrins for the formulation of supramolecular hydrogels in water: a proof of concept study **86**

1. Abstract	86
2. Introduction on the use of poly(urethane)s as PPR-forming polymers	87
3. Materials and Methods	89
3.1 Materials	89
3.2 Synthesis of PEUs	89
3.3 Chemical characterization of PEUs	90
3.3.1 Attenuated Total Reflectance – Fourier Transformed Infrared (ATR-FTIR) Spectroscopy	90
3.3.2 Size Exclusion Chromatography (SEC)	90
3.4 Preparation and characterization of PEU- and CD-based inclusion complexes (ICs)	90
3.4.1 Preparation of Supramolecular (SM) complexes	90
3.4.2 X-Ray powder diffraction (XRD) analysis	91
3.4.3 Attenuated Total Reflectance – Fourier Transformed Infrared (ATR-FTIR) Spectroscopy	91
3.4.4 Proton Nuclear Magnetic Resonance (¹ H-NMR) Spectroscopy	91
3.5 Preparation and characterization of PEU- and CD-based SM hydrogels	92

3.5.1 Preparation of SM hydrogels	92
3.5.2 Qualitative evaluation of gelation time in isothermal conditions and phase-separation	92
3.5.3 Rheological characterization	92
3.5.4 Swelling and stability in physiological-like conditions	93
3.5.5 Cytotoxicity evaluation	94
3.5.6 Release study of fluorescein isothiocyanate dextran (FD4)	94
3.6 Statistical analysis	94
4. Results	95
4.1 Chemical characterization of PEUs	95
4.2 Characterization of SM complexes based on PEUs and CDs	96
4.2.1 X-Ray powder diffraction (XRD) characterization	96
4.2.2 Attenuated Total Reflectance – Fourier Transformed Infrared (ATR-FTIR) spectroscopic analyses	97
4.2.3 Proton Nuclear Magnetic Resonance (¹ H-NMR) spectroscopy analyses	98
4.3 Supramolecular hydrogel characterization	101
4.3.1 SM hydrogel formulation and gelation kinetics	101
4.3.2 Rheological characterization of SM hydrogels	104
4.3.3 Responsiveness and stability in aqueous environment	110
4.3.4 Cytotoxicity tests	113
4.3.5 Evaluation of the release kinetics of FD4 model molecule from SM hydrogels	114
5. Conclusions	116
6. References	118

Chapter 2.3 – Investigation on hydrogel formulation, properties, and responsiveness in different aqueous media **120**

1. Abstract	120
2. Introduction	121
3. Materials and Methods	122
3.1 Materials	122
3.2 Preparation of SM hydrogels	122
3.4 Qualitative evaluation of gelation time in isothermal conditions	122
3.5 Rheological characterization	122
3.6 Swelling and stability test in physiological like conditions	123
3.7 Statistical analysis	123
4. Results and discussion	123
4.1 Gelation time evaluation	123
4.2 Rheological characterization	124
4.3 Swelling and stability tests	127
5. Conclusions	128
6. References	130

Chapter 2.4 – Application of poly(ether urethane)-based supramolecular hydrogels for curcumin encapsulation and release **131**

1. Abstract	131
2. Introduction	132
2.1 Curcumin: therapeutic effects and issues	132
2.2 Pharmaceutical formulations based on cyclodextrin for curcumin release	134
2.3 Supramolecular hydrogels for curcumin encapsulation and release	135
3. Materials and Methods	136
3.1 Materials	136
3.2 Synthesis of PEUs	137
3.3 De-protection of N-Boc Serinol-based PEUs	137
3.4 Chemical characterization of PEUs	137
3.4.1 Attenuated total reflectance – Fourier transformed infrared (ATR-FTIR) spectroscopy	137
3.4.2 Size exclusion chromatography (SEC) characterization	137
3.4.3 Proton nuclear magnetic resonance (¹ H-NMR) spectroscopy	137
3.4.4 Free primary amine quantification – Orange II Sodium Salt colorimetric assay	138
3.4.5 Critical micellar temperature (CMT) evaluation	138
3.5 Preparation and characterization of PEU- and CD-based SM complexes	138
3.5.1 Preparation of supramolecular (SM) complexes	138
3.5.2 X-ray powder diffraction (XRD) analysis	139
3.5.3 Attenuated Total Reflectance – Fourier Transformed Infrared (ATR-FTIR) spectroscopy	139
3.5.4 Proton Nuclear Magnetic Resonance (¹ H-NMR) Spectroscopy	139
3.6 Preparation and characterization of PEU- and CD-based SM hydrogels	139
3.6.1 Preparation of SM hydrogels	139
3.6.2 Qualitative evaluation of gelation time in isothermal conditions and phase-separation	140
3.6.3 Rheological characterization	140
3.6.4 Swelling and stability tests in physiological-like conditions	140
3.6.5 Cytotoxicity evaluation	140
3.6.6 Curcumin encapsulation and release studies	140
3.6.7 Statistical analysis	142
4. Results	142
4.1 Physico-chemical characterization of PEUs	142
4.1.1 ATR-FTIR spectroscopy and SEC	142
4.1.2 ¹ H-NMR spectroscopy and free primary amine quantification	143
4.1.3 Critical micellar temperature (CMT) evaluation	144
4.2 Physico-chemical characterization of SM complexes	147
4.2.1 X-Ray powder diffraction (XRD)	147
4.2.2 ATR-FTIR characterization	149
4.2.3 ¹ H-NMR spectroscopic analyses of SM structures	150
4.3 Supramolecular hydrogel characterization	151

4.3.1 SM hydrogel formulation and gelation kinetics	151
4.3.2 Rheological characterization of SM hydrogels	153
4.3.3 Swelling and stability in aqueous environment	157
4.3.4 Cytotoxicity evaluation	159
4.4 Curcumin encapsulation and release kinetics	160
4.4.1 Rheological characterization of curcumin-loaded SM hydrogels	160
4.4.2 Release studies of curcumin from PEU-based SM hydrogels	163
5. Conclusions	166
6. References	168

Section 2 – Chapter 2.5 – Case Study I: release studies of ciprofloxacin, a hydrophilic antibiotic drug for the treatment of infections **174**

1. Abstract	174
2. Introduction	174
3. Materials and Methods	177
3.1 Materials	177
3.2 Preparation of SM hydrogels encapsulating ciprofloxacin and qualitative evaluation of gelation time	177
3.3 Release studies of ciprofloxacin	177
4. Results	177
5. Conclusions	180
6. References	181

Section 2 – Chapter 2.6 – Case Study II: encapsulation of a PEU-based SM hydrogel within highly porous scaffolds composed of poly(ϵ -caprolactone) **183**

1. Abstract	183
2. Introduction	184
3. Materials and Methods	185
3.1 Materials	185
3.2 Preparation of PCL-based porous scaffolds through salt-leaching technique	186
3.3 Plasma treatment of PCL-based porous scaffolds	186
3.4 Characterization of PCL-based morphology	186
3.5 SHP407-based SM hydrogel formulation, preparation, and qualitative evaluation of gelation time	187
3.6 Rheological characterization of SHP407-based hydrogels	187
3.7 SM hydrogel loading within PCL-based scaffolds	187
3.8 Evaluation of mechanical properties	187
3.9 Release kinetics of FD4 from hybrid scaffold systems encapsulating SM hydrogels	188
4. Results	188
4.1 Physical evaluation of PCL-based scaffolds	188
4.2 Rheological characterization of SHP407-based hydrogel	189
4.3 SM hydrogel loading within PCL-based scaffolds and	

investigations of the mechanical properties of the resulting hybrid systems	191
4.4 Release studies of FD4 from hybrid hydrogel-scaffold systems	192
5. Conclusions	193
6. References	195

Section 3 – Highly functional supramolecular and photo-curable hydrogels based on poly(ether urethane)s **196**

Outline	196
---------	-----

Section 3 – Chapter 3.1 – Chemical hydrogels based on supramolecular architectures **197**

1. Abstract	197
2. Introduction	198
3. Materials and Methods	200
3.1 Materials	200
3.2 Synthesis of photo-sensitive PEU – HHP407	200
3.3 Chemical characterization of HHP407	201
3.4 CMT evaluation	201
3.5 Preparation and characterization of HHP407- and CD-based SM complexes	201
3.6 Preparation and characterization of HHP407- and CD-based SM hydrogels	202
3.6.1 Preparation of SM hydrogels	202
3.6.2 Qualitative evaluation of gelation time and phase-separation in isothermal conditions	202
3.6.3 Curcumin encapsulation with SM gels, characterization and release studies	202
3.6.4 Extrusion-based 3D printing of SM hydrogels	203
3.7 Statistical Analysis	204
4. Results	204
4.1 Physico-chemical characterization of HHP407	204
4.2 Characterization of HHP407-CD SM complexes	207
4.3 Physical characterization of HHP407-based SM hydrogels	209
4.4 Characterization of curcumin-loaded SM hydrogels based on HHP407 and CDs	210
4.4.1 Physical and mechanical characterization of curcumin-loaded SM hydrogels	210
4.4.2 Release profiles of Cur encapsulated within HHP407-based hydrogels	215
4.5 Preliminary studies on HHP407-based SM hydrogel extrudability	217
5. Conclusions	219
6. References	221

Section 3 – Chapter 3.2 – Development and engineering of bioartificial hydrogels based on supramolecular networks and gelatin methacryloyl **223**

1. Abstract	223
2. Introduction	224

3. Materials and Methods	226
3.1 Materials	226
3.2 Gelatin methacryloyl (GelMA) synthesis and physico-chemical characterization	226
3.2.1 GelMA synthesis protocol	226
3.2.2 Chemical characterization of GelMA	227
3.3 Biosynthetic and supramolecular hydrogels preparation and characterization	227
3.3.1 Preparation and physical characterization of bioartificial and supramolecular hydrogels based on GelMA, HHP407 and CDs	227
3.3.2 Curcumin encapsulation and release studies	228
3.4 Statistical Analysis	228
4. Results	228
4.1 Physico-chemical characterization of GelMA – ¹ H-NMR spectroscopy	228
4.2 Preparation and characterization of bioartificial hydrogels based on GelMA, HHP407 and CDs	229
4.2.1 Hydrogel formulation and gelation kinetics	229
4.3 Curcumin encapsulation and release studies	230
4.3.1 Rheological characterization of pure and Curcumin-loaded SM and bioartificial hydrogels	230
4.3.2 Curcumin release profiles from bioartificial hydrogels based on GelMA, HHP407 and CD	235
5. Conclusions	237
6. References	239
Section 4 – Conclusion	242

Acknowledgements – Ringraziamenti

Questo lavoro di dottorato è stato reso possibile da una iniziale proposta di tema, proveniente dal Professor Gianluca Ciardelli. Egli, infatti, proponendo come argomento “idrogeli sovramolecolari a base di poliuretani”, mi ha permesso di intraprendere un percorso di grande significato. Nonostante il lavoro avesse un importante livello di implicita incertezza iniziale, il processo di studio e avviamento delle attività di ricerca è subito divenuto molto stimolante. Infatti, oltre agli aspetti tecnico-scientifici, cioè oggettivi e che più mi appassionano, ad aver alimentato la mia motivazione nell’avanzare in tale lavoro sono stati i frequenti incontri con il professore stesso. In queste occasioni di stretto rapporto umano, l’interazione accademico-lavorativa veniva sublimata a un incentivo superiore, che ha veramente amplificato ogni mia buona intenzione e impegno. Devo pertanto ringraziare il Professor Gianluca Ciardelli per avermi consentito di procedere al meglio delle possibilità di fatto e soggettive, in quanto ciò non è da darsi mai per scontato, in generale, nei vari aspetti vita.

La presenza della Dottoressa e Ingegnere Monica Boffito è stata estremamente importante per me; è anzi stata fondamentale. Da questo punto a seguire, la chiamerò semplicemente Monica, a indicazione del grande legame umano che si è generato, al di là dei suoi titoli e notevoli risultati raggiunti. Sin dal principio della nostra interazione, ho sempre percepito la sua grande attenzione, il suo singolare zelo e la sua unica dedizione per ogni aspetto. Nell’evolversi di questo percorso di dottorato, ulteriori elementi di condivisione con Monica sono emersi, facendomi rendere conto dell’immensa fortuna che possedessi a potermi confrontare con ella nel contesto lavorativo e umano. Il suo singolare portamento al mestiere di ricercatrice e *co-supervisor* ha aggiunto un fondamentale contributo alla qualità del mio percorso e lavoro di Dottorato, facendomi sentire a mio agio e prendendo di buon grado ogni mia proposta, valutandola con oggettivo criterio e umana delicatezza. Le più salde fondamenta, sulle quali è stato costruito questo lavoro di dottorato, sono state permesse dal suo essenziale contributo. Oggi, a valle dello stesso lavoro di Dottorato, vedo Monica come esempio lavorativo da seguire e come amica sincera, per me estremamente cara e importante.

All’interno di questo lavoro, altre persone hanno avuto ruoli di alto significato per me. Rossella Laurano, mia collega di dottorato un anno avanti a me, è stata compagna di avventure e sventure lavorative. Insieme, confrontandoci ripetute volte, siamo cresciuti e migliorati, in modo sinergico e vicendevole. Abbiamo collaborato molto, senza mai competere, condividendo tutto in maniera disinteressata e sincera. Con questo approccio, abbiamo ottenuto risultati di lavoro e amicizia che ritengo molto preziosi per ciò che rappresentiamo oggi e saremo domani.

Nell’insieme dei miei altri colleghi di Alessandria, voglio ringraziare Arianna Grivet Brancot, Ornella Lima, Lucia Servello, Andrea Gallina, Alice Zoso, Andrea Desii e Roberta Pappalardo per aver contribuito alla collettività con spirito di condivisione e simpatia, rendendo la quotidianità nella quale ho svolto questo progetto di dottorato un contesto sereno. Voglio anche ringraziare Susanna Sartori, per la sua sincera empatia nei momenti di sconforto e più piacevoli. Facendo parte di un gruppo ampio, è per me necessario ringraziare anche tutti i membri della sede di Torino, ossia Chiara Tonda-Turo, Irene Carmagnola, Clara Mattu, Alice Zoso, Michela Licciardello e Viola Sgarminato, per aver attivamente partecipato alle riunioni di gruppo di ricerca nelle quali ho

presentato i graduali progressi del lavoro. Ringrazio anche Andrea Gallina, Mario Lavella e Claudio Cassino per aver contribuito a questo lavoro, con professionalità ed estrema gentilezza.

Devo anche ringraziare Subha Purkayastha, che è per me stimato scienziato e grande amico, con il quale ho condiviso discorsi molto importanti per la formulazione del mio lavoro e per la mia crescita personale.

Per quanto concerne le persone che sono state coinvolte nelle attività di ricerca di questo lavoro e delle quali sono stato parzialmente responsabile, voglio ringraziare di cuore Alice Stefani. Ella è stata talentuosa, precisa e sensibile tesista di laurea magistrale che ha preso parte a questo lavoro di dottorato. Alice mi ha permesso di crescere come persona e lavoratore, in uno scambio sincero di esperienza verso un vicendevole miglioramento. Le sono grato per la sincerità e immediatezza che ha sempre mostrato durante la sua attività. Infine, tra coloro che hanno partecipato alle attività sperimentali del mio lavoro di dottorato, mi sento di ringraziare anche Chiara Arduino e Lorenzo Galleani d'Agliano, tirocinanti di laurea triennale che hanno mostrato una rara e preziosa volontà nel proprio lavoro ed esperienza condivisa, dimostrando di essere anche splendide persone, nelle quali riporre serenamente fiducia.

Passando ora a coloro che non appartengono al contesto nel quale si è svolto direttamente questo lavoro di dottorato, voglio ringraziare tutta la mia famiglia. Mio padre, mia madre e mia sorella per avermi accompagnato e sostenuto in molti sensi, da quello morale a quello materiale, in questo tragitto di crescita personale, nonostante i tempi non abbiano presentato la migliore delle cornici. L'ascolto che ho ricevuto da parte dei miei familiari durante questa esperienza mi ha concesso di ricevere un importante appoggio umano. Mia madre, attraverso la sua particolare saggezza, buonsenso e percezione di me, mi ha spesso fornito una visione diversa dalla mia, ampliandola, con i suoi modi unici e a me tanto cari. Mio padre, nel suo ruolo di genitore e medico, mi ha fornito un sostegno tanto articolato e unico, quanto utile. Insieme, abbiamo condiviso sano divertimento e sobria serietà. Mia sorella, invece, pur appartenendo a una sfera lavorativa completamente differente dalla mia, si è impegnata per capire la mia situazione e fornirmi le sue sensazioni, che ancora oggi rielaboro e mi aiutano a crescere.

Infine, di fondamentale importanza è stata Valentina, la persona con la quale condivido l'interesse dei miei sentimenti e tutte le mie esperienze di vita che la Fortuna governa. Ella, insieme alla sua famiglia, mi hanno sostenuto durante le fasi più incerte e difficili del lavoro, attraverso gesti e parole che ho fatto miei in modo imperituro. Devo a Valentina momenti di sana evasione dagli oneri che sono stati da me sostenuti in questo percorso. Devo a lei, alla sua comprensione (specialmente negli ultimi giorni prima della consegna dell'elaborato) e ai suoi immensi e genuini sentimenti, il grande incentivo a proseguire al meglio delle mie possibilità, rendendomi sempre più conscio di quanto sia importante mantenersi umani e sostenersi a vicenda. Sempre.

A tutti voi, grazie infinite.

Alessandro Torchio

Brief Curriculum Vitae

Alessandro Torchio started his academic education in Biomedical engineering in 2011 at Politecnico di Torino (Italy). In 2014 he graduated obtaining the Bachelor degree with the thesis work *“Evaluation of cell adhesion on three novel ceramic materials: ATZ (alumina toughened zirconia), ZTA (zirconia toughened alumina) and nanoporous Alumina for dental implants”* under the supervision of Prof Cristina Bignardi (Politecnico di Torino) and Prof Federico Mussano (Università degli Studi di Torino). In the same year, Alessandro enrolled in the Master degree course in Biomedical engineering, selecting Bionanotechnologies and Biomechanics as specialist pathways, at Politecnico di Torino (Italy). He graduated *cum laude* in 2016 with the master thesis work *“Stimuli sensitive polyurethane-based hydrogels encapsulating mesoporous silica nanoparticles for drug release”* as part of the European H2020 Project *“Mesoporous matrices for localized pH-triggered release of therapeutic ions and drugs (MOZART)”* coordinated by Prof Chiara Vitale-Brovarone (Politecnico di Torino, Italy). The thesis work was supervised by Prof Gianluca Ciardelli, Dr Chiara Tonda Turo, Dr Monica Boffito and was awarded by Gruppo Nazionale di Bioingegneria (*“Laboratory of Biological Structure Mechanics”* award by Politecnico di Milano, Italy) in September 2017. From January 2017 to July 2017, Alessandro joined the Proof of Concept (PoC) project *“Optimization of bioartificial materials for the design of 3D structures for tissue engineering”* as research fellow under the supervision of Prof Valeria Chiono, actively collaborating with Prof Alberto Rainer from Università Campus Bio-medico in Rome, Italy. Subsequently, during the time frame from July 2017 to November 2017, he joined the IRMI project (Italian Regenerative Medicine Infrastructure project), in which he was involved in the development of *ad-hoc* injectable systems as carriers of biomolecules or inorganic phases. In November 2017 he was awarded a Ph.D. fellowship in the inter-university Doctoral Programme *Bioengineering and Medical Surgical Sciences* jointly activated by Politecnico di Torino (Italy) and Università degli Studi di Torino (Italy). Alessandro started his Ph.D. research activity on the development of supramolecular bioartificial hydrogels based on properly synthesized poly(ether urethane)s and cyclodextrins for drug delivery and tissue engineering application. During the Ph.D. Programme, Alessandro presented part of his work at the international congress TERMIS EU 2019 (Rhodes, Greece) and was awarded the 2nd place for Podium Presentation among RSC Journal of Materials Chemistry part B Winners.

List of publications

Research papers in peer-reviewed journals:

- “Hybrid injectable platforms for the *in situ* delivery of therapeutic ions from mesoporous glasses” - Pontremoli, C.; Boffito, M.; Fiorilli, S.; Laurano, R.; **Torchio, A.**; Bari, A.; Tonda-Turo, C.; Ciardelli, G.; Vitale-Brovarone, C. - In: CHEMICAL ENGINEERING JOURNAL. - ISSN 1385-8947. - 340(2018), pp. 103-113.
- “Plasma treatment of polymer powder as an effective tool to functionalize polymers: case study application on an amphiphilic polyurethane” – Laurano R.[#]; Boffito M.[#]; **Torchio A.**; Cassino C.; Chiono V.; Ciardelli G. In: POLYMERS. - ISSN 2073-4360. - . - 11:12(2019).
- “Hybrid Injectable Sol-Gel Systems Based on Thermo-Sensitive Polyurethane Hydrogels Carrying pH-Sensitive Mesoporous Silica Nanoparticles for the Controlled and Triggered Release of Therapeutic Agents” – Boffito M.; **Torchio A.**; Tonda-Turo C.; Laurano R.; Gisbert-Garzarán M.; Berkmann J.; Cassino C.; Manzano M.; Duda G.N.; Vallet-Regí M.; Schmidt-Bleek K.; Ciardelli G.; In: FRONTIERS IN BIOENGINEERING AND BIOTECHNOLOGY. - ISSN 2296-4185. - . - 8(2020), pp. 1-24.
- “Supramolecular hydrogels based on custom-made poly(ether urethane)s and cyclodextrins as potential drug delivery vehicles: design and characterization” – **Torchio A.**[#]; Boffito M.[#]; Gallina A.; Cassino C.; Lavella M.; Ciardelli G.; - In: JOURNAL OF MATERIALS CHEMISTRY B (RSC). ISSN 2050-7518. (2020). This paper is based on the findings reported in Section 2 – Chapter 2.2.
- “Inner strut morphology is the key parameter in producing highly porous and mechanically stable poly(ϵ -caprolactone) scaffolds via selective laser sintering” – Tortorici M.; Gayer C.; **Torchio A.**; Cho S.; Schleifenbaum J.H.; Petersen A.; - In: Materials Science and Engineering: C. February 2021, 111986.
- “Injectable supramolecular hydrogels based on custom-made poly(ether urethane)s and α -cyclodextrins as efficient delivery vehicles of curcumin” – **Torchio A.**; Cassino C.; Lavella M.; Gallina A.; Stefani A.; Boffito M.[§]; Ciardelli G.[§]; - Submitted to Materials Science and Engineering: C (under revision). This paper is based on the findings reported in Section 2 – Chapter 2.4.

Congress abstracts:

- “Nanotechnology-Based Strategies To Treat Chronic Wounds” - Tonda-Turo, C.*; Boffito, M.; Ruini, F.; **Torchio, A.**; Laurano, R.; Ceresa, C.; Fracchia, L.; Gentile, P.; Ferreira, A. M.; Ciardelli G. - (2017). (iSMIT 2017, Torino -Italy-, 09-10 November, 2017)
- “Injectable polyurethane-based hydrogels for smart drug release in the treatment of chronic skin wounds” - Laurano, R.*; **Torchio, A.**; Boffito, M.; Ciardelli, G. - (2017). (iSMIT 2017, Torino -Italy-, 09-10 November, 2017)

- “Novel thermo-responsive polyurethane-based hydrogels encapsulating pH-sensitive mesoporous silica nanocarriers” - **Torchio A.***; Boffito M.; Tonda Turo C.; Laurano R.; Gisbert Garzaran M.; Manzano M.; Vallet Regi M.; Ciardelli G. - (2018). (GNB2018, Milan – Italy, 25-27 June) (ORAL PRESENTATION)
- “Supramolecular hydrogels based on host-guest complexes between custom-made polyurethanes and cyclodextrins” - **Torchio A.***; Boffito, M.; Cassino C.; Ciardelli G. - pp. 79, 9th BSRT symposium - The art of failure: Regenerative therapies from experimental sketches to clinical masterpieces, Berlin, Germany, 28-30 November 2018. (ORAL PRESENTATION)
- “Polyurethane-based supramolecular hydrogels as drug delivery platforms of hydrophobic drugs” - **Torchio, A.***; Boffito, M.; Ciardelli, G. – ENIUS (COST) - Materials, Technology and Biomimetics as enabling tools for a new generation of Urinary Stents, Sofia, Bulgaria, 2 February 2019. (ORAL PRESENTATION)
- “Supramolecular hydrogels based on novel polyurethanes and cyclodextrins” **Torchio A.***, Boffito M., Gallina A., Cassino C., Ciardelli G., TERMIS EU 2019, Rhodes, Greece, 27-31 May 2019. (ORAL PRESENTATION) (BEST ORAL PRESENTATION AWARD, RSC Journal of Materials Chemistry Part B Winners, 2nd place)

These authors equally contributed to this work

§ These authors have contributed equally to the supervision of the first author

* presenting author

Abstract of the Thesis

Highly reversible and injectable devices represent important tools to answer modern clinical needs in both the tissue engineering/regenerative medicine and the pharmacology fields. Indeed, the local and minimally invasive administration of systems able to exert a therapeutic function has been continuously recording increasing interest over the last decades. To this aim, a particular kind of devices holds a huge potential, namely supramolecular (SM) hydrogels. The rationale underpinning their formulation relies in the possibility to design highly responsive and self-healing systems by taking inspiration from natural processes of self-assembly between compatible molecules. In this Ph.D. project, a plethora of newly designed poly(ether urethane)s (PEUs) was developed for the production of engineered SM hydrogels through their spontaneous self-assembly with α -cyclodextrins (CDs). To this aim, poly(ethylene oxide) (PEO) containing PEUs were designed and coupled with CDs to form poly(pseudo)rotaxanes (PPRs) as hydrogel forming SM crystals in aqueous media. Moreover, specific functionalities were additionally integrated into the PEU backbone to provide them with the capability to form hydrophobic interactions which could actively contribute to the formation of remarkably stable, handle and versatile hydrogel devices. Thence, various PEUs were synthesized utilizing commercially available thermo-sensitive triblock co-polymers based on PEO and poly(propylene oxide) (PPO): Poloxamer® 407 (P407, 70% wt PEO, M_n 12600 Da) and Pluronic® F68 (F68, 80% wt PEO, M_n 8400 Da), both characterized by a PEO-PPO-PEO block distribution. P407 and F68 were used as macrodiols for the synthesis of PEUs with the addition of an aliphatic diisocyanate (1,6-hexamethylene diisocyanate) and two different chain extenders (1,4-cyclohexanedimethanol or N-Boc serinol) or an end-capping photo-sensitive alcohol (2-hydroxyethyl methacrylate). A complete physico-chemical characterization was performed on the as-synthesized PEUs through Attenuated Total Reflectance – Fourier Transformed Infrared spectroscopy, Proton Nuclear Magnetic Resonance spectroscopy, and Size Exclusion Chromatography. Thermo-responsiveness of PEUs was assessed through the determination of the critical micellar temperatures of their aqueous solutions. PEU-CD SM structures were then produced and thoroughly characterized. In this regard, PEU chemical composition turned out to exert a fundamental role in determining the properties of the resulting complexes. In fact, P407-based PEUs were characterized by the highest yield in terms of self-assembly, while F68-based polymers were less suitable for SM network stabilization due to an insufficient hydrophobic character. SM structures were characterized in physico-chemical terms and through X-Ray powder diffraction, which evidenced the formation of channel-like SM crystals. A variety of SM hydrogel systems was then designed utilizing single PEU formulations or specific PEU blends to finely tune the physical properties of the resulting hydrogel systems (final PEU concentration ranging between 1 and 9% w/v, CD content between 7 and 10% w/v). Rheological characterization highlighted noteworthy mechanical properties and remarkable self-healing capacity of the developed SM networks. The best behavior in mechanical terms was observed for hydrogels with PEUs at low concentration (i.e., less than 5% w/v), thus indicating an enhanced and constructive interaction of the polymer chains with CDs. Swelling/stability tests performed by incubating the gels in contact with physiological aqueous milieus at 37 °C demonstrated good stability and responsiveness of SM hydrogels. Moreover, cytotoxicity tests were performed according to ISO 10993 proving the biocompatibility of SM gels, which turned

out to be suitable for advanced drug delivery studies. Indeed, after preliminary release studies utilizing a drug model molecule (i.e., fluorescein isothiocyanate dextran 4), curcumin (up to 570 $\mu\text{g ml}^{-1}$) and ciprofloxacin (up to 40 $\mu\text{g ml}^{-1}$) were successfully encapsulated at high concentration within SM hydrogels. Release studies evidenced progressive delivery kinetics of the loaded cargo over time in highly destabilizing conditions *in vitro*. Generally, PEU-based SM systems were able to guarantee the stability of the entire therapeutic payload in physiological-like environments and sustained its release up to five weeks in the case of photo-cured SM hydrogels prepared using the photo-sensitive PEU synthesized using 2-hydroxyethyl methacrylate. Moreover, the relevant versatility of the developed hydrogel systems allowed their easy integration within salt-leached poly(ϵ -caprolactone)-based porous scaffolds, providing a preliminary proof of concept of the possibility to use them to develop single stage strategies combining drug delivery and tissue engineering. In detail, a hydrogel loading a drug model molecule (i.e., fluorescein isothiocyanate dextran 4) was easily integrated within rigid polymeric supports and *in vitro* release studies indicated a progressive erosion and dissolution of the SM network, potentially allowing a consecutive maturation in biological terms of the remaining 3D framework.

In addition, preliminary 3D bioprinting tests were performed and one SM formulation showed the best performances as potential bioink for advanced applications in bioengineering. Finally, with the aim to develop a novel and alternative single stage strategy to combine regenerative pharmacology and tissue engineering, biosynthetic SM hydrogels were obtained by formulating systems based on CDs, a photo-sensitive PEU and gelatin methacryloyl (GelMA). The overall physical stability of the resulting hybrid hydrogels demonstrated a high reliability of PEU-based SM networks for the design of more complex and functional formulations. In fact, a thorough rheological characterization demonstrated well-structured hydrogel networks at their initial physical condition, while photo-rheological tests demonstrated good responsiveness to photo-stimulation through the formation of additional chemical crosslinking. Although the overall formulation of these systems was quite complex, the integration of all these components resulted to be effectively controllable. In fact, a high curcumin payload (i.e., 715 $\mu\text{g ml}^{-1}$) was easily integrated within these networks and release tests showed the sustained delivery of such drug up to three weeks.

To conclude, in this work the exploitation of a reliable and consistent synthesis process allowed the production of notably versatile multi-functional PEUs. These macromolecules turned out to be central elements for the formulation of a wide variety of promising devices specifically designed for drug delivery applications or for combined strategies including regenerative pharmacology and tissue engineering. The entire set of the designed formulations and the results attained in this work represents a reliable starting point for the further development of new *ad-hoc* engineered devices able to fulfil highly demanding clinical needs.

Section 1

General Introduction and Aim of the Thesis

Outline

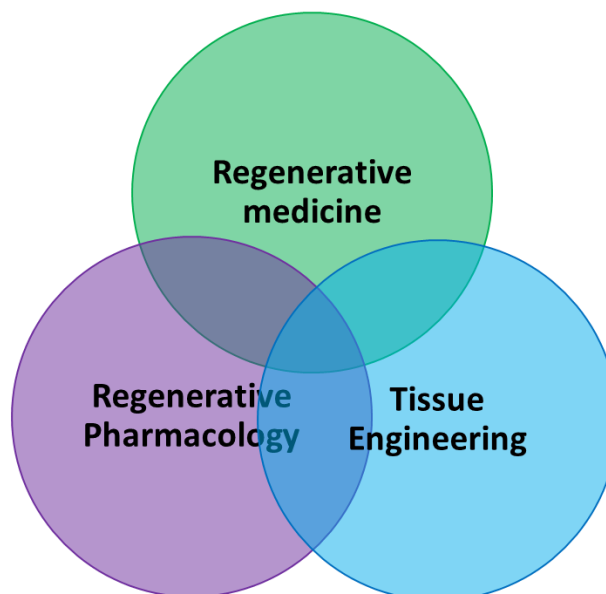
This section provides a general overview on the Drug Delivery and Tissue Engineering fields with the aim to introduce and properly identify the scenario in which this Ph.D. project has been conceived and developed. In *Chapter 1.1*, the general concepts, limitations and needs of modern medicine, such as organ transplantation, will be described and discussed. Then, the role of novel and pioneering solutions, namely regenerative pharmacology, tissue engineering and regenerative medicine, will be defined. The different available strategies to achieve the ultimate goals of these challenging and innovative approaches will be analyzed in scientific and technical terms. This section will thus provide the reader with an overall sight and focus on the main aspects that will be in-depth treated in the incoming sections of the Thesis. On the basis of this analysis, the general aim of this Ph.D. project will be described in *Chapter 1.2* in projection of the entire development of the work, which will be focused on the development of innovative and smart materials for drug delivery and tissue engineering.

Section 1 – Chapter 1.1 – Drug delivery and Tissue Engineering: general concepts, pros and cons of available approaches

1. Abstract

Organ transplantation represents a complex solution to modern clinical needs. Generally, the lack of organ donors and their appropriate storage are the main drawbacks, which significantly hinder the overall effectiveness of such approach. However, the technological development in the medical field has generated cutting edge strategies that rely on a multitude of disciplines, such as, materials science/engineering, biology and bionanotechnology. In this context, the pivoting idea consists in the complete regeneration of the original functions of damaged tissues and organs. The resulting multifaceted fields can be classified depending on specific perspectives and are known as *regenerative medicine*, *tissue engineering* and *regenerative pharmacology*. A relevant correlation exists among these three disciplines, as the final aim is widely shared. Indeed, they are sometimes used as synonyms. In this Chapter, the basic definitions and principles of these novel strategies are shown. Indeed, according to a bottom-up approach, the conducted research work encompasses various processes, from the specific design of polymeric macromolecules up to their concrete application and translation into devices for drug delivery and tissue engineering. Moreover, their most important achievements are described, starting from the conventional idea of pharmacology and culminating with the novel concepts of highly engineered and multi-functional strategies for tissue regeneration (i.e., particulate platforms, injectable hydrogels and solid scaffolds). The state of the art is reported and discussed, highlighting the advantages and drawbacks for each typology of platform in view of the development of new strategies towards clinical needs.

Graphical Abstract



The integration of novel and multidisciplinary fields towards clinical needs

2. Preface on Tissue Engineering and Regenerative Medicine

One of the most important achievements in medicine is represented by organ transplantation. However, the general need and the lack of organs to be transplanted as well as the commitment to long-life administration of anti-rejection therapies are concrete issues for worldwide healthcare. In the last few years, the World Health Organization conducted a set of studies concerning organ availability; as a result, it has been estimated that scarcely 10% of the total request is being satisfied.^{1,2} The United States of America represents a relevant example of this situation. In fact, it has been estimated that the real need for heart transplantation is at least ten-fold greater than the actual heart transplant waiting list. On the other side, only 0.3% of people who die in the USA effectively becomes a donor, since important constraints exist to determine organ suitability for storage and transplantation. In 2011, the totality of deaths due to end-stage organ diseases in the USA has been quantified to be fourteen-fold higher than the total waitlist additions. The combined need in the USA and Europe is quantified in millions of organs for transplantations every year, which is extensively relevant. The global scenario is further worsened by the situation of other eastern countries and Africa: these regions are characterized by the highest percentage of population in the world and, at the same time, by the lowest numbers of organ transplanted per population. As a comparison, the United States of America host *circa* the 4% of the world population and perform the 25% of the total organ transplants, while in Africa the population is around 16% of the world total and less than 0.5% of the total organ transplants are fulfilled (<http://www.transplant-observatory.org/summary/>).³

Organ transplantation generally requires the administration of relevant therapies such as immunosuppression, which has significantly increased the surgical rate of success, as well as graft acceptance and survival. Nevertheless, the 50% of grafts is subjected to organ failure in the time frame of 10 years from transplantation and immunosuppressive therapies could cause severe complications, such as the enhanced risk of fatal infections. Another important side effect of immunosuppressants is also the formation of cancer.⁴⁻¹⁰

Moreover, organ preservation before transplantation represents another important limitation. In fact, the availability of an organ generally lasts for the subsequent few hours after removal from the donor. An enhancement in organ storage and preservation procedures would result in a significant increase in the global availability of organs: this is the idea underpinning organ banking and could represent an important solution to the actual constraints.¹¹

Nevertheless, the continuous evolution of knowledge in medicine and the development of novel frontiers of engineering are generating strictly correlated strategies to answer to health-related needs caused by tissue or organ failure. Modern medicine is composed of many different branches and one of them is particularly formulated and addressed to this aim: *regenerative medicine*. The term “regeneration” derives from Latin (*regeneration*, from *regenerare*, which means “produce again”) and in case of medicine refers to a process that occurs and culminates in a complete reformation of a healthy tissue/organ. It is different from the idea of “reparation”, which usually results in a partial restoration of the physiological functions of the biological milieu. In fact, the “reparation” philosophy basically represents a traditional approach of medicine that relies on artificial prosthesis implantation or organ transplantation from a donor.¹² Differently, the purposes underpinning the philosophy of regenerative medicine are quite recent and remarkably challenging.¹³ Indeed, this branch of medicine requires a substantial integration from the technical environment. For this reason, a novel multi-disciplinary branch of engineering has been formulated

over the last decades and has been configured in *biomedical engineering*. More in detail, a wide sub-branch of the above-mentioned engineering field is involved, namely *tissue engineering*, which combines the most advanced technologies with biology-related sciences. Hence, regenerative medicine and tissue engineering are strictly overlapped multi-disciplinary fields. For this reason, these terms have often been used as synonyms.¹⁴

The constituting elements of tissue engineering are mainly three: i) a matrix (or scaffold), ii) cells and iii) regulators. A scaffold is basically a support for cell culture and proliferation. It is fundamental in order to reach a complete maturation of a final construct. Its properties, such as chemical composition, porosity and morphology represent key factors for the modulation of cell behavior. The importance of cells is certainly relevant in this field, since they are the living part of the system leading to a complete maturation of the construct when they are correctly stimulated by the scaffold and the external cues. These regulators are represented by a complex ensemble of variables, which can be chemical stimuli (e.g., growth factors, genes, or drugs) as well as physical regulations (e.g., mechanical or electrical stimuli). The strong interconnection that occurs between these three elements can be briefly summarized as represented in figure 1.

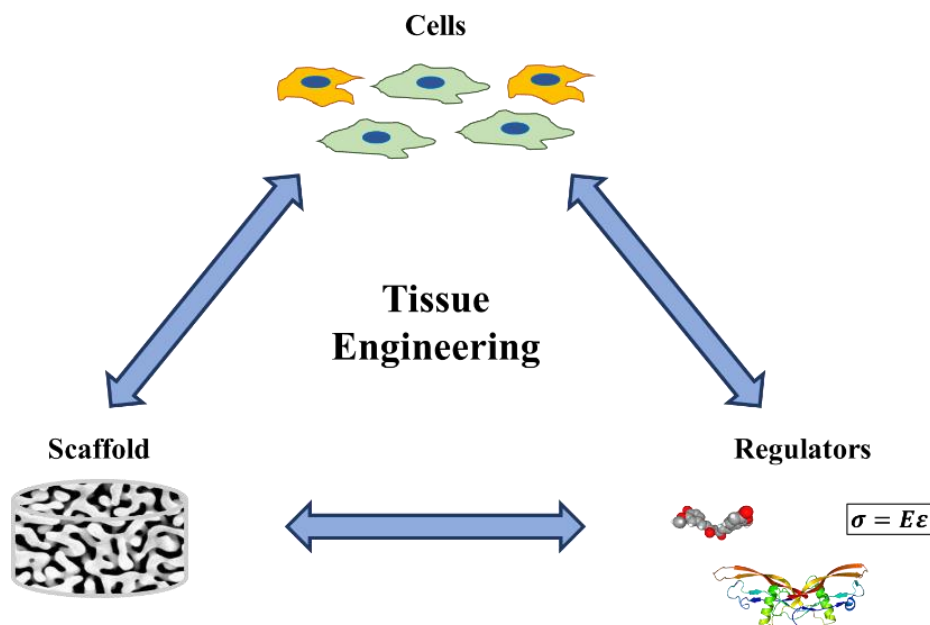


Figure 1 – Schematic representation of the basic elements of tissue engineering.

The importance of these components and their crosstalk is evident, but their co-presence is not mandatory to develop new and effective strategies for tissue engineering. Indeed, they can be used singularly by exploiting the relevant contribution of the hosting organism. From this point of view, the concept of cell and/or regulator delivery plays a fundamental role in the context of tissue engineering. Indeed, the development of smart platforms for targeted cargo release represents by itself an effective frontier in this scenario, as it can enhance the regeneration of a tissue where it is actually needed, thus increasing the overall efficacy and decreasing the eventuality of dangerous side-effects. Hence, delivery strategies constitute an essential branch of tissue engineering and regenerative medicine.

To summarize, the principal macro-disciplines that are related to the above-mentioned elements and define the tissue engineering/regenerative medicine field mainly are: i) human cell therapy, ii)

gene therapy, iii) molecular medicine, and iv) biomaterials science. Cell therapy is widely studied for cardiovascular and neurodegenerative diseases, neural injuries, diabetes and many others, in which cell supply is needed to allow a proper tissue or organ regeneration.¹⁵⁻¹⁷ Gene therapy relies on the use of specific gene-based molecules to rectify a missed or defective function or phenotype. It is extremely important to manage the correct delivery of DNA or genes to ensure an effective influence on target tissue. To this aim, the role of materials science and bionanotechnologies is fundamental.¹⁸ Contextually, molecular medicine refers to that field in which the role of included drug molecules enhances the generation of new tissue rather than the formation of an unfunctional scar.¹⁹ Instead, biomaterials science represents the needed technical field aimed to find solutions to ensure the correct function of the involved biological constituents, as, for example, the role of scaffolds in cell culture or engineered carriers for the delivery of therapeutic molecules. Thence, because of the above-mentioned complexity of this field, other fundamental branches of knowledge are the basic constituents of tissue engineering through a mutual interconnection. The following list reports some of them: materials science, mechanics, computational science, chemical engineering, cell biology, histology, genomics, pharmacology and biochemistry. In the following paragraphs, the basic principles of tissue engineering will be described and thoroughly discussed with the aim to highlight their importance for the development of novel strategies, with particular attention to the role of biomaterials science.

3. The basic concepts of traditional drug discovery and development

One of the most difficult and expensive processes in the medical and industrial fields concerns the development of new drugs for human health. It has been estimated that the total costs for drug development in the USA exceed a billion dollars and in the next years a further increase is foreseen. The total duration of the drug development process can require over 10 years and, once into the market, only 2 drugs out of 10 will cover the total development costs through revenues. The overall process encompasses various extended steps. Firstly, the target is identified when a needed correlation to a disease is confirmed by a clue. Subsequently, a high number of new molecules is synthesized and applied against the identified target with the aim to select which molecules, called *hits*, can exert the attended therapeutic effect. Based on the model of these molecules, new potential drugs are designed with slight differences in order to figure out which ones show an enhanced activity. A further procedure of selection on the previous molecules results in the definition of the most promising drugs, identified as *leads*, with enhanced pharmacological effects. However, only few of these *leads* are selected for following pre-clinical investigations. At the end, it is estimated that one molecule out of 10 which have been tested on humans can actually be sold into the pharmaceutical market.²⁰

In this complex scenario, the technological development plays a fundamental role in better optimizing the efficiency of the outputs of the drug development process. Nevertheless, the development process of any drug molecule is mainly hindered by one extremely important aspect, which is its delivery. It is well-known that physiological or pathological environments are characterized by the presence of biological barriers to drug efficacy and bioavailability. In particular, when a drug is delivered orally, its solubility, permeability and resistance to degradation in adverse environments (i.e., stomach) represent the major constraints. Moreover, the efficacy of

a drug is severely modulated by biological barriers, such as the blood brain barrier (BBB) or the intestinal mucosa when the target is represented by the brain or the intestine.

Because of the presence of these physico-chemical limitations, drug administration and delivery represent complex issues. In addition, it is necessary that an administered drug is delivered to the target sites at the therapeutic concentration with a sustained rate within a proper time frame, and reducing any side effect. From this point of view, the chemical properties and stability of a drug importantly influence the method for administration. In the book “Drug delivery: principles and applications”, Barich and co-authors schematically represented the correlation of three different aspects,²¹ namely physico-chemical properties, formulations and administration route, which affect the efficacy of a delivered drug, as reported in figure 2.

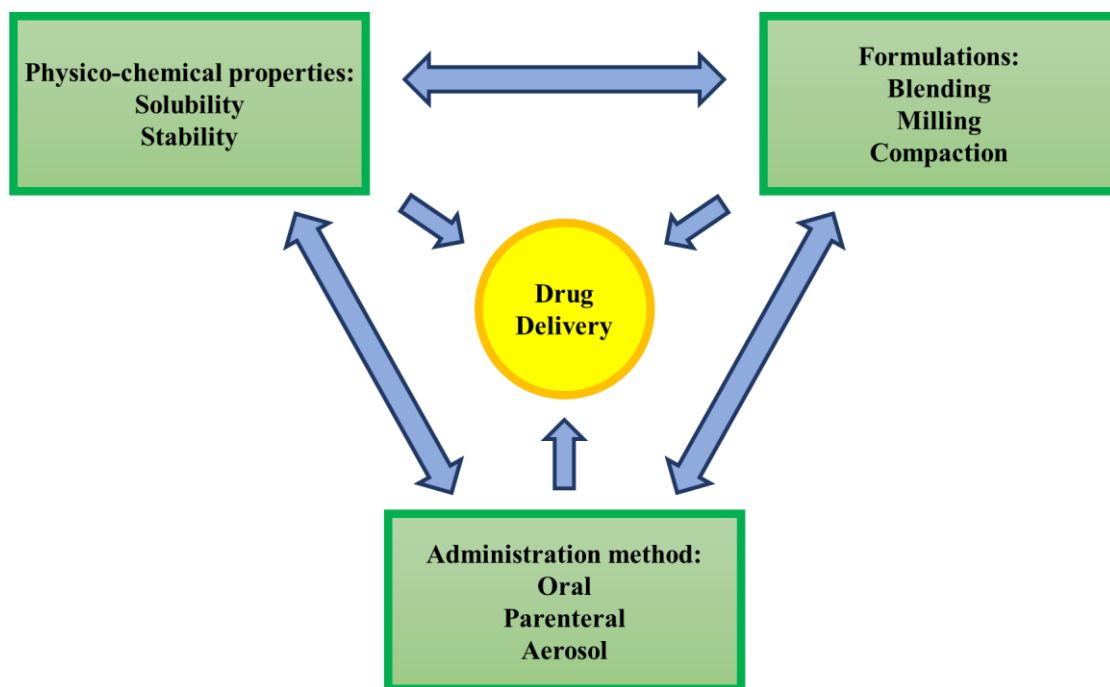


Figure 2 – Schematic and simplified representation of the overlap between administration method, physico-chemical properties and formulation method resulting in drug delivery.

A step forward in the evolution from this traditional approach occurred in 2007,²² when the idea of “regenerative pharmacology” was coined deriving from the potential overlapping between pharmacology, engineering, and medicine. In the following paragraph, the focus will move to this new and evolving frontier that combines medicine and pharmacology together to overcome the important limitations of traditional drug delivery approaches.

4. Regenerative pharmacology: a new answer to clinical needs

Regenerative pharmacology builds on the same aims of regenerative medicine. Therefore, these two disciplines are widely overlapped and can be associated as synonyms in certain cases. Indeed, regenerative pharmacology is finalized to treat a disease through a pharmacological approach able to re-establish the physiological functions of a tissue or an organ. This is significantly different from any usual pharmaceutical approach, which key target is the management and the alleviation of symptoms and pain without necessarily regenerating a physiological function. It is clear that traditional pharmacology represents an important field that significantly helps any patient to better

stand the symptoms of a pathology. Nevertheless, the idea of regenerative pharmacology is different and more ambitious. In fact, it exploits therapeutic formulations showing curative effects on the organism, trying to solve the disease at the first onset of symptoms. Undoubtedly, this approach results in a very complex strategy that will enable novel technologies to be realized; however, the impact of the expected outcomes corroborates the efforts spent in inducing a revolution in the clinical field.²² To demonstrate this and to better understand the central role of regenerative pharmacology, some of the principal elements of regenerative medicine, namely i) Cell culture, expansion and maturation, ii) Biomaterials science, iii) Enabling technologies, and iv) Implantation of the tissue, should be analyzed from a different perspective.

In the context of cell cultures, the role of applied pharmacology consists in modulating cell response through specific molecules, such as growth factors, hormones, cytokines, chemokines, and even small drugs. The importance of materials science is crucial to develop highly engineered platforms to manipulate and properly guide cell culture development, but also, in this particular case, to host and integrate enabling technologies to tune and manage the release kinetics of loaded molecules. In other words, this is the role of drug carriers for targeted and controlled release. In this scenario, even bioreactors are relevant devices for the advanced administration of drugs. Indeed, the automation that characterizes bioreactor design can represent a powerful tool in standardizing and controlling the evolution of an engineered tissue.²² Concerning tissue implantation, a wide array of regenerative and pharmacological strategies is applied to properly maintain and stimulate the construct during its integration *in vivo*.²³

For all the above-mentioned aspects, the role of pharmacology from a regenerative point of view is elemental and needs to be correctly implemented in order to induce a significant improvement in the efficacy of involved therapies. This represents a promising frontier, although new important challenges arise in the process for the design and development of these new therapeutic strategies, due to their overall increased complexity. To overcome these noteworthy challenges, it is mandatory to develop highly engineered and controllable biomaterials specifically addressed to drug release applications.

4.1 Biomaterials for regenerative pharmacology and tissue engineering

The development of biomaterials represents a highly branched field based on many disciplines, as chemistry, materials science, and biology. This subtle interconnection allows the design of highly functionalized biomaterials suitable for the development of drug delivery systems able to overcome traditional barriers in biological environments, thus widening the set of releasable molecules and enhancing their efficacy. Principally, two classes of strategies based on smart material application can be identified for drug payload release: i) particulate platforms, ii) scaffolding supports, or a combination of the two.

5. Particulate platforms based on nanotechnologies for drug release: general principles and considerations

Particulate systems have been developed in order to improve and tune pharmacokinetics, as well as to better overcome biological barriers that limit drug availability. In addition, these systems can

be specifically functionalized to show high specificity for a target to be treated, enhancing the efficacy of the drug treatment while reducing side effects. In regenerative medicine, these two aspects are extremely important, since the released molecules, such as growth factors, hormones, DNA segments, antioxidant or antitumor molecules, are generally characterized by short life in biological environments.^{24,25} In this scenario, the development of technologies at the micro- and nano-scales can represent an effective approach to overcome this obstacle. Materials science and engineering play a pivotal role in the achievement of this aim. In fact, regenerative pharmacology and medicine are addressed to realize functional devices of few hundreds nanometers or even less, opening the possibility to ensure higher availability, mobility and controllability of therapeutic agents that are delivered into the human body.²⁶

A set of general requirements for drug delivery vehicles can be defined based on the above-mentioned properties and finalities, highlighting the most important aspects to consider for an effective design of these devices.

Most importantly, i) the biological compatibility of a drug releasing nano-matrix should ideally prove the absence of toxicity, considering even degradation products that are generated over time in the organism. Moreover, to be effective, an engineered platform for advanced drug release should ensure ii) a relevant encapsulation stability, avoiding premature release of payload and maximizing the efficiency of the therapy in the targeted site. Additionally, a fundamental role is represented by iii) stimuli responsiveness. In fact, this aspect can allow a more precise and triggered release when it is effectively needed. The effectiveness of these systems is also dependent on iv) feasibility and simplicity of the synthesis process, which is mandatory for industrial production and final approval by regulatory commissions (e.g., Food and Drug Administration, FDA).

5.1. Physical and chemical principles for the development of drug delivery platforms

Different typologies of carriers can be found: metallic, inorganic, organic and polymer-based platforms. The physical nature and thus the chemical properties of a selected drug represent the key factors for the determination of carrier composition and design.

More specifically, the development of a drug delivery platform is based on a wide set of intermolecular interactions that occur spontaneously between the involved building units. The interdisciplinary field of materials science generally describes these physical phenomena as processes of self-assembly. Differently from covalent bond formation, physical interactions are significantly weaker and may negatively affect the overall stability of the systems. Nevertheless, when the involving variables are well understood and correctly controlled, the resulting devices can be characterized by high tuneability, versatility and reversibility. The involved interactions are i) hydrophobic interactions, ii) electrostatic bonds, iii) hydrogen bonds, and iv) π - π staking.

Hydrophobic effect represents the most important driving force in self-assembly processes. In nature, proteins, peptides and other polymers, such as lipids, can show an amphiphilic nature and their hydrophobicity can lead to microphase separation phenomena. In watery environments, hydrophobic domains can interact and collapse, thus forming aggregates with reduced interaction of hydrophobic domains with the polar solvent, while hydrophilic domains are exposed to it. This

is the principle of surfactants. Differently, electrostatic bonds are based on the interaction of opposite charged domains. Cationic molecules can assemble with anionic ones, thus forming intermolecular aggregates. Hydrogen bonds consist on the specific electrostatic interaction between hydrogen atoms and other elements showing marked electronegativity (e.g., O, N or F). Hydrogen bonds occur even between soluble molecules and water and are fundamental in the self-assembly process of DNA and proteins. π - π staking can be observed when the forming units are composed of aromatic domains, which are able to interact with other similar domains for their chemical and physical peculiarities resulting from their molecular orbitals.^{27,28} It is important to specify that these physical interactions can be observed simultaneously when systems composed of different chemical domains are developed.

Moreover, even chemical crosslinks can be exploited to design highly stable platforms for drug delivery. Indeed, the addition of covalent bonds is generally exploited to fix the structure derived from a previous physical self-assembly, thus enhancing circulating life and minimizing the risk of premature payload release. A wide variety of possible strategies based on covalent bonds can be exploited to develop drug delivery platforms. Among them, disulfide-, amine-, click chemistry-based and photo-induced crosslinking reactions are some relevant examples.^{29,30} Nevertheless, also in covalently stabilized platforms, physical interactions are extremely important for the primary intermolecular stabilization between the involved constituents before chemical crosslinking.³¹

5.2 Drug encapsulation strategies

Two approaches are mainly utilized for drug encapsulation: passive- and self-delivery. The former is based on the passive integration of a drug payload into carriers assembled through hydrophobic interactions. Examples of these systems are micelles, porous nanoparticles and polymeric nanocapsules, which are able to firmly encapsulate non-polar drugs.³¹ Nevertheless, this approach can result in a low drug loading or in an un-controlled and burst release. A possible solution to these drawbacks can be figured out through the direct drug conjugation to the nanocarriers.³² Whereas in the passive approach the encapsulated drug does not play any role in carrier assembly, in self-delivery drug molecules are properly exploited as forming units to build nanostructures. In this way, drug properties play a fundamental role for the tuning of release kinetics.³³ As delivery platforms are either molecular devices or molecule-based devices, further functionalities can be applied to achieve the desired targeting approach. In this regard, it is possible to classify two approaches: active and passive targeting.³⁴ In the former, specific molecular sensors, such as small proteins and antibodies are used to selectively recognize the target. Differently, in passive targeting physical and chemical variables are exploited to reach the site of interest. For example, the vessels generated from a growing tumor, which are particularly porous, represent the way for specifically sized carriers to reach the neoplastic target. The most relevant nanostructures and delivery strategies are discussed below with particular focus on polymer-based technologies.

5.3 Typologies of polymeric nanostructures for drug encapsulation and release

Because of their remarkable possibilities of functionalization, the development of polymeric systems represents an interesting solution for the design of drug carriers, which can effectively enhance drug solubility, stability, and efficiency. Natural or synthetic polymers can be selected to

produce engineered platforms having different nature and properties, as illustrated in figure 3 and discussed below.

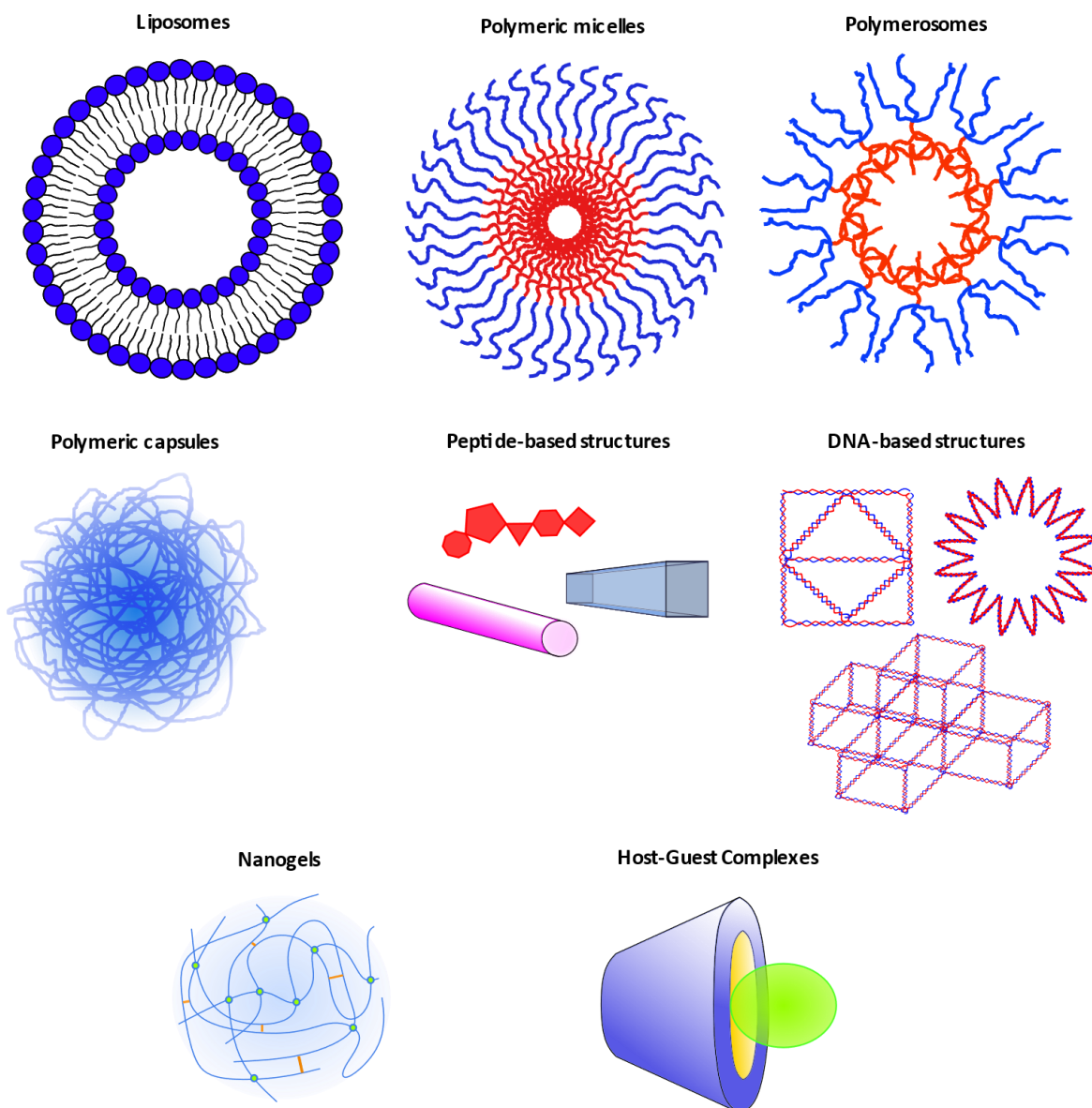


Figure 3 – Schematic representation of polymeric drug carriers.

Liposome-based nanocarriers have been studied from decades and are based on vesicles composed of low molecular weight phospholipids (e.g., phosphatidylcholine-functionalized molecules).³⁵ Their configuration could be based on one single lipid layer or a multilamellar wall, opening to way to the possibility to encapsulate both polar and non-polar molecules. Exceptional biocompatibility and tunable degradation rate can be properly achieved by modifying the lamellar nanostructure. Moreover, their chemical properties also allow the possibility for additional functionalization. As an example, X. Sun *et al.* designed biomineral-binding liposomes encapsulating icariin for the treatment of osteoporosis.³⁶ They found that liposomes effectively bound to biominerals and showed remarkable advantages with respect to pure drug for the treatment of osteoporosis. Another example can be found in the work by Nam *et al.*, which used liposomes for the targeted delivery of vascular endothelial growth factor (VEGF), observing an enhanced retention time, permeability, and then therapeutic effect in ischemic districts.³⁷

Nevertheless, liposomes are characterized by important limitations, such as the concrete risk of degradation through hydrolysis or oxidation, in addition to the relatively high costs for production and scaling-up.³⁸

Polymeric micelles and vesicles represent another type of drug carriers that can be developed in a wide range of sizes and shapes. In this context, amphiphilic polymers, which contain both hydrophilic and hydrophobic domains, are widely investigated forming materials of both micelles and vesicles. The nature of the constituent hydrophilic and hydrophobic domains and their balance are tunable parameters to modulate the properties of the resulting carriers.^{39,40} Strategy for drug loading relies on the spontaneous assembly of these macromolecules in solvents. Indeed, hydrophobic domains can assemble through weak interactions forming a stable core in which insoluble drugs can be encapsulated. Solubility in watery environment is guaranteed by hydrophilic blocks that constitute micelle shell. Many hydrophobic polymers can be used as amphiphilic polymer building blocks and the most diffused are poly(ϵ -caprolactone), poly(hydroxybutyrate), poly(lactic acid) or poly(propylene oxide). Hydrophilic domains are usually composed of poly(ethylene glycol) (PEG, traditionally used for low molecular weight polymers), also known as poly(ethylene oxide) (PEO, generally utilized for high molecular weight polymers); (PEG and PEO can be used as synonyms, since the literature reports various examples naming PEG and PEO polymers characterized by equal molecular weight, as reported below). The wide availability of designable polymers opens the way to the possibility to precisely tune dimensional properties, stability and drug encapsulation capability. In terms of applications in regenerative pharmacology, an interesting study was conducted by M. Gou and co-workers.⁴¹ Briefly, they designed a di-block co-polymer based on monomethoxy poly(ethylene glycol) and poly(ϵ -caprolactone) able to encapsulate curcumin as antitumor. They observed an inhibition of cancer growth and angiogenesis directly killing cancer cells *in vivo*. The development of polymeric micelles significantly enhanced the efficacy of the drug with respect to its free form. Many other examples of micelle-based delivery systems can be found in literature for the treatment of cancer^{42,43} and chronic wounds.⁴⁴ Differently, *polymeric vesicles* (or polymerosomes) are more complex entities, since they are based on bilayer walls containing a water-based solution into their core. In this way, the soluble payload is separated from the external environment that can be degradative for the drug. For example, P. Kulkarni and co-workers developed polymerosomes composed of poly(lactic acid)-azobenzene-poly(ethylene glycol) able to self-assemble in watery environment and encapsulate antitumor drugs (i.e., gemcitabine and erlotinib).⁴⁵ This platform was characterized by highly responsiveness to the external environment. In fact, most of cancers produce a hypoxic surrounding environment, which was exploited in this work to trigger vesicle disassembly and hence drug release. The application of the developed system showed a significant decrease of viability on pancreatic cancer cells (BxPC-3) spheroid cultures. Another interesting example of polymerosome-based drug delivery systems has been presented by P. Wei *et al.* through the development of ultrasound-sensitive polymerosomes based on poly(ethylene oxide)-*block*-poly(2-(diethylamino)ethyl methacrylate)-*stat*-poly(methoxyethyl methacrylate) [PEO-*b*-P(DEA-*stat*-MEMA)] co-polymer.⁴⁶ PEO was selected for its high hydrophilicity, cytocompatibility and enhanced circulation time *in vivo*, while PMEMA and PDEA were aimed to ultrasound- and pH-responsiveness, respectively. The resulting systems showed a pronounced endosomal escape ability and a high controllability of doxorubicin hydrochloride release *in vivo* due to ultrasound stimulation. Nevertheless, all the above-mentioned systems are based on

amphiphilic polymers and hence their stability and self-assembly are strongly dependent on many physical properties, such as polymer concentration and external temperature. In fact, the self-association among hydrophobic domains occurs above a critical micelle concentration (CMC) and a critical micelle temperature (CMT). Therefore, stochastic and uncontrollable variations of environmental parameters can significantly affect the response and the stability of these systems; for these reasons, further chemical stabilizations can be required. Indeed, through the addition of sites for chemical crosslinking on the constituting polymers, a better integrity in structural and chemical terms can be achieved. From a general point of view, such systems can be defined as *Polymeric nanogels*, although different definitions of this term can be found in literature.⁴⁷ An interesting example of polymeric nanogels for regenerative medicine is represented by the work of N. Kordalivand *et al.*, which developed cationic dextran-based nanogels loaded with synthetic long peptides containing different epitopes for T-helper cells.⁴⁸ Their strategy consisted in enhancing cell-mediated cancer immunotherapy through the effect of the loaded protein-based vaccines against cancer. The peptides were physically loaded or chemically bound into the nanogel-based platform. Results suggested that chemical stabilization of the therapeutic peptides represented the best strategy for the modulation of cell response. From a general perspective, chemical crosslinking or covalent drug tethering can represent a useful strategy for drug stabilization and release from nanogels. Nevertheless, in some cases, a higher stability may result in longer time and higher difficulty for total cleavage, thus enhancing toxic effects. As previously shown, polymeric nanogels have found many applications in the biomedical field,^{29,49} but they are contextually characterized by the potential risk to exhibit low responsiveness to the external environment. Moreover, the particulate platform as such and its degradation products can be characterized by local or systemic toxicity.

Polymeric nanocapsules constitute a delivery platform characterized by a different morphology compared to the above-described carriers. Drugs are confined into hollow cavities of polymer sheath through interfacial polymerization or solvent displacement method, thus protecting the payload from degradation and reducing drug-induced systemic toxicity. However, the high stability of the polymeric membranes can cause delayed release due to scarce permeability and therefore the controllability of the release kinetics represents a challenging aspect.⁵⁰ Despite these relevant drawbacks, M. Peleteiro and co-workers applied a delivery platform based on nanocapsules for vaccine delivery.⁵¹ In detail, three different carriers were designed utilizing protamine, polyarginine and chitosan, to investigate their interaction with specific cells of the immune system. Interestingly, they discovered that arginine-based systems were able to strongly modulate the involved biological processes and were then selected for the integration of the recombinant hepatitis B surface antigen through simple charge-mediated absorption onto the corona of the nanocapsules. The application of these systems *in vitro* and *in vivo* in mice suggested their potentiality for further similar applications aimed to vaccine delivery.

Nanostructures based on peptides represent an extremely promising strategy for the development of drug delivery systems.⁵² In fact, peptides can be characterized by high cytocompatibility, tunability and sensitivity to external stimuli. For their heterogeneous composition, they also show the ability to self-assemble, as occurs in protein synthesis and maturation. Their implementation opens the way to the possibility to produce highly functional and engineered devices with tunable final shape and size,⁵³ as peptide synthesis can be precisely controlled.⁵⁴ Hence, micelles, vesicle,

fibers, tapes and ribbons can be developed as drug carriers and can be easily functionalized with other biomolecules (e.g., antibodies) to actively target drug release. Moreover, the wide possibilities to tune peptide synthesis process also permit to design bioactive platforms for the treatment of various diseases or the stimulation of specific biological responses.⁵⁵ One interesting application of peptide-based nanostructures is the treatment of infected tissues or organs.⁵⁶ In detail, the involved molecules are known as antimicrobial peptides and are generally characterized by immunomodulatory activity and bactericidal power. In their work, S.L. Porter and co-authors developed a system based on self-assembling diphenylalanine peptide nanotubes showing the ability to selectively eradicate bacterial biofilms.⁵⁷ In this study, the singular tunability of peptide-based systems turned out to allow a fine modulation of bactericidal power and eukaryotic cell toxicity, thus reaching a complete *Staphylococcus aureus* biofilm kill within 24 hours exposure at 10 mg ml⁻¹ peptide concentration. The impact of these nanotechnologies can be revolutionary in the medical field. Nevertheless, the most important drawback can be represented by the relatively high costs for peptide synthesis,⁵⁸ which can hinder industrial scaling-up. For this reason, the spread of nanostructures based on peptides in the biomedical field is still a challenging aspect nowadays.

Nanostructures based on Nucleic Acids can be even utilized to produce interesting drug delivery platforms, since DNA and RNA show the ability to self-assemble into highly hierarchical structures. In particular, the DNA shows several interesting qualities, such as predisposition to chemical modifications, low immunogenicity, versatility, and release controllability.⁵⁹ Structures as nanotubes, dendrimers and polyhedra can be composed starting from DNA segments. In their work, Y. Huang and co-workers developed a novel DNA-based structure known as “DNA origami” with the enhanced ability to transport and release ruthenium polypyridyl metal complexes for cancer treatment, reducing systemic toxicity significantly.⁶⁰ Moreover, biotin was also conjugated to these systems to further enhance drug stability, cancer toxicity and cellular internalization. This strategy allowed the protection of other non-target organs from general side effects in nude mice. However, as for peptide-based drug delivery structures, these platforms require relevant expenses to be developed and produced. In addition, the tunability of pharmacokinetics of these structures is challenging since their bioavailability can be hindered *in vivo*.⁶¹

Nanostructures based on inclusion complexes are extremely interesting systems, in which the intimate interaction between a drug and a molecular carrier occurs and evolves at the supramolecular level. The formation of inclusion complexes can also be defined as the formation of *host-guest* structures, thus indicating self-delivery as drug encapsulation strategy. The carrier molecule must be characterized by unique morphology and physico-chemical properties to firmly host the involved drug. To this purpose, natural molecules, such as cyclodextrins, have been widely studied and show a great potentiality for future applications.⁶² Thanks to their toroidal shape and the intrinsic hydrophobicity that characterizes their inner cavity, cyclodextrins can encapsulate lipophilic drugs through hydrophobic interactions. Their geometrical properties can be tuned depending on the number of constituting monomers of glucose. The resulting host-guest complexes show the peculiarity to be water soluble, due to the hydrophilicity that characterizes the outer wall of these oligosaccharides. Generally, higher solubility, bioavailability, stability, and therapeutic effect of encapsulated drugs can be obtained through this strategy, but the formation

of complexes does not always improve drug properties in biological environments. Indeed, faster degradation of encapsulated drugs can be observed, depending on the involved interactions between the host and the guest molecules.^{63,64} Other macrocycles with a different chemical composition can be used for the same purpose: calixarenes,⁶⁵ cucurbiturils⁶⁶ and pillarenes.⁶⁷ Inclusion complexes can be formed even through the development of more convoluted molecules, such as dendrimers.⁶⁸ These molecules are extremely versatile for their highly complex and heterogeneous composition, allowing even covalent conjugation of drugs or active targeting. Nevertheless, the high complexity of dendrimers can hinder their predictability in real biological environments, where the number of uncontrollable variables is relevant.

5.4 Nanostructures for regenerative pharmacology as products into the market

As recently reported by Patra and co-authors,²⁶ nowadays more than 50 products based on the above-mentioned nanostructures are effectively used in the clinical field, as schematically reported in figure 4. *Circa* the 15% of these products is addressed to treat infections; the 19% for cancer treatment through chemotherapeutic drug delivery; the 30% is addressed to the resolution of autoimmune diseases or other physiological diseases; the 36% is aimed to the application of nucleic acid-based formulations. Nevertheless, even though an increasing interest for the development of novel bionanotechnologies is evident due to the high number of specific investments, an important set of issues is still affecting this multi-disciplinary field. In fact, because of their typical high complexity, it is generally difficult to find unique and clear definitions of the developed systems. Toxicity and safety assessments represent actual uncertainties, even because of specific and consistent regulations have not been developed yet. The lack of definitions and regulations is strictly related to the general variety of the emerging systems. Indeed, the significant number of variables that are involved in the application of these systems is the main hampering element for their development. Hence, it is common to find unforeseen results or to observe toxicity when these platforms are applied *in vivo* or in clinical trials. A partial solution to these issues has been individuated in the application of already existing regulations on conventional drugs. However, the application of such approach is questionable,^{69,70} since the risk to neglect relatively important aspects related to the behavior of involved nanostructures in real biological and pathological environments is concrete. From this perspective, if the complexity of the nanometric structures increases, the risk to negatively interfere with tissue or organs can be enhanced. Then, a concomitant and continuous advancement of knowledge in medicine at the molecular level and in nanotechnology is required to better set-up highly specific and controlled strategies. Ultimately, in order to carry out accurate analyses on the therapeutic impact, toxicity and industrial feasibility, long term studies are necessarily required. The development of specific and continuously updated regulations is now occurring in parallel to medical and nanotechnological progresses, thus widening the availability of optimized protocols for specific regulations.

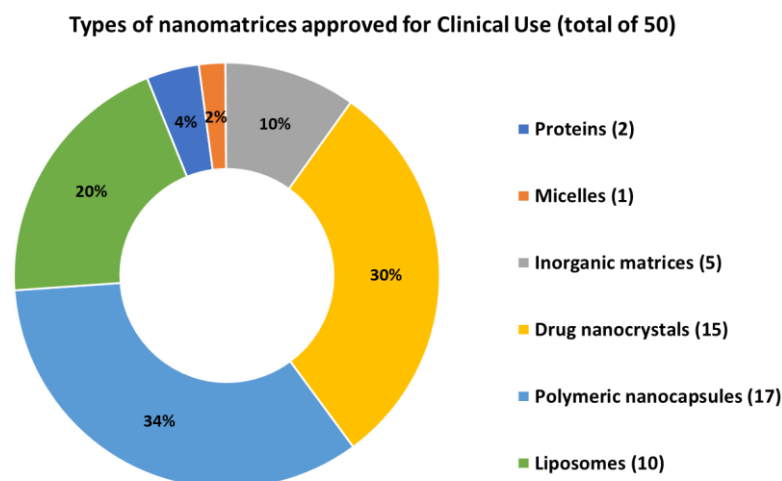


Figure 4 – Schematic representation of drug nanocarriers approved for clinical use⁷⁰.

6. Scaffold and injectable matrices as devices for regenerative medicine and pharmacology: general principles and considerations

Another strategy to induce tissue regeneration is based on the development of injectable matrices or implantable solid scaffolds. These structures strongly interact with the surrounding biological environment at different levels, thus enhancing regenerative processes.^{71,72} Their intrinsic chemical and morphological properties are the most influential for this purpose. In addition, the integration of additional features aimed to provide them with the ability to host and progressively deliver therapeutic molecules, represents an extremely valuable approach to enhance and accelerate tissue formation and growth. Nevertheless, the occurring of complex correlations between physical properties at the micro- and macro-scales, as well as the behavior at the molecular level, represent challenging aspects for the development of scaffolding platforms for drug release and tissue engineering. Hence, the design of new materials and production protocols are aimed to the achievement of the best controllability of biological response and in case release kinetics of stimulant molecules. Injectable systems generally show the possibility to reduce invasiveness, but may lack of mechanical qualities to sustain surrounding tissues and organs. From the opposite side, the development of solid porous scaffolds represents a valuable solution when a significant tissue lacuna characterizes the biological district where a therapy is needed. Although, in this case a more invasive surgical implantation can be required.

A set of various requirements characterizing scaffold-based platforms for drug release and tissue regeneration can be individuated. The most important aspect to consider is the *biocompatibility* of the system. Firstly, this property involves the surrounding biological environment through a direct contact. In this regard, the chemical composition is highly important. Natural materials can be used as constituents of engineered scaffolds and represent the best choice for biocompatibility. However, they may be defective in terms of controllability and repeatability for the intrinsic uncertainty related to extraction procedures.⁷³ Differently, synthetic materials (i.e., synthetic polymers or inorganic compounds (e.g., bioactive oxides and ceramics)) show the possibility to highly control and tune their physical properties, ensuring repeatability. Nevertheless, in this case

the integration into the organism and the biological response are more challenging with respect to systems based on natural materials. Bioartificial systems based on the combination of natural and synthetic materials can be also designed. The resulting devices can then show the advantages of the single components, while reducing the isolated limitations.

For all these aspects, biocompatibility is not a trivial property to characterize and control. Moreover, it is articulated on different levels, since it does not depend only on the chemical properties of the bulky material itself, but it is also correlated to the components that can be released during implantation as degradation/dissolution products. This facet introduces the ideas of biostable and biodegradable systems. In the first case, highly stable materials are used to compose the device (e.g., aliphatic polymers such as poly(ethylene) and poly(ether)s). In the second one, systems are based on materials that can progressively degrade (e.g., natural polymers, poly(ester)s and other hydrolysable polymers), thus allowing their progressive replacement with a newly regenerated tissue. Nevertheless, the controllability of degradation rate and the toxicity of released products represent important and challenging aspects to determine. In this regard, *morphological properties* play a pivotal role. Porosity as well as pore dimension and distribution are extremely important since they significantly modulate degradation kinetics and biological responses. Specifically, pore size and distribution initially modulate cell adhesion and migration. Tissue maturation depends on the mass exchange with the environment which is influenced by the properties of porosity at its higher level (i.e., hundreds of micrometers). In fact, nutrients and stimulating molecules are required for the correct tissue development, meanwhile metabolites need to be adequately washed out. The continuous and proper mass exchange and cell migration depend on the morphological properties of porosity and interconnectivity is fundamental in this regard. At lower levels (i.e., units and fraction of micrometers), porosity influences cell adhesion and response. In addition to morphological properties and the bulk composition of a scaffold for tissue engineering, the chemical properties at the interface with the biological matter is equally important. In fact, a specific functionalization of scaffold surface can be performed through the introduction of *bioactive domains*, such as proteins or peptides (e.g., RGD, IKVAV and similar) to properly control cell adhesion and behavior. Thence, a correct combination of micro-morphology and chemical composition is required to modulate cell fate.⁷⁴

In the following paragraphs, the main examples and applications of the above-mentioned devices are reported, with particular attention to their potentialities and challenges.

6.1 Drug delivery and tissue engineering applications of injectable systems

Injectable materials have been the topic of many research works since they represent the best promise for both drug delivery and tissue engineering. A well-developed injectable system allows localized deposition or parenteral delivery in the site of interest. Moreover, it can also be exploited as a proper template for the formation of a new tissue. Interestingly, a substantial resemblance exists between scaffolds addressed to cell-based applications and the ones developed for drug delivery. Generally, high tunability and processability characterize this kind of platforms. In the following paragraph, a general overview of their most recent applications in regenerative medicine is reported.

6.2 Hydrogels

Hydrogels are three-dimensional crosslinked networks with a pronounced hydrophilic nature. Hence, they are able to retain and exchange a relevant amount of water or biological fluids. For this reason, hydrogels show a set of properties in common with the extra-cellular matrix (ECM) and represent valuable candidates to mimic a physiological behavior when implanted in a biological environment. A high number of strategies can be found in the literature to form hydrogel networks, encompassing the use of natural or *ad-hoc* designed synthetic polymers, stabilized through physical or additional chemical crosslinking. The entire set of possibilities for hydrogel classification on the basis of various features (i.e., ionic charge, physical properties, biodegradability, source and crosslinking method) is reported in figure 5. Within this scenario, a subdomain of hydrogels exhibits injectability. From a general point of view, injectable gels must meet some requirements, which depend on their highly dynamic and responsive behavior. Firstly, their stabilization after deposition should be obtained under mild conditions, thus alleviating potential stressing processes (e.g., harmful chemical reactions) in the surrounding environment. Then, the time required for network formation should be as short as possible to avoid any potential mass loss outside the site of interest. Finally, hydrogel stability and biocompatibility of degradation products must be ensured in order to reduce the occurrence of any side effects. Physically crosslinked hydrogels can be preferred for the possibility to avoid the use of catalysts or potentially toxic small precursors for initiation, but the resulting mechanical properties are significantly worse with respect to chemically crosslinked networks. In the following paragraphs, typical crosslinking strategies are described, highlighting recent works and achievements in the field of tissue engineering.



Figure 5 – Hydrogel classification depending on various features: ionic charge, physical properties, biodegradability, source and crosslinking method.

6.2.1 Physical hydrogels

Gelation kinetics represents the most important variable for the definition of injection time window. Physical hydrogels can be significantly affected by this aspect in their final performances, depending on the nature of the interactions that lead to complete gelation. Potential reversibility is one important advantage derived from the physical nature of the interactions occurring in this kind of hydrogel networks.^{75,76} Depending on the nature of the occurring interactions, better mechanical properties or reversibility can be obtained. The most well-known categories of physical hydrogels are described and discussed below.

Thermo-sensitive hydrogels

External temperature is an extremely important variable for the development and control of physical hydrogels for drug delivery and tissue engineering. Different amphiphilic triblock polymers with an ABA-architecture (A: hydrophilic domain and B: hydrophobic domain) exhibit temperature-driven phase transitions upon solubilization in aqueous media. In fact, these systems can be characterized by a lower critical solution temperature (LCST) and are able to undergo phase-transition from sol to gel above this specific value. The temperature of human body is around 37 °C that is generally higher than ambient temperature (i.e., between 20 and 25 °C). The LCST value can be modulated working on the composition or the concentration of the constituting polymer in order to be lower than the one that characterizes human body. Hence, the occurrence of this thermal gradient can be exploited to design thermo-sensitive hydrogels able to ensure initial injectability and subsequent gelation after deposition. Moreover, because of their amphiphilic nature, these systems show the intrinsic possibility to increase the solubility and bioavailability of incorporated hydrophobic drugs.⁷⁷ Many applications of these systems can be found in the literature. Commercially available polymers forming thermo-sensitive hydrogels are Pluronics® (also known as Poloxamers®), which are triblock co-polymers with an ABA structure (poly(ethylene oxide)-poly(propylene oxide)-poly(ethylene oxide)). One recent work performed by Q. Wang *et al.* was based on the application of two different thermo-sensitive Pluronics® (i.e., F127 and F68) blended with chitosan.⁷⁸ The resulting bioartificial mixtures were tested for the intranasal delivery of a HIV-1 replication inhibitor (i.e., DB213), enhancing drug bioavailability and brain uptake significantly. The application of commercially available triblock co-polymers in drug delivery have been widely investigated in the last decades,^{79–81} but nowadays the general intention consists in synthesizing new amphiphilic polymers with the aim to enhance their physical and biological properties. For example, P. Patel and co-workers developed new ABA and BAB triblock co-polymers based on poly(ethylene glycol) (PEG, A-domain) and poly(ϵ -caprolactone) (PCL, B-domain). PCL-PEG-PCL-based systems resulted to be the most stable and were utilized to perform *in vitro* release studies of diclofenac sodium, an anti-inflammatory drug.⁸² In the field of tissue engineering, thermo-sensitive hydrogels based on poly(lactic acid-co-glycolic acid) (PLGA) and poly(ethylene glycol) blocks or graft co-polymers (PLGA-b-PEG-b-PLGA, PEG-g-PLGA, or PLGA-g-PEG) have been widely used in cartilage regeneration.⁸³ In particular, PLGA-PEG-PLGA co-polymers have been reported to form highly stable, biocompatible and biodegradable thermo-sensitive hydrogels able to sustain bone marrow mesenchymal stem cell proliferation, enhancing new cartilage formation *in vivo*.^{84,85} Another interesting study was conducted by X. Li and co-authors. Briefly, they encapsulated bone marrow mesenchymal stem cells and kartogenin, a chondro-inductive small drug, into PLGA-PEG-PLGA hydrogels,

observing a relevant cartilage formation in rabbits.⁸⁵ Another valuable approach for the production of thermo-sensitive hydrogels can be identified in the formulation of mixtures based on two enantiomeric triblock co-polymers, as reported in the work of Abebe and Fujiwara.⁸⁶ In more detail, PLA-PEG-PLA co-polymers having different PEG lengths were produced and hydrogels based on specific stereomixtures were designed, observing good resulting mechanical properties (i.e., storage modulus greater than 6 kPa) due to micelle self-organization and subsequent stereocomplexation. However, although the above-mentioned systems are characterized by extremely high versatility and reversibility, they can be affected by poor stability in watery environment when the hydrophilic domains constitute the majority of the overall content.⁸⁷ To reduce the impact of this disadvantage, the hydrophobic content of amphiphilic polymers can be increased, but this can negatively affect injectability, solubility and thermal reversibility. Differently, a very recent approach consists in producing more complex polymers through the polymerization of amphiphilic triblock chains. This can be possible thanks to the high versatility of novel protocols for polymer design and production, such as poly(urethane) synthesis.^{88,89} For instance, Boffito and co-workers developed different poly(urethane)s based on Poloxamer® 407 (i.e., Pluronic® F127), an aliphatic diisocyanate and small diols as chain extenders (e.g., N-Boc serinol or 1,4-cyclohexane dimethanol). As a result, poly(urethane)-based hydrogels showed faster gelation kinetics with respect to Poloxamer®-based ones with the same composition. Moreover, better mechanical properties and higher stability in physiological-like watery environment were obtained.

Ionic hydrogels

One important physical interaction utilized for the production of physical hydrogels is represented by ionic crosslinking. Essentially, charged polymers are mixed with counter-ions, which can be represented by other polymers or smaller ionized molecules or ions. The presence of net charges allows the formation of an interacting network, which is significantly sensitive to external factors. In fact, pH variations, ion diffusion and temperature modulate mechanical properties of the hydrogels and thus also their injectability.⁹⁰ In this field, alginate, a hydrophilic and anionic polysaccharide, is widely used. Its peculiarity consists in forming ionic crosslinks with Ca^{2+} , Mg^{2+} or Ba^{2+} in solution. In their interesting work, N.N. Ferreira and co-authors developed an alginate-based hydrogel to improve the therapeutic effect of bevacizumab (BVZ) as anti-angiogenic drug for cancer treatment.⁹¹ They proved the conformational stability of BVZ, which is a protein-based anti-VEGF drug, once encapsulated into calcium-alginate hydrogels. Moreover, the developed system containing BVZ (3 mg ml^{-1}) was easily syringable and showed enhanced therapeutic effect *in vivo* and high stability in cancer-related environments (i.e., low pH). Another typology of hydrogels based on ionic forces is represented by polyelectrolyte-based complexes. Charged natural and synthetic polymers can be mixed together to produce intermolecular and then supramolecular structures, thus forming hydrogel networks. The main weak point of this strategy is represented by the kinetics of interaction between the oppositely charged components, since inhomogeneous mixtures can be obtained due to the presence of aggregates. A recent work produced by X. Lv and co-workers described an interesting system composed of polyelectrolyte-based complexes.⁹² Briefly, a hydrogel system based on carboxymethyl chitosan and alginate was developed through the synergistic contribution of D-glucono- δ -lactone as donor of protons and chitosan oligosaccharides as building blocks and wound healing agents. Interestingly, upon

addition of chitosan oligosaccharides into the system two-step gelation process was observed, which resulted in gels with outstanding mechanical properties (i.e., elastic modulus about 1 MPa). The application of these systems in wound treatment *in vivo* demonstrated accelerated healing processes due to enhanced deposition of ECM and angiogenetic phenomena. Nevertheless, ionically crosslinked hydrogels can show issues related to the stability of their network. In fact, the external environment can negatively affect their stability by changing the local milieu through the diffusion of ions and water. Moreover, their versatility is limited in restricted time frames, as these systems are characterized by fast gelation kinetics which may impede injectability.⁷⁵ To overcome this issue, high controllability of ionic interactions on different molecular levels must be ensured through highly precise synthesis methods.⁹³

Hydrogels based $\pi - \pi$ stacking

$\pi - \pi$ stacking interactions are formed between aromatic molecules, as described before. When these functionalities are introduced as lateral or terminal groups in polymers, they can interact through the mutual affinity of π -electron-deficient and π -electron-rich regions. Their possibility to relatively arrange in two different ways (i.e., plane-to-plane and edge-to-plane) increases the probability of interaction and thus physical crosslinking formation. Due to their peculiarities, aromatic amino acids (i.e., tyrosine, phenylalanine and tryptophan) are widely used to form hydrogels.^{94,95} As such, the nature of these systems is based on natural oligomers or polymers (i.e., peptides and proteins), but also purely synthetic polymers can be produced showing the same side chains. For example, H. Cui and co-authors developed an highly functional and self-assembling system based on polylactide–poly(ethylene glycol)–polylactide (PLA-PEG-PLA) functionalized with carboxyl-capped tetra-aniline (CTA).⁹⁶ The resulting CTA-PLA-PEG-PLA-CTA-based aqueous solutions showed gelation properties that depended on different interactions, such as hydrogen bonding, stereo-complexation and $\pi - \pi$ stacking. Additionally, these hydrogels were injected subcutaneously and enhanced the proliferation of different cell phenotypes (i.e., cardiomyocytes, fibroblasts, and osteoblasts), appearing as highly promising scaffolding platforms for tissue regeneration. However, from a general point of view, these systems can suffer from different interferences that occur *in vivo*, since in real biological milieu the presence of aromatic molecules is not negligible. For this reason, the integrity of the above-described hydrogel systems can be compromised.

Host-guest interaction-based hydrogels

As previously described, the physical interactions that occur between two complementary molecules can result in the formation of inclusion complexes. Host molecules are generally characterized by a macrocyclic morphology and mainly are crown ethers, cucurbiturils, pillararenes and cyclodextrins. These interactions are based on both the physical and chemical matching between the host and the guest molecules. Generally, it is possible to determine specific constant of associations describing the general affinity between host and guest molecules. This peculiar interaction at the supramolecular level can confer to resulting hydrogels remarkable mechanical properties, enhanced reversibility, and good stability in water-based biological environments. Three different approaches can be exploited to produce supramolecular hydrogels: i) supramolecular interaction of linear polymer monomers as host and guest components, ii) complementary blending of host and guest polymer solutions, and iii) polymerization of reactive

and previously assembled host-guest inclusion complexes. In their recent study, Y. Takashima and co-authors developed a supramolecular hydrogel system based on the third strategy and using cyclodextrins as host molecule and dodecyl acetate as guest component, obtaining outstanding mechanical properties (e.g., strain at rupture of approx. 1000%) that can be considered promising for most biomedical applications. Nevertheless, this study needs further biological characterization to prove specific biocompatibility for tissue engineering applications.⁹⁷ Another valuable example was reported by K. H. Hong and S. Song.⁹⁸ In their work, they developed a hydrogel system based on the strong interaction between cyclodextrin and adamantane. Cyclodextrin were grafted to a thermo-sensitive polymer (i.e., poly(organophosphazene)), while adamantane was bounded to Arg-Gly-Asp peptide (i.e., RGD bioactive motif for focal adhesion formation). The interaction between these two components was highly controllable and effective to form a stable hydrogel system. The incorporation of mesenchymal stem cells into these systems was successful. Moreover, cell survival and differentiation turned out to be controllable *in vitro* and *in vivo* through the modulation of host-guest complexes. Furthermore, these macrocycles can even interact with linear polymers characterized by a backbone based on monomers suitable for the formation of host-guest complexes.⁹⁹ In this case, the gelation process is carried out through the formation of a highly hierarchical supramolecular structure, in which the general stabilization is ensured through hydrogen bonds between the outer surfaces of threaded macrocycles along polymer chains. Nonetheless, this strategy is based on non-specific interactions. As such, the overall stability of host-guest interactions and hence the cohesion of the hydrogel can be weakened by the potential interference with other molecular moieties.¹⁰⁰

Finally, the definition “physical hydrogels” denotes an extremely wide set of design strategies to answer to many clinical needs. Among the different investigated approaches, many disadvantages can be individuated. The main drawback is the potential instability of the systems that is correlated to the intrinsic reversibility of physical interactions. A general solution for this issue can be identified in the development of systems based on the synergistic contribution of different kinds of physical crosslinks. This is a widely comprehensive attitude, which can be correlated to the idea of mimicking the self-assembling processes that occur in nature.^{101–104} However, the exploitation of multiple physical principles to stabilize hydrogel networks can cause a significant increase in the overall complexity of the systems, thus weakening their predictability upon implantation into a real biological milieu. For these reasons, physical hydrogels can find a better and more consistent feasibility for drug delivery applications. In this case the physical integrity of the system is generally not addressed to be protracted for long periods. In fact, this property is a fundamental requirement for matrices properly designed for cell adhesion and tissue maturation. As for nanostructured platforms, the design of physical hydrogels should be driven by the extremely challenging intention to establish an effective compromise between simplicity, functionality and predictability.

6.2.2 Chemical hydrogels

The development of hydrogels through chemical crosslinking can answer to the need of increasing hydrogel stability for prolonged applications in the perspective of tissue growth. Nowadays, the possibility to synthesize specific polymers or modify the natural ones is widening the entire set of

available strategies for hydrogel design and tunability in chemical and physical terms. A general overview of the available chemical crosslinking processes to produce stable hydrogels is reported below, in order to highlight the differences with respect to physical crosslink-based approaches.

Hydrogels produced through radical polymerization

Radical polymerization represents a valuable strategy to quickly develop hydrogel networks.¹⁰⁵ In order to perform this kind of reactions, monomers characterized by reactive double bonds are necessary. Acrylamide, acrylic acid, 2-hydroxyethyl methacrylate are highly diffused monomers, but even polymers such as poly(ethylene glycol), poly(vinyl alcohol) and Pluronics® end-capped with double bond (i.e., acrylate or methacrylate groups) containing molecules can be produced or purchased. Moreover, natural polymers (e.g., hyaluronic acid, alginate, pullulan and gelatin) can be properly modified through the grafting of acrylate groups to perform radical polymerization. Nonetheless, the presence of reactive double bonds does not represent the only condition required for the formation of covalent crosslinking and/or polymerization. Indeed, an external stimulus provided through light exposure and the presence of specific catalysts are even necessary. Light-initiated crosslinking can be considered an interesting approach to initially manipulate hydrogel morphology and then stabilize it after injection *in vivo*. One of the most used sources is UV light. However, any biological environment can be sensitive to UV light exposure and formation of free radicals. Indeed, DNA damage and oxidative stress occur in these conditions.¹⁰⁶ Moreover, an important domain of drugs is light-sensitive and the irradiation for prolonged time intervals can cause a premature degradation of the payload.¹⁰⁷ A slight modulation of this negative effect can be obtained through a fine optimization of the crosslinking parameters. On the other hand, it is possible to use initiators able to be activated when irradiated with visible light, thus mitigating the potential DNA damage. Concerning advanced drug delivery applications, a recent study was conducted by K. McAvoy *et al.* that developed poly(ethylene glycol) diacrylate (PEGDA) hydrogels with tunable porosity for the release of different drugs (i.e., ovalbumin and triamcinolone acetonide).¹⁰⁸ They modulated drug release kinetics using PEGDA molecules at various molecular weights (i.e., M_w 250 and 700 Da). As a result, prolonged release kinetics were observed in systems characterized by a higher crosslink density (i.e., PEGDA at lower molecular weight) and encapsulating ovalbumin, which is the molecule with the highest molecular weight analyzed in this study. Additionally, the studied PEGDA-based hydrogels showed high cytocompatibility above a period of seven days, when tested with retinal epithelial cells. Hence, the overall characteristics elevated these systems as promising devices for the treatment of age-related macular degeneration and diabetic retinopathy. Concerning other strategies for tissue regeneration, one remarkably interesting example can be found in the work performed by X. Zhang and co-authors.¹⁰⁹ In their study, anisotropic scaffolds for heart valve tissue engineering were developed using PEGDA at different molecular weights (i.e., M_w 3.4 and 20 kDa) and a photolithographic patterning method. Moreover, a pronounced bioactivity was obtained through the addition of specific peptides for cell adhesion (i.e., RGDS) and collagenase-driven degradation (i.e., GGGPQGIWGQGK). In this study, the combined importance of morphological properties and bioactive domains resulted in controllable effects on the behavior of encapsulated cells and hence on the maturation of novel tissue. More complex polymeric systems can be even found for the development of multi-responsive hydrogels stabilized through photo-crosslinking. For example, photo- and thermo-responsive micelles based on block co-polymers have been stabilized

through radical polymerization in order to confer enhanced capability for drug encapsulation.¹¹⁰ Another interesting and recent work was performed by J. Wang and co-authors.¹¹¹ Through the mixing of alginate and polyacrylamide, they obtained hydrogels with remarkable mechanical properties derived from the co-presence of ionic and covalent crosslinks. Alginate was stabilized using trivalent cations, which are able to form stronger interactions than divalent ones. The combination and the proper modulation of this double crosslinking were the key points to obtain super-tough hydrogels with promising properties for tissue engineering. In fact, the systems characterized by the higher rate of covalent crosslinking were characterized by better mechanical properties than the ones having low content of crosslinker (i.e., N,N'-methylenebis(acrylamide)), differently from what usually occurs in double network systems.

Hydrogels based on carbon-nitrogen double bonds

Imines can be produced in physiological environment through the spontaneous reaction of ketones and aldehydes with available free amines. Moreover, these chemical domains are characterized by a simple synthesis procedure and the involved reactions are reversible. For this peculiarity, it is possible to design highly versatile and injectable hydrogels. The involved chemical groups are widely diffused in natural molecules and polymers, such as peptides, proteins, and polysaccharides, but even synthetic polymers can be designed.^{112,113} An interesting example is reported in the work performed by Y. Ma and co-authors.¹¹⁴ Briefly, they developed an injectable hydrogel system based on xanthan gum functionalized with aldehyde groups and phosphatidylethanolamine liposomes, which served as particulate cross-linkers. The resulting properties of this hydrogel were configured with fast gelation (within 5 minutes) and a high responsiveness to heat, pH and other biomolecules (e.g., histidine). Moreover, its biodegradation can be driven by enzymes that are present *in vivo*. Injectability and self-healing properties were guaranteed by the intrinsic reversibility of the involved interactions and bonds. High viability of encapsulated cells was maintained for two days and indicated a promising suitability of these systems for regenerative therapies through cell delivery in biological environments. Another kind of available chemical domains containing double carbon-nitrogen bonds is represented by oximes, as result of hydrazide- or hydroxyamine-based polymers reacting with aldehyde-based molecules. Chemical modification of natural polymers can be achieved exploiting the chemistry of carbodiimides, thus widening the plethora of available materials for hydrogel design.¹¹⁵ Nonetheless, it is also possible to find other cutting-edge strategies for the functionalization of traditional polymers. A recent work conducted by H. Sanchez-Moran and co-authors can be considered as a valuable example.¹¹⁶ The research group developed an interesting synthesis method to graft aldehyde and alkoxyamine moieties to sodium alginate backbone. The mixing of the developed counterparts in aqueous solutions resulted in oxime-crosslinked alginate-based hydrogels with highly tunable physical properties. The synergistic contribution of alginate-specific ionic crosslinking conferred further reversibility and processability to the resulting hydrogels. The possibility to control geometry and modulate mechanical response, in addition to the remarkable biological properties for 3D cell cultures, marked the developed systems as good candidates for effective applications in regenerative medicine. Another sophisticated example showing the here-discussed covalent strategy for hydrogel stabilization can be observed in the study developed by R. Mateen and colleagues.¹¹⁷ In detail, modified dextran was produced by the introduction of aldehyde and hydrazide groups with the aim to produce an injectable and biodegradable platform.

Moreover, inclusion complexes formed through cyclodextrins were exploited to encapsulate and stabilize dexamethasone. In addition, cyclodextrins were chemically modified to show hydrazide domains, which served to covalently bond them to the hydrogel network. In this way, cyclodextrins were utilized for drug encapsulation and hydrogel stabilization, both of which representing powerful parameters for the tuneability of drug release and hydrogel dissolution kinetics.

Hydrogels produced through Michael addition reaction

Michael addition reactions exploit the interaction between nucleophiles and electron-deficient olefins to synthesize polymers with highly different structures (e.g., linear, branched and so forth). In these reactions, thiols are widely used in combination with α,β -unsaturated carbonyls (e.g., acrylamides, acrylates) under mild conditions, resulting in high polymerization yield and controllability.¹¹⁸ Both natural and synthetic monomers or polymers can be used to develop hydrogel systems. In a recent study, R. Li and colleagues developed an *in situ* gelling system based on thiol-functionalized hyaluronan and maleilated collagen.¹¹⁹ Depending on the formulation and the degree of functionalization of the involved natural polymers, gelation kinetics and mechanical properties were highly tunable. Their suitability for regenerative medicine applications was proved by the good behavior they showed as cell culture supports for prolonged time. A similar strategy was developed by H. Hu and co-workers.¹²⁰ Briefly, they developed a system based on thiolated hyaluronan and maleilated chitosan. Because of the chemical functionalities of the involved polymers, a double crosslinking was obtained. In fact, chitosan behaves as a polycation, while hyaluronan as a polyanion, thus forming polyelectrolyte-based complexes. In conjunction to covalent crosslinking obtained through Michael addition reaction, the resulting hydrogel systems showed very fast gelation kinetics (i.e., within 4 minutes) and an effective antibacterial behavior was obtained due to the presence of chitosan. As an indicator of the continuously increasing interest and feasibility of this synthesis process, it is possible to find in literature an elevated number of works focused on the development of new materials and systems for the production of functional and bioactive hydrogels.^{121–123}

Hydrogels based on thiol-alkene reaction

This kind of chemistry is based on the click conjugation of thiols and double bond-based domains through the mediation of radical formations. Similarly to Michael addition reactions, thiol-ene click chemistry occurs under mild condition and is insensitive to oxygen. However, the presence of a photo-initiator sensitive to visible or UV light is needed. For this reason, considering the photo-sensitiveness of certain molecules (e.g., aromatic proteins and drugs) and the toxicity against cells that UV light might cause, it is necessary to opportunely modulate the irradiation process in order to minimize these side effects.¹²⁴ Generally, high controllability of hydrogel properties can be achieved by using this mechanism of reaction. In this regard, W. M. Gramlich and colleagues performed a study on the synthesis and photopatterning of hyaluronic acid-based hydrogels.¹²⁵ In detail, they attached norbornene groups to hyaluronic acid through a specific synthesis protocol. Hydrogel formulation consisted in the mixing of norbornene-functionalized hyaluronic acid and dithiothreitol, that acted as crosslinker and was exploited to finely tune the mechanical response of the resulting hydrogels. Indeed, the elastic modulus of the developed hydrogels ranged from 1 to 70 kPa. Moreover, the highly controlled technique for crosslinking allowed a defined patterning of multiple peptides, opening the way to the possibility to design

remarkably complex and functional hydrogels. One interesting example is reported in the work carried out by R. F. Pereira and co-authors.¹²⁶ Briefly, they developed a cell-instructive hydrogel system based on pectin for skin regeneration. Keratinocyte and dermal fibroblast behaviors were modulated by the presence of bioactive peptides, whereas mechanical properties and degradation profiles were tuned through crosslinking rate. As a result, the developed hydrogels were able to support the generation of physiological skin *in vitro*, thus representing promising devices for the realization of tissue models or for the treatment of severe skin wounds.

This method for crosslinking is still under investigation, with the aim to further elucidate all its potentiality for the production of highly stable and reversible hydrogels. Nevertheless, a crucial point can be identified in the challenging realization of predictable hydrogel systems that are intrinsically complex on both chemical and morphological aspects.

Hydrogels produced through enzymatically catalyzed reactions

Natural factors that can be found in biological environments can be exploited to form hydrogel networks as well. Thanks to their high selectivity and mild conditions, enzymes, as phosphatases, peroxidases, trans-glutaminase, oxidases and tyrosinase are extremely interesting biomolecules to induce gelation *in situ*. This approach retains particular effectiveness and safety due to the potential absence of toxic synthetic catalysts or external UV irradiation, thus minimizing the overall invasiveness.¹²⁷ In their work, H. Wang and co-authors developed a peptide-based hydrogel system based on self-assembly and enzymatic crosslinking through phosphatase.¹²⁸ The application of this system as vaccine adjuvants resulted highly promising. In fact, the response of immune system was enhanced through the release of an encapsulated model protein (i.e., ovalbumin). Additionally, the developed gels favored the maturation of dendritic cells, promoting the condensation of produced antigens into lymphatic nodes and hence hindering tumor development. As such, these hydrogels demonstrated to be eligible solutions for immunotherapy-related strategies. The main drawback of enzymatic-crosslinked hydrogels relies in the unknown variability of enzyme availability *in situ*. Therefore, the use of an external supplemented enzyme can represent a valuable solution to better control hydrogel behavior, but this may limit hydrogel versatility and injectability.¹²⁹

Hence, the development of chemical hydrogels includes various strategies, aiming to confer higher stability and better mechanical properties with respect to systems purely based on physical interactions. Nevertheless, as discussed above, their processability could be hindered by the quick occurrence of chemical reactions. It is also necessary to develop systems characterized by an extremely high controllability coupled with good handling. In this regard, combining the contributions of both chemical and physical interactions could efficiently answer to the most important requirements for effective hydrogel applications. Indeed, the controllability of hydrogel architecture and physical properties plays an elemental and extremely important role, which will be discussed hereafter. The main properties of physical and chemical hydrogels are summarized below (figure 6), thus highlighting the important correlation between these two crosslinking strategies in order to properly improve and engineer overall hydrogel functionality.

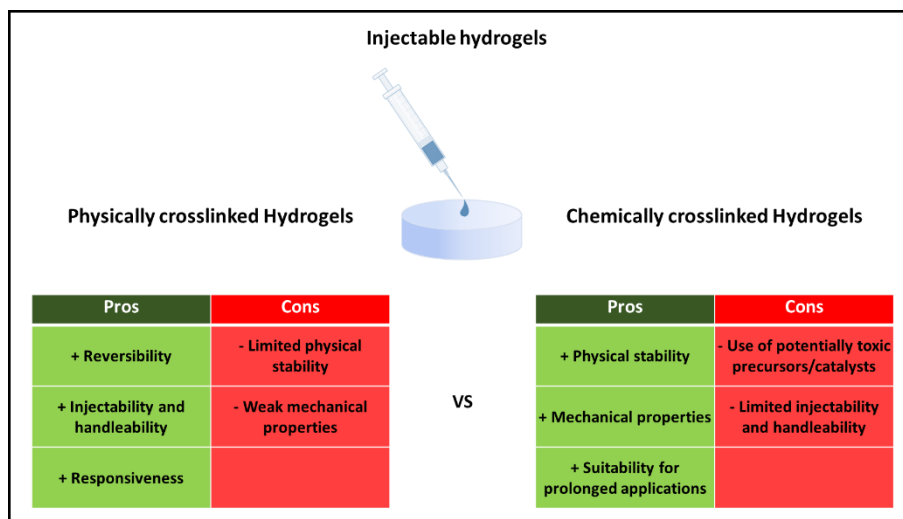


Figure 6 – Summary of the main properties (i.e., pros and cons) related to physical and chemical hydrogels as injectable matrices.

6.2.3 3D printing: the importance of hydrogel architecture

In its infancy, hydrogel design was characterized by structural homogeneity and isotropic response,¹³⁰ which fell later under debate due to the increasing awareness regarding the importance of a more specific control of morphological properties to properly mimic tissue behavior.^{131,132} In order to better control the architecture of hydrogel systems with respect to simple injection or molding, highly effective technologies have been developed, such as inkjet, micro-extrusion and light-based methods. The entire set of these techniques can be generally coded as “three-dimensional (3D) printing”, also known as “rapid prototyping” or “additive manufacturing”. All these terms identify a computer-assisted technique that permits the “layer by layer” development of highly complex morphologies based on different injectable matrices even based on living materials (i.e., cell encapsulating matrices). The exploitation of a CAD-CAM procedure allows a significative improvement in design, flexibility, rapidity, and cost reduction.¹³³ The characterizing high resolution of this approach allows the production of constructs in different shapes and sizes, that allow an effective replication of tissues and organ-like districts. In fact, a better mimesis of the native morphology and physical properties can ensure a better integration for either hydrogels aimed to the maturation of specific tissues or drug delivery systems. The water-based nature of hydrogels is particularly suitable for 3D printing approaches, relying on the remarkable tunability of their chemical composition, bioactivity, and physical response.¹³⁴ Hence, hydrogel design for specific 3D printing applications currently represents one of the most interesting and important challenges in regenerative medicine. In the following paragraphs, a general overview of hydrogel systems for cutting-edge 3D printing applications will be showed, highlighting the prevailing advantages and the concurrent limitations.

Extrusion-based and inkjet 3D printing

This technique is characterized by high simplicity and predictability for a wide set of already available hydrogel-based inks. The resonance into the market of this approach is remarkably strong. Indeed, many examples of commercially available extrusion-based 3D printer can be

found.¹³⁵ The available extrusion design can consist of pneumatic-, piston- or screw-driven systems, which are schematically represented in figure 7.

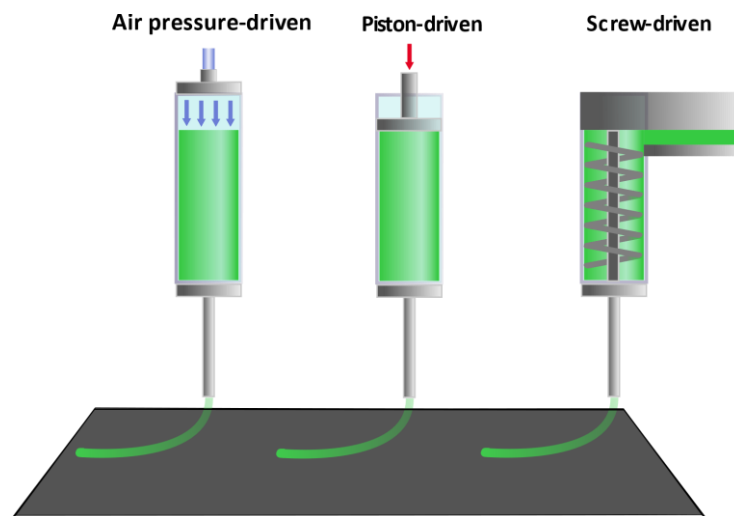


Figure 7 – Schematic representation of extrusion-based strategies for hydrogel 3D-printing.

One of the most important parameters for this technique is viscosity. In fact, its tunability determines printing performances and required time. Generally, the optimal viscosity of injectable systems for this application ranges between 30 and 6×10^7 mPa s,¹³⁶ which also permits the encapsulation of cells at high concentrations with good viability. However, the tight dependence of the printing process on this physical property also implies limited resolution and printing speed. A widely used approach is based on the extrusion of a liquid matrix that is stabilized after the deposition process. To this aim, photo-sensitive polymer-based systems allow a facilitated deposition at the liquid state and then an effective stabilization through photo-induced polymerization. Other strategies can be based on thermal or chemical crosslinking. Nonetheless, despite the remarkable versatility and high reversibility, the former may lack of stability in water-based biological environments,¹³⁷ while the latter might require extended time for chemical crosslinking causing consequent loss in resolution and shape fidelity.¹³⁸ To this aim, the exploitation of concurrent physical interactions can solve the relevant limitations in primary stability and resolution immediately after deposition. In fact, specific intermolecular interactions that produce supramolecular self-assembly phenomena can result in highly self-healing and thixotropic properties, which allow the direct deposition of matrices at the gel state while reducing shear stresses.¹³⁸ A notable example can be found in the work by L. Ouyang and co-workers.¹³⁹ In detail, they developed a printable matrix based on a modified polysaccharide in order to exploit a dual-crosslinking strategy. Indeed, they functionalized hyaluronic acid with cyclodextrins and adamantane, thus producing two counterparts able to form supramolecular crosslinks based on host-guest complexes. Moreover, they integrated methacrylated hyaluronic acid in their final system with the scope to form photo-induced covalent bonds between the constituting macromers. As a result, the novel material showed finely tunable mechanical properties and responsiveness. Additionally, the authors optimized the printing process obtaining complex structures at high morphological resolution. The constructs resulted to be optimal for cell encapsulation and thus bioprinting. The same approach was employed by L. Li and co-authors for the production of biomimetic hydrogel-based constructs for cartilage tissue engineering.¹⁴⁰ In this case, a double-

crosslinking was achieved through the exploitation of self-assembling peptides and photo-crosslinkable hyaluronic acid or multi-armed poly(ethylene glycol). The authors developed hydrogel networks with remarkable stiffness and compression limit (i.e., 200 kPa and >70%, respectively) in conjunction with self-healing ability. From a biological point of view, the here-mentioned systems enhanced the viability of encapsulated cells for several weeks. Additionally, a study conducted *in vivo* highlighted the remarkable regenerative potential of these hydrogels through histological evaluation.

Differently, inkjet bioprinting is based on inks characterized by low viscosity (i.e., <10 mPa s) and deposited through a discontinuous flow.¹³⁶ This peculiarity allows high velocity for fabrication and notably low costs, but implies limited cell density and scarce vertical printing ability. Three groups of inkjet printing methods can be defined, namely continuous-inkjet, electro-hydrodynamic and drop-on-demand bioprinting. More specifically, the approach consisting in drop-on-demand printing is one of the most used and it is based on other two principles: thermal and piezoelectric inkjet printing, as summarized in figure 8.

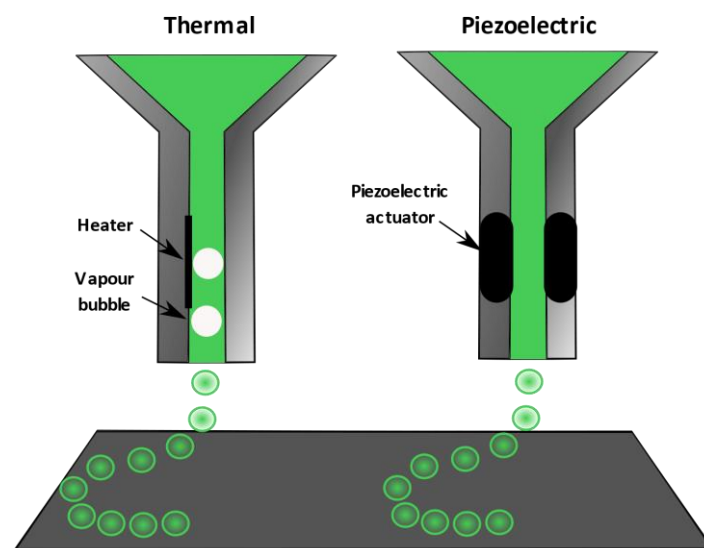


Figure 8 – Schematic representation of inkjet-based strategies for 3D-printing.

An interesting work carried out by Gao *et al.* showed the potentiality of this technique through the development of highly engineered materials.¹⁴¹ More specifically, they developed acrylated peptides that were blended with poly(ethylene glycol) diacrylate as photo-sensitive matrix. Human bone marrow-derived mesenchymal stem cells were encapsulated and showed high viability (i.e., 90%) due to the optimized printing and UV-curing processes. The bioactivity of printed constructs allowed a relevant deposition of extra-cellular matrix and minerals, thus making these systems eligible for cartilage and bone tissue regeneration. Moreover, the resulting physical properties were able to guarantee a controlled development of engineered tissues without inducing any hypertrophic phenomena. Another study based on drop-on-demand technique has been recently published by Part and co-workers.¹⁴² Briefly, they produced an organized three-dimensional papillary structure based on the ordered deposition of 3D microstructures containing fibroblasts into a pre-patterned collagen support. As a result, after different days of maturation in physiological conditions, the research group observed that the printed spheres were re-arranged through a modulated self-arrangement of fibroblasts.

In conclusion, 3D printing based on extrusion and inkjet systems can represent simple and rapid methods to produce engineered constructs for regenerative medicine. The most noteworthy facet of this technique is represented by the possibility to directly print cell-encapsulating matrices. As reported before, nowadays many research activities are focused on the development of novel materials as inks with the aim to improve morphological resolution and complexity, which represent the main challenges for extrusion-based 3D printing. Nonetheless, good physical properties and processability must be coupled with biocompatibility and bioactivity of developed systems at the end stage of their entire production. Generally, the complete and effective matching of the above-mentioned targets is not elementary.

Stereolithography-based 3D printing

This printing technique uses a light beam guided through digital micro-mirrors to precisely polymerize photo-sensitive materials.¹⁴³ In detail, the printing process proceeds step-by-step, each step consisting in the deposition of a fresh coat on the top of the construct in development, which is gradually lowered, and its photo-polymerization according to a CAD file. The additive procedure ends with a construct that contains non-crosslinked domains to be removed and in certain cases a further polymerization of the green-product can be performed to improve the adhesion between consecutive layers. Hence, being a nozzle-free technique, it does not require an intrinsic injectability of the involved hydrogels, ensuring the highest morphological resolution (e.g., up to 5 μm) and printing speed together with good viability of encapsulated cells. In fact, no pressure is required to shape the matrix and therefore no shear stresses are applied to cells. For these reasons, there are only slight limitations in terms of bioink viscosity: a low viscosity is preferable to more efficiently remove non-crosslinked material in the post-processing step. On the other hand, too low viscosity could result in sedimentation phenomena of encapsulated cells. A schematic illustration of stereolithography-based 3D printing is represented in figure 9.

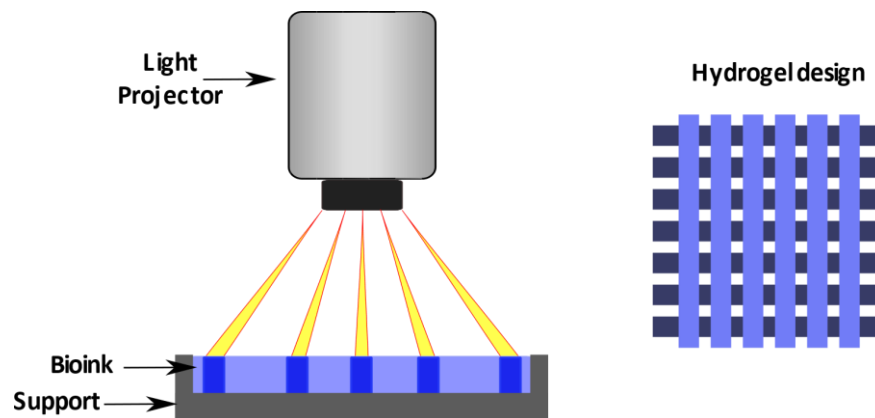


Figure 9 – Simple representation of stereolithography process for the realization of 3D-printed hydrogel matrices.

Nevertheless, the necessity to cure the matrix through light exposure can induce cytotoxic effects when the hydrogel system contains photo-initiators that are activated by wavelengths in the UV domain. A recently published study carried out by Zhu and co-workers showed an engineered and optimized strategy to print 3D structures based on methacrylated gelatin and poly(ethylene glycol) diacrylate using an UV source, reducing the negative effects of the curing step.¹⁴⁴ Furthermore, an additional electromagnetic stimulation in the visible domain (i.e., red light) was used after scaffold

photo-crosslinking to stimulate seeded neural stem cells with the aim to induce a therapeutic effect for degenerative neural diseases. The treatment resulted to exert a tunable effect on cultured cells. Indeed, cell growth and differentiation were modulated through light exposure. In another study, Creff *et al.* developed a 3D scaffold mimicking intestinal epithelium morphology.¹⁴⁵ The authors described an entire fabrication procedure that combines scaffold production based on poly(ethylene glycol) diacrylate and construct maturation through cell culture. As a result, they were able to produce a valuable *in vitro* model to produce organoid-like systems particularly aimed to drug screening. The continuous development of new optical technologies opened the way to the possibility to use modern and less invasive light sources, such as Bessel Beam,¹⁴⁶ which was recently exploited to produce highly precise structures based on different natural and synthetic materials, preserving cell viability in the printed constructs. As for other here-mentioned techniques, the main limit of this approach consists in the widespread utilization of UV-sensitive materials. Hence, a concrete need of novel photo-sensitive systems sensitive to less cytotoxic light sources (i.e., visible light) is nourishing the research activities nowadays. Finally, this technology is characterized by the main limitation to print one single cell culture each time.

Laser-assisted 3D printing

This method is based on the deposition of a matrix known as donor-slide onto a receiver-slide through the application of a focused laser beam. A simplified scheme of laser-assisted system is reported in the figure 10.

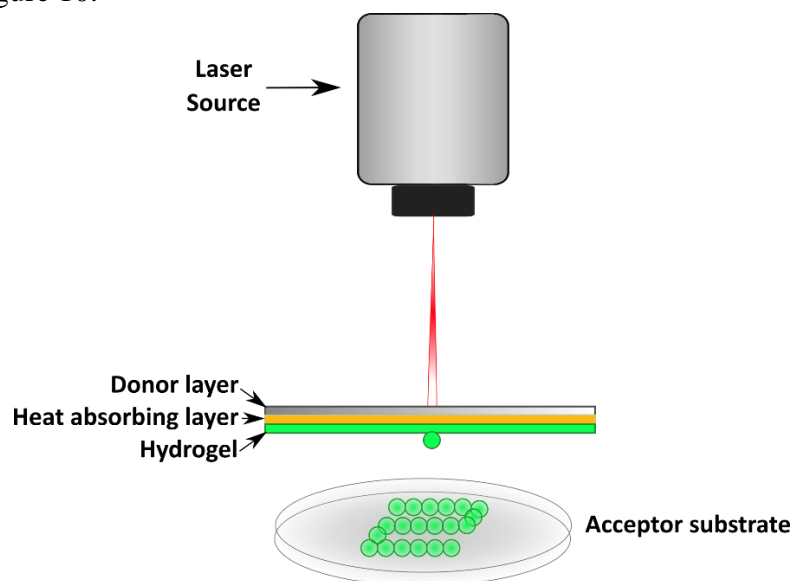


Figure 10 – Simplified representation of a laser-assisted 3D printer.

The donor-slide is generally composed by different layers. The first one that directly interacts with the pulsed laser is based on transparent glass, coupled with a subsequent thin metal sheet on which the bioink is applied. The incidence of the laser beam produces a localized vaporization between the metal and the bioink sheets. This phenomenon allows the precise deposition of bioink droplets on the receiver-slide. As for stereolithography-based 3D printing, this technique is not intrinsically based on injectable bioinks. However, some limitations in viscosity exist, as it should be lower than 300 mPa s. In a recent work, K erour dan *et al.* applied laser-assisted deposition to print collagen encapsulating endothelial cells and VEGF directly into bone defects *in vivo*.¹⁴⁷ This technique allowed the printing of different patterns in order to evaluate the best design to enhance

vascularization for bone regeneration. The authors highlighted the high potential for direct printing *in situ*. An additional and noteworthy work has been conducted by Sorkio and co-authors,¹⁴⁸ who developed a set of different corneal structures with two cell types (i.e., human adipose and pluripotent stem cells) using laminin and collagen as bioinks. As a result, they proved that laser-assisted bioprinting was a feasible approach for the production of highly complex and organized structures, such as corneal tissue. However, although this technique has great potentiality to effectively produce engineered constructs for regenerative medicine, the entire technology consists in relevantly expensive processes and scarce scalability, which limit its translation into the clinical field.

The here-described printing techniques for hydrogel matrices are characterized by different and complementary properties. Nowadays, the characteristic novelty of these approaches is limiting their potentiality, since their common main goal is still remote from their actual applicability, which is the total replacement of the autograft-based gold standard. One relevant limitation is also represented by the mismatch between the technological level and the availability of processable and reliable bioinks. This last aspect, indeed, represents the main frontier in the interdisciplinary field of biomaterials and would represent a substantial improvement towards the applicability of these techniques in the clinical environment. The continuous development of optimized bioprinting set-ups will improve the overall efficiency reducing the related high costs that contradistinguish inkjet- and laser-based bioprinting technologies. Another aim of the current research activities in this field is addressed to the scale-up of these techniques, in order to better answer to clinical needs. It is then clear that a common effort in the research field is being done to achieve a concrete applicability of these techniques as such or in smart combinations to properly control the biological development of tissue engineered constructs. Despite these transitional and noteworthy limitations, techniques based on rapid prototyping represent a valuable solution for the most important clinical needs in which regenerative medicine is involved.

6.2.4 Injectable hydrogels for the clinics

As previously shown, the available strategies to develop smart hydrogels are various and highly promising. Nonetheless, limiting the focus on drug delivery systems, which do not include biological components (i.e., cells), the number of available products for the clinics is remarkably limited.¹⁴⁹ This outcome is due to the notable set of limiting and challenging obstacles that researchers must overcome to achieve clinical application. In fact, many difficulties are affecting the overall development of hydrogel systems, starting from fabrication, scaling-up, storage and finishing with regulatory intricacy and costs. By the fact that hydrogels are mainly composed by water, final sterilization represents an important and articulated issue, since every component and process need to be validated. The dehydration of hydrogels can represent a potential alternative, but this may affect hydrogel behavior and drug activity. Hence, storage conditions are fundamental to protect the final functions and effectiveness of hydrogel-based delivery systems. Moreover, being systems based on a combination of components, regulatory approval procedures involve different aspects and can require up to 10 years to be completed, doubling the time with respect to scaffolding systems that do not contain drug payloads.

According to the data available at the end of the first semester of 2020 (www.clinicaltrials.gov), the number of registered clinical trials on hydrogels was around 481 studies, with 77 of them focused on tissue engineering. This represents an important indicator of the general interest in these systems. However, the available solutions are mostly related to simple tissues or organs (e.g., skin, bladder, and blood vessels). In fact, the development of more complex structures based on hydrogels faces more difficulties to overcome, such as the reproduction of highly specific morphological and mechanical properties, along with biological responses of incorporated cells and hosting tissues into a real organism. Nevertheless, an increasing number of clinical studies concerning hydrogels for more advanced tissue regeneration can be found in the last decade.¹⁵⁰ Hence, the development of injectable hydrogels in conjunction with novel production techniques (i.e., rapid prototyping) still represents a valuable strategy for the improvement of healthcare with the help of up-to-date regulations.¹⁵¹

6.3 Solid scaffold in tissue engineering

The necessity to reproduce the complexity of physical and mechanical properties of natural tissues has led to the continuous development of three-dimensional constructs based on solid materials, such as polymers, metals and inorganic matrices. In this regard, both conventional techniques or novel approaches based on additive manufacturing can produce highly promising and valuable supports for regenerative medicine. From a technical perspective, each strategy is finalized to control and tune the morphological properties (e.g., porosity, pore distribution and shape) to address the resulting product to specific applications. The continuous cross-talk between physical and chemical facets of scaffolds represents the complex ensemble of variables to be engineered to properly control biological response and hence tissue maturation. Then, there are different requirements to be fulfilled to properly develop scaffolds for tissue engineering: form, function, formation and fixation.¹⁵² *Form* is intended as the property to fully fill a tissue defect in order to properly exert its role. *Function* is referred to the ability of a scaffold to overcome initial mechanical and physical needs until the newly formed tissue is matured; this maturation properly represents the *formation* requisite. The overall ensemble of these properties has to be combined with the *fixation* demand that is related to the feasibility for surgeons to properly implant the device into the human body. Partially, these requirements are shared with hydrogels finalized to tissue maturation, but in case of solid scaffolds they are even more important. In fact, solid scaffolds are usually finalized to applications that include more relevant and highly incisive biomechanical facets (e.g., bone tissue engineering), that require higher stability after implantation. In the following paragraphs, a short overview on the available strategies for solid scaffold production aimed to regenerative medicine applications will be shown, reporting the most relevant and up-to-date examples.

6.3.1 Conventional methods for scaffold production

Conventional methods rely on solid technologies and are usually characterized by simplicity. Additionally, the scaling-up of most of these approaches can be achieved containing the costs to a reasonable level. However, the intrinsic limitations of conventional techniques can severely limit

the controllability of morphological properties. Despite this drawback, conventional methods can find widespread applications for tissue engineering, as reported below.

Solvent casting and particulate leaching

Solvent casting and particulate leaching (SC-PL) is based on the incorporation of a sacrificial dispersed phase (i.e., the porogen) into a continuous matrix that is usually constituted by a polymer.¹⁵³ The porogen can be based on soluble polymers, such as gelatin and glucose microparticles, or inorganic salts (e.g., NaCl or KCl). The particulate-based phase is finely dispersed into a solution containing the polymer; then, the suspension is casted into a mold. Once the solvent is evaporated, a solid structure composed of the matrix encapsulating the porogen is obtained. The pores are formed through the selective wash-out of the porogen by simple immersion in water. The main limitation related to this approach consists in the eventual presence of contaminants such as residual traces of salts or un-vapored solvent. Consequently, potential harmful effects can be induced. An interesting and cutting-edge application of this technique can be observed in the work performed by Sola and co-workers.¹⁵⁴ In brief, the exploitation of solvent-casting and particulate leaching permitted to obtain 3D scaffolds mimicking the structure of the bone marrow niche. As materials, poly(methyl methacrylate) and a commercially available and highly flexible poly(urethane) were selected for their good mechanical properties and cytocompatibility. The simplicity that characterizes the applied technique permitted to obtain porosity up to 91% with excellent cell response. This recent example demonstrates the potentiality that SC-PL still retains nowadays. Moreover, the extremely wide spectrum of suitable materials makes this technique highly versatile and interesting for advanced applications in regenerative tissue engineering. Nevertheless, some evident limitations can be highlighted. In fact, in addition to the above-mentioned risk of contamination, even non-interconnected porosity can result from the application of this procedure, limiting scaffold maturation and the mass exchange of nutrients and metabolites. Hence, the precise control of all the involved variables in SC-PL process is required to enhance the repeatability and the morphological quality of produced scaffolds.

Thermally induced phase separation

Among the traditional methods for scaffold production, thermally induced phase separation (TIPS) stands out for its reversibility and controllability. Indeed, it exploits the effects of temperature variations to cause a progressive de-mixing of a polymer solution into a porous matrix. Generally, it allows the production of highly interconnected pore structures. Physical parameters such as polymer concentration and molecular weight, as well as the cooling procedure and ratio between solvent and non-solvent play a fundamental role in the tuneability of the process.¹⁵⁵ For the resulting potentiality, this technique is continuously evolving and is still widely used for the production of engineered scaffolds for regenerative medicine. A recent example can be found in the work performed by Chen *et al.*, in which a macroporous scaffold system composed of poly(L-lactic acid) (PLLA) and chitosan has been developed for bone tissue regeneration.¹⁵⁶ In addition to the good mechanical properties deriving from PLLA, the developed scaffold resulted to be suitable for implantation into critical-size rat bone defects *in vivo*, showing good enhancement of new tissue formation due to the relevant contribution of chitosan. In another work, Guo and co-authors fabricated porous monoliths based on poly(propylene fumarate-co-caprolactone) with enhanced pores interconnectivity and biocompatibility *in vitro*.¹⁵⁷ Moreover, the process for

scaffold production allowed a relevant controllability of mechanical properties, biomineralization and cell response. Nonetheless, this technique may be limited to very simple geometries, such as simple monoliths (e.g., cylinders and parallelepipeds) and the utilization of different mold morphologies can induce significant variations in the entire set of the involved physical parameters.

Electrospinning

This technique is used for the fabrication of fibrous micro- and nano-structures based on simple polymers or composites. The instrumental set-up is composed of a syringe pump, a high-voltage generator and a collector. A charged polymeric solution is spun from the syringe to the collector once the electrostatic force produced by the generator overcome the specific surface tension. The consequent evaporation of the solvent results in the deposition of solid fibers. The resulting morphologies usually provide different advantages in terms of biological response. Indeed, highly interconnected porosity can be obtained through the deposition of fibres. Moreover, the wide availability of instrumental set-ups opens the way to the possibility to tune the morphological properties of the resulting scaffolds towards a fine mimesis of the properties of extra-cellular matrix and tissues.¹⁵⁸ In addition, specific molds can be integrated in the collector producing even complex geometries at the macro-scale having well-organized micro- and nano-structures. As an example, Xue and co-authors developed an ear-shaped electrospun scaffold composed of PCL and gelatin that showed remarkable mechanical properties and bioactivity *in vivo*.¹⁵⁹ Another noteworthy work was performed by Rajzer *et al.* who developed electrospun scaffolds based on PLA and PCL and encapsulating ossein-hydroxyapatite complexes, with enhanced mineralization, as well as cell adhesion and differentiation.¹⁶⁰ Hence, the potentialities of electrospinning are various and highly valuable. However, there are relevant limitations in the scaling-up of the entire process. In fact, the required time for the production of scaffolds is quite long and the overall process usually leads to mainly bidimensional constructs (i.e., membranes). Despite these relevant limitations, this technique holds the potential to fabricate unique morphologies able to finely modulate biological responses.^{161,162} Hence, electrospinning represents a valuable approach as such or in combination with other techniques for the production of highly bioactive scaffolds.

6.3.2 Non-conventional methods – 3D printing

The technological development based on CAD-CAM design induced a revolution even in the field of solid scaffold production. Similarly to 3D printed hydrogels, the development of 3D printed solid matrices allows to precisely control the morphology at different levels.

Fused deposition modeling

Fused deposition modeling (FDM) is one of the most popular and inexpensive approaches to additive manufacture solid materials. Differently from hydrogel 3D-bioprinting, a semi-molten matrix is deposited through extrusion from a nozzle on a support. The main involved variables are related to the thermoplastic polymer that is extruded. In fact, the molecular weight and the chemical composition of a material aimed to fused deposition modeling strongly influence the physical properties that must be controlled during the process, such as melting temperature, viscosity and printing speed. The most utilized and commercially available materials are PCL,

PLA and PLGA, which can be even found in composite forms with bioactive oxides (i.e., bioglasses or hydroxyapatite). A recent example of the relevant applicability of this approach has been provided by Ceretti and co-authors that fabricated multi-layered PCL-based scaffolds through an open source FDM-based printer and electrospinning.¹⁶³ The authors demonstrated how the involved FDM-related parameters can be finely controlled to produce 3D printed scaffolds for tissue engineering with specific geometrical and physical properties. Electrospun membranes were then applied on the 3D printed structures to enhance cell adhesion and proliferation. As a biological proof, a complete colonization of the resulting constructs was achieved with human fibroblasts, thus making this approach a suitable strategy for cartilage and bone tissue engineering. Another interesting work by Rebaioli *et al.* evidenced the versatility of FDM for scaffold production. In detail, they produced 3D-printed PLA scaffolds encapsulating carbon nanotubes (CNTs) with the aim to replicate the mechanical and electrical properties of bone extracellular matrix.¹⁶⁴ Differently, Chen and colleagues developed 3D scaffolds characterized by anisotropic properties.¹⁶⁵ As materials, they used a commercially available thermoplastic poly(urethane) blended with PLA and graphene oxide. The presence of the nanocomposites effectively enhanced the mechanical responses of the 3D printed scaffolds, acting as a reinforcing agent. FDM is continuously demonstrating to be a cutting-edge strategy to properly develop highly engineered scaffolds for regenerative medicine. However, a limiting aspect can be found in the maximum resolution obtainable from the printed filaments (i.e., between 100 and 200 μm).¹⁶⁶ For this reason, this technique is often coupled to other strategies (e.g., electrospinning or gas foaming¹⁶⁷) with the aim to obtain structures with features characterized at lower scales to specifically control cell behavior.

Selective laser sintering

Selective laser sintering (SLS) is a novel technology based on the precise and partial melting of powders through a focused and traced laser that follows a CAD-derived path translated into an STL file.¹⁶⁸ The formation of scaffolds proceeds layer-by-layer. The properties of the final construct, such as porosity and resolution, depend on laser- and powder-related variables. In fact, laser power, focusing radius and scan speed, as well as powder thermal properties, thickness, and size distribution (i.e., the granulometry) are key parameters influencing the outcomes of the process. Interestingly, in addition to the precise scaffold shape that can be obtained, the resulting micro-structure can be characterized by discrete powder particles bound with necks, thus generating a micro-porosity particularly useful for tissue engineering applications. However, the entire process involves non-trivial heat transfer phenomena, which require extremely precise preliminary optimization procedures. One extremely important advantage of SLS is represented by the possibility to produce complex structures without the necessity of any supports, thus significantly reducing or completely avoiding additional finishing processes. Generally, powder having 50 μm mean diameter are used for different polymers, such as poly(vinyl alcohol), poly(carbonate)s, poly(ether ether ketone)s, PCL, PLLA and poly(ethylene). The polymeric matrix can be reinforced through the addition of a mineral phase (e.g., hydroxyapatite). This approach was exploited by XiaoHui and co-authors in their work finalized to the production of poly(carbonate)-based scaffolds reinforced with hydroxyapatite (HA).¹⁶⁹ The optimized process allowed the development of composite constructs containing HA at 10% wt, having a porosity around 77% and a compressive modulus of 26 MPa. The resulting structures resulted to be

particularly suitable for bone tissue engineering. A different approach can be found in the work performed by Wu *et al.*, in which SLS-fabricated PCL templates were impregnated with a hydrogel phase to obtain solid scaffold-hydrogel system based on PCL/alginate/polyacrylamide with improved mechanical and biological performances.¹⁷⁰ In detail, elastic modulus was increased from 7 to 12.7 MPa, while the strain at break was almost doubled from 59% to 112%, when simple PCL sintered structures were embedded with bioartificial hydrogels based on alginate and polyacrylamide. Seeded and cultured cells on these substrates demonstrated excellent viability (94%) over 5 days.

Hence, SLS represents an extremely important technique for the production of unique structures for tissue engineering with noteworthy mechanical and biological properties. However, some limitations can be found in the restricted field of materials with suitable resistance to heat and shrinkage properties, since relevant temperatures can be locally reached during fabrication. Additionally, the SLS apparatus is relatively expensive when compared to FDM devices and requires extended time for processing and post-processing.

Stereolithography

As in the case of hydrogels, stereolithography (SLA) can be used for the production of solid constructs by varying the nature of the involved photo-sensitive materials. However, the number of available materials for SLA is limited and mainly based on photo-curable resins. In addition, the domain of available materials to be implemented has been limited by potential toxicity derived from photo-initiators or non-crosslinked monomers,^{171,172} as previously discussed. To properly process materials with SLA, viscosity is a fundamental parameter to be considered in order to increase curing effectiveness. In this regard, low molecular weight resins are thus preferable. In fact, a low viscosity (ranging from 0.25 and 10 Pa s) allows a better cleaning of uncured domains after fabrication. Although oligomer-based resins are preferable, also polymeric matrices have been developed to produce 3D printed structures at high resolution. For example, Elomaa and co-workers developed a bioartificial scaffold based on resins composed of gelatin methacryloyl (GelMA) and PCL functionalized with methacrylate end groups.¹⁷³ Interestingly, resins containing high content of GelMA (up to 70% wt) were formulated ensuring a suitable viscosity and a relevant resolution of the fabricated SLA-based 3D printed scaffolds. The resulting properties of the developed resins allowed the fabrication of small intestine-like scaffolds with enhanced bioactivity. Additionally, the here-developed strategy to formulate SLA-specific bioartificial resins has been transferred to decellularized and methacryloyl-functionalized murine ECM thus widening the plethora of promising materials for advanced applications in tissue engineering. As exemplified, nowadays a remarkable effort is being made to produce new available materials for SLA to continuously improve performances in biological milieu. Important limitations can also be found in the maximum dimensions of scaffolds that are obtainable through this strategy.

6.3.3 Translation of solid scaffolds to the clinics

The clinical translation of regenerative therapies based on scaffolds goes beyond the fundamentals of engineering by itself.^{152,174} As for hydrogel-based systems, regulatory procedures that involves specific organizations are mandatory and may have a critical impact on scaffold development. The already expensive and long pre-clinical process represents less than a half of the overall required

effort to actually translate a scaffold system into the clinics. Indeed, an extremely strict coordination among technical, scientific and medical requirements is fundamental to prove the real effectiveness of this kind of devices. In this regard, in addition to the evident and indisputable efficacy of a scaffold in terms of regenerative properties, a reasonable acceptance of practical feasibility for implantation must be provided by surgeons. It is necessary to take into account that the cost for the production of the final scaffold-based device must be as economical as possible, in order to enhance the feasibility of industrial scaling-up and hence the actual spread into the clinical field. The newer or the more complex is the material on which a scaffold is based, the longer and more arduous is the regulatory process.

To achieve these targets, the overall costs can overcome the value of 200 million dollars. Hence, the complete procedure from scaffold in sketch to real clinical applications is long, extremely expensive, and laborious, requiring at every step a solid collaboration between specialists that belong to all the involved disciplines. With the aim to simplify the subsequent regulatory processes, clinical needs should be pragmatically included in the early stages of development of a scaffold-based device for regenerative medicine. However, this is not easy and represents a concrete issue for investigators that develop novel materials for tissue engineering. The existence of guidelines (e.g., FDA and ISO) can effectively contribute to this purpose, but the rapid and persistent technological development requires continuous updates thus making the available protocols poor of consistency.

7. References

- (1) Shimazono, Y. Bulletin of the World Health Organization The State of the International Organ Trade: A Provisional Picture Based on Integration of Available Information. 9.
- (2) Israni, A. K.; Zaun, D.; Hadley, N.; Rosendale, J. D.; Schaffhausen, C.; McKinney, W.; Snyder, J. J.; Kasiske, B. L. OPTN/SRTR 2018 Annual Data Report: Deceased Organ Donation. *Am J Transplant* **2018**, *20* (s1), 509–541. <https://doi.org/10.1111/ajt.15678>.
- (3) <http://www.transplant-observatory.org/summary/>, 15 September 2020.
- (4) Anghel, D.; Tanasescu, R.; Campeanu, A.; Lupescu, I.; Podda, G.; Bajenaru, O. Neurotoxicity of Immunosuppressive Therapies in Organ Transplantation. *Maedica (Bucur)* **2013**, *8* (2), 170–175.
- (5) Goldberg, D.; French, B.; Abt, P.; Feng, S.; Cameron, A. M. Increasing Disparity in Waitlist Mortality Rates with Increased Model for End-Stage Liver Disease Scores for Candidates with Hepatocellular Carcinoma versus Candidates without Hepatocellular Carcinoma. *Liver Transpl* **2012**, *18* (4), 434–443. <https://doi.org/10.1002/lt.23394>.
- (6) Lai, J. C.; Feng, S.; Terrault, N. A.; Lizaola, B.; Hayssen, H.; Covinsky, K. Frailty Predicts Waitlist Mortality in Liver Transplant Candidates. *Am J Transplant* **2014**, *14* (8), 1870–1879. <https://doi.org/10.1111/ajt.12762>.
- (7) Knechtle, S. J.; Pirsch, J. D.; D’Alessandro, A. M.; Sollinger, H. W.; Kalayoglu, M.; Belzer, F. O. Renal Transplantation at the University of Wisconsin in the Cyclosporine Era. *Clin Transpl* **1993**, 211–218.
- (8) Knoll, G. Trends in Kidney Transplantation over the Past Decade: *Drugs* **2008**, *68* (Supplement 1), 3–10. <https://doi.org/10.2165/00003495-200868001-00002>.
- (9) Dunn, J.; Golden, D.; Van Buren, C. T.; Lewis, R. M.; Lawen, J.; Kahan, B. D. Causes of Graft Loss beyond Two Years in the Cyclosporine Era. *Transplantation* **1990**, *49* (2), 349–353. <https://doi.org/10.1097/00007890-199002000-00024>.
- (10) Morrissey, P. E.; Flynn, M. L.; Lin, S. Medication Noncompliance and Its Implications in Transplant Recipients. *Drugs* **2007**, *67* (10), 1463–1481. <https://doi.org/10.2165/00003495-200767100-00007>.
- (11) Lewis, J. K.; Bischof, J. C.; Braslavsky, I.; Brockbank, K. G. M.; Fahy, G. M.; Fuller, B. J.; Rabin, Y.; Tocchio, A.; Woods, E. J.; Wowk, B. G.; Acker, J. P.; Giwa, S. The Grand Challenges of Organ Banking: Proceedings from the First Global Summit on Complex Tissue Cryopreservation. *Cryobiology* **2016**, *72* (2), 169–182. <https://doi.org/10.1016/j.cryobiol.2015.12.001>.
- (12) Giwa, S.; Lewis, J. K.; Alvarez, L.; Langer, R.; Roth, A. E.; Church, G. M.; Markmann, J. F.; Sachs, D. H.; Chandraker, A.; Wertheim, J. A.; Rothblatt, M.; Boyden, E. S.; Eidbo, E.; Lee, W. P. A.; Pomahac, B.; Brandacher, G.; Weinstock, D. M.; Elliott, G.; Nelson, D.; Acker, J. P.; Uygun, K.; Schmalz, B.; Weegman, B. P.; Tocchio, A.; Fahy, G. M.; Storey, K. B.; Rubinsky, B.; Bischof, J.; Elliott, J. A. W.; Woodruff, T. K.; Morris, G. J.; Demirci, U.; Brockbank, K. G. M.; Woods, E. J.; Ben, R. N.; Baust, J. G.; Gao, D.; Fuller, B.; Rabin, Y.; Kravitz, D. C.; Taylor, M. J.; Toner, M. The Promise of Organ and Tissue Preservation to Transform Medicine. *Nat Biotechnol* **2017**, *35* (6), 530–542. <https://doi.org/10.1038/nbt.3889>.
- (13) Mason, C.; Dunnill, P. A Brief Definition of Regenerative Medicine. *Regenerative Medicine* **2008**, *3* (1), 1–5. <https://doi.org/10.2217/17460751.3.1.1>.
- (14) Dzobo, K.; Thomford, N. E.; Senthebane, D. A.; Shipanga, H.; Rowe, A.; Dandara, C.; Pillay, M.; Motaung, K. S. C. M. Advances in Regenerative Medicine and Tissue Engineering: Innovation and

Transformation of Medicine. *Stem Cells International* **2018**, 2018, 1–24. <https://doi.org/10.1155/2018/2495848>.

(15) Goradel, N. H.; Hour, F. G.; Negahdari, B.; Malekshahi, Z. V.; Hashemzahi, M.; Masoudifar, A.; Mirzaei, H. Stem Cell Therapy: A New Therapeutic Option for Cardiovascular Diseases. *J. Cell. Biochem.* **2018**, *119* (1), 95–104. <https://doi.org/10.1002/jcb.26169>.

(16) Marsh, S. E.; Blurton-Jones, M. Neural Stem Cell Therapy for Neurodegenerative Disorders: The Role of Neurotrophic Support. *Neurochemistry International* **2017**, *106*, 94–100. <https://doi.org/10.1016/j.neuint.2017.02.006>.

(17) El-Badawy, A.; El-Badri, N. Clinical Efficacy of Stem Cell Therapy for Diabetes Mellitus: A Meta-Analysis. *PLoS ONE* **2016**, *11* (4), e0151938. <https://doi.org/10.1371/journal.pone.0151938>.

(18) Ginn, S. L.; Amaya, A. K.; Alexander, I. E.; Edelstein, M.; Abedi, M. R. Gene Therapy Clinical Trials Worldwide to 2017: An Update. *J Gene Med* **2018**, *20* (5), e3015. <https://doi.org/10.1002/jgm.3015>.

(19) Lu, B.; Atala, A. Small Molecules and Small Molecule Drugs in Regenerative Medicine. *Drug Discovery Today* **2014**, *19* (6), 801–808. <https://doi.org/10.1016/j.drudis.2013.11.011>.

(20) Han, C.; Wang, B. Factors That Impact the Developability of Drug Candidates. In *Drug Delivery*; Wang, B., Hu, L., Siahaan, T. J., Eds.; John Wiley & Sons, Inc: Hoboken, NJ, 2016; pp 1–18. <https://doi.org/10.1002/9781118833322.ch1>.

(21) Barich, D. H.; Zell, M. T.; Munson, E. J. Physicochemical Properties, Formulation, and Drug Delivery. In *Drug Delivery*; Wang, B., Hu, L., Siahaan, T. J., Eds.; John Wiley & Sons, Inc: Hoboken, NJ, 2016; pp 35–48. <https://doi.org/10.1002/9781118833322.ch3>.

(22) Andersson, K.-E.; Christ, G. J. Regenerative Pharmacology: The Future Is Now. *Molecular Interventions* **2007**, *7* (2), 79–86. <https://doi.org/10.1124/mi.7.2.8>.

(23) Christ, G. J.; Saul, J. M.; Furth, M. E.; Andersson, K.-E. The Pharmacology of Regenerative Medicine. *Pharmacol Rev* **2013**, *65* (3), 1091–1133. <https://doi.org/10.1124/pr.112.007393>.

(24) Gainza, G.; Villullas, S.; Pedraz, J. L.; Hernandez, R. M.; Igartua, M. Advances in Drug Delivery Systems (DDSs) to Release Growth Factors for Wound Healing and Skin Regeneration. *Nanomedicine: Nanotechnology, Biology and Medicine* **2015**, *11* (6), 1551–1573. <https://doi.org/10.1016/j.nano.2015.03.002>.

(25) Lorden, E. R.; Levinson, H. M.; Leong, K. W. Integration of Drug, Protein, and Gene Delivery Systems with Regenerative Medicine. **2015**, *19*.

(26) Patra, J. K.; Das, G.; Fraceto, L. F.; Campos, E. V. R.; Rodriguez-Torres, M. del P.; Acosta-Torres, L. S.; Diaz-Torres, L. A.; Grillo, R.; Swamy, M. K.; Sharma, S.; Habtemariam, S.; Shin, H.-S. Nano Based Drug Delivery Systems: Recent Developments and Future Prospects. *J Nanobiotechnol* **2018**, *16* (1), 71. <https://doi.org/10.1186/s12951-018-0392-8>.

(27) Cui, W.; Li, J.; Decher, G. Self-Assembled Smart Nanocarriers for Targeted Drug Delivery. *Adv. Mater.* **2016**, *28* (6), 1302–1311. <https://doi.org/10.1002/adma.201502479>.

(28) Chang, Y.-C.; Chen, Y.-D.; Chen, C.-H.; Wen, Y.-S.; Lin, J. T.; Chen, H.-Y.; Kuo, M.-Y.; Chao, I. Crystal Engineering for Π - π Stacking via Interaction between Electron-Rich and Electron-Deficient Heteroaromatics. *J. Org. Chem.* **2008**, *73* (12), 4608–4614. <https://doi.org/10.1021/jo800546j>.

(29) Chacko, R. T.; Ventura, J.; Zhuang, J.; Thayumanavan, S. Polymer Nanogels: A Versatile Nanoscopic Drug Delivery Platform. *Advanced Drug Delivery Reviews* **2012**, *64* (9), 836–851. <https://doi.org/10.1016/j.addr.2012.02.002>.

- (30) Ulbrich, K.; Holá, K.; Šubr, V.; Bakandritsos, A.; Tuček, J.; Zbořil, R. Targeted Drug Delivery with Polymers and Magnetic Nanoparticles: Covalent and Noncovalent Approaches, Release Control, and Clinical Studies. *Chem. Rev.* **2016**, *116* (9), 5338–5431. <https://doi.org/10.1021/acs.chemrev.5b00589>.
- (31) Lu, H.; Wang, J.; Wang, T.; Zhong, J.; Bao, Y.; Hao, H. Recent Progress on Nanostructures for Drug Delivery Applications. *Journal of Nanomaterials* **2016**, *2016*, 1–12. <https://doi.org/10.1155/2016/5762431>.
- (32) Pasut, G.; Veronese, F. M. Polymer–Drug Conjugation, Recent Achievements and General Strategies. *Progress in Polymer Science* **2007**, *32* (8–9), 933–961. <https://doi.org/10.1016/j.progpolymsci.2007.05.008>.
- (33) Kita, K.; Dittrich, C. Drug Delivery Vehicles with Improved Encapsulation Efficiency: Taking Advantage of Specific Drug–Carrier Interactions. *Expert Opinion on Drug Delivery* **2011**, *8* (3), 329–342. <https://doi.org/10.1517/17425247.2011.553216>.
- (34) Hirsjarvi, S.; Passirani, C.; Benoit, J.-P. Passive and Active Tumour Targeting with Nanocarriers. *CDDT* **2011**, *8* (3), 188–196. <https://doi.org/10.2174/157016311796798991>.
- (35) He, H.; Lu, Y.; Qi, J.; Zhu, Q.; Chen, Z.; Wu, W. Adapting Liposomes for Oral Drug Delivery. *Acta Pharmaceutica Sinica B* **2019**, *9* (1), 36–48. <https://doi.org/10.1016/j.apsb.2018.06.005>.
- (36) Sun, X. Bone-Targeting Drug Delivery System of Biomineral-Binding Liposomes Loaded with Icaritin Enhances the Treatment for Osteoporosis. **2019**, 16.
- (37) Nam, M.; Lee, J.; Lee, K. Y.; Kim, J. Sequential Targeted Delivery of Liposomes to Ischemic Tissues by Controlling Blood Vessel Permeability. *ACS Biomater. Sci. Eng.* **2018**, *4* (2), 532–538. <https://doi.org/10.1021/acsbomaterials.7b00815>.
- (38) Wagner, A.; Vorauer-Uhl, K. Liposome Technology for Industrial Purposes. *J Drug Deliv* **2011**, *2011*, 591325. <https://doi.org/10.1155/2011/591325>.
- (39) Won, Y.-Y.; Brannan, A. K.; Davis, H. T.; Bates, F. S. Cryogenic Transmission Electron Microscopy (Cryo-TEM) of Micelles and Vesicles Formed in Water by Poly(Ethylene Oxide)-Based Block Copolymers. *J. Phys. Chem. B* **2002**, *106* (13), 3354–3364. <https://doi.org/10.1021/jp013639d>.
- (40) Battaglia, G.; Ryan, A. J. Bilayers and Interdigitation in Block Copolymer Vesicles. *J. Am. Chem. Soc.* **2005**, *127* (24), 8757–8764. <https://doi.org/10.1021/ja050742y>.
- (41) Gou, M.; Men, K.; Shi, H.; Xiang, M.; Zhang, J.; Song, J.; Long, J.; Wan, Y.; Luo, F.; Zhao, X.; Qian, Z. Curcumin-Loaded Biodegradable Polymeric Micelles for Colon Cancer Therapy in Vitro and in Vivo. *Nanoscale* **2011**, *3* (4), 1558. <https://doi.org/10.1039/c0nr00758g>.
- (42) Yuan, X.; Xie, Q.; Su, K.; Li, Z.; Dong, D.; Wu, B. Systemic Delivery of the Anticancer Agent Arenobufagin Using Polymeric Micelles. *IJN* **2017**, *Volume 12*, 4981–4989. <https://doi.org/10.2147/IJN.S139128>.
- (43) Hanafy, N.; Quarta, A.; Ferraro, M.; Dini, L.; Nobile, C.; De Giorgi, M.; Carallo, S.; Citti, C.; Gaballo, A.; Cannazza, G.; Rinaldi, R.; Giannelli, G.; Leporatti, S. Polymeric Nano-Micelles as Novel Cargo-Carriers for LY2157299 Liver Cancer Cells Delivery. *IJMS* **2018**, *19* (3), 748. <https://doi.org/10.3390/ijms19030748>.
- (44) Yu, H.; Chen, X.; Cai, J.; Ye, D.; Wu, Y.; Liu, P. Dual Controlled Release Micelle-in-Nanofiber System for Long-Term Antibacterial Medical Dressings. *Journal of Biomaterials Science, Polymer Edition* **2019**, *30* (1), 64–76. <https://doi.org/10.1080/09205063.2018.1549771>.

- (45) Kulkarni, P.; Haldar, M. K.; You, S.; Choi, Y.; Mallik, S. Hypoxia-Responsive Polymersomes for Drug Delivery to Hypoxic Pancreatic Cancer Cells. *Biomacromolecules* **2016**, *17* (8), 2507–2513. <https://doi.org/10.1021/acs.biomac.6b00350>.
- (46) Wei, P.; Sun, M.; Yang, B.; Xiao, J.; Du, J. Ultrasound-Responsive Polymersomes Capable of Endosomal Escape for Efficient Cancer Therapy. *Journal of Controlled Release* **2020**, *322*, 81–94. <https://doi.org/10.1016/j.jconrel.2020.03.013>.
- (47) Kousalová, J.; Etrych, T. Polymeric Nanogels as Drug Delivery Systems. *Physiol Res* **2018**, S305–S317. <https://doi.org/10.33549/physiolres.933979>.
- (48) Kordalivand, N.; Tondini, E.; Lau, C. Y. J.; Vermonden, T.; Mastrobattista, E.; Hennink, W. E.; Ossendorp, F.; Nostrum, C. F. van. Cationic Synthetic Long Peptides-Loaded Nanogels: An Efficient Therapeutic Vaccine Formulation for Induction of T-Cell Responses. *Journal of Controlled Release* **2019**, *315*, 114–125. <https://doi.org/10.1016/j.jconrel.2019.10.048>.
- (49) Li, Y.; Maciel, D.; Rodrigues, J.; Shi, X.; Tomás, H. Biodegradable Polymer Nanogels for Drug/Nucleic Acid Delivery. *Chem. Rev.* **2015**, *115* (16), 8564–8608. <https://doi.org/10.1021/cr500131f>.
- (50) Mayer, C. Nanocapsules as Drug Delivery Systems. *Int J Artif Organs* **2005**, *28* (11), 1163–1171. <https://doi.org/10.1177/039139880502801114>.
- (51) Peleteiro, M.; Presas, E.; González-Aramundiz, J. V.; Sánchez-Correa, B.; Simón-Vázquez, R.; Csaba, N.; Alonso, M. J.; González-Fernández, Á. Polymeric Nanocapsules for Vaccine Delivery: Influence of the Polymeric Shell on the Interaction With the Immune System. *Front. Immunol.* **2018**, *9*, 791. <https://doi.org/10.3389/fimmu.2018.00791>.
- (52) Acar, H.; Srivastava, S.; Chung, E. J.; Schnorenberg, M. R.; Barrett, J. C.; LaBelle, J. L.; Tirrell, M. Self-Assembling Peptide-Based Building Blocks in Medical Applications. *Advanced Drug Delivery Reviews* **2017**, *110–111*, 65–79. <https://doi.org/10.1016/j.addr.2016.08.006>.
- (53) Wei, G.; Su, Z.; Reynolds, N. P.; Arosio, P.; Hamley, I. W.; Gazit, E.; Mezzenga, R. Self-Assembling Peptide and Protein Amyloids: From Structure to Tailored Function in Nanotechnology. *Chem. Soc. Rev.* **2017**, *46* (15), 4661–4708. <https://doi.org/10.1039/C6CS00542J>.
- (54) Jaradat, D. M. M. Thirteen Decades of Peptide Synthesis: Key Developments in Solid Phase Peptide Synthesis and Amide Bond Formation Utilized in Peptide Ligation. *Amino Acids* **2018**, *50* (1), 39–68. <https://doi.org/10.1007/s00726-017-2516-0>.
- (55) Webber, M. J.; Kessler, J. A.; Stupp, S. I. Emerging Peptide Nanomedicine to Regenerate Tissues and Organs: Symposium: Peptide Nanomedicine. *Journal of Internal Medicine* **2010**, *267* (1), 71–88. <https://doi.org/10.1111/j.1365-2796.2009.02184.x>.
- (56) Lombardi, L.; Falanga, A.; Del Genio, V.; Galdiero, S. A New Hope: Self-Assembling Peptides with Antimicrobial Activity. *Pharmaceutics* **2019**, *11* (4), 166. <https://doi.org/10.3390/pharmaceutics11040166>.
- (57) Porter, S. L.; Coulter, S. M.; Pentlavalli, S.; Thompson, T. P.; Laverty, G. Self-Assembling Diphenylalanine Peptide Nanotubes Selectively Eradicate Bacterial Biofilm Infection. *Acta Biomaterialia* **2018**, *77*, 96–105. <https://doi.org/10.1016/j.actbio.2018.07.033>.
- (58) Agyei, D.; Danquah, M. K. Industrial-Scale Manufacturing of Pharmaceutical-Grade Bioactive Peptides. *Biotechnology Advances* **2011**, *29* (3), 272–277. <https://doi.org/10.1016/j.biotechadv.2011.01.001>.
- (59) Okholm, A. H.; Kjems, J. The Utility of DNA Nanostructures for Drug Delivery *in Vivo*. *Expert Opinion on Drug Delivery* **2017**, *14* (2), 137–139. <https://doi.org/10.1080/17425247.2017.1266335>.

- (60) Huang, Y.; Huang, W.; Chan, L.; Zhou, B.; Chen, T. A Multifunctional DNA Origami as Carrier of Metal Complexes to Achieve Enhanced Tumoral Delivery and Nullified Systemic Toxicity. *Biomaterials* **2016**, *103*, 183–196. <https://doi.org/10.1016/j.biomaterials.2016.06.053>.
- (61) Linko, V.; Ora, A.; Kostianinen, M. A. DNA Nanostructures as Smart Drug-Delivery Vehicles and Molecular Devices. *Trends in Biotechnology* **2015**, *33* (10), 586–594. <https://doi.org/10.1016/j.tibtech.2015.08.001>.
- (62) Santos, C. I. A. V.; Ribeiro, A. C. F.; Estes, M. A. Drug Delivery Systems: Study of Inclusion Complex Formation between Methylxanthines and Cyclodextrins and Their Thermodynamic and Transport Properties. *Biomolecules* **2019**, *9* (5), 196. <https://doi.org/10.3390/biom9050196>.
- (63) Qi, Z. H.; Mak, V.; Diaz, L.; Grant, D. M.; Chang, C. J. Molecular Recognition: .Alpha.-Cyclodextrin and Penicillin V Inclusion Complexation. *J. Org. Chem.* **1991**, *56* (4), 1537–1542. <https://doi.org/10.1021/jo00004a037>.
- (64) Loftsson, T.; Brewster, M. E. Pharmaceutical Applications of Cyclodextrins. 1. Drug Solubilization and Stabilization. *Journal of Pharmaceutical Sciences* **1996**, *85* (10), 1017–1025. <https://doi.org/10.1021/js950534b>.
- (65) Español, E. S.; Villamil, M. M. Calixarenes: Generalities and Their Role in Improving the Solubility, Biocompatibility, Stability, Bioavailability, Detection, and Transport of Biomolecules. **2019**, 15.
- (66) Das, D.; Assaf, K. I.; Nau, W. M. Applications of Cucurbiturils in Medicinal Chemistry and Chemical Biology. *Front. Chem.* **2019**, *7*, 619. <https://doi.org/10.3389/fchem.2019.00619>.
- (67) Song, N.; Lou, X.-Y.; Ma, L.; Gao, H.; Yang, Y.-W. Supramolecular Nanotheranostics Based on Pillarenes. *Theranostics* **2019**, *9* (11), 3075–3093. <https://doi.org/10.7150/thno.31858>.
- (68) Patri, A.; Kukowskalatallo, J.; Bakerjr, J. Targeted Drug Delivery with Dendrimers: Comparison of the Release Kinetics of Covalently Conjugated Drug and Non-Covalent Drug Inclusion Complex. *Advanced Drug Delivery Reviews* **2005**, *57* (15), 2203–2214. <https://doi.org/10.1016/j.addr.2005.09.014>.
- (69) Ventola, C. L. The Nanomedicine Revolution: Part 3: Regulatory and Safety Challenges. *P T* **2012**, *37* (11), 631–639.
- (70) Ventola, C. L. Progress in Nanomedicine: Approved and Investigational Nanodrugs. *P T* **2017**, *42* (12), 742–755.
- (71) Kretlow, J. D.; Klouda, L.; Mikos, A. G. Injectable Matrices and Scaffolds for Drug Delivery in Tissue Engineering. *Advanced Drug Delivery Reviews* **2007**, *59* (4–5), 263–273. <https://doi.org/10.1016/j.addr.2007.03.013>.
- (72) Jafari, M.; Paknejad, Z.; Rad, M. R.; Motamedian, S. R.; Eghbal, M. J.; Nadjmi, N.; Khojasteh, A. Polymeric Scaffolds in Tissue Engineering: A Literature Review. **2017**, *105* (2), 29.
- (73) Aravamudhan, A.; Ramos, D. M.; Nada, A. A.; Kumbar, S. G. Natural Polymers. In *Natural and Synthetic Biomedical Polymers*; Elsevier, 2014; pp 67–89. <https://doi.org/10.1016/B978-0-12-396983-5.00004-1>.
- (74) Kumar, G.; Tison, C. K.; Chatterjee, K.; Pine, P. S.; McDaniel, J. H.; Salit, M. L.; Young, M. F.; Simon, C. G. The Determination of Stem Cell Fate by 3D Scaffold Structures through the Control of Cell Shape. *Biomaterials* **2011**, *32* (35), 9188–9196. <https://doi.org/10.1016/j.biomaterials.2011.08.054>.
- (75) Uman, S.; Dhand, A.; Burdick, J. A. Recent Advances in Shear-thinning and Self-healing Hydrogels for Biomedical Applications. *J Appl Polym Sci* **2020**, *137* (25), 48668. <https://doi.org/10.1002/app.48668>.

- (76) Sun, Y.; Nan, D.; Jin, H.; Qu, X. Recent Advances of Injectable Hydrogels for Drug Delivery and Tissue Engineering Applications. *Polymer Testing* **2020**, *81*, 106283. <https://doi.org/10.1016/j.polymertesting.2019.106283>.
- (77) McKenzie, M.; Betts, D.; Suh, A.; Bui, K.; Kim, L.; Cho, H. Hydrogel-Based Drug Delivery Systems for Poorly Water-Soluble Drugs. *Molecules* **2015**, *20* (11), 20397–20408. <https://doi.org/10.3390/molecules201119705>.
- (78) Wang, Q.; Wong, C.-H.; Chan, H. Y. E.; Lee, W.-Y.; Zuo, Z. Statistical Design of Experiment (DoE) Based Development and Optimization of DB213 in Situ Thermosensitive Gel for Intranasal Delivery. *International Journal of Pharmaceutics* **2018**, *539* (1–2), 50–57. <https://doi.org/10.1016/j.ijpharm.2018.01.032>.
- (79) Liu, Y.; Lu, W.-L.; Wang, J.-C.; Zhang, X.; Zhang, H.; Wang, X.-Q.; Zhou, T.-Y.; Zhang, Q. Controlled Delivery of Recombinant Hirudin Based on Thermo-Sensitive Pluronic F127 Hydrogel for Subcutaneous Administration: In Vitro and in Vivo Characterization. *J Control Release* **2007**, *117* (3), 387–395. <https://doi.org/10.1016/j.jconrel.2006.11.024>.
- (80) Oshiro, A.; da Silva, D. C.; de Mello, J. C.; de Moraes, V. W. R.; Cavalcanti, L. P.; Franco, M. K. K. D.; Alkschbirs, M. I.; Fraceto, L. F.; Yokaichiya, F.; Rodrigues, T.; de Araujo, D. R. Pluronics F-127/L-81 Binary Hydrogels as Drug-Delivery Systems: Influence of Physicochemical Aspects on Release Kinetics and Cytotoxicity. *Langmuir* **2014**, *30* (45), 13689–13698. <https://doi.org/10.1021/la503021c>.
- (81) Shin, B.-K.; Baek, E. J.; Choi, S. G.; Davaa, E.; Nho, Y.-C.; Lim, Y.-M.; Park, J.-S.; Huh, K. M.; Park, J.-S. Preparation and Irradiation of Pluronic F127-Based Thermoreversible and Mucoadhesive Hydrogel for Local Delivery of Naproxen. *Drug Development and Industrial Pharmacy* **2013**, *39* (12), 1874–1880. <https://doi.org/10.3109/03639045.2012.665925>.
- (82) Patel, P.; Mandal, A.; Gote, V.; Pal, D.; Mitra, A. K. Thermosensitive Hydrogel-Based Drug Delivery System for Sustained Drug Release. *J Polym Res* **2019**, *26* (6), 131. <https://doi.org/10.1007/s10965-019-1771-z>.
- (83) Zhang, Y.; Yu, J.; Ren, K.; Zuo, J.; Ding, J.; Chen, X. Thermosensitive Hydrogels as Scaffolds for Cartilage Tissue Engineering. *Biomacromolecules* **2019**, *20* (4), 1478–1492. <https://doi.org/10.1021/acs.biomac.9b00043>.
- (84) Liu, H.; Ding, J.; Li, C.; Wang, C.; Wang, Y.; Wang, J.; Chang, F. Hydrogel Is Superior to Fibrin Gel as Matrix of Stem Cells in Alleviating Antigen-Induced Arthritis. *Polymers* **2016**, *8* (5), 182. <https://doi.org/10.3390/polym8050182>.
- (85) Li, X.; Ding, J.; Zhang, Z.; Yang, M.; Yu, J.; Wang, J.; Chang, F.; Chen, X. Kartogenin-Incorporated Thermogel Supports Stem Cells for Significant Cartilage Regeneration. *ACS Appl Mater Interfaces* **2016**, *8* (8), 5148–5159. <https://doi.org/10.1021/acsami.5b12212>.
- (86) Abebe, D. G.; Fujiwara, T. Controlled Thermoresponsive Hydrogels by Stereocomplexed PLA-PEG-PLA Prepared via Hybrid Micelles of Pre-Mixed Copolymers with Different PEG Lengths. *Biomacromolecules* **2012**, *13* (6), 1828–1836. <https://doi.org/10.1021/bm300325v>.
- (87) Volkmer, E.; Leicht, U.; Moritz, M.; Schwarz, C.; Wiese, H.; Milz, S.; Matthias, P.; Schloegl, W.; Friess, W.; Goettlinger, M.; Augat, P.; Schieker, M. Poloxamer-Based Hydrogels Hardening at Body Core Temperature as Carriers for Cell Based Therapies: In Vitro and in Vivo Analysis. *J Mater Sci: Mater Med* **2013**, *24* (9), 2223–2234. <https://doi.org/10.1007/s10856-013-4966-6>.
- (88) Boffito, M.; Gioffredi, E.; Chiono, V.; Calzone, S.; Ranzato, E.; Martinotti, S.; Ciardelli, G. Novel Polyurethane-Based Thermosensitive Hydrogels as Drug Release and Tissue Engineering Platforms: Design and *in Vitro* Characterization: Polyurethane-Based Thermosensitive Hydrogels. *Polym. Int.* **2016**, *65* (7), 756–769. <https://doi.org/10.1002/pi.5080>.

- (89) Boffito, M.; Pontremoli, C.; Fiorilli, S.; Laurano, R.; Ciardelli, G.; Vitale-Brovarone, C. Injectable Thermosensitive Formulation Based on Polyurethane Hydrogel/Mesoporous Glasses for Sustained Co-Delivery of Functional Ions and Drugs. *Pharmaceutics* **2019**, *11* (10), 501. <https://doi.org/10.3390/pharmaceutics11100501>.
- (90) Yang, J.-A.; Yeom, J.; Hwang, B. W.; Hoffman, A. S.; Hahn, S. K. In Situ-Forming Injectable Hydrogels for Regenerative Medicine. *Progress in Polymer Science* **2014**, *39* (12), 1973–1986. <https://doi.org/10.1016/j.progpolymsci.2014.07.006>.
- (91) Ferreira, N. N.; Ferreira, L. M. B.; Miranda-Gonçalves, V.; Reis, R. M.; Seraphim, T. V.; Borges, J. C.; Baltazar, F.; Gremião, M. P. D. Alginate Hydrogel Improves Anti-Angiogenic Bevacizumab Activity in Cancer Therapy. *European Journal of Pharmaceutics and Biopharmaceutics* **2017**, *12*.
- (92) Lv, X.; Liu, Y.; Song, S.; Tong, C.; Shi, X.; Zhao, Y.; Zhang, J.; Hou, M. Influence of Chitosan Oligosaccharide on the Gelling and Wound Healing Properties of Injectable Hydrogels Based on Carboxymethyl Chitosan/Alginate Polyelectrolyte Complexes. *Carbohydrate Polymers* **2019**, *205*, 312–321. <https://doi.org/10.1016/j.carbpol.2018.10.067>.
- (93) Luo, F.; Sun, T. L.; Nakajima, T.; King, D. R.; Kurokawa, T.; Zhao, Y.; Ihsan, A. B.; Li, X.; Guo, H.; Gong, J. P. Strong and Tough Polyion-Complex Hydrogels from Oppositely Charged Polyelectrolytes: A Comparative Study with Polyampholyte Hydrogels. *Macromolecules* **2016**, *49* (7), 2750–2760. <https://doi.org/10.1021/acs.macromol.6b00235>.
- (94) Hsu, S.-M.; Chakravarthy, R. D.; Cheng, H.; Wu, F.-Y.; Lai, T.-S.; Lin, H.-C. The Role of Aromatic Side Chains on the Supramolecular Hydrogelation of Naphthalimide/Dipeptide Conjugates. *New J. Chem.* **2018**, *42* (6), 4443–4449. <https://doi.org/10.1039/C7NJ03565A>.
- (95) Singh, N.; Kumar, M.; Miravet, J. F.; Ulijn, R. V.; Escuder, B. Peptide-Based Molecular Hydrogels as Supramolecular Protein Mimics. *Chem. Eur. J.* **2017**, *23* (5), 981–993. <https://doi.org/10.1002/chem.201602624>.
- (96) Cui, H.; Shao, J.; Wang, Y.; Zhang, P.; Chen, X.; Wei, Y. PLA-PEG-PLA and Its Electroactive Tetraaniline Copolymer as Multi-Interactive Injectable Hydrogels for Tissue Engineering. *Biomacromolecules* **2013**, *14* (6), 1904–1912. <https://doi.org/10.1021/bm4002766>.
- (97) Takashima, Y.; Sawa, Y.; Iwaso, K.; Nakahata, M.; Yamaguchi, H.; Harada, A. Supramolecular Materials Cross-Linked by Host–Guest Inclusion Complexes: The Effect of Side Chain Molecules on Mechanical Properties. *Macromolecules* **2017**, *50* (8), 3254–3261. <https://doi.org/10.1021/acs.macromol.7b00266>.
- (98) Hong, K. H.; Song, S.-C. 3D Hydrogel Stem Cell Niche Controlled by Host-Guest Interaction Affects Stem Cell Fate and Survival Rate. *Biomaterials* **2019**, *218*, 119338. <https://doi.org/10.1016/j.biomaterials.2019.119338>.
- (99) Zheng, Y.; Wyman, I. Supramolecular Nanostructures Based on Cyclodextrin and Poly(Ethylene Oxide): Syntheses, Structural Characterizations and Applications for Drug Delivery. *Polymers* **2016**, *8* (5), 198. <https://doi.org/10.3390/polym8050198>.
- (100) Hoque, J.; Sangaj, N.; Varghese, S. Stimuli-Responsive Supramolecular Hydrogels and Their Applications in Regenerative Medicine. *Macromol. Biosci.* **2019**, *19* (1), 1800259. <https://doi.org/10.1002/mabi.201800259>.
- (101) Zhang, Y.; Li, Y.; Liu, W. Dipole-Dipole and H-Bonding Interactions Significantly Enhance the Multifaceted Mechanical Properties of Thermoresponsive Shape Memory Hydrogels. *Adv. Funct. Mater.* **2015**, *25* (3), 471–480. <https://doi.org/10.1002/adfm.201401989>.

- (102) Mredha, Md. T. I.; Guo, Y. Z.; Nonoyama, T.; Nakajima, T.; Kurokawa, T.; Gong, J. P. A Facile Method to Fabricate Anisotropic Hydrogels with Perfectly Aligned Hierarchical Fibrous Structures. *Adv. Mater.* **2018**, *30* (9), 1704937. <https://doi.org/10.1002/adma.201704937>.
- (103) Shaikh, H.; Rho, J. Y.; Macdougall, L. J.; Gurnani, P.; Lunn, A. M.; Yang, J.; Huband, S.; Mansfield, E. D. H.; Peltier, R.; Perrier, S. Hydrogel and Organogel Formation by Hierarchical Self-Assembly of Cyclic Peptides Nanotubes. *Chem. Eur. J.* **2018**, *24* (71), 19066–19074. <https://doi.org/10.1002/chem.201804576>.
- (104) Liu, X.; Zhong, M.; Shi, F.; Xu, H.; Xie, X. Multi-Bond Network Hydrogels with Robust Mechanical and Self-Healable Properties. *Chin J Polym Sci* **2017**, *35* (10), 1253–1267. <https://doi.org/10.1007/s10118-017-1971-0>.
- (105) Hao, Y.; Fowler, E. W.; Jia, X. Chemical Synthesis of Biomimetic Hydrogels for Tissue Engineering: Chemical Synthesis of Biomimetic Hydrogels for Tissue Engineering. *Polym. Int.* **2017**, *66* (12), 1787–1799. <https://doi.org/10.1002/pi.5407>.
- (106) Shih, H.; Lin, C.-C. Visible-Light-Mediated Thiol-Ene Hydrogelation Using Eosin-Y as the Only Photoinitiator. *Macromol. Rapid Commun.* **2013**, *34* (3), 269–273. <https://doi.org/10.1002/marc.201200605>.
- (107) Ioele, G. Light-Sensitive Drugs in Topical Formulations: Stability Indicating Methods and Photostabilization Strategies. *Future Med. Chem.* **2017**, *14*.
- (108) McAvoy, K.; Jones, D.; Thakur, R. R. S. Synthesis and Characterisation of Photocrosslinked Poly(Ethylene Glycol) Diacrylate Implants for Sustained Ocular Drug Delivery. *Pharm Res* **2018**, *35* (2), 36. <https://doi.org/10.1007/s11095-017-2298-9>.
- (109) Zhang, X.; Xu, B.; Puperi, D. S.; Yonezawa, A. L.; Wu, Y.; Tseng, H.; Cuchiara, M. L.; West, J. L.; Grande-Allen, K. J. Integrating Valve-Inspired Design Features into Poly(Ethylene Glycol) Hydrogel Scaffolds for Heart Valve Tissue Engineering. *Acta Biomaterialia* **2015**, *14*, 11–21. <https://doi.org/10.1016/j.actbio.2014.11.042>.
- (110) Xiao, L.; Zhu, J.; Londono, D. J.; Pochan, D. J.; Jia, X. Mechano-Responsive Hydrogels Crosslinked by Block Copolymer Micelles. *Soft Matter* **2012**, *8* (40), 10233–10237. <https://doi.org/10.1039/C2SM26566D>.
- (111) Wang, J.; Lou, L.; Qiu, J. Super-tough Hydrogels Using Ionically Crosslinked Networks. *J Appl Polym Sci* **2019**, *136* (44), 48182. <https://doi.org/10.1002/app.48182>.
- (112) Morozowich, N. L.; Nichol, J. L.; Allcock, H. R. Hydrogels Based on Schiff Base Formation between an Amino-Containing Polyphosphazene and Aldehyde Functionalized-Dextrans. *J. Polym. Sci. Part A: Polym. Chem.* **2016**, *54* (18), 2984–2991. <https://doi.org/10.1002/pola.28184>.
- (113) Wu, X.; He, C.; Wu, Y.; Chen, X. Synergistic Therapeutic Effects of Schiff's Base Cross-Linked Injectable Hydrogels for Local Co-Delivery of Metformin and 5-FLUOROURACIL in a Mouse Colon Carcinoma Model. **2016**, *15*.
- (114) Ma, Y.-H.; Yang, J.; Li, B.; Jiang, Y.-W.; Lu, X.; Chen, Z. Biodegradable and Injectable Polymer-Liposome Hydrogel: A Promising Cell Carrier. *Polym. Chem.* **2016**, *7* (11), 2037–2044. <https://doi.org/10.1039/C5PY01773D>.
- (115) Jia, X.; Colombo, G.; Padera, R.; Langer, R.; Kohane, D. S. Prolongation of Sciatic Nerve Blockade by in Situ Cross-Linked Hyaluronic Acid. *Biomaterials* **2004**, *25* (19), 4797–4804. <https://doi.org/10.1016/j.biomaterials.2003.12.012>.

- (116) Sánchez-Morán, H.; Ahmadi, A.; Vogler, B.; Roh, K.-H. Oxime Cross-Linked Alginate Hydrogels with Tunable Stress Relaxation. *Biomacromolecules* **2019**, *20* (12), 4419–4429. <https://doi.org/10.1021/acs.biomac.9b01100>.
- (117) Mateen, R. Injectable, in Situ Gelling, Cyclodextrin–Dextran Hydrogels for the Partitioning-Driven Release of Hydrophobic Drugs. *Journal of Materials Chemistry B* **2014**, *11*.
- (118) Mather, B. D.; Viswanathan, K.; Miller, K. M.; Long, T. E. Michael Addition Reactions in Macromolecular Design for Emerging Technologies. *Progress in Polymer Science* **2006**, *31* (5), 487–531. <https://doi.org/10.1016/j.progpolymsci.2006.03.001>.
- (119) Li, R.; Cai, Z.; Li, Z.; Zhang, Q.; Zhang, S.; Deng, L.; Lu, L.; Li, L.; Zhou, C. Synthesis of In-Situ Formable Hydrogels with Collagen and Hyaluronan through Facile Michael Addition. *Materials Science and Engineering C* **2017**, *9*.
- (120) Hu, H.; Ye, B.; Lv, Y.; Zhang, Q. Preparing Antibacterial and In-Situ Formable Double Crosslinking Chitosan/Hyaluronan Composite Hydrogels. *Materials Letters* **2019**, *254*, 17–20. <https://doi.org/10.1016/j.matlet.2019.06.102>.
- (121) Khan, A. H.; Cook, J. K.; Wortmann, W. J.; Kersker, N. D.; Rao, A.; Pojman, J. A.; Melvin, A. T. Synthesis and Characterization of Thiol-acrylate Hydrogels Using a Base-catalyzed Michael Addition for 3D Cell Culture Applications. *J Biomed Mater Res* **2020**, *108* (5), 2294–2307. <https://doi.org/10.1002/jbm.b.34565>.
- (122) Kim, J.; Kong, Y. P.; Niedzielski, S. M.; Singh, R. K.; Putnam, A. J.; Shikanov, A. Characterization of the Crosslinking Kinetics of Multi-Arm Poly(Ethylene Glycol) Hydrogels Formed via Michael-Type Addition. *Soft Matter* **2016**, *12* (7), 2076–2085. <https://doi.org/10.1039/C5SM02668G>.
- (123) Moon, N. G.; Pekkanen, A. M.; Long, T. E.; Showalter, T. N.; Libby, B. Thiol-Michael ‘Click’ Hydrogels as an Imageable Packing Material for Cancer Therapy. *Polymer* **2017**, *125*, 66–75. <https://doi.org/10.1016/j.polymer.2017.07.078>.
- (124) Kharkar, P. M.; Rehmann, M. S.; Skeens, K. M.; Maverakis, E.; Kloxin, A. M. Thiol–ene Click Hydrogels for Therapeutic Delivery. **2016**, *15*.
- (125) Gramlich, W. M.; Kim, I. L.; Burdick, J. A. Synthesis and Orthogonal Photopatterning of Hyaluronic Acid Hydrogels with Thiol-Norbornene Chemistry. **2014**, *18*.
- (126) Pereira, R. F.; Barrias, C. C.; Bártolo, P. J.; Granja, P. L. Cell-Instructive Pectin Hydrogels Crosslinked via Thiol-Norbornene Photo-Click Chemistry for Skin Tissue Engineering. *Acta Biomaterialia* **2018**, *66*, 282–293. <https://doi.org/10.1016/j.actbio.2017.11.016>.
- (127) Teixeira, L. S. M.; Feijen, J.; van Blitterswijk, C. A.; Dijkstra, P. J.; Karperien, M. Enzyme-Catalyzed Crosslinkable Hydrogels: Emerging Strategies for Tissue Engineering. *Biomaterials* **2012**, *33* (5), 1281–1290. <https://doi.org/10.1016/j.biomaterials.2011.10.067>.
- (128) Wang, H.; Luo, Z.; Wang, Y.; He, T.; Yang, C.; Ren, C.; Ma, L.; Gong, C.; Li, X.; Yang, Z. Enzyme-Catalyzed Formation of Supramolecular Hydrogels as Promising Vaccine Adjuvants. *Adv. Funct. Mater.* **2016**, *26* (11), 1822–1829. <https://doi.org/10.1002/adfm.201505188>.
- (129) Zhao, L.; Li, X.; Zhao, J.; Ma, S.; Ma, X.; Fan, D.; Zhu, C.; Liu, Y. A Novel Smart Injectable Hydrogel Prepared by Microbial Transglutaminase and Human-like Collagen: Its Characterization and Biocompatibility. *Materials Science and Engineering: C* **2016**, *68*, 317–326. <https://doi.org/10.1016/j.msec.2016.05.108>.

- (130) Peppas, N. A.; Huang, Y.; Torres-Lugo, M.; Ward, J. H.; Zhang, J. Physicochemical Foundations and Structural Design of Hydrogels in Medicine and Biology. *Annu. Rev. Biomed. Eng.* **2000**, *2* (1), 9–29. <https://doi.org/10.1146/annurev.bioeng.2.1.9>.
- (131) Knets, I. Peculiarities of the Structure and Mechanical Properties of Biological Tissues. *Meccanica* **2002**, *37*, 375–384.
- (132) Sacks, M. S.; Sun, W. Multiaxial Mechanical Behavior of Biological Materials. *Annu. Rev. Biomed. Eng.* **2003**, *5* (1), 251–284. <https://doi.org/10.1146/annurev.bioeng.5.011303.120714>.
- (133) Weller, C.; Kleer, R.; Piller, F. T. Economic Implications of 3D Printing: Market Structure Models in Light of Additive Manufacturing Revisited. *International Journal of Production Economics* **2015**, *164*, 43–56. <https://doi.org/10.1016/j.ijpe.2015.02.020>.
- (134) Li, J.; Wu, C.; Chu, P. K.; Gelinsky, M. 3D Printing of Hydrogels: Rational Design Strategies and Emerging Biomedical Applications. *Materials Science and Engineering: R: Reports* **2020**, *140*, 100543. <https://doi.org/10.1016/j.mser.2020.100543>.
- (135) Thayer, P.; Martinez, H.; Gatenholm, E. History and Trends of 3D Bioprinting. In *3D Bioprinting*; Crook, J. M., Ed.; Methods in Molecular Biology; Springer US: New York, NY, 2020; Vol. 2140, pp 3–18. https://doi.org/10.1007/978-1-0716-0520-2_1.
- (136) Derakhshanfar, S.; Mbeleck, R.; Xu, K.; Zhang, X.; Zhong, W.; Xing, M. 3D Bioprinting for Biomedical Devices and Tissue Engineering: A Review of Recent Trends and Advances. *Bioactive Materials* **2018**, *3* (2), 144–156. <https://doi.org/10.1016/j.bioactmat.2017.11.008>.
- (137) Gioffredi, E.; Boffito, M.; Calzone, S.; Giannitelli, S. M.; Rainer, A.; Trombetta, M.; Mozetic, P.; Chiono, V. Pluronic F127 Hydrogel Characterization and Biofabrication in Cellularized Constructs for Tissue Engineering Applications. *Procedia CIRP* **2016**, *49*, 125–132. <https://doi.org/10.1016/j.procir.2015.11.001>.
- (138) Boere, K. W. M.; Blokzijl, M. M.; Visser, J.; Linssen, J. E. A.; Malda, J.; Hennink, W. E.; Vermonden, T. Biofabrication of Reinforced 3D-Scaffolds Using Two-Component Hydrogels. *J. Mater. Chem. B* **2015**, *3* (46), 9067–9078. <https://doi.org/10.1039/C5TB01645B>.
- (139) Ouyang, L.; Highley, C. B.; Rodell, C. B.; Sun, W.; Burdick, J. A. 3D Printing of Shear-Thinning Hyaluronic Acid Hydrogels with Secondary Cross-Linking. **2016**, *9*.
- (140) Li, L.; Zhang, K.; Wang, T.; Wang, P.; Xue, B.; Cao, Y.; Zhu, L.; Jiang, Q. Biofabrication of a Biomimetic Supramolecular-Polymer Double Network Hydrogel for Cartilage Regeneration. *Materials & Design* **2020**, *189*, 108492. <https://doi.org/10.1016/j.matdes.2020.108492>.
- (141) Gao, G.; Yonezawa, T.; Hubbell, K.; Dai, G.; Cui, X. Inkjet-Bioprinted Acrylated Peptides and PEG Hydrogel with Human Mesenchymal Stem Cells Promote Robust Bone and Cartilage Formation with Minimal Printhead Clogging. *Biotechnology Journal* **2015**, *10* (10), 1568–1577. <https://doi.org/10.1002/biot.201400635>.
- (142) Park, J. A.; Lee, H.; Park, S.; Jung, S. Self-Organization of Fibroblast-Laden 3D Collagen Microstructures from Inkjet-Printed Cell Patterns. *Adv. Biosys.* **2020**, *4* (5), 1900280. <https://doi.org/10.1002/adbi.201900280>.
- (143) Raman, R.; Bashir, R. Stereolithographic 3D Bioprinting for Biomedical Applications. In *Essentials of 3D Biofabrication and Translation*; Elsevier, 2015; pp 89–121. <https://doi.org/10.1016/B978-0-12-800972-7.00006-2>.

- (144) Zhu, W.; George, J. K.; Sorger, V. J.; Grace Zhang, L. 3D Printing Scaffold Coupled with Low Level Light Therapy for Neural Tissue Regeneration. *Biofabrication* **2017**, *9* (2), 025002. <https://doi.org/10.1088/1758-5090/aa6999>.
- (145) Creff, J.; Courson, R.; Mangeat, T.; Foncy, J.; Souleille, S.; Thibault, C.; Besson, A.; Malaquin, L. Fabrication of 3D Scaffolds Reproducing Intestinal Epithelium Topography by High-Resolution 3D Stereolithography. *Biomaterials* **2019**, *221*, 119404. <https://doi.org/10.1016/j.biomaterials.2019.119404>.
- (146) Liew, W. L. A. Laser-Based Fabrication of 3D Hydrogel Constructs Using Bessel Beams. **2018**, *8*.
- (147) Kérourédan, O.; Hakobyan, D.; Rémy, M.; Ziane, S.; Dusserre, N.; Fricain, J.-C.; Delmond, S.; Thébaud, N. B.; Devillard, R. *In Situ* Prevascularization Designed by Laser-Assisted Bioprinting: Effect on Bone Regeneration. *Biofabrication* **2019**, *11* (4), 045002. <https://doi.org/10.1088/1758-5090/ab2620>.
- (148) Sorkio, A.; Koch, L.; Koivusalo, L.; Deiwick, A.; Miettinen, S.; Chichkov, B.; Skottman, H. Human Stem Cell Based Corneal Tissue Mimicking Structures Using Laser-Assisted 3D Bioprinting and Functional Bioinks. *Biomaterials* **2018**, *171*, 57–71. <https://doi.org/10.1016/j.biomaterials.2018.04.034>.
- (149) Li, J.; Mooney, D. J. Designing Hydrogels for Controlled Drug Delivery. *Nat Rev Mater* **2016**, *1* (12), 16071. <https://doi.org/10.1038/natrevmats.2016.71>.
- (150) Foyt, D. A.; Norman, M. D. A.; Yu, T. T. L.; Gentleman, E. Exploiting Advanced Hydrogel Technologies to Address Key Challenges in Regenerative Medicine. *Adv Healthc Mater* **2018**, *7* (8), e1700939. <https://doi.org/10.1002/adhm.201700939>.
- (151) Mandal, A.; Clegg, J. R.; Anselmo, A. C.; Mitragotri, S. Hydrogels in the Clinic. **2004**, *12*.
- (152) Hollister, S. J. Scaffold Design and Manufacturing: From Concept to Clinic. *Adv. Mater.* **2009**, *21* (32–33), 3330–3342. <https://doi.org/10.1002/adma.200802977>.
- (153) Aram, E.; Mehdipour-Ataei, S. A Review on the Micro- and Nanoporous Polymeric Foams: Preparation and Properties. *International Journal of Polymeric Materials and Polymeric Biomaterials* **2016**, *65* (7), 358–375. <https://doi.org/10.1080/00914037.2015.1129948>.
- (154) Sola, A. Development of Solvent-Casting Particulate Leaching (SCPL) Polymer Scaffolds as Improved Three-Dimensional Supports to Mimic the Bone Marrow Niche. *Materials Science* **2019**, *13*.
- (155) Conoscenti, G.; Carrubba, V. L.; Brucato, V. A Versatile Technique to Produce Porous Polymeric Scaffolds: The Thermally Induced Phase Separation (TIPS) Method. *Arch Chem Res* **2017**, *01* (02). <https://doi.org/10.21767/2572-4657.100012>.
- (156) Chen, S.; Zhao, X.; Du, C. Macroporous Poly (l-Lactic Acid)/Chitosan Nanofibrous Scaffolds through Cloud Point Thermally Induced Phase Separation for Enhanced Bone Regeneration. *European Polymer Journal* **2018**, *109*, 303–316. <https://doi.org/10.1016/j.eurpolymj.2018.10.003>.
- (157) Guo, J.; Liu, X.; Lee Miller, A.; Waletzki, B. E.; Yaszemski, M. J.; Lu, L. Novel Porous Poly(Propylene Fumarate-Co-Caprolactone) Scaffolds Fabricated by Thermally Induced Phase Separation: SCAFFOLDS WITH POROUS STRUCTURES. *J. Biomed. Mater. Res.* **2017**, *105* (1), 226–235. <https://doi.org/10.1002/jbm.a.35862>.
- (158) Jun, I.; Han, H.-S.; Edwards, J.; Jeon, H. Electrospun Fibrous Scaffolds for Tissue Engineering: Viewpoints on Architecture and Fabrication. *IJMS* **2018**, *19* (3), 745. <https://doi.org/10.3390/ijms19030745>.
- (159) Xue, J.; Feng, B.; Zheng, R.; Lu, Y.; Zhou, G.; Liu, W.; Cao, Y.; Zhang, Y.; Zhang, W. J. Engineering Ear-Shaped Cartilage Using Electrospun Fibrous Membranes of Gelatin/Polycaprolactone. *Biomaterials* **2013**, *34* (11), 2624–2631. <https://doi.org/10.1016/j.biomaterials.2012.12.011>.

- (160) Rajzer, I.; Menaszek, E.; Castano, O. Electrospun Polymer Scaffolds Modified with Drugs for Tissue Engineering. *Materials Science and Engineering: C* **2017**, *77*, 493–499. <https://doi.org/10.1016/j.msec.2017.03.306>.
- (161) Licciardello, M.; Tonda-Turo, C.; Gallina, A.; Ciofani, G.; Ciardelli, G. Fabrication of Extracellular Matrix-like Membranes for Loading Piezoelectric Nanoparticles. *J. Phys. Mater.* **2020**, *3* (3), 034004. <https://doi.org/10.1088/2515-7639/ab8572>.
- (162) Nitti, P.; Gallo, N.; Natta, L.; Scalera, F.; Palazzo, B.; Sannino, A.; Gervaso, F. Influence of Nanofiber Orientation on Morphological and Mechanical Properties of Electrospun Chitosan Mats. *Journal of Healthcare Engineering* **2018**, *2018*, 1–12. <https://doi.org/10.1155/2018/3651480>.
- (163) Ceretti, E.; Ginestra, P.; Neto, P. I.; Fiorentino, A.; Da Silva, J. V. L. Multi-Layered Scaffolds Production via Fused Deposition Modeling (FDM) Using an Open Source 3D Printer: Process Parameters Optimization for Dimensional Accuracy and Design Reproducibility. *Procedia CIRP* **2017**, *65*, 13–18. <https://doi.org/10.1016/j.procir.2017.04.042>.
- (164) Rebaioli, L.; Pagano, C.; Fassi, I. Fabrication of PLA/CNT Composite Scaffolds by Fused Deposition Modeling. In *Volume 4: 23rd Design for Manufacturing and the Life Cycle Conference; 12th International Conference on Micro- and Nanosystems*; American Society of Mechanical Engineers: Quebec City, Quebec, Canada, 2018; p V004T08A032. <https://doi.org/10.1115/DETC2018-86097>.
- (165) Chen, Q.; Mangadla, J. D.; Wallat, J.; De Leon, A.; Pokorski, J. K.; Advincula, R. C. 3D Printing Biocompatible Polyurethane/Poly(Lactic Acid)/Graphene Oxide Nanocomposites: Anisotropic Properties. *ACS Appl. Mater. Interfaces* **2017**, *9* (4), 4015–4023. <https://doi.org/10.1021/acsami.6b11793>.
- (166) Do, A.-V.; Smith, R.; Acri, T. M.; Geary, S. M.; Salem, A. K. 3D Printing Technologies for 3D Scaffold Engineering. In *Functional 3D Tissue Engineering Scaffolds*; Elsevier, 2018; pp 203–234. <https://doi.org/10.1016/B978-0-08-100979-6.00009-4>.
- (167) Zhou, C.; Yang, K.; Wang, K.; Pei, X.; Dong, Z.; Hong, Y.; Zhang, X. Combination of Fused Deposition Modeling and Gas Foaming Technique to Fabricated Hierarchical Macro/Microporous Polymer Scaffolds. *Materials & Design* **2016**, *109*, 415–424. <https://doi.org/10.1016/j.matdes.2016.07.094>.
- (168) Mazzoli, A. Selective Laser Sintering in Biomedical Engineering. *Med Biol Eng Comput* **2013**, *51* (3), 245–256. <https://doi.org/10.1007/s11517-012-1001-x>.
- (169) XiaoHui, S.; Wei, L.; PingHui, S.; QingYong, S.; QingSong, W.; YuSheng, S.; Kai, L.; WenGuang, L. Selective Laser Sintering of Aliphatic-Polycarbonate/Hydroxyapatite Composite Scaffolds for Medical Applications. *Int J Adv Manuf Technol* **2015**, *81* (1–4), 15–25. <https://doi.org/10.1007/s00170-015-7135-x>.
- (170) Wu, J.; Yang, R.; Zheng, J.; Pan, L.; Liu, X. Fabrication and Improvement of PCL/Alginate/PAAm Scaffold via Selective Laser Sintering for Tissue Engineering. *Micro & Nano Letters* **2019**, *14* (8), 852–855. <https://doi.org/10.1049/mnl.2018.5806>.
- (171) Mota, C.; Puppi, D.; Chiellini, F.; Chiellini, E. Additive Manufacturing Techniques for the Production of Tissue Engineering Constructs. *J Tissue Eng Regen Med* **2015**, *9* (3), 174–190. <https://doi.org/10.1002/term.1635>.
- (172) Mondschein, R. J.; Kanitkar, A.; Williams, C. B.; Verbridge, S. S.; Long, T. E. Polymer Structure-Property Requirements for Stereolithographic 3D Printing of Soft Tissue Engineering Scaffolds. *Biomaterials* **2017**, *140*, 170–188. <https://doi.org/10.1016/j.biomaterials.2017.06.005>.
- (173) Elomaa, L.; Keshi, E.; Sauer, I. M.; Weinhart, M. Development of GelMA/PCL and DECM/PCL Resins for 3D Printing of Acellular in Vitro Tissue Scaffolds by Stereolithography. *Materials Science and Engineering: C* **2020**, *112*, 110958. <https://doi.org/10.1016/j.msec.2020.110958>.

(174) Youssef, A. Additive Manufacturing of Polymer Melts for Implantable Medical Devices and Scaffolds. *Biofabrication* **2017**, 9, 30.

Section 1 – Chapter 1.2 – Thesis Goal

As described in the previous Chapter, tissue engineering and regenerative medicine are based on common principles, which lay their foundation on different and correlated disciplines. In order to achieve the ambitious aims to administer highly effective pharmaceutical therapies and regenerate tissues and organ structures, relevantly complex or combined strategies need to be developed in most cases. In this scenario, the design of formulations based on specific physical phenomena represents a valuable strategy, resulting in surprisingly effective, versatile and handle devices. In this Ph.D. thesis, the above-mentioned approach will be pursued with the intention to develop innovative bioartificial injectable supramolecular formulations based on novel polyfunctional polymers and cyclodextrins. These newly designed systems will be engineered for drug delivery and regenerative medicine applications, relying on the technical and scientific principles that represent the newest available knowledge in the field. Poly(urethane)s will be properly designed as constituents of the newly developed formulations by exploiting their LEGO-like composition, which derives from a finely tunable synthesis process. In detail, a library of different amphiphilic poly(urethane)s will be developed covering a wide range of combined macromolecular properties finalized to the production of self-assembled supramolecular hydrogels. On the other hand, cyclodextrins will be exploited for their exceptional behavior in watery environment to host polymeric domains into their hydrophobic cavity, thus forming molecular complexes known as poly(pseudo)rotaxanes (PPRs). One specific type of cyclodextrins will be utilized in this work, namely α -cyclodextrins. These cyclic oligomers are in fact theoretically able to interact with poly(ethylene oxide) and other aliphatic blocks that will mainly constitute the backbone of the synthesized poly(urethane)s. The poly(pseudo)rotaxanes derived from the interaction of these two components will then further interact between each other forming channel-like crystals. By exploiting the spontaneous formation of these domains, highly injectable and self-healing hydrogels will be developed. Additionally, α -cyclodextrins will be easily exploited to encapsulate hydrophobic and non-soluble drugs through a self-delivery mechanism, leading to the development of drug-loaded systems with improved drug bioavailability and stability. The work will be structured in various sections with the intent to orderly show the consecutive achievements of the work, as described below.

In the first part, two poly(ether urethane)s (PEUs) based on a commercial amphiphilic triblock polyether (Poloxamer® 407, P407, PEO-PPO-PEO, 70% wt PEO and M_n 12600 Da) as macrodiol, a non-toxic aliphatic diisocyanate (1,6-hexamethylene diisocyanate) and two different chain extenders (i.e., N-Boc Serinol and 1,4-cyclohexanedimethanol) will be synthesized. In this section of the work, the interaction of these PEUs with α -cyclodextrins in pure water will be investigated. The formation of supramolecular complexes will be assessed through physico-chemical characterizations, such as X-Ray powder Diffraction, Attenuated Total Reflectance – Fourier Transform Infrared spectroscopy, Proton Nuclear Magnetic Resonance spectroscopy. Relying on the spontaneous self-assembly of these supramolecular structures, a wide library of novel hydrogels will be formulated and qualitatively characterized in terms of gelation kinetics and physical stability. Depending on the resulting properties, an accurate selection of the most

promising formulations will be carried out and a complete rheological characterization will be performed, even evaluating self-healing ability in dynamic conditions. The responsiveness and stability, as well as cytotoxicity of the resulting formulations in physiological-like environment will be studied to establish the best formulations for drug delivery applications. Finally, the most promising hydrogels will be selected for preliminary release studies.

As a transitory phase of this work, a comparative study of the effects of the solvent and other co-solutes (e.g., salts) on hydrogel gelation potential and timing will be performed to determine the best conditions for hydrogel formulation. To this aim, a complete rheological characterization, and a study for the evaluation of the hydrogel responsiveness in watery environment will also be performed.

In the second part of this work, the library of PEU-based supramolecular hydrogels will be further enriched with the aim to develop various formulations for specific drug delivery applications. To this purpose, novel poly(urethane)s will be synthesized to evaluate the role of PEU constituent blocks and their resulting chemical features on the gelation potential and physical properties of supramolecular formulations. In addition to Poloxamer® 407, a different Pluronic® will also be used as macrodiol for PEU synthesis. More specifically, Pluronic® F68 will be utilized due to its higher PEO content (80% wt) and lower molecular weight (M_n 8400 Da) compared to P407. As co-reagents, 1,6-hexamethylene diisocyanate and N-Boc Serinol will be used. The presence of the above-mentioned chain extender will open the way to the possibility to evaluate the effects of Boc cleavage and the exposure of free functional amino groups on the resulting supramolecular complexes and hydrogels. The entire set of physico-chemical characterizations will be performed as in the previous part (X-Ray powder Diffraction, Attenuated Total Reflectance – Fourier Transform Infrared spectroscopy, Proton Nuclear Magnetic resonance spectroscopy) with the aim to evaluate the behavior of this new PEU platform when mixed in aqueous solutions with α -cyclodextrins. An accurate comparative study between all the synthesized PEUs will be carried out, selecting the most promising materials for supramolecular hydrogel design. A set of supramolecular hydrogels containing PEUs at low concentration (i.e., less than 5% w/v) will be formulated and characterized through qualitative observations (gelation time in isothermal conditions) and rheological studies. Moreover, hydrogel responsiveness in contact with aqueous environments will be evaluated to assess their suitability as drug delivery platforms. In this regard, curcumin will be used as highly hydrophobic drug with wide therapeutic effects as antitumor, antioxidant and antibacterial agent. Then, the presence of α -cyclodextrins will be even exploited to encapsulate a high curcumin content, enhancing its availability. The differences induced by the presence of the drug into the hydrogel networks will be evaluated through rheological characterizations. Release studies will be conducted in physiological-like conditions for the most promising formulations.

To further prove the huge potential of the here-developed hydrogels, two different case studies will be carried out. The first will consist in the encapsulation and delivery of an antibiotic molecule (i.e., ciprofloxacin) from extremely mild hydrogel formulations. The robustness of the investigated gels for this specific drug delivery application will be evaluated through the encapsulation of different drug contents. The second case study will combine drug delivery and regenerative medicine towards the design of advanced therapeutic strategies. In detail, the integration of supramolecular hydrogels into three-dimensional porous scaffolds will be evaluated and

preliminary release studies of a model molecule from the resulting hybrid devices will be performed.

Besides, to further evaluate the versatility and suitability of PEU-based hydrogels as promising materials for regenerative medicine, a study on the development of photo-sensitive and supramolecular systems will be carried out. In particular, a photo-curable PEU based on P407 and 1,6-hexamethylene diisocyanate will be synthesized with the peculiarity to be end-capped through 2-hydroxyethyl methacrylate rather than being chain extended with other diols. The resulting photo-sensitive PEU will be chemically and physically characterized. Additionally, its ability to form supramolecular domains with α -cyclodextrins will be evaluated as for previous physical systems. 3D printed constructs composed of the most promising formulations will be fabricated and their stability in physiological-like environment will be assessed. Curcumin will also be encapsulated into these hydrogels and release kinetics will be tuned exploiting hydrogel photo-sensitivity.

Finally, a different approach will be investigated in the last part of the work. Indeed, a novel bioartificial mixture will be formulated by mixing a thermo- and photo-sensitive PEU, α -cyclodextrins and gelatin methacryloyl (GelMA), in order to compose an engineered platform with enhanced handling and bioactivity for tissue engineering applications. Curcumin will be encapsulated into these hydrogels in order to evaluate their overall stability and suitability as versatile scaffolding systems for combined drug delivery and tissue engineering approaches.

In conclusion, an overall analysis will be carried out in order to discuss how the developed systems could further evolve in the future, highlighting the open challenges to overcome in order to reach real clinical applications.

Section 2

Supramolecular hydrogels based on properly synthesized poly(ether urethane)s for smart applications in drug delivery

Outline

This section reports a thorough study regarding the development of supramolecular hydrogels based on newly synthesized poly(ether urethane)s and α -cyclodextrins for drug delivery applications. A brief introduction is reported in *Chapter 2.1*, in which the basic principles underpinning the formation of supramolecular hydrogels as a result of the self-assembly between linear polymers and α -cyclodextrins are explained. Moreover, this Chapter reports a wide discussion on the main requirements to be fulfilled for supramolecular hydrogel development inspired by the most recent approaches reported in the literature (i.e., the state of the art), highlighting main advantages and limitations.

Subsequently, an initial investigation on the suitability of poly(ether urethane)s to produce stable and responsive hydrogel networks was conducted, focusing on the importance of their chemical features (*Chapter 2.2*). An in-depth physico-chemical characterization was performed on complexes resulting from the self-assembly between two different poly(ether urethane)s and α -cyclodextrins. The importance of synthesis versatility was discussed and its potential in terms of modulation of hydrogel behavior was evidenced by the resulting good physical properties. A wide set of formulations was then evaluated with the aim to define a proper domain for hydrogel composition in view of future applications in drug delivery. In that regard, hydrogel formulations based on low polymer content were selected and showed good mechanical properties and self-healing ability. Swelling and stability tests in contact with physiological-like watery environments were also performed, showing a reliable hydrogel behavior, which resulted to be proper also in terms of cytotoxicity evaluated according to ISO 10993 standards. Drug release potential of the developed formulations was preliminary assessed using fluorescein isothiocyanate dextran 4 as a model molecule.

Chapter 2.3 deals with the evaluation of hydrogel gelation kinetics, mechanical properties, and responsiveness in watery environment as a function of the solvent used for their preparation, namely water or phosphate buffered saline. The conducted characterizations evidenced that the presence of salts in solution favored the formation of supramolecular hydrogels through the induction of the salting-out effect, thus significantly reducing gelation time and improving mechanical response. To completely characterize the resulting systems and the effects induced by salts within hydrogel networks, swelling and stability tests in contact with various watery environments (phosphate buffered saline as such and added with a lipophilic molecule (amphotericin B) to prevent mold formation) were additionally performed to assess hydrogel sensitivity.

On the basis of the previous data and findings, in *Chapter 2.4* novel poly(ether urethane)s were synthesized relying on the versatile synthesis procedure previously exploited. Different reagents

were selected (i.e., two different amphiphilic macrodiols and two chain extenders) in order to better evaluate the effects of poly(ether urethane) building blocks on hydrogel development. In detail, a set of poly(ether urethane)s characterized by various configurations, such as linearity, presence of pendant hydrophobic groups or presence of free primary amino domains, was developed. A thorough physico-chemical characterization was conducted to correlate the self-assembly ability with the composition of the investigated poly(ether urethane)s. Then, hydrogels were formulated in saline solution using a single poly(ether urethane) or a blend of poly(ether urethane)s with the intention to enhance the final hydrogel functionality. The resulting networks were tested in aqueous environment and turned out to be suitable to encapsulate a relevant amount of curcumin by exploiting the capability of α -cyclodextrins to form inclusion complexes with this molecule. Release tests of such extremely sensitive and therapeutic agent (i.e., curcumin) were conducted, also investigating the potential protective ability of hydrogel components.

To better validate the suitability of the here-developed polymers to design versatile platforms for drug delivery and regenerative medicine, two case studies are reported in *Chapter 2.5* and *Chapter 2.6*. In *Chapter 2.5*, the encapsulation of a totally different drug with respect to curcumin was conducted. In fact, ciprofloxacin, an antibiotic molecule, was encapsulated at two different concentrations within a hydrogel formulation based on one of the most promising poly(ether urethane)s previously selected and release studies were performed, after evaluating the general effects of the encapsulated drug on hydrogel network formation. In *Chapter 2.6* another promising poly(ether urethane) exposing free primary amino groups along its polymeric chains was selected for the formation of supramolecular hydrogels and their encapsulation within the void volume of rigid and highly porous scaffolds based on poly(ϵ -caprolactone) and produced through particulate-leaching technique. To enhance hydrogel encapsulation and biological potency, plasma treatment was conducted on porous scaffolds as well. A simple method for hydrogel encapsulation within solid scaffolds was developed and the properties of the resulting matrices were preliminary investigated through mechanical compression tests. Preliminary drug release evaluation was also conducted utilizing fluorescein isothiocyanate dextran 4 as a model molecule.

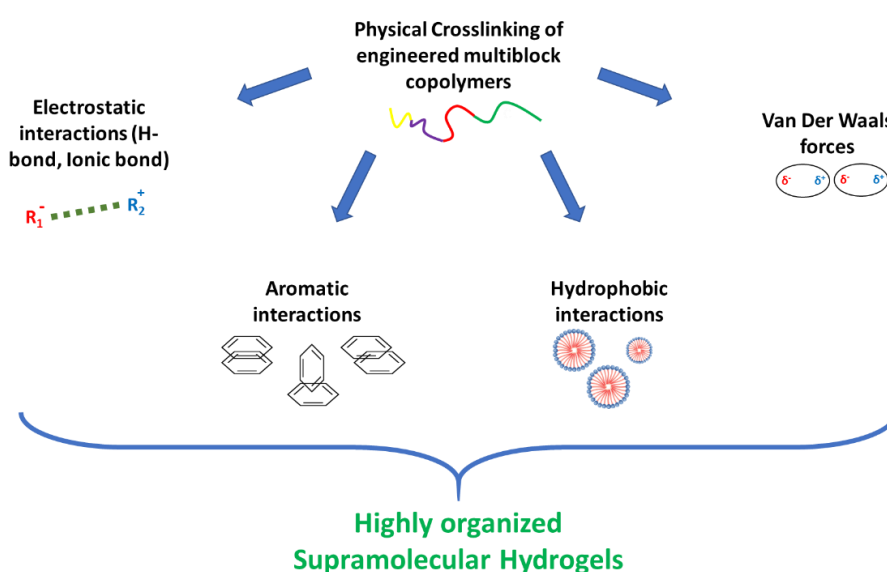
The entire set of data obtained from this section was fundamental in order to properly and critically overview the general potential and versatility of the here-developed poly(ether urethane)s for subsequent applications and developments.

Section 2 – Chapter 2.1 – Physical hydrogels as suitable tools for regenerative pharmacology and tissue engineering

1. Abstract

The importance of physical hydrogels in biomedical applications is remarkable. Indeed, these systems are generally characterized by a peculiar tunability and a relevant reversibility, which allow the design of highly handleable and injectable devices for drug delivery. Moreover, depending on the chemical functionalities of their constituents (i.e., natural and synthetic polymers), physical hydrogels could even show an enhanced sensitivity to external stimuli, thus widening the possibilities for the modulation of their final properties, especially in terms of mechanical response and drug release kinetics. Systems characterized by a particularly organized physically crosslinked network are known as “supramolecular hydrogels”. The hierarchical organization of the forming materials of such systems confers them interesting physical properties, such as self-healing ability and enhanced responsiveness to external environments. In this scenario, thermo-sensitive hydrogels based on amphiphilic polymers are highly interesting and potential platforms, as they retain the ability to undergo a sol-to-gel transition at body temperature through the formation of micelle-based networks. Additionally, the formation of host-guest inclusion complexes represents another strategy to form supramolecular hydrogel systems and cyclodextrins plays a fundamental role in this regard. In fact, cyclodextrins can form complexes with linear polymers known as “poly(pseudo)rotaxanes”, which are able to produce hydrogel networks. This Chapter discusses the main theoretical aspects underpinning the formation of supramolecular hydrogels, with the aim to highlight their most important properties and features, and survey the related state-of-the-art through noteworthy and recent works. In this regard, the development of highly functional LEGO-like poly(urethane)s as valuable raw materials for the production of cyclodextrin-based supramolecular hydrogels with improved physical properties and enhanced effectiveness for drug delivery applications will also be thoroughly discussed.

Graphical abstract



2. Physical hydrogels for biomedical applications: the importance of self-assembly

Physical hydrogels that rely on highly reversible and non-covalent bonds represent a class of devices particularly suitable for regenerative medicine applications. As reported before, different interactions can be utilized to formulate hydrogel networks, such as hydrophobic coalescence, hydrogen bonds and electrostatic interactions.¹⁻³ The exploitation of these phenomena in combination can lead to the formation of remarkably hierarchical and ordered inter- and intramolecular structures, resulting in supramolecular hydrogels. In this Ph.D. project, coordinated interactions at the supramolecular level will be exploited to obtain highly engineered physical hydrogels for drug delivery and tissue engineering. More specifically, the formation of thermo-sensitive micellar structures based on amphiphilic poly(ether urethane)s will be integrated with cyclodextrins, leading to the formation of assembled channel-like crystals based on poly(pseudo)rotaxanes. To better understand this particular arrangement at the molecular and higher levels, the involved scientific principles will be briefly discussed in the following paragraphs, highlighting the most noteworthy strategies specifically addressed to drug delivery for regenerative pharmacology.

3. Polymer-based supramolecular complexes for thermo-sensitive hydrogel formation

3.1 General aspects on polymer-based thermo-sensitive supramolecular constructs

Thermo-sensitive polymers can be defined as “smart” materials due to their ability to translate an external stimulus into specific supramolecular arrangements. Depending on the peculiarities of the involved polymers, two typologies of thermo-responsive polymeric systems can be identified, as previously anticipated in *Section 1*. A polymeric solution characterized by a lower critical solution temperature (LCST) shows an opposite gelling behavior and engineering applications with respect to a system that exhibits an upper critical solution temperature (UCST).⁴ Polymer solubility is the common feature of these two different systems. In fact, networks showing a LCST are characterized by a temperature above which two different phases are composed by the polymer and the solvent for specific temperature-driven self-assembly processes. The formation of two phases is achieved in an opposite manner in polymeric solutions characterized by an UCST (e.g., gelatin). The general behavior of these two types of hydrogels can be summarized as represented in figure 1. For biomedical applications, systems that show a LCST are more suitable. Indeed, the temperature of the body (i.e., 37 °C) can be exploited as a stimulus to induce gelation *in situ*, while preserving good handling properties as deposition can be carried out at room (i.e., 20-25 °C) or lower temperatures.

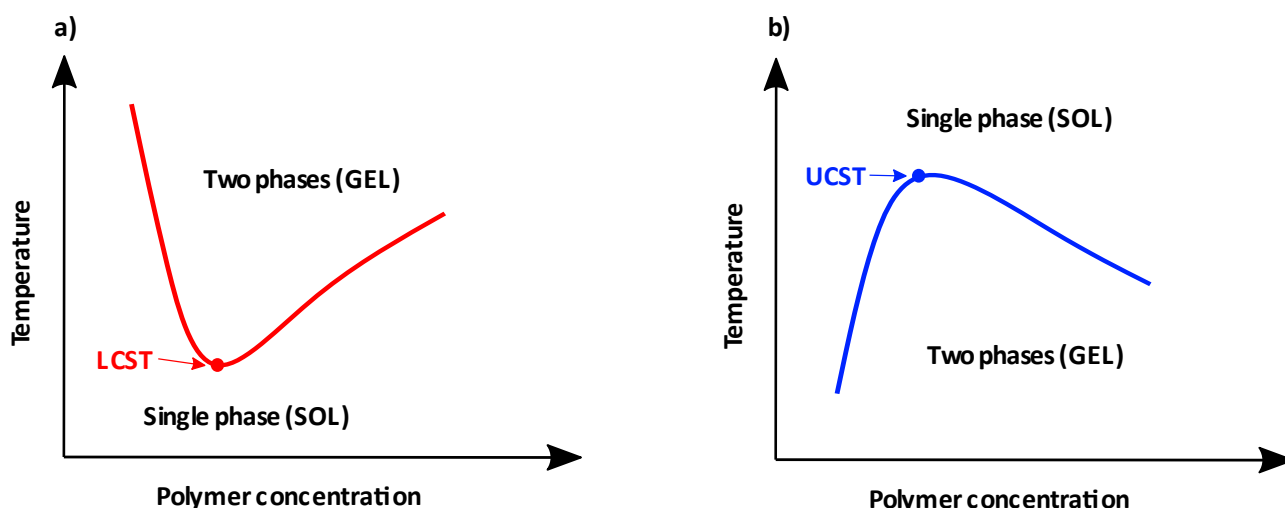


Figure 1 – Typical behavior of LCST (a) and UCST (b) gelling systems.

LCST polymeric solutions

Different amphiphilic polymers exhibit a temperature-dependent behavior showing a LCST upon solubilization in aqueous solutions. A well-known group of these materials is represented by Poloxamers® (ICI), also known as Pluronics® (BASF). These molecules are block copolymers composed of poly(ethylene oxide) (PEO)/poly(ethylene glycol) (PEG), which is hydrophilic, and poly(propylene oxide) (PPO), which is hydrophobic (figure 2).

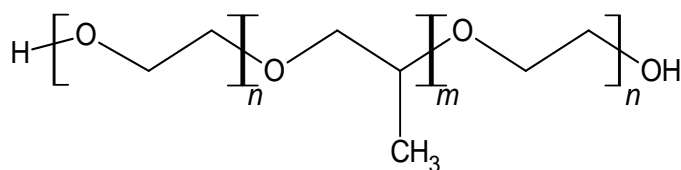


Figure 2 – Simplified molecular structure of Pluronics®/Poloxamers®.

As previously discussed in *Section 1*, the mechanism that leads amphiphilic copolymer-based solutions to gelation can be explained through the formation of hydrophobic interactions.⁵ These intra-molecular physical bonds are then the driving force for the self-assembly of polymeric chains into micelles, which are characterized by an inner hydrophobic core and an outer lipophobic corona. The formation of micelles occurs beyond defined polymer concentrations (i.e., at concentration higher than the critical micellization concentration, CMC) and temperatures (i.e., at temperature higher than the critical micellization temperature, CMT). The determination of these two parameters is extremely important to evaluate the thermo-responsiveness of systems based on amphiphilic copolymers in solution. Figure 3 reports a schematic representation of the micellization process. Under specific conditions, micelle formation and packing as a consequence of temperature increase can induce the formation of hydrogel networks. Indeed, solutions containing a sufficient amount of amphiphilic polymers (i.e., above a critical gelation concentration, CGC) show a sol-to-gel transition at specific temperatures (i.e., above a critical gelation temperature, CGT). This process is reversible, since the involved self-assembly depends on aggregation phenomena based on the formation of hydrophobic interactions.

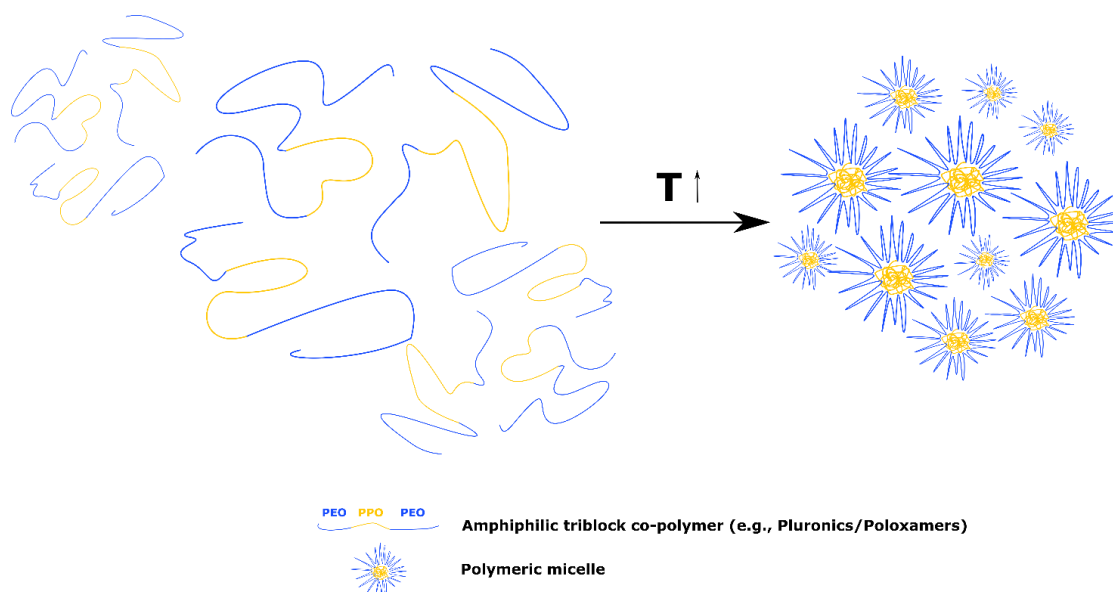


Figure 3 – Schematic representation of the micellization process. This phenomenon occurs in watery environments when the polymeric concentration is greater than the critical value (CMC), which depends on the chemical properties of the involved amphiphilic chains (i.e., molar mass, hydrophilic-hydrophobic balance, and distribution) in a specific range of temperatures (i.e., equal or greater than CMT).

In an extremely important study carried out in 1984, Vadnere and co-workers systematically evaluated the role of the involved variables in the micellization process that leads to gelation using a set of nine different block copolymers.⁶ They observed that the logarithm of polymer concentration and the reciprocal of the gelation temperature (T_m) were correlated through a linear function. Concerning the relationship between the logarithm of molecular mass and the reciprocal of the temperature of phase transition, no linear correlation was found, but an important dependency on the mass ratio between PPO and PEO domains was hypothesized. Generally, the gelation process was characterized by an endothermic variation of enthalpy. The effect of temperature change in the polymer solution can be summarized in the equation $\Delta G = \Delta H - T\Delta S$, in which ΔG is the negative free energy, ΔS is the entropy, ΔH is the enthalpy and T is the temperature of the system. Previous investigations evidenced a positive ΔH in the transition from solution to gel.⁷ The authors observed that at the equilibrium of this transition (i.e., $\text{sol} \rightleftharpoons \text{gel}$, T_m), ΔG assumed a value equal to zero, thus indicating that ΔS was also positive. Nonetheless, ΔS should result negative, as the gelation process induces the formation of an organized network. Vadnere and colleagues demonstrated that ΔH and ΔS were influenced by the solvent and the entity of hydrophobic domains present in the system. Their study demonstrated that at temperatures lower than T_m water molecules surrounding the hydrophobic domains are characterized by a higher order. Instead, when gelation process occurs, the formed hydrophobic interactions squeeze out these water molecules in the domain of less ordered solvent molecules. This process explained the incremental variation of entropy. In a subsequent study, Attwood and co-authors deepened the knowledge about one of the most promising triblock polymers in terms of gelation: Pluronic® F127, also known as Poloxamer® 407 (P407),⁸ which contains PEO at 70% wt and shows a molecular mass M_n around 12600 Da. They observed that the dehydration of micelles was concurrent with temperature increase. Their study demonstrated that this phenomenon is accompanied by an increment of the anhydrous volume given by micelle interaction and aggregation. To this purpose, it was observed that the dehydration and hence the interaction

between PEO domains of neighboring micelles are the elemental factors for the formation of the hydrogel network.

The knowledge about the above-mentioned mechanism of self-assembly has been further deepened during the last decades. Nowadays the availability of thermo-sensitive polymers able to form hydrogels is wide and the application of such systems in regenerative medicine is being consolidated.⁹ Poloxamer-based hydrogels are still utilized in the formulations of effective platforms for drug delivery and tissue engineering. Nonetheless, their limited stability in watery environments represents the major constraint in their use. Depending on different parameters, such as chemical properties, distribution and molecular mass of the constituent blocks, the thermo-responsiveness of Poloxamer aqueous solutions can be finely controlled. As anticipated before, the development of properly synthesized amphiphilic polymers is one of the most interesting strategies for the design of modern thermo-sensitive devices. To this aim, PPO can be substituted with another hydrophobic block, resulting in wider domain of tunability of hydrogel final properties. Poly(ϵ -caprolactone) (PCL), poly (lactic-*co*-glycolic acid) (PLGA) and poly (hydroxybutyrate) (PHB) are the most used blocks to produce copolymers (figure 4).

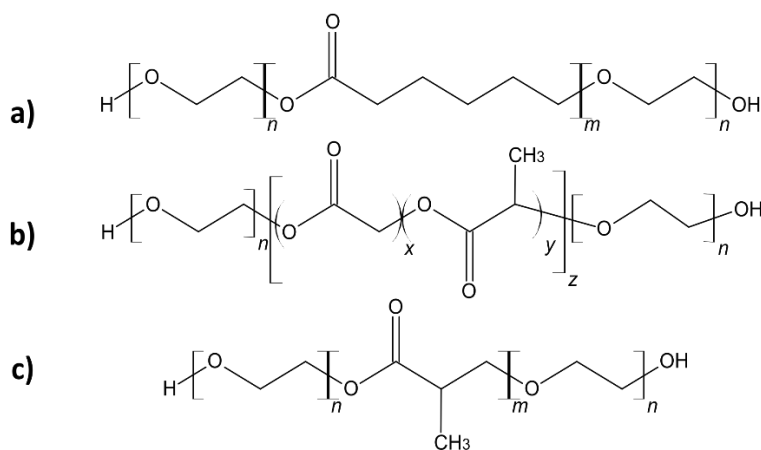


Figure 4 – Representations of other block copolymers based on a) PCL, b) PLGA, and c) PHB.

For example, PCL has a significantly higher hydrophobicity (up to ten-fold) than PPO blocks, which results in copolymers able to produce hydrogels at lower temperatures and concentrations.¹⁰ Other synthetic polymers showing a LCST can be synthesized (e.g., poly(N-isopropylacrylamide) (PNIPAAm)), as accurately reviewed by He *et al.*¹¹ However, a further advancement in the production of thermo-sensitive polymers has been performed through the development of multi-block amphiphilic copolymers through the exploitation of versatile synthesis procedures, such as the production of poly(urethane)s, as illustrated in the following paragraphs.

4. Development of self-assembling polyurethanes for hydrogel design

4.1 Polyurethanes: properties and potentiality in the biomedical field

The invention of poly(urethane)s (PUs) is dated between 1930 and 1940 and was carried out by Professor Otto Bayer, who developed a synthesis process based on the reaction that occurs between

an alcohol and an isocyanate.¹² The resulting chemical domain is also known as carbamate. In the following decades, this chemical reaction was widely exploited to develop various PUs that have found application in the industrial field for the production of coatings, solid materials or adhesives. The appearance of these polymers for medicine-related purposes is precisely dated in 1967, when a scientific paper described for the first time a PU-based elastomer that was classified as a “medical-grade” material.¹³

In chemical terms, PUs are synthesized through the addition polymerization that involves a polyisocyanate (typically, a diisocyanate) and a polyol (usually, a diol). The reaction is generally carried out in the presence of a catalyst and can be schematized as reported in figure 5. Most PUs are characterized by a thermoplastic nature, but even thermoset polymers can be produced using multifunctional isocyanates and branched polyols. In the biomedical field, linear polymers showing a thermoplastic behavior are generally preferable, since good workability and versatility (e.g., solubility or responsiveness to watery environments) are required for most applications.

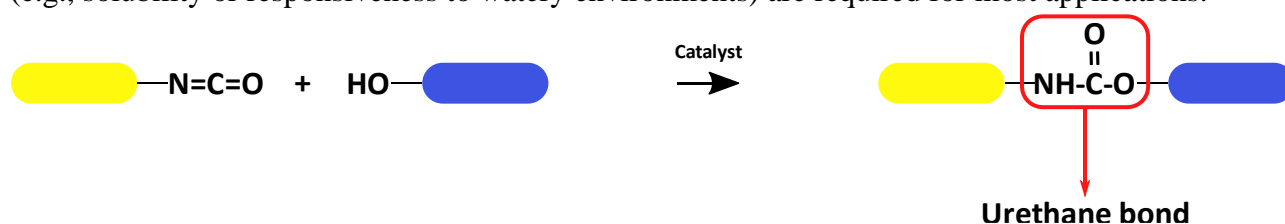


Figure 5 – Schematic representation of urethane bond formation.

The available diisocyanates can contain aliphatic (e.g., 1,6-hexamethylene diisocyanate or 1,4-diisocyanatobutane) or aromatic (e.g., 4,4'-diphenylmethane diisocyanate) domains. The reactivity of these molecules is derived by the positive partial charge induced on the carbon atom which is bound to more electronegative atoms (i.e., oxygen and nitrogen). Aromatic diisocyanates are more reactive due to a delocalization of the negative charge on the aromatic ring, but the resulting PUs are less resistant to oxidation and UV light irradiation and resulting degradation products can be highly toxic for human health (i.e., diamines showing carcinogenic effects). The nature of the diols can be various and principally includes polyesters and polyethers. Polyesters are characterized by an enhanced susceptibility to hydrolysis, while polyethers are sensitive to oxidation. PU synthesis reaction can be articulated in a subsequent step that can be exploited to induce a chain extension. To this aim, smaller diols are utilized and are known as *chain extenders* (e.g., 1,4-cyclohexanedimethanol). Even small diamines can be used for this step of reaction and in this case poly(urea-urethane)s are obtained. The presence of a catalyst is not compulsory, but it permits a better control on the reaction kinetics. Various catalysts are used in PU synthesis; for example, titanium tetrachloride, zinc naphthenate, butyl tin trichloride and dibutyltin dilaurate are some of them.

For this peculiar and versatile synthesis process, which involves different building blocks, PUs are characterized by a LEGO-like composition. The presence of a macrodiol, which can be a block-copolymer itself, is extremely determinant for the properties of the final polymers. Indeed, PUs are characterized by the presence of hard and soft domains. Soft segments derive from the macrodiol and are responsible of relevant elasticity and good mechanical properties at low temperatures. Differently, the presence of polarized domains into urethane groups determines the formation of hard regions constituted by the isocyanates and the chain extenders. These two phases are homogeneously distributed in most PUs and the molecular mass of the polymer plays a

fundamental role in this regard. A simplified representation of this arrangement is reported in figure 6. It has been demonstrated that the interaction between polarized domains (i.e., C=O and N-H groups) results in the formation of hydrogen bonds between the constituent blocks, thus conferring noteworthy mechanical properties to the overall polymer network.¹⁴ In fact, extremely high elasticity and toughness coupled with prolonged durability can be obtained through the synthesis of PUs. Thanks to this particular arrangement of polymer chains and the high predisposition to form widely diffused physical crosslinks, PUs also retain the great advantage to be suitable for various manufacturing processes.¹⁵

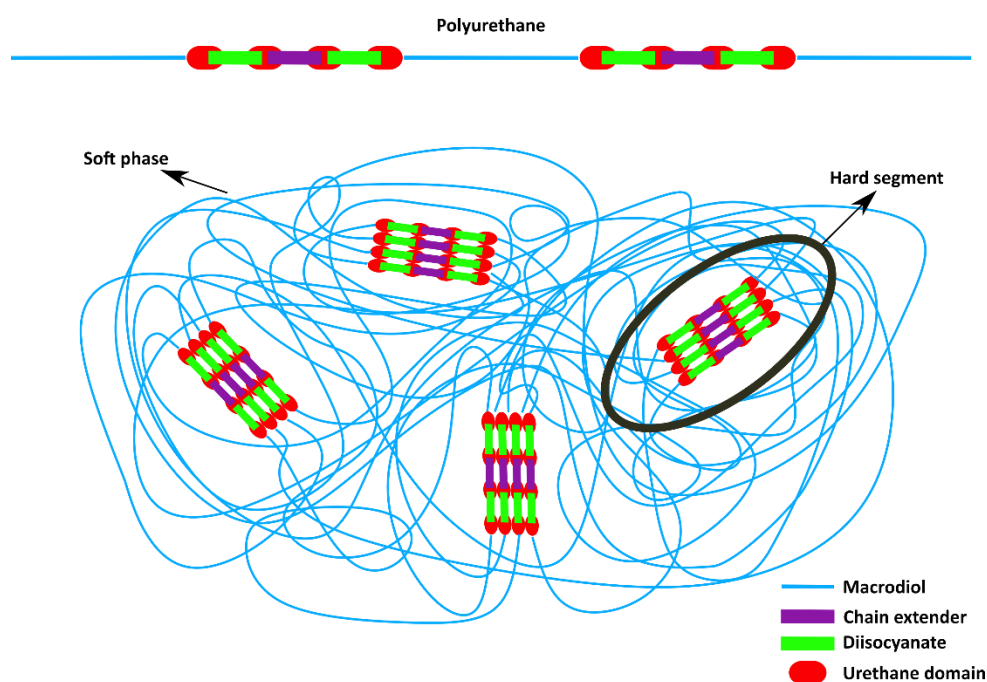


Figure 6 – Simplified representation of PU chains arrangement in hard and soft phases.

PUs are extremely important materials that have found different applications in biomedical engineering and medicine in general. The versatility of their synthesis process opens the way to the possibility to produce devices with different properties and morphologies, such as films, sponges, or even soluble matrices. Because of their highly interacting structures at the molecular level, the tunability of mechanical properties results to be excellent. In addition, the wide variety of available reagents (i.e., macrodiols, diisocyanates and chain extenders) allows to better control the interactions that occur with a specific biological environment, thus enhancing mechanical consistency and reducing the occurrence of unwanted phenomena (e.g., platelet adhesion). In this regard, the balance between hard and soft domains can be modulated to tune the chemical stability of the final PU-based systems. In fact, a PU characterized by a predominance of the soft phase, which is mainly amorphous or generally less stable than the hard one, can result in a biodegradable polymeric matrix. In this regard, segmented PUs generally show hydrolytic degradability, which can be properly tuned and engineered by means of composition and chemical properties of constituting blocks.¹⁶ Polyesters, such as PGA, PCL and PLA can be exploited to this aim and their different characteristics (e.g., hydrophobicity and molecular mass) represent other tuning parameters. One example of this approach is represented by the work carried out by Silvestri *et al.*¹⁷ The authors synthesized different PUs based on 1,4-diisocyanatobutane, and PCL and PEG as macrodiols, while a short peptide (Alanine-Alanine-Lysine, AAK) and L-lysine ethyl ester were

selected as chain extenders. The resulting PUs were characterized by different and controllable degradation rates. The further processing of these PUs by means of temperature-induced phase separation (TIPS) technique resulted in the production of porous scaffolds with mechanical properties suitable for applications for heart tissue regeneration. Finally, the chemical composition and the degradation products of the above-mentioned PUs resulted to be highly biocompatible. In another and more recent work, Boffito, Di Meglio, Mozetic and co-authors developed a highly engineered scaffold system based on a thermoplastic PU for the regeneration of myocardial tissue.¹⁸ More in detail and similarly to the previous work reported above, the PU developed in this work was synthesized using PCL diol (M_n 2000 Da), 1,4-butanediisocyanate and L-lysine ethyl ester. As a result, a PU characterized by a high molecular mass was obtained (i.e., M_n around 80000 Da). Scaffolds were produced through a 3D-printing process based on fused deposition modelling and subsequently functionalized with laminin-1 or gelatin, in order to confer an enhanced bioactive behavior and drive the differentiation of cardiac primitive cells. Moreover, *in vivo* experiments performed through subcutaneous implantation of scaffolds in mice showed a good integration of PU-based scaffolds with the surrounding tissues and the formation of new blood vessels.

Due to the remarkable mechanical properties that can be achieved using thermoplastic PUs, Ma and co-workers recently published a work in which a 3D-printed scaffold system based on a piperazine-functionalized poly(urethane urea) was developed.¹⁹ Through an optimized protocol of 3D-printing, scaffolds with interconnected pores were produced. In these systems, excellent mechanical properties (i.e., compressive modulus of c.a. 150 MPa) were coupled with enhanced osteoconductivity, which was intrinsic in the composition of the engineered polymer and was assessed through both *in vitro* and *in vivo* experiments.

Differently, in the case of biostable PUs, different PU-based commercial products can be found on the market, such as prosthesis for the cardiovascular systems (e.g., heart and blood valves). However, PUs are even widely used for the production of various other devices for clinical use (e.g., catheters, blood bags).

Finally, the synthesis process for PU production is extremely versatile and opens the way to the possibility to produce polymers that are soluble in water-based solutions. Indeed, as anticipated in the previous section, amphiphilic PUs can be produced as thermosensitive hydrogels having a LCST behavior. In the following paragraph, concrete examples of PUs forming hydrogels addressed to regenerative medicine applications will be shown with particular attention to their technical innovation and functionality in this field.

4.2 Thermo-sensitive poly(urethane)s as self-assembling molecules for drug delivery and tissue engineering

The production of thermo-sensitive amphiphilic PUs was driven by the intention to improve the properties of the resulting hydrogels in terms of stability in aqueous environment and concomitant reduction of synthetic polymer content. In fact, the idea behind the polymerization of amphiphilic polymers is finalized to the enhancement of the hydrophobic interactions occurring between polymers with high molecular weight. As a result, the formation of bigger micelles and their aggregates is facilitated, thus increasing thermal responsiveness and the stability of formed polymeric networks. Moreover, in the specific case of drug delivery, it has been demonstrated that

the production of chain extended amphiphilic polymers through PU synthesis significantly improves the overall capacity of drug payload encapsulation and release kinetics, as well as network stability for further applications for cell culture and release.^{20,21}

This approach has been applied since 2003 with the work performed by Cohn and co-authors.²² Interestingly, they followed two strategies to produce chain extended amphiphilic polymers: i) a bulk polymerization of Pluronic® F127/Poloxamer® 407 with 1,6-hexamethylene diisocyanate to produce a PU (or, more precisely, a poly(ether urethane) (PEU)), and ii) a covalent polymerization of PEO and PPO through the use of phosgene. The former polymer allowed the formulation of hydrogels with remarkably better mechanical properties through the formation of larger complexes with respect to native F127-based hydrogel networks. Additionally, PEU-based hydrogels at 30% w/v were utilized for the delivery of an anti-restenosis drug (RG-13577) up to 40 days, which represented a significant improvement with respect to the maximum period of 7 days obtained from native P407-based hydrogels. One interesting work was performed by Volkmer *et al.* demonstrating that the chain extension of a Pluronic® (P123, M_n 5800 Da, 30% wt PEO) resulted in better physical properties.²³ Pure P123-based hydrogels are characterized by thermo-induced gelation around the physiological temperature (i.e., 37 °C) at concentrations greater than 15% w/v. In their study, the authors developed a family of chain extended PEUs based on P123, 1,4-butane diisocyanate, 1,6-hexamethylene diisocyanate and hydrogenated diphenylmethane diisocyanate. A complete characterization of the resulting hydrogels led to the selection of those based on the PU composed of P123 and 1,4-butane diisocyanate. The selected hydrogels were suitable for cell-encapsulation and a further *in vivo* application into drill hole defects showed enhanced bone tissue regeneration. In another work carried out by Hsu and co-authors, different custom-made PUs were synthesized.²⁴ In short, PCL diol and PLA-PEG polymers were used to perform the PU synthesis at a mass ratio equal to 9:1. Moreover, different lengths of PLA domains were evaluated in order to tune the thermo-responsiveness of the resulting systems. Isophorone diisocyanate and ethylenediamine were used as co-reagents. PU solutions were able to undergo a sol-gel transition over a specific LCST, which resulted to be tunable through the modulation of PLA segments. Finally, due to their remarkable physical properties, PU-based thermo-sensitive and injectable hydrogels resulted to be suitable for the encapsulation and proliferation of mesenchymal stem cells (MSCs).

In other research activities, alternative and sophisticated synthesis procedures have been developed to further functionalize the resulting PUs. More specifically, Boffito and co-workers developed a two-step synthesis process for the production of a chain extended PEU.²⁵ In the first step of the polymerization, Pluronic® F127/Poloxamer® P407 was pre-polymerized with 1,6-hexamethylene diisocyanate. Then, a chain extender containing a Boc-protected primary amine (N-Boc serinol) was added to allow a further reaction of prepolymers. As a result, a PEU at high molecular weight (i.e., M_n 30000 Da) was obtained. A complete physico-chemical characterization of this polymer highlighted its ability to form stable micelle-based complexes and hydrogels at low concentrations. Indeed, the critical gelation concentration turned out to be around 6% w/v, which is significantly lower than the one that characterizes P407-based solutions (i.e., 18% w/v). Moreover, an accurate and thorough rheological study showed enhanced thermal responsiveness and noteworthy mechanical properties (e.g., storage moduli up to 40000 Pa) of the resulting physical hydrogels formulated at concentrations ranging between 10 and 20% w/v. In this work, the feasibility of PEU-based hydrogels for biomedical application was additionally proved by swelling and

dissolution tests coupled with absorption tests using a model molecule (fluorescein isothiocyanate dextran 4, FD4). The potential of such PEU has been further demonstrated in another recent work performed by Boffito and co-authors through the exploitation of primary amines derived from Boc cleavage on the chain extender.²⁶ In more detail, the PEU containing N-Boc serinol was subjected to acid treatment to expose free primary amines. The exposure of these functionalities along the polymer backbone opens the way to the possibility to exert a specific behavior (e.g., pH-responsiveness) or to perform functionalization procedures through the simple and mild carbodiimide chemistry. In this case, the presence of free amines was addressed to confer hydrogel network with responsiveness to acid environments, which often characterize various pathological milieus (e.g., tissues with acute inflammation or tumors). Hence, thermo- and pH-responsive hydrogels were formulated at 15% w/v containing drug carriers as mesoporous silica nanoparticles coated with a self-immolative polymer able to degrade in acid environments.²⁷ The resulting PEU-based hydrogels showed the ability to transmit the external pH through their network. To demonstrate the overall responsiveness of these multifunctional hydrogels encapsulating drug-loaded nanoparticles, *in vitro* release tests were performed at acid and physiological pH (i.e., pH equal to 5 and 7.4, respectively) using a Transwell® system to simulate the permeability of biological environments. As a result, a significantly higher release of payload (i.e., around two-fold) was observed when the systems were incubated in contact with the environment at low pH with respect to physiological conditions. In addition, *ex vivo* tests were performed in mice through the injection of the hybrid hydrogel system, observing a fast gelation and a good integration with the surrounding tissues. A simple scheme of the device developed in this work is reported in figure 7.

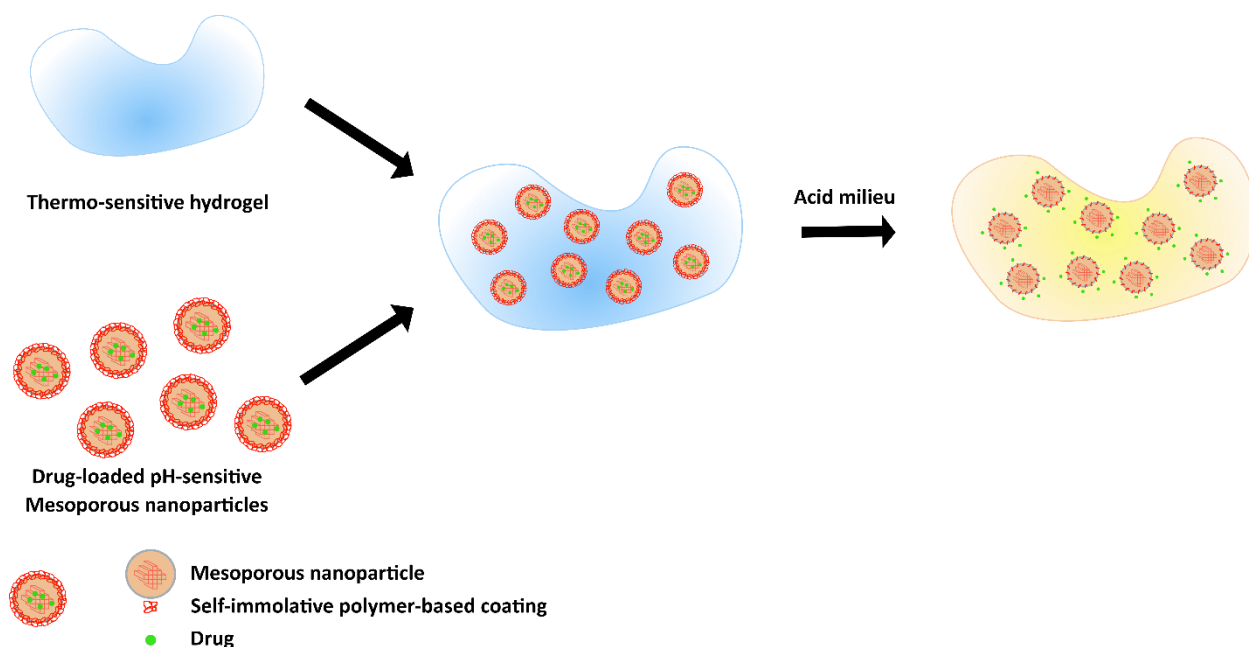


Figure 7– Schematic representation of the strategy exploited by Boffito and co-authors for the development and application of hybrid systems containing drug-loaded mesoporous silica nanoparticles.²⁶

The same protocol of PEU synthesis has been applied by the research group to produce similar polymers showing different properties. Another thermo-sensitive PEU has been synthesized using the same macrodiol and diisocyanate, but a different chain extender, which was characterized by a rigid aliphatic ring (i.e., 1,4-cyclohexanedimethanol).^{28,29} Hydrogels with high stability in

aqueous environment have been applied to encapsulate ion-doped and ibuprofen-bearing mesoporous silica nanoparticles with different compositions, demonstrating the overall feasibility of these hybrid hydrogel systems for antibacterial ion and anti-inflammatory drug co-release from inorganic particulate matrices.

Another example that shows the relevant versatility of the resulting P407-based PEUs in terms of functionalization has been reported in the work performed by Laurano *et al.*³⁰ Briefly, the synthesis process was optimized in order to enhance chain extension, using a diol containing Boc-protected secondary amines (N-Boc diethanolamine). After Boc group cleavage reaction, the obtained PEU showed a relevant number of -NH units, which were then exploited to graft thiol groups through carbodiimide chemistry using thioglycolic acid as functionalizing molecule. The high yield of thioglycolic acid grafting was proved through nuclear magnetic resonance spectroscopy, while thermo-responsiveness was evaluated by dynamic light scattering (DLS) and 1,6-diphenyl-1,3,5-hexatriene (DPH) assay for the evaluation of micellization temperature.

Hence, the possibility to produce highly functionalized, water-soluble, and thermo-sensitive PEUs for advanced application in regenerative medicine was proved in all the above-mentioned works, highlighting the noteworthy versatility of the involved synthesis process. A recently published review article written by Kausar represents an important reference concerning functional PUs.³¹ In summary, the author summarizes the typologies of functional PUs dividing them into many categories, such as photoactive, electroactive, pH-responsive, water-sensitive and thermo-sensitive PUs. Although the focus of this review article is not completely addressed to the biomedical field, important considerations are reported from the industrial perspective. Indeed, the author highlights that further advancements are needed for the emerging new molecules and synthesis processes (e.g., scale-up proofs) to meet industrial preferences. Specifically, concerning the biomedical field, in the book *“Polyurethane polymers: composites and nanocomposites”* edited by Thomas *et al.*, a similar discussion can be found in the chapter written by Hu and Tan.³² In this chapter, the authors report on the role of PUs even in combination with other molecules or materials, highlighting their multifaceted potentialities. The promising approaches based on the application of smart PUs are remarkably versatile and effective, but further characterizations are needed to better understand and optimally exploit all the functionalities that derive from the development of such macromolecules when addressed to specific applications in medicine. In this regard, the role of PUs and their functionalities in combinations with other components and factors will be considered and discussed in the field of supramolecular hydrogels based on inclusion complexes.

5. Supramolecular hydrogels based on inclusion complexes

5.1 Cyclodextrins: a fundamental family of macro-cycles

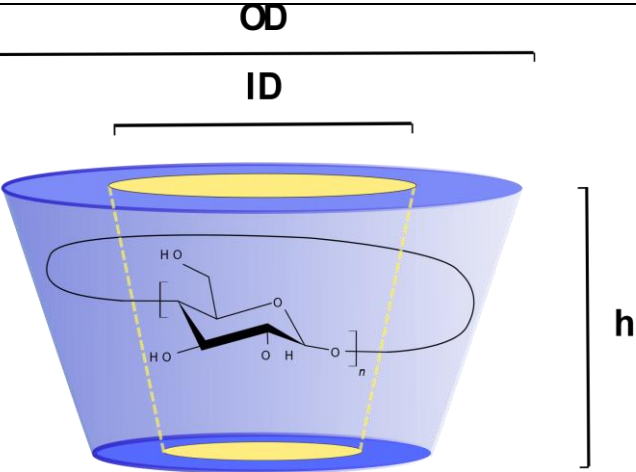
Between 1891 and 1892, Villiers discovered a crystalline matter isolated from the bacterial fermentation of starch.³³ He named the obtained substance “cellobiosine” and observed that it was highly stable and resistant to hydrolysis. Further investigations performed by Schardinger described the co-presence of two similar components into this crystalline matter that were coded as “ α -dextrin” and “ β -dextrin”. Nonetheless, the structures of the discovered compounds were still unknown until the 1950s, when more systematic investigations were performed by Freudenberg

and Cramer, who described their structures and basic properties.^{34,35} In 1953 the first patent related to these molecules was registered in Germany, describing three typologies of such molecules, which were coded as cyclodextrins (CDs) and differed in terms of dimensions.³⁶ This document even reported different chemical properties of these compounds which allow them to enhance the aqueous solubility of other molecules. Nonetheless, only few amounts of pure products were available at that time. The industrial revolution in the biotechnology field represented a great advancement that led to the production of pharmaceutical-grade CDs at large-scale and low price. The first product containing pure CDs for pharmacological purposes has been marketed in 1976 in Japan, while nowadays there are more than 40 products which contain CDs in their formulations.³⁵

In more chemical terms, CDs are cyclic oligosaccharides composed of $\alpha(1\rightarrow4)$ -linked D-glucopyranose monomers and are classified by the number of constituting units. α -, β - and γ -CDs refer to CDs with 6, 7 and 8 glucose monomers, respectively. Although other different typologies of CDs exist, α -, β - and γ -CDs are the most relevant and are widely utilized in the biomedical field. Due to the chemical properties and conformation (i.e., chair structure) of the constituent glucose units, CDs are characterized by a truncated-cone shape and an inner cavity. This configuration strongly influences the physico-chemical behavior of CDs. In fact, the inner cavity of these molecules shows a hydrophobic nature, while the outer wall is hydrophilic. Due to this particular property, CDs can interact with other hydrophobic molecules through encapsulation phenomena, thus forming host-guest complexes. In this manner, the included guest molecules, which are generally characterized by low wettability, can be solubilized and transported in watery environments.^{34,37} It is important to highlight that the interactions occurring between CDs and guest molecules are not specific. Indeed, the only requirements for the formation of inclusion complexes (ICs) are dimensional matching and hydrophobicity. Table 1 reports the basic structure and main parameters of CDs.

Additionally, CDs can be easily derivatized exploiting the reactivity of their hydroxyl groups at position C-6 (primary) and C-2 and C-3 (secondary). CD modification allows to further improve the advantages of the native molecules: i) solubility, ii) host recognition, and iii) biocompatibility. Because of the presence of various functionalities (3-fold the number of constituent glucoses), derivatizations are often statistical, but even regioselective modifications can be performed. Nonetheless, in the second case, the reproducibility of reaction conditions is not trivial and the overall yield can be low due to the further and necessary purification steps, which additionally increase the overall cost of production. However, native cyclodextrins are widely used for their versatility and cost-effective production. The intermolecular recognition that leads to the formation of ICs is mainly driven by physical bond formation, such as hydrophobic, dispersive and Van der Waals interactions. The solvent plays an important role, since the formation of host-guest complexes is permitted only in polar solvents and is driven by solvophobic interactions. Moreover, the interference of other small quantities of organic solvents can affect the stability of ICs. In fact, as these interactions are controlled by space filling, the more the non-polar domain of the guest fits with the internal cavity of CDs, the stronger the ICs will result. Thence, this process can be hindered by the interference of hydrophobic domains of organic solvents.

Table 1 – Schematic representation and main characteristics of native CDs.³⁵



CD type	α -Cyclodextrin	β -Cyclodextrin	γ -Cyclodextrin
n	6	7	8
Molar mass	972.84 Da	1134.98 Da	1297.12 Da
Height (h)	0.78 nm	0.78 nm	0.78 nm
Inner Diameter (ID)	0.50 nm	0.62 nm	0.80 nm
Outer Diameter (OD)	1.46 nm	1.54 nm	1.75 nm

More in detail, four different types of ICs can be found and classified. Type I ICs are based on a CD and a lipophilic guest molecule, mainly resulting in hydrophobic and insoluble complexes in water, since the hydroxyl groups of the CD are employed in the formation of the IC. Type II ICs are based on a cyclodextrin and an amphiphilic guest, thus forming potentially soluble ICs when the hydrophobic domain is relatively dominant. In this case, the solubility is guaranteed by the masking of the lipophilic region of the guest molecule. Type III interactions are based on the self-assembly of a CD with a *bola-amphiphile*, which presents two distinct hydrophilic regions that make these host-guest complexes highly soluble in water-based solutions. The last typology of ICs is classified as type IV and it is characterized by the presence of CD derivatives and a lipophilic guest.

It is possible to quantify the occurring molecular recognition with particular guest molecules through the determination of the binding constant K and the free energy ΔG^0 (Eq. 1 and 2).

$$K = \frac{[CD \cdot G]}{[CD][G]} \quad \text{Eq. 1}$$

$$\Delta G^0 = -RT \log K \quad \text{Eq. 2}$$

The accurate implementation of these equations is not immediate and is possible only for type II and type IV ICs, since the determination of K and ΔG^0 requires measurable concentrations of complexes in solution. Moreover, the molecular recognition that occurs in the formation of ICs is

also originated from the differentiation of the kinetics of association and dissociation (i.e., *kinetic recognition*). This kind of recognition mainly occurs in processes involving *bola-amphiphiles* due to the presence of big end-groups that hinder the association and the disassembly of host-guest complexes. Hence, the process of formation of ICs depends on an *activation energy*, which increases by increasing the size of end-groups. The activation free energy (ΔG^\ddagger) can be calculated through the Eyring equation, which depends on the rate constant k and also contains the constants of Boltzmann (k_B) and Plank (h), as reported in Eq. 3.

$$\Delta G^\ddagger = -RT \ln\left(\frac{kh}{k_B T}\right) \quad \text{Eq. 3}$$

The description of the process in terms of energy is represented in figure 8 for the case of amphiphiles, as an example.

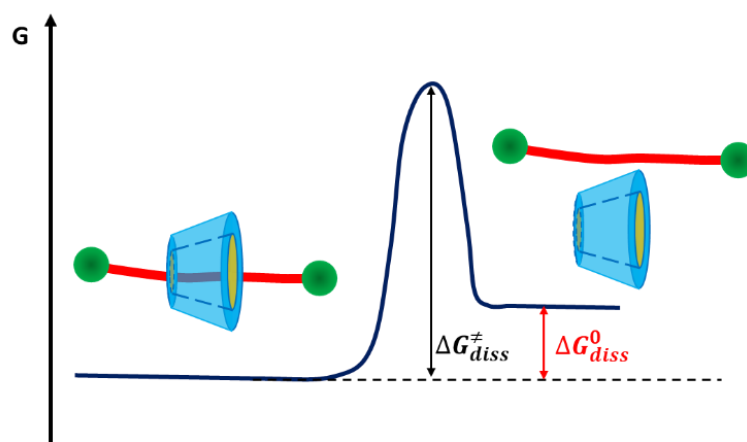
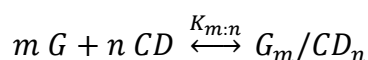


Figure 8 – Schematic representation of the energy diagram of the dissociation of host-guest complexes. Green circles: hydrophilic end groups of amphiphile, Red line: hydrophobic backbone of amphiphile. ΔG^\ddagger_{diss} is the activation free energy of disassembly, while $\Delta G^0_{diss} = -\Delta G^0$ is the free energy of dissociation.

Relying on non-covalent bonds, CD-based host-guest complexes are characterized by a strong dependency on the specific physical characteristics of the involved molecules. In addition to the binding constant, it is possible to determine a *stability constant*, which depends on different factors. Important variables are the number (m) of guest molecules (coded as G, usually a drug) and the number (n) of involved CDs into the complexes (G_m/CD_n). The condition of equilibrium is described by the following relationship:



In which $K_{m:n}$ characterizes the *stability constant* of a specific inclusion complex. n and m factors that represent the stoichiometry of complexes, and the stability constant can be calculated through phase-solubility diagrams. In these diagrams, the solubility of the guest molecule is represented as a function of overall CD content into the environment for complexation. Hence, different shapes of diagrams can be obtained from the occurring interactions between the involved molecules, as represented in figure 9. If the diagram appears as a linear function (A_L -type), first-order complexes are formed referring to involved CDs (n equal to 1), meanwhile first or greater order complexes are formed with respect to the guest ($m \geq 1$). It is then possible to obtain the function that defines the apparent solubility (S_{tot}) of the involved guest (Eq. 4):

$$S_{tot} = S_0 + m \left[\frac{G_m}{CD} \right] \quad (\text{Eq. 4})$$

where S_0 represents the intrinsic solubility of the guest molecule in the specific aqueous medium in which the complexation is occurring.

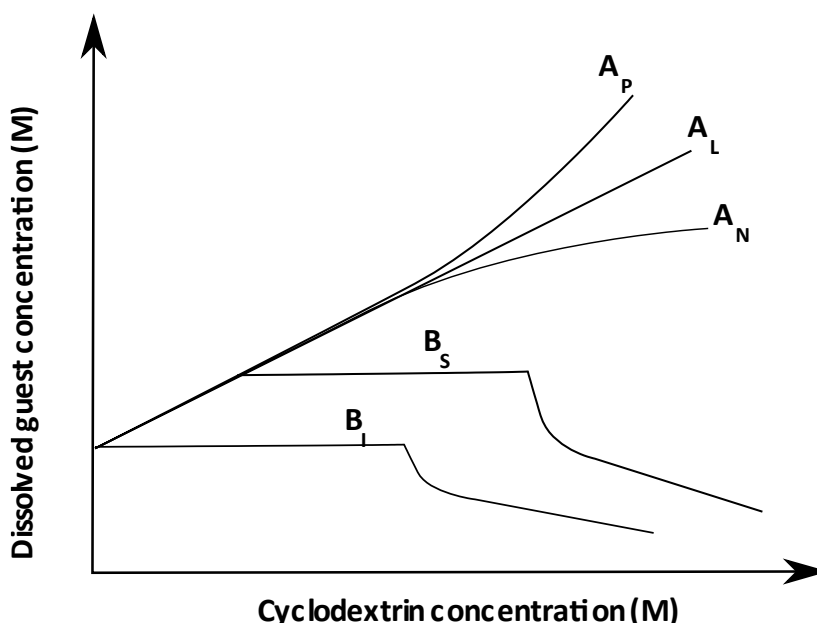


Figure 9 – Representation of solubilization diagrams of solution based on CDs.

Even formation of complexes based on a higher order stoichiometry is explained with a linear function, but the resulting slope is less than 2. More intricate cases compared to linear trend can be even found. Indeed, it is also possible to observe a positive deviation (A_P -type diagram) from the linear behavior when complexes at higher orders, are formed between already existing inclusion complexes having different molecular ratios (e.g., guest/CD molar ratio of 1:1, 1:2 or 1:3). Hence, it is evident that these diagrams do not properly represent and explain the kind of interactions occurring between host and guest components, but instead they describe the general influence of CDs on guest solubility. In fact, the solubility diagrams are based on guest saturated solutions, in which it is more probable to obtain higher order complexes rather than in diluted environments. Moreover, CDs retain the strong tendency to form aggregates in solution which significantly contribute in terms of guest solubilization through non-inclusion complexes. This remark explains the characteristic trend of A_N -type diagrams, in which the self-assembly between CDs plays a relevant role at high CD concentrations.

Differently, B-type diagrams are related to complexes characterized by low solubility. Native CDs (i.e., α -, β - and γ -CDs) are mainly involved in these phenomena that result in solubility diagrams with a plateau trend into a relatively wide range of CD concentrations. CD aggregates hinder the formation of smaller and more soluble complexes. In this case, at high CD concentrations the solubility diagrams are characterized by a progressive decline in guest solubility.

It is important to remind that solubility diagrams are obtained in non-ideal solutions (i.e., guest saturated aqueous environments). Only highly diluted solutions can properly adhere to more sophisticated mathematical models. In most applicative cases, instead, non-ideal environments are common. In fact, host-guest formulations are extremely sensitive to excipients or co-solutes (e.g.,

salts, polymers) and the ideal mathematical models are not correct. This is the case of drug formulations, which often require other additional elements that induce remarkable variations into the system. Nonetheless, the statement of mathematical and theoretical models can be generally useful to determine the most important variables that are involved in IC formation. In this regard, *in silico* models also represent a powerful tool.

Additionally, CDs are functional molecules even in chemical terms. Indeed, various derivatives can be synthesized and the most utilized in pharmacology are methylated, hydroxypropylated, alkylated and acylated CDs.^{38,39} Such chemical modifications can be exploited to properly tune CD physico-chemical properties and result in enhanced delivery of specific drug molecules in biological environments.

Focusing on the release of drugs from CD-based complexes, the most important factor is the simple dilution in the release medium. However, other more convoluted mechanisms can occur when the encapsulated drug or the complex interact with specific components of the biological environments. For example, some phenomena consist in drug-protein interaction/binding or direct drug release from the inclusion complex to the biological environment through competitive interactions (e.g., through the formation of hydrophobic interactions with an available domain in the extra-cellular matrix). In fact, the formation of ICs can occur with natural molecules such as cholesterol, vitamins or lipids that compose the membrane of cells. In particular, α -CDs can form ICs with the phospholipids of cell membrane, while β -CDs are mainly targeted to cholesterol. It has been demonstrated that native CDs, which are generally hydrophilic, show the ability to increase drug permeability through biological membranes and this behavior is enhanced when they are additionally combined with water-based carriers (e.g., hydrogels).^{40,41} In this regard, some hemolytic effects have been observed for β -CDs and their derivatives, while α -CDs and γ -CDs have shown neglectable toxicity at similar dosages. Additionally, native CDs in individuals having a physiological kidney function are generally excreted within 12 hours when administrated parenterally, thus preventing the organism from any accumulation phenomenon. For all the above-mentioned properties, CDs are generally considered harmless.

5.2 Cyclodextrins as building blocks of hydrogels through poly(pseudo)rotaxane formation and crystallization

As the interactions of CDs with their substrates are not specific, it is even possible to observe the formation of host-guest inclusion complexes between CDs and linear polymers. The diameter of α -, β - and γ -CDs represents the main variable for their interaction with the hydrophobic domains of linear polymers. Hence, the formation of ICs only depends on the physical match between the two involved components. The first work reporting a study on the complexation between CDs and a polymer dates back to 1990, when Li, Harada and Kamachi studied the formation of ICs between α -CDs and PEG/PEO.^{42,43} In detail, they analyzed the interaction between these two components by varying concentrations and molecular properties. Indeed, a wide range of PEG molar masses was investigated in order to evaluate the resulting role in complex formation. Interestingly, the authors found that two consecutive processes of self-assembly are involved in these water-based mixtures. The first involves the formation of structures called poly(pseudo)rotaxanes (PPRs), which derive from the threading of α -CDs along PEG chains. The term *pseudo* refers to the presence of free end groups, which allow the reverse process of de-threading of α -CDs.⁴⁴ A

schematic example of a PPR formed by α -CDs and a PEG chain in solution is reported in figure 10.

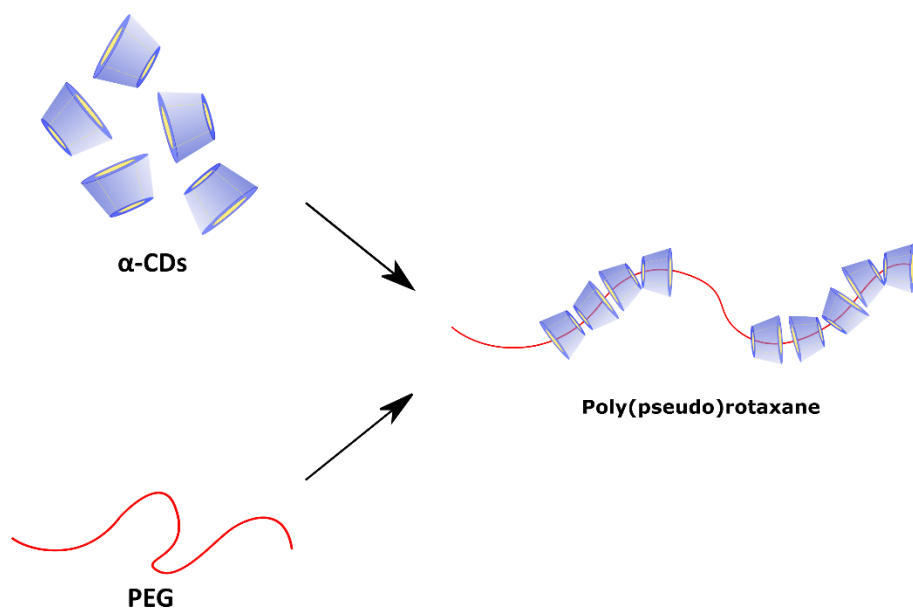


Figure 10 – Simple representation of a poly(pseudo)rotaxane formed by α -CDs and a PEG chain in water-based solutions.

The second process consists in the further coalescence of PPRs through the formation of hydrogen bonds between aligned α -CDs threaded along different PEG chains. The result of this phenomenon is the physical consumption of hydroxyl groups of α -CDs leading to the increase of their general hydrophobic character. Thence, the formation of turbidity and the precipitation of a white crystalline supramolecular matter occur.⁴⁵ Figure 11 reports the schematic conformation of the crystalline compound based on PPRs.

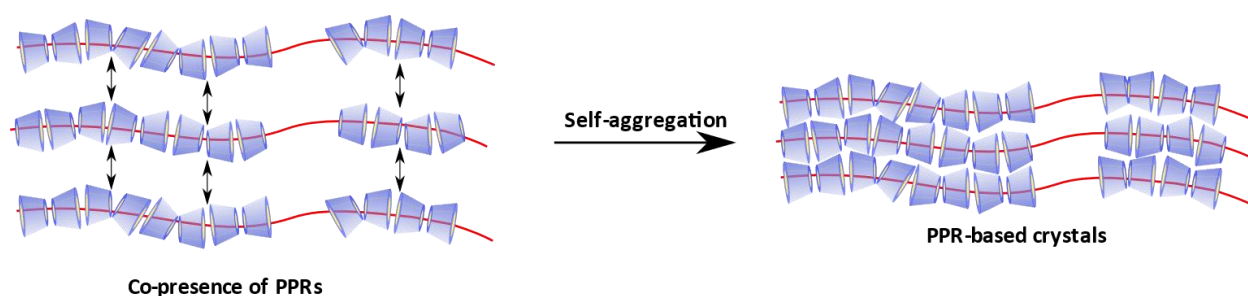


Figure 11 – Schematic representation of PPR crystallization in watery environments. Black arrows indicate the formation of hydrogen bonds between the outer walls of CDs.

X-Ray powder diffraction (XRD) studies showed a different crystallographic pattern from the resulting supramolecular matter with respect to the one obtained from pure α -CDs and PEG. Indeed, the XRD patterns related of these supramolecular structures were similar to those obtained from smaller linear molecules (e.g., valeric acid or octanol) which aggregate into “channel-type” supramolecular constructs composed of PPRs. Differently, native α -CDs, as well as β - and γ -CDs, are characterized by a different crystalline structure that is classified as “cage-type”. PPR based on β - and γ -CDs can be even produced with polymers having bigger and suitable dimensions (i.e., cross-sectional area).⁴⁶ Indeed, β - and γ -CDs can form complexes with poly(propylene glycol) chains and in particular γ -CDs can host two PEG chains,⁴⁷ thus forming a unique typology of

PPRs. However, in these cases, a slower self-assembly kinetics is observed due to lower affinity and stability.

Solutions that contain CDs and linear polymers forming PPRs can undergo sol-gel transitions under certain conditions.⁴⁸ In this regard, PEG is the most important polymer for the formation of hydrogels through the self-assembly with α -CDs. Indeed, thanks to the relatively high affinity of these two components, hydrogels based on a supramolecular structure can be obtained when a proper balance between PPR crystallization and free polymeric domains in solution is achieved (i.e., domains uncovered by α -CDs, since free hydrophilic regions are necessary to retain water inside hydrogel networks). Hence, it is necessary that the molar mass of the involved polymer is high enough to avoid crystal precipitation. Moreover, higher molar masses allow the formation of entanglements at different levels, thus acting as stabilizing elements for hydrogel network formation. The channel-like nano-crystals composed of PPRs represent the physical crosslinks that constitutes the hydrogel structure, as schematically represented in figure 12.

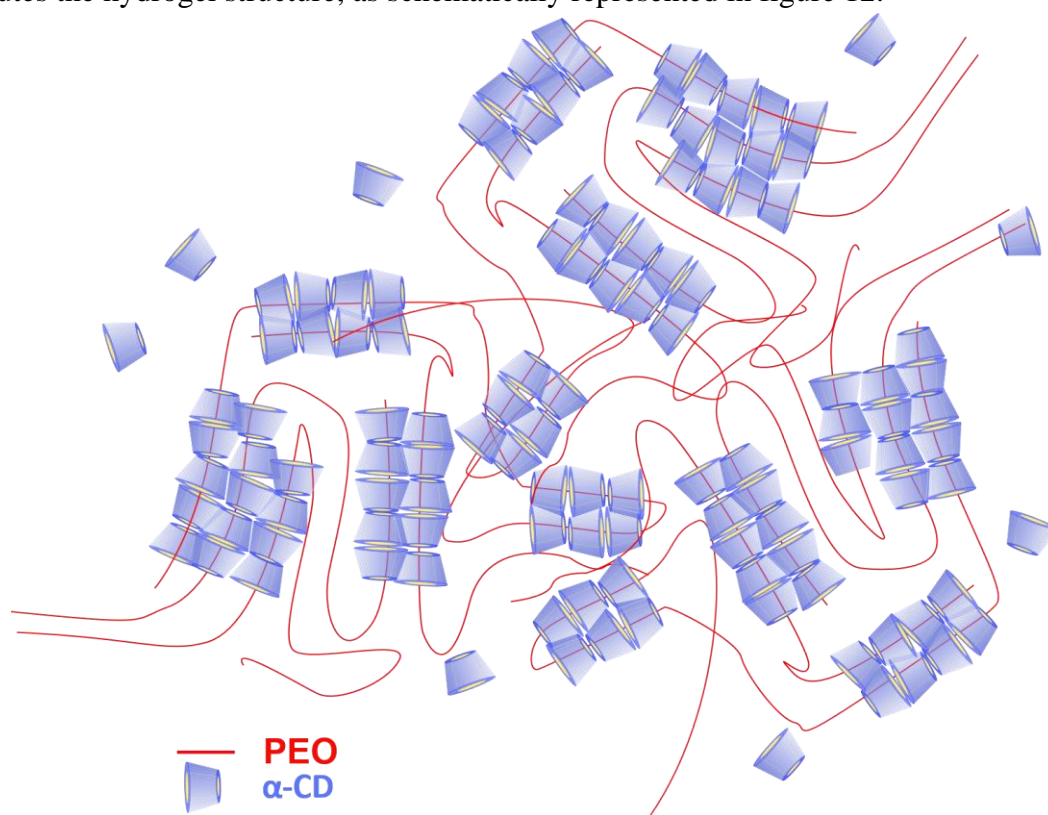


Figure 12 – Representation of a hydrogel network based on PEG chains and α -CD through the formation of PPR crystals and polymeric entanglements.

During the process of hydrogel formation, a continuous increase of viscosity and stiffness is observed. The higher the molar mass of PEO chains, the slower the process of hydrogel development. At the end of the transient of self-assembly, stable mechanical properties are achieved (i.e., storage and loss moduli reach asymptotic values). In this regard, mechanical (i.e., rheological) properties of hydrogels are important parameters to assess their suitability for specific applications in medicine. Interestingly, the ratio between α -CD and PEG represents the main variable for the modulation of physical properties. Indeed, high α -CDs/polymer mass ratios and generally high contents of α -CDs cause an enhanced formation of crystallized PPRs, which induce a relevant increment in hydrogel stiffness (i.e., elastic modulus, G') and affect the final

responsiveness of the network that is an important factor for drug delivery applications. Interestingly, the mechanical behavior of these hydrogels upon incremental shear stresses shows a thixotropic response, which is characterized by the concurrent decrease of viscosity and the ability to flow as a fluid. In addition to thixotropy, high reversibility characterizes these hydrogels. Indeed, when the application of shear stresses stops, the initial stiffness of hydrogel network can be partially or totally recovered, thus resulting in a self-healing behavior. These remarkable physical properties make PPR-based supramolecular hydrogels easily injectable through conventional syringes and needles. One of the earliest applications of α -CD- and PEG-based supramolecular hydrogels as potential platforms for drug delivery was reported by Li *et al.*⁴⁹ The authors explored the use of PEG characterized by different molecular masses to design supramolecular hydrogels for drug delivery applications. As a result, they observed that the optimal molar masses to produce self-eroding hydrogels for a progressive release of drug model molecules (i.e., fluorescein isothiocyanate-labeled dextran of different molar masses) ranged between 20 and 30 kDa, probably due to a proper balance of overall supramolecular crystallinity, polymeric entanglements and hydrophilic free domains. Another interesting example of the application of supramolecular hydrogels based on PEG homopolymer and α -CDs in drug delivery has been reported by Higashi and co-authors.⁵⁰ Briefly, they designed different hydrogels systems based on PEG and α -CDs and γ -CDs with the aim to perform sustained release of lysozyme *in vitro*. The resulting hydrogel networks were characterized by high responsiveness in watery environments, allowing an effective release of enzymatically active lysozyme. Another important work was carried out by Bilkova and co-workers, who developed star-PEG-based PPRs for the formation of pH-sensitive physical hydrogels.⁵¹ The exploitation of the acid catalysis of functional end-groups allowed the tunability of hydrogel responsiveness to external environment and thence the potential release of therapeutic molecules. The presence of PPR domains significantly delayed the hydrolysis of sensitive groups, thus making the overall systems suitable for peroral transport of prednisolone with tunable release kinetics through the digestive duct. Other interesting examples involving multi-armed PEG polymers can be found in the literature, since these polymeric systems result in supramolecular hydrogels with good mechanical properties.⁴⁵ Nonetheless, to the best of our knowledge, no recent studies concerning these specific systems in drug delivery have been conducted. Indeed, the use of simple PEG/PEO homopolymers in PPR formation is referred to as a relatively obsolete approach nowadays. On the other hand, the use of PEG to synthesize versatile and functional block copolymers represents an effective strategy to design PPR-based hydrogels with α -CDs, which are generally preferable with respect to the bigger β - and γ -CDs when PEG-based PPRs are formed in watery environments. In the following paragraphs, the evolution of novel polymers for the development of supramolecular hydrogels based on PPRs will be surveyed with the aim to highlight the most significant works and frontiers towards clinical applications.

5.3 Supramolecular hydrogels based on copolymers containing hydrophobic blocks and their applications in drug delivery: the state of the art

PPO-based copolymers (Pluronic®/Ploxamers®)

The introduction of hydrophobic domains into polymer backbone represents a valuable strategy to improve the properties of CD-based supramolecular hydrogel networks. The first application of

amphiphilic polymers to form such systems was carried out by Li *et al.* in 2001.⁵² In this study, a wide variety of Pluronic®/Poloxamer® copolymers has been investigated when mixed in solutions containing α -CDs. Interestingly, Pluronic® copolymers containing at least 25% wt PEO turned out to be able to form supramolecular hydrogels even at relatively low polymeric concentrations (i.e., at 13% wt). These observations highlighted that the amount of synthetic polymer required to observe gelation was significantly reduced in supramolecular formulations containing α -CDs at 9.7% wt with respect to the simple polymer-based systems. Indeed, solutions based on Pluronic® required polymeric concentrations up to 40% wt to show a sol-gel transition upon thermal stimulus (generally, greater than 20% wt). A significant contribution in the understating of the role of hydrophobic domains in α -CDs- and Pluronic-based supramolecular networks was given by the work of Pradal and co-workers in 2012.⁵³ Indeed, the authors supposed that hydrophobic interactions could induce a stabilizing effect on the self-assembly process that involves the threading of α -CDs along PEO domains. In order to validate this hypothesis, Pradal and colleagues carried out a complete set of rheological characterizations, in addition to small-angle X-ray scattering and dynamic light scattering to better investigate the mechanism of self-assembly. Pluronic® (i.e., Pluronic F127 (70% PEO, M_n 12600 Da) and F68 (80% PEO, M_n 8400 Da), also known as Poloxamer 407 and 188) concentrations of 10 and 20% w/v were mixed with α -CDs in order to cover the theoretical PEO content between 0 and 12%, which corresponded to α -CD concentrations up to 10% w/v. The authors observed that slight variations (i.e., 1% w/v) in α -CD content induced a significant modulation in the elastic shear modulus of the resulting hydrogel networks, which ranged between 3 kPa and 7 MPa. The authors also hypothesized that the gelation mechanism depends on the mass ratio between α -CDs and Pluronic®. In fact, they supposed that the gelation process was influenced by the threading of α -CDs along PEO domains of Pluronic® molecules (i.e., the formation of PPR-based domains) and the interpenetration between polymeric structures (i.e., both hydrophobic and hydrophilic regions). Hence, the authors observed that the predominance of PPRs or micellar structures was induced at specific concentrations of α -CDs and amphiphilic polymer, respectively. As a consequence, PPR precipitation phenomena occurred in systems characterized by a high α -CD content, while at high polymer concentration (e.g., F127 at 20% w/v, which represents a thermo-gelling condition) and low α -CD content the formation of inclusion complexes interferes with the formation of a micellar gel network. Nonetheless, the authors argued that an optimal interaction between the two components can be achieved at specific α -CD/Pluronic® mass ratios and figure 13 reports a simple scheme representing the resulting supramolecular configuration.

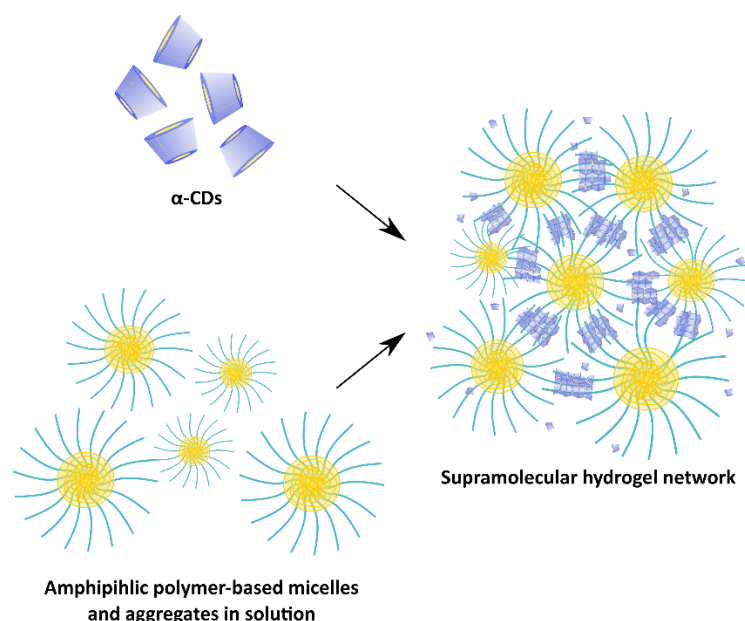


Figure 13 – Simplified representation of the supramolecular structure originated from the balanced interaction between thermo-sensitive amphiphilic polymers and α -CDs in watery environments.

In this case, the formation of polymeric micelles through hydrophobic interactions could contribute to hydrogel network stabilization for PPR arrangement within defined temperature ranges. In this regard, the authors observed that the role of temperature is fundamental. Indeed, too low temperatures impede the development of hydrophobic interactions, while even too high temperatures cause the formation of a strong and rigid micelle-based network and an excessive molecular agitation hindering the supramolecular interaction between α -CDs and PEO domains. F68-based solutions showed faster gelation kinetics with respect to F127-based ones when mixed to α -CDs, due to the higher PEO content and the formation of smaller polymeric aggregates with reduced steric hindrance. Hence, this work highlighted that a crucial role in the self-assembly process is played by a proper balance between several factors: i) the molar mass and the concentration of the involved polymer, ii) the content of PEO and its distribution, iii) α -CD/polymer ratio, and iv) the temperature of incubation. Interesting applications of Pluronic®/Poloxamer®-based systems for drug delivery can be found in more recent works. Simões and co-workers applied Pluronic® F127/Poloxamer® 407 for the production of engineered self-healing hydrogels for the progressive release of vancomycin.⁵⁴ The overall polymeric content of the most promising systems turned out to be greater than 13% w/v. Another interesting work was carried out by Di Donato and colleagues.⁵⁵ Briefly, they developed a hydrogel system based on the combination of Pluronic® F127/Poloxamer® 407 with α -CD and β -CD for the topical release of acyclovir as antiviral drug. The dual contribution of α -CDs and β -CDs resulted in the possibility to tune gelation properties and final hydrogel responsiveness. Lorenzo-Veiga and co-authors recently published a work describing a hydrogel system based on Soluplus (i.e., polyvinyl caprolactam-polyvinyl acetate-polyethylene glycol graft copolymer (PCL-PVAcPEG)), Pluronic® P103 and α -CD, and addressed to the release of natamycin in ocular delivery.⁵⁶ In this case, the role of both amphiphilic polymers was exploited to produce PPRs of mixed micelles for the encapsulation of natamycin, which was effectively released with increased solubility from the resulting PPR-based systems.

Additionally, even PEO-PPO non-linear copolymers can be exploited to produce supramolecular PPR-based hydrogels. Indeed, Poloxamines, which are star-shaped copolymers and are commercially known as Tetronics®, can be used to produce hydrogel systems suitable for drug delivery. Larraneta and Isasi described a Tetronic®-based system for the controlled delivery of bovine serum albumin via a hydrogel-network erosion mechanism.⁵⁷ In this case, a noteworthy increase in terms of complexity of the resulting systems can be deduced, which was coupled with a not significant improvement in terms of sustained release kinetics. Indeed, release profiles were limited within 6 hours. Differently, in the work conducted by Del Rosario and co-authors, the use of Poloxamine and α -CD resulted in highly functional and stable hydrogels, which were suitable to treat critical bone defects *in vivo* through the sustained release of simvastatin in combination with bone morphogenic protein 2 up to 15-20 days.⁵⁸ These works implicitly indicated once again the remarkable importance of the parameters involved in supramolecular formulation in properly tuning and optimizing the final behavior of such devices.

PHB-based copolymers

An important improvement in widening the possibilities of development of supramolecular networks based on amphiphilic copolymers was reported in the work carried out by Li and colleagues in 2006.⁵⁹ Their idea consisted in the synthesis of specific amphiphilic molecules as newly designed components of supramolecular hydrogels. The authors developed novel amphiphilic triblock copolymers based on PEO (M_n 5000 Da) and poly[(R)-3-hydroxybutyrate] (PHB) (PEO-PHB-PEO) at various molecular masses (M_n of 1750 and 3140 Da). Thermo-responsiveness of PEO-PHB-PEO polymers was compared to Pluronic® polyethers, evidencing significantly lower critical micellization concentrations (i.e., 1000-fold lower for PEO-PHB-PEO polymers with respect to Pluronic® as control samples) at similar temperatures (i.e., ranging between 22 and 25 °C). Hydrogel systems based on the two PEO-PHB-PEO polymers and α -CDs exhibited high stability and allowed a sustained release of a drug model molecule (i.e., Fluorescein isothiocyanate dextran 20, dextran-FTIC, 20 kDa). Nonetheless, in these formulations polymer concentration was maintained at relatively high values (i.e., 13.3% wt), which conferred high stability to the resulting hydrogel systems. The same research group also investigated the production of hydrogels based on reverse triblock copolymers with a PHB-PEO-PHB block configuration.⁶⁰ Such block distribution provided improved stabilization through hydrophobic interactions, which resulted in stiffer networks. Indeed, solutions based on relatively low polymer concentrations (i.e., around 5% wt) and molar masses (i.e., between 5 and 7 kDa) resulted in hydrogels having notable elastic shear modulus ranging between 10^4 and 10^5 Pa.

The balance between hydrophobic and hydrophilic components plays a pivotal role in determining the self-assembly of networks containing α -CDs and their suitability for drug encapsulation and release. Indeed, particularly marked hydrophobic behavior, while favoring the formation of highly stable and rigid hydrogels, could hinder or at least mitigate the release of hydrophobic drugs encapsulated into their cores. Thence, the development of properly balanced amphiphilic polymers that could meet the complex requirements to ensure hydrogel formation and stability through hydrophobic interactions and PPR formation, while simultaneously guaranteeing high drug encapsulation and sustained release, represents a noticeable challenge.

PCL-based copolymers

PCL represents another hydrophobic domain used as building block of amphiphilic copolymers. In an important study, Xu and Li developed a promising hydrogel system based on a PEO-PCL polymeric solution at 13.3% wt concentration in the presence of α -CDs at 8 and 9.7% wt concentrations.⁶¹ Preliminary dextran-FTIC (20 kDa) release studies evidenced good stability, as a confirmation of the measured rheological properties.⁶¹ The use of such polymers was also reported by Zhu and co-workers.⁶² In this example, an interesting system based on the copresence of PEG-PCL and PEG-poly(acrylic acid) (PAA) was developed to ensure a stepwise delivery of doxorubicin and cisplatin. Moreover, additives such as Pluronic® copolymers were exploited to properly tune gelation kinetics and release profiles. The release of the encapsulated drugs was hypothesized to be ascribed to the progressive delivery of micelles as drug-encapsulating vehicles. A cytotoxic effect of the released payload was observed on human bladder carcinoma cells, showing an enhanced cytotoxicity for the systems based on dual-drug encapsulation.

Triblock copolymers based on PCL have also been produced with both PEO-PCL-PEO and PCL-PEO-PCL configuration. The former has successfully been employed for the release of erythropoietin from supramolecular networks to treat myocardial infarction.^{63,64} The latter has been used to produce supramolecular gel systems in different contexts for the encapsulation and delivery of various drugs, such as vitamin B12 and naltrexone.⁶⁵ Additionally, PCL has been exploited to produce more complex linear polymers to optimize the interaction with α -CDs and DNA plasmids, thus producing an interesting dual supramolecular system for gene delivery.⁶⁶ In detail, Li and co-workers developed a cationic polymer based on PEG, PCL and poly[2-(dimethylamino)ethyl methacrylate] (PDMAEMA), which positive charge made it suitable for the formation of polyplexes with DNA plasmid. As a result, the polymer assumed a conformation based on a nanomatrix characterized by an inner core containing DNA plasmids and an outer corona formed by PEG domains. These units were then able to produce PPR-based supramolecular structures with α -CDs resulting in injectable hydrogels. The resulting DNA-loaded system showed progressive and effective release profiles, preserving the bioactivity of the payload.

PLA-based copolymers

Another effective hydrophobic block suitable for the production of copolymers with PEO is PLA. In a recent work, Poudel *et al.* described the design of a PEG-PLA copolymer able to form highly stable micelles in water-based environments.⁶⁷ The presence of PEG domains was exploited to interact with α -CDs and form PPRs in the external corona of micelles in solution. The remarkable aspect of this work relies on the design of micelle-based supramolecular hydrogels. Indeed, the polymeric content within hydrogels was set at 1% w/v, while the contribution of α -CDs was investigated at different concentrations ranging from 7 to 11% w/v. As expected, the higher α -CD concentration, the stiffer the resulting network (i.e., higher values of G'). Nonetheless, good mechanical properties were observed even at the lowest α -CD concentration (i.e., 7% w/v). Indeed, for the above-mentioned formulation, G' turned out to be around 3 kPa and a thixotropic response was observed through rheological characterizations when incremental shear stresses were applied. Finally, release studies of doxorubicin were performed, showing a progressive drug release up to

one week of incubation at 37 °C in contact with a physiological-like aqueous environment. The released drug showed an effective therapeutic action by exerting cytotoxicity against tumor HeLa cells *in vitro*.

6. General discussion and conclusions

The development of injectable hydrogels based on PPRs formed starting from properly designed amphiphilic polymers could actually contribute to the development of minimally invasive therapies directly addressed to disease sites. As recently analyzed in the review paper written by Domìnski and colleagues,⁶⁸ the importance of PPR-based hydrogels has been progressively increasing in the biomedical field. However, some limitations concerning this kind of systems can be identified. Indeed, their physical nature induces different complications in terms of handling and stability. Although these platforms can be considered as highly responsive systems, fast dissolution kinetics or limited mechanical properties could be observed in many formulations.^{50,66,69} One solution to this issue can be found in the design of hydrogels containing relatively high polymer concentrations (i.e., equal, or greater than 10% w/v).⁵⁴ However, in case of systems based on high polymer concentrations, the interactions with biological environments are neither trivial nor immediate.⁷⁰ Indeed, the biological effects of non-ionic amphiphilic polymers could be various. For example, Pluronic® F127/Poloxamer® 407 could cause an increment of lipid content in blood, as well as swelling and vacuolization of Kupffer and endothelial cells in the liver. Other polymers, such as Pluronic® L81, P85 and F68 could inhibit the secretion of lipoproteins in the intestine. These biological effects are intrinsic in the amphiphilic nature of these polymeric molecules and could be reduced by designing optimized devices with a lower polymeric content and/or enhanced stability. To this aim, nowadays a relevant effort is being made in the development of highly functional, reversible, stable and responsive systems containing thermo-sensitive amphiphilic polymers at low concentration. Highly branched natural or functional polymers have been developed for this purpose and a novel frontier of material development has been opened.⁶⁸ In this scenario, Pluronic®/Poloxamer®-based poly(urethane)s represent one of the newest strategies to meet the above-mentioned requirements.^{25,28-30} Indeed, better thermo-responsiveness, stability in aqueous environments and mechanical properties have been observed in pure PU-based thermo-sensitive hydrogels with respect to native Poloxamer®-based systems. These promising results were correlated with the attainment of a correct balance between molecular mass values and distribution (i.e., in other terms, the degree of polymerization and dispersity index, respectively). Additionally, even the resulting hydrophobic character and the presence of urethane domains have been considered as key factors in the resulting improvement of physical properties. Thence, the following Chapter of this work will investigate the application of properly synthesized Pluronic®/Poloxamer®-based PEUs as forming material of supramolecular hydrogels composed of PPRs. The main objective of the work will be the design of supramolecular hydrogels with low PEU concentration, and satisfactory handling properties, stability and responsiveness to external environments. The role of synthesis process will be discussed, and the most promising formulations will be selected for specific and advanced drug delivery studies.

7. References

- (1) Lim, J. Y. C.; Lin, Q.; Xue, K.; Loh, X. J. Recent Advances in Supramolecular Hydrogels for Biomedical Applications. *Mater. Today Adv.* **2019**, *3*, 100021. <https://doi.org/10.1016/j.mtadv.2019.100021>.
- (2) Jin, J.; Cai, L.; Jia, Y.-G.; Liu, S.; Chen, Y.; Ren, L. Progress in Self-Healing Hydrogels Assembled by Host–Guest Interactions: Preparation and Biomedical Applications. *J. Mater. Chem. B* **2019**, *7* (10), 1637–1651. <https://doi.org/10.1039/C8TB02547A>.
- (3) Ding, X.; Wang, Y. Weak Bond-Based Injectable and Stimuli Responsive Hydrogels for Biomedical Applications. *J. Mater. Chem. B* **2017**, *5* (5), 887–906. <https://doi.org/10.1039/C6TB03052A>.
- (4) Ward, M. A.; Georgiou, T. K. Thermoresponsive Polymers for Biomedical Applications. *Polymers* **2011**, *3* (3), 1215–1242. <https://doi.org/10.3390/polym3031215>.
- (5) Alexandridis, P.; Holzwarth, J. F.; Hatton, T. A. Micellization of Poly(Ethylene Oxide)-Poly(Propylene Oxide)-Poly(Ethylene Oxide) Triblock Copolymers in Aqueous Solutions: Thermodynamics of Copolymer Association. *Macromolecules* **1994**, *27* (9), 2414–2425. <https://doi.org/10.1021/ma00087a009>.
- (6) Vadnere, M.; Amidon, G.; Lindenbaum, S.; Haslam, J. Thermodynamic Studies on the Gel-Sol Transition of Some Pluronic Polyols. *Int. J. Pharm.* **1984**, *22* (2–3), 207–218. [https://doi.org/10.1016/0378-5173\(84\)90022-X](https://doi.org/10.1016/0378-5173(84)90022-X).
- (7) Eldridge, J. E.; Ferry, J. D. Studies of the Cross-Linking Process in Gelatin Gels. III. Dependence of Melting Point on Concentration and Molecular Weight. *J. Phys. Chem.* **1954**, *58* (11), 992–995. <https://doi.org/10.1021/j150521a013>.
- (8) Attwood, D.; Collett, J.; Tait, C. The Micellar Properties of the Poly(Oxyethylene) - Poly(Oxypropylene) Copolymer Pluronic F127 in Water and Electrolyte Solution. *Int. J. Pharm.* **1985**, *26* (1–2), 25–33. [https://doi.org/10.1016/0378-5173\(85\)90197-8](https://doi.org/10.1016/0378-5173(85)90197-8).
- (9) Liow, S. S.; Dou, Q.; Kai, D.; Karim, A. A.; Zhang, K.; Xu, F.; Loh, X. J. Thermogels: In Situ Gelling Biomaterial. *ACS Biomater. Sci. Eng.* **2016**, *2* (3), 295–316. <https://doi.org/10.1021/acsbiomaterials.5b00515>.
- (10) Hwang, M. J.; Suh, J. M.; Bae, Y. H.; Kim, S. W.; Jeong, B. Caprolactonic Poloxamer Analog: PEG-PCL-PEG. *Biomacromolecules* **2005**, *6* (2), 885–890. <https://doi.org/10.1021/bm049347a>.
- (11) He, C.; Kim, S. W.; Lee, D. S. In Situ Gelling Stimuli-Sensitive Block Copolymer Hydrogels for Drug Delivery. *J. Controlled Release* **2008**, *127* (3), 189–207. <https://doi.org/10.1016/j.jconrel.2008.01.005>.
- (12) Joseph, J.; Patel, R. M.; Wenham, A.; Smith, J. R. Biomedical Applications of Polyurethane Materials and Coatings. *Trans. IMF* **2018**, *96* (3), 121–129. <https://doi.org/10.1080/00202967.2018.1450209>.
- (13) Boretos, J. W.; Pierce, W. S. Segmented Polyurethane: A New Elastomer for Biomedical Applications. *Science* **1967**, *158* (3807), 1481–1482. <https://doi.org/10.1126/science.158.3807.1481>.
- (14) Szycher's Handbook of Polyurethanes By Michael Szycher (CardioTech International, Inc.). CRC Press: Boca Raton, FL. 1999. ISBN 0-8493-0602-7. *J. Am. Chem. Soc.* **2000**, *122* (16), 3983–3983. <https://doi.org/10.1021/ja004704k>.

- (15) Krol, P. Synthesis Methods, Chemical Structures and Phase Structures of Linear Polyurethanes. Properties and Applications of Linear Polyurethanes in Polyurethane Elastomers, Copolymers and Ionomers. *Prog. Mater. Sci.* **2007**, *52* (6), 915–1015. <https://doi.org/10.1016/j.pmatsci.2006.11.001>.
- (16) Mondal, S.; Martin, D. Hydrolytic Degradation of Segmented Polyurethane Copolymers for Biomedical Applications. *Polym. Degrad. Stab.* **2012**, *97* (8), 1553–1561. <https://doi.org/10.1016/j.polymdegradstab.2012.04.008>.
- (17) Silvestri, A.; Sartori, S.; Boffito, M.; Mattu, C.; Di Rienzo, A. M.; Boccafoschi, F.; Ciardelli, G. Biomimetic Myocardial Patches Fabricated with Poly(ϵ -Caprolactone) and Polyethylene Glycol-Based Polyurethanes: Biomimetic Polyurethane Scaffolds for Myocardial Repair. *J. Biomed. Mater. Res. B Appl. Biomater.* **2014**, *102* (5), 1002–1013. <https://doi.org/10.1002/jbm.b.33081>.
- (18) Boffito, M.; Di Meglio, F.; Mozetic, P.; Giannitelli, S. M.; Carmagnola, I.; Castaldo, C.; Nurzynska, D.; Sacco, A. M.; Miraglia, R.; Montagnani, S.; Vitale, N.; Brancaccio, M.; Tarone, G.; Basoli, F.; Rainer, A.; Trombetta, M.; Ciardelli, G.; Chiono, V. Surface Functionalization of Polyurethane Scaffolds Mimicking the Myocardial Microenvironment to Support Cardiac Primitive Cells. *PLOS ONE* **2018**, *13* (7), e0199896. <https://doi.org/10.1371/journal.pone.0199896>.
- (19) Ma, Y.; Hu, N.; Liu, J.; Zhai, X.; Wu, M.; Hu, C.; Li, L.; Lai, Y.; Pan, H.; Lu, W. W.; Zhang, X.; Luo, Y.; Ruan, C. Three-Dimensional Printing of Biodegradable Piperazine-Based Polyurethane-Urea Scaffolds with Enhanced Osteogenesis for Bone Regeneration. *ACS Appl. Mater. Interfaces* **2019**, *11* (9), 9415–9424. <https://doi.org/10.1021/acsami.8b20323>.
- (20) Ding, M.; Li, J.; Tan, H.; Fu, Q. Self-Assembly of Biodegradable Polyurethanes for Controlled Delivery Applications. *Soft Matter* **2012**, *8* (20), 5414. <https://doi.org/10.1039/c2sm07402h>.
- (21) Polo Fonseca, L.; Bergamo Trinca, R.; Isabel Felisberti, M. Thermo-Responsive Polyurethane Hydrogels Based on Poly(Ethylene Glycol) and Poly(Caprolactone): Physico-Chemical and Mechanical Properties: ARTICLE. *J. Appl. Polym. Sci.* **2016**, *133* (25). <https://doi.org/10.1002/app.43573>.
- (22) Cohn, D.; Sosnik, A.; Levy, A. Improved Reverse Thermo-Responsive Polymeric Systems. *Biomaterials* **2003**, *24* (21), 3707–3714. [https://doi.org/10.1016/S0142-9612\(03\)00245-X](https://doi.org/10.1016/S0142-9612(03)00245-X).
- (23) Volkmer, E.; Leicht, U.; Moritz, M.; Schwarz, C.; Wiese, H.; Milz, S.; Matthias, P.; Schloegl, W.; Friess, W.; Goettlinger, M.; Augat, P.; Schieker, M. Poloxamer-Based Hydrogels Hardening at Body Core Temperature as Carriers for Cell Based Therapies: In Vitro and in Vivo Analysis. *J. Mater. Sci. Mater. Med.* **2013**, *24* (9), 2223–2234. <https://doi.org/10.1007/s10856-013-4966-6>.
- (24) Hsu, S.; Chen, C.-W.; Hung, K.-C.; Tsai, Y.-C.; Li, S. Thermo-Responsive Polyurethane Hydrogels Based on Poly(ϵ -Caprolactone) Diol and Amphiphilic Polylactide-Poly(Ethylene Glycol) Block Copolymers. *Polymers* **2016**, *8* (7), 252. <https://doi.org/10.3390/polym8070252>.
- (25) Boffito, M.; Gioffredi, E.; Chiono, V.; Calzone, S.; Ranzato, E.; Martinotti, S.; Ciardelli, G. Novel Polyurethane-Based Thermosensitive Hydrogels as Drug Release and Tissue Engineering Platforms: Design and *in Vitro* Characterization: Polyurethane-Based Thermosensitive Hydrogels. *Polym. Int.* **2016**, *65* (7), 756–769. <https://doi.org/10.1002/pi.5080>.
- (26) Boffito, M.; Torchio, A.; Tonda-Turo, C.; Laurano, R.; Gisbert-Garzarán, M.; Berkmann, J. C.; Cassino, C.; Manzano, M.; Duda, G. N.; Vallet-Regí, M.; Schmidt-Bleek, K.; Ciardelli, G. Hybrid Injectable Sol-Gel Systems Based on Thermo-Sensitive Polyurethane Hydrogels Carrying PH-Sensitive Mesoporous Silica Nanoparticles for the Controlled and Triggered Release of Therapeutic Agents. *Front. Bioeng. Biotechnol.* **2020**, *8*, 384. <https://doi.org/10.3389/fbioe.2020.00384>.
- (27) Gisbert-Garzarán, M.; Lozano, D.; Vallet-Regí, M.; Manzano, M. Self-Immolative Polymers as Novel PH-Responsive Gate Keepers for Drug Delivery. *RSC Adv.* **2017**, *7* (1), 132–136. <https://doi.org/10.1039/C6RA26771H>.

- (28) Pontremoli, C.; Boffito, M.; Fiorilli, S.; Laurano, R.; Torchio, A.; Bari, A.; Tonda-Turo, C.; Ciardelli, G.; Vitale-Brovarone, C. Hybrid Injectable Platforms for the in Situ Delivery of Therapeutic Ions from Mesoporous Glasses. *Chem. Eng. J.* **2018**, *340*, 103–113. <https://doi.org/10.1016/j.cej.2018.01.073>.
- (29) Boffito, M.; Pontremoli, C.; Fiorilli, S.; Laurano, R.; Ciardelli, G.; Vitale-Brovarone, C. Injectable Thermosensitive Formulation Based on Polyurethane Hydrogel/Mesoporous Glasses for Sustained Co-Delivery of Functional Ions and Drugs. *Pharmaceutics* **2019**, *11* (10), 501. <https://doi.org/10.3390/pharmaceutics11100501>.
- (30) Laurano, R.; Cassino, C.; Ciardelli, G.; Chiono, V.; Boffito, M. Polyurethane-Based Thiomers: A New Multifunctional Copolymer Platform for Biomedical Applications. *React. Funct. Polym.* **2020**, *146*, 104413. <https://doi.org/10.1016/j.reactfunctpolym.2019.104413>.
- (31) Kausar, A. Review on Technological Significance of Photoactive, Electroactive, PH-Sensitive, Water-Active, and Thermoresponsive Polyurethane Materials. *Polym.-Plast. Technol. Eng.* **2017**, *56* (6), 606–616. <https://doi.org/10.1080/03602559.2016.1233279>.
- (32) Hu, J.; Tan, L. Polyurethane Composites and Nanocomposites for Biomedical Applications. In *Polyurethane Polymers*; Elsevier, 2017; pp 477–498. <https://doi.org/10.1016/B978-0-12-804065-2.00016-4>.
- (33) Villiers, A. Sur La Fermentation de La Fécule Par l'action Du Ferment Butyrique. *Compt. Rend. Acad. Sci.* 1891.
- (34) Wenz, G. Recognition of Monomers and Polymers by Cyclodextrins. In *Inclusion Polymers*; Wenz, G., Ed.; Advances in Polymer Science; Springer Berlin Heidelberg: Berlin, Heidelberg, 2009; Vol. 222, pp 204–254. https://doi.org/10.1007/12_2008_13.
- (35) Loftsson, T.; Brewster, M. E. Pharmaceutical Applications of Cyclodextrins: Basic Science and Product Development: Pharmaceutical Applications of Cyclodextrins. *J. Pharm. Pharmacol.* **2010**, *62* (11), 1607–1621. <https://doi.org/10.1111/j.2042-7158.2010.01030.x>.
- (36) Freudenberg, K.; Cramer, F.; Plieninger, H. A Process for the Preparation of Inclusion Compounds of Physiologically Active Organic Compounds. DE895769C.
- (37) Hedges, A. R. Industrial Applications of Cyclodextrins. *Chem. Rev.* **1998**, *98* (5), 2035–2044. <https://doi.org/10.1021/cr970014w>.
- (38) Jansook, P.; Ogawa, N.; Loftsson, T. Cyclodextrins: Structure, Physicochemical Properties and Pharmaceutical Applications. *Int. J. Pharm.* **2018**, *535* (1–2), 272–284. <https://doi.org/10.1016/j.ijpharm.2017.11.018>.
- (39) Arima, H.; Hayashi, Y.; Higashi, T.; Motoyama, K. Recent Advances in Cyclodextrin Delivery Techniques. *Expert Opin. Drug Deliv.* **2015**, *12* (9), 1425–1441. <https://doi.org/10.1517/17425247.2015.1026893>.
- (40) Haimhoffer, Á.; Ruzsnyák, Á.; Réti-Nagy, K.; Vasvári, G.; Váradi, J.; Vecsernyés, M.; Bácskay, I.; Fehér, P.; Ujhelyi, Z.; Fenyvesi, F. Cyclodextrins in Drug Delivery Systems and Their Effects on Biological Barriers. *Sci. Pharm.* **2019**, *87* (4), 33. <https://doi.org/10.3390/scipharm87040033>.
- (41) Ryzhakov, A.; Do Thi, T.; Stappaerts, J.; Bertoletti, L.; Kimpe, K.; Sá Couto, A. R.; Saokham, P.; Van den Mooter, G.; Augustijns, P.; Somsen, G. W.; Kurkov, S.; Inghelbrecht, S.; Arien, A.; Jimidar, M. I.; Schrijnemakers, K.; Loftsson, T. Self-Assembly of Cyclodextrins and Their Complexes in Aqueous Solutions. *J. Pharm. Sci.* **2016**, *105* (9), 2556–2569. <https://doi.org/10.1016/j.xphs.2016.01.019>.
- (42) Harada, A.; Kamachi, M. Complex Formation between Poly(Ethylene Glycol) and α -Cyclodextrin. *Macromolecules* **1990**, *23* (10), 2821–2823. <https://doi.org/10.1021/ma00212a039>.

- (43) Harada, A.; Li, J.; Kamachi, M. Preparation and Properties of Inclusion Complexes of Polyethylene Glycol with α -Cyclodextrin. *Macromolecules* **1993**, *26* (21), 5698–5703. <https://doi.org/10.1021/ma00073a026>.
- (44) Higashi, T.; Motoyama, K.; Arima, H. Cyclodextrin-Based Polyrotaxanes and Polypseudorotaxanes as Drug Delivery Carriers. *J. Drug Deliv. Sci. Technol.* **2013**, *23* (6), 523–529. [https://doi.org/10.1016/S1773-2247\(13\)50080-3](https://doi.org/10.1016/S1773-2247(13)50080-3).
- (45) Liu, G.; Yuan, Q.; Hollett, G.; Zhao, W.; Kang, Y.; Wu, J. Cyclodextrin-Based Host–Guest Supramolecular Hydrogel and Its Application in Biomedical Fields. *Polym. Chem.* **2018**, *9* (25), 3436–3449. <https://doi.org/10.1039/C8PY00730F>.
- (46) Harada, A.; Okada, M.; Li, J.; Kamachi, M. Preparation and Characterization of Inclusion Complexes of Poly(Propylene Glycol) with Cyclodextrins. *Macromolecules* **1995**, *28* (24), 8406–8411. <https://doi.org/10.1021/ma00128a060>.
- (47) Higashi, T.; Hirayama, F.; Misumi, S.; Arima, H.; Uekama, K. Design and Evaluation of Polypseudorotaxanes of Pegylated Insulin with Cyclodextrins as Sustained Release System. *Biomaterials* **2008**, *29* (28), 3866–3871. <https://doi.org/10.1016/j.biomaterials.2008.06.019>.
- (48) Li, J.; Harada, A.; Kamachi, M. Sol–Gel Transition during Inclusion Complex Formation between α -Cyclodextrin and High Molecular Weight Poly(Ethylene Glycol)s in Aqueous Solution. *Polym. J.* **1994**, *26* (9), 1019–1026. <https://doi.org/10.1295/polymj.26.1019>.
- (49) Li, J.; Ni, X.; Leong, K. W. Injectable Drug-Delivery Systems Based on Supramolecular Hydrogels Formed by Poly(Ethylene Oxide)s and α -Cyclodextrin. *J. Biomed. Mater. Res.* **2003**, *65A* (2), 196–202. <https://doi.org/10.1002/jbm.a.10444>.
- (50) Higashi, T.; Tajima, A.; Motoyama, K.; Arima, H. Cyclodextrin/Poly(Ethylene Glycol) Polypseudorotaxane Hydrogels as a Promising Sustained-Release System for Lysozyme. *J. Pharm. Sci.* **2012**, *101* (8), 2891–2899. <https://doi.org/10.1002/jps.23232>.
- (51) Bílková, E.; Sedlák, M.; Dvořák, B.; Ventura, K.; Knotek, P.; Beneš, L. Prednisolone- α -Cyclodextrin-Star PEG Polypseudorotaxanes with Controlled Drug Delivery Properties. *Org. Biomol. Chem.* **2010**, *8* (23), 5423. <https://doi.org/10.1039/c0ob00039f>.
- (52) Li, J.; Li, X.; Zhou, Z.; Ni, X.; Leong, K. W. Formation of Supramolecular Hydrogels Induced by Inclusion Complexation between Pluronics and α -Cyclodextrin. *Macromolecules* **2001**, *34* (21), 7236–7237. <https://doi.org/10.1021/ma010742s>.
- (53) Pradal, C.; Jack, K. S.; Grøndahl, L.; Cooper-White., J. J. Gelation Kinetics and Viscoelastic Properties of Pluronic and α -Cyclodextrin-Based Pseudopolyrotaxane Hydrogels. *Biomacromolecules* **2013**, *14* (10), 3780–3792. <https://doi.org/10.1021/bm401168h>.
- (54) Simões, S. M. N.; Veiga, F.; Torres-Labandeira, J. J.; Ribeiro, A. C. F.; Sandez-Macho, M. I.; Concheiro, A.; Alvarez-Lorenzo, C. Syringeable Pluronic- α -Cyclodextrin Supramolecular Gels for Sustained Delivery of Vancomycin. *Eur. J. Pharm. Biopharm.* **2012**, *80* (1), 103–112. <https://doi.org/10.1016/j.ejpb.2011.09.017>.
- (55) Di Donato, C.; Iacovino, R.; Isernia, C.; Malgieri, G.; Varela-Garcia, A.; Concheiro, A.; Alvarez-Lorenzo, C. Polypseudorotaxanes of Pluronic® F127 with Combinations of α - and β -Cyclodextrins for Topical Formulation of Acyclovir. *Nanomaterials* **2020**, *10* (4), 613. <https://doi.org/10.3390/nano10040613>.
- (56) Lorenzo-Veiga, B.; Sigurdsson, H. H.; Loftsson, T.; Alvarez-Lorenzo, C. Cyclodextrin–Amphiphilic Copolymer Supramolecular Assemblies for the Ocular Delivery of Natamycin. *Nanomaterials* **2019**, *9* (5), 745. <https://doi.org/10.3390/nano9050745>.

- (57) Larrañeta, E.; Isasi, J. R. Non-Covalent Hydrogels of Cyclodextrins and Poloxamines for the Controlled Release of Proteins. *Carbohydr. Polym.* **2014**, *102*, 674–681. <https://doi.org/10.1016/j.carbpol.2013.11.002>.
- (58) del Rosario, C.; Rodríguez-Évora, M.; Reyes, R.; Simões, S.; Concheiro, A.; Évora, C.; Alvarez-Lorenzo, C.; Delgado, A. Bone Critical Defect Repair with Poloxamine–Cyclodextrin Supramolecular Gels. *Int. J. Pharm.* **2015**, *495* (1), 463–473. <https://doi.org/10.1016/j.ijpharm.2015.09.003>.
- (59) Li, J.; Li, X.; Ni, X.; Wang, X.; Li, H.; Leong, K. W. Self-Assembled Supramolecular Hydrogels Formed by Biodegradable PEO–PHB–PEO Triblock Copolymers and α -Cyclodextrin for Controlled Drug Delivery. *Biomaterials* **2006**, *27* (22), 4132–4140. <https://doi.org/10.1016/j.biomaterials.2006.03.025>.
- (60) Liu, K. L.; Goh, S. H.; Li, J. Controlled Synthesis and Characterizations of Amphiphilic Poly[(R,S)-3-Hydroxybutyrate]-Poly(Ethylene Glycol)-Poly[(R,S)-3-Hydroxybutyrate] Triblock Copolymers. *Polymer* **2008**, *49* (3), 732–741. <https://doi.org/10.1016/j.polymer.2007.12.017>.
- (61) Li, X.; Li, J. Supramolecular Hydrogels Based on Inclusion Complexation between Poly(Ethylene Oxide)-*b*-Poly(ϵ -Caprolactone) Diblock Copolymer and α -Cyclodextrin and Their Controlled Release Property. *J. Biomed. Mater. Res. A* **2008**, *86A* (4), 1055–1061. <https://doi.org/10.1002/jbm.a.31710>.
- (62) Zhu, W.; Li, Y.; Liu, L.; Chen, Y.; Xi, F. Supramolecular Hydrogels as a Universal Scaffold for Stepwise Delivering Dox and Dox/Cisplatin Loaded Block Copolymer Micelles. *Int. J. Pharm.* **2012**, *437* (1–2), 11–19. <https://doi.org/10.1016/j.ijpharm.2012.08.007>.
- (63) Wu, D.-Q.; Wang, T.; Lu, B.; Xu, X.-D.; Cheng, S.-X.; Jiang, X.-J.; Zhang, X.-Z.; Zhuo, R.-X. Fabrication of Supramolecular Hydrogels for Drug Delivery and Stem Cell Encapsulation. *Langmuir* **2008**, *24* (18), 10306–10312. <https://doi.org/10.1021/la8006876>.
- (64) Wang, T.; Jiang, X.-J.; Lin, T.; Ren, S.; Li, X.-Y.; Zhang, X.-Z.; Tang, Q. The Inhibition of Postinfarct Ventricle Remodeling without Polycythaemia Following Local Sustained Intramyocardial Delivery of Erythropoietin within a Supramolecular Hydrogel. *Biomaterials* **2009**, *30* (25), 4161–4167. <https://doi.org/10.1016/j.biomaterials.2009.04.033>.
- (65) Tabassi, S. A. S.; Tekie, F. S. M.; Hadizadeh, F.; Rashid, R.; Khodaverdi, E.; Mohajeri, S. A. Sustained Release Drug Delivery Using Supramolecular Hydrogels of the Triblock Copolymer PCL–PEG–PCL and α -Cyclodextrin. *J. Sol-Gel Sci. Technol.* **2014**, *69* (1), 166–171. <https://doi.org/10.1007/s10971-013-3200-9>.
- (66) Li, Z.; Yin, H.; Zhang, Z.; Liu, K. L.; Li, J. Supramolecular Anchoring of DNA Polyplexes in Cyclodextrin-Based Polypseudorotaxane Hydrogels for Sustained Gene Delivery. *Biomacromolecules* **2012**, *13* (10), 3162–3172. <https://doi.org/10.1021/bm300936x>.
- (67) Poudel, A. J.; He, F.; Huang, L.; Xiao, L.; Yang, G. Supramolecular Hydrogels Based on Poly(Ethylene Glycol)-Poly(Lactic Acid) Block Copolymer Micelles and α -Cyclodextrin for Potential Injectable Drug Delivery System. *Carbohydr. Polym.* **2018**, *194*, 69–79. <https://doi.org/10.1016/j.carbpol.2018.04.035>.
- (68) Domiński, A.; Konieczny, T.; Kurcok, P. α -Cyclodextrin-Based Polypseudorotaxane Hydrogels. *Materials* **2019**, *13* (1), 133. <https://doi.org/10.3390/ma13010133>.
- (69) Abdul Karim, A.; Chee, P. L.; Chan, M. F.; Loh, X. J. Micellized α -Cyclodextrin-Based Supramolecular Hydrogel Exhibiting PH-Responsive Sustained Release and Corresponding Oscillatory Shear Behavior Analysis. *ACS Biomater. Sci. Eng.* **2016**, *2* (12), 2185–2195. <https://doi.org/10.1021/acsbmaterials.6b00383>.

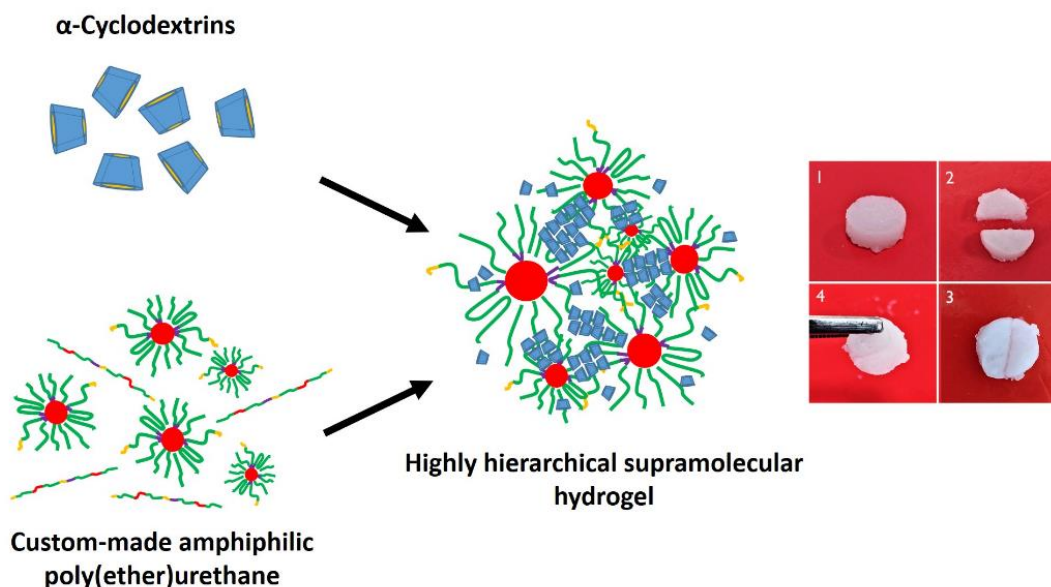
(70) Budkina, O. A.; Demina, T. V.; Dorodnykh, T. Yu.; Melik-Nubarov, N. S.; Grozdova, I. D. Cytotoxicity of Nonionic Amphiphilic Copolymers. *Polym. Sci. Ser. A* **2012**, *54* (9), 707–717. <https://doi.org/10.1134/S0965545X12080020>.

Section 2 - Chapter 2.2 - Combining Poloxamer® 407-based poly(ether urethane)s and cyclodextrins for the formulation of supramolecular hydrogels in water: a proof of concept study

1. Abstract

The need for engineered drug delivery systems characterized by high reversibility and handling is an actual and challenging demand in the clinical field. To this aim, hydrogels based on physical interactions can effectively contribute to the fulfilment of various requirements for tissue engineering and regenerative pharmacology applications, such as tunability and responsiveness. Nonetheless, proof of concept studies are necessary to evaluate the potential of novel polymers for the design of physical hydrogels for drug delivery. In this Chapter, the suitability of two properly synthesized PEUs (\bar{M}_n ca. 27-30 kDa) for the formulation of SM hydrogels based on inclusion complexes with α -CDs was evaluated. In detail, two PEUs were synthesized utilizing a commercially available amphiphilic triblock copolymer (i.e., Poloxamer® 407) and their capability to interact with α -CDs and form of PPR-based supramolecular crystals was investigated through X-Ray powder diffraction (XRD), Attenuated Total Reflectance – Fourier Transformed Infrared (ATR-FTIR) spectroscopy and Proton Nuclear Magnetic Resonance ($^1\text{H-NMR}$) spectroscopy. Thence, a library of highly stable supramolecular hydrogels was obtained at various PEU and α -CD concentrations (i.e., ranging between 1 and 9% w/v and 9 and 10% w/v, respectively). Gelation kinetics and mechanical properties improved as CD content increased from 9 to 10% w/v, while remarkable self-healing behavior (i.e., mechanical recovery greater than 80%) was observed for all the designed hydrogels. Two different hydrogel behaviors were found: low PEU containing hydrogel networks (i.e., 1-5% w/v concentration) were characterized by the predominance of PPR-based crystals, while high PEU containing systems (i.e., 7-9% w/v concentration) showed a preponderant thermo-sensitive behavior. Generally, hydrogels based on higher PEU contents (7-9% w/v) were characterized by non-fully developed networks at 37 °C and slight cytotoxicity, while residence time increased up to 7 days in physiological-like aqueous environment (i.e., pH 7.4, 37 °C). Differently, hydrogels based on lower PEU contents (1-5% w/v) were cytocompatible according to ISO 10993 standards and showed well-structured hydrogel networks, which turned out in the ability to maintain hydrogel shape up to 5 days when incubated in a watery milieu at 37 °C. PEU chemical composition affected the interaction with α -CDs and related effects were evaluated in hydrogel properties: the presence of pendant groups along PEU backbone resulted in slower gelation kinetics and inferior mechanical properties. Supramolecular hydrogels based on PEUs (at 1 and 5% w/v concentration) and α -CDs (at 10% w/v concentration) were able to release an encapsulated drug model molecule (i.e., fluorescein isothiocyanate dextran 4, \bar{M}_n 4 kDa) through a progressive kinetics (without burst release) within 4 days. Thence, the feasibility of PEUs as effective constituents of α -CD-based supramolecular hydrogels was demonstrated in this study, thus opening the way to further applications in drug delivery for regenerative medicine.

Graphical abstract



2. Introduction on the use of poly(urethane)s as PPR-forming polymers

The use of PUs in the development of supramolecular hydrogels based on PPRs has been quite investigated. One of the earliest examples reporting the formation of polyrotaxanes based on PU molecules is dated back to 1999.¹ In this work, Yamaguchi and colleagues utilized modified α - and β -CDs showing a permethyl functionality (PM- α -CDs and PM- β -CDs). Their strategy was based on performing the polyaddition of the involved reagents (aromatic diols and diisocyanates) in the presence of functionalized CDs in order to form inclusion complexes at high yield. This work represented an important demonstration of the high versatility that characterizes PU synthesis process. Another interesting example can be found in the work performed by Hasan *et al.*, who developed a linear PEU based on PEO and 1,6-hexamethylene diisocyanate (HDI).² The target of the authors of this work was the development of a water-soluble PEU based on defined units of PEO and HDI in order to tune its final thermo-sensitive behavior and self-assembly with α -CDs. Their hypothesis also relied on the idea of exploiting urethane domains to interact with α -CDs and hence significantly contribute to the overall integrity of PPRs. The synthesized PEU exhibited a molar mass around 3000 Da. The addition of α -CDs significantly affected the thermo-responsiveness of the PEU in solution. The authors hypothesized that this behavior could be ascribed to the interactions occurring between the nonpolar domains of α -CDs and PEU leading to inclusion complex (IC) formation. They also demonstrated that the formed ICs were decomposed through temperature increase. At defined PEU/ α -CDs ratios, hydrogel formation was observed and turned out to be dependent on a balanced coexistence of crystallized PPRs and hydrophobic interactions. The in-depth investigation through proton nuclear magnetic resonance spectroscopy demonstrated the dynamic state of threaded α -CDs, which were particularly concentrated on PEO domains. However, significant chemical shift changes were observed around the characteristic chemical shifts of HDI domains, thus indicating an important contribution of the hydrophobic domains of diisocyanates. Thence, a highly dynamic behavior was explained through the continuous transformation between free and complex components. Moreover, an exhaustive

characterization of the complexes at the solid state was performed through X-Ray powder diffraction, obtaining patterns that showed the typical peaks of crystallized PPRs, which formed an ordered supramolecular solid matter.

In terms of applications of PU hydrogels based on PPRs in drug delivery, one remarkable example can be found in the work performed by Cheng and co-authors.³ In detail, an innovative stimuli-sensitive injectable hydrogel was developed through the implementation of a linear amphiphilic PEU forming PPRs with α -CDs. pH- and redox-responsiveness were conferred through the exploitation of different chemical domains, such as dimethylolpropionic acid and di(1-hydroxyethylene) diselenide, respectively. The intrinsic ability to self-assemble of the here-developed PEU was exploited to form nanoparticles loading indomethacin, a hydrophobic drug, in watery environments. The subsequent formation of these nanostructures into a PPR-based hydrogel through the addition of α -CDs permitted the further integration of another molecule as hydrophilic drug molecule (rhodamine). The resulting hydrogels were characterized by low PEU concentration and high responsiveness to external stimuli, demonstrating the ability to trigger drug release. Moreover, enhanced reversibility and hence good injectability were also observed. The overall properties of these hydrogel systems represent highly promising factors for future clinical investigations.

For all the above-mentioned examples and many others, in which the use of PUs in drug delivery is explored,⁴ the development of novel drug delivery systems based on highly tunable PU-based supramolecular hydrogels seems to be an effective, interesting and promising frontier to further overcome the limitations of already existing drug delivery platforms. Indeed, the possibility to confer relevant and multiple functions to a polymeric system could give the possibility to decrease the amount of synthetic polymers required for formulation fabrication, while simultaneously enhancing tunability, handling, stability and responsiveness to external environment.

In the following part of the work, two custom-made PEUs were utilized to investigate the formation and design of supramolecular hydrogels based on PPRs. In detail, the two PEUs were produced through a two-step synthesis process using Poloxamer® 407 (P407, PEO-PPO-PEO, 70% wt PEO, \bar{M}_n 12600 Da), a non-toxic hydrophobic diisocyanate (1,6-hexamethylene diisocyanate, HDI) and two chain extenders, specifically an aliphatic cyclic diol (1,4-cyclohexanedimethanol) and an amino acid-derived diol (N-Boc Serinol).⁵⁻⁷ The peculiarity of these PEUs resides on their pronounced thermo-responsiveness. Indeed, these PEUs in solutions showed remarkably lower critical gelation concentrations (i.e., around 6% w/v) with respect to the native macrodiol P407 (i.e., around 18% w/v). In addition to this notable thermo-responsiveness, the presence of large PEO domains and HDI aliphatic regions into PEU polymer chains could allow these materials to spontaneously form supramolecular complexes with α -CDs. To investigate the nature of these interactions, X-Ray powder diffraction (XRD), Attenuated Total Reflectance - Fourier Transformed Infrared (ATR-FTIR) Spectroscopy and Proton Nuclear Magnetic Resonance (¹H-NMR) Spectroscopy were performed. Then, hydrogels were formulated with PEU content ranging between 1 and 9% w/v and α -CDs from 7 to 10% w/v. Hydrogel qualitative properties (i.e., gelation time) were evaluated through tube inverting test at different temperatures (i.e., 25 and 37 °C). Mechanical properties and reversibility of hydrogels were assessed through rheological characterizations. Hydrogel responsiveness and stability in physiological-like environment were evaluated up to 7 days incubation at 37 °C, while cytotoxicity on pure hydrogel extracts was investigated according to ISO 10993 recommendations. Finally, in

order to evaluate the suitability of such hydrogel systems as drug delivery platforms, encapsulation and release studies of Fluorescein isothiocyanate-dextran 4 (FD4, \bar{M}_n 4000 Da) were performed utilizing formulations characterized by low PEU content (i.e., ranging between 1 and 5% w/v).

3. Materials and Methods

3.1 Materials

Poloxamer® 407 (P407, \bar{M}_n 12.6 kDa, 70% PEO), 1,6-hexamethylene diisocyanate (HDI), 1,4-cyclohexanedimethanol (CDM), N-Boc serinol (NBoc), dibutyltin dilaurate (DBTDL) and 3-(trimethylsilyl)propionic-2,2,3,3-d 4 acid sodium salt (TSP) were obtained from Merck/Sigma-Aldrich (Milan, Italy). α -CDs (from now on simply indicated with the acronym “CDs”) were obtained from TCI Chemicals Europe (Zwijndrecht, Belgium). P407 was dehydrated for 8 h at 100 °C at low pressure (i.e., c.a. 200 mbar) and then maintained at 40 °C until use. CDM and NBoc were dried overnight into a desiccator at low pressure and room temperature. HDI was purified through distillation under vacuum. The utilized solvents were purchased from Carlo Erba Reagents at analytical grade (Milan, Italy). Overnight anhydrication of 1,2-dichloroethane (DCE, Carlo Erba Reagents, Milan, Italy) was performed by storing it over activated (overnight drying at 120 °C, atmospheric pressure) molecular sieves (Sigma Aldrich, Milan, Italy) under N₂ atmosphere.

3.2 Synthesis of PEUs

In this part of the work, two PEUs based on different chain extenders were synthesized through an optimized two-step procedure. In detail, P407 was dissolved in anhydrous DCE at 20% w/v concentration and equilibrated at 80 °C. Then, HDI and DBTDL were added at 2:1 molar ratio and 0.1% w/w concentration with respect to solubilized P407, respectively. The step of pre-polymerization was carried out for 2.5 hours under stirring (*ca.* 250 rpm) at 80 °C, thus obtaining a pre-polymer with isocyanate end-groups. The second step of the synthesis consisted in a chain extension of the pre-polymer. The chain extender (CDM or NBoc) was solubilized at 60 °C in DCE (3% w/v) and at 1:1 molar ratio with respect to P407 and added to the pre-polymer solution. The reaction was carried out for 1.5 hours at 60 °C. Subsequently, the solution was cooled at room temperature (25 °C) and methanol was added in excess (6 ml every 16 g of theoretical PEU) to passivate any unreacted isocyanate domain. The solution containing the newly produced PEU was then precipitated in petroleum ether (4:1 v/v ratio with respect to overall DCE volume) under vigorous stirring. The precipitated PEU was separated from the supernatant and kept under a fume hood overnight. Subsequently, the dried PEU was solubilized in DCE at 20% w/v concentration and purified through precipitation in a diethyl ether (DEE)/methanol mixture (98/2% v/v and 5:1 with respect to utilized DCE). PEU separation was performed through centrifugation (Hettich, MIKRO 220R) for 20 minutes at 6000 rpm and 0 °C. Then, the PEU was dried overnight under a fume hood, collected, and stored under vacuum at 3 °C. From now on, the obtained PEUs will be coded as NHP407 and CHP407, where P407 represents the macrodiol used for the synthesis, H identifies the diisocyanate, while N and C indicate NBoc and CDM, respectively.

3.3 Chemical characterization of PEUs

3.3.1 Attenuated Total Reflectance – Fourier Transformed Infrared (ATR-FTIR) Spectroscopy

The successful synthesis of PEUs was proved through ATR-FTIR spectroscopy, which was performed at room temperature on PEU powder utilizing a Perkin Elmer Spectrum 100 Instrument equipped with an ATR accessory with diamond crystal (UATR KRSS). Each spectrum was obtained from 16 scans (4 cm⁻¹ resolution) in the spectral domain from 4000 to 600 cm⁻¹. The analysis of data was conducted utilizing the Perkin Elmer Spectrum software. As control sample, the spectrum of P407 was obtained using the same protocol.

3.3.2 Size Exclusion Chromatography (SEC)

Molar mass distributions of NHP407 and CHP407 were characterized through an Agilent Technologies 1200 Series (California, USA) SEC supplied with a refractive index detector (RID) and two Waters Styragel columns (HR1 and HR4). N,N-dimethylformamide (DMF, HPLC grade, Carlo Erba, Milan, Italy) containing LiBr at 0.1% w/v concentration was utilized as mobile phase at a flow rate of 0.5 ml min⁻¹. Registered RID and elution volume data were then exported as .CSV file. Number average molar mass (\bar{M}_n), weight average molar mass (\bar{M}_w) and dispersity index ($D = \bar{M}_w/\bar{M}_n$) were calculated using Microsoft Excel (Office 365, Microsoft Corporation, USA) and a specific calibration curve obtained from PEO standards having peak molecular weight (\bar{M}_p) ranging from 982 to 205500 Da. For sample preparation, 2 mg of PEU were dissolved in 1 ml of DMF added with LiBr and filtered using poly(tetrafluoroethylene) (PTFE) syringe filters (0.45 μm, LLG International, Meckenheim, Germany).

3.4 Preparation and characterization of PEU- and CD-based inclusion complexes (ICs)

3.4.1 Preparation of Supramolecular (SM) complexes

The formation of ICs between PEUs and CDs was evaluated in double distilled water (ddH₂O) by mixing their respective solutions. More in detail, concentrated solutions of PEUs were produced by solubilizing the required amount of polymer in ddH₂O at 3 °C overnight. Subsequently, a transparent solution of CDs at 14% w/v concentration was prepared, added to the previously obtained PEU solutions and homogenized with a vortex (40 Hz for *ca.* 30 seconds). The final samples were characterized by a PEU concentration of 1% w/v and the required amount of CDs to theoretically cover the 100% of available PEO domains (i.e., CD at 7.6% w/v concentration). Then, the samples were incubated for 72 hours at room temperature (i.e., 25 °C) to form ICs. The resulting crystalline matter composed of PPR-based aggregates was separated through centrifugation (Mikro 220R, Hettich, Germany) at 4500 rpm and 10 °C for 15 minutes. The samples containing SM complexes were quenched and frozen through immersion in liquid nitrogen and freeze dried (Martin Christ ALPHA 2-4 LSC, Germany) for 24 hours. Hereafter, the obtained SM complexes based on PEUs will be coded as NHP407 SM_100% and CHP407

SM_100% to indicate that were designed to theoretically reach a complete coverage of PEO domains through CDs.

3.4.2 X-Ray powder diffraction (XRD) analysis

XRD patterns of NHP407 SM_100% and CHP407 SM_100% were obtained using an X-Ray diffractometer D5005 assembled with a Bragg-Brentano geometry and vertical goniometer theta - theta (the specimen holder is fixed while tube and detector rotate). The instrument was also equipped with a Ni-filtered Cu K α (1.542 Å) radiation source set at 40 kV and 40 mA. Tests were performed in step scan mode within the 2 θ range from 5° to 30° at increment rate of 0.1° step⁻¹ and scan speed of 10 s step⁻¹. As control samples, NHP407 and CHP407 were also analyzed using the same protocol.

3.4.3 Attenuated Total Reflectance – Fourier Transformed Infrared (ATR-FTIR) Spectroscopy

NHP407 SM_100% and CHP407 SM_100% were also characterized through ATR-FTIR spectroscopy in order to further characterize their constituents and occurring SM interactions. Spectra were obtained at room temperature and by averaging 32 scans in the spectral range from 4000 and 600 cm⁻¹ at a resolution of 1 cm⁻¹. Analyses were performed on three different batches of each sample and recorded spectra were averaged. Pure PEUs and CDs were also analyzed for comparative purposes.

3.4.4 Proton Nuclear Magnetic Resonance (¹H-NMR) Spectroscopy

¹H-NMR characterization was performed using an AVANCE III Bruker spectrometer equipped with an 11.75 T superconducting magnet (500 MHz ¹H Larmor frequency) and a Bruker BVT-3000 unit for temperature control. The NMR spectra were obtained at 300 K after 10 min for temperature stabilization at 25 °C. Each spectrum was obtained as the average of 12 scans, with 10 s relaxation time. A sealed capillary containing 1 mM TSP in D₂O was inserted in the NMR tube and used as reference for the zero of the chemical shift scale.

Samples for ¹H-NMR spectroscopy were obtained through solubilization of NHP407 SM_100% and CHP407 SM_100% in deuterium oxide (D₂O, 99.8%, Sigma Aldrich, Italy) at a concentration of 5 mg ml⁻¹. Analyses were additionally performed on self-assembling samples based on the mixture of PEU (1% w/v) and CD solutions in D₂O. In this case, CDs (14% w/v) were added in order to cover the theoretical 50% of available PEO domains (i.e., resulting CD concentration at 3.8% w/v in D₂O) and avoid crystal formation and precipitation (acronyms for these samples are: NHP407 SM_50% and CHP407 SM_50%). Spectra of control samples of CD, NHP407 and CHP407 were also obtained according to the same protocol. MNova software (Mestrelab Research, S.L, Spain, www.mestrelab.com) was utilized for spectra elaboration.

Additionally, 2D ¹H-NMR spectra were obtained through Nuclear Overhauser Effect Spectroscopy (NOESY, 2D homonuclear correlation via dipolar coupling) and Rotating frame Overhauser Effect (ROESY) spectroscopy for the samples NHP407 SM_50% and CHP407 SM_50% in order to better investigate the occurring interactions between PEUs and CDs. NOESY

spectra were obtained as average of 24 scans with a spectral window size $f1$ 10 ppm and $f2$ 10 ppm (mixing time 0.3 s and relaxation delay 3 s). ROESY spectra were obtained as average of 24 scans with a spectral window size $f1$ 10 ppm and $f2$ 10 ppm (continuous wave spinlock for mixing and relaxation delay 3 s).

3.5 Preparation and characterization of PEU- and CD-based SM hydrogels

3.5.1 Preparation of SM hydrogels

SM hydrogels were prepared in ddH₂O by mixing PEU and CD solutions. Briefly, PEUs were weighted in the required amount in Bijou sample containers (17 mm diameter, 7 ml, Carlo Erba Reagents, Milan, Italy) and firstly solubilized in ddH₂O at 3 °C overnight. Subsequently, specific aliquots of a clear solution of CDs in ddH₂O (14% w/v) were added to the previously prepared PEU solutions and the obtained mixtures were homogenized using a vortex (40 Hz, 30 seconds). The samples were then incubated in isothermal conditions (i.e., 25 and 37 °C) to allow gelation through SM structure development. Various formulations containing PEUs (1, 5, 7 and 9% w/v) and CDs (7, 8, 9 and 10% w/v) were produced to obtain a library of SM hydrogels to characterize. Hereafter, SM hydrogels will be indicated with the acronym PEU X% - CD Y%, in which PEU refers to the specific poly(ether urethane) that constitutes the synthetic component of the hydrogel (i.e., NHP407 or CHP407), while X and Y identify PEU and CD concentrations, respectively.

3.5.2 Qualitative evaluation of gelation time in isothermal conditions and phase-separation

Gelation kinetics of SM hydrogels was qualitatively investigated through visual inspection at room temperature (25 °C) and at 37 °C. In detail, at precise time steps (i.e., every 1 and 5 minutes up to 1 hour observation and then every 10 minutes), the samples were inverted and the flowing of solutions containing PEUs and CDs was assessed. The condition of “gel” state was characterized by a “no-flow” condition after 30 seconds of vial inversion. Once the gelation process was completed, the samples were maintained at the gelling temperature (25 or 37 °C) and visually evaluated every day to assess the occurrence of phase-separation phenomena.

3.5.3 Rheological characterization

Rheological characterizations on PEU-based SM gels were carried out with a stress-controlled rheometer (MCR302, Anton Paar GmbH, Graz, Austria) equipped with a Peltier system for temperature control and a 25 mm parallel plate configuration. Hydrogels (PEU concentration between 1 and 9% w/v and CD concentrations at 9 and 10% w/v) were injected through a 5 ml syringe (2 mm needle, *ca.* 0.4 ml) on the lower plate of the rheometer previously equilibrated at 25 °C. The normal force was imposed at 0 N and the thickness of the sample was set at 0.6 mm for all the characterizations.

Strain sweep tests were carried out at 37 °C and 1 rad s⁻¹ angular frequency by varying strain values from 0.01 to 500%. Samples that were analyzed through strain sweep test were analyzed again after 15 minutes of recovery in quiescent state and isothermal conditions (37 °C) with the aim to evaluate hydrogel capability to self-heal after a relevant strain has been applied (i.e., 500%).

Frequency sweep tests were performed within the linear viscoelastic region (strain at 0.1%) at 25, 30 and 37°C and angular frequency from 0.1 to 100 rad s⁻¹.

Self-healing tests were also executed to evaluate the physical reversibility of hydrogels when a variable strain was cyclically applied over time at 37 °C, according to the protocol described by Wu and co-workers with few modifications.⁸ Specifically, SM hydrogels were initially subjected to a constant strain (0.1%, 1 Hz, recovery phase) for 120 seconds; subsequently, a complete breakage of hydrogel network was induced through the application of a significantly higher strain (100%, 1 Hz, rupture phase) for 60 seconds. The above-mentioned procedure was applied on each sample for three cycles and finally the starting strain (0.1%, 1 Hz, recovery phase) was applied again to evaluate residual mechanical properties.

3.5.4 Swelling and stability in physiological-like conditions

The behavior of SM hydrogels (1 ml in Bijou sample containers with 7 ml capacity and an inner diameter of 17 mm) in aqueous environments was evaluated through incubation at 37 °C in contact with phosphate buffered saline (PBS, 1 ml, pH 7.4) added with sodium azide (NaN₃, 0.1% w/v, Sigma Aldrich, Milan, Italy). In detail, swelling and dissolution of hydrogel network were quantified. The hydrogels were initially weighted (W_{gel_i}) and acclimatized at 37 °C for 15 minutes. Subsequently, PBS added with NaN₃ (1 ml, 37 °C) was gently poured to each sample and the hydrogels were then incubated at 37 °C. At specific time frames (24h, 3 days, 5 days and 7 days) the residual PBS was removed, and the hydrogels were weighted again (W_{gel_f}) to quantify their swelling ability (i.e., PBS absorption %) according to equation 1. The same hydrogels were freeze dried (Martin Christ ALPHA 2-4 LSC, Germany) and weighted again ($W_{dried\ gel_f}$) to measure network weight loss (Weight loss %) using the formula in equation 2. Reference samples were also prepared according to the same protocol, freeze dried and weighted ($W_{dried\ gel_i}$), without being incubated in contact with PBS.

$$PBS\ Absorption\ \% = \frac{W_{gel_f} - W_{gel_i}}{W_{gel_f}} \times 100 \quad Eq.1$$

$$Weight\ loss\ \% = \frac{W_{dried\ gel_i} - W_{dried\ gel_f}}{W_{dried\ gel_i}} \times 100 \quad Eq.2$$

Additionally, the responsiveness of SM hydrogels to watery environments was evaluated through the calculation of the swelling ratio values at each time frame. In fact, the swelling ratio represents a useful parameter to highlight the ratio between water and polymer contents within the hydrogel systems over time. Equation 3 was applied to calculate swelling ratios of hydrogels. Control samples were prepared and used as reference (i.e., swelling ratio equal to 1).

$$Swelling\ ratio = \frac{W_{gel_f} - W_{dried\ gel_f}}{W_{dried\ gel_f}} \quad Eq.3$$

Analyses were conducted in quintuplicate and results are reported as mean \pm standard deviation.

3.5.5 Cytotoxicity evaluation

The evaluation of cytotoxicity was performed on various formulations containing PEUs (from 1 to 9% w/v concentration) and CDs (9 and 10% w/v concentration). In detail, SM gels (250 mg) were prepared in Bijou sample containers (7 ml, 17 mm inner diameter), sterilized through UV light exposure (290 nm) for 30 minutes and acclimatized at 37 °C for 15 minutes. Subsequently, Dulbecco's Modified Eagle Medium (37 °C, high glucose, Carlo Erba Reagents, Italy) added with foetal bovine serum (10% v/v, Carlo Erba Reagents, Italy) was poured in contact with SM hydrogels (1 ml every 100 mg of hydrogel). The samples were then incubated for 24 hours at 37 °C and the hydrogel extracts were collected. Simultaneously, murine fibroblasts (NIH 3T3 cell line, ATCC, USA) were cultured utilizing the same medium (37 °C, 5% CO₂) on a 96 well plate (20000 cell well⁻¹, 100 µl culture medium) for 24 hours. The previously collected hydrogel extracts were filtered (0.22 µm, PTFE, LLG labware) and then 100 µl were administered to the cultured cells for 24 hours at 37 °C. Afterwards, the medium was totally renewed with fresh one (100 µl) added with resazurine (0.1 mg ml⁻¹, Sigma Aldrich, Milan, Italy) and the plate was incubated for 1 hour at 37 °C. Cell viability was estimated using a multimode plate reader (Perkin Elmer Victor X3) by quantifying the reduced resazurine at 595 nm (excitation at 530 nm). Control samples (i.e., cells that were cultured in pure medium) were also prepared and analyzed. Three independent experiments were conducted and results are reported as mean ± standard deviation.

3.5.6 Release study of fluorescein isothiocyanate dextran (FD4)

Release studies of FD4 loaded into SM hydrogels (PEU concentrations at 1 or 5% w/v, CDs concentration at 10% w/v) were conducted. FD4 (4 kDa, Sigma Adrich, Milan, Italy) was utilized as model molecule of small hydrophilic drugs and macromolecules, such as antibiotics and proteins, respectively. FD4 was encapsulated into SM hydrogels through solubilization in a solution containing CDs at 14% w/v in ddH₂O. Then, the required aliquot of CD/FD4 solution was mixed with PEU solutions in Bijou sample containers (7 ml capacity, inner diameter 17 mm, Carlo Erba, Milan, Italy) obtaining a CD and FD4 concentration of 10% w/v and 1 mg ml⁻¹, respectively, and final sample volume of 1 ml. Hydrogel network development was ensured through incubation at room temperature (25 °C) for 48 hours in the dark. Then, SM hydrogels were acclimatized at 37 °C for 15 minutes and PBS (1 ml, 37 °C) was added as medium for FD4 release. The quantification of FD4 was carried out through a multimode plate reader (Perkin Elmer Victor X3) by evaluating the absorbance at 490 nm on a 96 well plate (200 µl per well). Hydrogels were prepared in quintuplicate for each investigated formulation. A calibration curve based on standard samples with FD4 concentration ranging from 0.05 to 1 mg ml⁻¹ was obtained as reference for FD4 quantification. In order to select a proper condition for FD4 quantification, a set of calibration curves based on standard samples prepared in PBS containing CDs at different concentrations (i.e., 0, 1, 2.5, 5 and 10% w/v) was investigated. Data are shown as average ± standard deviation.

3.6 Statistical analysis

Statistical analysis was conducted through GraphPad Prism 8 for Windows 10 (GraphPad Software, La Jolla, CA, USA; www.graphpad.com). Two-way ANOVA analysis coupled with

Bonferroni multiple comparison test was performed to compare results, assessing the statistical significance according to Boffito *et al.*⁵

Significance level were assigned depending on p-values: $p < 0.0001$ Extremely significant (****), $0.0001 < p < 0.001$ Extremely significant (***), $0.001 < p < 0.01$ Very significant (**), $0.01 < p < 0.05$ Significant (*), $p \geq 0.05$ Not significant (ns).

4. Results

4.1 Chemical characterization of PEUs

ATR-FTIR spectroscopy and SEC analyses were conducted to demonstrate the successful synthesis of NHP407 and CHP407 PEUs. ATR-FTIR spectra of PEUs and P407 as reference are reported in figure 1. The presence of new bands referred to urethane domains was observed in both NHP407 and CHP407 spectra. In detail, the stretching vibration of free carbonyl groups (C=O) at 1720 cm^{-1} and the concurrent bending of N-H and stretching and C-N domains at 1530 cm^{-1} were observed. Additionally, N-H stretching was also detected at 3350 cm^{-1} . The absence of any vibration around 2200 cm^{-1} clearly demonstrated a total conversion of isocyanate groups. The presence of the typical absorption bands of P407 was also observed in PEU spectra at 2880 and 1250 cm^{-1} (CH_2 stretching and rocking, respectively) and at 1100 cm^{-1} (C-O-C stretching).

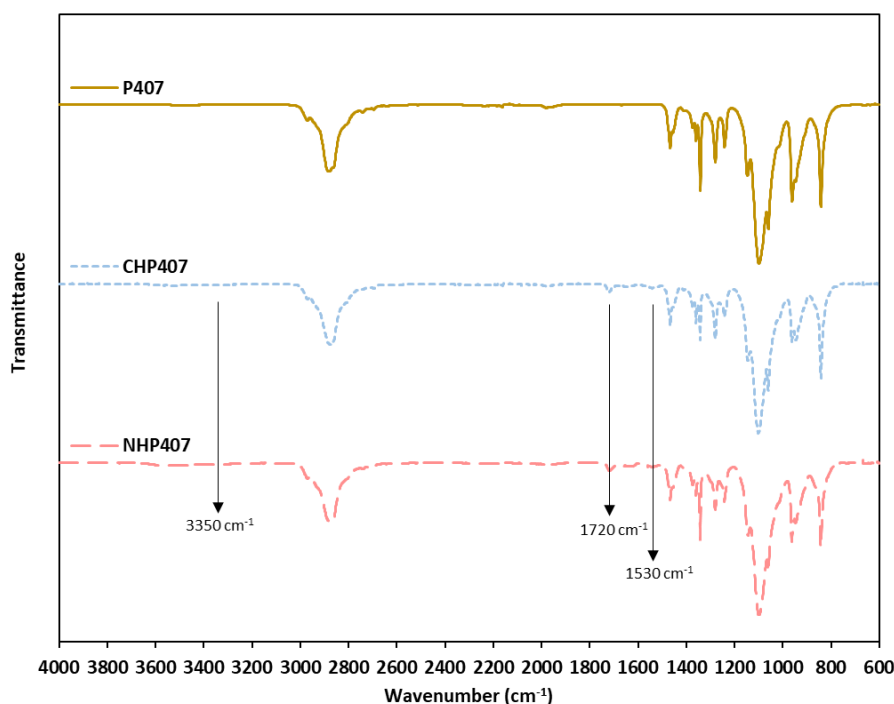


Figure 1 – ATR-FTIR spectra of P407 (ochre continuous line), CHP407 (light blue dotted line) and NHP407 (light red long dashed line). Typical urethane vibration bands are specifically indicated through vertical arrows at 3350 , 1720 and 1530 cm^{-1} .

CHP407 and NHP407 were characterized by similar number average molar masses (\bar{M}_n) which were quantified around 30 kDa and 27 kDa, respectively. As the typical error of SEC measurements is around 10%, the observed difference was not significant.⁹ Dispersity index

resulted to be 1.8 for both PEUs. The SEC profiles of both PEUs and P407 as reference (\bar{M}_n around 8 kDa, $D = 1.2$) are reported in figure 2. Moreover, the molecular mass distribution of both PEUs showed a residual peak resulting from polymers derived by typical P407 di-blocks¹⁰. This indicated the presence partially polymerized chains that were not completely removed through purification processes. However, the effect of such components on final hydrogel behavior can be considered negligible, because of their limited contribution within the entire molecular mass distribution.

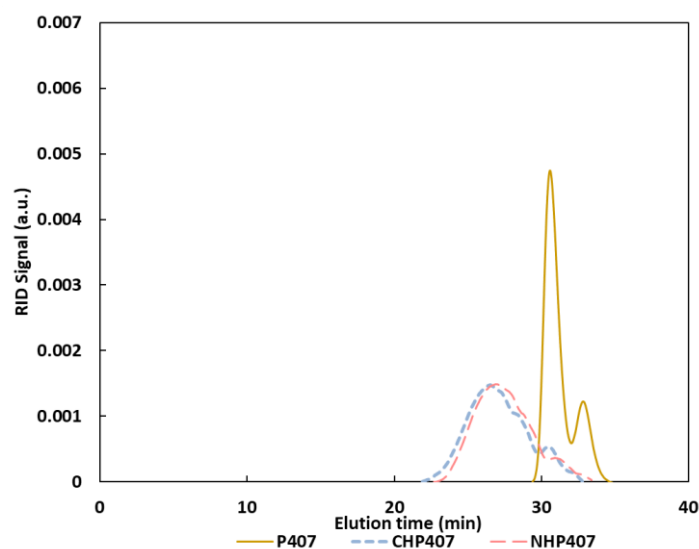


Figure 2 – SEC profiles (RID signal vs. elution time) of P407 (ochre continuous line), CHP407 (light blue dotted line) and NHP407 (light red dashed line).

4.2 Characterization of SM complexes based on PEUs and CDs

4.2.1 X-Ray powder diffraction (XRD) characterization

XRD analyses were performed to demonstrate the formation of SM inclusion complexes between PEUs and CDs and characterize the potential morphology of PPR-based crystals. XRD patterns of P407 reported in the literature show the presence of two peaks at *ca.* 19°-19.3° and 23.1°-23.5°, which are related to the presence of PEO domains (approx. 70% w/v).¹¹ Pure PEU spectra (figure 3) exhibited two main peaks at 2θ equal to 19.1° and 23.2°, demonstrating the presence of P407 typical crystalline domains. Curiously, PEU increased molar mass did not significantly interfere with the process of crystallization with respect to native P407.

In the presence of CDs, it has been widely demonstrated that typical peaks of a hexagonal channel-like crystal lattice can be found at 2θ around 7.3°-7.6°, 12.7°-13° and 19.5°-20°.¹¹⁻¹³ XRD patterns of PEUs-based SM structures (figure 3) evidently showed the presence of PPR-based crystalline domains. In fact, a relevant peak at 2θ around 19.8°-20° was observed in both NHP407 SM_100% and CHP407 SM_100% spectra. Moreover, additional peaks were observed at values of 2θ around 7.6° and 13°, thus further confirming the hexagonal channel-like morphology of PEU-based SM crystals. The absence of multiple reflections in these patterns demonstrated the absence of free crystalline domains based on pure CDs.¹⁴ In physical terms, the overall yield of collected crystalline mass resulted to be $58 \pm 0.5\%$ and $30 \pm 0.5\%$ for CHP407 SM_100% and NHP407

SM_100% (average of three measurements), respectively. In this regard, the different composition of PEUs could be an important factor. Indeed, CHP407 did not possess pendant groups (i.e., Boc domains) along its backbone that could cause steric hindrance as for NHP407. This difference could be the reason of the enhanced SM self-assembly that was observed for CHP407 SM_100%, even though CDM is notably a more rigid chain extender with respect to NBoc due to the presence of the cyclic monomer cyclohexane. Thence, it has been hypothesized that the steric hindrance of lateral pendant Boc groups most likely impeded the threading of CDs along NHP407 chains.

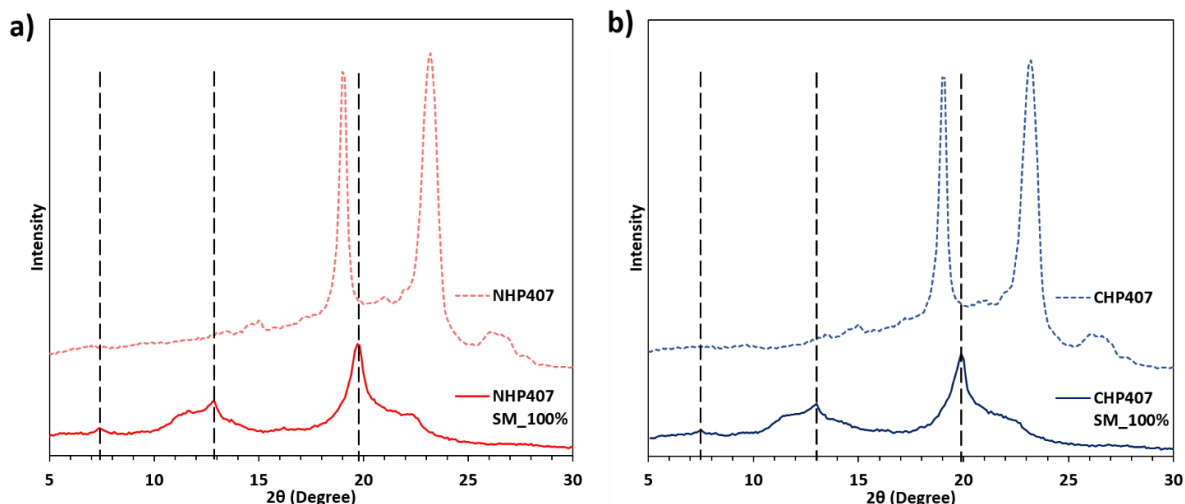


Figure 3 – XRD patterns of PEUs and their related SM samples. a) NHP407 (light red dashed line) and NHP407 SM_100% (red continuous line), and b) CHP407 (light blue dashed line) and CHP407 SM_100% (blue continuous line). Pure PEU samples resulted in patterns very similar to the one that characterizes P407. This result suggested that no significant variations in chemical conformation were caused by neither presence of hydrophobic domains (i.e., PPO, ca. 30% wt) nor the chain extension process. Differently, the typical peaks of PPR-based crystals are highlighted by vertical black dashed lines (2θ equal to 7.6° , 13° and 19.8°) in the patterns of samples resulting from the self-assembly of PEUs and CDs. Moreover, the obtained spectra were characterized by the absence of peaks related to pure PEU domains and native CD-based crystals.

4.2.2 Attenuated Total Reflectance – Fourier Transformed Infrared (ATR-FTIR) spectroscopic analyses

CHP407 SM_100% and NHP407 SM_100% samples were also characterized through ATR-FTIR spectroscopy. ATR-FTIR analyses of SM samples evidenced noteworthy differences with respect to pure PEU- and CD-based control samples. The simultaneous presence of typical absorption peaks of both native PEUs and CDs demonstrated the occurrence of a clear self-assembly process (figure 4). For example, typical peaks of CDs were detected in SM sample spectra at 1075 , 1155 and 2954 cm^{-1} , which were due to C-O, C-O-C and -CH stretching excitations, respectively. Moreover, another important signal in CD spectrum appeared at 3308 cm^{-1} and was originated by the asymmetric and symmetric stretching of -OH domains. In SM samples, in which CDs were forming PPR-based crystals, this peak resulted to be upshifted to 3340 cm^{-1} , thus indicating that the involved CDs were not disposed in the typical cage-like packing that characterizes pure CD powders.^{15–17} In fact, it could be hypothesized that CDs were packed along PEU chains and formed hydrogen bonds between -OH domains that belonged to adjacent outer faces of aligned molecules. The resulting arrangement could cause variations in the vibration of -OH domains with respect to

the typical cage-type conformation, by lowering the energy of the spontaneous assembly of CDs. Another element further confirming this hypothesis was found in the upshift of the peak related to urethane C=O domains, which was found at 1740 cm^{-1} rather than 1720 cm^{-1} . This shift could be most likely caused by SM domains hindering the spontaneous crystallization of PEU chains. These results were in accordance with other previous studies^{16,17} and the discussed XRD results, thus further demonstrating the hypothesis on the formation of PPR-based channel-like SM crystals between PEUs and CDs, with an additional contribution from urethane domains.

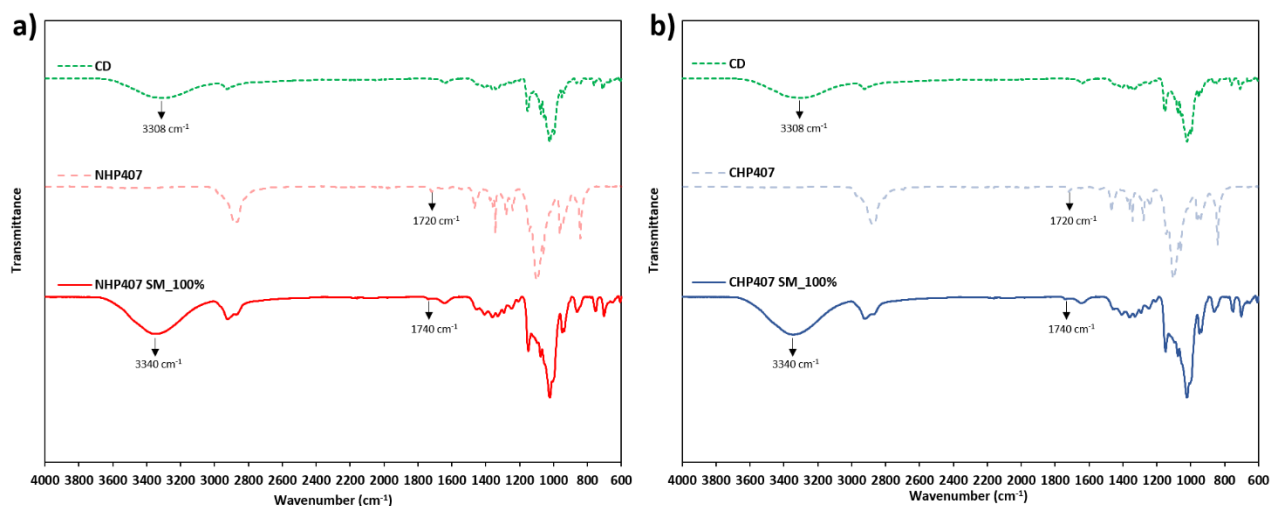


Figure 4 – ATR-FTIR spectra of CD, PEU and SM complexes. a) comparative evaluation among CD (green dotted line), NHP407 (light red dashed line) and NHP407 SM_100% (red continuous line), and b) comparative evaluation among CD (green dotted line), CHP407 (light blue dashed line) and CHP407 SM_100% (blue continuous line). Shifts of -OH (from 3308 to 3340 cm^{-1}) and C=O (from 1720 to 1740 cm^{-1}) due to the presence of SM domains are highlighted by black arrows in their respective spectra.

4.2.3 Proton Nuclear Magnetic Resonance (^1H -NMR) spectroscopy analyses

In order to complete the physico-chemical characterization of SM samples, ^1H -NMR spectroscopy was also carried out on NHP407 SM_100% and CHP407 SM_100% samples solubilized in D_2O . As observed in ATR-FTIR results, the concomitant presence of the main characteristic chemical shifts of both CDs (ranging from 4.05 to 3.55 ppm and at 5.07 ppm) and PEUs (ranging from 1.60 to 0.95 ppm and at 3.75 ppm) confirmed that the obtained crystalline matter was based on complexes between CDs and PEUs, as reported in figure 5.

Moreover, ^1H -NMR spectroscopy was performed on self-assembling samples (i.e., NHP407 SM_50% and CHP407 SM_50%) with the aim to better understand the interactions occurring between PEUs and CDs in solution. However, no significant variation in chemical shifts were observed for the specific domains of CDs that could be involved in the formation of PPRs, in opposition with already published results regarding similar PEUs with significantly lower molar mass (i.e., \bar{M}_n around 3.1 kDa).² Indeed, only non-relevant variations in the chemical shifts related to the inner protons of CDs (i.e., H3 and H5) were observed in NHP407 SM_50% and CHP407 SM_50%, as indicated in figure 6a. Additionally, potential variations of the main peak of PEO were not detectable due to highly broad and non-uniform peaks, in accordance with the results reported by Hasan and colleagues.²

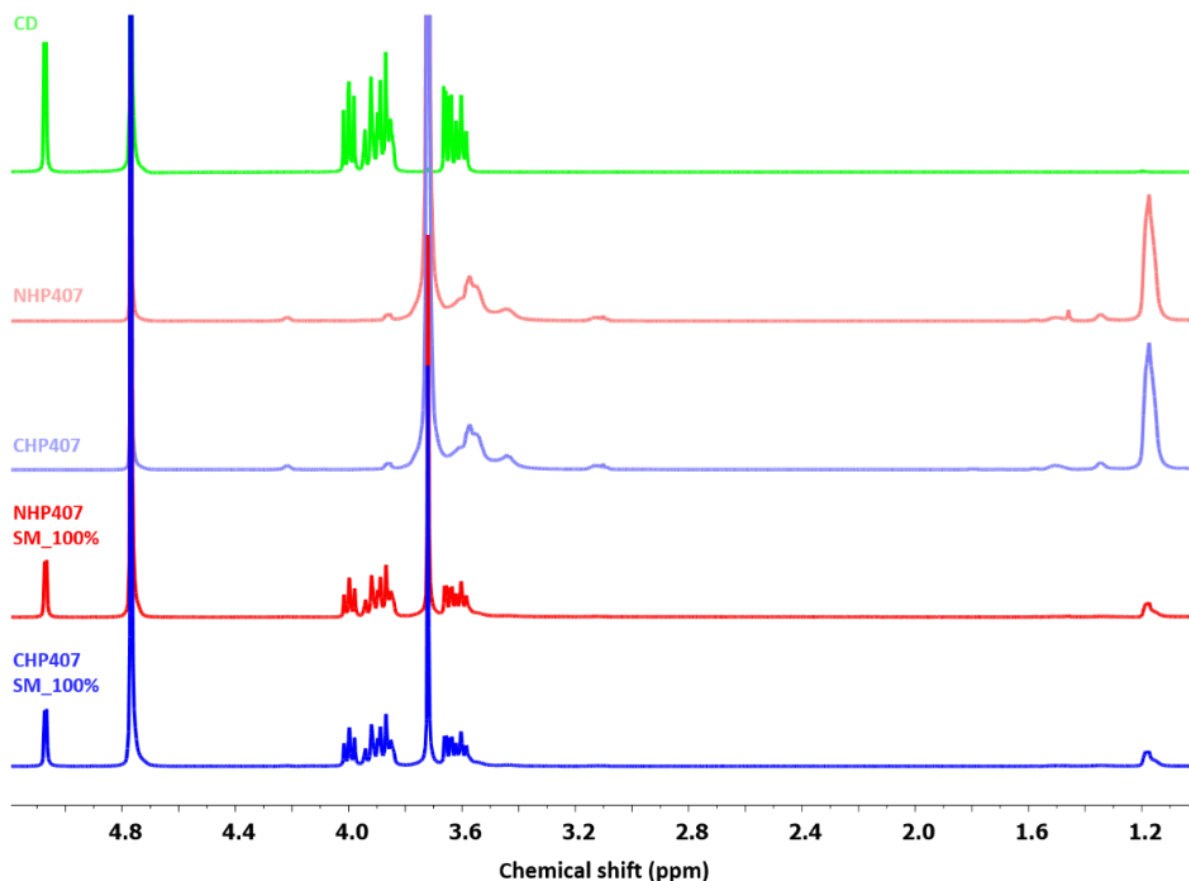


Figure 5 – $^1\text{H-NMR}$ spectra of CDs (light green), NHP407 (light red), CHP407 (light blue), NHP407 SM_100% (red) and CHP407 SM_100% (blue). The appearance of the chemical shifts related to both CDs and PEUs in NHP407 SM_100% and CHP407 SM_100% spectra demonstrates the co-presence of both components in the obtained SM crystals.

Moreover, a potentially lower stability of SM structures based on PEUs and CDs in mild conditions (i.e., relatively low CD concentration) could be supposed, as a consequence of the high molecular complexity and molar mass of PEUs. Thence, it could be hypothesized that the majority of CDs of NHP407 SM_50% and CHP407 SM_50% samples were in the free form and the amount of CDs forming PPRs was too restricted to result in significant variations of the involved chemical shifts in the NMR spectra.

Nonetheless, the peaks related to PEU HDI domains (chemical shifts ranging between 1.55 and 1.30 ppm) resulted to be broaden in $^1\text{H-NMR}$ spectra of the complexed samples (Figure 6b and 6c). This result could be an indication of occurring interactions between CDs and urethane domains, as previously supposed in the discussion of ATR-FTIR spectra of similar samples. Ultimately, because of the relevant complexity of the involved systems, the implementation of NMR shift titration analyses to obtain constants of association between PEUs and CDs was not possible.

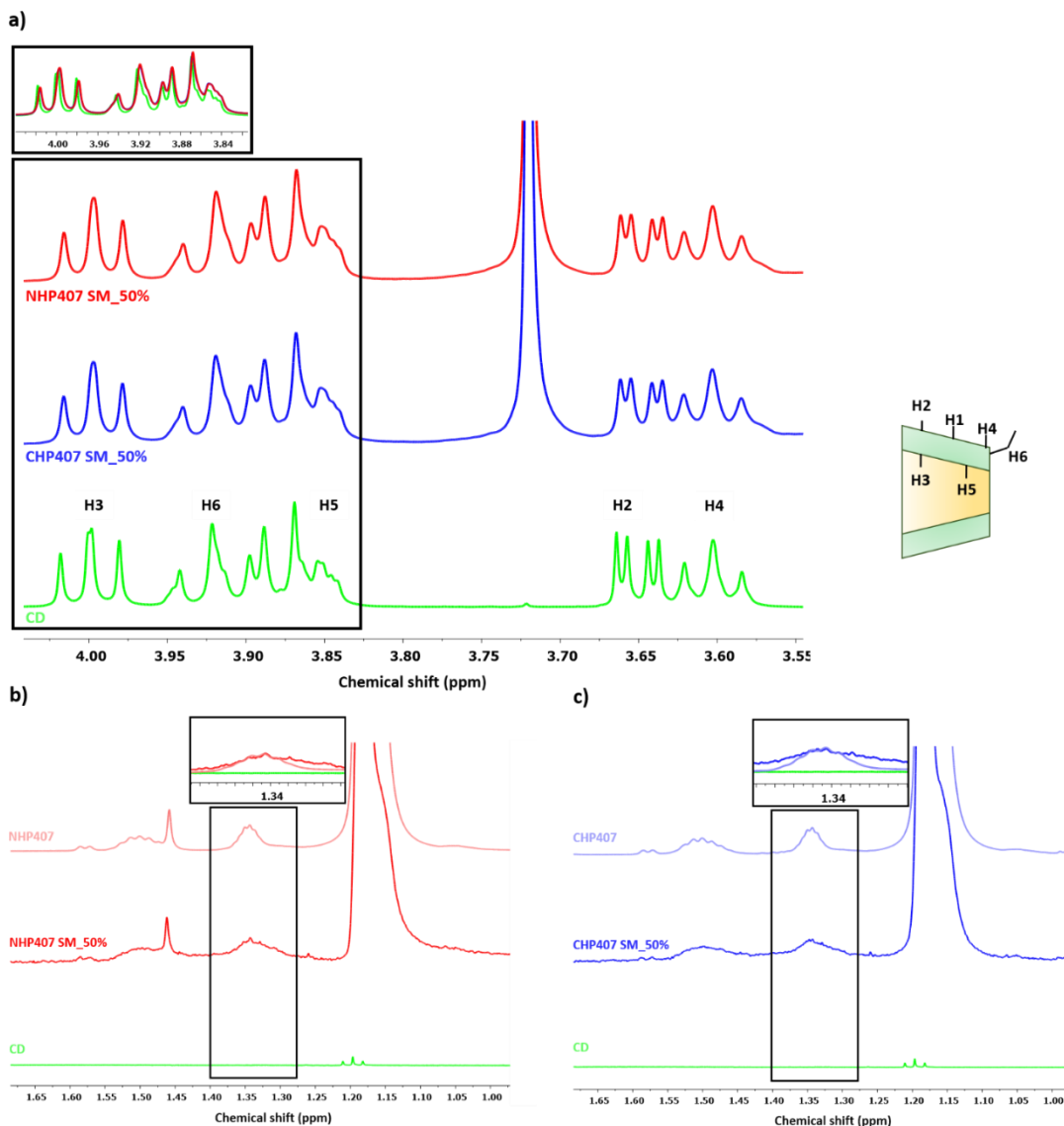


Figure 6 – a) ¹H-NMR spectra of NHP407 SM_50%, CHP407 SM_50% and CDs for comparative purposes. The insert on top reports the overlapped ¹H-NMR spectra within the chemical shift range from 3.81 to 4.40 ppm in order to highlight the presence of only unimportant variations of the shifts related to CD inner protons (i.e., H3 and H5) in NHP407 SM_50% and CHP407 SM_50% in comparison to CDs as such. b) ¹H-NMR spectra of NHP407 (light red), NHP407 SM_50% (red) and CDs (green) in the chemical shift range from 1.70 to 0.95 ppm. The insert on top reports overlapped ¹H-NMR spectra in the chemical shift range from 1.25 to 1.55 ppm to highlight the broadening of signals referred to HDI domains in NHP407 SM_50% with respect to native NHP407. c) ¹H-NMR spectra of CHP407 (light blue), CHP407 SM_50% (blue) and CDs (green) in the chemical shift range from 1.70 to 0.95 ppm. The insert on top reports overlapped ¹H-NMR spectra in the chemical shift range from 1.25 to 1.55 ppm to highlight the broadening of signals referred to HDI domains in CHP407 SM_50% with respect to native CHP407.

Additionally, NOESY and ROESY ¹H-¹H-NMR characterizations were performed on a sample containing CHP407 at 1% w/v and CDs in order to cover the 50% of total EO domains (i.e., 3.8% w/v). These conditions for sample preparation are consistent with the ¹H-NMR characterization reported in figure 6, in which the formation of PPRs in solution has been investigated. The following figure 7a and b show the results obtained through NOESY characterization, while figure

7c and d contain the results obtained through ROESY characterization. However, under these specific conditions of analysis the expected interactions between PEO domains and CDs were neglectable. In fact, no correlation peaks were identified between chemical shifts around 3.6 ppm (EO) and 3.9-3.75 ppm (H3 and H5 internal protons of CDs). These observations further suggested and consolidated the fact that nontrivial interactions occurred between PEUs and CDs. In fact, it is likely that the self-assembly of PEU chains into micelles and wider aggregates can hinder the formation of PPRs in solution at low CD concentrations (i.e., 3.8% w/v). Hence, higher CD contents may be required to clearly appreciate PEU-CD interaction. However, in these conditions the precipitation of PPR-based channel-like crystals most likely occurs. In conclusion, because of the complexity of PEU polymer chains, an in-depth characterization analytically explaining the phenomena underpinning PPR formation was notably complex. Nonetheless, XRD measurements demonstrated that the physical nature of these supramolecular networks was based on PPR-based channel-like crystals, which turned out to be stabilized by the intermolecular interactions (e.g., hydrophobic interactions) that generally occur into PEU-based networks.

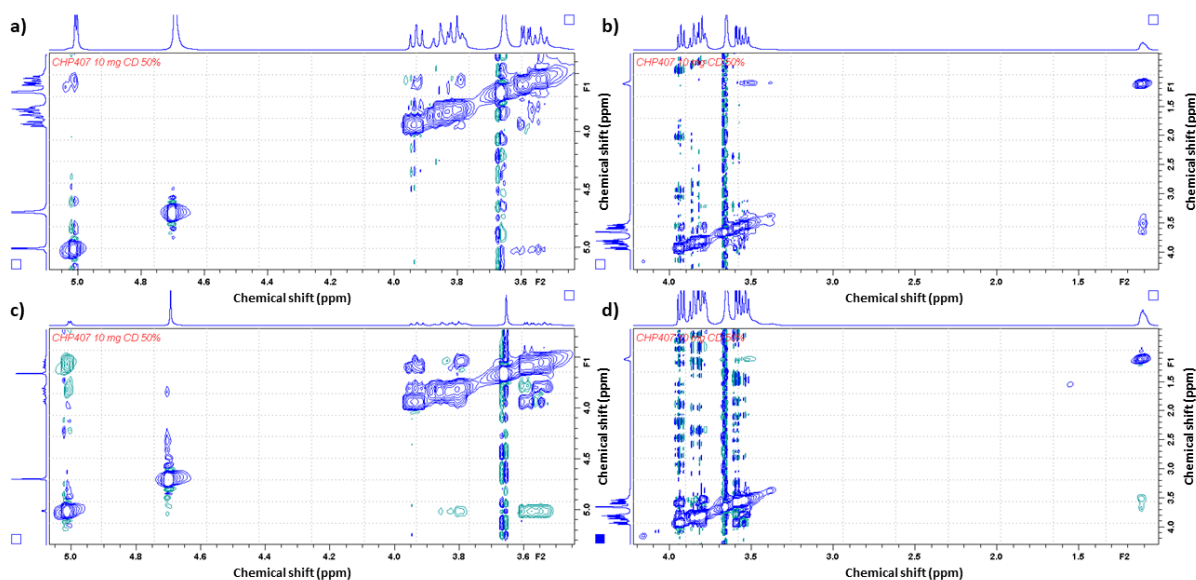


Figure 7 – a) and b) represent NOESY 2D spectra of CHP405 SM_50%, while c) and d) report ROESY ^1H - ^1H -NMR spectra of the same sample. No relevant cross-peaks were observed between the protons of the inner CD cavity (H3 and H5, between 4.1 and 3.8 ppm) and the signal related to EO domains (3.72 ppm), thus indicating that remarkably complex phenomena were involved in the formation of SM networks based on PPRs.

4.3 Supramolecular hydrogel characterization

4.3.1 SM hydrogel formulation and gelation kinetics

Hydrogel gelation ability and kinetics were evaluated on mixtures based on PEUs and CDs at various concentrations, as reported in table 1. Mixtures based on P407 were also produced as control samples. Gelation time test was performed at 25 and 37 °C with the aim to evaluate the role of temperature on gel development and its relationship with hydrogel formulation.

A complete gelation was observed for formulations composed of CDs at 9 and 10% w/v even at remarkably low PEU contents (i.e., 1 and 3% w/v). This observation resulted to be quite

interesting, as previous studies reported that aqueous PEU solutions at low polymer concentration (i.e., less than 5% w/v) did not exhibit a sol-to-gel transition even upon relevant thermal stimuli.⁵ This peculiarity thus demonstrated that CDs were the main factor to induce the physical gelation of PEU-CD mixtures characterized by low PEU concentrations. Moreover, this result represented an important achievement in terms of hydrogel design. Indeed, the development of hydrogels containing a low content of synthetic polymers could be considered an important feature to minimize the response of biological environments to material implantation, and to reduce the entity of potential side effects. Interestingly, hydrogel systems containing PEU up to 5% w/v showed significantly faster gelation kinetics at 25 °C with respect to 37 °C, regardless of CD content. These properties could be correlated with the already known thermo-responsiveness of PEU solutions. Indeed, PEUs in aqueous environments were characterized by the ability to form highly stable supramolecular structures based on micelles and their aggregates upon thermal stimulus. This arrangement of PEU chains into organized structures could work as a hindering factor to CD threading along PEU chains. In fact, samples containing PEUs and CDs were contradistinguished by a slower appearance of turbidity (indicative of the formation of PPR-based SM crystals) when incubated at 37 °C rather than 25 °C. Differently, formulations containing PEUs at higher concentrations (i.e., 7 and 9% w/v) were characterized by faster gelation times when incubated at 37 °C with respect to 25 °C. This opposite behavior could be correlated with a more relevant contribution of temperature-driven gelation in the overall sol-to-gel transition of the samples. Indeed, solutions characterized by a PEU content higher than a critical concentration (i.e., the critical gelation concentration (CGC), that was found to be around 5% w/v for solutions based on PEUs showing similar composition⁵) were able to undergo sol-to-gel transition upon thermal stimulus. Thence, a significant increase of physical crosslinking based on hydrophobic interactions represented the main factor for the gelation processes that characterized such formulations (i.e., PEU content of 7 and 9% w/v). In addition, these systems showed a slight formation of turbidity, thus indicating a weak self-assembly of SM structures. This evidence supported the hypothesis that such formulations exhibited unfavorable conditions for PPR formation (i.e., at 37 °C) and the main role in the gelation process was assigned to PEU thermo-responsiveness.

Gelation time generally decreased with increasing CD content in SM hydrogels as a consequence of the enhanced SM interactions that can occur at higher CD concentrations (i.e., 9 and 10% w/v). Indeed, solutions with CD concentrations of 7 and 8% w/v were characterized by remarkably slow gelation kinetics, which turned out to be typically over 3 days incubation. Differently, sample containing higher CD contents of 9 and 10% w/v showed fast turbidity appearance and hydrogel formation within few hours of incubation.

At equivalent PEU and CD contents, SM hydrogels based on CHP407 were characterized by faster gelation kinetics with respect to systems composed of NHP407. Some exceptions were observed for samples containing PEUs below 5% w/v and CDs at 9% w/v when incubated at 37 °C. This peculiar response could be correlated with the different molecular conformation of the PEUs. Indeed, CHP407 polymer chains were characterized by the absence of pendant groups, which instead were present in NHP407 (i.e., Boc domains). Hence, this conformational difference probably made CD threading and packing along CHP407 chains enhanced and faster even at 37 °C, which represented an adverse condition for the threading process due to the presence of micelles and micelle-based aggregates in the samples. Moreover, CHP407-based solutions were probably characterized by a slightly lower thermo-responsiveness and slower micelle formation

kinetics because of the higher chain rigidity due to the presence of aliphatic rings (i.e., cyclohexane) of CDM. Hence, at higher PEU contents (i.e., 7 and 9% w/v) CHP407 polymeric structures were facilitated in the interaction with CDs even at 37 °C, as demonstrated by the faster gelation kinetics of CHP407-based hydrogels with respect to NHP407-based ones. For example, in unfavorable conditions (i.e., 37 °C), CHP407 7% - CD 9% underwent sol-gel transition in 12 minutes, while NHP407 7% - CD 9% sample required 33 minutes of incubation. These observations were in complete accordance with the higher yield of SM crystalline matter obtained from CHP407 SM_{100%} ($58 \pm 0.5\%$) with respect to NHP407 SM_{100%} ($30 \pm 0.5\%$), as previously discussed. Differently, NHP407-based hydrogels showed faster gelation kinetics at 37 °C at PEU concentration below 5% w/v and CD content at 9% w/v. No simple explanation can be given to such behavior, which could be probably ascribed to a particular balance between PEU/CD mass ratio and overall PEU concentration, as well as to hydrophobicity and chain rigidity. In such adverse environment for PPR formation (i.e., at 37 °C), better conditions for gelation could probably occur in NHP407-based systems due to a likely higher chain mobility with respect to those composed of CHP407.

At polymeric content below 5% w/v, P407-based solutions were characterized by faster gelation with respect to PEU-based formulations at 37 °C. This behavior could be ascribed to the higher molar mass and molecular complexity of PEUs compared to native P407, thus inducing a delay in the overall SM gelation process. These results are in accordance with the marked thermo-responsiveness of solutions based on PEUs when compared to systems composed of P407,⁵ since the formation of highly stable micelle-based aggregates could hinder and retard PPR formation and hence gelation process based on SM crystals. An opposite response was observed at 37 °C and higher polymer contents (i.e., 7 and 9% w/v). Indeed, PEU-based solutions were characterized by faster temperature-driven gelation kinetics due to a relevant increase of viscosity compared to P407-based ones. In this regard, CGC for P407-based aqueous systems was quantified around 18% w/v, which is *ca.* three-fold greater than CGC of solutions based on PEUs (i.e., *ca.* 6%).⁵

Differently, at a significantly lower temperature (i.e., 25 °C) than the critical gelation temperature of PEU solutions at 7 and 9% w/v concentration,⁵ systems based on P407 generally showed remarkably faster gelation processes with respect to formulations composed of PEUs. Nonetheless, in order to obtain highly stable P407-based SM systems with good mechanical response, high polymer concentrations are required (i.e., greater than 10% w/v), as demonstrated in previous works.^{12,18,19} Indeed, phase-separation phenomena were frequent in P407-based systems, while in PEU-based solutions the precipitation of SM crystals was quite rare. Only after prolonged incubation (i.e., up to 5 days) at 37 °C, hydrogels containing PEU at concentration between 5 and 9% w/v and CDs at 7% w/v were subjected to an evident precipitation of the SM crystalline phase. A different response was observed for PEU 1% - CD 8% samples, which did not undergo SM gelation and were characterized by phase-separation phenomena at both 25 and 37 °C.

Beyond the above-mentioned exceptions, most PEU-based SM samples that were characterized by sol-gel transition did not exhibit phase-separation phenomena up to 4 weeks incubation time at any investigated temperature (i.e., 25 or 37 °C).

Hereafter, SM gels were produced through incubation at 25 °C with the aim to design suitable protocols for hydrogel practical preparation in different scenarios and laboratories.

Table 1 – Gelation kinetics of the formulated SM hydrogels at different concentrations of synthetic polymers (CHP407, NHP407 and P407 at 1, 3, 5, 7 and 9% w/v) and CDs (7, 8, 9 and 10% w/v). ON: overnight gelation; x: non-gelling solutions; (*): phase separation occurrence within 5 days incubation.

T = 25 °C														
CHP407	CD 7%	CD 8%	CD 9%	CD 10%	NHP407	CD 7%	CD 8%	CD 9%	CD 10%	P407	CD 7%	CD 8%	CD 9%	CD 10%
1%	x	x (*)	24h	ON	1%	x	x (*)	24h	ON	1%	360'	360'	360'	360'
3%	x	4d	ON	4h30'	3%	x	4d	ON	4h30'	3%	110'	90'	65'	45'
5%	x	4d	ON	4h	5%	x	4d	ON	4h10'	5%	90'	60'	45'	45'
7%	x	4d	ON	3h40'	7%	x	4d	ON	3h50'	7%	90'	55'	45' (*)	40' (*)
9%	x	4d	ON	2h30'	9%	x	4d	ON	3h	9%	75' (*)	50' (*)	45' (*)	40' (*)
T = 37 °C														
CHP407	CD 7%	CD 8%	CD 9%	CD 10%	NHP407	CD 7%	CD 8%	CD 9%	CD 10%	P407	CD 7%	CD 8%	CD 9%	CD 10%
1%	x	x (*)	4d	ON	1%	x	x (*)	ON	ON	1%	ON	ON	ON	ON
3%	x	4d	4d	ON	3%	x	4d	ON	ON	3%	ON	ON	70'	70'
5%	x (*)	4d	4d	ON	5%	x (*)	4d	ON	ON	5%	ON	ON	60'	45'
7%	33' (*)	12'	12'	10'	7%	20' (*)	22'	33'	12'	7%	ON	160'	50'	25'
9%	12' (*)	7'	7'	6'	9%	16' (*)	16'	12'	7'	9%	ON	160'	45'	22'

4.3.2 Rheological characterization of SM hydrogels

Based on the results obtained from tube inverting test, a complete rheological characterization was performed on a selection of SM hydrogels consisting in PEU at 1, 5, 7 and 9% w/v concentration and CD content of 9 and 10% w/v. These formulations were selected for their relatively quick gelation kinetics.

Strain sweep tests were carried out to identify the region of viscoelastic linearity (LVE) of the hydrogels and investigate their mechanical resistance upon applied deformation. In the range of deformations within the LVE domain, all SM hydrogels exhibited constant mechanical properties (i.e., storage modulus G' and loss modulus G''), with G' that resulted higher than G'' , thus indicating that all hydrogels were in a “gel” condition at the imposed temperature of 37 °C and angular frequency (i.e., 1 rad s^{-1}). When a critical value of strain was reached (γ_L), the mechanical properties started to vary. In detail, G' initially decreased, indicating the occurrence of cracks into the hydrogel network, and then, upon the complete rupture of the sample, become lower than G'' , as typical of viscoelastic fluids. From a general perspective, superior mechanical properties were observed for samples based on PEUs at 1 and 5% w/v concentrations and CDs at 10% w/v with respect to those based on lower CD content (i.e., 9% w/v). Indeed, higher values of G' within the LVE domain (i.e., G'_{LVE}) were observed, as indicated in table 2. This behavior could be probably due to the development of a better assembled SM hydrogel network based on crystals of PPRs at low PEU content and higher CD concentrations. In these conditions, the interactions between CDs and PEUs were probably enhanced, as previously hypothesized from gelation time test results. The increment of PEU content within the hydrogels did not generally induce significant improvements in terms of mechanical properties and this feature was shared by both families of formulations containing CDs at 9 or 10% w/v concentration. This behavior was in accordance with previously discussed observations on tube inverting test results. Indeed, this response could represent another

confirmation that temperature-driven gelation plays the main role in the sol-gel transition of formulations at high PEU content, over the formation of SM structures based on PPRs. In fact, in these testing conditions, an interesting pyramidal trend was observed for G'_{LVE} values as a function of PEU content at a specific CD concentration (i.e., 9 or 10% w/v). This behavior suggested a reciprocal effect of PPR- or micelle- based gelation mechanisms. The former resulted to be predominant at low PEU concentrations (1 and 5% w/v), while the latter at higher PEU contents (7 and 9% w/v). γ_L values improved with increasing PEU concentration within the SM hydrogel systems. For example, for hydrogels based on CHP407 containing CDs at 10% concentration, γ_L increased from 0.7 to 7.3% with increasing PEU content from 1 to 9% w/v, thus indicating a toughening role of PEUs within the hydrogels. Hydrogel resistance to applied strains was comparable between systems based on CHP407 or NHP407 at equal concentrations (e.g., NHP407 1% - CD 10% and CHP407 1% - CD 10% showed γ_L of 0.4 and 0.7%, respectively). Simultaneously, a non-clear dependence of γ_L over CD concentration within SM hydrogels was observed (e.g., NHP407 5% - CD 9% and NHP407 5% - CD 10% were characterized by γ_L of 0.7 and 0.3%, respectively). In these terms, no significant differences were thus observed, but a partial embrittlement due to a relevant increment of hydrogel stiffness could be supposed.

Additionally, strain sweep tests were even performed to evaluate an eventual self-healing ability of the here-developed SM systems by repeating the test on the same hydrogel sample after a recovery of 15 minutes in quiescent state at 37 °C. Interestingly, a hydrogel network recovery greater than 80% of the initial G'_{LVE} was quantified for all the tested SM systems and no significant differences were observed between systems based on CHP407 and NHP407. To better clarify the self-healing behavior of these SM networks, a wide set of G' and G'' curves as a function of incremental strain for CHP407- and NHP407-based hydrogels is reported in figure 8, as obtained through measurements before and after network recovery (i.e., quiescent state for 15 minutes at 37 °C).

Table 2 – Storage (G'_{LVE}) and loss moduli (G''_{LVE}) within the LVE domain, and recovery (%) of G' (G' recovery after complete gel rupture and 15 minutes of recovery in quiescence at 37 °C), as obtained through strain sweep tests.

	G'_{LVE} (Pa)	G''_{LVE} (Pa)	G' recovery (%)		G'_{LVE} (Pa)	G''_{LVE} (Pa)	G' recovery (%)
NHP407 1% - CD 9%	665	50	90	CHP407 1% - CD 9%	1100	70	83
NHP407 1% - CD 10%	2300	150	94	CHP407 1% - CD 10%	2690	150	87
NHP407 5% - CD 9%	6840	1110	86	CHP407 5% - CD 9%	8670	1120	87
NHP407 5% - CD 10%	14320	1880	81	CHP407 5% - CD 10%	17580	3230	92
NHP407 7% - CD 9%	5520	1510	91	CHP407 7% - CD 9%	7700	2790	96
NHP407 7% - CD 10%	5170	1530	96	CHP407 7% - CD 10%	18750	3910	89
NHP407 9% - CD 9%	4400	2650	88	CHP407 9% - CD 9%	3000	1570	93
NHP407 9% - CD 10%	4890	2770	94	CHP407 9% - CD 10%	4400	2160	93

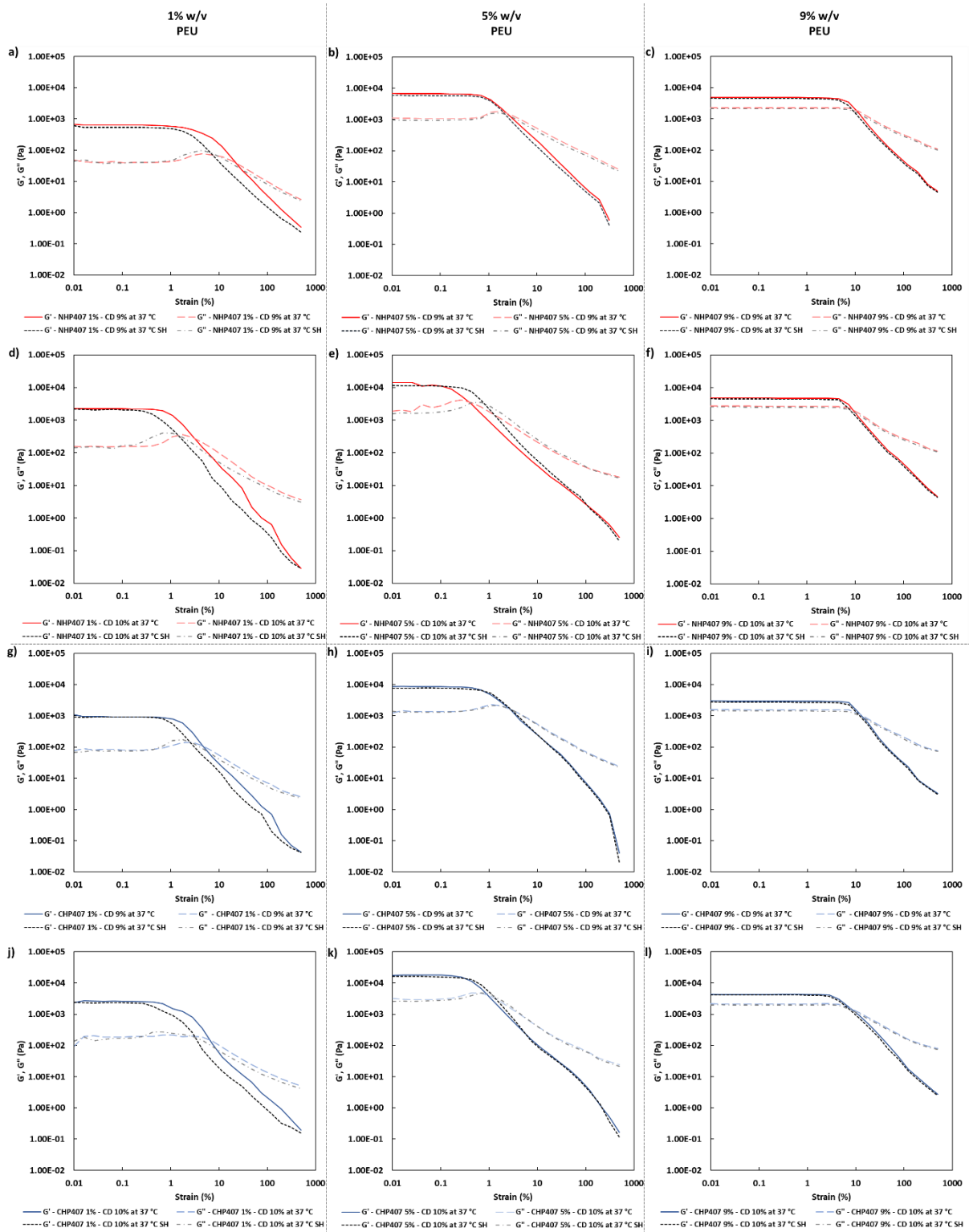


Figure 8 – Trends of G' (continuous lines) and G'' (long dashed lines) as a function of applied incremental strain for a) NHP407 1% - CD 9%, b) NHP407 5% - CD 9%, c) NHP407 9% - CD 9%, d) NHP407 1% - CD 10%, e) NHP407 5% - CD 10%, f) NHP407 9% - CD 10%, g) CHP407 1% - CD 9%, h) CHP407 5% - CD 9%, i) CHP407 9% - CD 9%, j) CHP407 1% - CD 10%, k) CHP407 5% - CD 10%, and l) CHP407 9% - CD 10%. Curves of NHP407-based hydrogels are represented in red, while those of CHP407 formulations are reported in blue. For each sample, the trends of G' (black short dashed lines) and G'' (dark grey dash-dotted lines) after complete rupture and 15 minutes of recovery in quiescence at 37 °C are also reported for comparative purposes with starting values.

The attainment of fully developed SM gels was also demonstrated through frequency sweep tests. As an emblematic example of the broad complete set of frequency sweep tests, figure 9 reports the entire characterization of hydrogels composed of CHP407 and CDs at 10% (i.e., CHP407 1% - CD 10%, CHP407 5% - CD 10% and CHP407 9% - CD 10%). Generally, all the formulations containing PEU concentrations below 7% w/v showed G' higher than G'' within the entire domain of investigated frequencies, suggesting that all the SM systems were characterized by a gel state within the range of tested temperatures (i.e., 25, 30 and 37 °C). Although a slight dependency of the moduli over frequency was found, SM systems containing a low amount of PEUs were characterized by a marked gel state, thus indicating the formation of a highly organized PPR-based network. Differently, in agreement with previous observations, hydrogel systems containing PEU at 9% w/v showed an evident dependency of G' and G'' over frequency due to the thermo-sensitive nature of the prevalent micelle-based network. As a matter of fact, this behavior was similar to the one observed for purely PEU-based thermo-sensitive hydrogels.⁵ Cross-over points between G' and G'' were found at 25 and 30 °C, thus indicating a biphasic nature of these systems, which were then simultaneously composed of both sol and gel domains. Differently, at 37 °C these hydrogels resulted to mainly be in gel phase, but the mechanical properties (i.e., G' and G'') showed a relevant dependence on frequency. Nevertheless, also SM domains based on PPRs relevantly contributed to the overall mechanical response. In fact, hydrogels containing PEUs at a concentration of 9% w/v showed G' values around 10^4 Pa at 100 rad s^{-1} and 37 °C, while for purely PEU-based hydrogels a concentration of synthetic polymer around 15% w/v was necessary to reach similar values.^{5,6} In agreement with strain sweep test results, mechanical properties improved by increasing CD concentration within the hydrogels at each temperature. As an example, at 100 rad s^{-1} and 37 °C NHP407 1% - CD 9% and NHP407 1% - CD 10% were characterized by G' values of 1150 and 3260 Pa, respectively. By comparing NHP407- with CHP407-based systems, hydrogels composed of CHP407 were characterized by better mechanical properties, in agreement with previous hypothesis on the enhanced formation of PPRs between CHP407 and CDs due to chemical composition of the polymer chains. Although the contribution of SM crystals based on PEUs and CDs resulted to be highly relevant for hydrogel development, a slight thermo-responsive behavior was observed for all the hydrogel formulations. In fact, an improvement of mechanical properties was observed when the temperature increased from 25 to 37 °C (e.g., G' at 100 rad s^{-1} of CHP407 1% - CD 10% improved from 1920 to 3970 Pa when the temperature increased from 25 to 37 °C). This thermo-responsiveness could be ascribed to the well-known behavior PEU amphiphilic chains, which maintained their ability to form hydrophobic interactions through their free domains with increasing temperature. Table 3 reports the G' values at 100 rad s^{-1} for the entire set of SM hydrogels as measured at 25, 30 and 37 °C. From a general perspective, formulations with intermediate PEU concentrations (i.e., 5 and 7% w/v) turned out to show the best mechanical properties, irrespective of CD content. This peculiarity could be probably due to a balanced and synergistic dual contribution of both PPR-based crystals and hydrophobic interactions among free PEU chains in gel network formation and development.

Table 3 – Storage modulus values of NHP407- and CHP407-based hydrogels measured at 100 rad s⁻¹ through frequency sweep tests performed at 25, 30 and 37 °C

	G' (Pa) at 100 rad/s - 25 °C	G' (Pa) at 100 rad/s - 30 °C	G' (Pa) at 100 rad/s - 37 °C		G' (Pa) at 100 rad/s - 25 °C	G' (Pa) at 100 rad/s - 30 °C	G' (Pa) at 100 rad/s - 37 °C
NHP407 1% - CD 9%	760	900	1150	CHP407 1% - CD 9%	985	985	1290
NHP407 1% - CD 10%	2080	2740	3260	CHP407 1% - CD 10%	1920	3430	3970
NHP407 5% - CD 9%	10240	12500	12500	CHP407 5% - CD 9%	8080	11590	11980
NHP407 5% - CD 10%	15230	18000	18000	CHP407 5% - CD 10%	14500	25260	26260
NHP407 7% - CD 9%	6080	11500	12370	CHP407 7% - CD 9%	11850	19940	21040
NHP407 7% - CD 10%	6900	11870	12620	CHP407 7% - CD 10%	18440	26300	25770
NHP407 9% - CD 9%	5040	11600	13820	CHP407 9% - CD 9%	1890	5970	7410
NHP407 9% - CD 10%	3110	8930	11100	CHP407 9% - CD 10%	2860	8900	11400

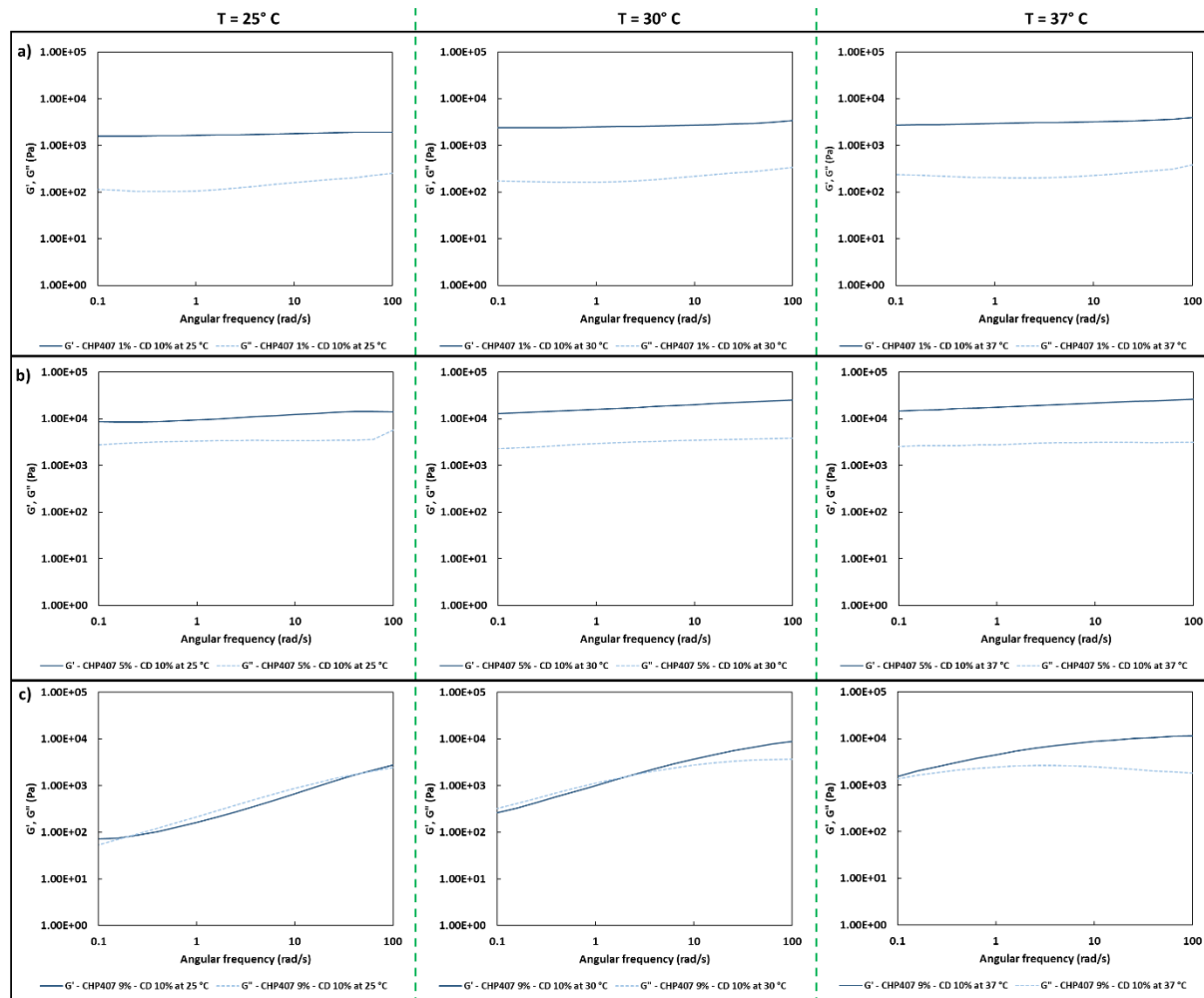


Figure 9 – G' (blue continuous lines) and G'' (light blue dashed lines) curves of a) CHP407 1% - CD 10%, b) CHP407 5% - CD 10%, and c) CHP407 9% - CD 10% as a function of angular frequency at 25, 30 and 37 °C.

Additionally, self-healing ability was evaluated through specific strain tests performed on SM hydrogels. The obtained results confirmed the ability of SM networks to restore their starting mechanical properties. Indeed, a minimum recovery of 80% of G' after complete network rupture at high strain (i.e., 100%) was observed at every cycle within 30 seconds of restoration at low strain (i.e., 0.1%). Table 4 reports the percentage of restored of G' (%) after 3 breakage cycles for the most representative formulations within the investigated PEU concentration range (i.e., 1, 5

and 9% w/v). Additionally, the trends of G' and G'' of the most representative SM hydrogels are reported in figure 10 as a function of time as measured through strain tests.

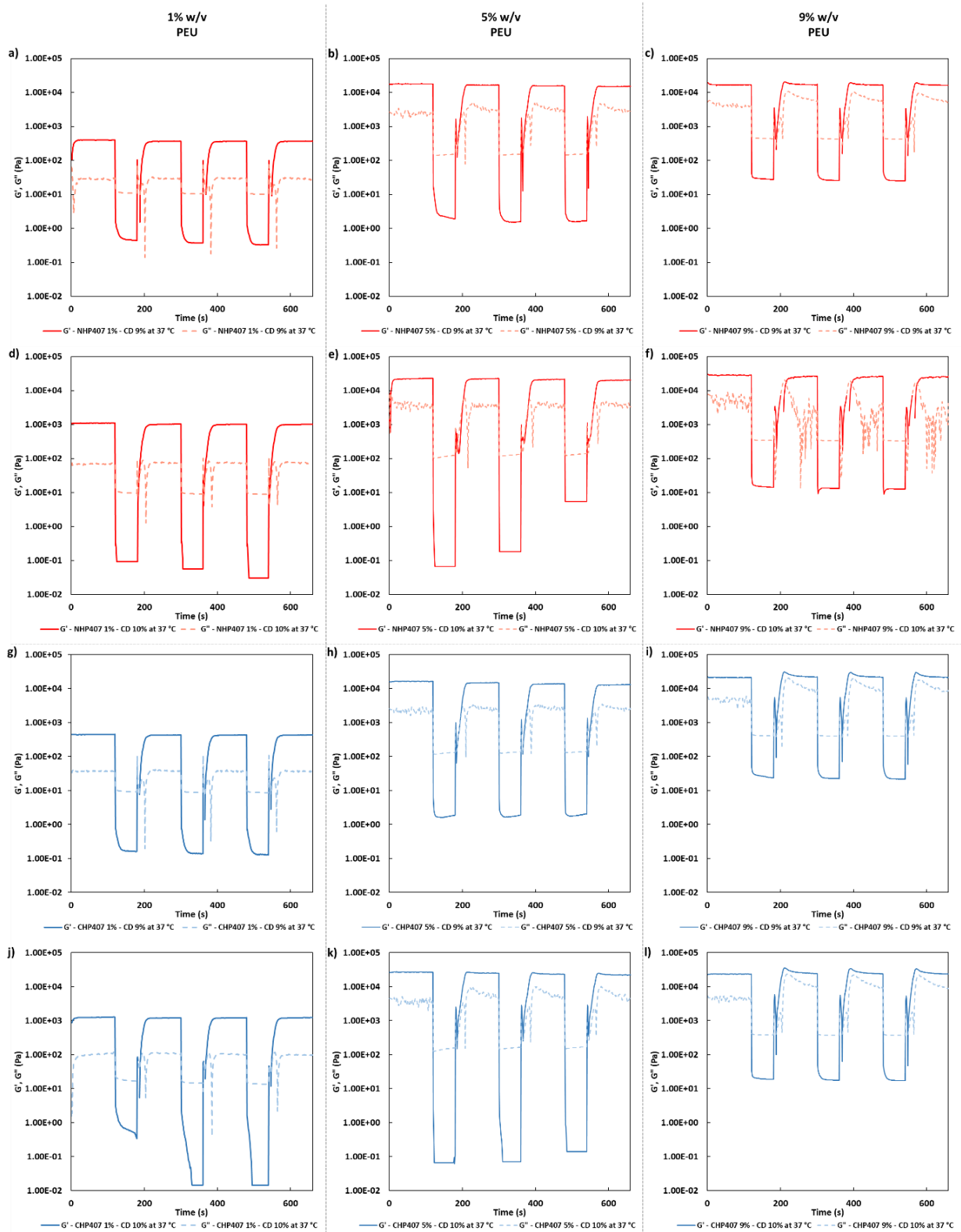


Figure 10 – Trends of G' (continuous lines) and G'' (long dashed lines) as a function of time upon low and high strains (i.e., 0.1 and 100%, respectively) application for a) NHP407 1% - CD 9%, b) NHP407 5% - CD 9%, c) NHP407 9% - CD 9%, d) NHP407 1% - CD 10%, e) NHP407 5% - CD 10%, f) NHP407 9% - CD 10%, g) CHP407 1% - CD 9%, h) CHP407 5% - CD 9%, i) CHP407 9% - CD 9%, j) CHP407 1% -

CD 10%, k) CHP407 5% - CD 10%, and l) CHP407 9% - CD 10%. G' and G'' trends for NHP407-based hydrogels are figured in red, while those of CHP407-based formulations are represented in blue.

An interesting response was observed for hydrogels containing PEUs at 9% concentration. Indeed, after each cycle of hydrogel rupture, G' trends indicated a hardening effect during the first 30 seconds of recovery phase at low strain (i.e., 0.1%). This response could be caused by a continuous adaptation of micellar-based networks as a consequence of applied deformations, in accordance with already published observations for purely PEU-based thermo-sensitive gels.^{5,6}

Table 4 – Percentage of recovered storage modulus (G'_{recovery}) after three rupture cycles with respect to starting G' values (i.e., average of recorded G' within the interval from 600 to 660 seconds of strain test).

	G'_{recovery} (%)		G'_{recovery} (%)
NHP407 1% - CD 9%	91	CHP407 1% - CD 9%	98
NHP407 1% - CD 10%	91	CHP407 1% - CD 10%	97
NHP407 5% - CD 9%	88	CHP407 5% - CD 9%	80
NHP407 5% - CD 10%	89	CHP407 5% - CD 10%	82
NHP407 9% - CD 9%	96	CHP407 9% - CD 9%	100
NHP407 9% - CD 10%	86	CHP407 9% - CD 10%	100

The evaluation of gelation kinetics and the characterization of mechanical properties of SM hydrogels evidenced the presence of three main categories of systems based on PEUs and CDs. In detail, low, medium and high PEU containing hydrogels were distinguished. The two boundary conditions were characterized by the predominant behavior determined by PPR structures (i.e., 1% w/v, low PEU containing hydrogels) and PEU-based thermo-responsive micellar aggregates (i.e., 9% w/v, high PEU containing hydrogels), while the condition in between represented a mixed behavior of both of them (i.e., 5% w/v, medium PEU containing hydrogels).

According to such findings, hydrogels with a PEU concentration of 1, 5, and 9% w/v were selected as representative of the above-mentioned categories of SM hydrogels (i.e., low, medium and high PEU content, respectively) for further investigations and characterizations in terms of responsiveness (swelling) and stability (dissolution) in aqueous environments.

4.3.3 Responsiveness and stability in aqueous environment

The determination of responsiveness and stability is essential when hydrogel systems are addressed to drug and/or gene delivery. Indeed, the evaluation of mass exchange that occurs between the external aqueous milieu and the hydrogel represents an important factor for the definition of the potential release kinetics of encapsulated drugs. Hence, swelling and dissolution response of SM hydrogels were evaluated in physiological-simulated conditions by incubating samples in contact with PBS (pH 7.4) at 37 °C. Interestingly, all SM hydrogels showed good stability in these conditions and concentration-dependent swelling and dissolution responses were observed. Indeed, as reported in figure 11, even the SM systems containing the lowest PEU concentration (1% w/v) showed the ability to maintain their shape and wet mass up to 5 days of

incubation in contact with PBS, while they were completely solubilized at the time step of 7 days. This behavior was deducible from weight loss trends. Indeed, although the wet mass was maintained almost constant and only slight de-swelling phenomena were quantified (maximum negative swelling values around -8%), the dry weight loss resulted to be relevant (greater than 50%). For these reasons, a significant release of mostly non-assembled and less stable components (i.e., free PEU molecules/aggregates and CDs) occurred during incubation in physiological-like conditions, as demonstrated by weight loss data. Thence, as the wet weight resulted to be almost constant, a concomitant and noteworthy absorption of fluids from external PBS-based aqueous environment was taking place. Similarly, even hydrogels containing PEU at 5% concentration were characterized by good responsiveness. Nonetheless, a lower stability was observed for these samples, which showed a significantly higher wet weight loss with respect to the samples at lower PEU content (i.e., 1% w/v). This datum suggested a prevalence of erosion and dissolution phenomena over fluid absorption. These results even indicated that SM gels designed at lower PEU/CD ratio were potentially able to form more stable networks due to an enhanced formation of SM structures composed of PPRs. Differently, SM hydrogels containing PEUs at 9% w/v showed a behavior similar to pure thermo-sensitive systems, in agreement with our previous hypotheses. In addition, such hydrogels showed the longest residence time in aqueous environment: after 7 days incubation, hydrogel samples were characterized by a dry weight loss around 50%. However, considering the relevant differences in terms of concentration, the dry weight loss of samples at 9% PEU concentration was comparable with that of hydrogels containing significantly lower PEU amounts (i.e., 1 and 5% w/v). This result suggested that higher PEU contents were correlated with an enhanced hydrogel network dissolution. Hence, although a dependence of dissolution behavior on PEU content have been identified, a non-trivial composition-related response was observed in contact with aqueous environment. In fact, systems containing PEUs at 1 and 9% w/v concentrations showed higher stability in wet conditions, thus suggesting a stabilizing contribution of the involved structures forming the hydrogel network (i.e., PPR- or micelle-based systems, respectively). Differently, hydrogels at medium PEU concentration (i.e., 5% w/v) exhibited a more relevant weight loss in wet conditions probably as a consequence of their hybrid nature between a fully PPR- or micelle-based network. The increment of CD concentration from 9 to 10% w/v resulted in a further stabilizing element leading to better organized SM networks, showing a more evident impact on samples based on PEU at 1 and 5% w/v concentrations.

Additionally, the determination of swelling ratio allowed a better understanding of the behavior of SM hydrogels when incubated in contact with watery environments. Indeed, this parameter considers the mutual contribution of water and polymer contents simultaneously and summarizes hydrogel network responsiveness when in contact with watery environments. As reported in figure 12, all formulations showed a marked responsiveness. Hydrogels containing PEUs at low concentration (1% w/v) were characterized by the highest values of swelling ratio. This result suggested that hydrogels containing PEU at 1% w/v concentration were not only more stable than SM networks with higher PEU amounts (i.e., 5 and 9% w/v), but they were also more responsive showing a more relevant mass exchange with the external milieu. Such behavior could be related to the enhanced formation of PPR-based SM structures at low PEU/CD mass ratio, in accordance with the previous hypothesis. Differently, hydrogels based on PEUs at higher concentrations (i.e., 5 and 9% w/v) showed less pronounced responsiveness in terms of swelling ratio and a

simultaneous less stability, as evident from PBS absorption and hydrogel weight loss data reported in figure 11. Thence, these results further confirmed the importance of finely modulating PEU/CD mass ratio to favor the formation of hydrogels with better responsiveness and superior stability.

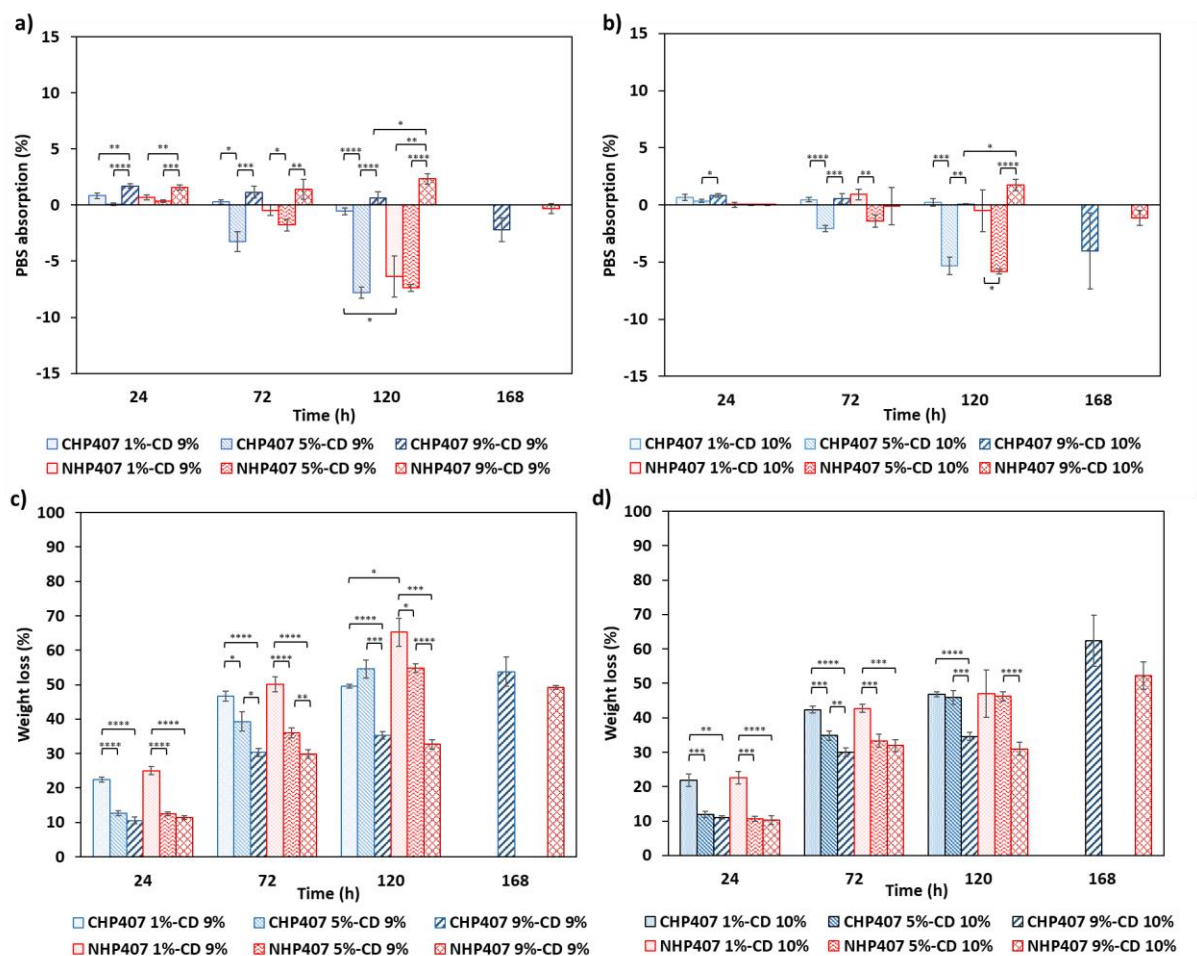


Figure 11 – Bar diagrams reporting the swelling (a and b figures related to CD content at 9 and 10% w/v, respectively) and weight loss (c and d figures related to CD content at 9 and 10% w/v, respectively) percentages for hydrogel systems based on CHP407 (blue) and NHP407 (red).

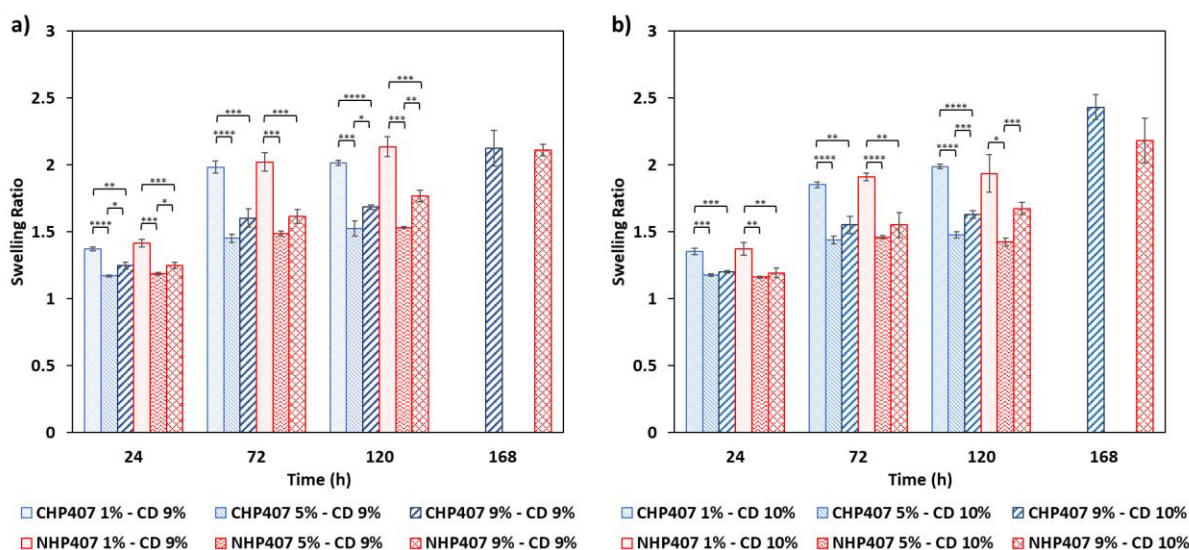


Figure 12 – Bar diagrams showing the swelling ratio (a and b figures related to CD content at 9 and 10% w/v, respectively) values of hydrogel systems based on CHP407 (blue) and NHP407 (red).

4.3.4 Cytotoxicity tests

SM hydrogel biocompatibility was evaluated on sample extracts according to ISO rules (figure 13). The evaluation of cytotoxicity suggested that the content of CDs did not represent an important parameter negatively affecting the biocompatibility of SM hydrogels. Instead, SM hydrogel cytotoxicity resulted to be dependent on the concentration of PEUs. In fact, hydrogel formulations containing PEUs at 1 and 5% concentrations did not show any cytotoxic effect. In that regard, the slight improvement in cell viability for the formulations containing PEUs at 1% w/v could be due to the presence of a relevant amount of free CDs within hydrogel extracts.^{20,21} Moreover, this observation can be considered intrinsically correlated to resazurine-based tests, which provide a combined information between cell number and activity. Differently, systems composed of PEUs at 9% w/v concentration (NHP407 9% - CD 9% and CHP407 9% - CD 9%) showed slight cytotoxicity (i.e., around 55% cell viability). As discussed above, this response could find explanation in the nature of SM systems containing a high PEU content (i.e., 9% w/v) that exhibited an unstable hydrogel network resulting from a not proper PEU/CD mass ratio. In fact, as previously hypothesized, SM systems containing PEU at high concentration (9% w/v) could be associated to a behavior characterized by a prevalent thermo-sensitivity that partially hindered the formation of PPR-based SM crystals. In addition, as demonstrated through rheological tests, these samples were characterized by a non-fully developed gel state (G' strongly depended over frequency even at 37 °C) suggesting that CDs did not adequately stabilize the polymeric network of these formulations. Hence, these properties could play a fundamental role in terms of stability of less stable and potentially cytotoxic entities (i.e., PEU micelle/aggregates²²) in conditions in which hydrogel dynamic response is enhanced, as indicated by the ISO 10993 guidelines. For these reasons, the observed cytotoxicity could be originated by the relatively higher weight loss with respect to samples containing lower PEU amounts (i.e., 1 and 5% w/v concentration). Nevertheless, it has been proved that thermo-sensitive hydrogels purely based on PEUs at higher concentration compared to the here-developed systems (e.g., 15% w/v) did not show any cytotoxic response. Indeed, the enhanced thermo-responsiveness due to higher PEU

content led to hydrogels characterized by high stability and low dissolution rates in watery environments.⁵ Hence, even a probable contribution in cytotoxicity due a residual presence of the catalyst used for PEU synthesis (i.e., DBTDL) could be excluded.

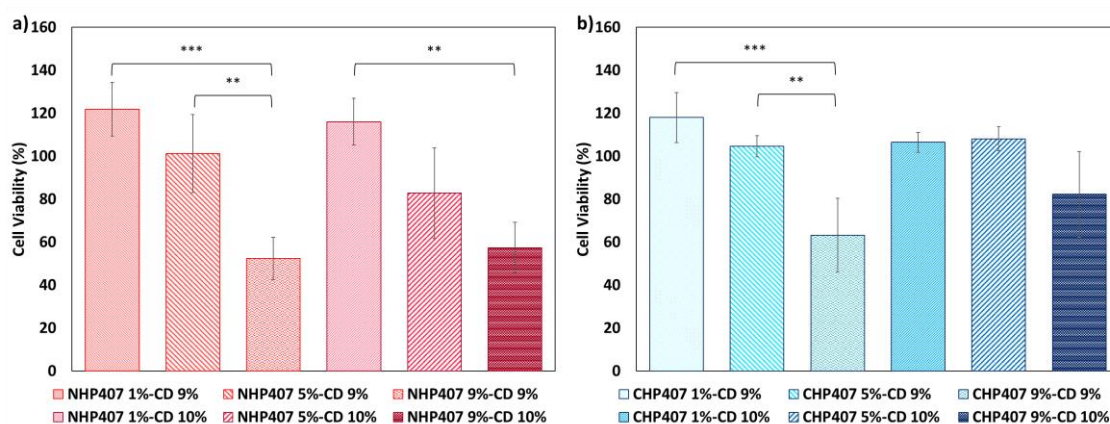


Figure 13 – Bar diagrams reporting cytotoxicity evaluation according to ISO 10993 guidelines for a) NHP407- (red) and b) CHP407-based (blue) hydrogels.

On the basis of these observations and considerations, the hydrogels containing PEUs at the concentration of 9% w/v were no longer investigated and characterized in this work. Moreover, the SM systems containing CD at 10% w/v concentration were selected for further investigations for their faster gelation, better stability and superior mechanical properties. In addition, a higher amount of CDs within SM hydrogels potentially allows the design of systems able to encapsulate higher drug contents, reducing the potential risk of interference with the development of PPR-based SM networks.

4.3.5 Evaluation of the release kinetics of FD4 model molecule from SM hydrogels

The selection of FD4 as model molecule to perform studies on release kinetics was driven by its molecular properties. Indeed, it represents an intermediate condition between small drugs (e.g., antibiotics and anti-inflammatory molecules) and biomacromolecules (e.g., peptide sequences, growth factors and proteins). Figure 14 shows the effects of CD presence into the samples (at concentration ranging from 0 to 10% w/v) on the trend of FD4 calibration curves. Indeed, some interactions between CDs and FD4 aromatic domains cannot be completely excluded and some variations in terms of FD4 spectrometric response could be envisaged. Nonetheless, the contribution of CDs was not relevant within the range of considered CD concentrations (i.e., up to 10% w/v). Moreover, the spectrometric properties of FD4/CD-based solutions were comparable within a wide range of FD4 concentrations (i.e., up to 0.6 mg ml⁻¹). Thence, even considering the relevant stability of the SM hydrogels observed from the previously discussed swelling and stability tests, the calibration curve obtained from standards with CD content at 0% w/v was selected for the quantification of released FD4. As reported in figure 15, all the investigated systems were characterized by the ability to release the 100% of theoretical payload within 4 days. Interestingly, the release of FD4 was concomitant with the progressive hydrogel dissolution in external milieu due to complete medium refreshes performed at each release medium collection. Additionally, the presence of FD4 could also interfere with the development of SM hydrogels

through the presence of aromatic pendant groups, which could attract CDs by means of hydrophobic interactions.

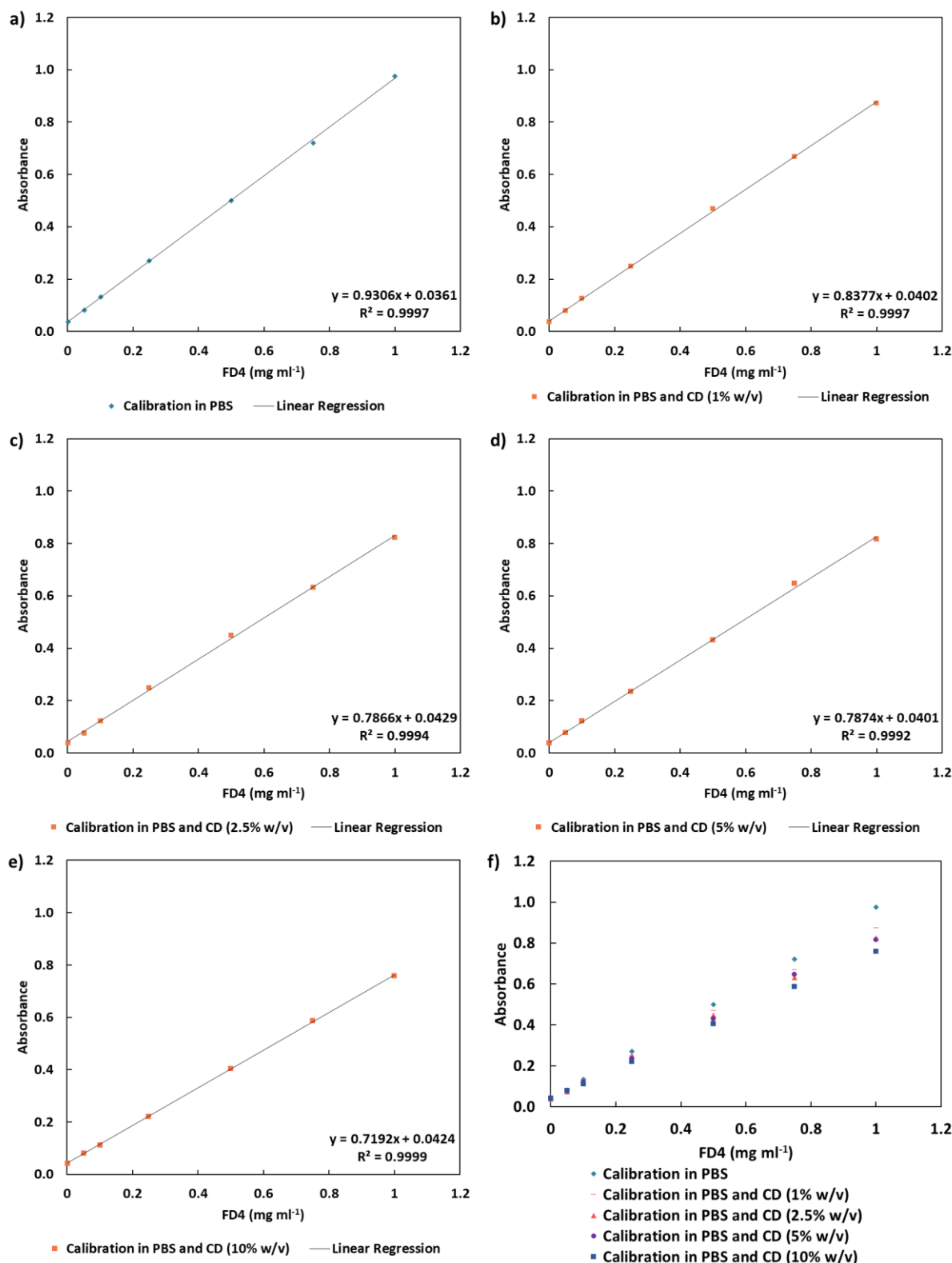


Figure 14 – Calibration curves of FD4 obtained using FD4 standard samples containing CDs at different concentrations: a) 0%, b) 1%, c) 2.5%, d) 5% and e) 10% w/v. The parameters obtained from linear regression are also reported. f) entire set of registered absorbance values highlighting the relevant data similarity within the FD4 range up to 0.5-0.6 mg ml⁻¹.

Moreover, although FD4 notably is a highly hydrophilic molecule (water solubility over 50 mg ml⁻¹), it was progressively released from hydrogels without any burst release. In fact, 20% of total payload was released within the first 6 hours of incubation. Systems based on different PEUs (i.e., NHP407 and CHP407) did not show significant differences in release profiles. SM samples at 1% w/v PEU concentration showed a faster FD4 release within the first 6 hours of observation with respect to hydrogel samples at 5% w/v PEU concentration. Then, the profiles become almost completely overlapped and hydrogels containing PEU at 5% w/v concentration sustained the release of FD4 for a longer period, probably due to their intrinsic higher density deriving from the higher PEU content. Interestingly, these results showed release kinetics comparable to those reported in other previous works for similar hydrogel systems designed at higher polymer concentrations (i.e., greater than 10% w/v).^{12,18,23–25} Finally, the here-designed PEUs demonstrated to be suitable for the development of stable hydrogel networks at low polymeric concentration (i.e., 1% w/v), without negatively affecting the overall physical properties.

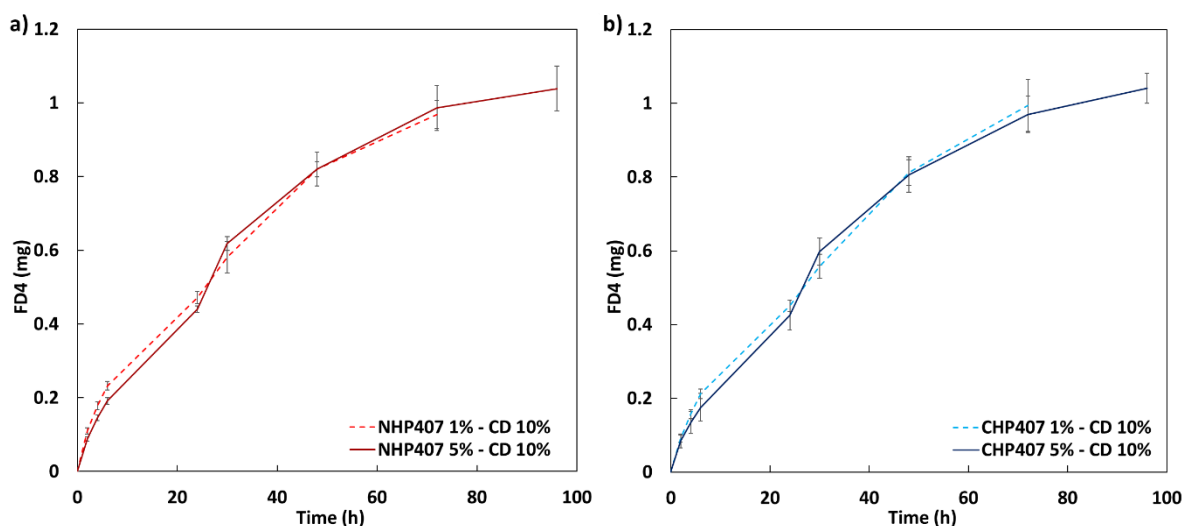


Figure 15 – Release profiles of FD4 from SM systems composed of NHP407 (a, red) and CHP407 (b, blue) at 1% (dashed lines) and 5% (continuous lines) w/v concentration and CD at 10% w/v content.

5. Conclusions

In the present Chapter, the suitability of newly synthesized amphiphilic PEUs as constituents of smart supramolecular hydrogels based on CDs has been demonstrated. An initial thorough physico-chemical characterization proved NHP407 and CHP407 capability to interact with CDs in solution forming PPRs. Their molecular complexity made notably difficult the determination of specific parameters, such as their constant associations with CDs. Nonetheless, the effects of self-assembly resulted in the clear formation of a crystalline matter, which was characterized by highly ordered PPR-based crystalline domains, as showed through XRD measurements. Thence, a wide library of SM hydrogels based on these PEUs was developed and characterized in physical and mechanical terms. Fast gelation kinetics and good SM network stability (i.e., absence of phase-separation phenomena) were observed for PEU-based hydrogels containing sufficient PEU and CD amounts (i.e., greater than 1 and 9% w/v, respectively). Rheological characterizations highlighted notable values of storage modulus even at low PEU content (i.e., greater than 1 kPa at 1% w/v PEU concentration) and self-healing behavior of all the SM hydrogels. In this scenario,

the balance between PEU and CD mass contents (i.e., PEU/CD mass ratio) turned out to be an important factor for the explanation of the different behaviors that were observed. Indeed, low PEU/CD ratios resulted in completely developed and highly stable hydrogel networks, while at higher ratios (i.e., higher PEU content) SM hydrogels were probably characterized by a lower PPR formation and crystallization yield due to PEU-based structures (i.e., micelles and their bigger aggregates) hindering PEU-CD interactions. In particular, SM hydrogels containing PEU at 9% w/v concentration in bi-distilled water were characterized by a predominant thermo-sensitive behavior resulting in non-fully developed and poorly stable gel networks. In fact, a slight cytotoxicity was observed for these SM gels which could be ascribed to their enhanced dissolution in watery media. Differently, the formulations designed at lower PEU concentrations (i.e., 1 and 5% w/v) generally resulted to be more stable and cytocompatible. Hence, such formulations were selected for preliminary release studies of FD4 (1 ml SM hydrogels containing FD4 at 1 mg ml^{-1} concentration in contact with PBS (1 ml) at $37 \text{ }^\circ\text{C}$), demonstrating the ability of the developed systems to allow a progressive and sustained release of their payload.

The entire set of these results established for the first time that even remarkably low concentrations of PEUs (i.e., less than 5% w/v) could form stable PPR-based hydrogels, as demonstrated through swelling and stability tests and preliminary release studies. For these reasons, further investigations were focused on the tunability of hydrogel properties by utilizing other solvents for hydrogel preparation (i.e., PBS instead of ddH₂O, *Chapter 2.3*). Moreover, relying on a solid and repeatable synthesis process, novel PEUs (e.g., composed of different macrodiols and/or exposing pendant functional groups, such as primary amines) were prepared in order to better understand the effects of their chemical and physical features on the formation of PEU-based PPRs as constituting units of SM networks (*Chapter 2.4*). As a result, new possibilities in the design of efficient drug-encapsulating hydrogels were investigated.

6. References

- (1) Yamaguchi, I.; Takenaka, Y.; Osakada, K.; Yamamoto, T. Preparation and Characterization of Polyurethane–Cyclodextrin Pseudopolyrotaxanes. *Macromolecules* **1999**, *32* (6), 2051–2054. <https://doi.org/10.1021/ma9805452>.
- (2) Hasan, E. A.; Cosgrove, T.; Round, A. N. Nanoscale Thin Film Ordering Produced by Channel Formation in the Inclusion Complex of α -Cyclodextrin with a Polyurethane Composed of Polyethylene Oxide and Hexamethylene. *Macromolecules* **2008**, *41* (4), 1393–1400. <https://doi.org/10.1021/ma071484n>.
- (3) Cheng, X.; Jin, Y.; Sun, T.; Qi, R.; Li, H.; Fan, W. An Injectable, Dual PH and Oxidation-Responsive Supramolecular Hydrogel for Controlled Dual Drug Delivery. *Colloids and Surfaces B: Biointerfaces* **2016**, *141*, 44–52. <https://doi.org/10.1016/j.colsurfb.2016.01.034>.
- (4) Cherng, J. Y.; Hou, T. Y.; Shih, M. F.; Talsma, H.; Hennink, W. E. Polyurethane-Based Drug Delivery Systems. *Int J Pharm* **2013**, *450* (1–2), 145–162. <https://doi.org/10.1016/j.ijpharm.2013.04.063>.
- (5) Boffito, M.; Gioffredi, E.; Chiono, V.; Calzone, S.; Ranzato, E.; Martinotti, S.; Ciardelli, G. Novel Polyurethane-Based Thermosensitive Hydrogels as Drug Release and Tissue Engineering Platforms: Design and *in Vitro* Characterization: Polyurethane-Based Thermosensitive Hydrogels. *Polym. Int.* **2016**, *65* (7), 756–769. <https://doi.org/10.1002/pi.5080>.
- (6) Pontremoli, C.; Boffito, M.; Fiorilli, S.; Laurano, R.; Torchio, A.; Bari, A.; Tonda-Turo, C.; Ciardelli, G.; Vitale-Brovarone, C. Hybrid Injectable Platforms for the *in Situ* Delivery of Therapeutic Ions from Mesoporous Glasses. *Chemical Engineering Journal* **2018**, *340*, 103–113. <https://doi.org/10.1016/j.cej.2018.01.073>.
- (7) Laurano, R.; Boffito, M.; Torchio, A.; Cassino, C.; Chiono, V.; Ciardelli, G. Plasma Treatment of Polymer Powder as an Effective Tool to Functionalize Polymers: Case Study Application on an Amphiphilic Polyurethane. *Polymers* **2019**, *11* (12), 2109. <https://doi.org/10.3390/polym11122109>.
- (8) Wu, L.; Yu, L.; Fu, X.; Li, Z. Injectable Supramolecular Hydrogels via Inclusion Complexation of MPEG-Grafted Copolyglutamate with α -Cyclodextrin. *Chin J Polym Sci* **2015**, *33* (8), 1140–1149. <https://doi.org/10.1007/s10118-015-1640-0>.
- (9) Trathnigg, B. Size-Exclusion Chromatography of Polymers. In *Encyclopedia of Analytical Chemistry*; Meyers, R. A., Ed.; John Wiley & Sons, Ltd: Chichester, UK, 2006; p a2032. <https://doi.org/10.1002/9780470027318.a2032>.
- (10) Fakhari, A.; Corcoran, M.; Schwarz, A. Thermogelling Properties of Purified Poloxamer 407. *Heliyon* **2017**, *3* (8), e00390. <https://doi.org/10.1016/j.heliyon.2017.e00390>.
- (11) Chung, J. W.; Kang, T. J.; Kwak, S.-Y. Supramolecular Self-Assembly of Architecturally Variant α -Cyclodextrin Inclusion Complexes as Building Blocks of Hexagonally Aligned Microfibrils. *Macromolecules* **2007**, *40* (12), 4225–4234. <https://doi.org/10.1021/ma0625105>.
- (12) Simões, S. M. N.; Veiga, F.; Torres-Labandeira, J. J.; Ribeiro, A. C. F.; Sandez-Macho, M. I.; Concheiro, A.; Alvarez-Lorenzo, C. Syringeable Pluronic– α -Cyclodextrin Supramolecular Gels for Sustained Delivery of Vancomycin. *European Journal of Pharmaceutics and Biopharmaceutics* **2012**, *80* (1), 103–112. <https://doi.org/10.1016/j.ejpb.2011.09.017>.
- (13) Dang, Z.; Xin Song, L.; Qing Guo, X.; Yun Du, F.; Yang, J.; Yang, J. Applications of Powder X-Ray Diffraction to Inclusion Complexes of Cyclodextrins. *COC* **2011**, *15* (6), 848–861. <https://doi.org/10.2174/138527211794518899>.

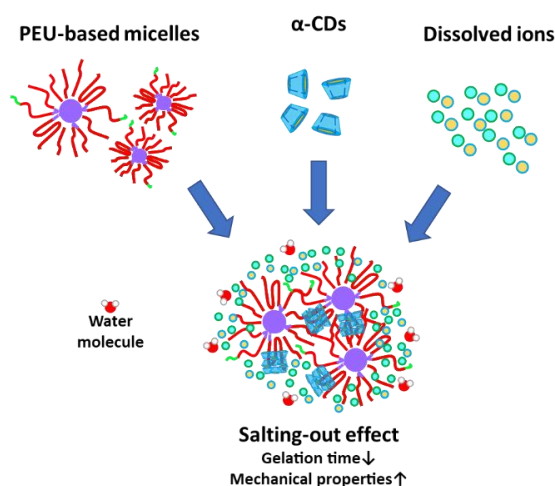
- (14) Wang, J.; Li, L.; Zhu, Y.; Liu, P.; Guo, X. Hydrogels Assembled by Inclusion Complexation of Poly(Ethylene Glycol) with Alpha-Cyclodextrin. *Asia-Pacific Jnl of Chem. Eng* **2009**, *4* (5), 544–550. <https://doi.org/10.1002/apj.280>.
- (15) Huang, L.; Allen, E.; Tonelli, A. E. Study of the Inclusion Compounds Formed between α -Cyclodextrin and High Molecular Weight Poly(Ethylene Oxide) and Poly(ϵ -Caprolactone). *Polymer* **1998**, *39* (20), 4857–4865. [https://doi.org/10.1016/S0032-3861\(97\)00568-5](https://doi.org/10.1016/S0032-3861(97)00568-5).
- (16) Lazzara, G.; Milioto, S.; Muratore, N. Solubilization of an Organic Solute in Aqueous Solutions of Unimeric Block Copolymers and Their Mixtures with Monomeric Surfactant: Volume, Surface Tension, Differential Scanning Calorimetry, Viscosity, and Fluorescence Spectroscopy Studies. *J. Phys. Chem. B* **2008**, *112* (18), 5616–5625. <https://doi.org/10.1021/jp712126j>.
- (17) Xie, D. M.; Yang, K. S.; Sun, W. X. Formation and Characterization of Polylactide and β -Cyclodextrin Inclusion Complex. *Current Applied Physics* **2007**, *7*, e15–e18. <https://doi.org/10.1016/j.cap.2006.11.006>.
- (18) Li, J.; Li, X.; Ni, X.; Wang, X.; Li, H.; Leong, K. W. Self-Assembled Supramolecular Hydrogels Formed by Biodegradable PEO–PHB–PEO Triblock Copolymers and α -Cyclodextrin for Controlled Drug Delivery. *Biomaterials* **2006**, *27* (22), 4132–4140. <https://doi.org/10.1016/j.biomaterials.2006.03.025>.
- (19) Pradal, C.; Jack, K. S.; Grøndahl, L.; Cooper-White, J. J. Gelation Kinetics and Viscoelastic Properties of Pluronic and α -Cyclodextrin-Based Pseudopolyrotaxane Hydrogels. *Biomacromolecules* **2013**, *14* (10), 3780–3792. <https://doi.org/10.1021/bm401168h>.
- (20) Róka, E.; Ujhelyi, Z.; Deli, M.; Bocsik, A.; Fenyvesi, É.; Szente, L.; Fenyvesi, F.; Vecsernyés, M.; Váradi, J.; Fehér, P.; Gesztelyi, R.; Félix, C.; Perret, F.; Bácskay, I. Evaluation of the Cytotoxicity of α -Cyclodextrin Derivatives on the Caco-2 Cell Line and Human Erythrocytes. *Molecules* **2015**, *20* (11), 20269–20285. <https://doi.org/10.3390/molecules201119694>.
- (21) Szente, L.; Singhal, A.; Domokos, A.; Song, B. Cyclodextrins: Assessing the Impact of Cavity Size, Occupancy, and Substitutions on Cytotoxicity and Cholesterol Homeostasis. *Molecules* **2018**, *23* (5). <https://doi.org/10.3390/molecules23051228>.
- (22) Budkina, O. A.; Demina, T. V.; Dorodnykh, T. Yu.; Melik-Nubarov, N. S.; Grozdova, I. D. Cytotoxicity of Nonionic Amphiphilic Copolymers. *Polym. Sci. Ser. A* **2012**, *54* (9), 707–717. <https://doi.org/10.1134/S0965545X12080020>.
- (23) Poudel, A. J.; He, F.; Huang, L.; Xiao, L.; Yang, G. Supramolecular Hydrogels Based on Poly(Ethylene Glycol)-Poly(Lactic Acid) Block Copolymer Micelles and α -Cyclodextrin for Potential Injectable Drug Delivery System. *Carbohydrate Polymers* **2018**, *194*, 69–79. <https://doi.org/10.1016/j.carbpol.2018.04.035>.
- (24) Xu, S.; Yin, L.; Xiang, Y.; Deng, H.; Deng, L.; Fan, H.; Tang, H.; Zhang, J.; Dong, A. Supramolecular Hydrogel from Nanoparticles and Cyclodextrins for Local and Sustained Nanoparticle Delivery. *Macromol. Biosci.* **2016**, *16* (8), 1188–1199. <https://doi.org/10.1002/mabi.201600076>.
- (25) Li, J. Self-Assembled Supramolecular Hydrogels Based on Polymer–Cyclodextrin Inclusion Complexes for Drug Delivery. *NPG Asia Mater* **2010**, *2* (3), 112–118. <https://doi.org/10.1038/asiamat.2010.84>.

Section 2 – Chapter 2.3 – Investigation on hydrogel formulation, properties, and responsiveness in different aqueous media

1. Abstract

The watery environment in which SM hydrogels are developed represents an important parameter for the fine tuning and engineering of their final properties. For this reason, in the present Chapter CHP407 and NHP407 poly(ether urethane)s were investigated as forming materials of SM hydrogels in phosphate buffered saline (PBS, pH 7.4) at low PEU contents (1 and 5% w/v) and 10% w/v CD concentration. These newly designed SM hydrogels were then compared with similar systems formulated in double distilled water (ddH₂O) and already characterized in the previous Chapter (*Chapter 2.2*). Salting-out effects were observed through the qualitative evaluation of gelation kinetics in isothermal conditions (i.e., 25 °C). In this regard, gelation time resulted to be significantly reduced for PBS-based samples with respect to ddH₂O-based ones. Rheological characterization highlighted that the use of PBS induced a further improvement by increasing the storage modulus of SM hydrogels containing PEUs at 1% w/v concentration, while no significant differences were observed for samples composed of PEUs at 5% w/v concentration. Self-healing behavior resulted to be independent from the presence of ions in solutions and relevant values of mechanical properties recovery (over 83% recovery in storage modulus) were observed. The responsiveness and stability of SM hydrogels were evaluated through swelling and stability tests, revealing that the systems prepared in bi-distilled water were characterized by an initial higher responsiveness and dissolution (within 24 hours incubation at 37 °C in contact with PBS). Nonetheless, for longer incubation time (i.e., 120 hours) no significant differences were observed between samples prepared in either ddH₂O or PBS, suggesting a progressive diffusion of ions into SM hydrogels based on ddH₂O from the external environment and a concomitant occurrence of a late salting-out effect over time. Hence, in this chapter the huge versatility and potential of PEU-based SM networks as remarkably tunable hydrogel devices were further proved, opening the way to the possibility to finely modulate their residence time and payload release kinetics according to therapeutic requirements.

Graphical Abstract



2. Introduction

Nowadays it is well known that the behavior of thermo-sensitive polymers is also dependent on other and various external factors in addition to temperature. Indeed, although temperature represents the most important variable on phase transition of amphiphilic polymer-based solutions, other stimuli can act on hydrogel networks and modulate their thermal and mechanical properties.¹ An important reference in this regard is represented by the Hofmeister series, which describes the specific interactions that occur between ions and natural or synthetic polymers.² Generally, a superior and pronounced effect has been observed for anions with respect to cations. The anionic species can be in fact classified into specific series, referring to a set of physical parameters that can influence the overall properties of solubilized macromolecules. One of the most important factors is the effect on water solubility. Indeed, two opposite ion actions can be found in solutions containing natural or synthetic macromolecules: the salting-in and the salting-out effects. The former induces a general increase in solubility, while the latter causes a decrease in solubility depending on the size, charge, and hydration parameters of the involved ions. As an example, small anions, such as chloride anion (Cl^-), show enhanced hydration in water and induce a salting-out effect resulting in the dehydration of polymeric domains. An opposite behavior is observed in the presence of perchlorate anion (ClO_4^-), which is able to induce salting-in effects, thus increasing the solubility of involved macromolecules. The effects of these ions have been investigated in the literature even in terms of property modulation of polymer-based hydrogels. For instance, Khamari and co-workers evaluated the specific ion effects of chloride and perchlorate ions on hydrogels based on Poloxamer® 407.³ The authors observed that the addition of salts to P407-based solutions influenced aggregation and gelation ability of the involved polymeric structures, as observed even for other triblock co-polymers.^{4,5}

Additionally, it has been demonstrated that the presence of salts can affect the formation of poly(pseudo)rotaxanes in watery environments containing PEG/PEO- and PPG-based polymers and cyclodextrins (α -, β - and γ -CDs).⁶ Indeed, from a general perspective, the process of threading of CDs along polymer chains depends on the interactions occurring between the hydrophobic cavities of CDs and the repeating groups of the involved polymers. These interactions are strongly related to the concurrent presence of water molecules, which compose the polar solvent that is necessary for the self-assembly process. Moreover, the formation of hydrogen bonds between adjacent cyclodextrins that are packed onto polymer chains induces a further expulsion of water molecules. In this scenario, the concurrent presence of salts can significantly affect the interactions occurring among the involved entities, since chemical and thermodynamic properties (i.e., solubility, hydration energy and surface tension) strongly depend on the kind and quantity of involved ions.

Thence, the use of electrolytes in solutions can represent an effective strategy to improve gelation and mechanical properties of hydrogel systems based on supramolecular networks composed of cyclodextrins and amphiphilic polymers, such as the PEU-based SM hydrogels designed and characterized in the previous Chapter. In addition, the use of saline solutions also allows the formulation of systems in potentially isotonic or buffered conditions with respect to external biological environments. In this Chapter, the role of salts in the formation and responsiveness of PEU-based SM systems was evaluated using Phosphate Buffered Saline (PBS, pH 7.4) to develop SM hydrogels based on NHP407 or CHP407 and CDs (PEU at 1 and 5% w/v concentration and CDs at 10% w/v concentration). Comparative studies between purely water- and PBS-based

systems were initially performed through the qualitative evaluation of gelation kinetics in isothermal conditions (i.e., at 25 °C). Additionally, the effects of salts on hydrogel mechanical properties were assessed through rheological characterizations. Finally, swelling and stability tests (at 37 °C) were performed on hydrogels based on ddH₂O or PBS solution in contact with pure PBS or PBS added with a hydrophobic antimycotic molecule (i.e., Amphotericin B) with the aim to also observe potential effects of lipophilic species in the external environments of hydrogel behavior in watery media.

3. Materials and Methods

3.1 Materials

In this study, NHP407 and CHP407 PEUs were synthesized as reported before in *Section 2 – Chapter 2.2 – Materials and methods – Synthesis of poly(ether urethane)s*. Phosphate buffered saline (PBS, disodium hydrogen phosphate and potassium dihydrogen phosphate at 0.01 M, potassium chloride 0.0027 M and sodium chloride at 0.137 M concentrations, pH 7.4 at 25 °C) and amphotericin B were purchased from Sigma Aldrich (Milan, Italy). α -CDs (from now on abbreviated with the acronym “CDs”) were obtained from TCI Chemicals Europe (Zwijndrecht, Belgium).

3.2 Preparation of SM hydrogels

SM hydrogels based on PEUs (i.e., NHP407 and CHP407) and CDs were prepared according to the protocol reported in *Section 2 – Chapter 2.2 – Materials and methods – Preparation of SM hydrogels* with slight modifications. Briefly, PEU-based hydrogels were prepared utilizing ddH₂O or PBS as solvents. Then, hydrogel SM gelation was carried out in isothermal conditions (i.e., at 25 °C). SM systems will be identified with the acronyms PEU X% - CD Y% H₂O and PEU X% - CD Y% PBS (X and Y indicate PEU and CD contents) for ddH₂O- and PBS-based networks, respectively.

3.4 Qualitative evaluation of gelation time in isothermal conditions

Gelation time evaluation of SM systems prepared in ddH₂O or PBS was carried out as indicated in *Section 2 – Chapter 2.2 – Materials and methods – Qualitative evaluation of gelation time in isothermal conditions*.

3.5 Rheological characterization

Rheological characterizations were performed on SM hydrogel systems based on ddH₂O and PBS as indicated in *Section 2 – Chapter 2.2 – Materials and methods – Rheological characterization*.

3.6 Swelling and stability test in physiological like conditions

Swelling and stability tests were performed on ddH₂O- and PBS-based SM hydrogel systems as indicated in *Section 2 – Chapter 2.2 – Materials and methods – Swelling and stability in physiological-like conditions* with slight modifications. SM hydrogels (1 ml) were prepared in Bijou sample containers (7 ml capacity and an inner diameter of 17 mm) and their swelling and stability were evaluated through incubation at 37 °C in contact with PBS (1 ml, pH 7.4) or PBS added with amphotericin B (1 ml, 2.5 µg ml⁻¹ amphotericin B concentration) previously equilibrated at 37 °C. Fluid absorption (%), Weight loss (%) and swelling ratio were calculated at different time steps (i.e., 24h and 5 days incubation) through equations 1, 2 and 3 reported in *Section 2 – Chapter 2.2 – Materials and methods – Swelling and stability in physiological-like conditions*. Analyses were conducted in quintuplicate and results are reported as mean ± standard deviation.

3.7 Statistical analysis

Statistical analysis was conducted as indicated in *Section 2 – Chapter 2.2 – Materials and methods – Statistical analysis*.

4. Results and discussion

4.1 Gelation time evaluation

Gelation time evaluation was conducted to assess the effects of dissolved ions on the overall gelation process of SM hydrogels. As reported in table 1, SM hydrogel systems containing PEUs at 5% w/v concentration in PBS were characterized by significantly faster gelation kinetics compared to similar samples prepared in ddH₂O. As an example, the gelation time of CHP407 5% - CD 10% PBS resulted to be around 1 hour and 30 minutes, while the same formulation prepared in pure water (i.e., ddH₂O) formed a stable and static hydrogel network after 4 hours incubation in the same isothermal conditions (i.e., at 25 °C). Additionally, CHP407-based SM hydrogels maintained their tendency to more quickly complete the sol-to-gel transition compared to NHP407-based ones. In addition, differences in gelation time between NHP407 and CHP407 become more relevant when hydrogels were prepared in PBS instead of ddH₂O. In fact, the gelation time of NHP407 5% - CD 10% PBS formulation resulted to be 1 hour longer than for CHP407 5% - CD 10% PBS, while the difference for the same samples formulated in pure water resulted to be around 10 minutes. Such different response of the two PEUs could be correlated with their different chemical composition. Indeed, pendant Boc groups present in NHP407 backbone could represent an additional variable influencing the interaction of the polymer chains with water molecules and ions. More in detail, they probably hindered or at least delayed the overall stabilization of NHP407 network in PBS (i.e., salting-out effect) with respect to CHP407-based systems.

Table 1 – Gelation time of NHP407- and CHP407-based hydrogels formulated in PBS and ddH₂O. ON: overnight gelation.

	Gelation Time		Gelation Time	
NHP407 1% - CD 10% H ₂ O	ON	CHP407 1% - CD 10% H ₂ O	ON	ON
NHP407 1% - CD 10% PBS	ON	CHP407 1% - CD 10% PBS	ON	ON
NHP407 5% - CD 10% H ₂ O	4h10'	CHP407 5% - CD 10% H ₂ O	4h	4h
NHP407 5% - CD 10% PBS	2h30'	CHP407 5% - CD 10% PBS	1h30'	1h30'

4.2 Rheological characterization

A complete rheological characterization was performed on CHP407-based samples with the aim to assess the general influences of the salting-out effect over PEU-based SM networks. Strain sweep test were performed to evaluate any variation in mechanical properties (i.e., G' and G'') and critical strain (γ_L) within the LVE region. Figure 1 reports the measured G' and G'' trends before and after self-healing for 15 minutes in quiescent state at 37 °C. Interestingly, hydrogel formulation using PBS as aqueous medium resulted in better mechanical properties by increasing storage and loss moduli for samples containing PEU at 1% w/v concentration.

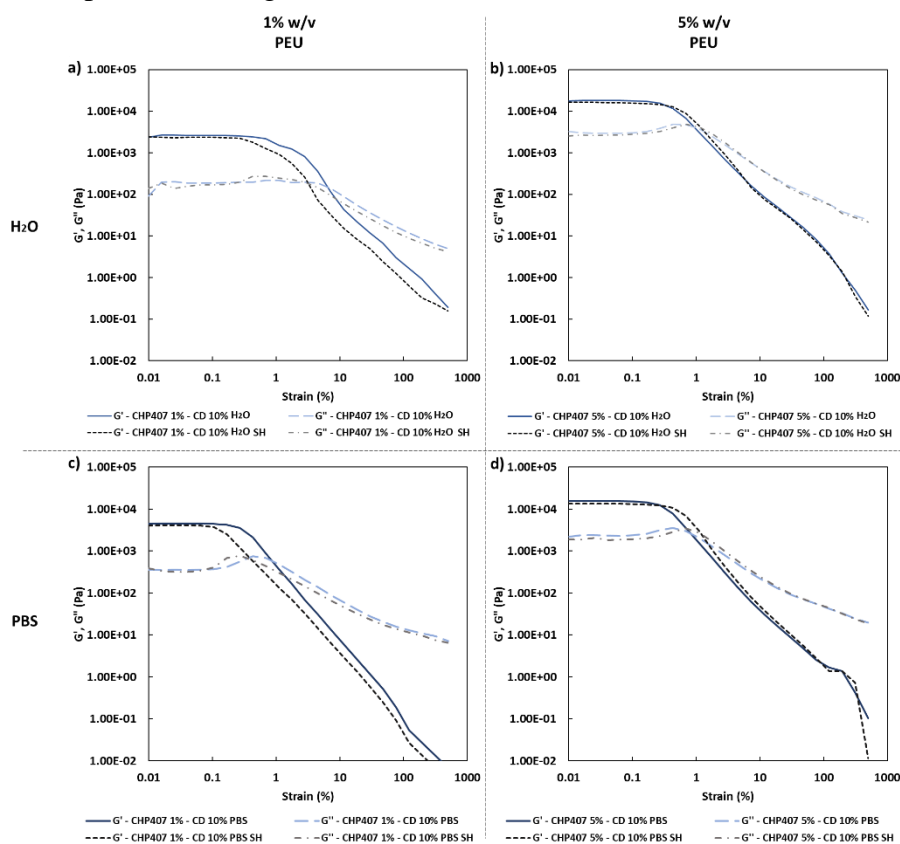


Figure 1 – Trends of G' and G'' before rupture (blue continuous and light blue dashed lines, respectively) and after recovery in quiescent state (black dotted lines and grey dash-dotted lines, respectively) as a function of applied strain for a) CHP407 1% - CD 10% H₂O, b) CHP407 5% - CD 10% H₂O, c) CHP407 1% - CD 10% PBS, and d) CHP407 5% - CD 10% PBS at 37 °C.

In detail, G'_{LVE} resulted to be around 4.5 kPa and 2.7 kPa for CHP407 1% - CD 10% PBS and CHP407 1% - CD 10% H₂O (i.e., 70% G' increase due to salting-out effect), respectively. Differently, for higher PEU concentrations (5% w/v) no significant differences were observed in terms of G'_{LVE} values (G'_{LVE} values for CHP407 5% - CD 10% PBS and CHP407 5% - CD 10% H₂O were measured around 15700 and 16200 Pa, respectively). Moreover, no changes in self-healing ability were observed for SM systems uniquely differing for the solvent used during their preparation (e.g., G'_{LVE} recovery values for CHP407 5% - CD 10% PBS and CHP407 5% - CD 10% H₂O resulted to be around 87% and 90%, respectively). Nonetheless, slightly lower γ_L values were observed for the sample containing CHP407 at 1% w/v concentration and formulated in PBS with respect to its counterpart prepared in ddH₂O (i.e., 0.3% and 0.7% for CHP407 1% - CD 10% PBS and CHP407 1% - CD 10% H₂O, respectively). This observation is in agreement with the higher values of G'_{LVE} characterizing PBS-based hydrogels, since a higher rigidity of hydrogel network could be generally correlated to enhanced fragility and hence lower critical strain values before rupture. Frequency sweep tests were also performed with the aim to assess the influence of dissolved ions in terms of mechanical properties measured as a function of applied angular frequencies at different temperatures (i.e., 25, 30 and 37 °C). The registered G' and G'' profiles are reported in figure 2.

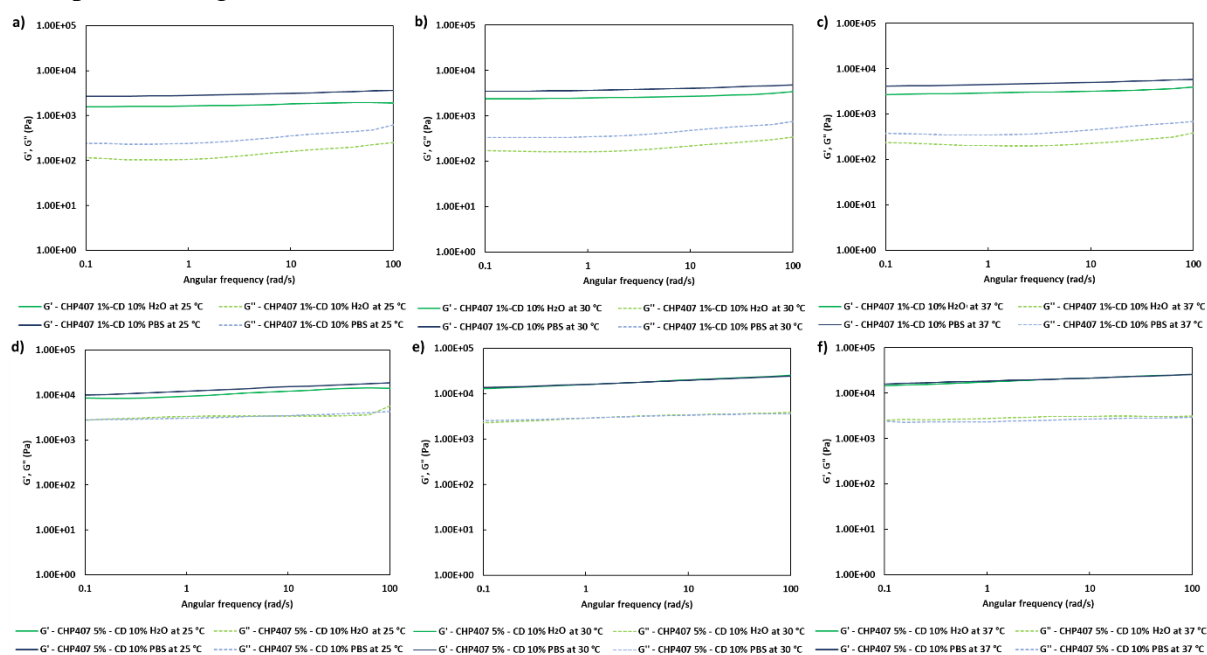


Figure 2 - G' (continuous lines) and G'' (dashed lines) trends of PBS- (in blue, a, b and c) for CHP407 1% - CD 10% PBS and d, e, and f) for CHP407 5% - CD 10% PBS) and ddH₂O-based gels (in green, a, b and c) for CHP407 1% - CD 10% H₂O and d, e, and f) for CHP407 5% - CD 10% H₂O) as a function of angular frequency at different temperatures (i.e., 25, 30 and 37 °C).

These data were in complete accordance with strain sweep test results. Indeed, irrespective of the testing temperature, a slight improvement of elastic and viscous moduli (i.e., higher values of G' and G'' , respectively) was observed for SM hydrogels containing PEU at 1% w/v concentration and prepared in PBS compared to the reference samples formulated in ddH₂O. Differently, at higher PEU content (i.e., 5% w/v concentration) no significant differences were observed. These consistent results between strain sweep and frequency sweep tests further confirmed the enhanced formation of SM networks based on crystallized PPRs within hydrogels characterized by a low

PEU/CD mass ratio (i.e., SM systems at 1% w/v PEU concentration). Indeed, it is likely that in these conditions the stabilizing effect of dissolved ions (i.e., salting-out effect) more evidently contributed to the formation of PPR-based SM networks, thus increasing the mechanical properties of the resulting hydrogels and reducing their gelation time. The salting-out effect could be supposed to act on the formation of PEU complexes (i.e., micelles and micelle-based aggregates) and even on the threading and packing of CDs along PEU chains and thus on the formation of PPR-based crystals. Although a negligible contribution of salting-out effect on mechanical properties was observed on SM hydrogels containing PEU at 5% w/v concentration, a significantly faster gelation kinetics was observed for these systems formulated in PBS compared to their counterpart prepared in ddH₂O (see previous paragraph). This curious behavior could be ascribed to the relevant contribution of not well-organized domains of free PEU chains and the weaker character in terms of PPR self-assembly of systems prepared at such PEU concentration, as previously hypothesized. Indeed, it is likely that a better stabilization on PEU network in solution could occur in the presence of dissolved ions, thus improving gelation kinetics. Nonetheless, the main impediment to the formation of PPR-based SM networks could derive from the intrinsic presence of notable PEU aggregates in these systems, resulting in the absence of improvements in mechanical properties for PEU 5% - CD 10% PBS systems compared to PEU 5% - CD 10% ddH₂O. Figure 3 reports G' and G'' trends as a function of time in response to different strains (i.e., recovery phase at 0.1% strain and rupture phase at 100% strain), highlighting the self-healing behavior of the here-investigated SM hydrogels. In this case, solubilized ions did not affect the overall mechanical reversibility of SM hydrogels. Nonetheless, slight differences were observed in terms of recovery of starting mechanical properties. Indeed, CHP407 1% - CD 10% H₂O showed an almost total recovery of G' after three rupture cycles (i.e., 97%), while the sample CHP407 1% - CD 10% PBS was characterized by a lower self-healing (i.e., 89%). These results were in accordance with the previous consideration on the improvement of mechanical properties resulting from the contribution of salting-out effect. Indeed, SM samples formulated in PBS exhibited higher G' values, indicating a higher rigidity (i.e., enhanced fragility) and, as a consequence, a less pronounced reversibility of the network after cyclic rupture. The variation of the recovery values with respect to the measured through strain sweep tests could be related to the relevant differences in the testing conditions (i.e., different strain values and recovery conditions). In fact, strain tests were performed by cyclically applying constant strains for defined time intervals (i.e., 0.1 and 100% for 120 and 60 seconds, respectively), while strain sweep tests were conducted at incremental strain values until rupture followed by a prolonged recovery phase in quiescent state (i.e., 0% strain for 15 minutes at 37 °C). No significant differences were observed for samples containing PEU at 5% w/v concentration (around 83% recovery for both ddH₂O and PBS-based systems), probably due to an enhanced damping role exerted by the PEU that resulted in amorphous domains, as previously hypothesized.

Thence, the entire set of rheological characterizations suggested that the use of PBS as watery medium for the development of SM networks based on PPRs could contribute in improving gelation kinetics and mechanical properties, without negatively affecting the overall reversibility of hydrogel systems.

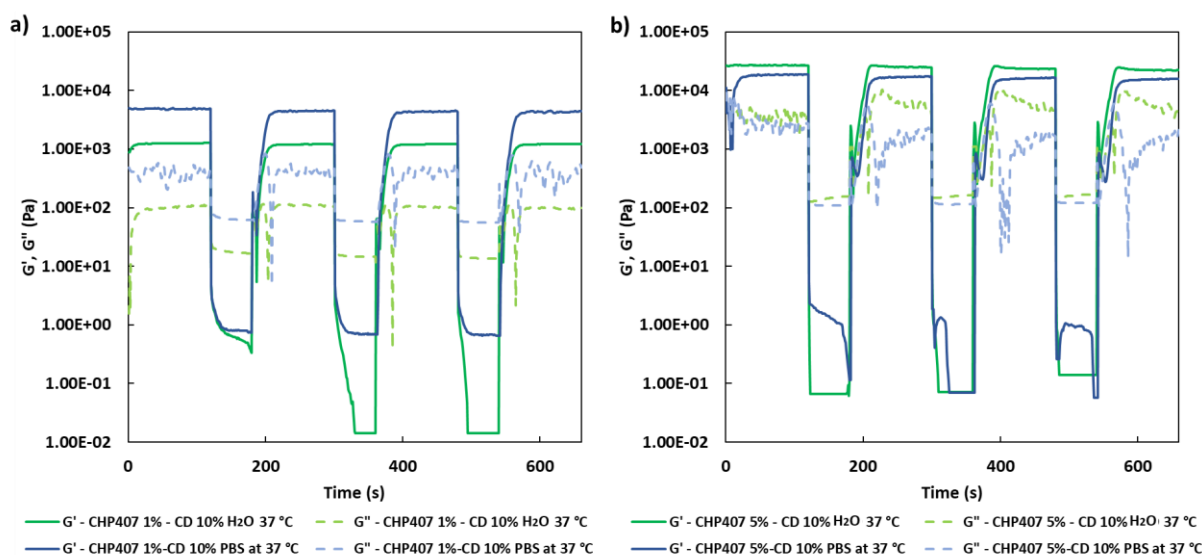


Figure 3 - G' (continuous lines) and G'' (dashed lines) trends of PBS- (in blue, a) CHP407 1% - CD 10% PBS, and b) CHP407 5% - CD 10% PBS) and ddH₂O-based gels (i.e., in green, a) CHP407 1% - CD 10% H₂O and b) CHP407 5% - CD 10% H₂O) as a function of time in response of low (recovery phase) and high (rupture phase) strains (i.e., 0.1% and 100%, respectively) at 37 °C.

4.3 Swelling and stability tests

The evaluation of swelling, dissolution and swelling ratio of SM hydrogels prepared using different solvents (i.e., ddH₂O and PBS) in contact with pure PBS and PBS added with Amphotericin B (i.e., AMPBS) was elemental in order to characterize the general responsiveness of SM networks in a watery milieu. Figure 4 reports the entire set of data describing hydrogel behavior in contact with the selected aqueous environments. SM hydrogels based in ddH₂O showed higher responsiveness and hence enhanced weight loss with respect to PBS-based samples when incubated in contact with the same external environment at 37 °C. As an example, the system NHP407 1% - CD 10% formulated in ddH₂O (i.e., NHP407 1% - CD 10% H₂O) showed a weight loss of 26.6 ± 0.5 % while the equivalent hydrogel based on PBS (i.e., NHP407 1% - CD 10% PBS) was characterized by values around 19.2 ± 0.6 % after 24 hours of incubation in contact with pure PBS at 37 °C (significant difference, p value < 0.0001). In these conditions, significant differences were observed even in terms of swelling ratio, while comparable values of fluid absorption were quantified. In this regard, it is likely that the presence of dissolved ions in hydrogel networks could act as a further stabilizing factor when the systems were in contact with the same saline solution (i.e., PBS) with respect to the ones based on pure water (i.e., ddH₂O). Differently, after 120 hours of incubation at 37 °C, the behavior of ddH₂O- and PBS-based hydrogels was comparable in general terms. Interestingly, these data suggest that the marked dissolution of the hydrogels prepared in ddH₂O was limited to the first hours of incubation. Indeed, it is likely that during the incubation process a continuous diffusion of PBS ions into ddH₂O hydrogel networks was occurring, thus inducing a late salting-out effect. The contribution of amphotericin B was generally negligible, as reported in figure 4, thus further indicating that the here-developed SM networks were stable even in the presence of highly hydrophobic molecules (i.e., amphotericin B), which could negatively affect the integrity of hydrogel network through their potentially relevant affinity with the inner cavity of CDs. NHP407 and CHP407-based hydrogels showed the same

behavior in terms of responsiveness in contact with different water-based external environments, in complete accordance with the data discussed in the previous chapter (*Section 2 – Chapter 2.2 – Results – Swelling and stability in physiological-like conditions*). The different composition of PEUs probably plays a more relevant role in determining hydrogel gelation kinetics and mechanical properties rather than in influencing network responsiveness to aqueous environments. Thence, it can be deduced that the production of SM hydrogels in PBS solutions could further contribute to enhancing their typical stability and progressive erosion in watery environments.

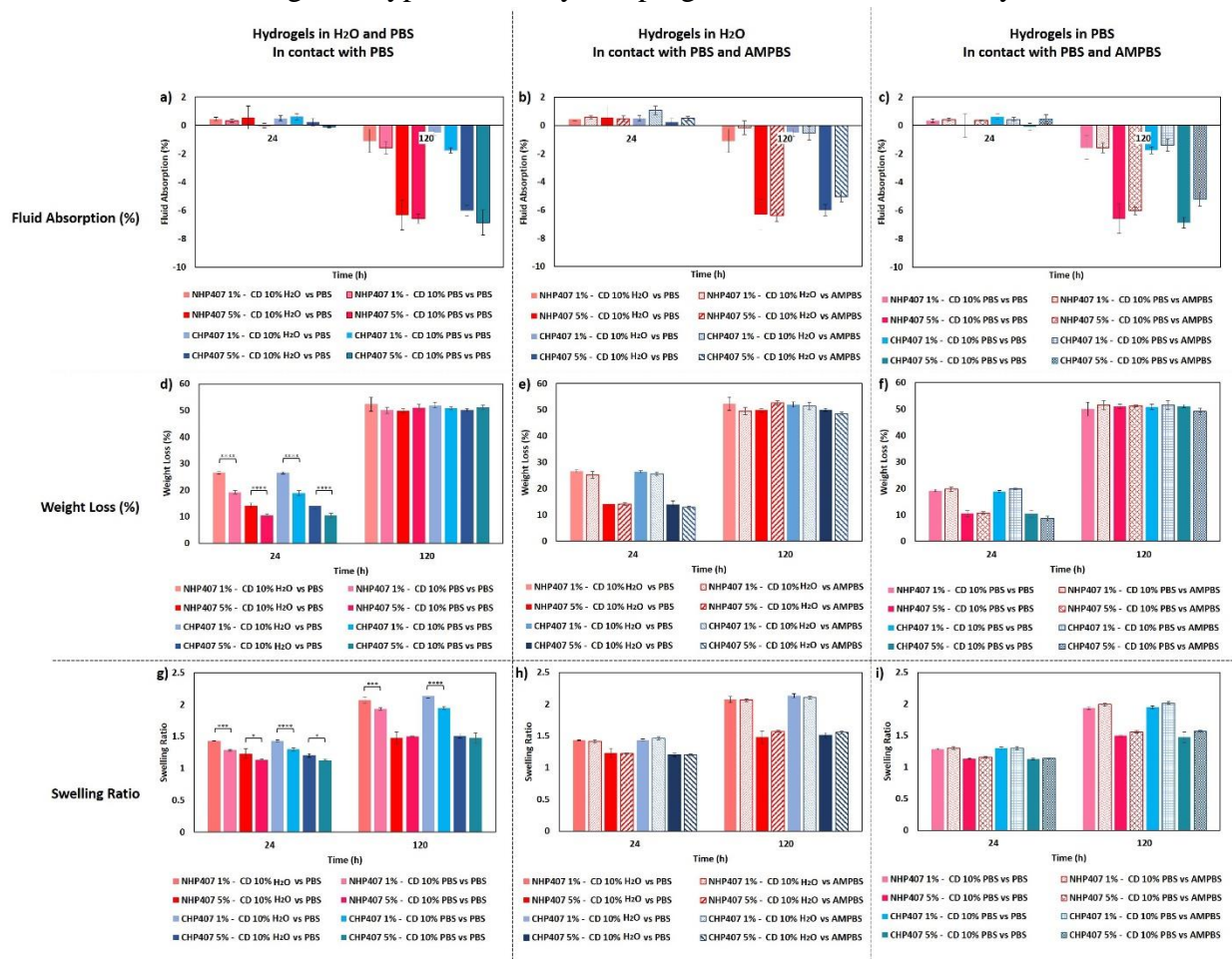


Figure 4 – Bar diagrams in vertical disposition for: a, d and g) PEU X% - CD 10% H₂O compared with PEU X% - CD 10% PBS in contact with PBS; b, e and h) PEU X% - CD 10% H₂O in contact with PBS and AMPBS; c, f and i) PEU X% - CD 10% PBS in contact with PBS and AMPBS. In horizontal disposition, fluid absorption (%) (a, b and c), weight loss (%) (c, d and e) and swelling ratio (g, h and i) are reported for the above-mentioned hydrogel systems.

5. Conclusions

The continuous research for new strategies to effectively tune final properties of drug eluting systems is of key importance to facilitate their effective use in regenerative pharmacology for modern medicine. To this aim, the design of novel and engineered molecules by exploiting PEU synthesis process is a promising solution for the development of responsive hydrogels devices. The study reported in this chapter represents an elemental passage within this context, as it aimed to evaluate the feasibility of exploiting different watery environments for hydrogel preparation as

tuning factors for their properties. Indeed, the ability of the here-developed SM hydrogels to consistently respond to various and remarkably different solvents (i.e., ddH₂O and PBS) in terms of self-assembly could broaden the domain of hydrogel designs, allowing a fine modulation of final responsiveness and mechanical properties. It is likely that the chemical heterogeneity of PEUs substantially contributed to the achievement of tunable networks, which were even characterized by a consistent behavior and good repeatability within the entire set of performed characterizations. Moreover, the possibility to develop solid hydrogel devices in a wide range of different environments could even broaden the possibilities for the *ad-hoc* design of drug-loaded systems. Indeed, the internal milieu of hydrogel systems is fundamental for drug solubilization, stabilization and storage before any release process.⁷ Thence, the observed stability and robustness of the formulated PEU-based hydrogel devices as such and in contact with various environments represent reinforcing elements of the rationale underpinning the development of SM hydrogels for specific and critical drug delivery applications. On the basis of these observations, the next Chapter will be focused on the specific design of functional hydrogels for the encapsulation and delivery of highly hydrophobic and scarcely bioavailable drugs, such as curcumin.

6. References

- (1) Sadeghi, R.; Jahani, F. Salting-In and Salting-Out of Water-Soluble Polymers in Aqueous Salt Solutions. *J. Phys. Chem. B* **2012**, *116* (17), 5234–5241. <https://doi.org/10.1021/jp300665b>.
- (2) Zhang, Y.; Cremer, P. Interactions between Macromolecules and Ions: The Hofmeister Series. *Current Opinion in Chemical Biology* **2006**, *10* (6), 658–663. <https://doi.org/10.1016/j.cbpa.2006.09.020>.
- (3) Khamari, L. Specific Ion Effects on F127 Hydrogel_ FCS, Anisotropy and Solvation Dynamics. *Chemical Physics Letters* **2019**, *6*.
- (4) Ganguly, R.; Aswal, V. K. Improved Micellar Hydration and Gelation Characteristics of PEO–PPO–PEO Triblock Copolymer Solutions in the Presence of LiCl. *J. Phys. Chem. B* **2008**, *112* (26), 7726–7731. <https://doi.org/10.1021/jp801940m>.
- (5) Alexandridis, P.; Holzwarth, J. F. Differential Scanning Calorimetry Investigation of the Effect of Salts on Aqueous Solution Properties of an Amphiphilic Block Copolymer (Pluronic). *Langmuir* **1997**, *13* (23), 6074–6082. <https://doi.org/10.1021/la9703712>.
- (6) Lo Nostro, P.; Lopes, J. R.; Ninham, B. W.; Baglioni, P. Effect of Cations and Anions on the Formation of Polypseudorotaxanes. *J. Phys. Chem. B* **2002**, *106* (9), 2166–2174. <https://doi.org/10.1021/jp012915l>.
- (7) Bye, J. W.; Platts, L.; Falconer, R. J. Biopharmaceutical Liquid Formulation: A Review of the Science of Protein Stability and Solubility in Aqueous Environments. *Biotechnol Lett* **2014**, *36* (5), 869–875. <https://doi.org/10.1007/s10529-013-1445-6>.

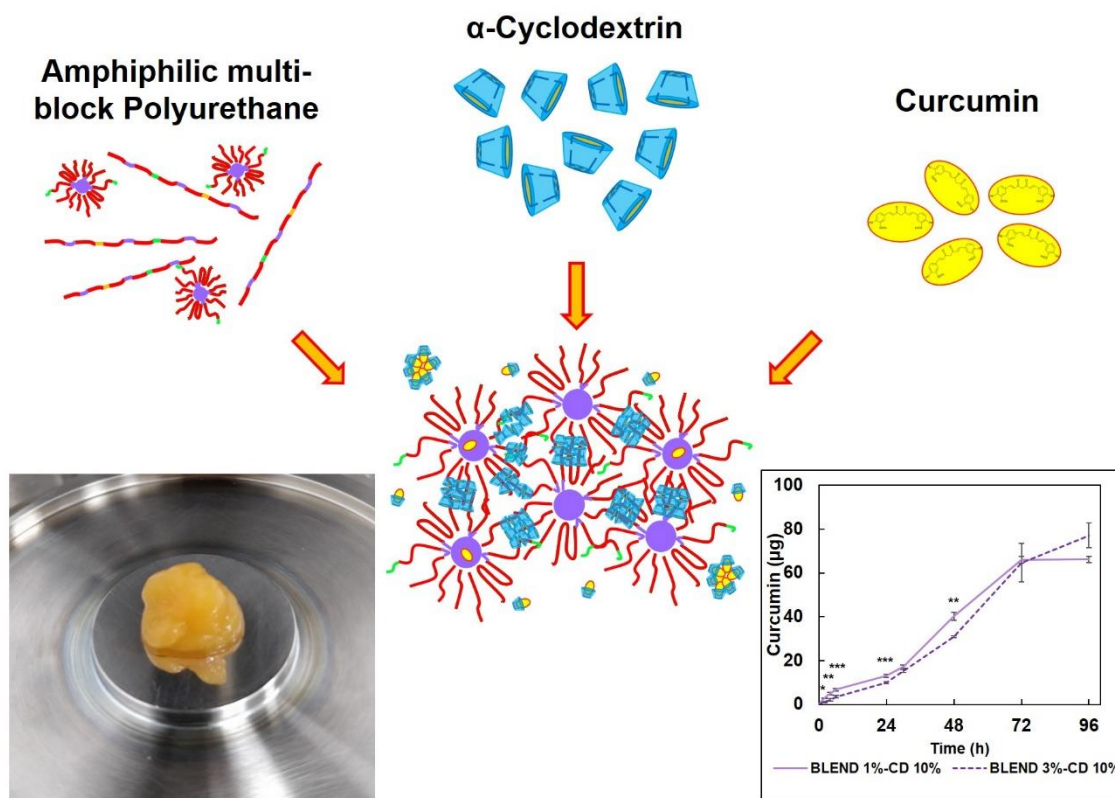
Section 2 – Chapter 2.4 – Application of polyurethane-based supramolecular hydrogels for curcumin encapsulation and release

1. Abstract

The development of novel drugs represents a highly complex and expensive process. In addition, the therapeutic potential of a drug not only depends on its intrinsic properties, but also on its delivery strategies. Indeed, notably functional drugs can be characterized by low bioavailability and fast degradation kinetics in real biological environments, which hinder their overall effectiveness. This is the case of highly hydrophobic and chemical sensitive drugs, such as curcumin, which has been studied from decades and is considered a potential remedy for various diseases. Indeed, curcumin exerts antitumoral, anti-inflammatory, antioxidative, antimicrobial effects as well as highly regenerative potential on various tissues. Nonetheless, curcumin is not practically soluble in water-based solutions and undergoes quick degradation phenomena. In this regard, one modern approach to overcome the previously listed issues consists in developing novel systems (e.g., nanocarriers and smart hydrogels) able to enhance the therapeutic effect of highly cost-effective and promising drugs, which are generally not easily administrable. In this section of the work, novel PEUs were synthesized to this aim. In detail, SM hydrogels were designed utilizing already existing and newly synthesized functional PEUs in combination with CDs for the encapsulation and release of high amounts of curcumin. PEU based on Poloxamer 407 (70% wt PEO, \bar{M}_n 12600 Da) and Pluronic F68 (80% wt PEO, \bar{M}_n 8400 Da) were synthesized utilizing two different chain extenders (1,4-cyclohexanedimethanol and N-Boc serinol). A variety of five PEUs was produced showing specific chemical properties (i.e., molar mass, linear structure, presence of pendant hydrophobic or primary amino groups) with the aim to study their effects on final hydrogel devices, thus further widening the possibilities for system engineering. Physico-chemical characterizations on PEU-CD complexes were conducted through X-ray powder diffraction, Attenuated Total Reflectance – Fourier Transformed Infrared spectroscopy and Proton Nuclear Magnetic Resonance spectroscopy. The formation of PPR-based crystals was found to be dependent on the chemical structure of PEUs. A set of hypotheses on the importance of chain length and distribution of hydrophobic domains was made in this regard. P407-based PEUs showed better physico-chemical properties to produce stable hydrogels. Moreover, pendant hydrophobic moieties or primary amino groups resulted to be other important variables for the modulation of the self-assembly yield. SM hydrogels were developed at PEU content ranging between 1 and 5% w/v and CDs at 10% w/v concentration. On the basis of physico-chemical characterizations and gelation ability, a set of PEUs and specific PEU blends was selected for the production of SM hydrogels with the aim to enhance functionality and tunability of the resulting SM gel platform. A complete rheological characterization was conducted to confirm overall stability and responsiveness of SM hydrogels. In this regard, the investigated hydrogel systems showed good mechanical properties (e.g., elastic modulus greater than 10^4 Pa) and resulted to be self-healing, showing a recovery of mechanical properties over 80% after complete network breakage. An evident ability to exchange mass with the external milieu while maintaining hydrogel shape was observed by incubating the gels in contact with a physiological-like watery environment (i.e., pH 7.4, 37 °C). Then, curcumin was encapsulated at high concentration (i.e., 80 $\mu\text{g ml}^{-1}$)

within SM systems and *in vitro* delivery studies showed progressive release profiles of the entire amount of the drug. Korsmeyer-Peppas drug release model was implemented as a tool to better explain the mechanism of curcumin delivery from the here-developed highly organized SM hydrogels, thus highlighting a principal role of SM network features for curcumin release kinetics.

Graphical abstract



2. Introduction

2.1 Curcumin: its therapeutic effects and issues

Curcumin represents the most important curcuminoid of *Curcuma Longa*, a turmeric. Historically, curcuminoids were discovered in 1815 by Vogel and Pelletier¹⁻³ and various constituents of *Curcuma Longa* were identified: curcumin I at 77%, curcumin II at 17%, curcumin III at 3% and cyclocurcumin at 3% w/w. The chemical structure, properties and synthesis of curcumin were investigated in 1913 by Lampe and Milobedzka.⁴ In structural terms, this molecule can exist in the enol and keto tautomeric forms, as represented in figure 1. These domains, in addition to the particular structure of curcumin, result in highly evident anticancer,⁵⁻⁷ antiviral,⁸ antibacterial,⁹⁻¹¹ anti-inflammatory,¹² antioxidant^{12,13} and antidiabetic¹⁴ properties. Moreover, other advantages make this family of molecules notably interesting and important, such as their negligible chemical hazard, biological tolerability¹⁵ and cost-effectiveness.¹⁶ For these relevant reasons, curcumin has been studied for decades to develop highly effective therapies in traditional medicine. More in detail, curcumin can interact with a wide variety of protein-based complexes (e.g., nuclear,

transcription and growth factors, enzymes, inflammatory cytokines, receptors, kinases and apoptotic regulators).¹ Hence, curcumin is characterized by the relevant ability to interact with many cellular pathways related to various severe and chronic diseases.¹⁷ In fact, recent studies have highlighted the use of curcumin even for the treatment of neurological disorders.¹⁸ Moreover, in addition to the all above-mentioned properties, curcumin is also characterized by a relevantly effective regenerative function for various tissues (e.g., cartilage and cardiac tissue).^{19,20} Interestingly, in most of these applications the therapeutic window of curcumin is characterized by very low required concentrations (i.e., in the order of micromolar).²¹

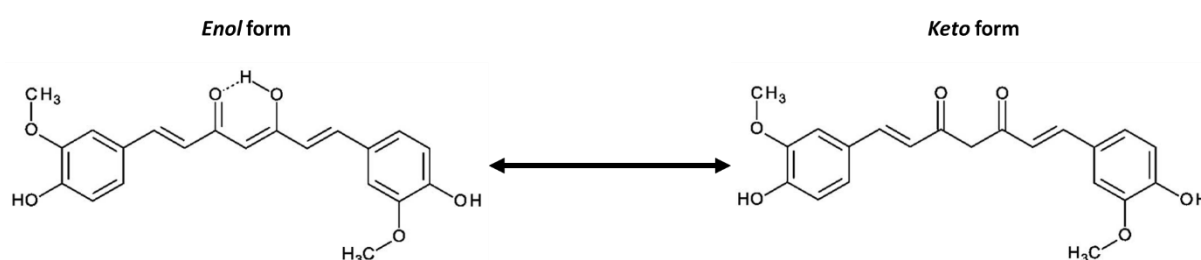


Figure 1 – Representation of the reversible structures of curcumin (i.e., enol and keto curcumin).

Generally, the assumption of curcumin can be considered safe. Indeed, various organizations (e.g., WHO Expert Committee on food additives) indicate an adequate daily intake up to 3 mg kg^{-1} .²² Nonetheless, such drug even retains great limitations. Indeed, due to its marked hydrophobicity and pronounced tendency to form highly stable crystals through lipophilic and aromatic interactions, its bioavailability is generally extremely low if administrated through conventional methodologies.²³ Indeed, curcumin is insoluble in water at neutral or acidic pH. Slight solubility of curcumin can be achieved in alkaline environments, but in these conditions enhanced hydrolytic degradation kinetics are observed.^{24–26} The main degradation products of curcumin are ferulic acid, feruloyl methane and vanillin, which however retain a therapeutic potential. Thence, the low solubility in combination with the relevant sensibility to degradation make curcumin extremely difficult to administer at specific doses. In this regard, the role of active methylene domains and β -diketone moieties is crucial in terms of chemical stability and availability in biological environments. For instance, many studies have evidenced that curcumin shows extremely low or even undetectable concentration in extraintestinal tissue and blood due to poor absorption, chemical instability, rapid metabolism, and systemic elimination.²³ Several investigations on animals demonstrated that oral administration of curcumin results in relevant excretion through the faeces (up to 90%).²⁷ In the past, a great effort has been made to overcome these important issues related to curcumin application as therapeutic agent aiming at maximally exploiting the notable therapeutic effects of such drug. One possible solution relies in the use of curcumin synthetic analogues (e.g., demethoxycurcumin and bide-methoxycurcumin) with enhanced stability and bioavailability. Nonetheless, a relevant and concrete frontier for the effective exploitation of the therapeutic potential of curcumin as such is being pursued by biomedical engineering through its particular facet concerning bionanotechnology. Indeed, the wide use of liposomes, polymer-based micelles and hydrogels only partially represents the wide set of strategies available for the production of engineered carriers for curcumin.^{2,13,28–30} In this scenario, the role of specific natural and synthetic macromolecules, such as proteins, polysaccharides and amphiphilic polymers,¹³ is

crucial to produce water-soluble curcumin-based complexes. Cyclodextrins (CDs) represent one of the most important categories of molecules to this aim.

2.2 Pharmaceutical formulations based on cyclodextrins for curcumin release

CDs (α -, β - and γ -CDs) can form soluble inclusion complexes through the self-assembly of host-guest structures based on the encapsulation of hydrophobic molecules, as previously documented in *Section 2 – Chapter 2.1 – Cyclodextrins: a fundamental family of macro-cycles*. For this peculiarity, CDs are widely used in the pharmaceutical field as excipients (i.e., solubilizing and stabilizing agents).^{31,32} Indeed, CDs can exert a protective action on highly hydrolysable molecules; they even show a photo-protective behavior on photo-sensitive molecules, such as curcumin. In this regard, a wide set of relevant studies evaluating the ability of CDs to form specific complexes with curcumin has been conducted.^{33–35} More in detail, Tønnesen and co-workers investigated the effects of CDs as solubilizing agents of curcumin.³³ Interestingly, they observed that water solubility of curcumin was improved by a factor greater than 10^4 in adverse conditions (i.e., pH 5). Moreover, the chemical stability of curcumin was significantly improved even in alkaline environments (up to 500-fold increase), thus suggesting that the interaction with CDs could protect curcumin molecules from hydrolytic degradation in water-based solutions. Nonetheless, an enhanced photo-induced decomposition of such drug was observed in organic solvents. The dimension of CD cavity also influences the overall stabilizing effect of the resulting complexes depending on the specific parameters of association. β - and γ -CDs and their derivatives have been demonstrated to be the most suitable for the formation of specific and highly stable inclusion complexes at various curcumin/CD molecular ratios (e.g., 1:1 or 1:2).³⁴ Differently, α -CDs result in complexes with a weaker stability due to their lower affinity with curcumin. Nonetheless, they have found remarkably interesting applications in this regard. Indeed, although α -CD-based complexes with curcumin result from a more intricate and less controllable process of aggregation, a relatively high versatility of the corresponding supramolecular structures has been observed in various applications.^{36–39} As an example, in the work performed by Gerola and co-workers α -CD turned out to be suitable for the formation of inclusion complexes with curcumin showing an overall enhanced solubility of the resulting supramolecular structures due to the intrinsic higher solubility of α -CDs with respect to β -CDs.³⁸ In biological terms, the work carried out by Li and co-authors reports interesting results regarding the intestinal absorption of curcumin complexed with α -CDs.⁴⁰ Compared with β - and γ -CDs, the complexes composed of α -CDs allowed a better absorption without showing significant toxicity. Moreover, α -CDs-based complexes promoted the permeation of curcumin through paracellular and transcellular pathways. Another noteworthy example is represented by the work performed by Jana *et al.*, who described the specific interaction occurring between α -CD-curcumin complexes with tubulin surface of cancer cells.³⁷ Interestingly, the authors reported a dual beneficial contribution of both α -CDs and curcumin. Indeed, curcumin did not represent the only therapeutic agent, but even a central role of α -CDs was found in the interaction with intracellular tubulin and microtubules, thus further acting as additional inhibitor of cancer cell replication. The highly engineered supramolecular system that was described in this work resulted in relevant toxic effect on lung cancer cells (A549) with no significant negative action on healthy lung fibroblasts (W138). Moreover, the activation of protein-based functional biomolecules, such as tumor suppressor protein p53 and cyclin-dependent

kinase inhibitor 1 p21, was observed, thus hindering the formation of three-dimensional spheroids based on cancer cells.

All the above-mentioned aspects are extremely important and can be even extended to composite systems based on nano-matrices and injectable hydrogel networks, in order to enhance local release of highly therapeutic drugs with prolonged bioavailability.

2.3 Supramolecular hydrogels for curcumin encapsulation and release

To date, various examples of curcumin-loaded hydrogels can be found in the literature. The exploitation of supramolecular architectures could represent a powerful strategy to design highly stable, reversible and functional hydrogels able to encapsulate a high amount of hydrophobic drugs, such as curcumin. As a recent example, Khan and co-authors conducted a study on a self-assembled and thermosensitive hydrogel system based on β -CDs, PEO and difunctional Pluronic® F127 for the controlled release of curcumin.⁴¹ Interestingly, the authors designed a PPR-based SM hydrogel exploiting PEO domains and β -CDs. The further addition of a Pluronic® F127 solution encapsulating curcumin into its micelle core resulted in highly thermo-sensitive systems characterized by a LCST. *In vitro* delivery studies evidenced the release of active and bioavailable curcumin over time, showing a toxic effect against cancer cells. In another work, Zhou and colleagues designed a supramolecular hydrogel based on methoxy poly(ethylene glycol)-*block*-poly(ϵ -caprolactone) (MPEG-PCL) micelles encapsulating curcumin and assembling a supramolecular network through crystalline PPRs composed of α -CDs.⁴² The use MPEG-PCL micelles increased curcumin water solubility up to 1.87 mg ml⁻¹ (i.e., at least 1.87 x 10⁶ higher than simple curcumin). The resulting hydrogels showed a relevant release of curcumin up to 4.5 hours and their application in *ex vivo* experiments resulted in high permeability of the released drug. Additionally, *in vivo* tests showed a higher effectiveness of curcumin-loaded hydrogels compared to dexamethasone ointments against croton oil-induced ear edema, thus resulting in notably promising formulations for the effective treatment of skin inflammation. Another recent study by Li *et al.* reported the design of a supramolecular network based on liposomes encapsulating curcumin.⁴³ The stabilization of liposome-based hydrogels was performed by coating the liposomes with a chitosan-based thiomers. *In vitro* studies and *in vivo* applications of such systems containing curcumin at 200 μ M concentration showed an effective inhibition of breast cancer progression, while no cytotoxicity was observed for healthy cells.

Thence, the application of curcumin to actively constitute (i.e., self-delivery) highly engineered supramolecular hydrogels represents an open field, in which novel and promising strategies for the treatment of many diseases can be developed. The advantages related to the use curcumin can be found in its cost-effectiveness and low toxicity, in addition to the already known and evident therapeutic effects. In this scenario, this Ph.D. work proceeded in the development of PEU-based SM hydrogels containing high dosages of curcumin for local injection and treatment of various diseases, such as cancer and chronic infection. The potential that contradistinguishes the synthesis procedure of PEUs represented a powerful tool to be exploited, aiming at enhancing the final functionality of therapeutic hydrogel-based devices while reducing their content in constituents of synthetic origin. In fact, the previously characterized mechanical reversibility and the related easy handling of PEU-based SM hydrogels generally represent highly important features for the

development of proper devices for smart drug delivery. Hence, to further extend the domain of possibilities for hydrogel design, novel amphiphilic macromolecules were synthesized utilizing Poloxamer® 407 (P407) and Pluronic® F68 (80% wt PEO, \bar{M}_n 8400 Da). As co-reagents, 1,6-hexamethylene diisocyanate (HDI) was used as diisocyanate and two different chain extenders (i.e., 1,4-cyclohexanedimethanol (CDM) and N-Boc Serinol (NBoc)) were used to produce three novel PEUs. Additionally, two properly synthesized NBoc-based polymers were treated in acid environment to expose free primary amines along PEU backbone and hence improve their functionality. In fact, amino-based amphiphilic polymers show an additional responsiveness to the external pH that characterizes the milieu of acute inflammations and various cancers.⁴⁴ This feature could be highly important in order to tune cargo release kinetics of smart hydrogels.⁴⁵ Moreover, the presence of free amines along PEU backbone can be even exploited to perform other chemical modifications through carbodiimide chemistry, as accurately reported by Laurano *et al.* for similar PEUs.⁴⁶ Herein, the formation of PPRs based on the newly synthesized PEUs and α -CDs was first evaluated through X-Ray powder diffraction (XRD), Attenuated Total Reflectance – Fourier Transformed Infrared (ATR-FTIR) and Proton Nuclear Magnetic Resonance (¹H-NMR) spectroscopies. On the basis of the results discussed in the previous Chapters, novel supramolecular hydrogels were then formulated in phosphate buffered saline (PBS, pH 7.4 at 25 °C) at low PEU concentration (i.e., between 1 and 5% w/v concentration) and α -CDs at 10% w/v concentration. The entire set of SM hydrogels was characterized in terms of gelation kinetics through qualitative visual inspections (i.e., tube inverting test) and mechanical properties through rheological characterizations. Biocompatibility of SM hydrogels was evaluated on pure extracts according to ISO 10993 guidelines. Then, the suitability of PEU-based SM hydrogels for drug delivery applications was evaluated through the encapsulation of a high amount of curcumin (i.e., 80 $\mu\text{g ml}^{-1}$) that was made possible by the simultaneous copresence of PEUs and α -CDs.³⁹ Finally, release tests of curcumin were performed in physiological-like environment (pH 7.4, 37 °C) and the resulting set of curcumin delivery profiles was studied through the implementation of the Korsmeyer-Peppas model.

3. Materials and methods

3.1 Materials

Poloxamer® 407 (P407) and Pluronic® F68 (F68), HDI, NBoc, CDM, dibutyltin dilaurate (DBTDL), 3-(trimethylsilyl)propionic-2,2,3,3-d 4 acid sodium salt (TSP), trifluoroacetic acid (TFA), amphotericin B and curcumin (from *Curcuma Longa*) were purchased from Merck/Sigma Aldrich (Milan, Italy). All the utilized solvents were purchased from Carlo Erba Reagents (Milan, Italy). P407 and F68 were dehydrated before use at 100 °C for 8 hours at low pressure (*ca.* 150 mbar) and subsequently maintained at 40 °C. CDM and NBoc were dried using a desiccator under partial vacuum (i.e., *ca.* 1 mbar) at room temperature. HDI was distilled under vacuum before use. 1,2-dichloroethane (DCE) was utilized as solvent for PEU synthesis after anhydrication over activated molecular sieves (Merck/Sigma Aldrich, Milan, Italy) under inert atmosphere (i.e., N₂) before use. α -CDs (hereafter indicated as “CDs”) were obtained from TCI Chemical Europe (Zwijndrecht, Belgium) and used as supplied.

3.2 Synthesis of PEUs

The synthesis of PEUs was carried out as reported in *Section 2 – Chapter 2.2 – Materials and methods – Synthesis of PEUs*. The obtained PEUs were coded depending on their reagents as CHP407, NHP407 and NHF68, where “P407” and “F68” indicate the amphiphilic triblock copolymer used as macrodiol, while “C”, “N” and “H” refer to CDM, NBoc and HDI, respectively.

3.3 De-protection of N-Boc Serinol-based PEUs

The reaction for Boc-domain cleavage was conducted on NHP407 and NHF68 through acid treatment as reported by Boffito *et al.*⁴⁷ In detail, 10 g of PEU were solubilized in chloroform (CF) at room temperature for 2.5 hours under stirring (250 rpm). After complete solubilization, trifluoroacetic acid (TFA) was added to polymer solution reaching a final concentration of 4% w/v with a CF/TFA volume ratio of 90:10. The reaction was conducted for 1 hour under stirring at 250 rpm and then the resulting solution was concentrated using a rotary evaporator (RII Rotavapor, Buchi) at 60 °C. Subsequently, the concentrated solution was washed twice with CF (100 ml) and then 200 ml of bi-distilled water were added forming a suspension, which was maintained at 3 °C under vigorous stirring overnight. In order to remove potentially residual traces of TFA and CF, dialysis was conducted (cellulose membrane, cut-off 10-12 kDa, Sigma Aldrich, Italy) for 48 hours against distilled water at 3 °C (complete dialysis medium refresh twice/day). The de-protected PEU was then collected after freeze drying (Martin Christ ALPHA 2-4 LSC, Germany) and stored under vacuum at 3 °C. The resulting PEUs were coded as SHP407 and SHF68 referring to their native forms (i.e., NHP407 and NHF68, respectively) and the name of the Boc-cleaved chain extender (i.e., serinol, “S”).

3.4 Chemical characterization of PEUs

3.4.1 Attenuated total reflectance – Fourier transformed infrared (ATR-FTIR) spectroscopy

ATR-FTIR spectroscopy was performed as reported in *Section 2 – Chapter 2.2 – Materials and methods – Chemical characterization of PEUs – ATR-FTIR spectroscopy*.

3.4.2 Size exclusion chromatography (SEC) characterization

SEC characterization was performed as indicated in *Section 2 – Chapter 2.2 – Materials and methods – Chemical characterization of PEUs – SEC characterization*.

3.4.3 Proton nuclear magnetic resonance (¹H-NMR) spectroscopy

¹H-NMR spectroscopy was conducted on native PEUs (i.e., CHP407, NHP407 and NHF68) and the de-protected derivatives (i.e., SHP407 and SHF68). PEU samples were prepared in D₂O (10 mg ml⁻¹) and spectra were obtained through an Avance III Bruker spectrometer equipped with a 11.74 T superconductor magnet (500 MHz ¹H Larmor frequency), a Bruker BBFO direct probe and a Bruker BVT 3000 unit for temperature control. The analyses were conducted at 25 °C and

the spectra were obtained from 12 scans (10 seconds relaxation time) referring to D₂O peak at 4.675 ppm. The obtained spectra were analyzed through MNOVA software (Mestrelab Research, S.L., Spain, www.mestrelab.com).

3.4.4 Free primary amine quantification – Orange II Sodium Salt colorimetric assay

Primary amino groups in de-protected PEUs were quantified according to the protocol reported by Laurano *et al.*⁴⁶ Briefly, PEUs were dissolved at 0.04% w/v concentration in a solution of Orange II Sodium Salt (0.175 mg ml⁻¹, Sigma Aldrich, Italy) in ddH₂O previously adjusted at pH 3 and then incubated at room temperature (i.e., 25 °C) for 18 hours in the dark. Subsequently, dialysis (cut-off membrane 10-12 kDa) against ddH₂O was conducted for 3 days (three total refreshes per day) in the dark at room temperature. PEU samples were collected after freeze drying (Martin Christ ALPHA 2-4 LSC). The quantification of amines was conducted after dye detachment through sample solubilization in ddH₂O adjusted at pH 12 for 2 hours at room temperature. Then, the samples were centrifuged at 6000 rpm for 10 minutes at 15 °C and supernatants were analyzed with a UV-Vis spectrophotometer (Perkin Elmer Lambda 25 UV/Vis spectrometer, Waltham, MA, USA) in the wavelength domain from 700 to 400 nm by quantifying the main peak at 485 nm that is characteristic of the utilized dye molecule. As a reference for free amino groups quantification, a calibration curve was obtained through the preparation of specific samples of Orange II Sodium Salt in ddH₂O (pH 12) in the concentration range from 1.75 to 29.2 µg ml⁻¹. Virgin PEUs containing Boc-protected amines were also subjected to the same protocol and used as reference samples.

3.4.5 Critical micellar temperature (CMT) evaluation

The evaluation of CMT was performed with the aim to investigate the temperature-dependent behavior of PEU solutions at low concentration. In detail, 1,6-diphenyl-1,3,5-hexatriene (DPH, Sigma Aldrich, Milan, Italy) fluorescent dye (4 x 10⁻⁴ mol L⁻¹ in methanol) was added to PEU solutions at 1% w/v previously prepared in ddH₂O or PBS at a final concentration of 2 x 10⁻⁵ mol L⁻¹. Then, micelle formation was studied through a UV-Visible spectrophotometer (Perkin Elmer Lambda 25 UV/VIS spectrometer, Waltham, MA, USA) in the temperature range between 5 and 40 °C at a rate of 1 °C step⁻¹ with an equilibration time of 5 minutes step⁻¹. As documented by Boffito *et al.*,⁴⁸ the absorbance peak at 356 nm, which is as an indicator of DPH solubilization within micelle core, was represented as a function of temperature and the CMT value was obtained at the intercept between the linear regions before and after the inflection point that indicates the beginning of the micellization process.^{49,50}

3.5 Preparation and characterization of PEU- and CD-based SM complexes

3.5.1 Preparation of SM complexes

SM inclusion complexes based on PEUs were produced according to the protocol indicated in Section 2 – Chapter 2.2 – Materials and methods – Preparation and characterization of PEU- and CD-based SM complexes – Preparation of SM complexes. The obtained SM samples were coded

as PEU X% - SM Y%, where X represents the specific concentration (% w/v) of the PEU and Y indicates the content (%) of CDs with respect to the total amount of EO domains, with the assumption that 1 CD molecule can contain 2 EO groups into its cavity.⁵¹

3.5.2 X-ray powder diffraction (XRD) analysis

XRD analysis was conducted on SM samples of PEUs and CDs and their corresponding control samples as reported in *Section 2 – Chapter 2.2 – Materials and methods – Preparation and characterization of PEU- and CD-based SM complexes – XRD analysis*.

3.5.3 Attenuated Total Reflectance – Fourier Transformed Infrared (ATR-FTIR) spectroscopy

ATR-FTIR spectroscopy was performed on SM and control samples according to the protocol reported in *Section 2 – Chapter 2.2 – Materials and methods – Preparation and characterization of PEU- and CD-based SM complexes – ATR-FTIR spectroscopy*.

3.5.4 Proton Nuclear Magnetic Resonance (¹H-NMR) Spectroscopy

¹H-NMR spectroscopy was conducted according to the protocol reported in *Section 2 – Chapter 2.2 – Materials and methods – Preparation and characterization of PEU- and CD-based SM complexes – ¹H-NMR spectroscopy* with slight modifications. In detail, ¹H-NMR spectroscopy was performed only on re-solubilized SM samples based on crystalline PPRs. Differently, self-assembling samples were not prepared based on previous considerations (*Section 2 – Chapter 2.2 – Materials and methods – Preparation and characterization of PEU- and CD-based SM complexes – ¹H-NMR spectroscopy*).

3.6 Preparation and characterization of PEU- and CD-based SM hydrogels

3.6.1 Preparation of SM hydrogels

SM hydrogels based on PEUs and CDs were prepared in Bijou sample containers (17 mm inner diameter, 7 ml, Carlo Erba, Milan, Italy) utilizing PBS (pH 7.4, Sigma Aldrich, Milan, Italy) as solvent. In detail, the specific amount of PEU was dissolved in PBS into Bijou sample containers at 3 °C overnight. Then, a clear solution of CDs in PBS (14% w/v concentration) was prepared and aliquots were added to the previously prepared PEU solutions to reach the final and operative concentrations of both PEUs (1, 3 and 5% w/v) and CDs (i.e., 10% w/v). The mixtures were homogenized using a vortex (40 Hz for 30 seconds) and then incubated at 25 °C to allow gelation. In addition to SM hydrogels based on single PEU-based solutions, novel samples characterized by the blend of two PEUs were also prepared using CHP407 and SHF68, maintaining a mass ratio of 80:20 (%w/w) and a total PEU concentration as that of systems composed of one single PEU (i.e., 1, 3 and 5% w/v). The resulting hydrogels will be indicated as PEU X% - CD Y%, where PEU refers to the specific poly(ether urethane) that constitutes the hydrogel (i.e., NHP407, CHP407, NHF68, SHP407, SHF68), while X and Y specify the concentrations of PEU and CD, respectively.

For the systems based on the mixture of CHP407 and SHF68, the utilized codes were BLEND X% - CD Y%, in which X and Y are defined as reported above for single PEU-based samples.

3.6.2 Qualitative evaluation of gelation time and phase-separation in isothermal conditions

The evaluation of gelation time and phase separation of SM hydrogels was carried out as reported in *Section 2 – Chapter 2.2 – Materials and methods – Preparation and characterization of PEU- and CD-based SM hydrogels – Qualitative evaluation of gelation time and phase-separation in isothermal conditions.*

3.6.3 Rheological characterization

A complete rheological characterization was performed on SM hydrogels as indicated in *Section 2 – Chapter 2.2 – Materials and methods – Preparation and characterization of PEU- and CD-based SM hydrogels – Rheological characterization.*

3.6.4 Swelling and stability tests in physiological-like conditions

Responsiveness and stability of SM hydrogels were evaluated as reported in *Section 2 – Chapter 2.2 – Materials and methods – Preparation and characterization of PEU- and CD-based SM hydrogels – Swelling and stability tests in physiological-like conditions* with slight modifications. Tests were performed through gel incubation at 37 °C in contact with PBS added with amphotericin B (2.5 µg ml⁻¹) in order to prevent mold formation. As indicated in *Section 2 – Chapter 2.2 – Materials and methods – Preparation and characterization of PEU- and CD-based SM hydrogels – Swelling and stability tests in physiological-like conditions*, at predefined time steps (6h, 24h, 3 days and 5 days) PBS Absorption (%), Weight Loss (%) and Swelling ratio were calculated utilizing equations 1, 2 and 3, respectively. Analyses were conducted in quintuplicate and results are represented as mean ± standard deviation.

3.6.5 Cytotoxicity evaluation

Cytotoxicity tests were performed as indicated in *Section 2 – Chapter 2.2 – Materials and methods – Preparation and characterization of PEU- and CD-based SM hydrogels – Cytotoxicity evaluation* for SM hydrogels containing PEUs at 1 and 5% w/v and CDs at 10% w/v concentration.

3.6.6 Curcumin encapsulation and release studies

In order to encapsulate curcumin (Cur) into hydrogel systems (1 ml) reducing the risk of its degradation due to ions and alkaline pH,^{21,52} the required amount of CDs to produce SM hydrogels was equally divided in two parts. The first 50% (%v) of CD solution at 14% w/v concentration was prepared in PBS as previously described and mixed with PEU solutions (prepared in PBS as previously indicated). The remaining 50% (%v) of required CDs to produce the hydrogel systems was prepared in ddH₂O (pH around 5.5-6) at equal concentration (i.e., 14% w/v) in the presence of Cur at 225 µg ml⁻¹ content. To ensure complete solubilization of Cur within CD solution,

ultrasound sonication (52 W, 20 kHz, Vibracell VCX130, Sonics, USA) was applied for 3 minutes using a probe while stirring in contact with a cold water-ice bath at 0 °C to prevent solvent evaporation. Finally, the remaining amount of Cur-loaded CD solution was added to the samples, thus obtaining final CD concentration of 10% w/v, PEU content at 1 and 3% w/v and curcumin at 80 µg ml⁻¹ concentration. Gelation was ensured through incubation at room temperature (25 °C) for 48 hours.

A thorough rheological characterization was performed as indicated in *Section 2 – Chapter 2.2 – Materials and methods – Preparation and characterization of PEU- and CD-based SM hydrogels – Rheological characterization* on SM hydrogels containing Cur and control samples based on the same mixture of PBS and ddH₂O in order to evaluate separately the effects of the drug and the solvents on hydrogel mechanical response. The novel formulations that were investigated were identified as PEU X%-CD Y%-PBS/H₂O and PEU X%-CD Y%-Cur 80 mg/ml in order to indicate the systems that showed the single contribution of the solvents and the additional presence of Cur, respectively.

Release studies of Cur were performed after acclimatization of SM hydrogels in Bijou sample containers (1 ml, 17 mm inner diameter) at 37 °C for 15 minutes. Then, PBS (1 ml at 37 °C) was added to each sample. At specific time steps (2, 4, 6, 24, 48, 72 and 96 hours), elutes were collected and completely refreshed with new PBS. Then, curcumin quantification was conducted through a multimode plate reader (Perkin Elmer Victor X3) by transferring 200 µl of eluates into a 96 well plate and measuring the absorbance peak at 450 nm. A set of reference curves was obtained by producing Cur standards in PBS in the concentration range between 1 and 10 µg ml⁻¹ starting from either a storage solution of Cur (1 mg ml⁻¹ concentration) in ethanol or storage solutions prepared in PBS (50 µg ml⁻¹) and containing CDs at various concentrations (i.e., 2.5, 5 and 10% w/v). Additionally, the Korsmeyer-Peppas model (power law) was implemented within the first 6 hours of Cur release in order to better hypothesize the occurring mechanism of drug release. In fact, this model is particularly suitable for polymer-based systems (i.e., hydrogels having different morphologies) characterized by unknown or multiple drug release mechanisms (drug diffusion and/or transport) with respect to other models which are more suitable to characterize planar or particulate systems, as accurately discussed by Bruschi.⁵³ More specifically, the following equation 4 was used to calculate the exponent of release n :

$$\frac{M_t}{M_\infty} = Kt^n ; \text{Log} \left(\frac{M_t}{M_\infty} \right) = n\text{Log}(t) + \text{Log}(K) \text{ Eq.4}$$

in which M_t corresponds to the mass of drug released at the time step t , M_∞ represents the total amount (i.e., total mass) of Cur loaded into the systems and K is a constant of incorporation of structural modification (i.e., release velocity constant). In the case of cylindrical hydrogels, n equals to 0.45 indicates a release mechanism based on diffusion, while n equal to 0.89 characterizes a release behavior that depends on swelling. n values in the range between 0.45 and 0.89 indicate a combination of the above-mentioned release mechanisms, thus resulting in an anomalous transport. Instead, n values greater than 0.89 suggest an extreme way of transport, which corresponds to the presence of relevant inner tensions within the hydrogel network due to concomitant solvent absorption and important mass exchange from the external watery environment. Analyses were conducted in quintuplicate and results are represented as mean \pm standard deviation.

3.6.7 Statistical analysis

Statistical analysis was conducted as reported in *Section 2 – Chapter 2.2 – Materials and methods – Statistical analysis*.

4. Results

4.1 Physico-chemical characterization of PEUs

4.1.1 ATR-FTIR spectroscopy and SEC

Infrared spectroscopy was performed with the aim to assess the successful synthesis of PEUs. Figure 2 reports the spectra of P407- and F68-based polymer backbones. The presence of new vibration bands at 1720 cm^{-1} was related to the stretching of carbonyl groups (C=O). Moreover, the convoluted peak at 1530 cm^{-1} represented the simultaneous excitation of N-H and C-N domains as bending and stretching vibrations, respectively. Another important indication of urethane domain formation was provided by the wide excitation band at 3350 cm^{-1} due to N-H stretching. The absence of any peak around 2200 cm^{-1} proved the complete conversion of isocyanate groups. The typical vibration bands of P407 and F68 were found at 1250 cm^{-1} (CH_2 stretching), 2880 cm^{-1} (CH_2 rocking) and 1100 cm^{-1} (C-O-C stretching). The consistent overlapping between the spectra of de-protected PEUs with the ones of their native counterparts (i.e., SHP407 and SHF68 for NHP407 and NHF68, respectively) indicated that the reaction for Boc group cleavage did not induce any evident chemical modification on urethane domains.

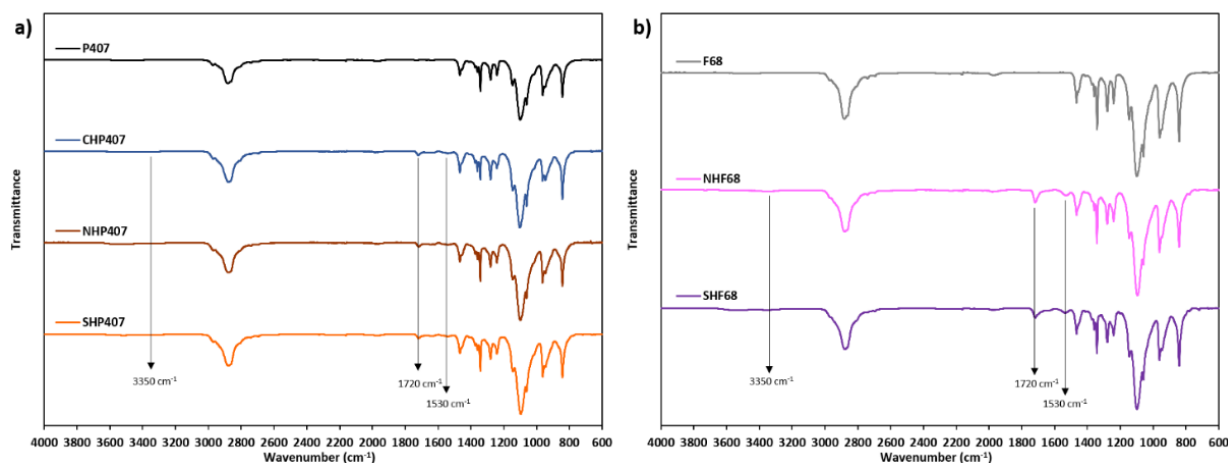


Figure 2 – ATR-FTIR spectra of a) P407-based PEUs (CHP407 in blue, NHP407 in brown and SHP407 in orange) and P407 as control (black), and b) F68-based PEUs (NHF68 in pink and SHF68 in purple) and F68 as control (grey). The typical peaks of urethane domains are indicated by vertical black arrows at 3350 , 1720 and 1530 cm^{-1} .

SEC results are summarized in table 1 and RID profiles are represented in figure 3. Considering the intrinsic error of SEC measurements (i.e., around 10%),⁵⁴ PEU molar masses generally were significantly greater with respect to their native macrodiols (i.e., P407 and F68). P407-based PEUs did not show significant differences when compared among each other, as well as for F68-based ones. Hence, these results further confirmed the efficacy of both PEU synthesis process and Boc-

cleavage reaction, as demonstrated in previous works.^{46,47} P407-based PEUs showed a significantly higher molar mass with respect to F68-based ones, as expectable from the nature of the involved macrodiols. Nonetheless, a good consistency was observed in terms of dispersity indexes, which were quantified around 1.8 for all PEUs. Moreover, as discussed in *Chapter 2.2*, a residual peak resulting from short polymers mainly composed of P407 di-blocks⁵⁵ was observed in all PEUs. This indicated the presence partially polymerized chains that were not completely removed through purification processes. However, the effect of such components on final hydrogel behavior can be considered negligible, because of their limited contribution within the entire molecular mass distribution.

Table 1 – Number average molar mass, Weight average molar mass and dispersity index of the macrodiols (i.e., P407 and F68) and the synthesized PEUs (i.e., CHP407, NHP407, SHP407, NHF68 and SHF68).

	<i>Number average Molar mass (Da)</i>	<i>Weight average Molar mass (Da)</i>	<i>Dispersity index</i>
P407	8000	9500	1.2
CHP407	30000	54000	1.8
NHP407	27000	49000	1.8
SHP407	29000	53000	1.8
F68	6300	6800	1.1
NHF68	22000	38000	1.8
SHF68	24000	40000	1.8

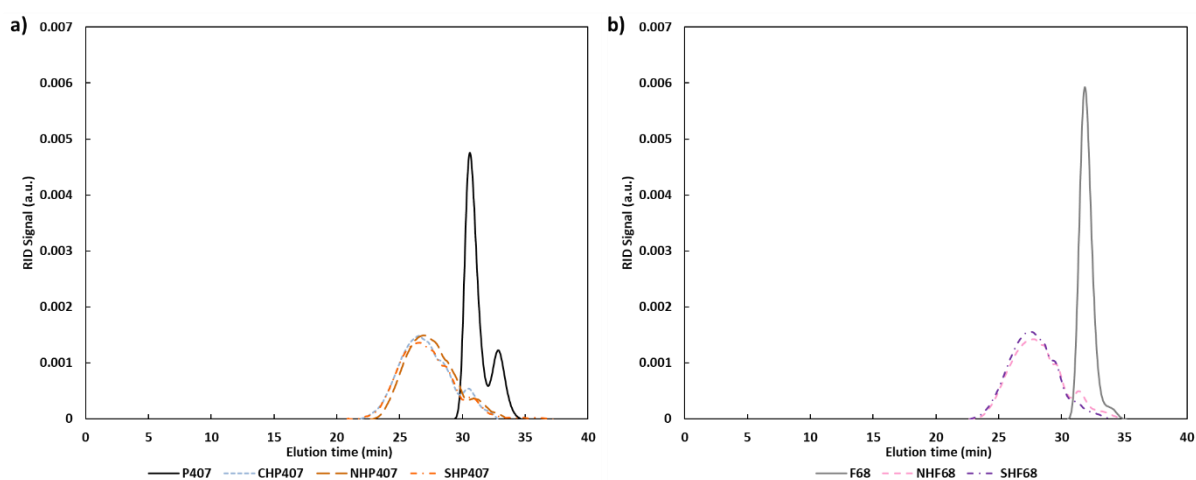


Figure 3 – SEC profiles (i.e., RID signal vs. elution time) of a) P407-based PEUs (CHP407 as blue dotted line, NHP407 as brown dashed line and SHP407 as orange dash-dotted line) and P407 (black continuous line), and b) F68-based PEUs (NHF68 as pink dashed line and SHF68 as purple dash-dotted line) and F68 (grey continuous line).

4.1.2 ¹H-NMR spectroscopy and free primary amine quantification

¹H-NMR spectroscopy was performed with the aim to evaluate whether the de-protection procedure was successfully performed. As reported in figure 4, no differences were observed between the spectra of PEUs based on the same macrodiol, thus further confirming a repeatable and consistent synthesis procedure and a conservative Boc-cleavage reaction in terms of molecular

structures, in accordance with ATR-FTIR and SEC results. Moreover, the amino group bearing PEUs (i.e., SHP407 and SHF68) showed a relevant decrease of the typical peak of Boc domains in the chemical shift range around 1.36 ppm in comparison with their original structures (i.e., NHP407 and NHF68), thus proving the effectiveness of the de-protection reaction for amine exposure. In addition, the intensity of the Boc-related peak reached higher relative values in NHF68 with respect to NHP407. Indeed, by comparing the peak related to Boc groups (1.35-1.36 ppm) with the bands derived from HDI domains (i.e., chemical shift between 1.46 and 1.37 ppm) the spectrum of NHF68 was characterized by a peak approximately 50% greater with respect to NHP407. This datum could indicate an enhanced chain extension process for NHF68 compared to NHP407 as a result of the probable higher reactivity of smaller F68-based pre-polymers, which were obtained at the end of the first step of the PEU synthesis process. As a consequence, Boc cleavage reaction performed on NHP407 resulted in an almost total deprotection of primary amines (i.e., Boc cleavage yield > 90%), while a lower yield (approx. 83%) resulted from NHF68. This hypothesis was further reinforced by the identified correlation between these results and those obtained from the quantification of free primary amines through Orange II sodium salt colorimetric assay. Indeed, the quantification of free primary amines resulted to be around $3.5E18 \pm 5.4E17$ NH_2/g_{SHP407} and $1.7E19 \pm 3.9E18$ NH_2/g_{SHF68} for SHP407 and SHF68, respectively. In this regard, the presence of a noteworthy amount of free primary amines generally represents an important factor for the suitability of such functionalized polymers for the design of devices for drug delivery. In fact, it has been demonstrated that the presence of $-NH_2$ groups can be exploited to perform specific functionalization reactions through carbodiimide chemistry⁴⁶ or confer enhanced responsiveness to acid environments⁴⁷ that characterize the milieu of acute inflammations or tumors in various tissues.⁵⁶ Additionally, amino-functionalized amphiphilic polymers can be used to design effective strategies for the encapsulation and delivery of therapeutic agents with improved bioavailability and efficacy into tumor environments,⁵⁷ as previously discussed in the introduction of this Chapter.

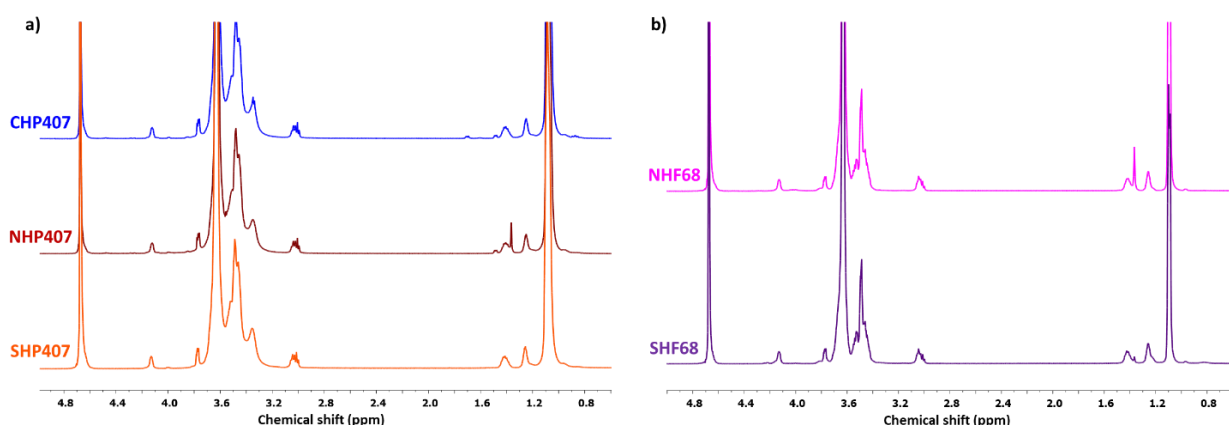


Figure 4 – 1H -NMR spectra of a) P407-based (CHP407 (blue), NHP407 (brown) and SHP407 (orange)) and b) F68-based (NHF68 (pink), SHF68 (purple)) PEUs.

4.1.3 Critical micellar temperature (CMT) evaluation

The study of the self-assembly process that induces micelle formation is an important information to properly understand and evaluate the thermo-responsiveness of amphiphilic polymers in watery

environments. Indeed, the here-developed PEUs are expected to form supramolecular structures composed of a lipophilic core and a hydrophilic external corona upon thermal stimulus. The characterization of CMT allows a better definition of PEU thermo-sensitivity, which represents an elemental factor for the formation of PPR-based SM networks. Indeed, it has been demonstrated that hydrophobic interactions act as stabilizing factors within polymeric networks, thus enhancing the formation of SM hydrogels based on crystallized PPRs.⁵⁸⁻⁶⁰ Moreover, as discussed in the previous Chapter, the presence of dissolved ions can induce significant variations in the kinetics of micelle formation by decreasing the CMT, thus acting as a further stabilizing element. Thence, it can be deduced that various behaviors of PEUs in forming SM structures could be ascribed to the above-mentioned factors (i.e., amphiphilic nature of PEUs and presence of ions in solution). Figure 5 reports the quantified absorbance at 356 nm as a function of temperature for PEU solutions at 1% w/v concentration in PBS and the two linear regressions used for CMT quantification. Interestingly, significant differences were found between the two PEU families. P407-based PEUs were characterized by a sharp increase of absorbance due to DPH internalization and solubilization into micelle cores, thus resulting in specific values of CMTs, which are reported synthetically in table 2. Interestingly, for all P407-based PEUs CMTs values in PBS were in the range between 19.5 and 20.1 °C, thus indicating a consistent responsiveness upon thermal stimulus. This common behavior resulted to be in complete agreement with the previously discussed results from ATR-FTIR, SEC and ¹H-NMR characterizations. Instead, F68-based PEUs did not show the ability to form micellar structures within the investigated temperature range (i.e., from 5 to 40 °C). In detail, no absorbance signal variations were observed for NHF68, while a slight increase of absorbance was observed for SHF68-based solutions. It is likely that the dimension, the relative quantity and the distribution of PPO domains into PEU backbone were not suitable for the formation of micelles around body temperature (i.e., 37 °C), although the synthesis process resulted in highly chain-extended PEUs. This behavior was in accordance with the results obtained for solutions based on native F68 macrodiol.⁶¹ Thence, even though F68-based PEUs showed relatively high molar mass, the influence of the characteristics of PPO domains of such macrodiol could play the most important role in the formation of micelles. In this case, even the presence of dissolved ions did not contribute to form substantial hydrophobic interactions within the investigated range of temperatures. PEU solutions in ddH₂O were characterized by slightly higher values of CMT due to the absence of salting-out effect,^{62,63} as indicated in figure 6 and table 2. Such observations represented an important set of information in order to better explain the behavior of similar PEU solutions (i.e., at 1% w/v concentration) upon the addition of CDs and curcumin. Moreover, these observations could be even helpful for the interpretation of systems based on higher PEU contents.

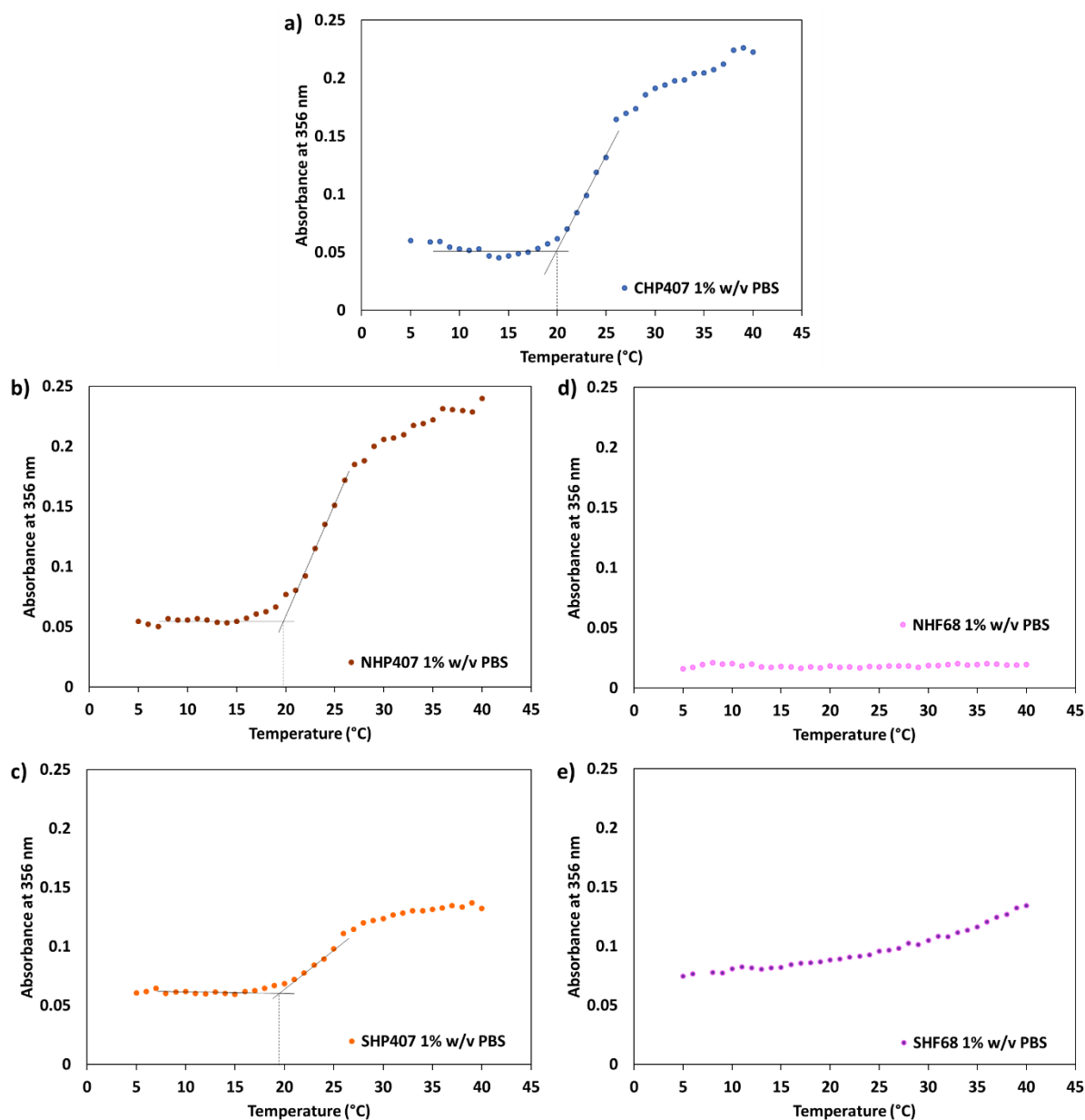


Figure 5 – CMT curves (i.e., absorbance at 356 nm vs. temperature) of a) CHP407 (blue), b) NHP407 (brown), c) SHP407 (orange), d) NHF68 (pink) and e) SHF68 (purple) solutions (1% w/v) in PBS. CMT values are indicated by black vertical lines.

Table 2 – CMT values for all the synthesized PEUs solubilized in PBS and ddH₂O at 1% w/v concentration.

PEU	CMT in PBS (°C)	CMT in ddH ₂ O (°C)
CHP407	20.1	21.5
NHP407	19.8	22.0
SHP407	19.5	22.3
NHF68	-	-
SHF68	-	-

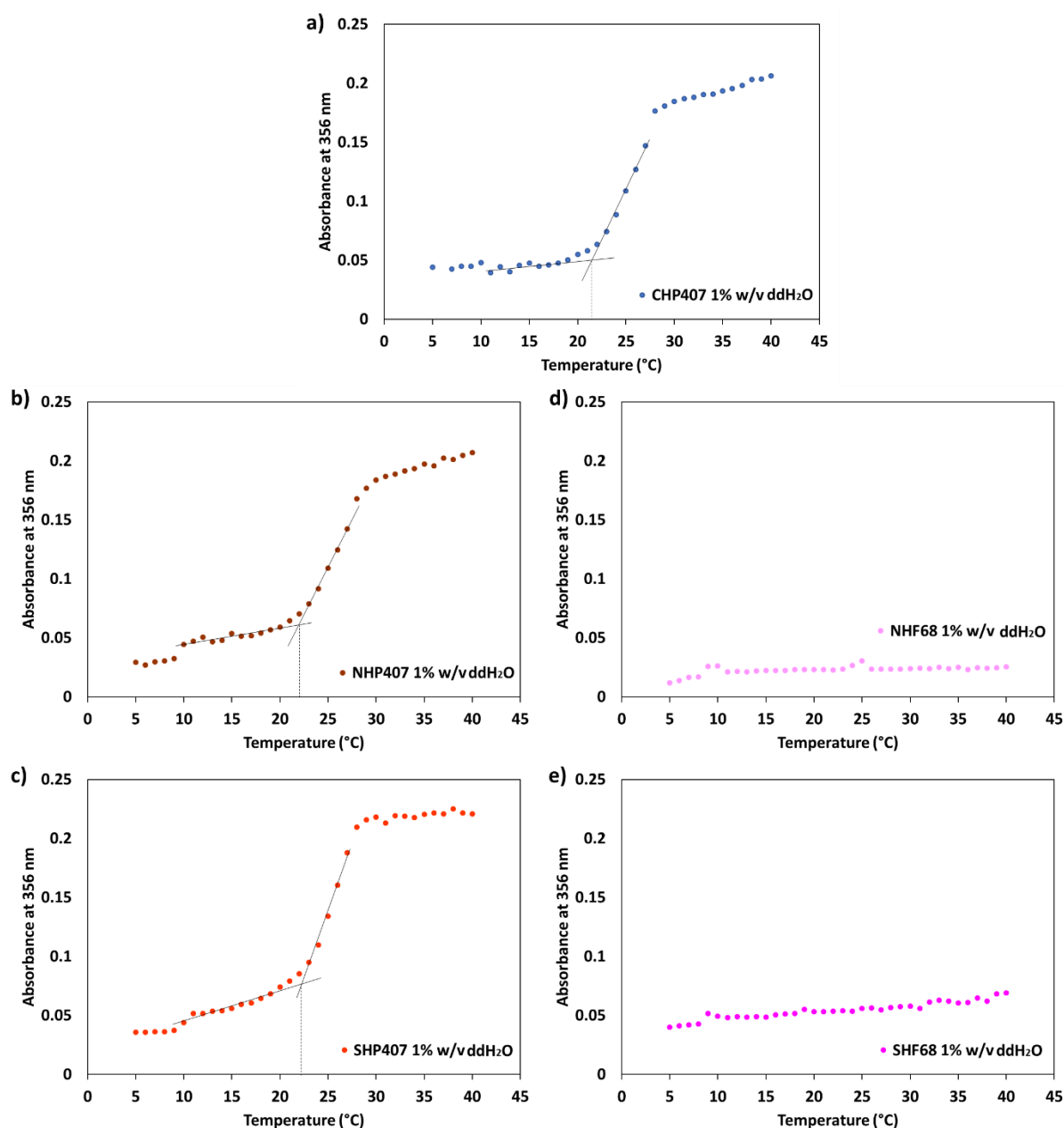


Figure 6 – CMT curves (i.e., absorbance at 356 nm vs. temperature) of a) CHP407 (blue), b) NHP407 (brown), c) SHP407 (orange), d) NHF68 (pink) and e) SHF68 (purple) solutions (1% w/v) in ddH₂O. CMT values are indicated by black vertical lines.

4.2 Physico-chemical characterization of SM complexes

4.2.1 X-Ray powder diffraction (XRD)

XRD tests were performed with the aim to detect the presence of PEU-based SM crystals composed of packed PPRs. The typical patterns of PEO-based polymers exhibit specific peaks around 19.1° and 23.3°, which were detected also in pure PEU samples, as reported in figure 7. Nonetheless, the presence of CDs in solution with PEUs resulted in the formation of a turbid suspension and the consecutive precipitation of a crystalline matter. The patterns related to the SM self-assembly of PEUs and CDs are reported in figure 7. Interestingly, as expected from our

previous findings, the resulting crystalline samples were characterized by the presence of the typical peaks of PPRs forming channel-like crystals. Indeed, the diffractograms showed peaks at 2θ equal to 19.8° , 13° and 7.6° .⁶⁴ The simultaneous absence of multiple reflections demonstrated the complete transformation of free CDs into PPRs and the consecutive coalescence into SM crystals. Nonetheless, although a successful formation of SM domains was observed for most PEUs, some differences and exceptions were evidenced by this investigation. Indeed, the PEUs investigated in the previous chapters (i.e., CHP407 and NHP407) were used to prepare formulations with a polymeric content of 1% w/v and a CD concentration required to cover the theoretical 100% of PEO domains (i.e., 7.6% w/v). In these conditions, CHP407- and NHP407-based samples resulted in yield of PPR crystallization around $58 \pm 0.5\%$ and $30 \pm 0.5\%$, respectively. Differently, with the here-investigated novel PEUs (i.e., SHP407, NHF68 and SHF68), formulations containing higher PEU and/or CD concentrations were required to achieve a comparable yield of crystallization (i.e., yield greater than 30%) that was necessary for the preparation of samples for XRD crystallography. In detail, the designed formulations were different depending on the involved PEU: SHP407 1% - SM 130% (i.e., SHP407 at 1% w/v concentration, 10% w/v CD concentration, $74.4 \pm 1.5\%$ yield) and SHF68 2% - SM 70% (i.e., SHF68 at 1% w/v concentration, 12% w/v CD concentration, $84.8 \pm 0.4\%$ yield). Instead, NHF68-based systems did not result in a suitable amount of crystalline matter for XRD characterization (i.e., yield $< 10\%$). These data can be ascribed to the different PEU thermo-sensitivity that was previously investigated and discussed. In this regard, it is highly probable that P407-based PEUs exhibited the highest yield of SM crystals due to their marked ability to form hydrophobic interactions, which acted as effective stabilizing physical crosslinks for the formation and the subsequent crystallization of PPRs in watery environments. Differently, although the PEUs based on F68 were characterized a lower molecular mass (i.e., approx. 20% lower than P407-based PEUs), which would generally enhance the SM self-assembly process, these PEUs were characterized by smaller PPO domains and hence a lower capacity to stabilize the polymeric network. This peculiarity could probably represent the most important factor influencing the production of SM crystals based on PPRs starting from PEUs. However, significant differences were observed between NHF68 and SHF68. Indeed, in addition to the above-mentioned common properties, the presence of Boc domains represented a further factor affecting SM network development. It is likely that the presence of Boc domains as pendant groups acted as hindering elements for CD threading along NHF68 chains. For these reasons, the inclusion complexes based on NHF68 were no longer characterized in physico-chemical terms. Interestingly, an opposite behavior was observed for NHP407 and SHP407. Indeed, NHP407 was able to produce a relatively higher amount of SM crystalline powder (i.e., around $30\% \pm 0.5\%$) at lower PEU and CD concentrations (i.e., 1% w/v and 7.6% w/v, respectively) when compared to SHP407, which in same conditions produced a negligible amount of crystalline matter (i.e., $< 10\%$). This particular relationship could be attributed to the lower degree of polymerization of these materials, which resulted in a lower number of Boc groups present along NHP407 chains with respect to NHF68, as previously hypothesized through ¹H-NMR measurements. It is then probable that for NHP407 the presence of a balanced number of Boc domains, which are hydrophobic, could act as further stabilizing factor for the formation of hydrophobic interactions with other in-chain domains (i.e., PPO and HDI), thus enhancing the formation of PPRs without significantly impeding CD threading along PEU chains. Nonetheless, the best PEU for PPR formation and crystallization

resulted to be CHP407, probably due to its best balance between hydrophobicity and molar mass, in the absence of lateral steric hindrance. Thence, these results were in complete accordance with previous $^1\text{H-NMR}$ and CMT characterizations, thus further demonstrating that PEU composition and behavior could play an elemental role in the formation of SM networks and tuning of final hydrogel properties.

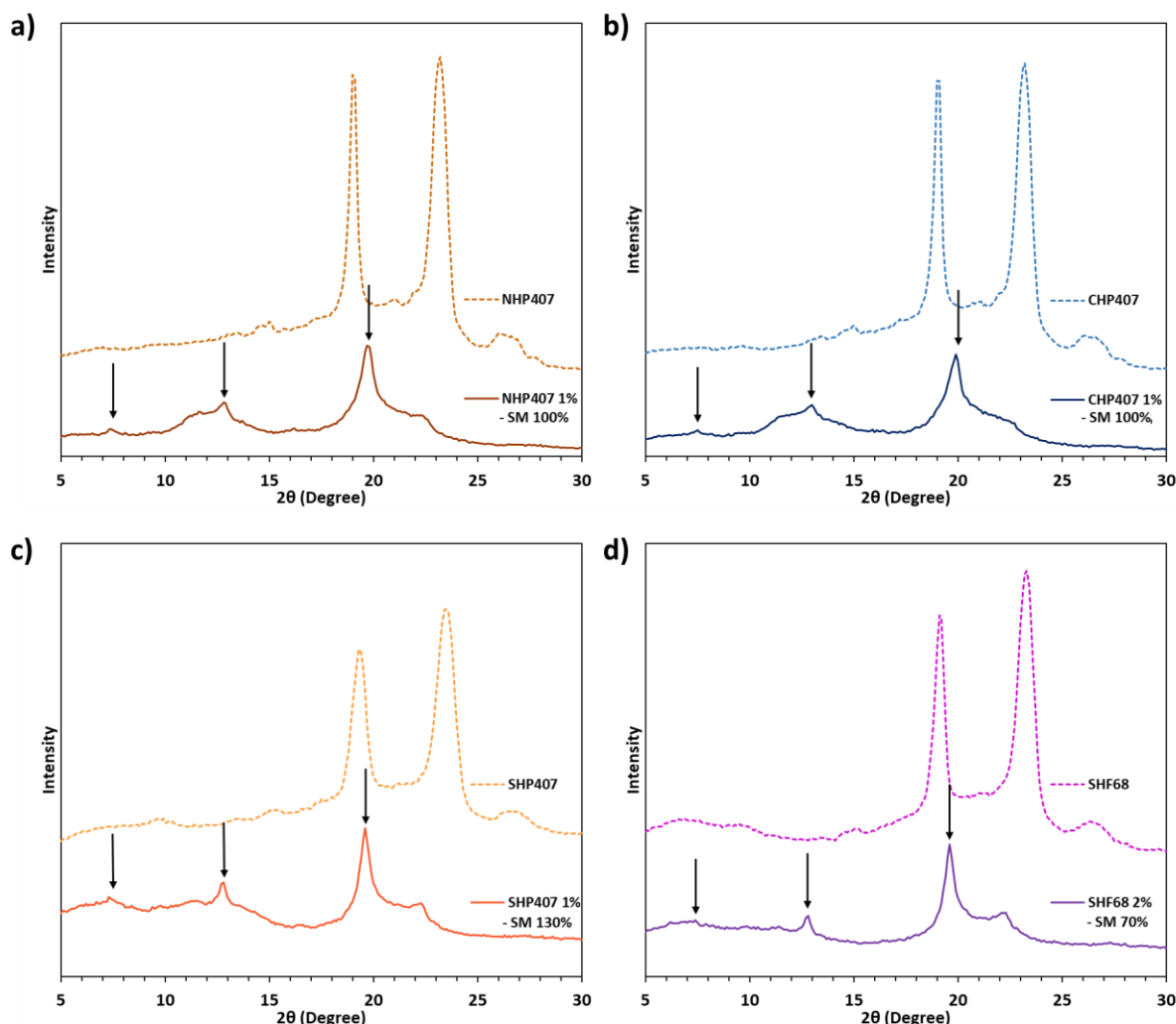


Figure 7 – XRD spectra of a) NHP407 (brown), b) CHP407 (blue), c) SHP407 (orange) and d) SHF68 (purple). Patterns of pure PEU powders are represented as dashed lines (light colors), while those of the SM crystalline powders resulting from their crystallization with CDs are reported as continuous lines (dark colors). The typical peaks (approx. 2θ equal to 7.2° , 12.8° and 19.8°) of SM crystals composed of packed PPRs are highlighted by vertical black arrows.

4.2.2 ATR-FTIR characterization

The simultaneous co-presence of PEUs and CDs in the crystalline matter resulting from the self-assembly process in ddH₂O was proved also through ATR-FTIR spectroscopy. The samples previously characterized using XRD crystallography were evaluated and the data are reported in figure 8, in which each SM sample is compared with native CD and PEU. From a general perspective, all the typical peaks of both PEUs and CDs were observed even in the spectra of SM samples. In detail, the presence of CDs was confirmed by the characteristic peaks at 1075, 1155

and 2954 cm^{-1} for C-O, C-O-C and CH stretching vibrations, respectively. Moreover, even the peak related to the asymmetric stretching of -OH domains that belong to CDs was detected in SM samples. Nonetheless, such vibration band resulted upshifted up to 3340 cm^{-1} in SM samples, thus indicating a different conformation of CDs composing PPRs. In this regard, it is likely that the linear head-tail arrangement of CDs could result in a different excitation energy with respect to the typical cage-like conformation of native CDs. In addition, also the characterizing peaks of urethane domains were found upshifted. Indeed, the stretching vibration of C=O groups at 1720 cm^{-1} was upshifted up to 1740 cm^{-1} in SM samples, thus indicating an inhibition of crystallization and packing mediated from hydrogen bonds in PEU chains. Interesting differences were also observed between the different investigated PEUs. Indeed, the entity of the observed upshifts was different for SHF68, probably due to the formation of a less-organized SM network for the previously indicated reasons (i.e., weaker hydrophobicity that could hinder the stabilization of the polymeric network for CD threading along PEO domains).

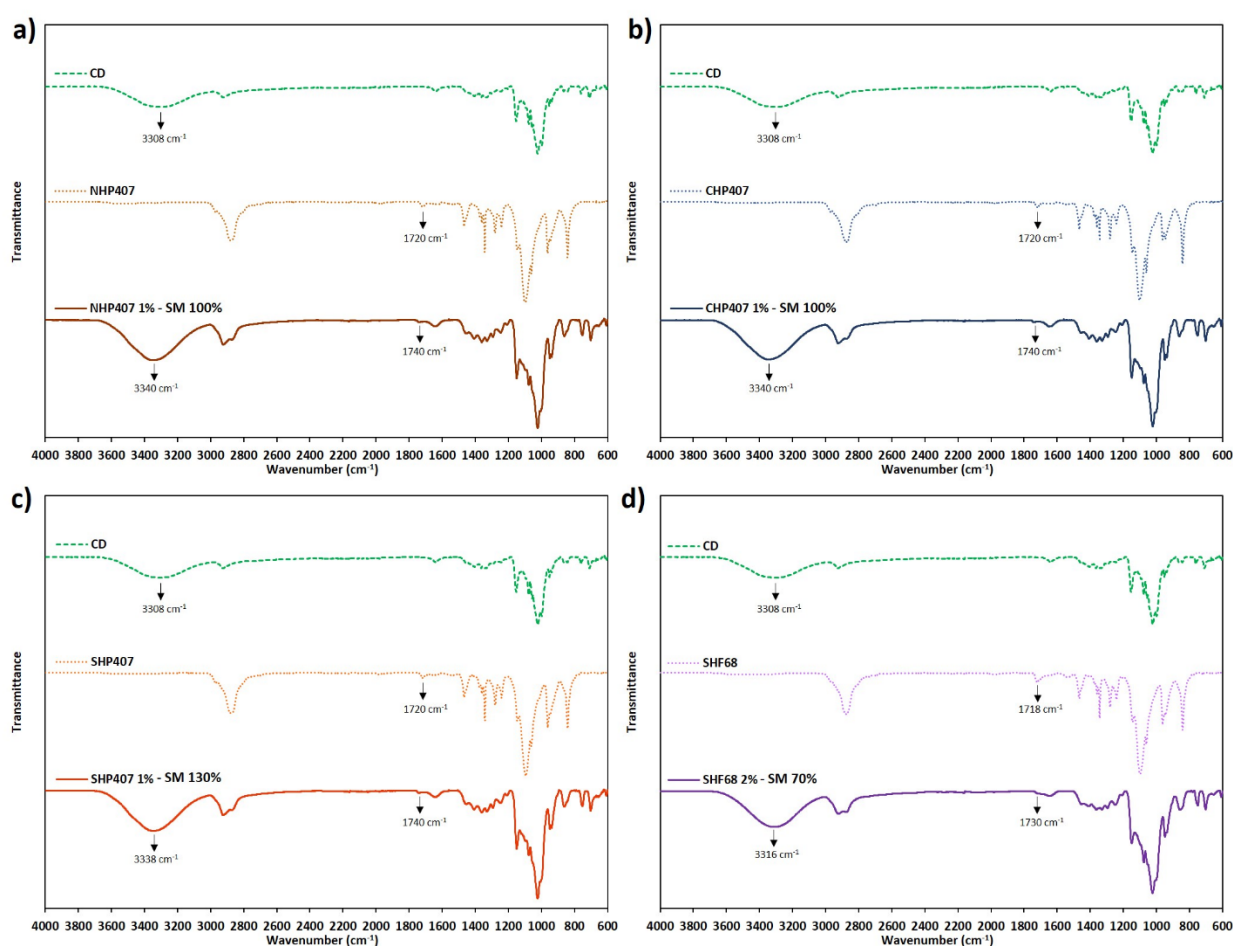


Figure 8 – ATR-FTIR spectra of CDs (green dashed lines), pure PEUs (dotted lines) and SM crystalline samples (continuous lines) for a) NHP407 (brown), b) CHP407 (blue), c) SHP407 (orange), and d) SHF68 (purple). All peaks subjected to significant shifts are highlighted by black vertical arrows.

4.2.3 $^1\text{H-NMR}$ spectroscopic analyses of SM structures

$^1\text{H-NMR}$ spectroscopy was performed in order to complete the set of characterizations that proved the self-assembly of PPRs within PEU- and CD-based mixtures in ddH_2O . To this aim, the same

formulations previously characterized through XRD crystallography and ATR-FTIR spectroscopy were re-solubilized in D₂O and were analyzed by ¹H-NMR spectroscopy. Figure 9 reports the entire set of recorded spectra. The presence of chemical shifts around 3.63 ppm and in the domain ranging between 1.5 and 0.9 ppm proved the presence of PEU in the resulting SM crystals. The contribution of CDs was demonstrated by the occurrence of multiple peaks in the chemical shift domains from 4.0 to 3.7 ppm, from 3.55 to 3.45 and at 5.08 ppm. Thence, the strong correlation between XRD, ATR-FTIR and ¹H-NMR results demonstrated the successful utilization of PEUs as PPR-forming polymeric materials and their chemical composition significantly influenced the final assembly process with CDs. Generally, the resulting molecular complexity of PEUs made notably difficult the calculation of specific parameters that describe the formation of SM complexes, such as the constant of associations with CDs. Nonetheless, such investigations were not elemental for the development of this work and a general dependence of SM complexes over PEU composition and chemical properties was reliably assessed through the performed studies.

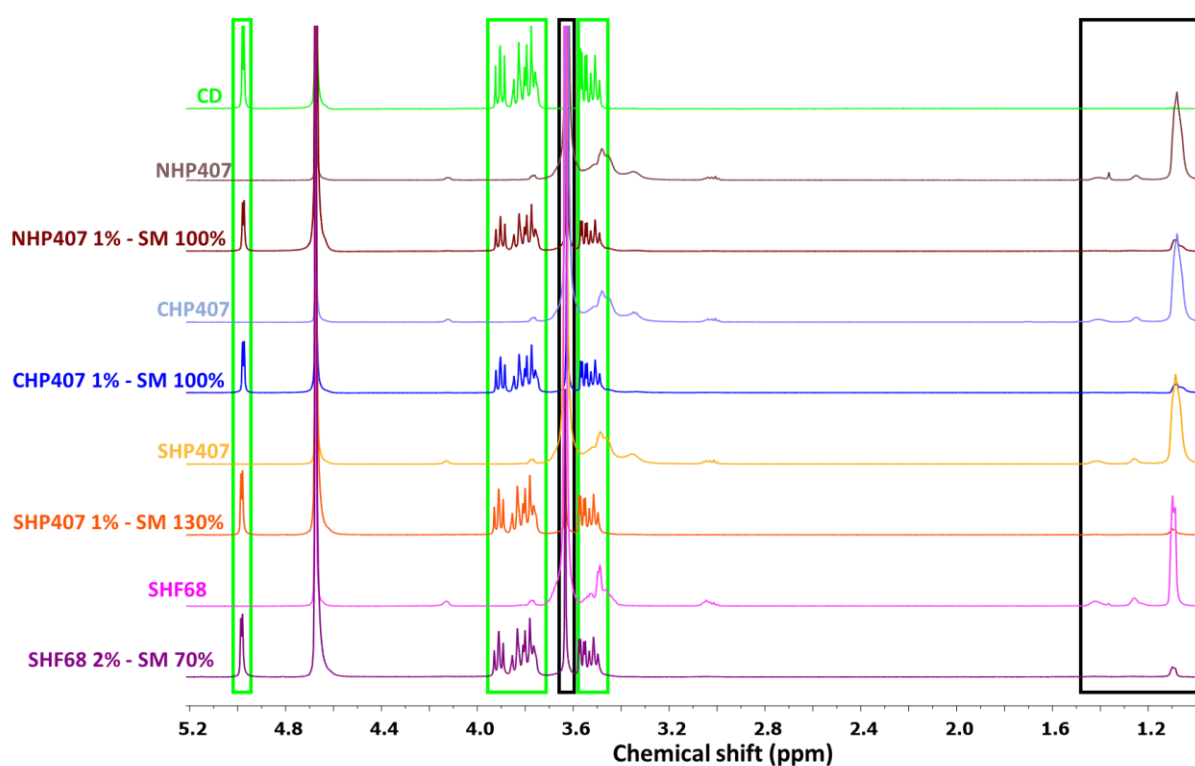


Figure 9 – ¹H-NMR spectra of CDs (green), NHP407 (light brown), NHP407 1% - SM 100% (brown), CHP407 (light blue), CHP407 1% - SM 100% (blue), SHP407 (light orange), SHP407 1% - SM 130% (orange), SHF68 (pink) and SHF68 1% - SM 70% (purple) samples solubilized in D₂O. CD and PEU typical chemical shifts are embedded in green and black squares, respectively.

4.3 Supramolecular hydrogel characterization

4.3.1 SM hydrogel formulation and gelation kinetics

SM hydrogels were formulated at PEU and CD concentrations defined based on data reported in the previous Chapters. In detail, a PEU concentration range between 1 and 5% w/v was investigated, while CD content was fixed at 10% w/v concentration. Table 3 reports gelation time

results for all the tested systems. NHF68-based formulations exhibited non-gelling behavior (i.e., NHF68 1% - CD 10%) or significantly more extended gelation time when compared to all the other systems at PEU concentration of 3% and 5% w/v. These observations were in total agreement with the previous considerations. Thence, for the limited suitability of NHF68 to form stable and solid hydrogel networks, such PEU was excluded from the following characterizations. Differently, SHF68 was characterized by still acceptable gelation properties and presented a relevant number of free amino groups along its backbone, which make it suitable for further functionalization or for the design of pH-sensitive formulations. Because of these reasons, such PEU was maintained in the subsequent studies as constituent of BLEND samples together with CHP407 (BLEND samples were composed of CHP407 at 80% wt and SHF68 at 20% wt with respect to the total mass of PEU present within the gel). Such composition for BLEND-based hydrogels was defined to take the advantages of the best PEU in terms of gelation properties (i.e., CHP407) and the one with the higher degree of functionalization in terms of quantity of free primary amines (i.e., SHF68). As these two PEUs were characterized by similar chemical structures, but different properties (i.e., hydrophobic character and molar mass), it was expected that their mixture in watery environment could result in an interesting behavior. Indeed, the sample BLEND 5% - CD 10% was characterized by the fastest gelation kinetics with respect to the other samples at the same PEU concentration (i.e., 5% w/v). Such result could be related to probable constructive interactions occurring between CHP407 and SHP407 chains, thus inducing the formation of a more interconnected polymeric network. It is likely that the chains of SHF68, which is characterized by a lower molar mass and higher hydrophilicity, could act as polymeric crosslinkers through the formation of entanglements with the domains of the highly organized network based on CHP407.^{65,66} SM hydrogels based on pure CHP407 showed remarkably fast gelation kinetics due to the absence of any pendant group along PEU backbone and a pronounced hydrophobicity derived by the presence of various lipophilic domains (i.e., CDM, HDI and PPO). Interestingly, SHP407-based hydrogels showed slightly faster gelation with respect to NHP407-based systems. This observation resulted to be in contrast with the previous results in terms of SM self-assembly yield in ddH₂O. The reason for such behavior could be related to the different aqueous environment used for the production of SM hydrogels compared to the one exploited for the formation of pure crystals for physico-chemical analyses. Indeed, PBS contains dissolved anions (i.e., phosphate), which could interact with the polar domains resulting from the presence of primary amines as pendant groups within SHP407 chains, thus acting as a further stabilizing factor of the hydrogel network. This behavior was in complete accordance with the previous CMT results. In fact, SHP407-based solutions in PBS were characterized by slightly lower values of CMT (19.5 °C) with respect to NHP407-based ones (19.8 °C), while an opposite behavior was observed for formulations based on ddH₂O. The same phenomenon could be supposed for SHF68-based systems. In fact, SHF68 was characterized by a relevant number of free primary amines (i.e., 6-fold greater than SHP407). However, differences in gelation timing between NHP407- and SHP407-based hydrogels at 3% w/v PEU concentration followed an opposite trend with respect to the systems designed at higher PEU contents (i.e., 5% w/v). Indeed, the system composed of NHP407 at 3% w/v concentration was characterized by a faster gelation kinetics with respect to the one based on SHP407 and identically formulated. This peculiar behavior could be dependent on highly complex physical interactions (e.g., hydrophobic interactions, hydrogen bonds, salting-out effect, entanglements and steric hindrance), which undoubtedly influenced the convoluted self-

assembling process in a non-linear fashion. Thence, at lower PEU content, i.e., lower PEU/CD mass ratio, the additional effect of Boc groups as hydrophobic regions probably retains a more evident role in determining gelation kinetics, rather than the presence of free primary amino groups. Indeed, in agreement with our previous hypothesis, in these conditions the presence of Boc groups most likely stabilizes the network composed of PEU units, while at higher PEU/CD mass ratio (i.e., PEU at higher concentration, 5% w/v) Boc regions probably hamper the mobility of the network and a superior balance could be reached by means of a more linear structure characterized by polar groups as in SHP407. Hereafter, CHP407, SHP407 and BLEND were selected for the further characterizations of their hydrogel systems, since such PEUs open the way to the possibility to produce a plethora of SM systems with different chemical properties and best gelation kinetics.

Table 3 – Gelation time of PEU-based hydrogels incubated at 25 °C. O.N. = overnight.

	Gelation time
CHP407 1% - CD 10%	O.N.
CHP407 3% - CD 10%	2 h 20 min
CHP407 5% - CD 10%	1 h 30 min
NHP407 1% - CD 10%	O.N.
NHP407 3% - CD 10%	2 h 20 min
NHP407 5% - CD 10%	2 h 30 min
SHP407 1% - CD 10%	O.N.
SHP407 3% - CD 10%	3 h
SHP407 5% - CD 10%	2 h
BLEND 1% - CD 10%	O.N.
BLEND 3% - CD 10%	2 h 20 min
BLEND 5% - CD 10%	1h
NHF68 1% - CD 10%	SOL
NHF68 3% - CD 10%	72 h
NHF68 5% - CD 10%	72 h
SHF68 1% - CD 10%	O.N.
SHF68 3% - CD 10%	O.N.
SHF68 5% - CD 10%	5h 30 min

4.3.2 Rheological characterization of SM hydrogels

In order to better investigate the role of PEUs on the properties of the resulting SM hydrogel networks, a complete set of rheological tests was performed on formulations with the highest and the lowest PEU concentration within the investigated range (i.e., 1 and 5% w/v). Moreover, rheological characterizations are elemental to assess whether a hydrogel system could be suitable for the clinical practice as injectable platform for drug delivery. Strain sweep tests were performed in order to characterize the ability of the gels to withstand mechanical load and self-heal. Moreover, such rheological tests permitted the definition of the region of viscoelastic linearity (LVE). Figure 10 reports the trends of G' and G'' (i.e., storage and loss moduli, respectively) as a function of applied strain at 37 °C and table 4 collects the most significant parameters that can be obtained from these tests.

Table 4 – Summary of strain sweep test main parameters: G'_{LVE} , G''_{LVE} , G'_{LVE} recovered (percentage of recovery of the starting storage modulus measured by repeating the test after sample quiescence for 15 minutes at 37 °C), strain at which network rupture occurs (γ_L), $\gamma_{L_recovery}$ (γ_L measured by repeating the test after sample quiescence for 15 minutes at 37 °C).

	G'_{LVE} (Pa)	G''_{LVE} (Pa)	G'_{LVE} recovered (%)	γ_L (%)	$\gamma_{L_recovery}$ (%)
CHP407 1% - CD 10%	4500	350	91	0.29	0.13
CHP407 5% - CD 10%	15400	2300	87	0.29	0.50
SHP407 1% - CD 10%	4000	240	88	1.00	0.45
SHP407 5% - CD 10%	10000	1400	91	0.48	0.56
BLEND 1% - CD 10%	3600	280	97	0.70	0.38
BLEND 5% - CD 10%	14700	1500	83	0.55	0.50

All the samples showed constant values of G' and G'' within the LVE region (i.e., G'_{LVE} and G''_{LVE}). Over a critical value of strain (γ_L), all the formulations showed a relevant decrease of G' and a crossover point between G' and G'' , in which G'' became greater than G' , indicating that the samples started to behave as viscoelastic fluids as a consequence of hydrogel network rupture due to crack formation. The concomitant decrease of G' and G'' was typical of a thixotropic behavior of such PPR-based networks, in accordance with other similar systems reported in the literature.⁶⁷ Then, upon the achievement of relevant strain values (i.e., 500%) the hydrogels were maintained in quiescent state at 37 °C for 15 minutes and tested again in order to evaluate their self-healing ability. As expected, all the hydrogels resulted to be self-healing and a recovery of at least 83% of their starting G' was observed for all the formulations. CHP407-based hydrogels showed the highest values of G'_{LVE} and G''_{LVE} but the lowest values of γ_L . Such response could be explained by the probable higher yield of SM crystallization that resulted from the marked hydrophobicity and linearity of CHP407, thus forming stiffer and more fragile networks. A similar response was observed for SHP407- and BLEND-based systems at 1% w/v PEU concentration, while at 5% w/v PEU content BLEND-based system was characterized by better mechanical properties, which were slightly lower with respect to those of the sample with the same composition but based on CHP407. In this regard, the presence of SHF68 within BLEND formulations could induce a toughening effect on the resulting networks. From a general perspective, no clear dependency of γ_L over recovery process was assessed. However, it was observed that the hydrogels containing PEU at 1% w/v concentration were negatively affected by the rupture process, since $\gamma_{L_recovery}$ values decreased for all the PEU-based formulations, while not significant decrements were observed for samples at 5% w/v PEU concentrations. These different behaviors could be ascribed to the nature of the formed networks that depends on the PEU/CD mass ratio, as hypothesized in the previous Chapters. Indeed, PEU 1% - CD 10% systems were characterized by a low PEU/CD ratio, which could result in highly crystalline SM networks. Differently, higher PEU/CD ratios (i.e., PEU 5% - CD 10%) could result in more diffused free PEU domains that are less sensitive to applied deformation with respect to highly crystalline PPR-based regions.

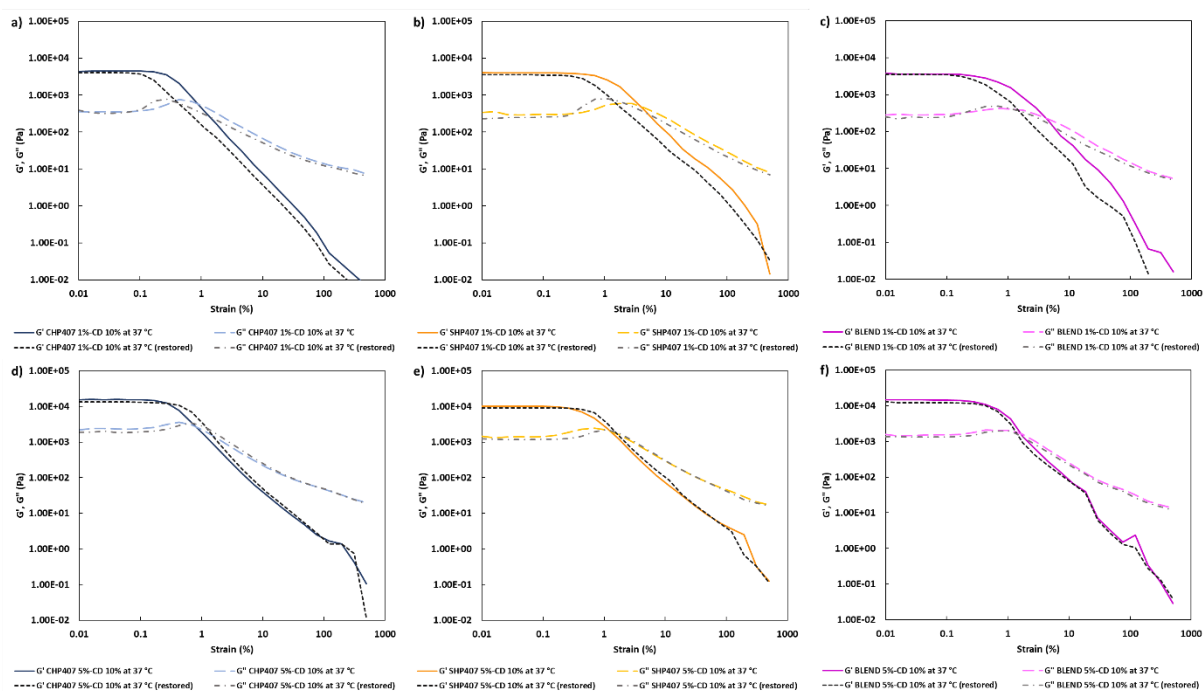


Figure 10 – G' (continuous lines) and G'' (dashed lines) curves as a function of applied deformation for a,d) CHP407 (blue), b,e) SHP407- (orange), and c,f) BLEND- (purple) based hydrogels. G' (black dotted lines) and G'' (grey dash-dotted lines) trends registered after recovery in quiescent state for 15 minutes at 37 °C are also plotted to evaluate self-healing ability.

Frequency sweep tests were performed at 25, 30 and 37 °C to evaluate the gelation process of the SM networks, since all the here-synthesized PEUs showed a thermo-responsive behavior. Figure 11 reports the trends of G' and G'' as a function of applied frequency within the investigated temperature range. Generally, all the hydrogels were characterized by a fully developed “gel” state. Indeed, G' was greater than G'' within the whole investigated range of angular frequencies and temperatures. However, a slight dependence over temperature was observed. Indeed, a thermo-thickening effect was observed due to the thermo-sensitive nature of the amphiphilic PEUs. As an example, G' at 100 rad s⁻¹ for SHP407 1% - CD 10% was equal to 2450 Pa at 25 °C, while the same parameter resulted to be equal to 4200 Pa at 37 °C. Even in this case, CHP407-based hydrogels were characterized by the highest values of G' and G'' , while SHP407-based ones exhibited the lowest ones. BLEND-based hydrogels were characterized by intermediate mechanical properties compared to other systems based on CHP407 and SHP407.

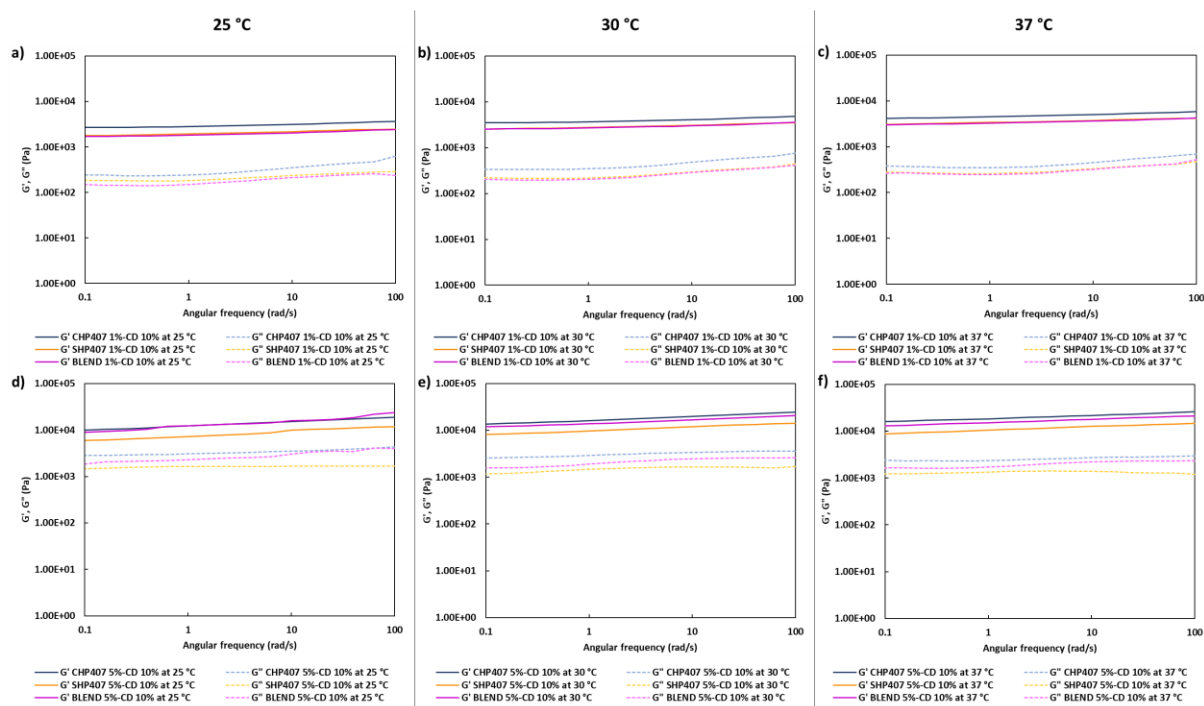


Figure 11 – Trends of G' (continuous line) and G'' (dashed line) as a function of angular frequency for hydrogels based on CHP407 (blue), SHP407 (orange), and BLEND (purple) at three different temperatures (i.e., 25, 30 and 37 °C).

The ability of the SM hydrogels to self-heal upon cyclic deformations was evaluated through strain tests. As reported in figure 12, all the investigated formulations were characterized by a quick recovery (i.e., within 30 seconds) at low deformation (0.1%) after complete rupture of hydrogel network through the application of a high strain (100%) for 60 seconds. During the rupture phases, higher values of G'' were registered with respect to G' , as typical of viscoelastic fluids. The overall recovery of G' after three complete rupture cycles was quantified to be greater than 84% for all formulations, as summarized in table 5. Interestingly, the system SHP407 5% - CD 10% was characterized by a complete recovery of its starting mechanical properties (i.e., 100% recovery of starting G'). This behavior could be correlated with the previously supposed lower degree of development of the PPR-based SM network for this sample, resulting in a less rigid and more reversible hydrogel system. A parallel and less relevant contribution of salting-out effect could be hypothesized in the case of SHP407-based hydrogel networks. A similar explanation could be attributed to the behavior of BLEND-based hydrogels, since the observed recovery ability turned out to be greater with respect to CHP407-based ones. Probably, the mixed contribution of a less developed SM network and polymeric crosslinks composed of SHF68 domains represent features enhancing the reversibility of BLEND-based hydrogels after cyclic stress application. These results indicated that the here-designed SM hydrogels were characterized by remarkable mechanical properties and reversibility, thus suggesting a good suitability in terms of stability, responsiveness and handling properties.

Table 5 – Percentage of G' recovered (%) after 3 complete rupture cycles at 100% strain.

	G' recovered (%) after 3 cyclic ruptures
CHP407 1% - CD 10%	89
CHP407 5% - CD 10%	84
SHP407 1% - CD 10%	88
SHP407 5% - CD 10%	100
BLEND 1% - CD 10%	90
BLEND 5% - CD 10%	92

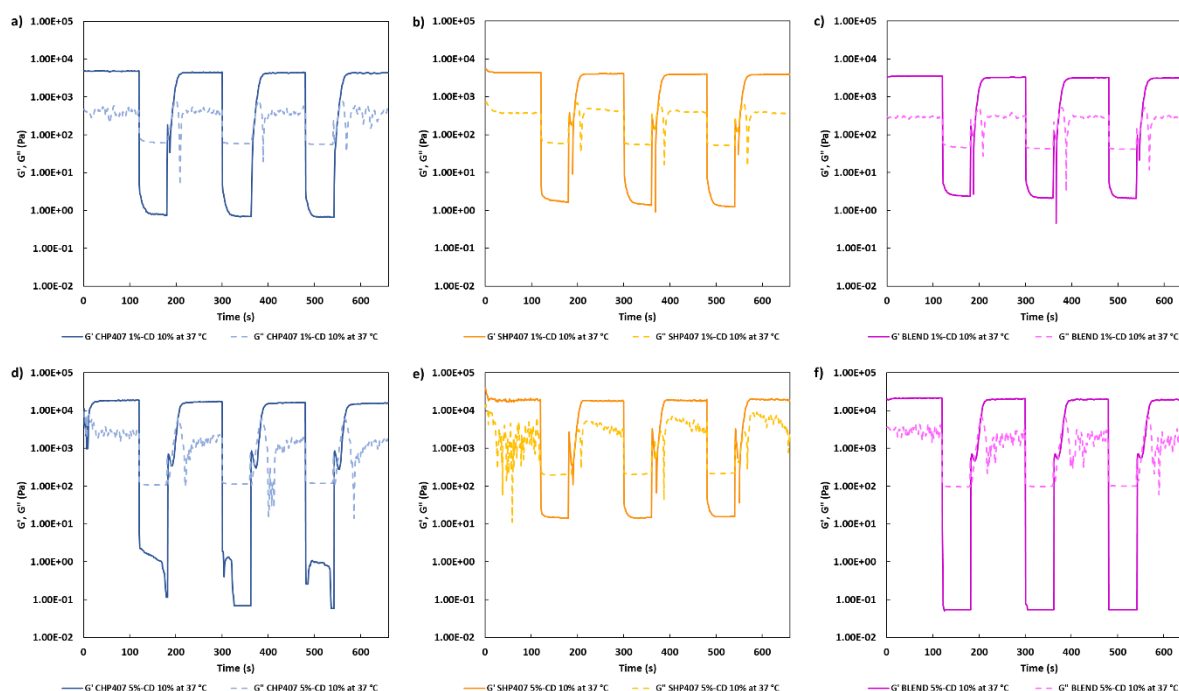


Figure 12 – Self-healing test reporting the trends of G' (continuous line) and G'' (dashed line) for CHP407 (blue, a) 1% and d) 5% w/v), SHP407 (orange, b) 1% and e) 5% w/v), and BLEND (purple, c) 1% and f) 5% w/v) hydrogels. Recovery phases (0.1 % strain for 120 s) are characterized by $G' > G''$, while rupture phases (100 % strain for 60 s) are characterized by $G'' > G'$, thus indicating a complete hydrogel breakage and a thixotropic response.

4.3.3 Swelling and stability in aqueous environment

The responsiveness to external environments of the here-designed SM hydrogels was evaluated in physiological-like milieu (i.e., PBS, pH 7.4, 37 °C). The obtained data regarding PBS absorption and weight loss are reported in figure 13. Generally, the results were comparable to the ones reported in the literature^{58,68,69} and in accordance with previous observations in *Chapter 2.2* and *Chapter 2.3* of *Section 2*. As previously discussed, the entire set of investigated hydrogels showed a good stability, as highlighted by the maintenance of an approximately constant network wet weight. Nonetheless, a simultaneous and evident release of hydrogel components was measured through the determination of weight loss. Thence, these observations suggested the occurrence of a relevant mass exchange between the hydrogel network and the external watery environment, as previously observed through preliminary studies. The integration of these two aspects can be

observed by estimating the swelling ratio value. In fact, the SM hydrogels showed a continuously increasing swelling ratio, thus indicating an incremental fluid content over time, as indicated in figure 14. Swelling ratio calculation was characterized by values even greater than 2, thus indicating that the ratio between fluid and polymeric content was at least doubled over incubation. Hence, the hydrogels continuously released instable components, such as free CDs and PEU aggregates. Once this process terminated, the hydrogels were dissolved within the next incubation step. The novel formulations based on SHP407 and BLEND showed a behavior that was consistent with CHP407-based systems. The hydrogels formulated at 1% w/v PEU concentration were characterized by a lower tendency to de-swell when compared to the formulations at higher PEU content (i.e., 3 and 5% w/v). It is likely that the hydrogels at low PEU contents (i.e., low PEU/CD mass ratio) showed such behavior due to a marked development of PPR-based SM structures, which are notably more stable than other kinds of physical crosslinking (i.e., hydrophobic interactions). In systems at higher PEU concentrations (i.e., 5% w/v) a similar behavior was observed, but a higher release of hydrogel components occurred in absolute terms. Indeed, no significant differences were observed between the formulations containing PEU at 5% w/v and the ones at 3% w/v. Such observations indicated that the higher PEU/CD mass ratio, the lower the stability within the investigated range of concentrations. A different responsiveness was observed among the formulations based on different PEUs. Indeed, SHP407 showed the highest rate of dissolution in both wet and dry conditions. Such behavior could be related to the less developed SM network that characterized these samples, as previously discussed through the results obtained from XRD analysis, gelation time and rheological tests. Generally, no significant differences were observed between CHP407- and BLEND-based samples. Nonetheless, slightly higher dissolution rates were quantified for BLEND samples with respect to CHP407 ones at the time frame of 24 hours. For example, BLEND 1% - CD 10% resulted in a weight loss equal to $34.9 \pm 1.8\%$, while for CHP407 1%-CD 10% weight loss was $30.3 \pm 1.5\%$ (p-value = 0.0043); for BLEND 3% - CD 10% and CHP407 3% - CD 10% the weight loss value was $26.8 \pm 0.8\%$ and $20.3 \pm 1.4\%$, respectively (p-value = 0.025). Moreover, higher swelling ratio values were estimated for BLEND-based SM hydrogels at different time frames with respect to CHP407-based ones. As an example, at 24 hours, the swelling ratio of BLEND 1% - CD 10% was greater than CHP407 1% - CD 10% (1.63 ± 0.04 and 1.52 ± 0.04 (p-value = 0.048), respectively). Significant differences were observed also for the samples at 3 and 5% w/v PEU concentration at the same time step (p-values equal to 0.0039 and 0.0084, respectively). This set of observations indicated a general higher responsiveness of BLEND-based samples with respect to CHP407-based ones. Mutually, the hydrogels composed of CHP407 were characterized by the highest stability even at the lowest PEU concentration (i.e., 1% w/v). Indeed, CHP407 1% - CD 10% showed the ability to exchange mass with the external environment up to 5 days of incubation, while the corresponding samples based on SHP407 and BLEND were completely solubilized. These observations were in accordance with the previous XRD and rheological characterizations, in which CHP407-based SM systems turned out to be the best in terms of SM crystallization yield and hence stability of the resulting hydrogel networks.

Thence, through the complete set of physical characterizations, the here-developed SM hydrogels showed promising properties for the encapsulation and release of hydrophobic drugs. Indeed, the sustained release over time of less stable components (i.e., free CDs and PEU aggregates) represented a fundamental factor for the validation of the feasibility of these hydrogels as drug

delivery systems. Indeed, the observed mechanism of mass exchange could be exploited for the release of Cur, which is a highly hydrophobic and insoluble drug.

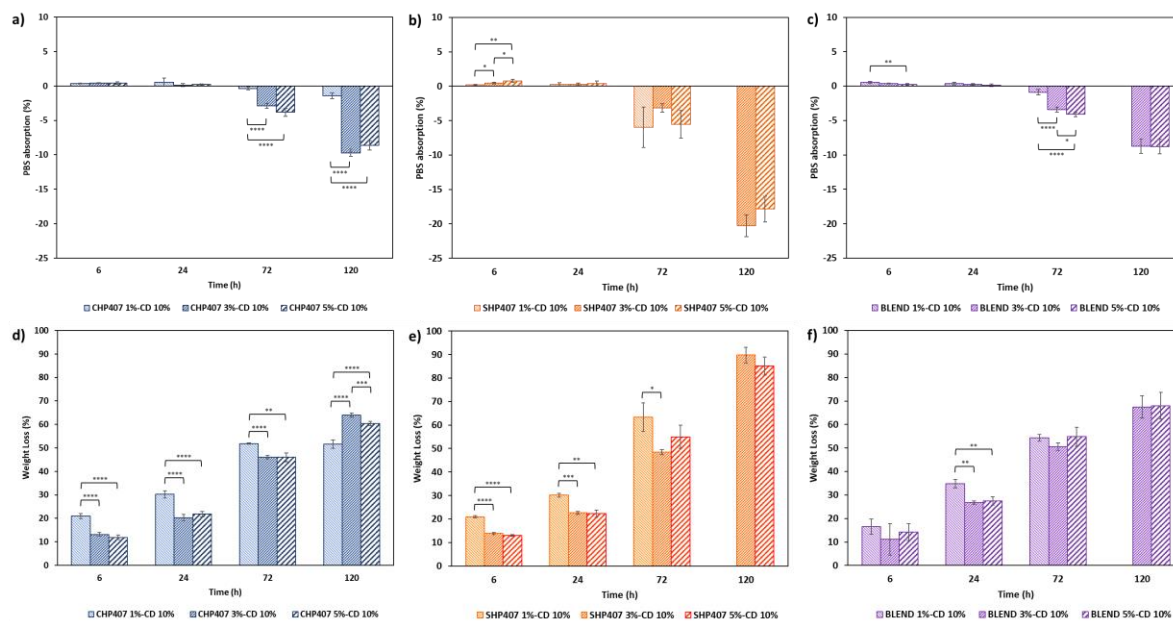


Figure 13 – Bar diagrams of PBS absorption (%) and weight loss (%) for a,d) CHP407- (blue), b,e) SHP407- (orange) and c,f) BLEND-based (purple) hydrogels.

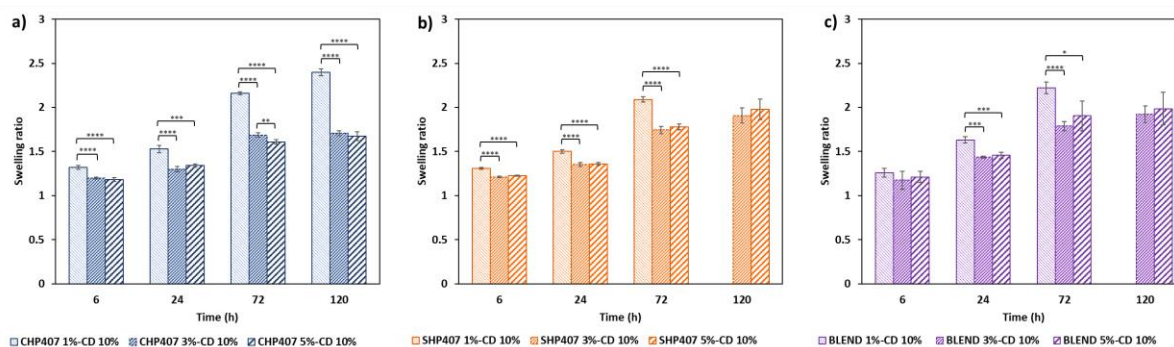


Figure 14 – Bar diagrams of swelling ratio values for a) CHP407- (blue), b) SHP407- (orange) and c) BLEND-based (purple) hydrogels.

4.3.4 Cytotoxicity evaluation

Cytotoxicity was assessed on formulations based on only one PEU with the aim to evaluate the single effect of PEU physico-chemical properties separately. As reported in figure 15, the investigated hydrogel systems did not show any cytotoxic effect of their pure eluates. A generally enhanced cell viability was observed, probably due to the relevant release of CDs.^{70,71} The lower enhancement of cell viability that was found for CHP407-based hydrogels could be considered not stochastic, since these systems showed the best results in terms of stability and then the lowest potential for the release of free CDs. Hence, in addition to the promising results obtained from rheological test and responsiveness in aqueous environments, the here-designed PEUs were elected as highly suitable polymers for the development of promising drug delivery systems. In this regard, the PEU concentrations of 1 and 3% w/v were selected to design curcumin-loaded

systems. The formulations containing PEUs at 5% w/v were excluded, due to their higher instability and unnecessary PEU content.

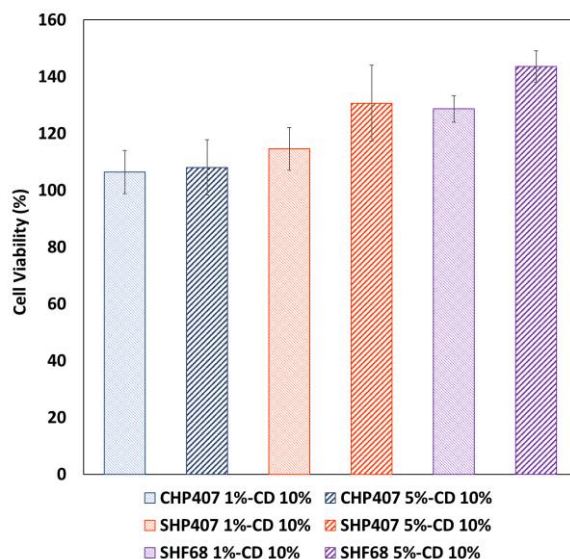


Figure 15 – Bar diagrams representing cell viability results for CHP407 (blue), SHP407 (orange) and BLEND (purple).

4.4 Curcumin encapsulation and release kinetics

4.4.1 Rheological characterization of curcumin-loaded SM hydrogels

The protocol for the formulation of SM hydrogels containing Cur was *ad-hoc* defined with the aim to preserve drug molecules for degradation by avoiding drug solubilization in the presence of ions (e.g., Cl^-) and alkaline pH. Thence, the total amount of CDs was divided in two equal fractions using ddH₂O (for Cur solubilization) and PBS as solvents. The presence of ddH₂O and Cur could slightly influence the network of hydrogels. In fact, ddH₂O as fraction of total volume of hydrogel solvent could reduce the salting-out effect that stabilizes the polymeric network for PPR formation and crystallization. Simultaneously, Cur highly interacts with CDs and hydrophobic domains of PEUs, thus potentially reducing CD availability for the self-assembly of PPRs and the ability to form lipophilic interactions. Then, it is likely that detrimental effects could occur during hydrogel network development. The effects of solvent composition and Cur encapsulation were evaluated on the formulation that showed the most evident SM character, namely the SM hydrogels composed of PEUs at 1% w/v concentration. A complete rheological characterization was conducted on SM systems to evaluate hydrogel network development. Three conditions of hydrogel composition were tested, thus separating the contribution of solvents (i.e., PEU 1% - CD 10%-PBS/H₂O) from that deriving from the additional encapsulation of the drug (i.e., PEU 1% - CD 10%- Cur 80 $\mu\text{g}/\text{ml}$) with respect to the reference hydrogels based on pure PBS solvent in the absence of Cur (i.e., PEU 1% - CD 10%). Frequency sweep tests allowed an overall evaluation of hydrogel development and mechanical properties. The obtained trends of G' and G'' at different temperatures (i.e., 25, 30 and 37 °C) are reported in figure 16.

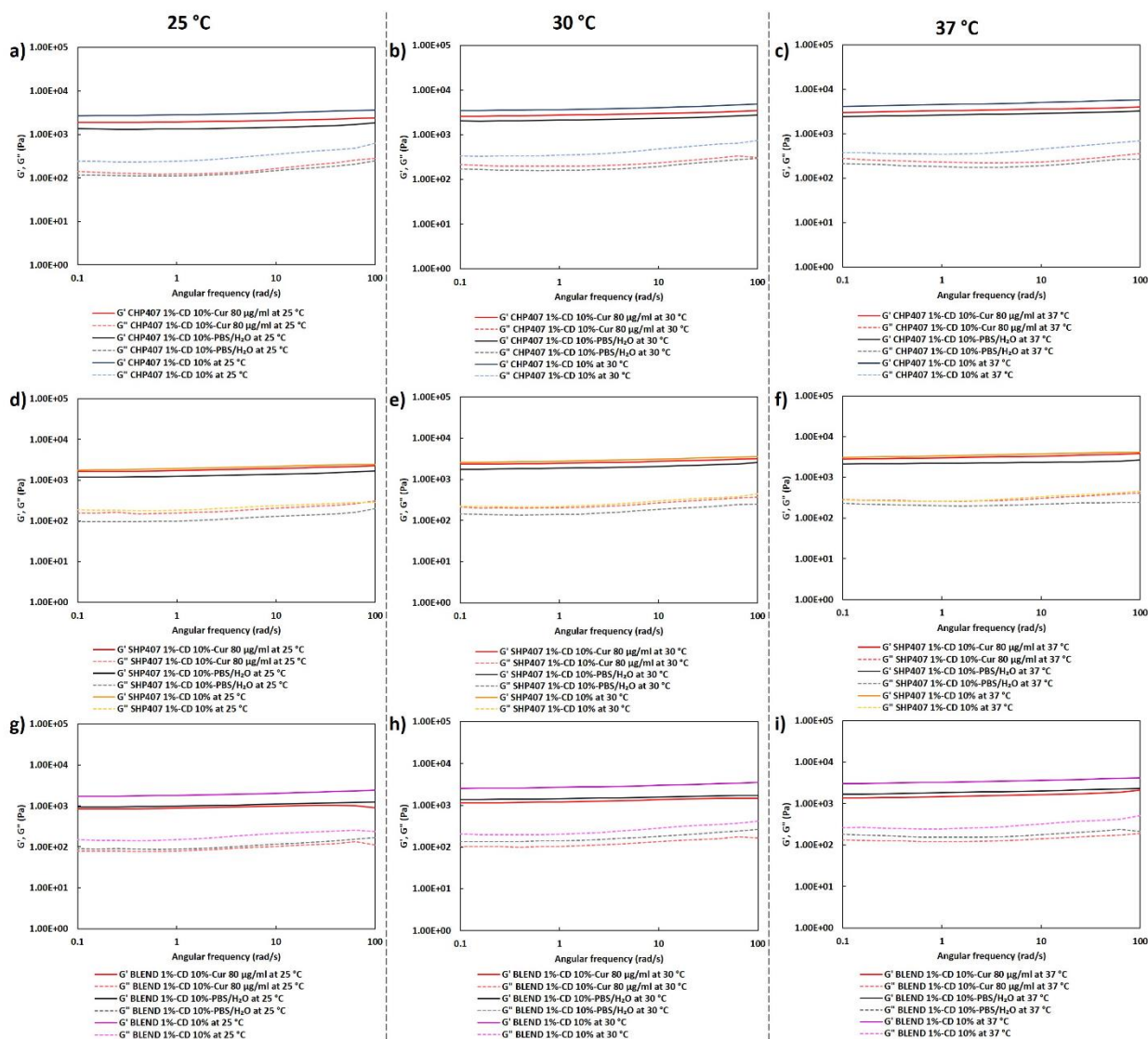


Figure 16 – G' (continuous lines) and G'' (dashed lines) as a function of applied angular frequency at 25, 30 and 37 °C for SM hydrogels formulated in different environments: PBS/H₂O (65/35 % v/v, dark continuous line (G') and grey dashed line (G'')), Cur 80 µg/ml (in PBS/H₂O, red continuous line (G') and light red dashed line (G'')), and pure PBS. CHP407- (a,b,c), SHP407- (d,e,f) and BLEND-based (g,h,i) hydrogels are represented in blue, orange and purple, respectively. The comparisons are represented among hydrogels based on the same PEU but having different solvent composition and Cur content. A decrement of mechanical properties can be observed at each temperature caused by the reduction of the salting-out effect in the samples based on PBS/H₂O and Cur 80 µg/ml (in PBS/H₂O). Nonetheless, Cur could be supposed to form hydrophobic interactions with PEU domains, thus inducing a further stabilizing effect with respect to the hydrogel formulations that are characterized by the single contribution of the solvent.

All the hydrogels were characterized by a fully developed hydrogel network. Indeed, G' resulted higher than G'' within the whole range of investigated frequencies and temperatures for all the formulations. Nonetheless, a general decrease of mechanical properties was observed in both PEU 1% - CD 10%-PBS/H₂O and PEU 1% - CD 10%- Cur 80 µg/ml systems with respect to control samples in pure PBS (PEU 1% - CD 10%). In more detail, the greatest effect in terms of mechanical properties decrease was observed in the case of isolated solvents with respect to the samples containing even Cur. This interesting result could be correlated to the fact that Cur could

represent a stabilizing element for hydrophobic interactions of PEU structures thus compensating the weaker salting out effect that was induced by the presence of ddH₂O. Then, a contribution in Cur encapsulation and stabilization within the hydrogel network could be ascribed even to the PEUs themselves due to their amphiphilic nature. More evident effects were found for CHP407- and BLEND-based samples with respect to SHP407-based ones. Such behavior could be caused by the less developed SM structure of SHP407-based networks with respect to the other systems. Probably, SHP407-based SM hydrogels resulted to be less sensitive to solvent formulation and Cur encapsulation due to their intrinsic lower ability to interact with CDs and form SM hydrogel structures based on PPRs. Hence, the hydrogels based on SHP407 could be less sensitive to the partial lack of CDs that are implemented for Cur solubilization. It could be also likely that the additional presence of pendant amino groups could be the cause of the less enhanced SM network development due to the intrinsic polarity of such chemical domains. The above-mentioned hypothesis is in accordance with the previous observations related to SM crystal yield for XRD analysis.

The presence of ddH₂O or Cur did not negatively affect the self-healing ability of the resulting hydrogels, as reported in figure 17, which summarizes the results from strain sweep and self-healing tests. Consistently with the previous frequency sweep tests, the contribution of both the solvent and the additional presence of Cur prevalently influenced the entity of mechanical properties (i.e., G' and G''), while hydrogel responsiveness and reversibility were not significantly affected. This peculiarity allows to consider PEU-based SM hydrogels as proper systems for the encapsulation of drugs with limited solubility, such as Cur. It is then probable that the well-balanced amphiphilic nature of the here-developed PEUs could be particularly suitable for both hydrogel formation and drug encapsulation.

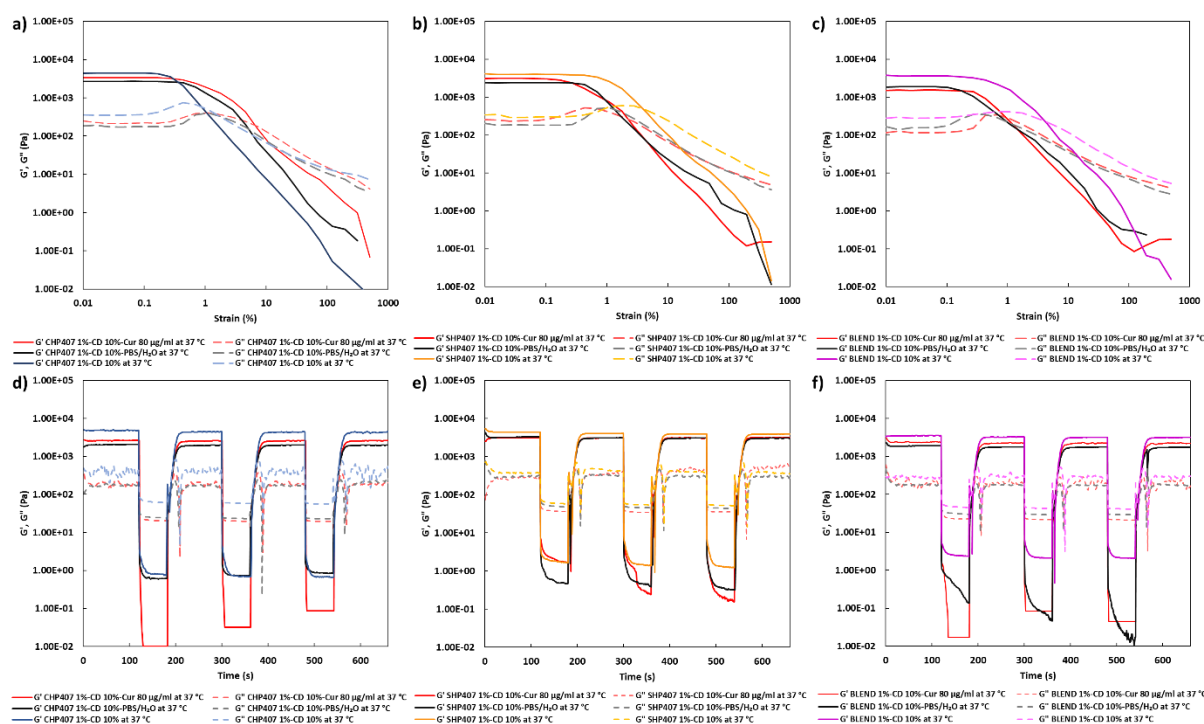


Figure 17 – G' (continuous lines) and G'' (dashed lines) as a function of applied strain (a,b and c) and time (d, e and f) with alternated phases of recovery (0.1 % strain) and rupture (100 %) at 37 °C for SM hydrogels formulated in different environments: PBS/H₂O (65/35 % v/v, dark continuous line (G') and grey

dashed line (G'')), Cur 80 $\mu\text{g/ml}$ (in PBS/ H_2O , red continuous line (G') and light red dashed line (G'')), and pure PBS. CHP407- (a,d), SHP407- (b,e) and BLEND-based (c,f) hydrogels are represented in blue, orange and purple, respectively. The comparisons are represented between hydrogels based on the same PEU but having different solvent composition and Cur content. No significant differences were observed in terms of self-healing ability among the investigated systems.

4.4.2 Release studies of curcumin from PEU-based SM hydrogels

In order to properly quantify the released Cur over time, a complete set of reference curves was produced using standard samples of different composition. Indeed, CDs can interact with Cur leading to the formation of inclusion complexes and less organized aggregates, which could exhibit different spectroscopic properties. Hence, the spectrometric properties of the solutions containing CDs and Cur were evaluated at different CD concentrations (i.e., in PBS containing CDs at 0, 2.5, 5 and 10% w/v). The obtained reference curves are reported in figure 18. Interestingly, no relevant effects within the wide range of tested CD concentrations were observed in terms of absorbance of Cur samples at equal content. Thence, also considering the results obtained from swelling and stability test, the contribution of CDs was generally negligible in terms of spectroscopic response and the reference curve characterized by the absence of CDs was selected for the quantification of Cur into hydrogel extracts obtained from release tests.

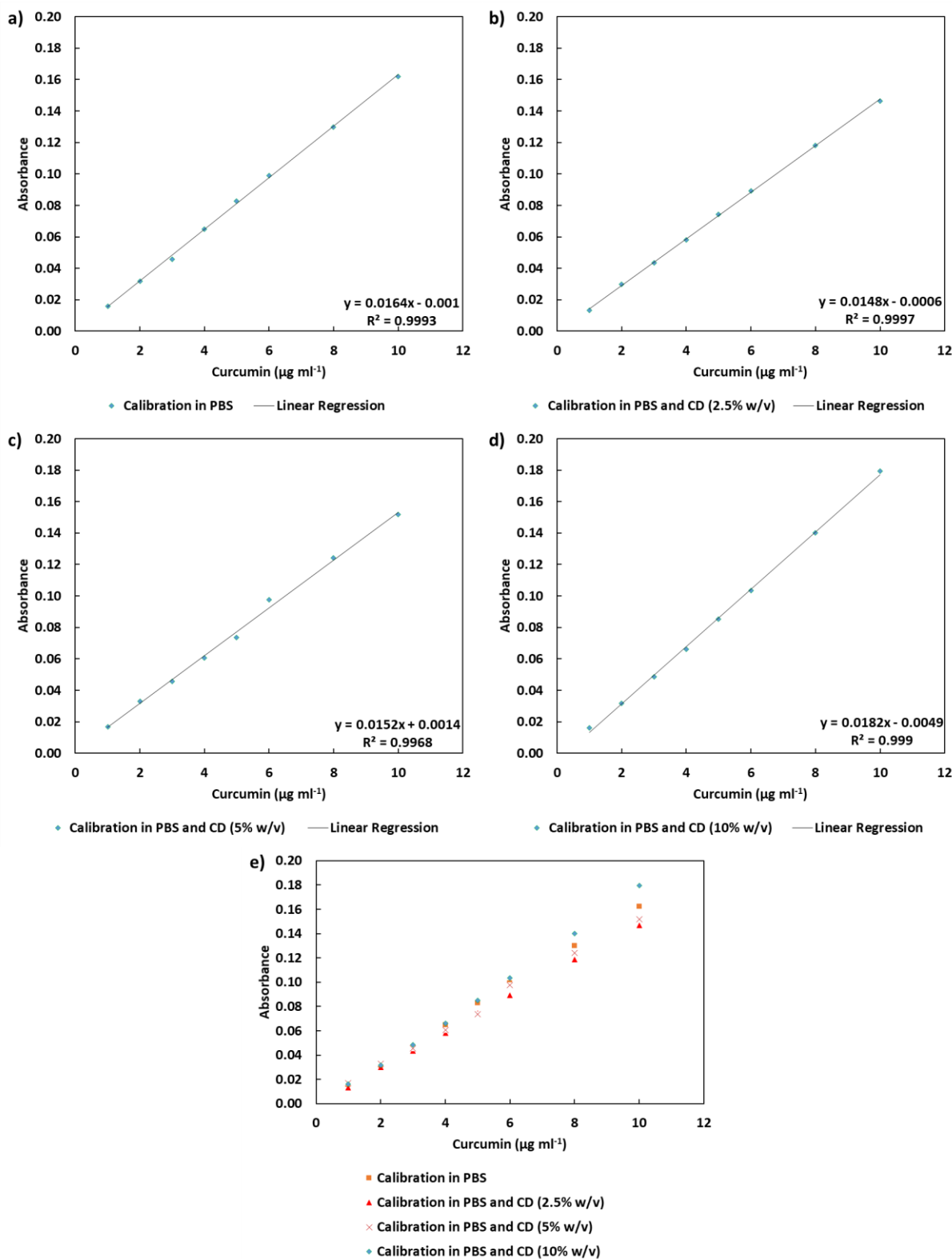


Figure 18 – Calibration curves of Cur in PBS at various CD concentrations: a) 0%, b) 2.5%, c) 5% and d) 10% w/v. The parameters obtained from the linear regression of data are also reported on the bottom right of each graph. f) summary of all the obtained data for comparative purposes.

Release studies of Cur from SM gels (1 ml) highlighted notably progressive release kinetics, which can be divided into different intervals. Figure 19 reports the obtained trends of Cur delivery over time. All the investigated formulations were characterized by the absence of any burst release

phenomena. The SM systems at 1% w/v PEU concentration showed significantly higher Cur release (i.e., *ca.* two-fold) with respect to the samples at 3% w/v PEU content within the first 6 hours of incubation. Such different behaviors could be explained by referring to the data obtained from swelling and stability tests. Indeed, the samples PEU 1% - CD 10% were characterized by significant higher swelling ratios and dissolution rates, indicating a favored dissolution of free components which allowed a faster release of Cur with respect to PEU 3% - CD 10% samples within 6 hours of incubation. The observed amounts of released Cur were quantified in the range of concentrations that turned out to be potentially therapeutic (i.e., micromolar) for many applications, such as the treatment of tumors and acute inflammatory processes.^{5,15,21} Additionally, Peppas release exponents were calculated within 6 hours of Cur release. The obtained values ranged between 0.7 and 0.89 for PEU 1% - CD 10% samples, thus indicating a mechanism of Cur release based on a hybrid behavior between swelling and diffusion (anomalous transport). PEU 3% - CD 10% samples were characterized by release exponents generally greater than 0.89, thus indicating a super Case II release mechanism, which indicated an extremized Cur release process due to the induction of relevant mechanical tensions into hydrogel networks. Such response could be explained by the higher stiffness of SM hydrogels with higher PEU contents. Indeed, the hypothesized tension within the hydrogels PEU 3% - CD 10% could be due to a release of free components and a concomitant absorption of fluid from the external environment while maintaining the overall hydrogel shape over time, as observed from swelling and stability tests. In these conditions, such mass exchange could cause the formation of relevant tensions into highly stiff SM networks. An exception was represented by CHP407 3% - CD 10% hydrogels (*n* equal to 0.82) with respect to SHP407 3% - CD 10% and BLEND 3% - CD 10% (*n* greater than 0.89). This different responsiveness could be related to the higher stability of CHP407 3% - CD 10%, as suggested by swelling and stability tests. The enhanced responsiveness of SHP407 3% - CD 10% and BLEND 3% - CD 10% could be due to a faster kinetics of fluid absorption originated by the presence of water-attracting domains (i.e., free primary amines) thus increasing the mass exchange through the release of hydrogel components. In addition, a further contribution for such behavior could be related to the intrinsic higher dissolution rates of SHP407- and BLEND-based SM networks. The release profiles of Cur showed a relevant acceleration after 48 hours of incubation in physiological-like conditions. Such variation in release kinetics could be due to the continuous erosion of SM hydrogels that led to a spontaneous dissolution of the residual physical network that occurred for prolonged incubation times (i.e., 96 hours). During this phase, no significant differences were generally observed between the samples containing PEUs at 1 and 3% w/v concentrations. These data confirmed the previous hypothesis on the importance of low PEU/CD mass ratio in allowing the formation of more stable SM hydrogel networks. The total amount of encapsulated Cur within the hydrogels (i.e., 80 µg ml⁻¹) was cumulatively released over time, thus indicating that no significant degradation phenomena of Cur occurred during release tests. It is likely that the contribution of CDs and PEU-based micelles as drug carriers was highly important for the chemical stability of Cur in alkaline pH over time.

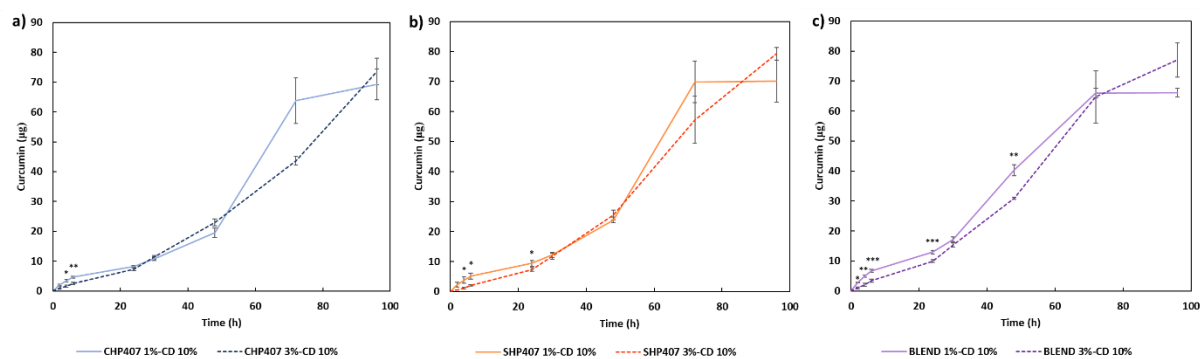


Figure 19 – Cur release profiles as a function of incubation time for CHP407- (a, blue), SHP407 (b, orange) and BLEND-based (c, purple) SM gels. PEU 1% - CD 10% (dashed line) and PEU 3% - CD 10% (continuous line) are represented for each PEU.

5. Conclusions

In this Chapter of the work, a library of novel PEU-based SM hydrogels (and their blends) was developed. Indeed, the already optimized and reliable PEU synthesis process was exploited to produce newly engineered PEUs. Two amphiphilic triblocks were selected for their different chemical properties: P407 and F68. The other reagents (i.e., HDI, CDM and NBoc) were chosen with the aim to improve the domain of available parameters to tune the final properties of hydrogel systems. In this regard, all PEUs were characterized by a peculiar ability to form PPR-based structures depending on their hydrophobic character. P407-based PEUs (CHP407, NHP407 and SHP407) showed the highest yields in terms of PPR self-assembly and crystallization. Conversely, F68-based PEUs (NHF68 and SHF68) showed low crystallization yield and slow gelation kinetics, despite their higher PEO content (i.e., 80% wt) and lower molecular mass (approx. 20% lower than P407-based PEUs), which were expected to enhance PPR-based network formation. Probably because of the additional steric hindrance of pendant Boc groups, NHF68 resulted to be not suitable for the development of stable PPR-based SM networks. In this regard, such different behavior could be ascribed to the overall composition of PEU backbones. Indeed, since the here-developed PEUs were characterized by a multi-block configuration, their responsiveness could be attributed to relevant intermolecular interactions. On the basis of this hypothesis, the presence of hydrophobic domains (i.e., PPO, HDI and CDM) and their properties (i.e., PPO block length and overall content) were elemental parameters for the stabilization of the resulting polymeric networks and then PPR formation through CD threading along the polymer chains. The formation of PPR-based channel-like crystals was proved through XRD crystallography, FTIR-ATR and $^1\text{H-NMR}$ spectroscopies. Then, SM hydrogels were designed containing PEUs at low concentration (i.e., ranging from 1 to 5% w/v) and CDs at 10% w/v. In order to further investigate the potential of PEUs as constituting polymers of SM hydrogels, systems based on blends of CHP407 and SHF68 were also designed (BLEND samples, containing CHP407 and SHF68, 80:20 mass ratio). The complete plethora of SM hydrogels was represented by CHP407, SHP407 and BLEND samples, which were tested in terms of gelation kinetics, rheological properties, stability in physiological-like watery environments and cytocompatibility. All the developed hydrogel systems were characterized by good stability when incubated in contact with PBS at 37 °C, showing the ability to maintain their shape while releasing potential drug carriers (i.e., free CDs

and PEU aggregates). However, the SM hydrogels characterized by the lowest PEU/CD ratio (i.e., 1% w/v PEU concentration) turned out to be highly stable and comparable to the systems containing PEUs at concentrations three- to five-fold higher (i.e., 3 and 5% w/v). Thence, it was hypothesized that the SM development was enhanced at low PEU content, thus further confirming their suitability for the interaction with CDs to form PPR-based networks, despite their high molar mass. This achievement was generally notable. Indeed, the reduction of the required amount of synthetic polymer to produce stable SM hydrogels represents an important target for the design of drug delivery systems. Nonetheless, the mechanical properties were significantly improved through the design of hydrogels containing a higher PEU content (5% w/v) opening the way to the possibility to design self-healing hydrogel systems characterized by elastic moduli over 10^4 Pa, which is relevant for physical networks at low polymer content. The resulting mechanical response (i.e., thixotropic behavior and self-healing ability) made the here-developed hydrogels suitable for injection through conventional syringes and needles. Moreover, the SM networks based on PEUs did not show any cytotoxic effects according to ISO 10993 guidelines.

Then, curcumin was easily integrated at high concentration (i.e., $80 \mu\text{g ml}^{-1}$) within SM hydrogels by exploiting its complexation with CDs and no relevant detrimental effects were observed in mechanical terms. *In vitro* tests showed highly tunable and progressive release kinetics of the total curcumin payload, thus potentially preserving the bioavailability of such natural drug.

Finally, it can be concluded that this study further highlighted the suitability of properly synthesized PEUs as raw materials to develop engineered drug delivery systems for regenerative medicine. Generally, the most relevant features of the here-designed systems can be individuated in the wide tunability of the final properties of the hydrogel systems relying on the important possibility to functionalize PEUs. In fact, these synthetic polymers were able to exert their specific behaviors at remarkably low contents. Indeed, slight variations on PEU composition and hydrogel formulation can result in a relevant modulation of physical and mechanical properties. The possibility to easily design hydrogels containing a high payload of poorly bioavailable drugs represents an interesting feature for future applications. In order to better investigate the general suitability of PEU-based SM systems for regenerative medicine, two case studies were also carried out, as reported in the following Chapters of this work.

6. References

- (1) Kunnumakkara, A. B.; Bordoloi, D.; Padmavathi, G.; Monisha, J.; Roy, N. K.; Prasad, S.; Aggarwal, B. B. Curcumin, the Golden Nutraceutical: Multitargeting for Multiple Chronic Diseases: Curcumin: From Kitchen to Clinic. *British Journal of Pharmacology* **2017**, *174* (11), 1325–1348. <https://doi.org/10.1111/bph.13621>.
- (2) Ahangari, N.; Kargozar, S.; Ghayour-Mobarhan, M.; Baino, F.; Pasdar, A.; Sahebkar, A.; Ferns, G. A. A.; Kim, H.; Mozafari, M. Curcumin in Tissue Engineering: A Traditional Remedy for Modern Medicine. *BioFactors* **2019**, *45* (2), 135–151. <https://doi.org/10.1002/biof.1474>.
- (3) Vogel, H.A.; Pelletier, J. Curcumin-Biological and Medicinal Properties. *J. Pharma.* 1815.
- (4) Lampe, V.; Milobedzka, J. Studien über Curcumin. *Ber. Dtsch. Chem. Ges.* **1913**, *46* (2), 2235–2240. <https://doi.org/10.1002/cber.191304602149>.
- (5) Wright, L.; Frye, J.; Gorti, B.; Timmermann, B.; Funk, J. Bioactivity of Turmeric-Derived Curcuminoids and Related Metabolites in Breast Cancer. *CPD* **2013**, *19* (34), 6218–6225. <https://doi.org/10.2174/1381612811319340013>.
- (6) Schmidt, K. T.; Figg, W. D. The Potential Role of Curcumin in Prostate Cancer: The Importance of Optimizing Pharmacokinetics in Clinical Studies. *Transl. Cancer Res* **2016**, *5* (S6), S1107–S1110. <https://doi.org/10.21037/tcr.2016.11.04>.
- (7) Tan, B. L.; Norhaizan, M. E. Curcumin Combination Chemotherapy: The Implication and Efficacy in Cancer. **2019**, 21.
- (8) Mathew, D.; Hsu, W.-L. Antiviral Potential of Curcumin. *Journal of Functional Foods* **2018**, *40*, 692–699. <https://doi.org/10.1016/j.jff.2017.12.017>.
- (9) Liu, C.-H.; Huang, H.-Y. Antimicrobial Activity of Curcumin-Loaded Myristic Acid Microemulsions against *Staphylococcus Epidermidis*. *Chem. Pharm. Bull.* **2012**, *60* (9), 1118–1124. <https://doi.org/10.1248/cpb.c12-00220>.
- (10) Mahady, G. B.; Pendland, S. L.; Yun, G.; Lu, Z. Z. Turmeric (*Curcuma Longa*) and Curcumin Inhibit the Growth of *Helicobacter Pylori*, a Group 1 Carcinogen. *Anticancer Res* **2002**, *22* (6C), 4179–4181.
- (11) Reddy, R. C.; Vatsala, P. G.; Keshamouni, V. G.; Padmanaban, G.; Rangarajan, P. N. Curcumin for Malaria Therapy. *Biochemical and Biophysical Research Communications* **2005**, *326* (2), 472–474. <https://doi.org/10.1016/j.bbrc.2004.11.051>.
- (12) Shimizu, K.; Funamoto, M.; Sunagawa, Y.; Shimizu, S.; Katanasaka, Y.; Miyazaki, Y.; Wada, H.; Hasegawa, K.; Morimoto, T. Anti-Inflammatory Action of Curcumin and Its Use in the Treatment of Lifestyle-Related Diseases. *Eur Cardiol* **2019**, *14* (2), 117–122. <https://doi.org/10.15420/ecr.2019.17.2>.
- (13) Kant, V.; Gopal, A.; Pathak, N. N.; Kumar, P.; Tandan, S. K.; Kumar, D. Antioxidant and Anti-Inflammatory Potential of Curcumin Accelerated the Cutaneous Wound Healing in Streptozotocin-Induced Diabetic Rats. *International Immunopharmacology* **2014**, *20* (2), 322–330. <https://doi.org/10.1016/j.intimp.2014.03.009>.
- (14) Den Hartogh, D. J.; Gabriel, A.; Tsiani, E. Antidiabetic Properties of Curcumin I: Evidence from In Vitro Studies. *Nutrients* **2020**, *12* (1), 118. <https://doi.org/10.3390/nu12010118>.
- (15) Hewlings, S.; Kalman, D. Curcumin: A Review of Its Effects on Human Health. *Foods* **2017**, *6* (10), 92. <https://doi.org/10.3390/foods6100092>.

- (16) Priyadarsini, K. The Chemistry of Curcumin: From Extraction to Therapeutic Agent. *Molecules* **2014**, *19* (12), 20091–20112. <https://doi.org/10.3390/molecules191220091>.
- (17) He, Y.; Yue, Y.; Zheng, X.; Zhang, K.; Chen, S.; Du, Z. Curcumin, Inflammation, and Chronic Diseases: How Are They Linked? *Molecules* **2015**, *20* (5), 9183–9213. <https://doi.org/10.3390/molecules20059183>.
- (18) Qureshi, M.; Al-Suhaimi, E. A.; Wahid, F.; Shehzad, O.; Shehzad, A. Therapeutic Potential of Curcumin for Multiple Sclerosis. *Neurol Sci* **2018**, *39* (2), 207–214. <https://doi.org/10.1007/s10072-017-3149-5>.
- (19) Henrotin, Y.; Clutterbuck, A. L.; Allaway, D.; Lodwig, E. M.; Harris, P.; Mathy-Hartert, M.; Shakibaei, M.; Mobasheri, A. Biological Actions of Curcumin on Articular Chondrocytes. *Osteoarthritis and Cartilage* **2010**, *18* (2), 141–149. <https://doi.org/10.1016/j.joca.2009.10.002>.
- (20) Kargozar, S.; Baino, F.; Hoseini, S. J.; Verdi, J.; Asadpour, S.; Mozafari, M. Curcumin: Footprints on Cardiac Tissue Engineering. *Expert Opinion on Biological Therapy* **2019**, *19* (11), 1199–1205. <https://doi.org/10.1080/14712598.2019.1650912>.
- (21) Heger, M.; van Golen, R. F.; Broekgaarden, M.; Michel, M. C. The Molecular Basis for the Pharmacokinetics and Pharmacodynamics of Curcumin and Its Metabolites in Relation to Cancer. *Pharmacol Rev* **2014**, *66* (1), 222–307. <https://doi.org/10.1124/pr.110.004044>.
- (22) Kocaadam, B.; Şanlıer, N. Curcumin, an Active Component of Turmeric (*Curcuma Longa*), and Its Effects on Health. *Critical Reviews in Food Science and Nutrition* **2017**, *57* (13), 2889–2895. <https://doi.org/10.1080/10408398.2015.1077195>.
- (23) Lopresti, A. L. The Problem of Curcumin and Its Bioavailability: Could Its Gastrointestinal Influence Contribute to Its Overall Health-Enhancing Effects? *Advances in Nutrition* **2018**, *9* (1), 41–50. <https://doi.org/10.1093/advances/nmx011>.
- (24) Tønnesen, H. H.; Karlsen, J. Studies on Curcumin and Curcuminoids. VI. Kinetics of Curcumin Degradation in Aqueous Solution. *Z Lebensm Unters Forsch* **1985**, *180* (5), 402–404. <https://doi.org/10.1007/BF01027775>.
- (25) Tønnesen, H.H.; Karlsen, J. Studies on Curcumin and Curcuminoids. V. Alkaline Degradation of Curcumin. *Zeitschrift für Lebensmittel-Untersuchung und -Forschung*. 1985, pp 132–134.
- (26) Tonnesen, H.; Karlsen, J. Studies on Curcumin and Curcuminoids. X. The Use of Curcumin as a Formulation Aid to Protect Light-Sensitive Drugs in Soft Gelatin Capsules. *International Journal of Pharmaceutics* **1987**, *38* (1–3), 247–249. [https://doi.org/10.1016/0378-5173\(87\)90121-9](https://doi.org/10.1016/0378-5173(87)90121-9).
- (27) Metzler, M.; Pfeiffer, E.; Schulz, S. I.; Dempe, J. S. Curcumin Uptake and Metabolism. *BioFactors* **2013**, *39* (1), 14–20. <https://doi.org/10.1002/biof.1042>.
- (28) Sarkar, N.; Bose, S. Liposome-Encapsulated Curcumin-Loaded 3D Printed Scaffold for Bone Tissue Engineering. *ACS Appl. Mater. Interfaces* **2019**, *11* (19), 17184–17192. <https://doi.org/10.1021/acsami.9b01218>.
- (29) Tsai, W.-H.; Yu, K.-H.; Huang, Y.-C.; Lee, C.-I. EGFR-Targeted Photodynamic Therapy by Curcumin-Encapsulated Chitosan/TPP Nanoparticles. *IJN* **2018**, *Volume 13*, 903–916. <https://doi.org/10.2147/IJN.S148305>.
- (30) Mitra, T.; Manna, P. J.; Raja, S. T. K.; Gnanamani, A.; Kundu, P. P. Curcumin Loaded Nanographene Oxide Reinforced Fish Scale Collagen - A 3D Scaffold Biomaterial for Wound Healing Application. *RSC Advances* **43**.

- (31) Haimhoffer, Á.; Ruzsnyák, Á.; Réti-Nagy, K.; Vasvári, G.; Váradi, J.; Vecsernyés, M.; Bácskay, I.; Fehér, P.; Ujhelyi, Z.; Fenyvesi, F. Cyclodextrins in Drug Delivery Systems and Their Effects on Biological Barriers. *Sci. Pharm.* **2019**, *87* (4), 33. <https://doi.org/10.3390/scipharm87040033>.
- (32) Carneiro, S.; Costa Duarte, F.; Heimfarth, L.; Siqueira Quintans, J.; Quintans-Júnior, L.; Veiga Júnior, V.; Neves de Lima, Á. Cyclodextrin–Drug Inclusion Complexes: In Vivo and In Vitro Approaches. *IJMS* **2019**, *20* (3), 642. <https://doi.org/10.3390/ijms20030642>.
- (33) Tønnesen, H. H.; Másson, M.; Loftsson, T. Studies of Curcumin and Curcuminoids. XXVII. Cyclodextrin Complexation: Solubility, Chemical and Photochemical Stability. *International Journal of Pharmaceutics* **2002**, *244* (1–2), 127–135. [https://doi.org/10.1016/S0378-5173\(02\)00323-X](https://doi.org/10.1016/S0378-5173(02)00323-X).
- (34) Tomren, M. A.; Másson, M.; Loftsson, T.; Tønnesen, H. H. Studies on Curcumin and Curcuminoids XXXI. Symmetric and Asymmetric Curcuminoids: Stability, Activity and Complexation with Cyclodextrin. *Int J Pharm* **2007**, *338* (1–2), 27–34. <https://doi.org/10.1016/j.ijpharm.2007.01.013>.
- (35) Singh, R.; Tønnesen, H. H.; Vogensen, S. B.; Loftsson, T.; Másson, M. Studies of Curcumin and Curcuminoids. XXXVI. The Stoichiometry and Complexation Constants of Cyclodextrin Complexes as Determined by the Phase-Solubility Method and UV–Vis Titration. *J Incl Phenom Macrocycl Chem* **2010**, *66* (3–4), 335–348. <https://doi.org/10.1007/s10847-009-9651-5>.
- (36) Ryzhakov, A.; Do Thi, T.; Stappaerts, J.; Bertoletti, L.; Kimpe, K.; Sá Couto, A. R.; Saokham, P.; Van den Mooter, G.; Augustijns, P.; Somsen, G. W.; Kurkov, S.; Inghelbrecht, S.; Arien, A.; Jimidar, M. I.; Schrijnemakers, K.; Loftsson, T. Self-Assembly of Cyclodextrins and Their Complexes in Aqueous Solutions. *Journal of Pharmaceutical Sciences* **2016**, *105* (9), 2556–2569. <https://doi.org/10.1016/j.xphs.2016.01.019>.
- (37) Jana, B.; Mohapatra, S.; Mondal, P.; Barman, S.; Pradhan, K.; Saha, A.; Ghosh, S. α -Cyclodextrin Interacts Close to Vinblastine Site of Tubulin and Delivers Curcumin Preferentially to the Tubulin Surface of Cancer Cell. *ACS Appl. Mater. Interfaces* **2016**, *8* (22), 13793–13803. <https://doi.org/10.1021/acsami.6b03474>.
- (38) Gerola, A. P.; Silva, D. C.; Jesus, S.; Carvalho, R. A.; Rubira, A. F.; Muniz, E. C.; Borges, O.; Valente, A. J. M. Synthesis and Controlled Curcumin Supramolecular Complex Release from PH-Sensitive Modified Gum-Arabic-Based Hydrogels. *RSC Adv.* **2015**, *5* (115), 94519–94533. <https://doi.org/10.1039/C5RA14331D>.
- (39) Patro, N. M.; Sultana, A.; Terao, K.; Nakata, D.; Jo, A.; Urano, A.; Ishida, Y.; Gorantla, R. N.; Pandit, V.; Devi, K.; Rohit, S.; Grewal, B. K.; Sophia, E. M.; Suresh, A.; Ekbote, V. K.; Suresh, S. Comparison and Correlation of in Vitro, in Vivo and in Silico Evaluations of Alpha, Beta and Gamma Cyclodextrin Complexes of Curcumin. *J Incl Phenom Macrocycl Chem* **2014**, *78* (1–4), 471–483. <https://doi.org/10.1007/s10847-013-0322-1>.
- (40) Li, X.; Uehara, S.; Sawangrat, K.; Morishita, M.; Kusamori, K.; Katsumi, H.; Sakane, T.; Yamamoto, A. Improvement of Intestinal Absorption of Curcumin by Cyclodextrins and the Mechanisms Underlying Absorption Enhancement. *International Journal of Pharmaceutics* **2018**, *535* (1–2), 340–349. <https://doi.org/10.1016/j.ijpharm.2017.11.032>.
- (41) Khan, S.; Minhas, M. U.; Ahmad, M.; Sohail, M. Self-Assembled Supramolecular Thermoreversible β -Cyclodextrin/Ethylene Glycol Injectable Hydrogels with Difunctional Pluronic[®] 127 as Controlled Delivery Depot of Curcumin. Development, Characterization and *in Vitro* Evaluation. *Journal of Biomaterials Science, Polymer Edition* **2018**, *29* (1), 1–34. <https://doi.org/10.1080/09205063.2017.1396707>.

- (42) Zhou, F.; Song, Z.; Wen, Y.; Xu, H.; Zhu, L.; Feng, R. Transdermal Delivery of Curcumin-Loaded Supramolecular Hydrogels for Dermatitis Treatment. *J Mater Sci: Mater Med* **2019**, *30* (1), 11. <https://doi.org/10.1007/s10856-018-6215-5>.
- (43) Li, R.; Lin, Z.; Zhang, Q.; Zhang, Y.; Liu, Y.; Lyu, Y.; Li, X.; Zhou, C.; Wu, G.; Ao, N.; Li, L. Injectable and *In Situ* -Formable Thiolated Chitosan-Coated Liposomal Hydrogels as Curcumin Carriers for Prevention of *In Vivo* Breast Cancer Recurrence. *ACS Appl. Mater. Interfaces* **2020**, *12* (15), 17936–17948. <https://doi.org/10.1021/acsami.9b21528>.
- (44) Casimir, G. J.; Lefèvre, N.; Corazza, F.; Duchateau, J.; Chamekh, M. The Acid-Base Balance and Gender in Inflammation: A Mini-Review. *Front Immunol* **2018**, *9*, 475. <https://doi.org/10.3389/fimmu.2018.00475>.
- (45) Yu, J.; Ha, W.; Chen, J.; Shi, Y. PH-Responsive Supramolecular Hydrogels for Codelivery of Hydrophobic and Hydrophilic Anticancer Drugs. *RSC Adv.* **2014**, *4* (103), 58982–58989. <https://doi.org/10.1039/C4RA11311J>.
- (46) Laurano, R.; Cassino, C.; Ciardelli, G.; Chiono, V.; Boffito, M. Polyurethane-Based Thiomers: A New Multifunctional Copolymer Platform for Biomedical Applications. *Reactive and Functional Polymers* **2020**, *146*, 104413. <https://doi.org/10.1016/j.reactfunctpolym.2019.104413>.
- (47) Boffito, M.; Torchio, A.; Tonda-Turo, C.; Laurano, R.; Gisbert-Garzarán, M.; Berkmann, J. C.; Cassino, C.; Manzano, M.; Duda, G. N.; Vallet-Regí, M.; Schmidt-Bleek, K.; Ciardelli, G. Hybrid Injectable Sol-Gel Systems Based on Thermo-Sensitive Polyurethane Hydrogels Carrying PH-Sensitive Mesoporous Silica Nanoparticles for the Controlled and Triggered Release of Therapeutic Agents. *Front. Bioeng. Biotechnol.* **2020**, *8*, 384. <https://doi.org/10.3389/fbioe.2020.00384>.
- (48) Boffito, M.; Gioffredi, E.; Chiono, V.; Calzone, S.; Ranzato, E.; Martinotti, S.; Ciardelli, G. Novel Polyurethane-Based Thermosensitive Hydrogels as Drug Release and Tissue Engineering Platforms: Design and *in Vitro* Characterization: Polyurethane-Based Thermosensitive Hydrogels. *Polym. Int.* **2016**, *65* (7), 756–769. <https://doi.org/10.1002/pi.5080>.
- (49) Wright, M.; Kurumada, K.; Robinson, B. Rates of Incorporation of Small Molecules into Pluronic Micelles. In *Trends in Colloid and Interface Science XVI*; Miguel, M., Burrows, H. D., Eds.; Springer Berlin Heidelberg: Berlin, Heidelberg, 2004; pp 8–11. https://doi.org/10.1007/978-3-540-36462-7_3.
- (50) Loh, X. J.; Cheng, L. W. I.; Li, J. Micellization and Thermogelation of Poly(Ether Urethane)s Comprising Poly(Ethylene Glycol) and Poly(Propylene Glycol). *Macromol. Symp.* **2010**, *296* (1), 161–169. <https://doi.org/10.1002/masy.201051024>.
- (51) Harada, A.; Li, J.; Kamachi, M. Preparation and Properties of Inclusion Complexes of Polyethylene Glycol with .Alpha.-Cyclodextrin. *Macromolecules* **1993**, *26* (21), 5698–5703. <https://doi.org/10.1021/ma00073a026>.
- (52) Schneider, C.; Gordon, O. N.; Edwards, R. L.; Luis, P. B. Degradation of Curcumin: From Mechanism to Biological Implications. *J. Agric. Food Chem.* **2015**, *63* (35), 7606–7614. <https://doi.org/10.1021/acs.jafc.5b00244>.
- (53) Mathematical Models of Drug Release. In *Strategies to Modify the Drug Release from Pharmaceutical Systems*; Elsevier, 2015; pp 63–86. <https://doi.org/10.1016/B978-0-08-100092-2.00005-9>.
- (54) Trathnigg, B. Size-Exclusion Chromatography of Polymers. In *Encyclopedia of Analytical Chemistry*; Meyers, R. A., Ed.; John Wiley & Sons, Ltd: Chichester, UK, 2006; p a2032. <https://doi.org/10.1002/9780470027318.a2032>.
- (55) Fakhari, A.; Corcoran, M.; Schwarz, A. Thermogelling Properties of Purified Poloxamer 407. *Heliyon* **2017**, *3* (8), e00390. <https://doi.org/10.1016/j.heliyon.2017.e00390>.

- (56) Pang, X.; Jiang, Y.; Xiao, Q.; Leung, A. W.; Hua, H.; Xu, C. PH-Responsive Polymer–Drug Conjugates: Design and Progress. *Journal of Controlled Release* **2016**, *222*, 116–129. <https://doi.org/10.1016/j.jconrel.2015.12.024>.
- (57) Liu, J.; Huang, Y.; Kumar, A.; Tan, A.; Jin, S.; Mozhi, A.; Liang, X.-J. PH-Sensitive Nano-Systems for Drug Delivery in Cancer Therapy. *Biotechnology Advances* **2014**, *32* (4), 693–710. <https://doi.org/10.1016/j.biotechadv.2013.11.009>.
- (58) Li, J.; Li, X.; Ni, X.; Wang, X.; Li, H.; Leong, K. W. Self-Assembled Supramolecular Hydrogels Formed by Biodegradable PEO–PHB–PEO Triblock Copolymers and α -Cyclodextrin for Controlled Drug Delivery. *Biomaterials* **2006**, *27* (22), 4132–4140. <https://doi.org/10.1016/j.biomaterials.2006.03.025>.
- (59) Domiński, A.; Konieczny, T.; Kurcok, P. α -Cyclodextrin-Based Polypseudorotaxane Hydrogels. *Materials* **2019**, *13* (1), 133. <https://doi.org/10.3390/ma13010133>.
- (60) Pradal, C.; Jack, K. S.; Grøndahl, L.; Cooper-White., J. J. Gelation Kinetics and Viscoelastic Properties of Pluronic and α -Cyclodextrin-Based Pseudopolyrotaxane Hydrogels. *Biomacromolecules* **2013**, *14* (10), 3780–3792. <https://doi.org/10.1021/bm401168h>.
- (61) Lee, C.-F.; Tseng, H.-W.; Bahadur, P.; Chen, L.-J. Synergistic Effect of Binary Mixed-Pluronic Systems on Temperature Dependent Self-Assembly Process and Drug Solubility. *Polymers* **2018**, *10* (1), 105. <https://doi.org/10.3390/polym10010105>.
- (62) Anderson, B. C.; Cox, S. M.; Ambardekar, A. V.; Mallapragada, S. K. The Effect of Salts on the Micellization Temperature of Aqueous Poly(Ethylene Oxide)-b-poly(Propylene Oxide)-b-poly(Ethylene Oxide) Solutions and the Dissolution Rate and Water Diffusion Coefficient in Their Corresponding Gels. *Journal of Pharmaceutical Sciences* **2002**, *91* (1), 180–188. <https://doi.org/10.1002/jps.10037>.
- (63) Sadeghi, R.; Jahani, F. Salting-In and Salting-Out of Water-Soluble Polymers in Aqueous Salt Solutions. *J. Phys. Chem. B* **2012**, *116* (17), 5234–5241. <https://doi.org/10.1021/jp300665b>.
- (64) Chung, J. W.; Kang, T. J.; Kwak, S.-Y. Supramolecular Self-Assembly of Architecturally Variant α -Cyclodextrin Inclusion Complexes as Building Blocks of Hexagonally Aligned Microfibrils. *Macromolecules* **2007**, *40* (12), 4225–4234. <https://doi.org/10.1021/ma0625105>.
- (65) Jeong, B.; Bae, Y. H.; Kim, S. W. Thermoreversible Gelation of PEG–PLGA–PEG Triblock Copolymer Aqueous Solutions. *Macromolecules* **1999**, *32* (21), 7064–7069. <https://doi.org/10.1021/ma9908999>.
- (66) Brown, W.; Schillen, K.; Hvidt, S. Triblock Copolymers in Aqueous Solution Studied by Static and Dynamic Light Scattering and Oscillatory Shear Measurements: Influence of Relative Block Sizes. *J. Phys. Chem.* **1992**, *96* (14), 6038–6044. <https://doi.org/10.1021/j100193a072>.
- (67) Liu, K. L.; Zhu, J.; Li, J. Elucidating Rheological Property Enhancements in Supramolecular Hydrogels of Short Poly[(R,S)-3-Hydroxybutyrate]-Based Amphiphilic Triblock Copolymer and α -Cyclodextrin for Injectable Hydrogel Applications. *Soft Matter* **2010**, *6* (10), 2300. <https://doi.org/10.1039/b923472a>.
- (68) Abdul Karim, A.; Chee, P. L.; Chan, M. F.; Loh, X. J. Micellized α -Cyclodextrin-Based Supramolecular Hydrogel Exhibiting PH-Responsive Sustained Release and Corresponding Oscillatory Shear Behavior Analysis. *ACS Biomater. Sci. Eng.* **2016**, *2* (12), 2185–2195. <https://doi.org/10.1021/acsbmaterials.6b00383>.
- (69) Tong, L.; Yang, Y.; Luan, X.; Shen, J.; Xin, X. Supramolecular Hydrogels Facilitated by α -Cyclodextrin and Silicone Surfactants and Their Use for Drug Release. *Colloids and Surfaces A: Physicochemical and Engineering Aspects* **2017**, *522*, 470–476. <https://doi.org/10.1016/j.colsurfa.2017.03.026>.

(70) Róka, E.; Ujhelyi, Z.; Deli, M.; Bocsik, A.; Fenyvesi, É.; Szente, L.; Fenyvesi, F.; Vecsernyés, M.; Váradi, J.; Fehér, P.; Gesztelyi, R.; Félix, C.; Perret, F.; Bácskay, I. Evaluation of the Cytotoxicity of α -Cyclodextrin Derivatives on the Caco-2 Cell Line and Human Erythrocytes. *Molecules* **2015**, *20* (11), 20269–20285. <https://doi.org/10.3390/molecules201119694>.

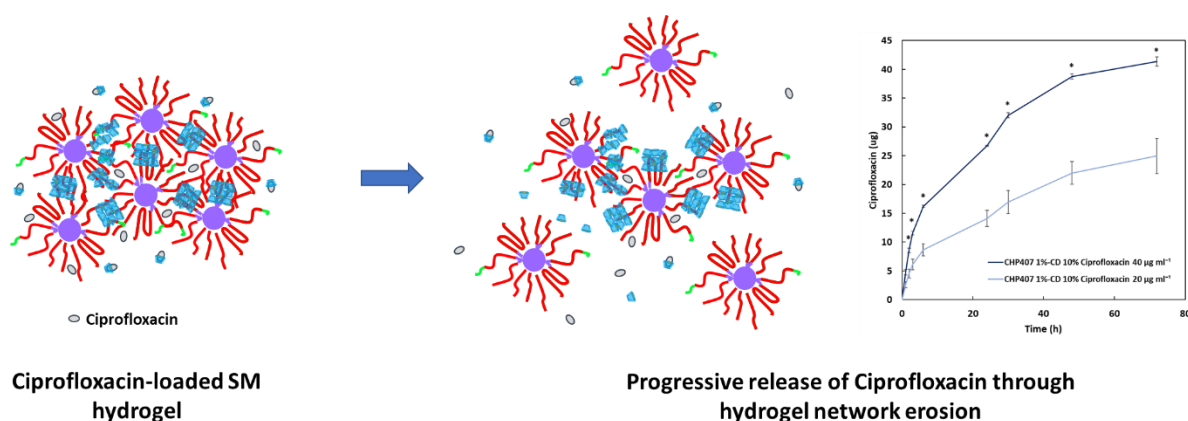
(71) Szente, L.; Singhal, A.; Domokos, A.; Song, B. Cyclodextrins: Assessing the Impact of Cavity Size, Occupancy, and Substitutions on Cytotoxicity and Cholesterol Homeostasis. *Molecules* **2018**, *23* (5). <https://doi.org/10.3390/molecules23051228>.

Section 2 – Chapter 2.5 – Case Study I: release studies of ciprofloxacin, a hydrophilic antibiotic drug for the treatment of infections

1. Abstract

The presence of acute or chronic infections can importantly hinder the process of reparation of tissues and organs. The effective resolution of these pathologies is highly dependent on the methodology of administration of antibiotic drugs. In this regard, the application of injectable hydrogels for the local delivery of antibiotics is a promising strategy for regenerative purposes. Indeed, such an approach would enhance the therapeutic action of antibiotic drugs, while reducing their systemic adverse effects. In this Chapter, a specific application of a custom-made PEU was investigated with the aim to provide a proof-of-concept of the suitability of the synthetic polymers developed in the present work for the design of versatile drug delivery hydrogel platforms. In particular, CHP407 PEU was utilized for the design of SM hydrogel systems containing ciprofloxacin, which is a powerful antibiotic, showing bactericidal action against a wide spectrum of micro-organisms. Ciprofloxacin (i.e., 20 and 40 $\mu\text{g ml}^{-1}$) was successfully encapsulated within SM hydrogels at low CHP407 concentration (i.e., 1% w/v) and CD content at 10% w/v. The effects of drug loading on hydrogel gelation process were qualitatively evaluated by tube inverting tests and a significant increase of gelation time (up to 33%) was observed. Release studies were performed in physiological-like conditions (i.e., PBS, 37 °C) and showed progressive release profiles of ciprofloxacin within the therapeutic window up to 3 days, when complete dissolution of hydrogel systems was concurrently observed. Moreover, 100% of total payload was quantified after release studies, thus indicating a good chemical preservation of ciprofloxacin.

Graphical Abstract



2. Introduction

Ciprofloxacin is a powerful antibiotic drug that shows evident bactericidal effects. It belongs to the class of fluoroquinolones and is the most effective one against gram-negative bacteria (e.g.,

Pseudomonas aeruginosa, *Escherichia coli*, *Enterobacteriaceae*, *Shigella spp.* and *Salmonella spp.*). Its chemical structure is reported in figure 1.

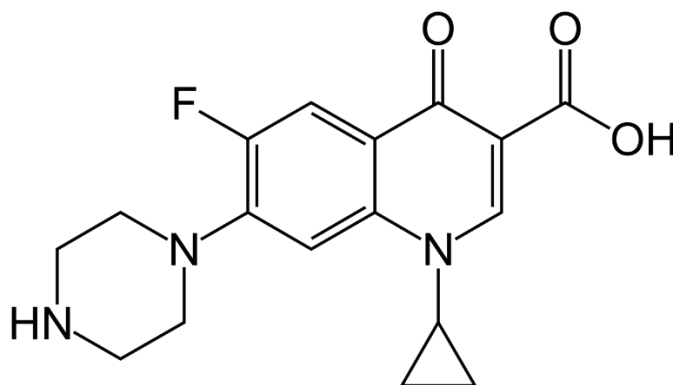


Figure 1 – Chemical structure of ciprofloxacin, a fluoroquinolone.

However, ciprofloxacin shows toxicity also against gram-positive bacteria. Its mechanism of action is based on the inhibition of DNA replication by interacting with DNA topoisomerase and gyrase. For these reasons, ciprofloxacin and generally fluoroquinolones are widely used for the treatment of infection of urinary and gastrointestinal ducts, as well as for respiratory tracts and skin. Moreover, ciprofloxacin is used for the treatment of sexually transmitted diseases and chronic osteomyelitis.^{1,2} It has also been observed that ciprofloxacin can exert anti-proliferative and apoptotic effects on neoplastic cells, such as osteosarcoma and leukemia cells.³ Moreover, Aranha and co-workers observed that ciprofloxacin acts as therapeutic agent for transitional cell carcinoma of the bladder.⁴ Thence, an unquestionable efficacy of such antibiotic drug even for the treatment of tumors has been demonstrated and a lower general toxicity was observed with respect to other chemotherapeutic drugs.⁵ Ciprofloxacin has a general bioavailability around 70% after oral administration and a maximum plasma concentration ranging between 0.8 and 3.9 mg L⁻¹ within 2 hours (administration doses of 250 and 740 mg, respectively). Nonetheless, it is generally excreted almost completely unmetabolized via urine and faeces. Generally, the side effects of ciprofloxacin do not induce severe complications if compared to the overall beneficial activities. At therapeutic dosages, mild toxicity is observed in the gastrointestinal district as nausea, vomiting and diarrhea.⁶ Reactions due to skin photo-sensitivity have been also reported in some cases.^{1,7} Moreover, due to the role exerted by the blood brain barrier, the brain uptake is extremely low.⁸ The most severe effects have been observed after relevant administration doses as induced aseptic meningitis and arthritis damages.^{9,10} In this regard, the most important concern with the use of ciprofloxacin regards its application in children. Indeed, cartilage and bone damages have been observed in such patients.¹¹ For all the above-mentioned controversial effects, the development of highly effective drug carriers, which could enhance the therapeutic activity of ciprofloxacin, represents a valuable strategy to elevate an already existing drug to novel and more advanced applications. According to such approach, innovative and cutting-edge research works are continuously published nowadays. For example, Mahdavinia and colleagues developed a nanocomposite hydrogel system based on κ -carrageenan-crosslinked chitosan/hydroxyapatite for the sustained release of ciprofloxacin.¹² The presented device was addressed to the treatment of relevantly infected bone defects. The importance to avoid burst release of ciprofloxacin was discussed in that work and the developed system showed a sustained delivery kinetics *in vitro* for

several days. In another example, Prusty *et al.* designed a bioartificial nanocomposite hydrogel based on silver nanoparticles encapsulated into soy protein/polyacrylamide polymeric networks.¹³ Highly effective antibacterial and also bactericidal effects were observed by testing the system against *Escherichia Coli*, *Shigella Flexneri*, *Bacillus Cereus* and *Listeria Inuaba*. Nonetheless, a relatively fast drug release was observed. Indeed, over 95% of the total ciprofloxacin was released *in vitro* within 6 hours. The observed fast release was ascribed to the method selected for delivery studies (i.e., hydrogel reswelling).

Release studies of ciprofloxacin could be hindered by the relative solubility of ciprofloxacin. Indeed, such drug molecule is only soluble in acidic condition.² In this regard, it was demonstrated that cyclodextrins enhance the solubilization of ciprofloxacin in a wider range of aqueous environments through the formation of inclusion complexes. Aithal and Udupa conducted a pioneering study on the complexation between ciprofloxacin and β -CDs, thus suggesting the use of the resulting supramolecular structures rather than the drug as such.¹⁴ In the work conducted by Rajendiran and colleagues, the evaluation of self-assembly between α - and β -CDs and ciprofloxacin was studied through UV-Vis, IR and ¹H-NMR spectroscopies.¹⁵ Moreover, computational studies were also conducted to better clarify the physical compatibility existing between these molecular entities. They observed that α - and β -CDs differently interacted with the drug molecules due to their specific cavity diameters. Nonetheless, both of these cyclic molecules were able to form stable inclusion complexes with ciprofloxacin, thus enhancing solubility and stability of such drug. Macocinschi and colleagues developed an engineered film system based on a polyurethane and β -CDs for the controlled release of ciprofloxacin.¹⁶ The formation of drug-containing composite films was studied and characterized, revealing an enhanced activity of released ciprofloxacin from the developed devices. A similar idea is also reported in the study conducted by Masoumi *et al.*, who developed PCL-based nanofibers encapsulating inclusion complexes between cyclodextrins (i.e., α - and β -CDs) and ciprofloxacin.¹⁷ Physico-chemical studies demonstrated the formation of proper inclusion complexes between the cyclic molecules and the drug. Then, such supramolecular structures were encapsulated into PCL-based nanofibers and release studies were conducted, showing controlled release profiles of the drug.

As demonstrated in the above-mentioned works, supramolecular complexes obtained from intramolecular interactions represent valuable systems for the development of promising strategies for drug release. On the basis of this knowledge, in this part of the work PEUs were investigated as constituents of SM gels encapsulating ciprofloxacin. In detail, CHP407 PEU was selected as synthetic counterpart of SM gels due to its better gelation properties and mechanical response with respect to the other investigated PEUs in previous Chapters. The lowest analyzed concentration of CHP407 (i.e., 1% w/v) was used for the design of the novel antimicrobial systems. Qualitative evaluation of gelation properties upon encapsulation of ciprofloxacin at various concentrations was conducted and release kinetics were studied via gel incubation in contact with aqueous environment mimicking physiological-like conditions (i.e., pH 7.4, 37 °C). The implementation of Korsmeyer-Peppas drug release model was exploited to better understand the kinetics of drug release and a comparative evaluation with respect to the previous hydrogel systems encapsulating curcumin was conducted.

3. Materials and Methods

3.1 Materials

For this study, CHP407 was synthesized as reported in the previous Chapters and utilized as PEU for the development of ciprofloxacin-loaded SM hydrogels for its superior ability to form PPR-based networks. Ciprofloxacin (Cip) and phosphate buffered saline (PBS, pH 7.4) were purchased from Sigma Aldrich (Milan, Italy), while α -CDs (from now on simply indicated as “CDs”) were purchased from TCI Chemicals Europe (Zwijndrecht, Belgium).

3.2 Preparation of SM hydrogels encapsulating ciprofloxacin and qualitative evaluation of gelation time

The required mass of CHP407 was solubilized into Bijou sample containers (17 mm inner diameter, Carlo Erba Reagents, Milan, Italy) in PBS at 3 °C overnight. Then, precise volumes of a clear solution of CDs at 14% w/v concentration and a solution of Cip (1 mg ml⁻¹) prepared in HCl (0.1 M) were added to the previously prepared CHP407-based solutions, thus obtaining the final hydrogel formulations composed of CHP407 at 1% w/v, CDs at 10% w/v and Cip at 20 and 40 μ g ml⁻¹ concentrations. Gelation time was evaluated through tube inverting test according to the protocol reported in the previous *Chapter 2.2*.

3.3 Release studies of ciprofloxacin

CHP407 1% - CD 10% samples (1 ml in Bijou sample containers with 17 mm inner diameter) containing Cip at 20 and 40 μ g ml⁻¹ were acclimatized for 15 minutes at 37 °C. Then, PBS (1 ml, 37 °C) was gently added to each sample and at precise time frames (1, 2, 3, 6, 24, 30, 48 and 72 hours) the elutes were withdrawn and analyzed using a UV-Vis spectrometer (Perkin Elmer Lambda 25 UV/Vis spectrometer, Waltham, MA, USA) by quantifying the absorbance peak at 270 nm. Three samples were prepared for each condition and data are reported as mean \pm standard deviation. Reference curves were obtained from standard Cip samples with concentration in the range between 1 and 10 μ g ml⁻¹ and in the presence of CDs at various contents (0, 1, 2.5, 5 and 10% w/v) in order to evaluate the contribution of possible supramolecular interactions to Cip quantification. Korsmeyer-Peppas model was implemented as reported in previous Chapters (Equation 4, *Section 2 – Chapter 2.4 – Materials and methods – Curcumin encapsulation and release studies*) to evaluate the involved mechanism of drug delivery.

4. Results

The encapsulation of Cip within SM hydrogels based on CHP407 resulted in a delaying effect of the gelation process. Indeed, CHP407 1% - CD 10% was characterized by a gelation time at room temperature around 10 hours and 30 minutes, while hydrogel systems containing Cip at 20 and 40 μ g ml⁻¹ concentration required 12 and 14 hours to complete gelation, respectively. Thence, some interactions between CDs and Cip probably occurred, as expected.¹⁵ However, no significant differences were observed in the UV-Vis spectroscopic responses obtained from standard Cip samples containing CDs at different concentrations ranging from 0 to 10% w/v. Figure 2 reports

the obtained data and the resulting linear regressions. Then, on the basis of previous data on the evaluation of SM hydrogel responsiveness in contact with watery environments (i.e., swelling and stability tests) and on the observed good stability of the involved networks, the calibration curve based on Cip standards not containing CDs was selected for drug quantification.

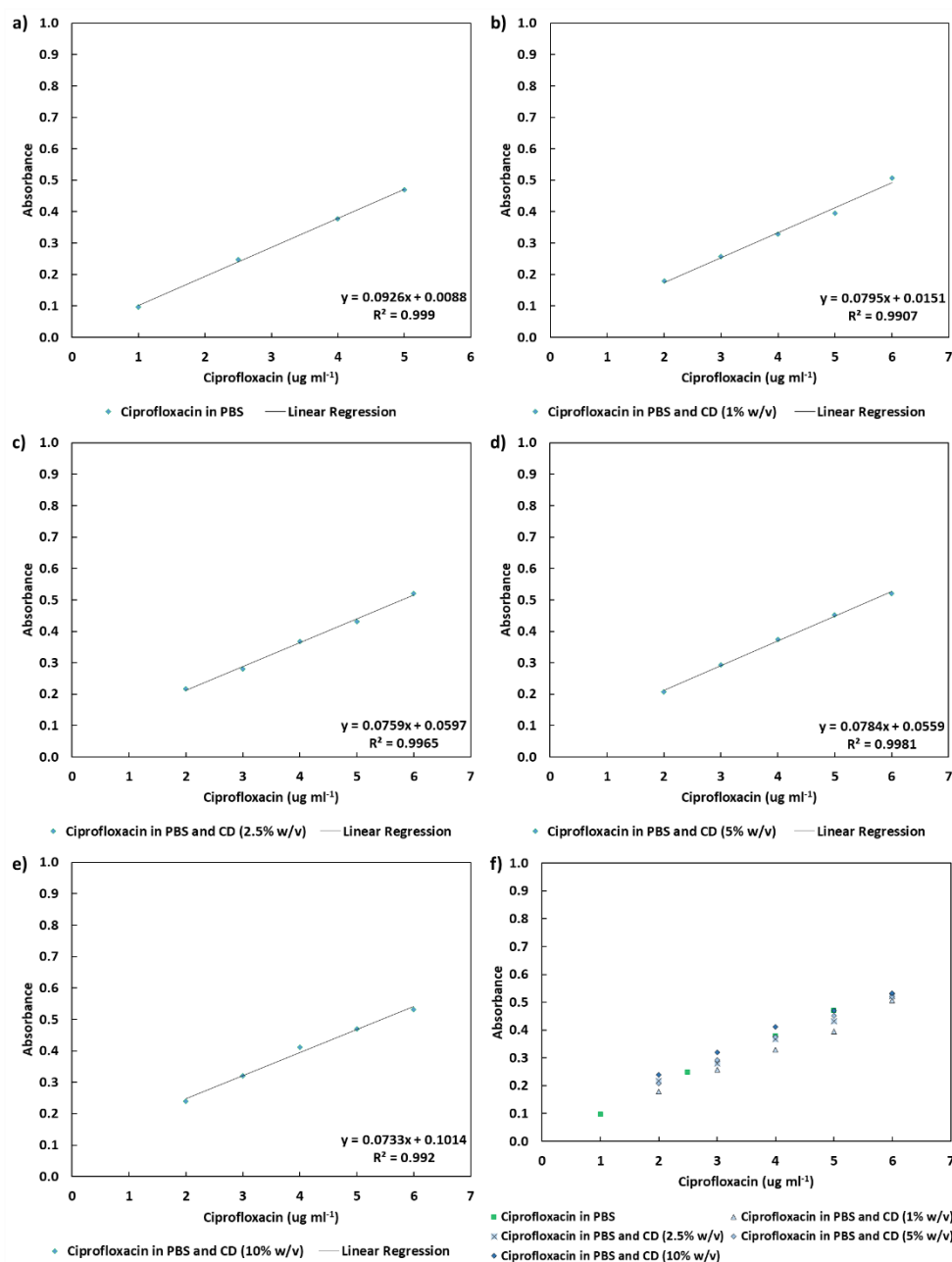


Figure 2 – Calibration curves of Cip in PBS in the absence (a) and in the presence of CDs at b) 1%, c) 2.5%, d) 5%, and e) 10% w/v concentration. A general comparison is also reported (f) to appreciate the slight differences that occurred among the entire domain of tested conditions.

The spectra of Cip (0% w/v CD content) at various concentrations in PBS within the spectral range between 200 and 400 nm are reported in figure 3. Release profiles of Cip are reported in figure 4 and showed highly progressive kinetics up to 100% of the encapsulated payload. In fact, no burst release was observed. Moreover, the calculation of Korsmeyer-Peppas parameters indicated a non-Fickian delivery mechanism. In detail, the obtained values of n for CHP407 1% - CD 10%

containing Cip at 20 and 40 $\mu\text{g ml}^{-1}$ resulted equal to 0.66 ± 0.03 and 0.69 ± 0.05 , respectively. Interestingly, the calculated n values for Cip were not significantly different from the ones obtained from the release studies of Cur conducted in the previous Chapter from the same hydrogel system, thus indicating a consistent responsiveness of the here-designed formulations. Nonetheless, significantly different release rates were observed between the release profiles of Cip and Cur. In fact, the K values that were obtained through the implementation of the Korsmeyer-Peppas model were significantly greater for Cip release profiles, thus indicating a faster kinetics. In detail, K for the hydrogel system containing Cip resulted equal to 0.11 ± 0.02 for both Cip payloads, while K value for Cur-loaded hydrogels was quantified around 0.02 ± 0.006 (significant difference, p value = 0.044). In this regard, although Cip and Cur show similar molecular mass (i.e., 331.35 Da and 368.38 Da, respectively), Cur is characterized by a marked hydrophobicity, which could retard its release in watery environments, thus indicating a strong dependence of release on the progressive dissolution of hydrogel components (i.e., CDs and CHP407 chains). These observations further highlighted the suitability of PEU-based hydrogel networks to stabilize and progressively release encapsulated drugs with different nature (i.e., lipophilic or hydrophilic).

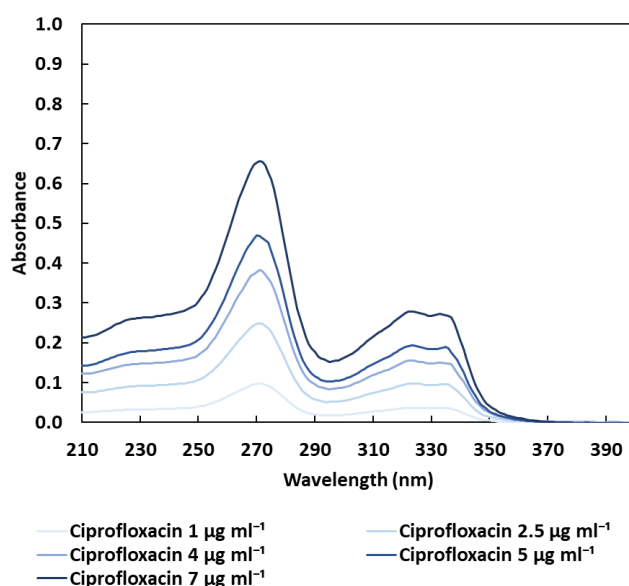


Figure 3 – UV spectra of Cip in pure PBS at the different concentrations tested for the construction of the calibration curve by quantifying the peak at 270 nm.

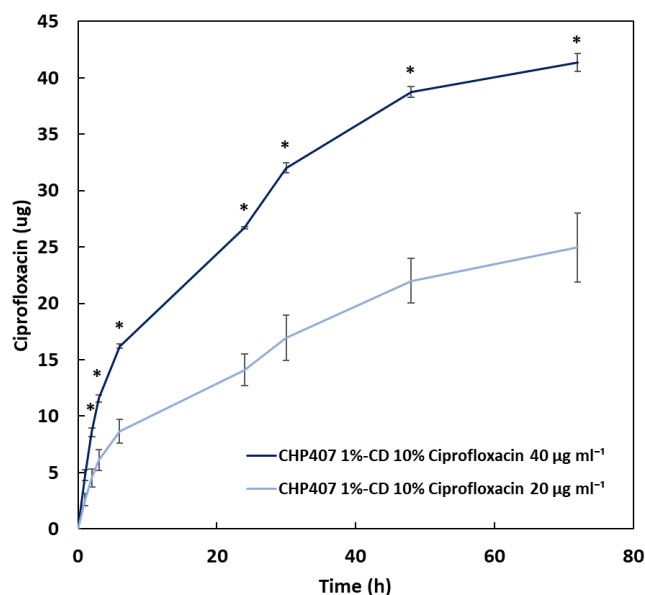


Figure 4 – Release profiles of Cip from CHP407 1% - CD 10% hydrogels (1 ml) containing Cip at 20 (light blue) and 40 (blue) $\mu\text{g ml}^{-1}$ concentration.

5. Conclusions

In this part of the work, the specific case of Cip release from PEU-based SM hydrogels was evaluated. For the encapsulation of such drug, CHP407 was selected to form SM networks due to its superior physical and mechanical properties with respect to the other PEUs investigated in the previous Chapters. The hydrogel formulation based on CHP407 at 1% w/v concentration resulted to be again suitable for the attainment of progressive release profiles of the encapsulated drug. These observations confirmed the important role exerted by SM networks with low PEU/CD ratios in the formation of highly stable and responsive hydrogels for local drug release after injection. This proof-of-concept study reinforced the rationale underpinning the development of functional hydrogels at low polymeric content. In this regard, PEUs have been demonstrated to play a pivotal role. Moreover, this short study further proved the high versatility of properly synthesized PEUs in the field of drug delivery for regenerative medicine. In fact, the here-developed systems showed promising features as drug carriers enhancing drug therapeutic action while simultaneously reducing the controversial effects and the potential interactions of hydrogel components with real biological environments.

6. References

- (1) Appelbaum, P. C.; Hunter, P. A. The Fluoroquinolone Antibacterials: Past, Present and Future Perspectives. *International Journal of Antimicrobial Agents* **2000**, *16* (1), 5–15. [https://doi.org/10.1016/S0924-8579\(00\)00192-8](https://doi.org/10.1016/S0924-8579(00)00192-8).
- (2) Davis, R.; Markham, A.; Balfour, J. A. Ciprofloxacin: An Updated Review of Its Pharmacology, Therapeutic Efficacy and Tolerability. *Drugs* **1996**, *51* (6), 1019–1074. <https://doi.org/10.2165/00003495-199651060-00010>.
- (3) Sharma, P. C.; Jain, A.; Jain, S.; Pahwa, R.; Yar, M. S. Ciprofloxacin: Review on Developments in Synthetic, Analytical, and Medicinal Aspects. *Journal of Enzyme Inhibition and Medicinal Chemistry* **2010**, *25* (4), 577–589. <https://doi.org/10.3109/14756360903373350>.
- (4) Aranha, O.; Wood, D. P.; Sarkar, F. H. Ciprofloxacin Mediated Cell Growth Inhibition, S/G2-M Cell Cycle Arrest, and Apoptosis in a Human Transitional Cell Carcinoma of the Bladder Cell Line. *Clinical Cancer Research* **2000**, *6*, 891–900.
- (5) Aranha, O.; Grignon, R.; Fernandes, N.; McDONNELL, T. J.; Jr, D. P. W.; Sarkar, F. H. Suppression of Human Prostate Cancer Cell Growth by Ciprofloxacin Is Associated with Cell Cycle Arrest and Apoptosis. *INTERNATIONAL JOURNAL OF ONCOLOGY* **2003**, *8*.
- (6) Sárközy, G. Quinolones: A Class of Antimicrobial Agents. *Veterinarni Medicina* **2001**, *46* (No. 9–10), 257–274. <https://doi.org/10.17221/7883-VETMED>.
- (7) Blandeau, J. M. Expanded Activity and Utility of the New Fluoroquinolones: A Review. *Clinical Therapeutics* **1999**, *21* (1), 3–40. [https://doi.org/10.1016/S0149-2918\(00\)88266-1](https://doi.org/10.1016/S0149-2918(00)88266-1).
- (8) Oliphant, C. M.; Green, G. M. Quinolones: A Comprehensive Review. **2002**, *65* (3), 10.
- (9) Kepa, L.; Oczko-Grzesik, B.; Stolarz, W.; Sobala-Szczygiel, B. Drug-Induced Aseptic Meningitis in Suspected Central Nervous System Infections. *Journal of Clinical Neuroscience* **2005**, *12* (5), 562–564. <https://doi.org/10.1016/j.jocn.2004.08.024>.
- (10) Mao, Z.; Ma, L.; Gao, C.; Shen, J. Preformed Microcapsules for Loading and Sustained Release of Ciprofloxacin Hydrochloride. *Journal of Controlled Release* **2005**, *104* (1), 193–202. <https://doi.org/10.1016/j.jconrel.2005.02.005>.
- (11) Velissariou, I. M. The Use of Fluoroquinolones in Children: Recent Advances. *Expert Review of Anti-infective Therapy* **2006**, *4* (5), 853–860. <https://doi.org/10.1586/14787210.4.5.853>.
- (12) Mahdavinia, G. R.; Karimi, M. H.; Soltaniniya, M.; Massoumi, B. In Vitro Evaluation of Sustained Ciprofloxacin Release from κ -Carrageenan-Crosslinked Chitosan/Hydroxyapatite Hydrogel Nanocomposites. *International Journal of Biological Macromolecules* **2019**, *126*, 443–453. <https://doi.org/10.1016/j.ijbiomac.2018.12.240>.
- (13) Prusty, K.; Biswal, A.; Biswal, S. B.; Swain, S. K. Synthesis of Soy Protein/Polyacrylamide Nanocomposite Hydrogels for Delivery of Ciprofloxacin Drug. *Materials Chemistry and Physics* **2019**, *234*, 378–389. <https://doi.org/10.1016/j.matchemphys.2019.05.038>.
- (14) K. Shrinivas Aithal; N. Udupa. Physicochemical Study of Ciprofloxacin with B-Cyclodextrin. *Pharmacy and Pharmacology Communications*. 1996, pp 451–455.

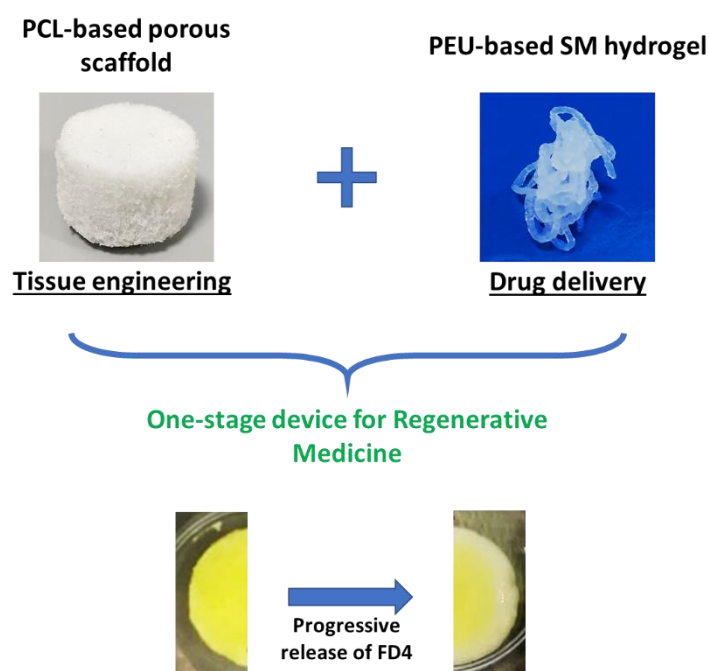
- (15) Rajendiran, N.; Mohandoss, T.; Thulasidhasan, J. Encapsulation of Ciprofloxacin, Sparfloxacin, and Ofloxacin Drugs with α - and β -Cyclodextrins: Spectral and Molecular Modelling Studies. *Physics and Chemistry of Liquids* **2016**, *54* (2), 193–212. <https://doi.org/10.1080/00319104.2015.1074046>.
- (16) Macocinschi, D.; Filip, D.; Vlad, S.; Tuchilus, C. G.; Cristian, A. F.; Barboiu, M. Polyurethane/ β -Cyclodextrin/Ciprofloxacin Composite Films for Possible Medical Coatings with Antibacterial Properties. *J. Mater. Chem. B* **2014**, *2* (6), 681–690. <https://doi.org/10.1039/C3TB21361G>.
- (17) Masoumi, S.; Amiri, S.; Bahrami, S. H. PCL-Based Nanofibers Loaded with Ciprofloxacin/Cyclodextrin Containers. *The Journal of The Textile Institute* **2018**, *109* (8), 1044–1053. <https://doi.org/10.1080/00405000.2017.1398625>.

Section 2 – Chapter 2.6 – Case Study II: encapsulation of a PEU-based SM hydrogel within highly porous scaffolds composed of poly(ϵ -caprolactone)

1. Abstract

Biomedical engineering aims to develop multi-functional devices able to induce a successful regeneration of damaged tissues and organs. In this regard, the design of systems that combine drug delivery and tissue engineering represents an extremely attractive strategy. Hence, in this part of the work, a case study was conducted with the intention to provide a proof of concept about the feasibility to use a PEU-based SM hydrogel for the development of a “one-stage” regenerative approach resulting from its integration into a porous matrix. To this aim, SHP407 PEU was selected for the production of SM hydrogels. Indeed, such PEU is characterized by the presence of free primary amino groups that can enhance network responsiveness in acidic milieus, which distinguish acute inflammation and tumor environments. 3D-porous scaffolds were produced through a simple and conventional method (i.e., salt-leaching) using poly(ϵ -caprolactone) (\bar{M}_n 80 kDa) as forming material. The implementation of this technique allowed the preparation of homogeneous and highly porous systems (up to 89% interconnected porosity). Plasma treatment was performed on the resulting scaffolds in order to improve surface hydrophilicity and hydrogel loading. Hydrogels containing SHP407 at 2% w/v and CDs at 10% w/v were selected as a good compromise between good mechanical properties and low PEU content. In this regard, rheological characterizations showed that hydrogels composed of PEU at 2% w/v concentration exhibited significantly better mechanical properties when compared with formulations containing the same polymer at 5% w/v (up to 30% higher G' values for hydrogels containing SHP407 at 2% w/v with respect to 5% w/v), thus indicating an enhanced formation of PPR-based SM network at lower PEU/CD mass ratios. A simple and effective method for hydrogel encapsulation within the void volume of scaffolds was developed by exploiting the temporal window for gelation. During this period, the scaffolds were immersed into a gelling mixture of SHP407 2% - CD 10% and gently compressed, thus resulting in a high hydrogel encapsulation yield (i.e., approx. 80%). A qualitative evaluation of mechanical properties through compression tests showed an enhanced mechanical resistance of the hybrid systems compared to virgin scaffolds at strain values over 10%. Finally, preliminary studies of drug release were conducted by loading a precise amount of a model molecule (i.e., FD4) with the hydrogel counterpart of the hybrid systems and highly progressive release profiles up to 48 hours were obtained in contact with physiological-like aqueous environments (i.e., PBS, pH 7.4, 37 °C).

Graphical Abstract



2. Introduction

Injectable hydrogels and solid porous scaffolds represent two elemental tools of regenerative medicine. In fact, reversible and injectable matrices are particularly useful to locally deliver pharmacological therapies, which can be addressed to various aims, such as infection treatment, inflammation reduction and regeneration enhancement. On the other hand, porous scaffolds are mainly designed to host specific cells and engineered to be bioactive, thus inducing a proper tissue regeneration after substrate implantation and maturation *in vivo*. Nonetheless, to date a wide number of hydrogel-scaffolds and drug-eluting scaffolds can be found in the literature, since both strategies show a wide domain of possibilities for property engineering and are notably overlapped in terms of final intent.¹⁻³ Generally, the attainment of satisfactory properties in both the aspects of drug release and scaffold maturation is not trivial. An interesting and alternative approach consists in developing single-stage devices based on both solid scaffold and water-based hydrogels to exert a dual function. Indeed, such hybrid systems are generally designed to initially deliver therapeutic agents to treat the involved pathologies; subsequently, the scaffold aims to regenerate the tissues by exerting its bioactivity. It is clear that the complexity of such systems represents a hindering element for the overall development and validation for real clinical uses. However, extremely important advantages can be attributed to this approach. In fact, the possibility to include a therapeutic potential and a bioactive functionality within a single device could allow a significant reduction of both the invasiveness of multiple surgeries and hospitalization periods, thus alleviating the overall impact on the involved patients. Thence, the rationale underpinning the development of these relatively complex hybrid devices can be considered notably valid. In this regard, it is possible to find various examples in the literature finalized to the design of highly engineered hybrid systems. For instance, Hernandez and co-authors developed a hybrid system based on a 3D-printed PCL gyroid containing a composite hydrogel system formulated with alginate, gelatin and nano-hydroxyapatite.⁴ The soft gel component of this system was exploited

to encapsulate human mesenchymal stem cells with the aim to induce an effective regeneration of bone tissue. The overall effectiveness of this device was demonstrated by evaluating the induced biomineralization and hydrogel dissolution through *in vitro* tests. A similar approach was reported by Gupta *et al.*, who developed a 3D-printed PLA monolith impregnated with a dual crosslinked hydrogel network based on alginate and collagen.⁵ The hydrogel network was stabilized through ionic crosslinking and the formation of reversible Schiff-base domains. Chondrogenic differentiation of human stem cells was evaluated through *in vitro* tests, while *in vivo* implantation demonstrated good biocompatibility and suitability for meniscal regeneration. A different approach was illustrated by Ilomuanya and co-workers.⁶ In brief, PLA-based scaffolds were produced through electrospinning and loaded with hydrogels composed of hyaluronic acid encapsulating valsartan and ascorbic acid. A set of studies conducted *in vitro* demonstrated the progressive release of valsartan as potential wound healing co-factor, while *in vivo* evaluations showed enhanced re-epithelization induced by this hybrid device.

The entire set of these recent studies highlights the general interest of the research community in the development of particular systems sharing the same hybrid nature. Thence, in this part of the work, a different typology of single-stage device was developed as a further proof of the versatility of the here-developed supramolecular hydrogels based on custom-made PEUs. In detail, by exploiting an easy protocol based on salt leaching, highly porous scaffolds composed of PCL were produced and physically characterized. In order to increase scaffold surface hydrophilicity, argon plasma treatment was carried out. Then, SHP407 was selected for the production of SM hydrogels due to its responsiveness in water-based environments and ability to exert a pH-sensitive behavior.⁷ A physical characterization in general terms was conducted on SHP407-based hydrogels by qualitatively evaluating gelation kinetics and performing rheological tests. Hydrogel encapsulation was conducted through gentle compression of PCL-based scaffolds within gelling solution of SHP407 and CDs. A preliminary mechanical characterization of the hybrid systems was conducted through compression tests to evaluate the effects of the loaded SM hydrogel on the overall mechanical behavior. Finally, release kinetics of a drug model molecule (i.e., FD4) from SHP407-based hydrogels loaded within the porous scaffolds was evaluated to assess the suitability of these newly designed hybrid systems for regenerative pharmacology applications.

3. Materials and Methods

3.1 Materials

PCL (\bar{M}_n 80000 Da) and sodium chloride were purchased from Sigma Aldrich (Milan, Italy). CDs were purchased from TCI Chemical Europe (Zwijndrecht, Belgium). All solvents were obtained from Carlo Erba Reagents (Milan, Italy). SHP407 was produced from NHP407, which was synthesized as reported in *Section 2 – Chapter 2.2 – Materials and methods – Synthesis of PEUs*, and subjected to Boc group cleavage as indicated in *Section 2 – Chapter 2.4 – Materials and methods – De-protection of N-Boc serinol-based PEUs*.

3.2 Preparation of PCL-based porous scaffolds through salt-leaching technique

For the preparation of highly porous PCL-based scaffolds, the polymer was solubilized in chloroform at a concentration of 30% w/v. In parallel, NaCl was sieved (particle diameter ranging between 250 and 500 μm). Then, 2 g of PCL solution at 30% w/v were transferred into a 20 ml beaker and 8 g of sieved NaCl were added. The mixture was manually homogenized using a spatula, transferred into a syringe (5 ml, outlet diameter equal to syringe barrel) and compacted. Then, glass cylindrical molds (10 mm inner diameter, 15 mm height) with reference marks were filled with the prepared paste (approx. 0.5 ml). The cut-off end of the syringe was used to extrude the paste and then the samples were stabilized within the mold through gentle compression using a 5 ml syringe plunger. The samples were maintained under a fume hood overnight to ensure the complete evaporation of chloroform. Finally, the obtained samples were immersed in excess distilled water for 5 days to leach out the porogen (i.e., NaCl) and dried for 48 hours under a fume hood.

3.3 Plasma treatment of PCL-based porous scaffolds

Plasma treatment was exploited to improve the hydrophilicity of PCL-based scaffolds. The presence of polar domains generally enhances and improves the interaction of biomaterials with biological environments (e.g., cell adhesion and proliferation).^{8,9} In addition, it can even enhance water-based hydrogel encapsulation within the void volume of porous scaffolds. To this aim, surface etching was performed through argon (Ar) plasma to induce the formation of polar chemical domains. A standard procedure was conducted to this aim. In detail, one batch of PCL-based scaffolds was loaded into a plasma reactor (Diener electronic, Ebhausen, Germany). A supply of Ar gas was conducted for 10 minutes at a pressure of 0.27 mbar. Then, the surface etching procedure was conducted at 50 W direct power supply for 15 minutes. For each batch, the entire process was repeated twice by rotating upside down the samples in order to treat all scaffold surfaces.

3.4 Characterization of PCL-based morphology

The fabricated scaffolds were geometrically characterized by measuring their diameter and height (three measurements were performed). The resulting scaffold density ($\rho_{porous\ scaffold}$) was calculated by dividing the obtained cylindrical volume by its measured mass and the overall porosity (%) was calculated as indicated in equation 1.

$$p = \left(1 - \frac{\rho_{porous\ scaffold}}{\rho_{bulk\ PCL}}\right) \times 100 \quad \text{Eq. 1}$$

in which $\rho_{bulk\ PCL}$ indicates the density of bulk PCL (1.145 g cm^{-3}).¹⁰ Two batches consisting in 10 scaffolds each were produced in order to evaluate the repeatability of the process.

A qualitative evaluation of the presence of residual porogen and the resulting pore morphology was conducted through optical microscopy using an inverted microscope (Leica DM IL LED, Leica Microsystems, Milan, Italy). Analyses were conducted on scaffold sections obtained through rigid slicing at extremely low temperatures (i.e., immediately after removal from 1 minute immersion in liquid nitrogen).

3.5 SHP407-based SM hydrogel formulation, preparation, and qualitative evaluation of gelation time

For this study, SHP407 was selected for its enhanced responsiveness in aqueous environments due to the presence of free primary amines as pendant groups. Indeed, in previous studies SHP407 PEU resulted to be suitable for the design of pH-responsive and thermo-sensitive hydrogels for advanced applications in drug delivery,⁷ in addition to the promising results discussed in *Chapter 2.4* regarding the formation of PPR-based gel systems. SM hydrogels were formulated containing SHP407 at 2% w/v and CDs at 10% w/v concentrations according to the protocol described in previous Chapters dedicated to SM hydrogel preparation. In this case, the higher PEU content (2% w/v) with respect to previous studies (i.e., 1% w/v) was selected to enhance the interaction of hydrogel polymer chains with the polymeric surface of PCL-based porous scaffolds and confer superior mechanical properties to the resulting hybrid system. Gelation time was qualitatively evaluated as indicated in the previous protocols through tube inverting test of hydrogels samples (1 ml) prepared in Bijou sample containers (17 mm inner diameter, Carlo Erba Reagent, Milan, Italy) and incubated in isothermal conditions (i.e., 25 °C).

3.6 Rheological characterization of SHP407-based hydrogels

In order to characterize the mechanical response of the here-formulated SHP407-based hydrogel, a set of rheological tests was conducted (i.e., frequency sweep, strain sweep and self-healing tests) at various temperatures (i.e., 25 and 37 °C) as indicated in the previous Chapter (*Section 2 – Chapter 2.2 – Materials and method – Rheological characterization*).

3.7 SM hydrogel loading within PCL-based scaffolds

The integration of SHP407-based hydrogels within the porous PCL scaffolds composed was carried out through simple immersion and compression of the solid systems into a self-assembling solution of SHP407 and CDs. In detail, a storage solution of SHP407 2% - CD 10% was prepared as previously indicated. Then, 1 ml of this mixture was transferred into a Bijou sample container (17 mm inner diameter, Carlo Erba Reagents, Milan, Italy) and one scaffold was inserted after weight measurement. The permeation of the gelling solution within the porous network was enhanced through gentle compression of the immersed scaffold using a syringe plunger (conventional syringe, 5 ml volume capacity). Complete gelation of the loaded SM mixture was ensured through incubation for 48 hours at room temperature (i.e., 25 °C). Finally, the obtained hybrid systems were removed from sample containers and weighted to evaluate the theoretical hydrogel loading within the solid scaffolds referring to the void volume defined from scaffold porosity.

3.8 Evaluation of mechanical properties

Preliminary compression tests were conducted as indicated in the work performed by Guarino and co-authors with slight modifications.¹¹ In detail, plasma-treated PCL-based scaffolds loaded with SHP407 2% - CD 10% were tested using an MTS Q-Test 10 device (MTS, USA) equipped with two parallel plates and a 500 N load cell. The tests were conducted at a deformation speed of 1

mm min⁻¹ (sampling frequency equal to 1 Hz) up to 20% of total height at room temperature (25 °C). Three hybrid samples were prepared by integrating SHP407-based SM hydrogels within PCL-based scaffolds and three control samples were also produced by repeating the same loading procedure with simple PBS rather than gelling solutions.

3.9 Release kinetics of FD4 from hybrid scaffold systems encapsulating SM hydrogels

Release studies of FD4-loaded hydrogels encapsulated within PCL-based scaffolds were conducted in physiological-like conditions (i.e., through immersion in PBS, pH 7.4, 37 °C). In detail, hybrid samples were prepared as reported before through the loading of self-assembling SHP407- and CD-based solutions containing a precise amount of FD4. Then, FD4-loaded hybrid systems were transferred into a 24 well-plate and acclimatized at 37 °C for 15 minutes. In order to avoid evaporation phenomena and consecutive dehydration of samples, free wells were filled with bi-distilled water (37 °C). Then, 0.5 ml of PBS (37 °C) were added to the samples. At predefined time steps (2, 4, 6, 24, 30 and 48 hours) the eluates were collected and fully refreshed with new PBS. The obtained samples were centrifuged at 4500 rpm for 10 minutes at 15 °C with the aim to remove any SM structures in suspension that could induce optical interference. 200 µl of each sample were transferred into a 96-well plate and FD4 quantification was performed utilizing a plate reader (Victor X3, Perkin Elmer) by evaluating the absorbance of the samples at 490 nm and referring to a curve obtained from FD4 standards prepared in PBS at concentration ranging between 0 and 1 mg ml⁻¹.

4. Results

4.1 Physical evaluation of PCL-based scaffolds

The main physical parameters of PCL-based scaffolds belonging to two different batches are reported in table 1. Interestingly, the investigated parameters (i.e., volume, density, and porosity) were characterized by low variability within the same batch and the main difference between the two batches was represented by scaffold height (i.e., approx. 20% difference). Such outcome can be ascribed to the intrinsic variability related to the extrusion process of the paste into the mold. Nonetheless, these results suggested a solid procedure for scaffold preparation with highly repeatable physical properties. Indeed, the obtained values of porosity were statistically identical among the two batches (i.e., 89.2-89.3%). Figure 1 shows scaffold morphology as evidenced through optical microscopy.

Table 1 – Main physical parameters characterizing PCL-based scaffolds belonging to two different batches (10 scaffolds each).

	Batch 1	Batch 2
Volume (ml)	0.45 ± 0.03	0.56 ± 0.02
Density (g cm⁻³)	0.125 ± 0.006	0.123 ± 0.006
Porosity (%)	89.2 ± 0.5	89.3 ± 0.5

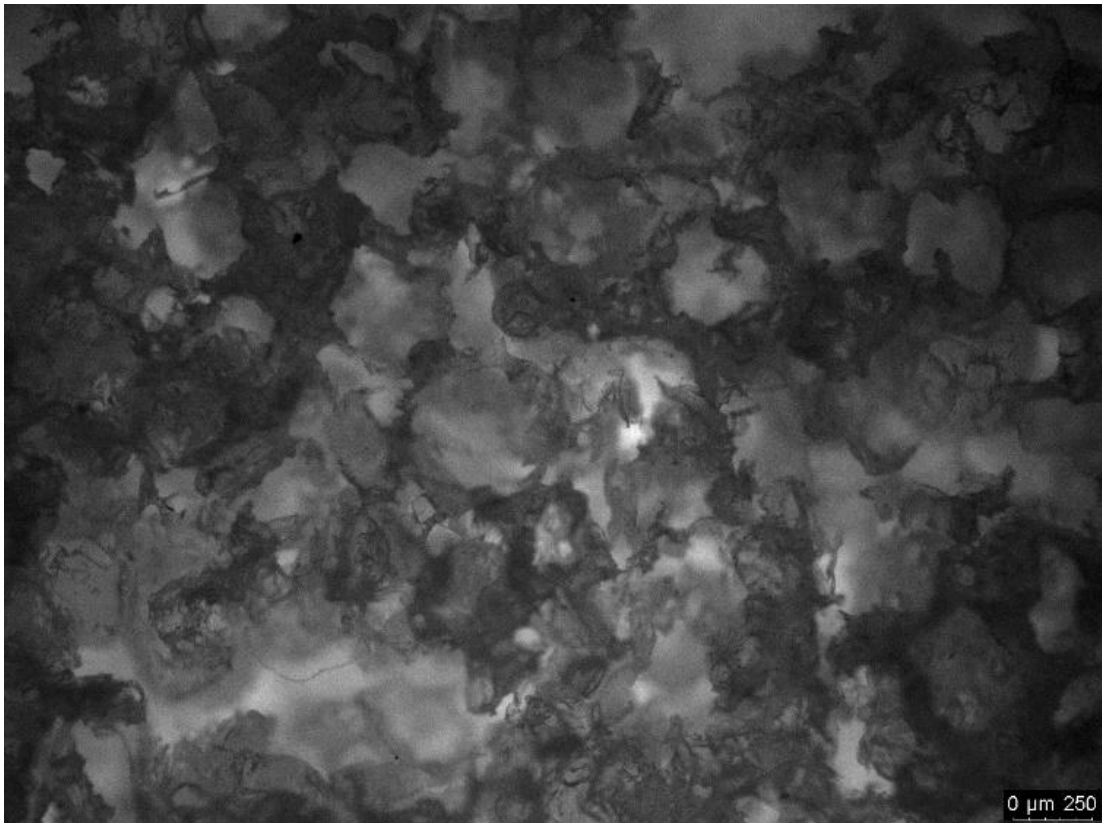


Figure 1 – Optical microscope image of the resulting porosity that characterized PCL-based scaffolds. It is possible to observe the typical pore morphology derived from the cubic structure of NaCl crystals. No residual particles of porogen were detected.

4.2 Rheological characterization of SHP407-based hydrogel

A formulation based on SHP407 at 2% w/v and CDs at 10% w/v concentrations was selected as a compromise between low content of synthetic polymer and mechanical properties. Indeed, a relevant increment of mechanical properties was expected by increasing PEU concentration from 1 to 2% w/v, while maintaining the overall synthetic content relatively low. Gelation time of SHP407 2% - CD 10% turned out to be around 3 hours, which represented a suitable temporal window for further manipulation in view of hydrogel encapsulation within the porous scaffolds. In order to characterize the mechanical responsiveness of the resulting SHP407 2% - CD 10% hydrogel system, a general set of rheological tests was conducted (i.e., frequency sweep tests at 25 and 37 °C, strain sweep and self-healing tests at 37 °C). The results are entirely reported in figure 2.

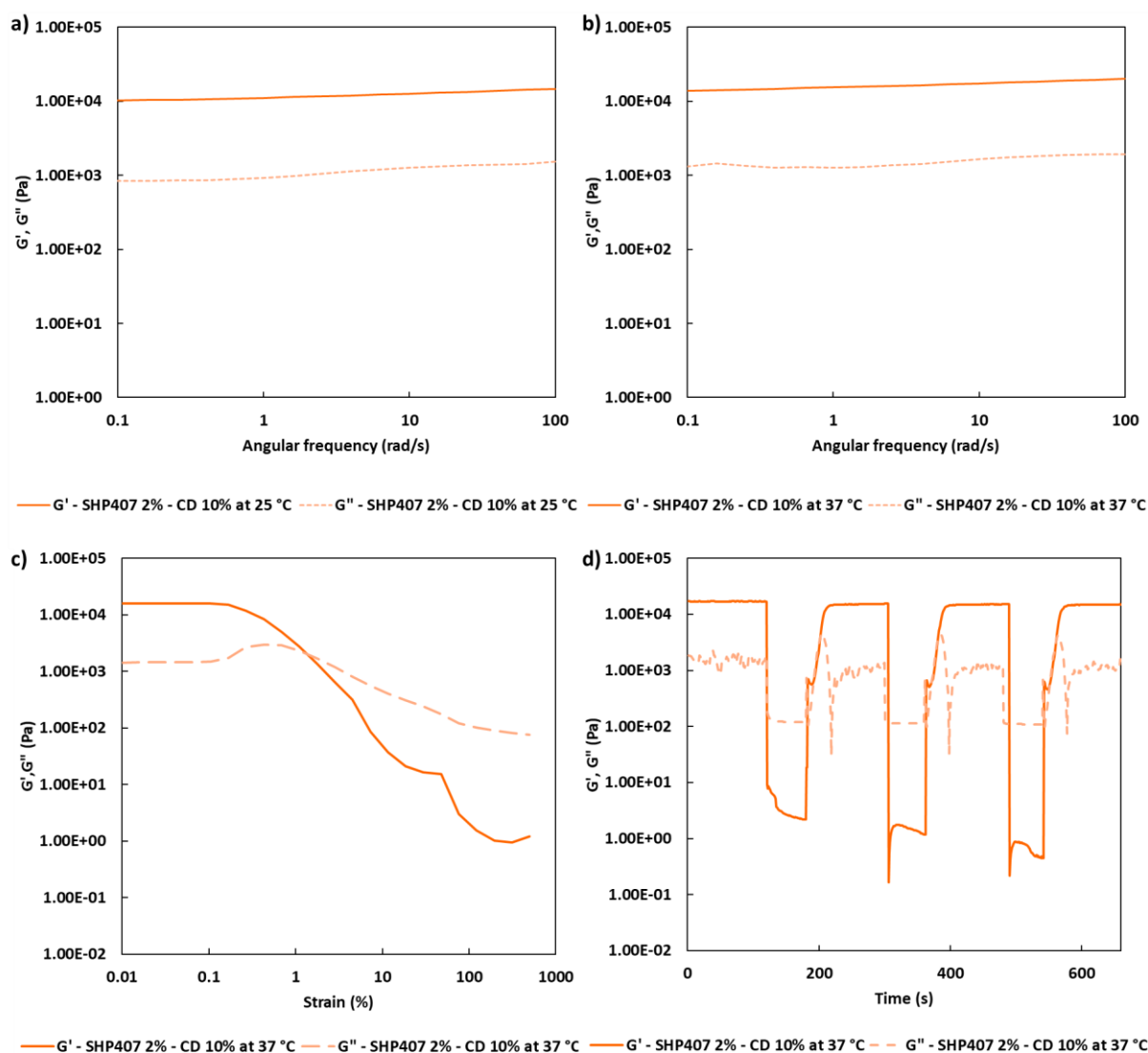


Figure 2 – Rheological characterization of SHP407 2% - CD 10%. Frequency sweep tests at a) 25 °C and b) 37 °C, c) Strain sweep test at 37 °C, and d) recovery tests at 37 °C are reported, representing G' (orange continuous lines) and G'' (light orange dashed lines) trends.

SHP407 2% - CD 10% showed the typical responsiveness of a fully developed and self-healing hydrogel network. Indeed, no crossover points between G' and G'' were observed within the entire range of investigated frequencies and temperatures (i.e., 25 and 37 °C), as illustrated in figure 2a and 2b. Self-healing ability was demonstrated by alternating recovery (0.1% strain) and rupture (100% strain) phases over time. In this regard, an overall recovery of starting G' around 88% was observed after three complete rupture cycles. Interestingly, the investigated formulation resulted to be a remarkably good compromise between PEU content and mechanical properties. In fact, G' values greater than the ones that characterized formulations containing higher SHP407 contents were observed. In detail, SHP407 2% - CD 10% showed G' around 20 kPa at 37 °C and 100 rad s^{-1} , while in the same conditions SHP407 5% - CD 10% hydrogel was characterized by G' approximately equal to 15 kPa, as assessed in *Chapter 2.4*. This interesting result further reinforced our previous hypothesis that SM network formation enhances with decreasing PEU/CD mass ratios. It could be additionally deduced that the PEU concentration domain ranging between 1 and 3% w/v corresponded to the best condition in terms of SM hydrogel development through a

maximization of the interaction between PEU and CDs. In detail, the specific PEU concentration of 2% w/v resulted in a significant improvement compared to 1 % w/v. Indeed, a four-fold increase in G' was observed in SHP407 2% - CD 10% with respect to SHP407 1% - CD 10%, thus confirming the above-mentioned hypothesis and indicating that the SHP407 concentration of 2% w/v represented a better enhancing condition for the development of SM structures based on PPRs.

4.3 SM hydrogel loading within PCL-based scaffolds and investigations of the mechanical properties of the resulting hybrid systems

The encapsulation of SHP407 2% - CD 10% was conducted at room temperature (25 °C) in a specific temporal window, in which the solution is characterized by low viscosity (i.e., immediately after mixing of PEU and CD components). Scaffolds belonging to batch 1 were selected for these studies. Simple immersion of scaffolds into gelling solutions did not result in an acceptable loading yield (i.e., <10%). Differently, the addition of a slight compression resulted in relatively high hydrogel encapsulation yield within the solid structures. In detail, an encapsulation yield around 80 ± 4 % was obtained for plasma-treated samples, while 50 ± 13 % resulted from the application of the same method on native scaffolds. This result suggested a successful enhancement of surface hydrophilicity on plasma-treated PCL-based scaffolds. Mechanical tests were performed on samples belonging to batch 2. Each sample was investigated by measuring its mass to ensure a hydrogel encapsulation yield around 80%. Figure 3 reports the trends of compressive stress-strain curves of the scaffolds loaded with either SM hydrogel or simple PBS for comparative purposes.

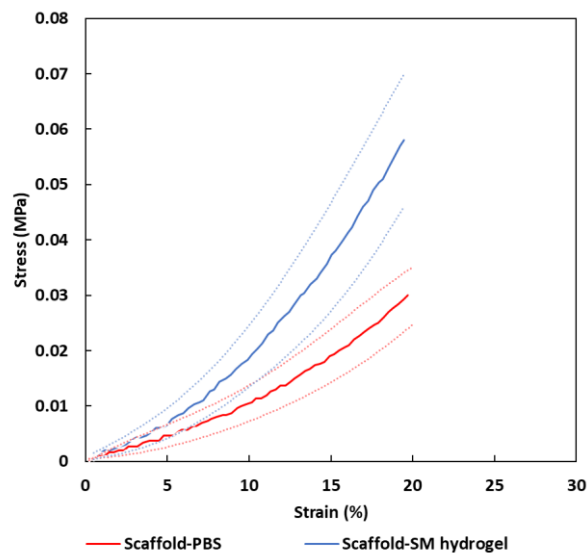


Figure 3 – Mean stress-strain curves of scaffolds encapsulating pure PBS (red continuous line) and SM hydrogels (blue continuous line). Dotted lines delimitate the respective upper and lower curves deduced by the calculated standard deviations.

A good curve repeatability was observed, thus indicating that the utilized method for hydrogel and PBS loading within the produced scaffolds was reliable. Interestingly, this characterization showed that the two different systems behaved similarly within a specific domain of applied compressive strain (i.e., up to 5% strain). Then, higher stress values were recorded for the scaffold systems encapsulating SHP407 2% - CD 10% at equal strains with respect to the control samples. This

marked resistance to applied deformation suggests a probable hardening effect induced by the loaded SM hydrogels within the void volume of PCL-based scaffolds. Thence, the encapsulated SM hydrogel systems most likely induced an improvement in the overall mechanical response of the hybrid scaffolds, as expected. Nonetheless, this study represented only a superficial investigation on the potential role of SM networks in forming more complex hybrid systems with solid and porous scaffolds. Further characterizations are thus needed to validate these preliminary observations in mechanical terms. For instance, it could be useful to investigate the general mechanical response as a function of strain rate. In this regard, it could be envisaged that higher mechanical resistance and fragility could be observed with increasing strain rate.

4.4 Release studies of FD4 from hybrid hydrogel-scaffold systems

The encapsulation of FD4 within the developed hybrid systems was based on the previously obtained results regarding hydrogel loading yield within the void volume of porous scaffolds. In detail, according to the obtained hydrogel loading yield (i.e., around 80%), FD4 was solubilized into CD solutions (14% w/v concentration) in order to obtain a final FD4 content within the hybrid system equal to 0.75 mg. Thence, the gelling solution was formulated containing FD4 at 2.35 mg ml⁻¹. The resulting release profile of FD4 evaluated in physiological-like conditions (i.e., PBS, 37 °C) is reported in figure 4.

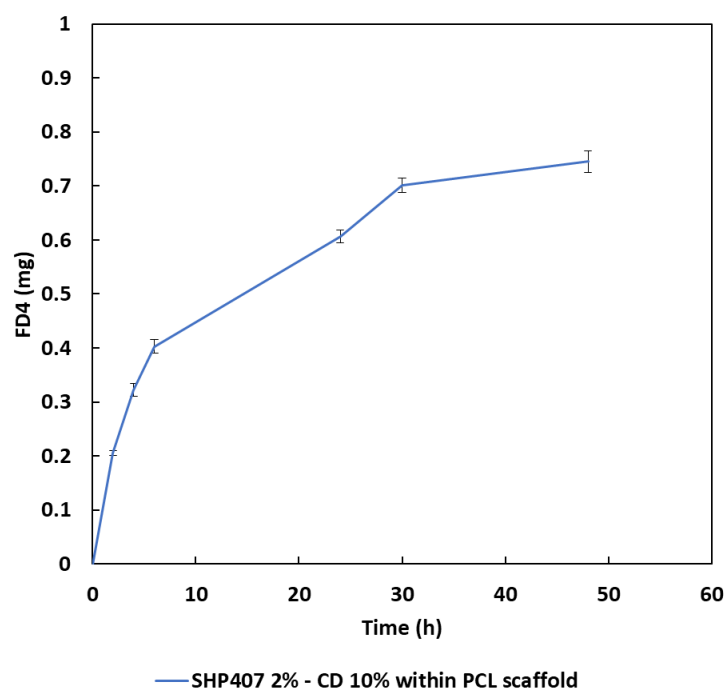


Figure 4 – Release profile of FD4 from hybrid systems composed of PCL-based scaffolds encapsulating FD4-loaded SM hydrogels (SHP407 2% - CD 10%).

A progressive trend of FD4 delivery from the hybrid systems was observed and the process was sustained up to 48 hours incubation, when 100% of theoretical FD4 was delivered. This datum confirmed the reliability of hydrogel loading process within the porous scaffolds. The gradual nature of FD4 release profile can be further clarified by observing the images in figure 5. In fact, the hydrogels were released through their continuous erosion from the external surfaces to the

inner core of the hybrid systems. It is important to highlight that this process could be enhanced by the intrinsic nature of the *in vitro* release tests, which were conducted by placing the samples in direct contact with a watery environment having a comparable volume. However, no burst release behavior was observed even in the case of FD4 which is a highly hydrophilic molecule, thus indicating a good integration of the hydrogel systems within the scaffolds and thus a relevant stability of the resulting hybrid platforms.

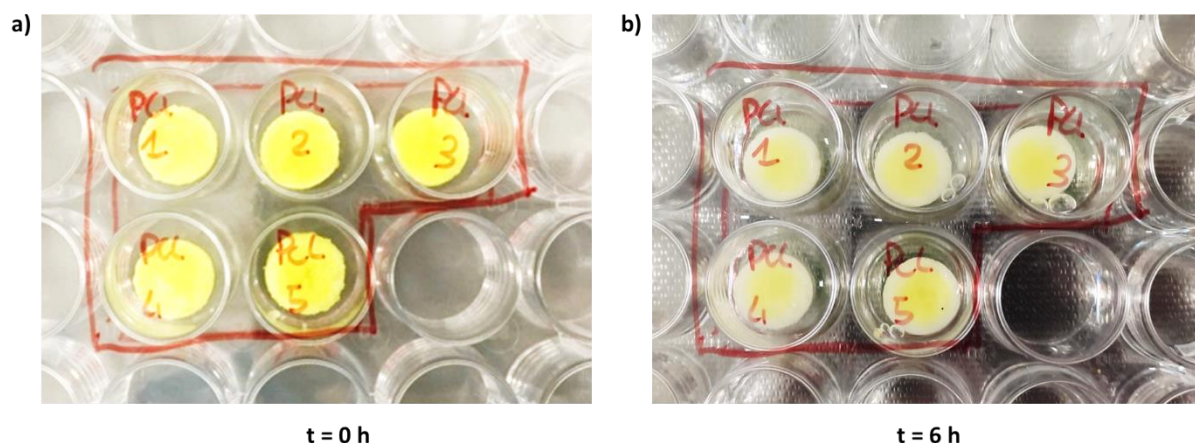


Figure 5 – Hybrid systems based on PCL scaffolds and SM hydrogels (SHP407 2% - CD 10%) encapsulating FD4 at a) 0 and b) 6 hours incubation in contact with PBS at 37 °C. The erosion of loaded hydrogels is clearly indicated by the progressive formation of a white corona from the external surface of the hybrid systems.

5. Conclusions

In this study, a new particular application of SM hydrogels was evaluated, namely their potential integration into 3D porous matrices aiming to the design of hybrid systems for regenerative pharmacology application. In detail, a SM hydrogel based on PEUs was successfully encapsulated into the void volume of PCL-based porous scaffolds produced through salt-leaching technique. In this regard, a reliable method for the production of highly porous scaffolds composed of PCL was implemented and allowed the production of highly homogeneous systems. Moreover, plasma treatment was exploited to increase surface hydrophilicity and potential biocompatibility of the supports for 3D cell culture. Then, with the aim to minimize synthetic polymer concentration within the hydrogel while improving mechanical properties, a hydrogel containing SHP407 at 2% w/v and CDs at 10% w/v concentrations (i.e., SHP407 2% - CD 10%) was formulated and thoroughly characterized. The gelation window of around 3 hours was exploited to load such hydrogel into PCL-based scaffolds and the resulting encapsulation yield indicated a relevant role of plasma treatment in enhancing the hydrogel loading phase. Moreover, improved mechanical properties were preliminary observed on hybrid systems with respect to reference samples encapsulating simple water-based saline solution (i.e., PBS). In this regard, a proof of concept on the idea of improving mechanical properties of polymeric scaffolds through the integration of SM PEU-based hydrogels was provided, although more specific and exhaustive mechanical characterizations are needed in order to better clarify the role of such water-based networks integrated within remarkably stiffer solid structures. Nonetheless, SM hydrogels showed a huge potential towards the development of highly engineered and multi-functional devices for

regenerative medicine based on the synergistic role of drug delivery and tissue engineering strategies. In the future, the presented approach could be extended to other specific applications involving particular therapeutic agents and porous scaffolds based on natural or synthetic polymers. Hence, this short study represented a further proof of the wide versatility of PEU-based SM hydrogels, which owe their good properties to reliable synthesis procedure and effective design.

6. References

- (1) Spicer, C. D. Hydrogel Scaffolds for Tissue Engineering: The Importance of Polymer Choice. *Polym. Chem.* **2020**, *11* (2), 184–219. <https://doi.org/10.1039/C9PY01021A>.
- (2) Nezhad-Mokhtari, P.; Ghorbani, M.; Roshangar, L.; Soleimani Rad, J. A Review on the Construction of Hydrogel Scaffolds by Various Chemically Techniques for Tissue Engineering. *European Polymer Journal* **2019**, *117*, 64–76. <https://doi.org/10.1016/j.eurpolymj.2019.05.004>.
- (3) Mohammed, A.; Elshaer, A.; Sareh, P.; Elsayed, M.; Hassanin, H. Additive Manufacturing Technologies for Drug Delivery Applications. *International Journal of Pharmaceutics* **2020**, *580*, 119245. <https://doi.org/10.1016/j.ijpharm.2020.119245>.
- (4) Hernandez, I.; Kumar, A.; Joddar, B. A Bioactive Hydrogel and 3D Printed Polycaprolactone System for Bone Tissue Engineering. **2017**, 13.
- (5) Gupta, S. Meniscal Tissue Engineering via 3D Printed PLA Monolith with Carbohydrate Based Self-Healing Interpenetrating Network Hydrogel. *International Journal of Biological Macromolecules* **2020**, 14.
- (6) Ilomuanya, M. O.; Okafor, P. S.; Amajuoyi, J. N.; Onyejekwe, J. C.; Okubanjo, O. O.; Adeosun, S. O.; Silva, B. O. Poly(lactic Acid)-Based Electrospun Fiber and Hyaluronic Acid-Valsartan Hydrogel Scaffold for Chronic Wound Healing. *Beni-Suef Univ J Basic Appl Sci* **2020**, *9* (1), 31. <https://doi.org/10.1186/s43088-020-00057-9>.
- (7) Boffito, M.; Torchio, A.; Tonda-Turo, C.; Laurano, R.; Gisbert-Garzarán, M.; Berkmann, J. C.; Cassino, C.; Manzano, M.; Duda, G. N.; Vallet-Regí, M.; Schmidt-Bleek, K.; Ciardelli, G. Hybrid Injectable Sol-Gel Systems Based on Thermo-Sensitive Polyurethane Hydrogels Carrying PH-Sensitive Mesoporous Silica Nanoparticles for the Controlled and Triggered Release of Therapeutic Agents. *Front. Bioeng. Biotechnol.* **2020**, *8*, 384. <https://doi.org/10.3389/fbioe.2020.00384>.
- (8) Lee, H.-U.; Jeong, Y.-S.; Jeong, S.-Y.; Park, S.-Y.; Bae, J.-S.; Kim, H.-G.; Cho, C.-R. Role of Reactive Gas in Atmospheric Plasma for Cell Attachment and Proliferation on Biocompatible Poly ϵ -Caprolactone Film. *Applied Surface Science* **2008**, *254* (18), 5700–5705. <https://doi.org/10.1016/j.apsusc.2008.03.049>.
- (9) Morent, R.; De Geyter, N.; Desmet, T.; Dubruel, P.; Leys, C. Plasma Surface Modification of Biodegradable Polymers: A Review: Plasma Surface Modification of Biodegradable Polymers: A Review. *Plasma Processes Polym.* **2011**, *8* (3), 171–190. <https://doi.org/10.1002/ppap.201000153>.
- (10) Reignier, J.; Huneault, M. A. Preparation of Interconnected Poly(ϵ -Caprolactone) Porous Scaffolds by a Combination of Polymer and Salt Particulate Leaching. *Polymer* **2006**, *47* (13), 4703–4717. <https://doi.org/10.1016/j.polymer.2006.04.029>.
- (11) Guarino, V.; Causa, F.; Ambrosio, L. Porosity and Mechanical Properties Relationship in PCL Porous Scaffolds. *Journal of Applied Biomaterials & Biomechanics* **2007**, *5* (3), 149–157.

Section 3

Highly functional supramolecular and photo-curable hydrogels based on poly(ether urethane)s

Outline

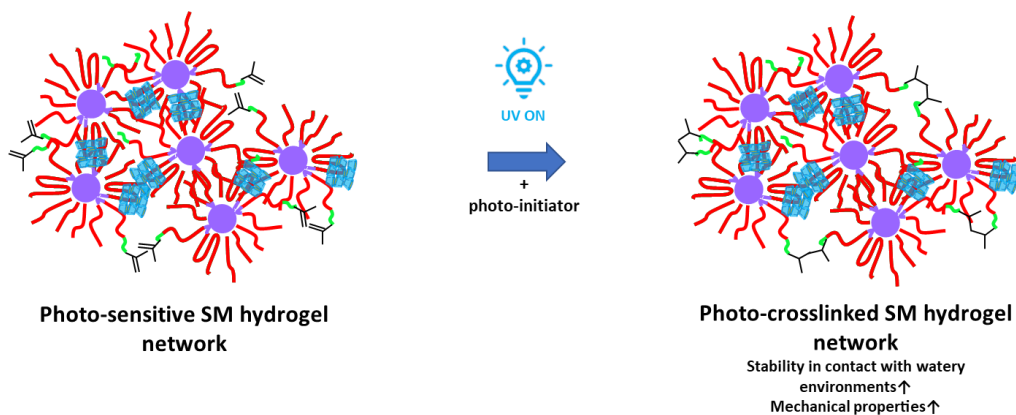
This section deals with the investigation of a novel approach exploiting the dual contribution of supramolecular features in synergy with chemical crosslinking with the ultimate aim to design hydrogel networks showing even more stability and tunability compared to purely SM systems. In detail, the adaptability of the synthesis process to produce poly(ether urethane)s was utilized to design a polymer functionalized with photo-sensitive end-groups (*Chapter 3.1*). A complete physico-chemical characterization was carried out on such newly synthesized macromolecule, in order to assess its potential photo-sensitivity and suitability to form supramolecular hydrogels. The chemical features of the involved poly(ether urethane) resulted to be proper for the formation of a wide plethora of supramolecular hydrogels. A mannerly selection of the best formulations and the exploitation of α -cyclodextrins led to the possibility to integrate high dosages of curcumin within the developed supramolecular networks. Rheological and photo-rheological characterizations were conducted to evaluate the stability and responsiveness of the investigated hydrogels. Tunable release kinetics of such drug was achieved by means of photo-induced crosslinking. Moreover, a proof of concept of hydrogel printability was achieved through an extrusion-based 3D printer to evaluate the potential of such systems for additive manufacturing techniques and thence for the production of precise morphologies. A further step forward the potential development of single-stage strategies combining drug delivery and tissue engineering was conducted in *Chapter 3.2* as well. In detail, the designed photo-sensitive poly(ether urethane) was utilized to integrate gelatin methacryloyl, which is a notably bioactive natural polymer bearing photo-curable domains, within its deriving supramolecular network. A library of various formulations was investigated and the best ones were selected for the evaluation of mechanical properties and release studies of curcumin, thus further widening the potential of the developed multi-functional formulations in the regenerative medicine scenario.

Section 3 – Chapter 3.1 – Chemical hydrogels based on supramolecular architectures

1. Abstract

Physical and chemical hydrogels represent two wide domains of potential strategies for regenerative medicine applications. Generally, their natures can be considered opposite. Indeed, physical hydrogels are particularly suitable for the design of drug delivery systems due to their enhanced reversibility and responsiveness. Differently, chemical hydrogels represent the best strategy to produce stable supports for 3D cell cultures in the tissue engineering/regenerative medicine (TERM) field. In this part of the work, these two strategies have been combined with the aim to develop multi-functional formulations integrating into one device both drug delivery potential with TERM approaches. Specifically, a novel PEU was synthesized in order to form SM networks with CDs suitable for further photo-induced crosslinking, thus connecting the pros of both physical and chemical hydrogel systems and hence improving the overall network properties. The usual PEU synthesis process was slightly modified to perform an end-capping reaction on pre-polymers for the grafting of methacrylate terminal groups. To this aim, 2-hydroxyethyl methacrylate (HEMA) was utilized to functionalize pre-polymers based on P407 and HDI, thus obtaining HHP407 PEU. A complete physico-chemical characterization was performed through ATR-FTIR spectroscopy, SEC and $^1\text{H-NMR}$ spectroscopy to assess successful PEU synthesis. A lower molecular mass (\bar{M}_n 22000 Da) was calculated with respect to previous PEUs and a good yield of PEU functionalization through HEMA addition was achieved (i.e., up to 75%). Thermo-responsiveness was characterized through CMT evaluation which suggested an optimized compromise between molecular mass and overall hydrophobicity (i.e., lipophilic block length and distribution). In fact, CMT values comparable to chain-extended PEUs (i.e., 19.4 °C) were measured. XRD and $^1\text{H-NMR}$ spectroscopy demonstrated the satisfactory performance of HHP407 PEU in terms of self-assembly with CDs due to such particularly suitable polymeric features. These properties were translated into the possibility to produce a plethora of SM hydrogels with remarkably fast gelation kinetics (i.e., few minutes). Hence, novel hydrogel systems were developed at low PEU concentration ($\leq 5\%$ w/v) and with a 20% lower content of CDs (i.e., 8% w/v) with respect to the previously designed systems. Good mechanical properties and self-healing ability were characterized through rheological tests, while photo-sensitivity was evaluated through photo-rheological characterization. Fast photo-crosslinking was observed (i.e., within 30 seconds) for the resulting networks. A high payload of Cur ($570 \mu\text{g ml}^{-1}$) was encapsulated within HHP407-based SM hydrogels and release kinetics was studied in physiological-simulated environment. In this regard, high tunability was allowed by hydrogel composition and photo-crosslinking, thus obtaining progressive Cur release up to 5 weeks. Finally, a preliminary evaluation of the printability of HHP407-based hydrogels was performed through an extrusion-based bioprinter obtaining 3D-printed structures showing good resolution and morphological fidelity with respect to original design.

Graphical Abstract



Hybrid SM networks based on both physical and chemical crosslinking for prolonged drug release studies

2. Introduction

Physical hydrogels are extremely interesting systems due to their marked reversibility and processability. Indeed, the main advantage of physically crosslinked networks is represented by the possibility to easily perform injection and to adapt to the external morphologies. High tunability is also another advantage of these systems. Nonetheless, some limitations can be individuated. Most importantly, the development of highly stable and durable hydrogel networks based on physical interactions is challenging. Indeed, a relevant number of weak crosslinks is necessary to properly stabilize a polymeric network in watery environments. However, the indispensable hydrophilicity that is required and characterizes these systems induces relevant absorption of fluids from the external environments. Such natural process of swelling can lead to a relevant mass exchange with the adjacent milieu and complete dissolution may occur within few days, as observed in the previous Section of this work. Although this behavior is ideal for most drug delivery applications, since a relevant number of therapeutic drugs is characterized by high hydrophobicity and low bioavailability and hence needs specific carriers to be delivered, it could even represent a strong limitation for the integration of biological elements (e.g., cells). This issue is well-known and has been widely discussed by various authors.¹ A possible solution to overcome this relative drawback can be found in the development of chemically crosslinked networks, as discussed in the first Section of this work. However, low responsiveness and limited handling are generally correlated to this strategy.² Moreover, chemical additives are often necessary to carry out the crosslinking process and hence toxic effects may be induced.³ A relatively wider approach consists in the integration of both the typologies of hydrogel network crosslinking aiming at combining the advantages of both strategies while reducing related deficiencies. In this regard, a proper selection of the chemical composition and the resulting physical properties are elemental factors to successfully develop hybrid strategies based on both chemical and physical crosslinking. Indeed, the tuning of physical interactions originated by the constituent polymeric units in combination with additional chemical crosslinking can result in highly stiff and stable hydrogels, as reported, for example, in the work of Li *et al.*, in which a hydrogel system characterized by an elastic modulus around 5 MPa and a strength equal to 2.5 MPa was described.⁴ In detail, the

authors discussed the importance of a well-organized hydrogel network and the nature of the occurring interactions to provide hydrogel networks with remarkable mechanical response. In this work, they developed a hydrogel network stabilized through crystalline (physical) and covalent (chemical) domains using poly(vinyl alcohol) (PVA) to form crystallites and polyacrylamide (PAA) to generate chemical bonds. As a result, they obtained a hydrogel system able to show mechanical properties very similar to the ones of natural tissues, such as cartilage and skin. In this case, chemical crosslinking was pursued through overnight *in situ* polymerization of acrylamide in the presence of N,N'-methylenebisacrylamide (MBAA) and tetramethyl-ethylenediamine (TEMED), at room temperature. Such approach can be considered as a “macromolecular” strategy, in which the organization of the resulting network is based on standard intermolecular interactions. Nonetheless, a more sophisticated approach can be pursued, that is supramolecular self-assembly. In this case, the initial processability of physical hydrogels is preserved due to the notable adaptivity of SM networks and a subsequent *in situ* stabilization can be performed through chemical crosslinking. Indeed, it is possible to develop highly organized SM networks suitable for a further and fast chemical stabilization that induces mechanical strengthening and improves resistance to solubilization. In this regard, the chemical composition of all the components of the deriving hydrogel systems is even more important in terms of tuning and engineering. An interesting example describing this approach can be found in the work conducted by Zhao and co-authors.⁵ In this case, a modified di-acryloyl block co-polymer was synthesized utilizing Pluronic F68 (i.e., Poloxamer 188, P188) and PCL with the aim to exploit its photo-sensitivity to ensure fast polymerization after complete self-assembly into PPRs with α -CDs. The resulting hydrogel systems were characterized by notably high mechanical properties (i.e., G' greater than 100 kPa) and good responsiveness in aqueous environments. Another similar work was conducted by these authors utilizing the same macromer in the presence of β -CDs, thus further proving the versatility of properly synthesized amphiphilic polymers.⁶ Differently, Wei and co-workers developed an interesting system composed of star-shaped photo-curable macromers and α -CDs.⁷ In detail, they synthesized a methacryol-terminated PLA-*b*-PEG copolymer consisting in three or four arms and formulated SM hydrogels by adding α -CDs in aqueous solutions. The authors observed that the addition of photocurable domains induced an improvement in terms of mechanical strength and stability in aqueous environment of the deriving SM networks. Moreover, these systems showed a highly tunable responsiveness in watery environments and demonstrated the potentiality to reach values of swelling ratio up to 500% within 7 days incubation in contact with watery environments. The same research group developed other similar systems based on the same strategy.^{8,9} Although, over the last decade, only few research works have focused on the specific design of photo-crosslinkable PPR-based networks, the general importance of developing shear-thinning and self-healing hydrogels retaining the possibility of secondary crosslinking has gained a continuously increasing interest. Indeed, the combined possibility to easily process a hydrogel matrix that is intrinsically self-sustaining and then further stabilize it through fast photo-crosslinking also represents an extremely important feature for the development of bioinks for extrusion-based 3D printing. The most recent and relevant strategies underpinning this idea have been reviewed by Chimene and co-workers.¹⁰ Moreover, the authors discussed on the importance of mechanical features in order to develop highly effective and functional hydrogel bioinks. In this regard, supramolecular-based matrices represent one of the most promising strategies to ensure self-

healing and shear thinning responses, which are elemental features for injection or printing of even cell-laden hydrogels.

Within this scenario and on the basis of the promising results reported in the previous Section of this Ph.D. thesis, in this Chapter novel SM and photo-curable systems based on a properly synthesized PEU were developed. In detail, the previous results indicated P407-based PEUs as the best ones in terms of suitability for the formation of PPR-based networks with α -CDs due to their balanced match among molecular mass, hydrophobicity and overall macromolecular functionality (i.e., thermo-responsiveness) induced by chemical domains and structures. For these reasons, a new photo-sensitive PEU based on P407 and HDI was synthesized by end-capping the pre-polymer chains resulting at the end of the first step of reaction through the addition of 2-hydroxyethyl methacrylate (HEMA) instead of a chain extender. In this manner, a further improvement of the gelling ability of the resulting formulations was expected due to a significant reduction of molar mass and a concomitant preservation of the hydrophobic character derived from the partial polymerization reaction. A complete physico-chemical characterization was performed on the resulting PEU through SEC, ATR-FTIR and $^1\text{H-NMR}$ spectroscopies. Evaluations on the resulting thermo-responsiveness were conducted through CMT characterization in watery environments. A new plethora of photo-curable SM hydrogels was designed by mixing PEU and α -CDs solutions and the most promising formulations were selected for rheological and photo-rheological characterizations. The encapsulation of an extremely high payload of curcumin (i.e., $570 \mu\text{g ml}^{-1}$) was performed within these novel PEU-based hydrogels and release profiles were obtained from physical and photo-cured hydrogels through incubation in contact with physiological-like environments in highly destabilizing conditions. Finally, the suitability of the developed formulations for rapid prototyping was evaluated through extrusion-based 3D-printing. Thence, the work reported in this chapter was finalized to further prove the versatility of PEU synthesis process as an effective tool for the production of highly functional and tunable hydrogel systems. Moreover, in this study the developed plethora of PEU-based SM hydrogels was further widened towards potential application in regenerative medicine.

3. Materials and Methods

3.1 Materials

P407, HDI, HEMA, DBTDL and TSP were obtained from Merck/Sigma-Aldrich (Milan, Italy). α -CDs (from now on simply indicated with the acronym “CDs”) and lithium phenyl-2,4,6-trimethylbenzoylphosphinate (LAP, a photo-initiator) were obtained from TCI Chemicals Europe (Zwijndrecht, Belgium). All solvents were obtained from Carlo Erba Reagents (Milan, Italy). P407, HEMA and DCE were dried as indicated in *Section 2 – Chapter 2.2 – Materials and Methods – Materials* before use for PEU synthesis.

3.2 Synthesis of photo-sensitive PEU – HHP407

An innovative photo-sensitive PEU was synthesized according to the same protocol reported in the previous Chapters with slight modifications. In detail, the first step of the reaction aiming at

the production of the prepolymer was conducted in the same manner. Differently, the second step of the reaction was characterized by the end-capping of the isocyanate-terminated prepolymer chains through the addition of HEMA, which indeed has only one reactive -OH group. In detail, HEMA was solubilized in DCE at 3% w/v and added to the reaction mixture at 2:1 molar ratio with respect to P407 (i.e., 1:1 molar ratio with respect to HDI). The reaction was conducted for 3 hours at room temperature under stirring and protected from any source of light to avoid the occurrence of any side reaction. Then, the reaction was stopped through the addition of methanol (6 ml every 16 g of theoretical PEU) to passivate any exposed and unreacted isocyanate group. The solution containing the end-capped PEU was precipitated in petroleum ether (4:1 v/v ratio with respect to total DCE volume) at room temperature under vigorous agitation and in the dark. The supernatant was separated from the precipitated PEU, which was kept under a fume hood overnight to allow drying. Subsequently, the dried PEU was solubilized again in DCE at 20% w/v concentration and purified through precipitation in a mixture of diethyl ether and methanol (98:2 v/v, 5:1 with respect to DCE volume) in the dark. The purified PEU was obtained through centrifugation at 0 °C for 20 minutes at 6000 rpm and dried under a fume hood overnight. The resulting dry polymer was collected and stored under vacuum at 3 °C in the dark to avoid any reaction due to its interaction with light sources. The obtained PEU was identified with the acronym HHP407, where P407 indicates the macrodiol, while the first H refers to the chain extender (HEMA) and the second one to the diisocyanate (HDI).

3.3 Chemical characterization of HHP407

SEC, ATR-FTIR and ¹H-NMR spectroscopies were conducted as reported in *Section 2 – Chapter 2.2 – Materials and Methods – Chemical characterization of PEUs*.

3.4 CMT evaluation

The characterization of CMT of HHP407-based solutions at 1% w/v concentration in PBS and ddH₂O was conducted as reported *Section 2 – Chapter 2.4 – Materials and Methods – Critical micellar temperature (CMT) evaluation*.

3.5 Preparation and characterization of HHP407- and CD-based SM complexes

SM complexes composed of HHP407 and CDs were prepared and characterized through XRD, ATR-FTIR and ¹H-NMR spectroscopies as indicated in *Section 2 – Chapter 2.2 – Materials and Methods – Preparation and characterization of PEU- and CD-based complexes*. HHP407-based SM crystals were formulated in ddH₂O at PEU concentration of 1% w/v and the CD content required to cover the theoretical 100% of PEO domains (i.e., 7.6% w/v).

3.6 Preparation and characterization of HHP407- and CD-based SM hydrogels

3.6.1 Preparation of SM hydrogels

SM hydrogels were prepared in Bijou sample containers (17 mm inner diameter, 7 ml volume capacity, Carlo Erba Reagents, Milan, Italy) utilizing PBS (pH 7.4, Sigma Aldrich, Milan, Italy) added with LAP at 0.05% w/v as solvent (PBS/LAP). HHP407 was firstly solubilized in the required amount in PBS/LAP overnight at 3 °C. Then, a clear solution of CDs in PBS/LAP was prepared at 14% w/v and added to HHP407 solutions, thus obtaining gelling systems containing HHP407 between 1 and 5% w/v and CDs between 7 and 10% w/v concentrations. Homogenization of the obtained mixtures was performed using a vortex (40 Hz, 30 seconds), while gelation was conducted at room temperature (25 °C). HHP407-based samples were protected from any source of light during their preparation and characterization.

3.6.2 Qualitative evaluation of gelation time and phase-separation in isothermal conditions

Gelation time and phase-separation were evaluated at room temperature (25 °C) as indicated in *Section 2 – Chapter 2.2 – Preparation and characterization of PEU- and CD-based SM hydrogels - Qualitative evaluation of gelation time and phase-separation in isothermal conditions.*

3.6.3 Curcumin encapsulation with SM gels, characterization and release studies

The previously obtained results on curcumin (Cur) encapsulation and release evidenced a good stability of this drug within SM hydrogel samples and during the release studies in a potentially degradative environment (i.e., PBS). This result was ascribed to the protective role of CDs and PEUs, which are known to retain the ability to encapsulate and delivery Cur in watery environments. Based on these results, in this study, a further improvement in terms of Cur payload encapsulation within SM hydrogels was experimented. To this aim, a CD solution at 14% w/v in PBS/LAP was utilized to produce a suspension of Cur at 1 mg ml⁻¹. Cur stabilization was carried out through ultrasound sonication (52 W, 20 kHz, Vibracell VCX130, Sonics, USA) that was applied for 3 minutes using a probe and a water-ice bath to avoid significant evaporation phenomena. The stability of the obtained suspension was evaluated through visual inspection at room temperature (25 °C) in order to assess a temporal window for practical use. This suspension was then added to HHP407-based solution in PBS/LAP thus composing SM hydrogels at specific HHP407, CD and Cur contents. Overnight incubation was carried out to ensure complete sample gelation.

An entire set of rheological characterizations was conducted on SM-based hydrogels as such and loaded with Cur as indicated in *Section 2 – Chapter 2.2 – Preparation and characterization of PEU- and CD-based SM hydrogels – Rheological characterization.* Moreover, due to the photo-responsive nature of HHP407, a photo-rheological characterization was also performed on the same samples. In detail, G' of SM hydrogels was evaluated as a function of time in oscillation (1 Hz, 0.1% strain, 0 N normal force) for 1 minute before UV irradiation. Then, UV light exposure was applied for 1 minute at 365 nm and 10 mW cm⁻² and G' was registered for other 2 minutes in order to assess the overall stability of the photo-crosslinked networks.

SM hydrogels (0.5 ml) for release studies of Cur were prepared in glass vial (10 mm inner diameter, 4 ml volume capacity, Sigma Aldrich, Milan, Italy) and indicated with sample code HHP407 X% - CD Y% Cur, where X indicates PEU concentration (% w/v), while Y% refers to CD concentration (% w/v). For all selected formulations, two sets of 5 samples each were prepared in order to evaluate the behavior of purely physical hydrogel networks and the additional contribution of photo-crosslinking. UV light exposure (up to 1 minute at 365 nm and 10 mW cm⁻²) was performed on both sides of the hydrogels in order to guarantee a homogeneous crosslinking, thus obtaining samples coded as HHP407 X% - CD Y% Cur UV. Release studies were conducted on SM hydrogels at 37 °C after acclimatization for 15 minutes. Then, 1 ml of PBS (37 °C) was gently added on top of each hydrogel sample. At precise time steps (2, 4, 6, 24 hours and 3, 4, 7, 14, 21, 28 and 35 days) elutes were withdrawn and completely refreshed with PBS. Cur quantification was performed through a UV/Vis spectrometer (Perkin Elmer Lambda 25 UV/VIS spectrometer, Waltham, MA, USA) by evaluating the absorbance peak around 430 nm. Reference curves were obtained by specific standard solutions produced through hydrogel dissolution and subsequent dilution (Cur concentration ranging between 1 and 20 µg ml⁻¹).

3.6.4 Extrusion-based 3D printing of SM hydrogels

A preliminary evaluation of the printability of HHP407-based hydrogels was performed utilizing a Cellink Inkredible+ bioprinter (Cellink, USA). The printed CAD design was characterized by a squared grid (15x15 mm) based on two layers (0.45 mm filament diameter and 0.35 mm filament gap). The top view of the resulting geometry is reported in figure 1.

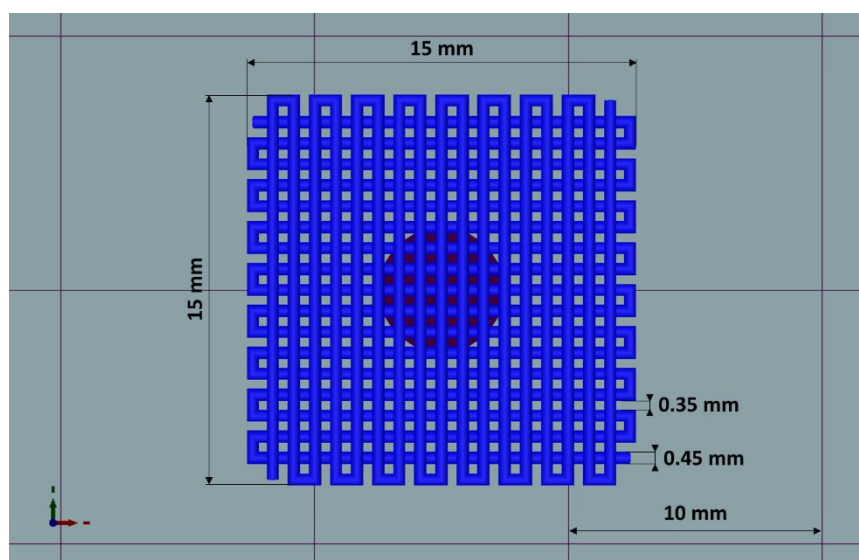


Figure 1 – Top view of the CAD model used to evaluate HHP407-based hydrogel 3D-printability.

Hydrogel preparation was conducted as reported in the specific section above with slight modifications. In detail, solutions composed of HHP407 and CDs were transferred immediately after mixing (i.e., during gelation) into syringes appositely supplied for the 3D-printer. After overnight incubation at room temperature (i.e., 25 °C), the resulting hydrogel networks were kept at 37 °C and their extrudability was tested with three different syringe tips (200, 250 and 450 µm diameter). Constructs were printed into Petri supports (polystyrene, 5 cm diameter, Carlo Erba Reagents, Milan, Italy) and were evaluated through optical microscopy (Leica DM IL LED, Leica

Microsystems, Milan, Italy), while geometrical parameters were characterized through ImageJ software (<https://imagej.nih.gov/ij/index.html>). Photo-induced crosslinking was performed after the printing procedure utilizing a UV light source at 365 nm (10 mW cm⁻²). Qualitative evaluation of the stability of 3D-printed structures was carried out through incubation in contact with PBS (pH 7.4, 5 ml) at room temperature (i.e., 25 °C).

3.7 Statistical Analysis

Statistical analysis was conducted as indicated in *Section 2 – Chapter 2.2 – Materials and Methods – Statistical Analysis*.

4. Results

4.1 Physico-chemical characterization of HHP407

ATR-FTIR spectroscopy was conducted with the aim to assess the successful synthesis of HHP407 PEU. The spectra of HHP407 and P407 are reported in figure 2. As for previous PEUs, the typical vibration bands of urethane domains were detected. In detail, the peak around 1720 cm⁻¹ was ascribed to the stretching of C=O domains, while the peak at 1530 cm⁻¹ was attributed to the simultaneous bending and stretching of N-H and C-N chemical regions, respectively. Moreover, the typical broad vibration band around 3350 cm⁻¹ was referred to N-H stretching. The complete absence of signal at 2200 cm⁻¹ suggested a complete conversion of the isocyanate groups of HDI into urethane moieties. In addition, the characterizing vibration bands of P407 were detected at 1250 cm⁻¹ (CH₂ stretching), 2880 cm⁻¹ (CH₂ rocking) and 1100 cm⁻¹ (C-O-C stretching). Nonetheless, no peaks characterizing the end-capping molecule (i.e., HEMA) were detectable, probably because they overlapped with peaks related to the macrodiol and in-chain urethane domains.

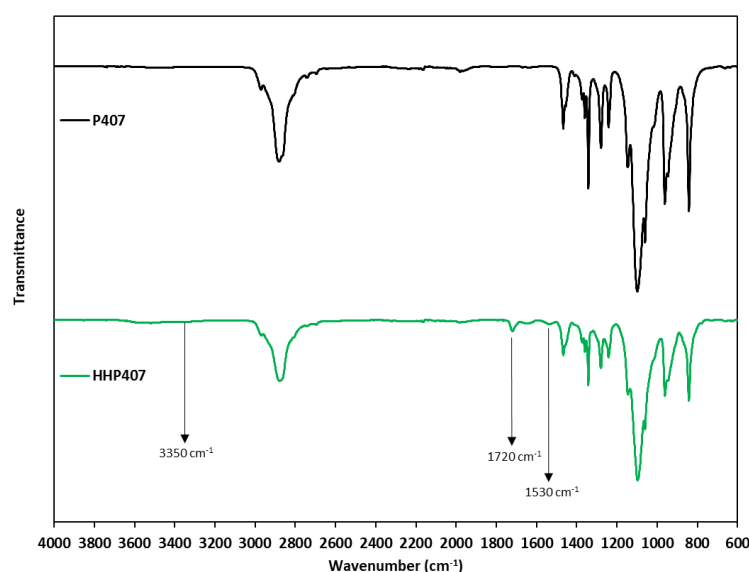


Figure 2 – ATR-FTIR spectra of P407 (black continuous line) and HHP407 (green continuous line). The typical peaks of urethane domains are indicated by vertical black arrows at 3350, 1720 and 1530 cm⁻¹.

SEC results evidenced a significantly higher molecular mass for HHP407 with respect to P407. Figure 3 reports the two different molecular mass distributions. Interestingly, the end-capping procedure resulted in a significantly lower molecular mass for HHP407 (i.e., \bar{M}_n equal to 22000 Da, $D = 1.7$) with respect to chain-extended PEUs (i.e., \bar{M}_n equal to 30000 Da, $D = 1.8$). Nonetheless, these observations indicated that a probable and partial chain extension was also occurring during the first step of the reaction leading to HHP407 synthesis. In this regard, specific modifications should be applied on the synthesis protocol in order to optimize the formation of smaller pre-polymers, which could enhance chain extension or end-capping procedures, as recently observed and discussed by Laurano *et al.* for similar PEUs.¹¹ However, no modifications were made and HHP407 was produced with the same protocol of the previously studied PEUs with the aim to isolate the effects of the end-capping reaction of prepolymer chains on the resulting PEU structure and evaluate their contribution on the final behavior in terms of SM self-assembly with CDs. Indeed, as for chain-extended PEUs, also in the case of HHP407 a residual peak resulting from polymers derived by typical P407 di-blocks was found.¹² This indicated the presence partially polymerized chains that were not totally removed through purification processes. However, the effect of such components on final hydrogel behavior can be considered negligible, because of their limited contribution within the entire molecular mass distribution.

¹H-NMR characterization of HHP407 in D₂O was performed in order to detect the presence of HEMA domains, thus proving the effectiveness of the end-capping procedure. As reported in figure 4, the typical peaks of HEMA were detected at 6.15, 5.85 and 1.95 ppm. Moreover, on the basis of SEC results, the end-capping procedure allowed the production of polymeric chains containing approximately 1.25-1.5 HEMA units per chain (i.e., up to 75% end-capping yield), when the maximum theoretical value is 2 (i.e., 100% end-capping yield). This result indicated a reliable end-capping reaction during the second step of PEU synthesis, although relatively high molecular mass (i.e., $\bar{M}_n = 22000$ Da) and dispersity index were obtained (i.e., 1.7) for HHP407. The entire overview resulting from these characterizations demonstrated an effective synthesis procedure to obtain potentially photo-sensitive PEUs.

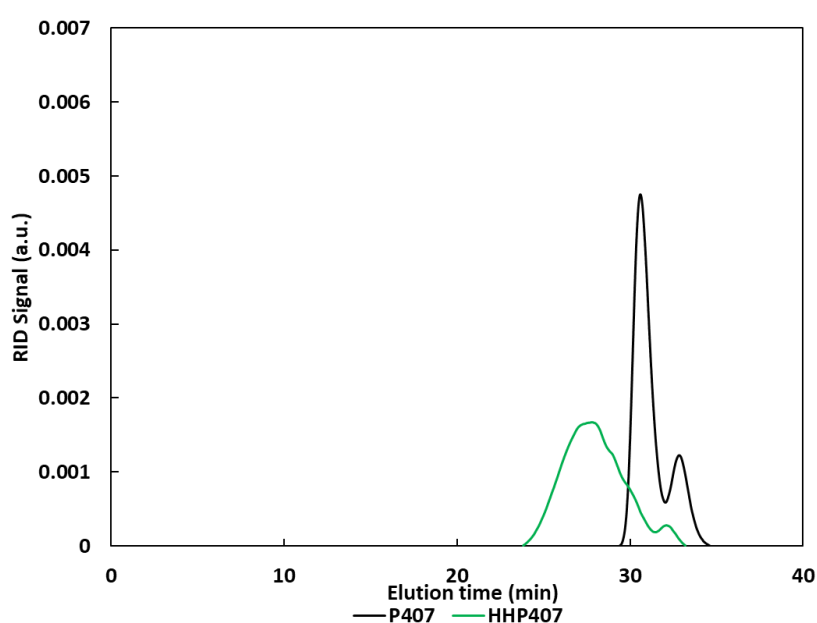


Figure 3 – SEC profiles of P407 (black continuous line) and HHP407 (green continuous line).

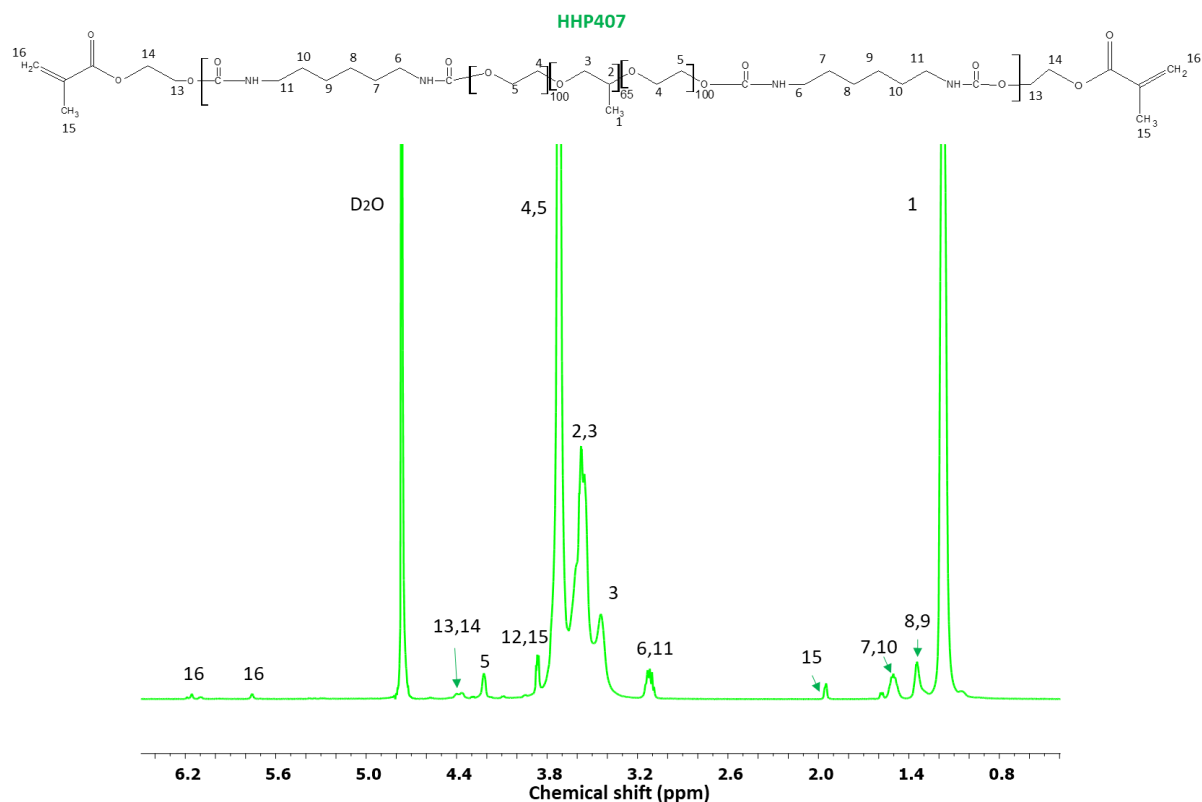


Figure 4 – $^1\text{H-NMR}$ spectrum of HHP407. All PEU-related proton peaks are indicated by specific numbers and arrows. The presence of typical HEMA domains is indicated by protons 13 and 14 (around 4.2-4.4 ppm), 15 (1.95 ppm) and 16 (5.85 and 6.1 ppm).

The thermo-sensitive behavior of HHP407-based solutions (1% w/v concentration) was evaluated in PBS and ddH₂O. Figure 5 reports CMT curves of HHP407 solutions at 1% w/v concentration. Interestingly, HHP407 solubilized in pure water showed a CMT value of 22.2 °C, while the same formulation prepared in PBS was characterized by a CMT equal to 19.6 °C. This relevant difference can be ascribed to a probable salting-out effect generated by the presence of dissolved ions of PBS in a similar way as for the previously studied P407-based PEUs. Nonetheless, an important and additional remark should be discussed. In fact, HHP407 was characterized by comparable CMT values to those of chain extended P407-based PEUs at equal concentration (i.e., 1% w/v), although its molecular mass was significantly lower (i.e., around 30%). The correlation between these results suggested an enhancement in the thermo-induced self-assembly of HHP407 chains into micelles probably originated by a better balance between the overall hydrophobicity and length of polymer chains. It is also plausible that the presence of end-methacrylate groups could induce a significant contribution in this regard.

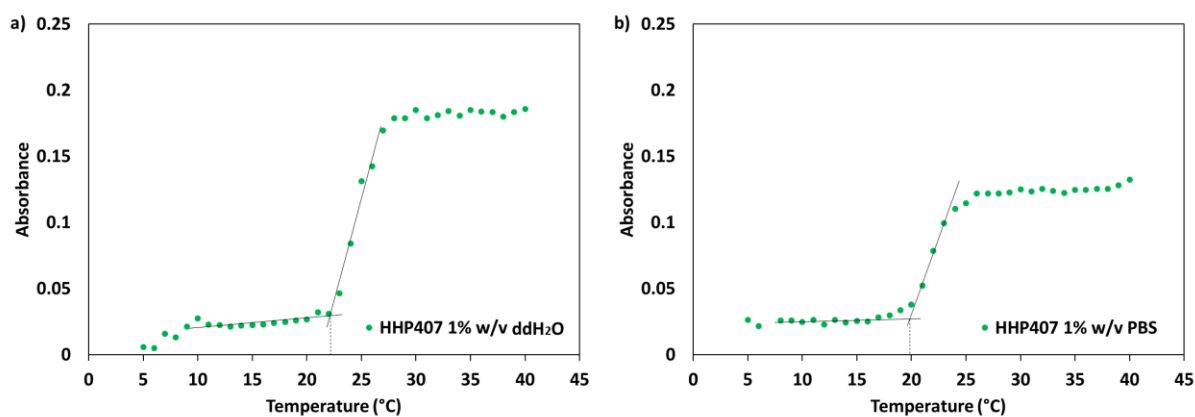


Figure 5 – CMT curves for HHP407 at 1% w/v concentration in a) ddH₂O and b) PBS representing the measured absorbance at 356 nm as a function of temperature. CMT values are indicated by black vertical dotted lines.

4.2 Characterization of HHP407-CD SM complexes

The mixture containing HHP407 at 1% w/v and CDs at 7.6% w/v (i.e., 100% theoretical PEO domain coverage, HHP407 1% - SM 100%) in ddH₂O resulted in a 100% crystallization yield, thus indicating the formation of a proper SM hydrogel network. This datum indicated that HHP407 was the best PEU in terms of interaction with CDs in watery environments when compared to the previously characterized PEUs. Indeed, as expected from the previous data obtained from SEC and CMT evaluation, HHP407 was probably characterized by the best match between molecular mass and resulting hydrophobicity that could enhance its self-assembling ability in forming micelles and thence PPR-based networks in solution. XRD patterns demonstrated the formation of PPR-based channel-like crystalline structures, as reported in figure 6. Indeed, three main peaks at 2θ equal to 7.4° , 12.8° and 19.6° were detected and clearly represented the formation of SM crystals within HHP407-based networks, as notably indicated in the literature.¹³ The pattern of native HHP407 powders was characterized by the presence of the same peaks that were found in previous PEUs (i.e., 2θ equal to 19° and 23.3°), which were comparable to the ones derived from P407 and PEO samples, thus further confirming the hypothesis that the molecular mass and hydrophobic domains were not particularly affecting the crystallization process of chain-extended PEO-based amphiphilic tri-blocks in morphological terms.

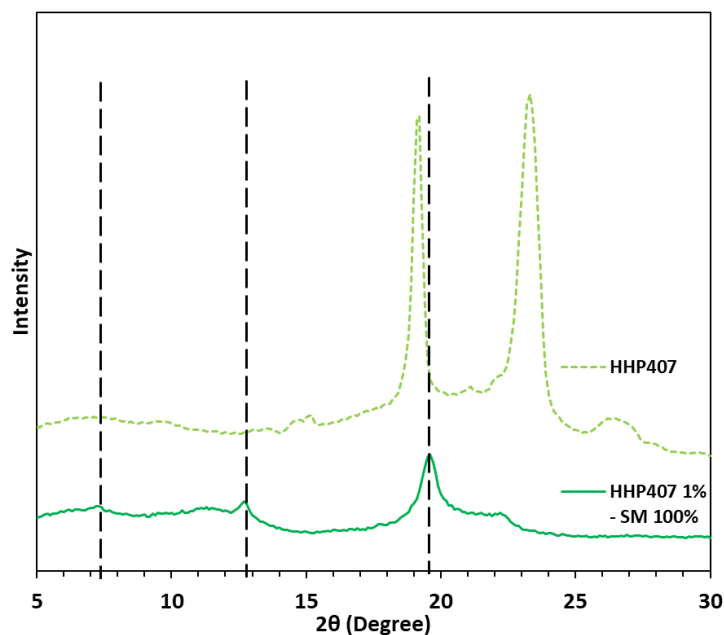


Figure 6 – XRD patterns of HHP407 (light green dashed line) and HHP407 1% - SM 100% (green continuous line). Typical peaks of channel-like PPR-based crystals are indicated by black vertical dashed lines at 2θ equal to 7.4° , 12.8° and 19.6° . The pattern of pure HHP407 is reported for comparative purposes.

ATR-FTIR characterization on the produced SM crystalline powder demonstrated the co-presence of HHP407 and CDs, as reported in figure 7. However, slightly lower up-shifts of the characterizing peaks of PEU (1720 cm^{-1}) and CDs (3308 cm^{-1}) were observed in HHP407 1% - SM 100% with respect to the previously analyzed SM samples. In fact, the asymmetrical and symmetrical vibration peak of -OH domains belonging to CDs were upshifted at 3324 cm^{-1} and the C=O stretching signal appeared around 1725 cm^{-1} , while the same peaks were found at 3340 cm^{-1} and 1740 cm^{-1} for the previous PEUs (i.e., CHP407 and NHP407, which were the best PEUs in terms of SM self-assembly with CDs in the previous studies), respectively. This difference can be ascribed to the formation of a stiff hydrogel network that did not allow the complete removal of potentially free CDs and PEU chains in solution through centrifugation, thus causing an overlap of the involved excitations. Nonetheless, the detection of urethane domains through ATR-FTIR was relatively hindered, due to the substantially higher CD content. Thence, $^1\text{H-NMR}$ characterization on the resolubilized crystalline powder more clearly confirmed the co-presence of HHP407 and CDs, as reported in figure 8. In fact, the presence of characteristic peaks of CDs was found within the chemical shift range from 4.05 to 3.55 ppm and at 5.08 ppm, while PEU resonance domains were detected within the chemical shift region between 1.60 and 0.95 and at 3.75 ppm.

Finally, the entire set of physico-chemical characterizations marked HHP407 as the best PEU for the formation of SM crystalline domains with CDs, thus bringing different benefits for SM hydrogel design.

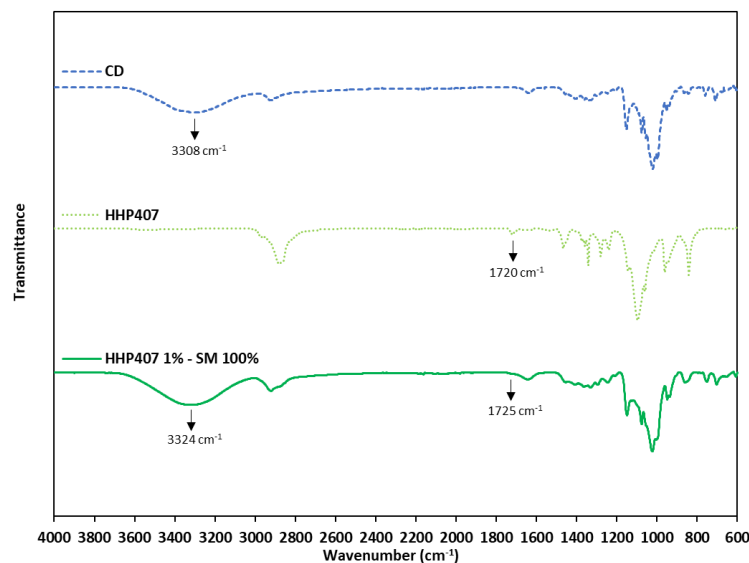


Figure 7 – ATR-FTIR spectra of CD (blue dashed line), HHP407 (light green dotted line) and HHP407 1% - SM 100% (green continuous line). Typical peaks of PEU and CD domains are indicated by vertical black arrows.

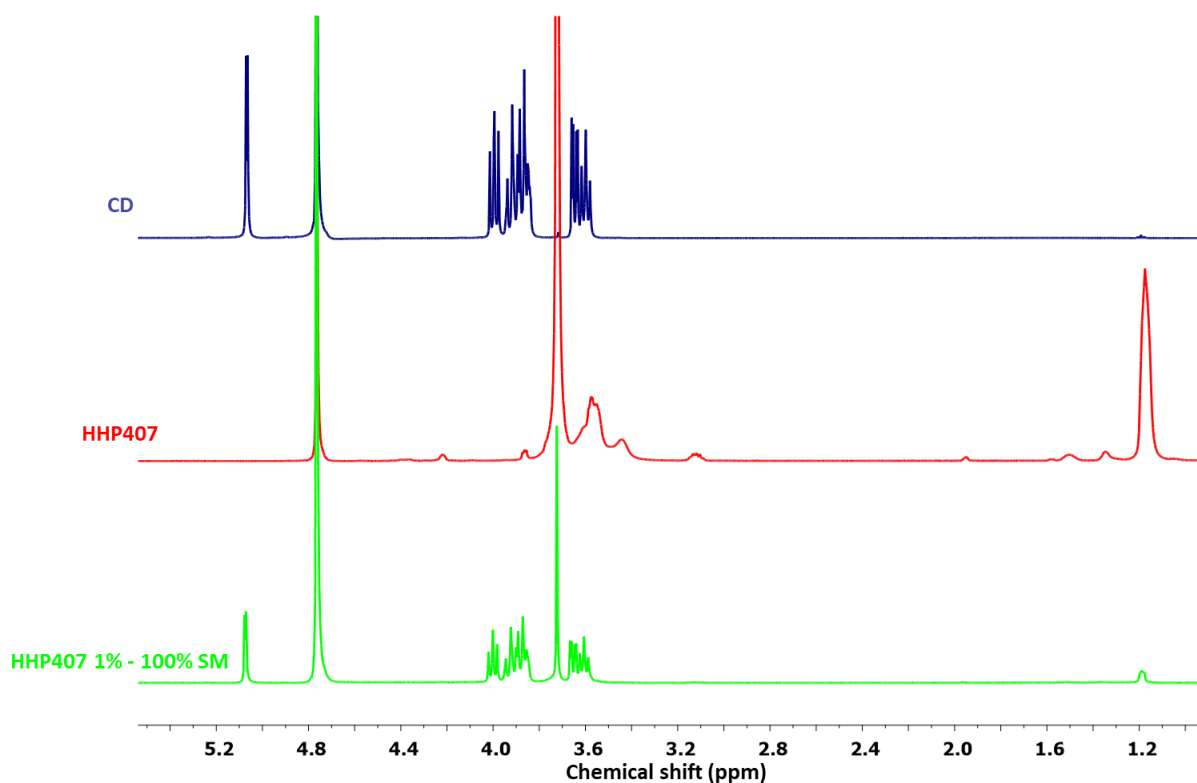


Figure 8 – ¹H-NMR spectra of CD (blue), HHP407 (red) and HHP407 1% - SM 100% (green). The simultaneous presence of CD and PEU in the produced SM powder is confirmed by the appearance of the respective typical resonance bands in HHP407 1% - SM 100% spectrum.

4.3 Physical characterization of HHP407-based SM hydrogels

The higher affinity of HHP407 for the interaction with CDs indicated that deeper investigations on hydrogel formulation design were needed. For this reason, a wide plethora of hydrogel

formulations was produced at a maximum PEU content of 5% w/v and gelation time was qualitatively evaluated, as reported in table 1. Interestingly, no phase-separation phenomena were observed and all the estimated gelation time values were significantly lower with respect to those of identically formulated samples based of the other PEUs developed in this Ph.D. work. Indeed, HHP407 1% - CD 10% hydrogel sample was characterized by a gelation time around 1 hour and 5 minutes at room temperature (i.e., 25 °C), while an overnight incubation was necessary for identical formulations based on chain-extended PEUs. By decreasing CD concentration to 8% w/v, the gelation process was still characterized by extremely fast kinetics. In detail, HHP407 1% - CD 8% required only 4 hours and 20 minutes to result in a turbid hydrogel, while 3 hours were necessary for HHP407 5% - CD 8%. These results further confirmed the previous hypothesis on the remarkably better interaction of HHP407 with CDs with respect to the chain-extended PEUs. Thence, HHP407 properties in terms of balance between molecular mass and hydrophobicity (i.e., PPO block dimension and distribution along PEU chain) could be validated as the best ones to improve interactions with CDs.

Table 1 – Gelation time at 25 °C for SM hydrogel formulations containing HHP407 at 1 and 5% w/v and CDs between 7 and 10% w/v. O.N. = overnight incubation to complete sol-gel transition

	CDs 7% w/v	CDs 8% w/v	CDs 9% w/v	CDs 10% w/v
HHP407 1% w/v	O.N.	4h 20'	2h 15'	1h 5'
HHP407 5% w/v	O.N.	3h	50'	20'

For all the above-mentioned reasons, a selection among these HHP407-based hydrogel formulations was conducted and the hydrogels containing CD at 8% w/v were selected for further investigations. Such selection was driven by the concurrent possibility to significantly decrease CD content (i.e., 20% lower than the previously designed hydrogels based on chain-extended PEUs) with respect to the previously developed formulations, while keeping gelation relatively fast. Indeed, this novel design allowed the production of highly promising SM hydrogels with significantly lower CD content, thus indicating a potential advantage in terms of hydrogel production-related costs.

4.4 Characterization of curcumin-loaded SM hydrogels based on HHP407 and CDs

4.4.1 Physical and mechanical characterization of curcumin-loaded SM hydrogels

HHP407 1% - CD 8% and HHP407 5% - CD 8% were selected for Cur encapsulation and release tests. In this study, a novel protocol for the production of SM hydrogels containing higher Cur payloads was designed. Indeed, CDs were exploited to produce an initial suspension of highly concentrated Cur. In detail, a solution containing CDs at 14% w/v in PBS/LAP was exploited to suspend Cur at 1 mg ml⁻¹ concentration. A homogeneous suspension of Cur was obtained through the aid of ultrasound sonication for 3-4 minutes under vigorous stirring and the final product is represented in figure 9. The overall stability of the resulting suspension of Cur- and CD-based

complexes was restricted within a temporal range of 30 minutes in static condition at 25 °C, then precipitation phenomena started to occur.



Figure 9 – Visual comparison among a Cur solution (1 mg ml^{-1}) in ethanol (left) and a Cur suspension (1 mg ml^{-1}) in a solution of CD at 14% w/v concentration in PBS/LAP (right).

Within the temporal frame of stability of the produced Cur suspension, specific aliquots were added to previously prepared HHP407-based solutions in PBS/LAP, thus producing SM hydrogels containing CD at 8% w/v and Cur at $570 \mu\text{g ml}^{-1}$. The resulting samples (i.e., HHP407 1% - CD 8% Cur and HHP407 5% - CD 8% Cur) were compared with the corresponding control samples not containing Cur (i.e., HHP407 1% - CD 8% and HHP407 5% - CD 8%).

The effects of Cur loading on hydrogel gelation were evaluated through rheological and photo-rheological characterizations. Figure 10 reports the trends of G' and G'' as a function of applied strain (i.e., strain sweep tests). Interestingly, SM hydrogels based on HHP407 at 1% w/v concentration revealed better mechanical properties with respect to formulations at higher PEU content, both in the presence and in the absence of Cur. For example, G' within the linear viscoelastic region (i.e., G'_{LVE}) for HHP407 1% - CD 8% was equal to 6400 Pa, while for HHP407 5% - CD 8% the same parameter was 3800 Pa (i.e., approx. 40% lower than the G'_{LVE} of HHP407 1% - CD 8%). This interesting result could be ascribed to the lower PEU/CD ratio that characterized HHP407 1% - CD 8% with respect to HHP407 5% - CD 8%, as hypothesized in the previous studies. Moreover, the resulting enhancement of such phenomenon could be attributed to the higher ability of HHP407 to interact with CDs with respect to the previously evaluated PEUs due to its physico-chemical features. The presence of Cur induced a G'_{LVE} decrease of 20% and 26% for formulations containing HHP407 at 1 and 5% w/v, respectively. Moreover, slightly lower critical strain values (γ_L) were observed for the hydrogels containing Cur with respect to the control samples. For example, γ_L value for HHP407 1% - CD 8% was around 0.3%, while for the system containing Cur the same parameter was measured around 0.1%. However, the encapsulation of a notably high payload of Cur (i.e., $570 \mu\text{g ml}^{-1}$) did not significantly induce any detrimental effect from a general perspective. Additionally, all the investigated hydrogels showed a relevant self-healing ability. Indeed, G'_{LVE} after complete rupture at 500% strain and recovery in quiescent state at 37 °C for 15 minutes was greater than 88% for all the investigated hydrogel systems. In this regard, hydrogels composed of HHP407 at 1% w/v concentration showed a higher self-healing capacity compared to the formulations at higher PEU content. Indeed, HHP407 1% - CD 8% systems exhibited recovery values of 97% for the control condition and 93% for the network containing Cur, while for hydrogel systems at 5% w/v HHP407 concentration a consistent 88% recovery was calculated for both cases. This different response could be a consequence of a

hindered SM crystallization due to a relevant formation of micelle-based structures within samples containing a higher amount of HHP407 (i.e., 5% w/v), which has been observed to be highly thermo-sensitive by means of CMT evaluation. The concomitant presence of CDs at a lower concentration (i.e., 8%) with respect to the previous Chapters could also have an important role. In this regard, the decrement of CD concentration from 10% to 8% w/v indicated an increased PEU/CD mass ratio, which resulted in a set of conditions that are not completely proper for PPR crystallization and probably made the effects induced by differences in PEU content more evident. However, these observations generally indicated a good consistency with the previous results concerning chain-extended PEUs.

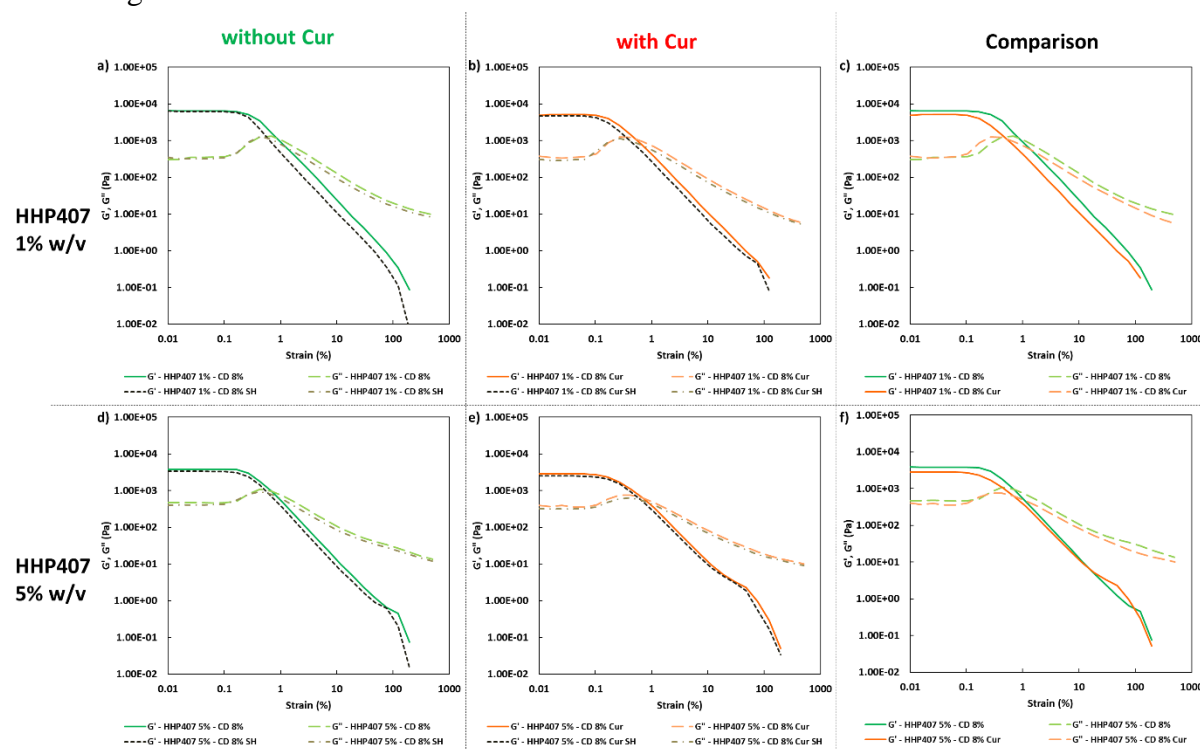


Figure 10 – G' (continuous lines) and G'' (long dashed lines) trends as a function of applied strain at 37 °C for a) HHP407 1% - CD 8%, b) HHP407 1% - CD 8% Cur (i.e., 570 $\mu\text{g ml}^{-1}$), d) HHP407 5% - CD 8%, and e) HHP407 5% - CD 8% Cur (i.e., 570 $\mu\text{g ml}^{-1}$). G' (black short dashed lines) and G'' (grey dash-dotted lines) trends after recovery in quiescent state for 15 minutes at 37 °C are also reported for each formulation. Figures c) and f) represent direct comparisons between hydrogels not containing (in green) and containing Cur (in orange).

Frequency sweep tests were also conducted at 25, 30 and 37 °C with the aim to evaluate the behavior of HHP407-based hydrogels in terms of network development and thermo-responsiveness. All the investigated formulations were characterized by a fully developed gel state at each tested temperature and no cross-over points between G' and G'' were identified, as reported in figure 11. A slight dependence of G' and G'' trends over temperature was observed for all the hydrogel systems. For example, even the formulation containing the lowest amount of thermo-sensitive PEU (i.e., HHP407 1% - CD 8%) showed a G' equal to 5700 Pa at 25 °C (at 100 rad s^{-1} applied angular frequency), while the same parameter turned out to be 7400 Pa at 37 °C. Interestingly, the formulation containing HHP407 at 1% w/v showed a better developed hydrogel network with respect to the one containing such PEU at 5% w/v. Indeed, the former was characterized by a less marked dependency of G' and G'' over frequency compared to the latter.

Even frequency sweep tests evidenced better mechanical properties for the hydrogel composed of HHP407 at 1% w/v concentration with respect to the one containing such PEU at 5% w/v. As an example, G' at 37 °C (100 rad s⁻¹) was 7400 Pa for HHP407 1% - CD 8% and 5000 Pa for HHP407 5% - CD 8%. Cur loading induced a slight decrease of mechanical properties, as previously observed and discussed. Cur contribution was more evident in the samples containing HHP407 at 5% w/v with respect to the ones at 1% w/v, probably because of the presence of a less developed SM hydrogel network at a higher PEU/CD mass ratio (i.e., HHP407 at 5% w/v). However, no significant effects of Cur on hydrogel development were generally observed, since G' and G'' characterizing Cur-loaded hydrogels showed consistent trends over applied frequency at the investigated temperatures (i.e., 25, 30 and 37 °C) with respect to control samples.

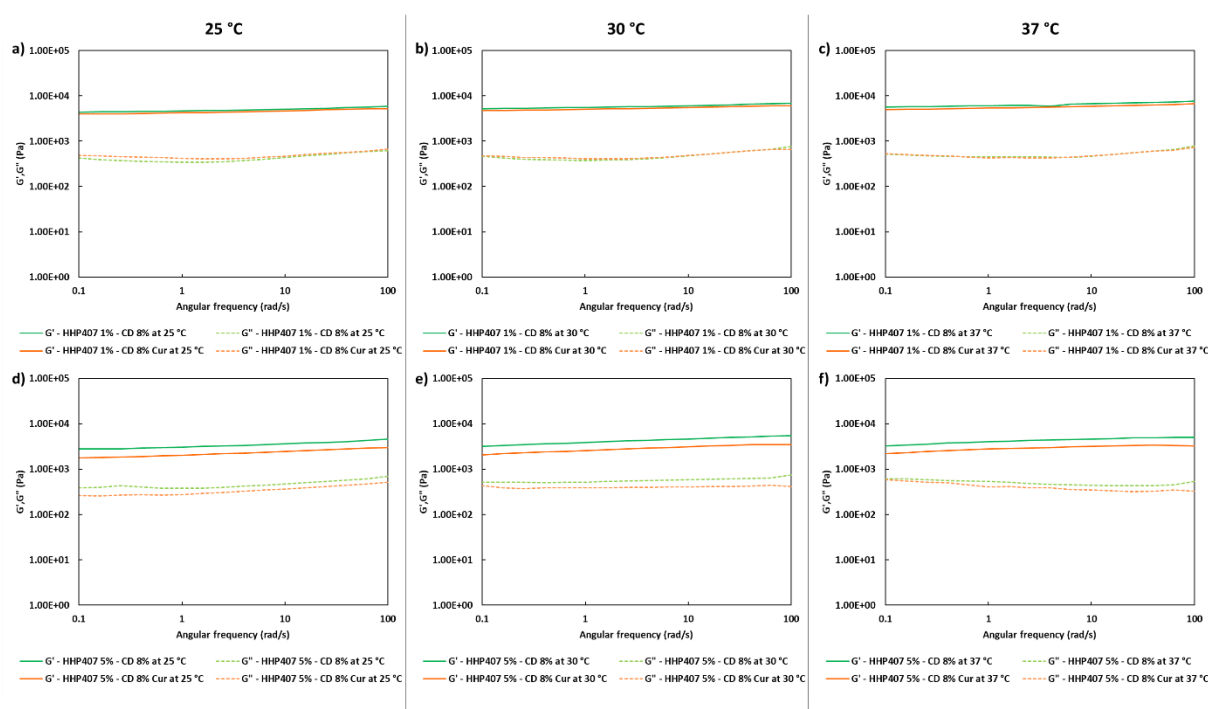


Figure 11 – G' (continuous lines) and G'' (dashed lines) trends as a function of applied angular frequency at 25, 30 and 37 °C for a,b,c) HHP407 1% - CD 8%, and d,e,f) HHP407 5% - CD 8% as such (green) and containing Cur (orange) at 570 $\mu\text{g ml}^{-1}$.

Self-healing tests were also performed, and remarkable recovery ability of all HHP407-based hydrogels was typically observed, as reported in figure 12. In fact, a G' recovery greater than 85% after 3 rupture cycles was observed for all the investigated systems. Higher recovery values were measured for samples at 5% w/v HHP407 concentration (i.e., around 95%) with respect to the ones at 1% w/v (i.e., around 88%). This difference could be ascribed to a better fatigue resistance of the hydrogel systems containing the PEU at higher concentration (i.e., 5% w/v), due to a relatively higher damping effect originated by more diffused and interacting amorphous domains¹⁴ (i.e., PEU chains not involved in the formation of SM crystals) with respect to hydrogel networks with lower PEU/CD ratio (i.e., 1% w/v). Indeed, this condition generally enhanced the organization of available PEU chains into stiffer PPRs-based networks. Finally, the presence of Cur did not significantly affect the mechanical response of the resulting hydrogels to applied rupture cycles and recovery phases.

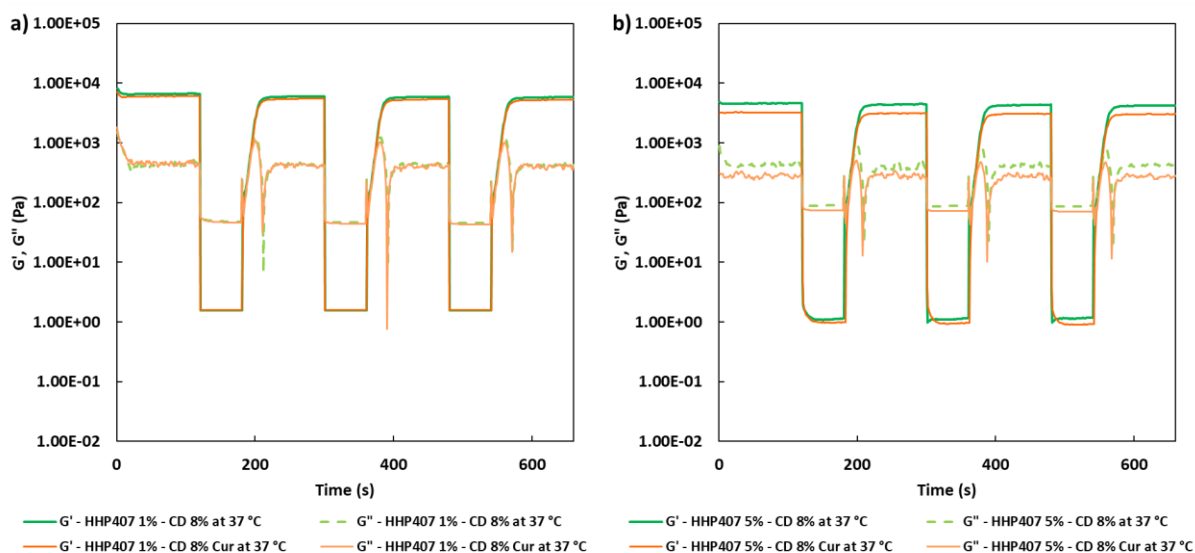


Figure 12 – Strain test curves reporting the trends of G' (continuous lines) and G'' (dashed lines) as a function of time during cyclic rupture (100% strain, 60 seconds) and recovery (0.1% strain, 120 seconds) of hydrogel networks at a) 1% and b) 5% w/v HHP407 concentrations at 37 °C. Control hydrogels (green lines) are compared to the ones containing Cur (orange lines) at $570 \mu\text{g ml}^{-1}$.

Photo-rheological tests were also performed with the aim to assess the photo-responsiveness of the developed SM hydrogels. In this regard, the typical turbidity of these systems could represent an important impediment to light transmission within the entire hydrogel volume. Nonetheless, all gels showed a good responsiveness to UV light exposure, as reported in figure 13. In fact, G' increase after UV light exposure was quantified around 21% and 17% for HHP407 1% - CD 8% and HHP407 5% - CD 8% hydrogels, respectively. Differently, a 8% and 11% G' increase after UV irradiation was observed in average for hydrogel systems containing Cur at $570 \mu\text{g ml}^{-1}$ and PEU at 1 and 5% w/v concentration, respectively. These results suggested a lower photo-sensitivity of Cur-loaded systems due to the high content of encapsulated Cur, which is a photo-sensitive dye, thus contributing in terms of UV light dissipation. Interestingly, the visual inspection of the sample containing HHP407 at 1% w/v and Cur indicated a significant reduction of the original intense orange color. This observation indicated an indisputable degradation of an important amount of Cur payload within the hydrogel network containing PEU at low concentration. Differently, no significant color changes were observed for the sample HHP407 5% - CD 8%, thus suggesting that the higher content of photo-sensitive PEU helped in the preservation of the Cur payload. Such behavior could be ascribed to two main aspects. First, a significantly higher number of photo-sensitive groups was intrinsically present in the formulation containing HHP407 at 5% w/v compared to 1% w/v, thus competing with Cur degradation process in terms of UV light absorbance through the formation of chemical crosslinking. Second, it could be likely that a higher content of PEU could help in terms of Cur stabilization and protection from degradation through its encapsulation into the more available hydrophobic domains. In conclusion, these photo-rheological characterizations suggested that a shorter UV light exposure could be sufficient to achieve complete crosslinking and this aspect was particularly important for the samples containing HHP407 at low concentration (i.e., 1% w/v). More specifically, the results suggested that an almost complete crosslinking was obtainable within 20-30 seconds of UV light

irradiation for all the investigated hydrogels, as observable from the G' curves reported in the graphs in figure 13.

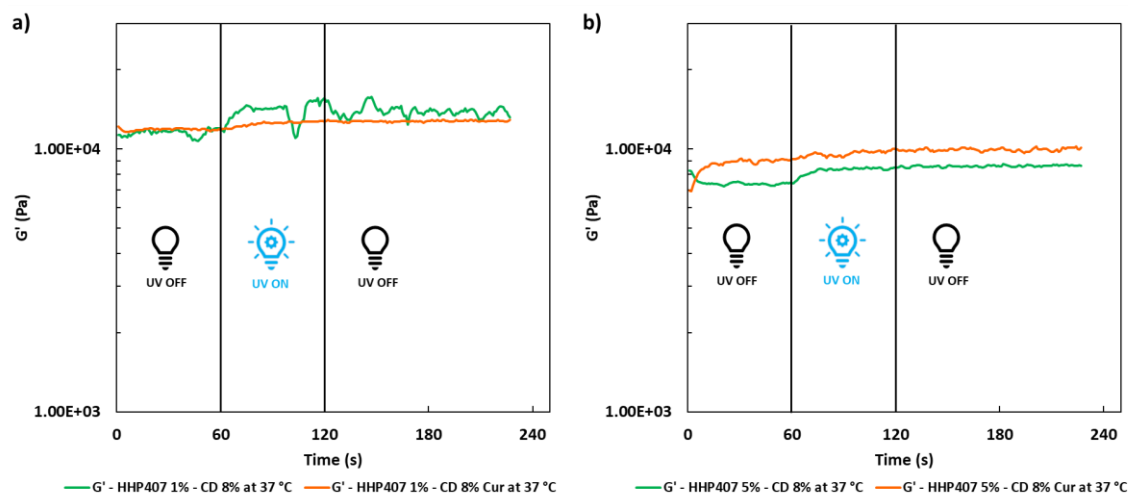


Figure 13 – G' trends as a function of time for hydrogels at a) 1 and b) 5% w/v HHP407 concentration as such (green lines) and containing curcumin (orange lines) at $570 \mu\text{g ml}^{-1}$. Hydrogels were characterized before photo-crosslinking for 60 seconds. Then, exposure to UV light (365 nm , 10 mW cm^{-2}) was conducted for 60 seconds and resulting mechanical properties were observed for additional 120 seconds.

4.4.2 Release profiles of Cur encapsulated within HHP407-based hydrogels

The previous characterizations proved the physical stability and the photo-sensitivity of the designed Cur-loaded ($570 \mu\text{g ml}^{-1}$) SM hydrogels (i.e., HHP407 1% - CD 8% and HHP407 5% - CD 8%). Release studies were performed using 0.5 ml hydrogel samples in 4 ml glass vial (10 mm inner diameter). HHP407 1% - CD 8% Cur was exposed to UV light at 365 nm (10 mW cm^{-2}) for 15 seconds per each side of the vial, thus obtaining HHP407 1% - CD 8% Cur UV. For HHP407 5% - CD 8% Cur 1 minute UV light exposure was implemented according to the same procedure, thus producing HHP407 5% - CD 8% Cur UV. Release studies were conducted on the basis of specific calibration lines obtained through the re-solubilization of hydrogel systems in PBS. Such procedure was necessary in this case because the high amount of encapsulated Cur (i.e., $570 \mu\text{g ml}^{-1}$) induced a highly more important contribution of the involved PEU in terms of solubilization and delivery with respect to the previous studies, in which instead PEU contribution was negligible, since all hydrogels (i.e., 1 and 3% w/v PEU content and $80 \mu\text{g ml}^{-1}$ Cur payload) behaved similarly. In this study, the involvement of specific PEU-dependent structures was hypothesized, as suggested from the available literature on the design of Cur loaded systems based on amphiphilic polymers.^{15,16} Calibration curves obtained from HHP407 1% - CD 8% and HHP407 5% - CD 8% re-solubilization are reported in figure 14. Totally different calibration curves were obtained, although the only difference among these samples was related to PEU content. In detail, a higher molar extinction coefficient was observed for the system containing HHP407 at 5% w/v with respect to 1% w/v concentration, thus probably indicating an enhanced Cur integration and solubilization at higher PEU concentration. Moreover, notably good linear fittings were calculated.

Cur release profiles from all hydrogels (i.e., HHP407 1% - CD 8% Cur, HHP407 1% - CD 8% Cur UV, HHP407 5% - CD 8% Cur, HHP407 5% - CD 8% Cur UV) showed significantly different trends, which were correlated to hydrogel formulation, as shown in figure 15. Generally, the systems exposed to UV light showed delayed delivery of Cur and were able to sustain this process up to 35 days incubation in physiological-like conditions (i.e., in contact with PBS at 37 °C). Surprisingly, the entire payload of Cur (i.e., 285 µg) was released also from UV cured systems, thus indicating an optimal preservation of its chemical stability within the SM networks, which indeed acted as protective elements for such highly sensitive drug. An exception was represented by the hydrogel HHP407 1% - CD 8% Cur, which showed a total release slightly lower than the other systems (i.e., approx. 5%). This behavior can be probably correlated with the low PEU content (i.e., less capability as drug carrier) of such formulation and the highly destabilizing external aqueous milieu which induced the precipitation of an aliquot of released Cur (i.e., greater than 200 µg ml⁻¹ in 18 hours), thus resulting in an under-estimation of the released drug. Hence, the limit of Cur solubility into the released PEU and CD carriers was probably overtaken, as previously suggested by the specific calibration curve obtained for the formulation containing HHP407 at 1% w/v. Interestingly, SM hydrogels based on HHP407 at 1% w/v concentration exhibited a slower release kinetics compared to those containing such PEU at 5% w/v concentration. In particular, at each time point a significantly higher release rate was observed for HHP407 5% - CD 8% Cur UV with respect to HHP407 1% - CD 8% Cur UV (data not shown, P value < 0.0012). This observation could be correlated to the previous rheological and photo-rheological characterizations, in which the hydrogels composed of HHP407 at 1% w/v concentration showed the highest values of G', thus indicating the formation of highly rigid networks, due to an enhanced SM self-assembly into PPR-based crystals.^{17,18} Even in this case, the characterizing PEU/CD ratio suggested the formation of differently organized networks that were also able to perform photo-induced crosslinking and hence open the way to the possibility to finely tune the resulting release kinetics. The entire set of these data proved the suitability of HHP407 as building block of remarkably tunable and engineered devices at notably low concentrations.

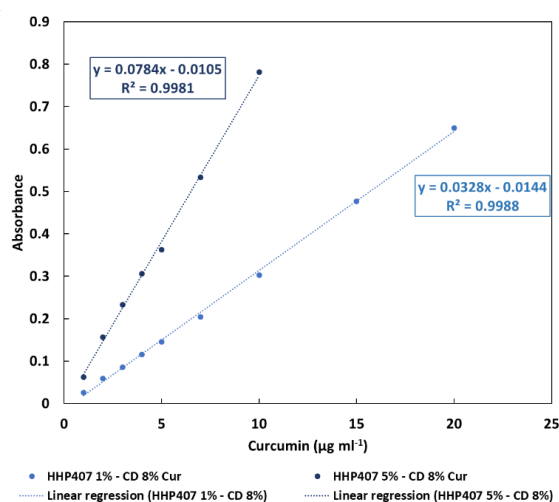


Figure 14 – Calibration curves showing the absorbance of standard samples as a function of Cur concentration after dissolution of HHP407 1% - CD 8% Cur (light blue) and HHP407 5% - CD 8% Cur (blue) in order to obtain storage solutions at 100 µg ml⁻¹ Cur concentration. Linear regressions are also reported with the resulting equations, which showed a good fitting.

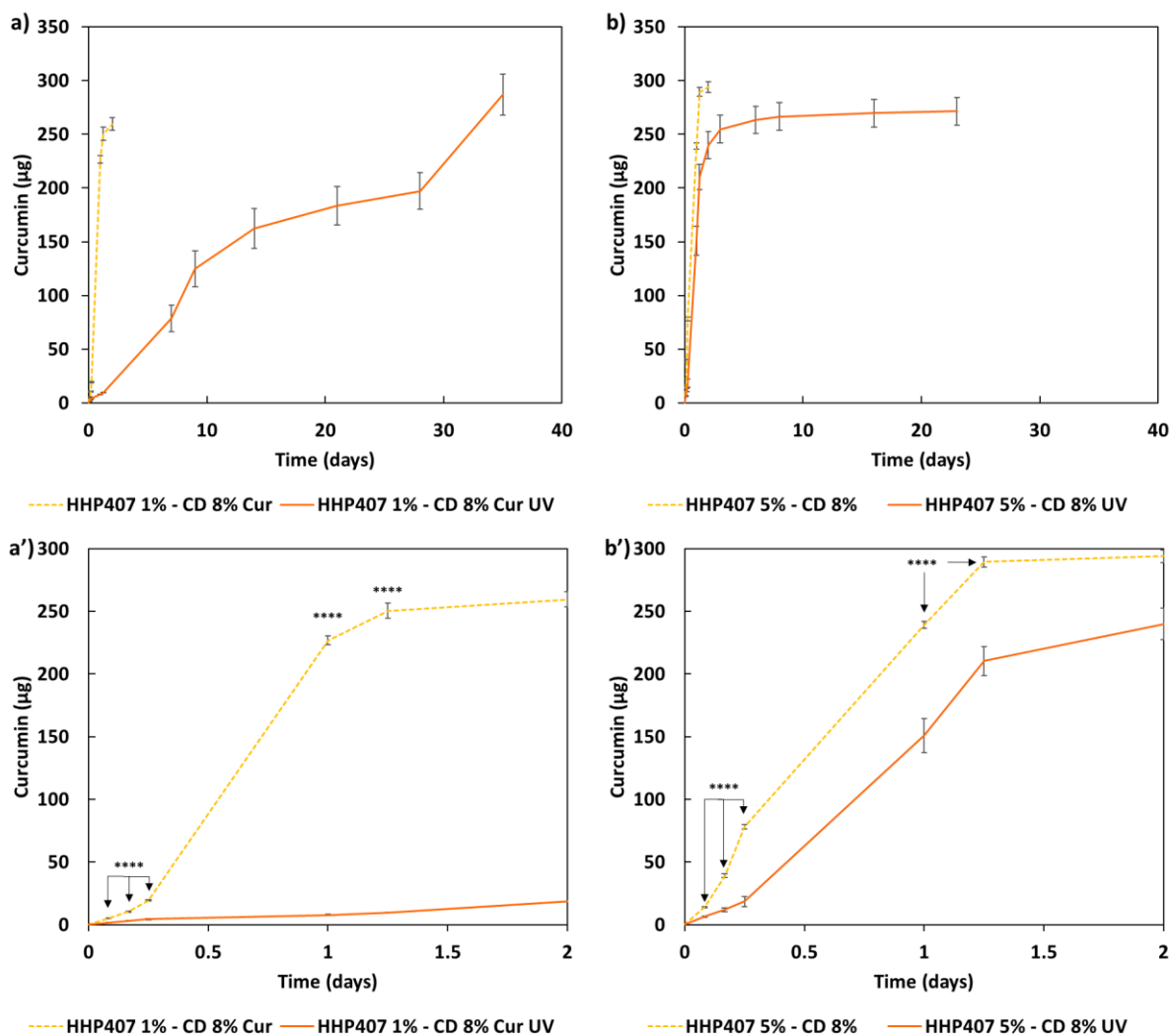


Figure 15 – Cur release profiles of hydrogel systems in contact with PBS at 37 °C and characterized by different HHP407 contents: a,a') 1% w/v (HHP407 1% - CD 8% Cur and HHP407 1% - CD 8% Cur UV) and b,b') 5% w/v (HHP407 5% - CD 8% Cur and HHP407 5% - CD 8% Cur UV). Physical hydrogels (light orange dashed lines) are compared with photo-cured systems (orange continuous lines). a') and b') graphs represent in detail the release profile measured within 2 days observation.

4.5 Preliminary studies on HHP407-based SM hydrogel extrudability

In this study, a preliminary evaluation of the general printability of HHP407-based hydrogel systems was conducted. The formulation HHP407 5% - CD 8% was selected for its lower rigidity and generally higher damping/self-healing ability that were observed through rheological characterizations. These parameters are fundamental aspects to consider for the selection of a potential bioink.¹⁹ Printing procedure was conducted by controlling different parameters: tip extrusion diameter (D_E), extrusion pressure (P_E), printhead velocity (v_P), syringe temperature (T_S) and bed temperature (T_B). The printing process was conducted at 37 °C for both the syringe and bed in order to enhance the stabilization of the hydrogel network through a major contribution of hydrophobic interactions. A preliminary set of optimized parameters was obtained and reported in Table 2. Figure 16 reports the produced 3D-printed construct and a qualitative comparison with the resulting geometry compared to the theoretical CAD design.

Table 2 – Selected parameters for printing process.

D_E	P_E	VP	T_s	T_B
250 μm	35-40 kPa	10 mm s^{-1}	37 $^{\circ}\text{C}$	37 $^{\circ}\text{C}$

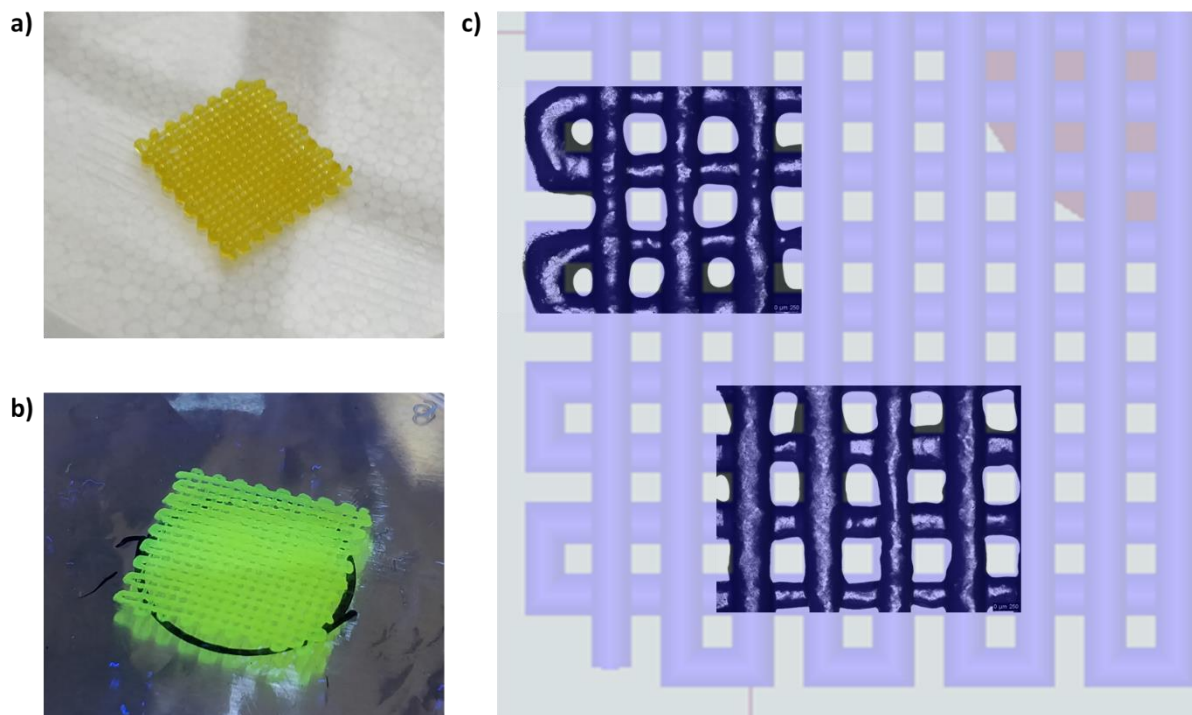


Figure 16 – a) 3D-printed construct based on HHP407 5% - CD 8% Cur, b) UV curing of HHP407 5% - CD 8% Cur, c) qualitative geometrical match in 2D of 3D-printed HHP407 5% - CD 8% Cur.

The printing process set with the parameters reported in table 2 produced constructs with good definition and acceptable printing fidelity. In fact, filament diameter turned out to be 0.46 ± 0.08 mm (average of 5 measurements obtained from 4 different filaments), while the theoretical value was 0.45 mm, thus proving extrudability and filament formation. The selection of a smaller tip diameter (0.25 mm) with respect to the theoretical value (0.45 mm) was driven by the definition of a compromise between printing velocity and required extrusion pressure: in the case of a larger tip diameter (0.45 mm), a slower printing velocity was necessary to obtain filaments having a proper geometry. In the selected conditions, the production of grids composed by two layers required an overall printing time around 1 minute. Pore dimension was larger than the theoretical design. Indeed, the calculation of pore area of constructs resulted to be 0.17 ± 0.04 mm^2 , while the theoretical value was 0.1225 mm^2 , thus indicating an excess around 40%. This difference could be ascribed to defects in proximity of the intersections between the two layers. Nonetheless, a general good printability could be deduced from these preliminary results. Further optimizations could be achieved by using more precise methodologies for geometry investigation (e.g., computed tomography or optical coherence tomography) in order to better find the correlation between morphological features and printing parameters. Another qualitative characterization was conducted in terms of stability in contact with a large volume of an aqueous medium (PBS, 5 ml, 25 $^{\circ}\text{C}$). UV cured systems (HHP407 5% - CD 8% Cur UV) showed a significantly improved residence time with respect to the physical sample (HHP407 5% - CD 8% Cur). In fact, as shown

in figure 17, the system treated through UV light irradiation preserved its geometrical integrity for 3 days in a highly destabilizing aqueous environment, while the physical sample was completely solubilized within an incubation time of 3 hours. Moreover, an evident color change was observed after UV curing for 1 minute, thus indicating that the resulting relevant interfacial surface and the limited thickness of the construct probably enhanced the exposure of Cur to photo-degradation. Nonetheless, an evident yellowish was maintained, indicating a relevant protective effect of HHP407 and CDs on Cur even in such particularly degradative conditions. Indeed, the same UV curing protocol applied to the samples utilized for release studies did not induce any evident degradation phenomena, due to a combination between the protective effect of HHP407/CDs and geometry (i.e., thickness, overall volume).

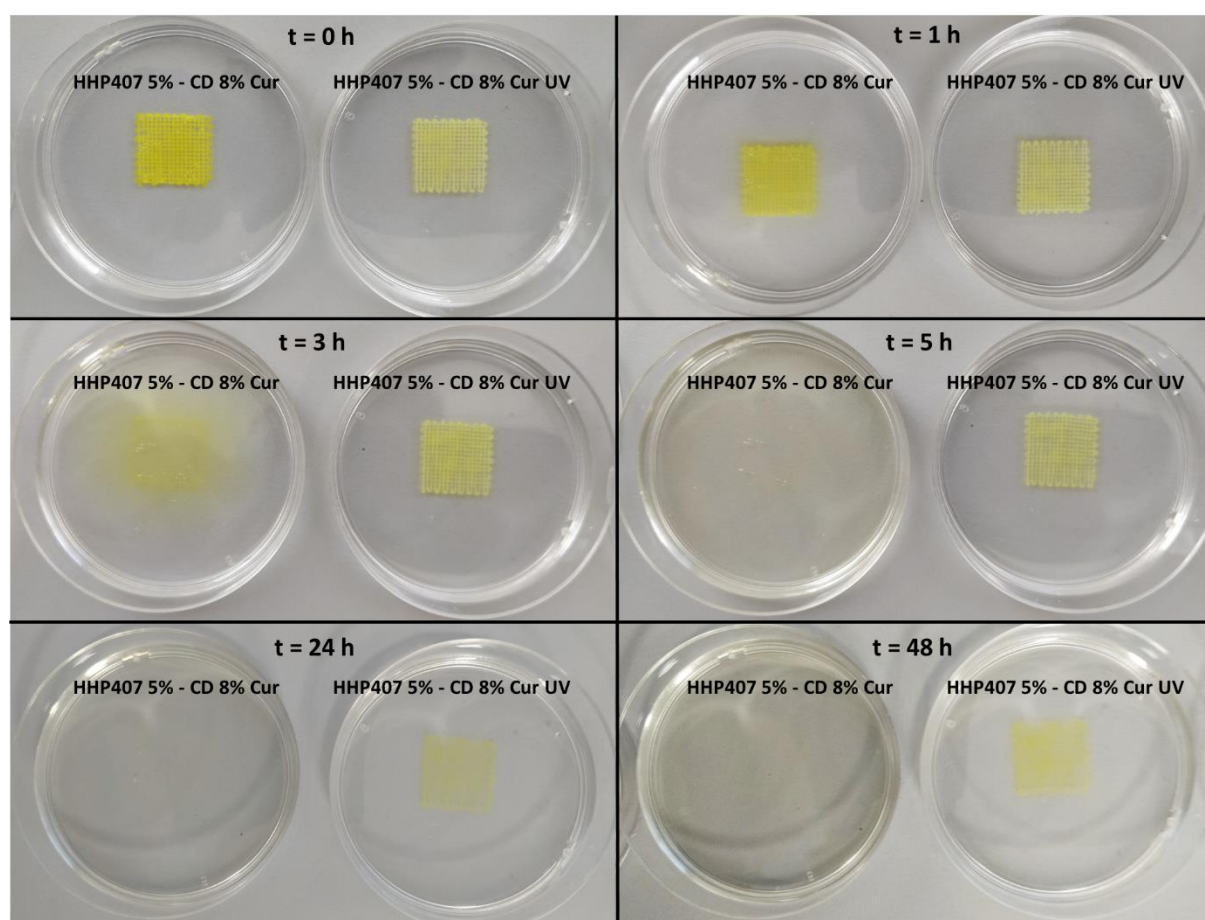


Figure 17 – Qualitative evaluation of stability for 3D-printed HHP407 5% - CD 8% Cur and HHP407 5% - CD 8% Cur UV structured in contact with 5 ml of PBS at 25 °C (within a Petri support - 50 mm diameter).

5. Conclusions

In this part of the work, a novel photo-sensitive PEU was synthesized implementing a modification of the usual synthesis process described before in *Chapter 2.2 of Section 2*. Indeed, HHP407 PEU was synthesized by using HEMA as end-capping alcohol of the prepolymer chains resulting from the prepolymerization reaction. A complete physico-chemical characterization indicated a good functionalization through the addition of methacrylate end-groups to the resulting PEU chains. Moreover, a notably good thermo-sensitivity was assessed by CMT evaluation, although a lower molecular mass was obtained. This behavior suggested the achievement of a well-balanced

polymer structure among its overall molecular mass and hydrophobicity in terms of length and distribution of available domains (i.e., PPO, HDI and probably also HEMA). Because of these physico-chemical properties, HHP407 turned out to be suitable for the formation of PPR-based crystals in aqueous environments. Moreover, it resulted to be the best PEU for the formation of SM networks among the whole plethora of PEUs investigated in this thesis work. Thence, it is likely that its structural features represented an optimized set of properties for the constructive interaction with CDs, thus resulting in highly stable and simultaneously responsive networks. This particular behavior allowed the design of SM hydrogels at low HHP407 content (i.e., $\leq 5\%$ w/v) and the significant reduction of CD concentration (i.e., 20%, from 10% to 8% w/v) for the development of SM hydrogels with good mechanical properties. In this regard, the formulations showing a lower PEU/CD mass ratio (i.e., 1% and 8% w/v HHP407 and CD concentration, respectively) were characterized by better mechanical properties with respect to the systems containing HHP407 at 5% w/v, as assessed through rheological characterizations. This observation was in evident agreement with the previous results obtained for similar systems, thus further reinforcing the hypothesis of the high functionality of PEU macromolecules at low concentrations in combination with CDs. Although HHP407 produced highly crystalline hydrogel networks with CDs, thus inducing a relevant risk of the formation of fragile hydrogels, a notorious self-healing ability was even observed. Photo-sensitivity was assessed by means of photo-rheological characterizations. Cur delivery studies demonstrated the protective ability of HHP407 and CDs on this photo-sensitive drug, opening the way to the possibility to sustain the release of Cur in aqueous environments up to 5 weeks. Moreover, a central role of hydrogel composition and consecutive photo-crosslinking was found for the tunability of Cur release kinetics from HHP407-based networks. Finally, one formulation among the developed hydrogels was preliminary evaluated for the production of 3D-printed structures with good resolution. Such results further indicated HHP407 as a highly versatile polymer for the development of engineered devices for regenerative medicine. Hence, this study further confirmed the great potential of properly synthesized PEUs as raw materials for the design of SM hydrogels at low synthetic polymer content, and showing good mechanical performances, progressive release profiles of encapsulated drugs, and additional promising properties for future insights into 3D cell culture and delivery.

6. References

- (1) Eelkema, R.; Pich, A. Pros and Cons: Supramolecular or Macromolecular: What Is Best for Functional Hydrogels with Advanced Properties? *Adv. Mater.* **2020**, *32* (20), 1906012. <https://doi.org/10.1002/adma.201906012>.
- (2) Tian, B.; Hua, S.; Tian, Y.; Liu, J. Chemical and Physical Chitosan Hydrogels as Prospective Carriers for Drug Delivery: A Review. *J. Mater. Chem. B* **2020**, *8* (44), 10050–10064. <https://doi.org/10.1039/D0TB01869D>.
- (3) Zhang, Y. S.; Khademhosseini, A. Advances in Engineering Hydrogels. *Science* **2017**, *356* (6337), eaaf3627. <https://doi.org/10.1126/science.aaf3627>.
- (4) Li, J.; Suo, Z.; Vlassak, J. J. Stiff, Strong, and Tough Hydrogels with Good Chemical Stability. *J. Mater. Chem. B* **2014**, *2* (39), 6708–6713. <https://doi.org/10.1039/C4TB01194E>.
- (5) Zhao, S.-P.; Zhang, L.-M.; Ma, D.; Yang, C.; Yan, L. Fabrication of Novel Supramolecular Hydrogels with High Mechanical Strength and Adjustable Thermosensitivity. *J. Phys. Chem. B* **2006**, *110* (33), 16503–16507. <https://doi.org/10.1021/jp063005c>.
- (6) Zhao, S.-P.; Xu, W.-L. Thermo-Sensitive Hydrogels Formed from the Photocrosslinkable Polypseudorotaxanes Consisting of β -Cyclodextrin and Pluronic F68/PCL Macromer. *J Polym Res* **2010**, *17* (4), 503–510. <https://doi.org/10.1007/s10965-009-9337-0>.
- (7) Wei, H.; Zhang, A.-Y.; Qian, L.; Yu, H.; Hou, D.; Qiu, R.; Feng, Z.-G. Supramolecular Structured Hydrogel Preparation Based on Self-Assemblies of Photocurable Star-Shaped Macromers with α -Cyclodextrins. *J. Polym. Sci. A Polym. Chem.* **2005**, *43* (13), 2941–2949. <https://doi.org/10.1002/pola.20773>.
- (8) Wei, H.; Yu, H.; Zhang, A.; Sun, L.; Hou, D.; Feng, Z. Synthesis and Characterization of Thermosensitive and Supramolecular Structured Hydrogels. *Macromolecules* **2005**, *38* (21), 8833–8839. <https://doi.org/10.1021/ma050887p>.
- (9) Wei, H.; He, J.; Sun, L.; Zhu, K.; Feng, Z. Gel Formation and Photopolymerization during Supramolecular Self-Assemblies of α -CDs with LA-PEG-LA Copolymer End-Capped with Methacryloyl Groups. *European Polymer Journal* **2005**, *41* (5), 948–957. <https://doi.org/10.1016/j.eurpolymj.2004.11.041>.
- (10) Chimene, D.; Kaunas, R.; Gaharwar, A. K. Hydrogel Biointerface Reinforcement for Additive Manufacturing: A Focused Review of Emerging Strategies. *Adv. Mater.* **2020**, *32* (1), 1902026. <https://doi.org/10.1002/adma.201902026>.
- (11) Laurano, R.; Cassino, C.; Ciardelli, G.; Chiono, V.; Boffito, M. Polyurethane-Based Thiomers: A New Multifunctional Copolymer Platform for Biomedical Applications. *Reactive and Functional Polymers* **2020**, *146*, 104413. <https://doi.org/10.1016/j.reactfunctpolym.2019.104413>.
- (12) Fakhari, A.; Corcoran, M.; Schwarz, A. Thermogelling Properties of Purified Poloxamer 407. *Heliyon* **2017**, *3* (8), e00390. <https://doi.org/10.1016/j.heliyon.2017.e00390>.
- (13) Chung, J. W.; Kang, T. J.; Kwak, S.-Y. Supramolecular Self-Assembly of Architecturally Variant α -Cyclodextrin Inclusion Complexes as Building Blocks of Hexagonally Aligned Microfibrils. *Macromolecules* **2007**, *40* (12), 4225–4234. <https://doi.org/10.1021/ma0625105>.

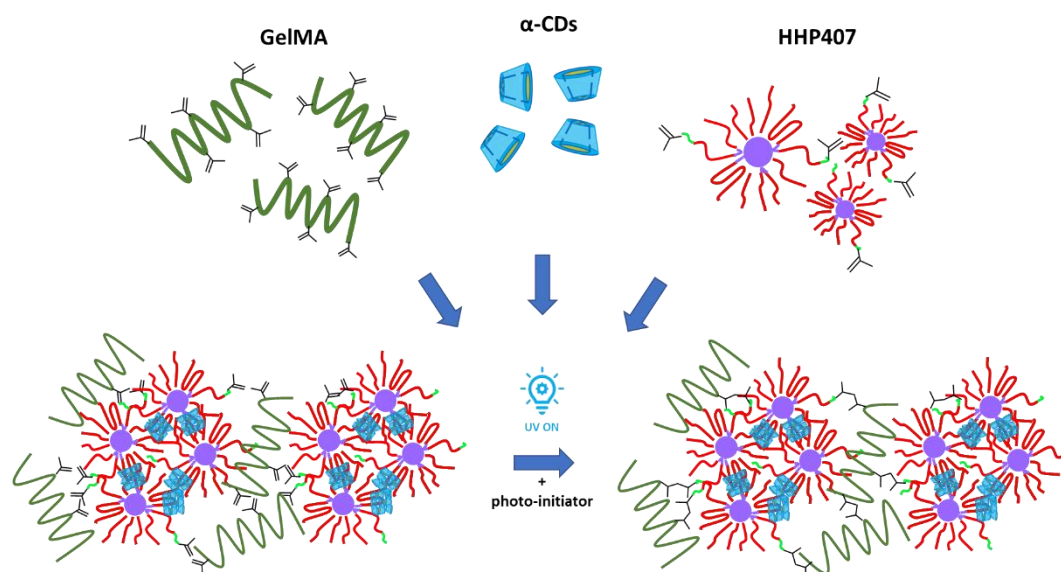
- (14) Henderson, K. J.; Zhou, T. C.; Otim, K. J.; Shull, K. R. Ionically Cross-Linked Triblock Copolymer Hydrogels with High Strength. *Macromolecules* **2010**, *43* (14), 6193–6201. <https://doi.org/10.1021/ma100963m>.
- (15) Kant, V.; Gopal, A.; Kumar, D.; Pathak, N. N.; Ram, M.; Jangir, B. L.; Tandan, S. K.; Kumar, D. Curcumin-Induced Angiogenesis Hastens Wound Healing in Diabetic Rats. *Journal of Surgical Research* **2015**, *193* (2), 978–988. <https://doi.org/10.1016/j.jss.2014.10.019>.
- (16) Khan, S.; Minhas, M. U.; Ahmad, M.; Sohail, M. Self-Assembled Supramolecular Thermoreversible β -Cyclodextrin/Ethylene Glycol Injectable Hydrogels with Difunctional Pluronic[®] 127 as Controlled Delivery Depot of Curcumin. Development, Characterization and *in Vitro* Evaluation. *Journal of Biomaterials Science, Polymer Edition* **2018**, *29* (1), 1–34. <https://doi.org/10.1080/09205063.2017.1396707>.
- (17) Stowers, R. S.; Allen, S. C.; Suggs, L. J. Dynamic Phototuning of 3D Hydrogel Stiffness. *Proc Natl Acad Sci USA* **2015**, *112* (7), 1953–1958. <https://doi.org/10.1073/pnas.1421897112>.
- (18) Domiński, A.; Konieczny, T.; Kurcok, P. α -Cyclodextrin-Based Polypseudorotaxane Hydrogels. *Materials* **2019**, *13* (1), 133. <https://doi.org/10.3390/ma13010133>.
- (19) Schwab, A.; Levato, R.; D'Este, M.; Piluso, S.; Eglin, D.; Malda, J. Printability and Shape Fidelity of Bioinks in 3D Bioprinting. *Chem. Rev.* **2020**, *120* (19), 11028–11055. <https://doi.org/10.1021/acs.chemrev.0c00084>.

Section 3 – Chapter 3.2 – Development and engineering of bioartificial hydrogels based on supramolecular networks and gelatin methacryloyl

1. Abstract

Single stage repair/regenerative strategies rely on the idea to exert multiple functions through a unique device. Indeed, one of the recently emerging frontiers in regenerative medicine aims to develop systems able to couple the administration of a pharmaceutical therapy with a biomimetic action with the ultimate goal to properly allow new tissue growth and hence regeneration. In this manner, the overall invasiveness of a regenerative therapy can be significantly reduced, thus accelerating the entire process, and improving acceptance from patients. However, the development of such devices is not trivial and requires highly versatile and tunable components. Within this context, in this part of the work, the previously characterized HHP407 poly(ether-urethane) was implemented for the production of novel biosynthetic systems containing gelatin methacryloyl (GelMA), which is a modified natural protein contraddistinguished by good bioactivity. In order to realize this aim, the fast self-assembly of HHP407 with CDs was exploited to stably encapsulate GelMA within its network. The integration of a well-developed supramolecular system and GelMA could result in a highly handy and potentially functional device in terms of combined regenerative pharmacology and tissue engineering. A plethora of nine newly formulated hydrogels was investigated and the two most promising systems were selected to conduct rheological characterization and studies on the encapsulation and release of curcumin as potential therapeutic agent. In this regard, hybrid bioartificial systems containing HHP407 at 3 and 5% w/v and α -cyclodextrins at 10% w/v were utilized to integrate GelMA at 3% w/v, resulting in highly stable and easy injectable formulations. Mechanical properties were investigated through strain sweep, frequency sweep and self-healing rheological tests. In this regard, even purely physical hydrogels turned out to be notably reliable and responsive when subjected to various mechanical stimuli. Generally, high values of elastic modulus were observed (greater than 10^4 Pa) and high self-healing ability was quantified (over 75% elastic modulus recovery). The good mechanical responsiveness was attributed to the aptness of HHP407 in forming poly(pseudo)rotaxane-based supramolecular networks. Photo-sensitivity was demonstrated through photo-rheological characterization. The encapsulation of high curcumin dosages ($715 \mu\text{g ml}^{-1}$) was carried out by exploiting a combined effect of α -cyclodextrins and HHP407. No detrimental effect on both physical and photo-crosslinked hydrogel network was observed due to curcumin loading through rheological and photo-rheological characterizations. Release studies evidenced a progressive curcumin delivery in watery environment and highly destabilizing conditions for hydrogel networks. Generally, curcumin release was sustained up to three weeks with a significant improvement due to the photo-induced crosslinking. Moreover, 100% of total payload was released over time, thus indicating a protective ability of the here-developed hydrogel systems for curcumin payload.

Graphical Abstract



Hybrid SM networks based on both physical and chemical crosslinking as potential one-stage injectable devices

2. Introduction

Natural polymers are extremely effective materials for the production of highly biocompatible and bioactive hydrogels. Indeed, from a general perspective, these macromolecules are preferred to synthetic polymers for the production of hydrogel-based scaffolds.^{1,2} In this regard, Bhatia and co-workers recently published a critical review in which they discussed the importance and superiority of natural polymers over synthetic ones in terms of biological performances due to their chemical composition and functionalities.³ The most diffused natural polymers used for the formation of hydrogels can be mainly and approximately categorized into proteins and polysaccharides. Widely used proteins for this purpose are collagen,⁴ elastin,⁵ fibrin,⁶ silk fibroin⁷ and gelatin,⁸ while highly used polysaccharides are chitosan,⁹ alginate¹⁰ and hyaluronic acid.¹¹ In this wide set of materials, gelatin represents one of the most interesting. In fact, it is derived from collagen and hence contains a variety of bioactive domains for cell adhesion (i.e., peptide sequences for integrin interactions) and guided biodegradation (i.e., peptide sequences for metalloproteinase action). Moreover, gelatin is generally characterized by a cost-effective production and shows a thermo-sensitive behavior guided by a self-assembly process that is translated into an upper critical solution temperature (UCST) response. For this reason, it is not suitable as such for the formation of gel networks at body temperature (i.e., 37 °C) and requires further chemical modifications to enhance crosslinking in this thermal condition. Nonetheless, chemical functionalization and crosslinking of gelatin are easy, due to its high number of available functionalities.¹² A highly common strategy in this regard consists in coupling the available primary amino groups of (hydroxy)lysine with the carboxylic acid domains exposed by aspartic and glutamic acid through carbodiimide chemistry,¹³ thus forming a “zero length” crosslinking. Another approach is represented by the exploitation of nucleophilic domains of gelatin for the interaction with glutaraldehyde as crosslinker.¹⁴ However, the two above-mentioned strategies importantly hinder construct design and property tuning for their intrinsic short manipulation

window. A different approach that has been widely diffused in the last two decades is represented by the possibility to easily functionalize gelatin with photo-sensitive domains, thus producing an interesting derivative, namely gelatin methacryloyl (GelMA).^{15,16} Such functionalization, which is easy and cheap to conduct, is based on the exploitation of available free primary amino groups of gelatin for the interaction with methacrylic anhydride. Thence, GelMA has been elected as a gold standard for the production of photo-curable hydrogels with marked bioactivity. Other crosslinking strategies have continuously emerged through the exploitation of thiol-ene click chemistry, disulphide bonds, Schiff-base reaction, photo-oxidation and enzymatic crosslinking.¹² Nonetheless, a general drawback can be highlighted regarding the utilization and modification of natural polymers such as gelatin, that is the chemical variability due to its natural origin.^{17,18} For this reason, a widely shared approach consists in the production of hydrogel systems showing a bioartificial/biosynthetic composition (i.e., the general integration of natural and synthetic polymers/materials within the same system). The rationale underpinning this attractive approach lies in the synergistic combination of the advantages of both natural and synthetic materials. Indeed, materials of synthetic origins can improve repeatability and technological features in terms of processability and property engineering of final hydrogel constructs.¹⁹ One interesting example in this regard is represented by the work carried out by Bektas and Hasirci.²⁰ In brief, the authors developed a system based on GelMA and poly(2-hydroxyethyl methacrylate) (poly(HEMA)) characterized by the dual contribution of interpenetrating networks and photo-sensitivity. The resulting mechanical properties showed a valuable contribution of the poly(HEMA), which improved the elastic modulus of purely GelMA-based hydrogels from 6.5 to 150 kPa. The successful encapsulation of stromal keratocytes and the resulting high transparency indicated a huge potential of the developed formulation for the treatment of corneal blindness. Another example of a simple but highly engineered photo-sensitive biosynthetic system is reported in the work performed by Gao and co-authors.²¹ Aiming at developing a bioprinted system for bone and cartilage tissue regeneration, the authors of this work designed a novel bioink based on the mixture between poly(ethylene glycol) dimethacrylate and GelMA. Good mechanical properties, printability and biological properties were ensured by a well-balanced integration between the two counterparts. Additionally, good cell response was observed through the occurrence of both osteogenic and chondrogenic differentiation. However, a more interesting strategy can be found in the idea of designing supramolecular (SM) and photo-sensitive hydrogel networks based on GelMA and other synthetic counterparts. In this regard, the role of cyclodextrins is elemental. Indeed, the well-known ability of cyclodextrin to form SM complexes can be further improved with their additional contribution in terms of tissue adhesiveness.²² As an example, Wang *et al.* developed a 3D-printable hydrogel characterized by self-healing ability and photo-sensitivity.²³ To realize this target, a three-armed SM macromolecule was developed exploiting the self-assembly between isocyanatoethyl acrylate-modified β -cyclodextrin (β -CD-AOI₂) and acryloylated tetra-ethylene glycol-modified adamantane (A-TEG-Ad). Then, a copolymerization with GelMA was performed and a covalently crosslinked SM and bioartificial hydrogel was obtained. High resistance to fatigue and fast self-healing characterized such novel gel system and for these properties a good performance in terms of extrusion-based 3D printing was also observed. In this regard, the highest contribution was provided by the synthetic components. Parallely, good biological properties were observed for 3D cell cultures and were attributed to the well-known bioactivity of GelMA. The mechanical reinforcement induced by slidable SM crosslinking derived

from the presence of poly(pseudo)rotaxanes (PPRs) on gelatin-based hydrogels has been also discussed over the last two decades in other works present in the literature.^{24,25} However, in this scenario, the development of easily processable devices is not effortless. Indeed, the most important requirement consists in a proper integration between the natural and the synthetic counterparts, which is not elementary to satisfy. The possibility to properly control the synthesis outcomes and the resulting physico-chemical properties denotes an important feature to successfully integrate different materials. In this regard, the role of poly(urethane)s as synthetic components should be considered important, since the exploitation of these molecules could be an effective answer to the challenging need to integrate many different features, such as miscibility, physical stability, chemical functionality and low polymeric content.

Thence, in this part of the work, the newly synthesized PEU containing methacrylate photo-sensitive domains (i.e., HHP407) was exploited to assemble a biosynthetic hydrogel system in combination with GelMA, with the aim to design networks suitable for both regenerative pharmacology and tissue engineering. HHP407 and GelMA were synthesized and characterized in physico-chemical terms. Then, a wide plethora of bioartificial formulations composed of GelMA, HHP407 and α -CDs was designed and physically characterized. The evaluation of gelation kinetics and injectability was qualitatively conducted and a selection of the most promising formulations was carried out. Moreover, the encapsulation of curcumin at high concentration (i.e., 715 $\mu\text{g ml}^{-1}$) was guaranteed through the exploitation of α -CDs and stability of resulting drug-loaded networks was evaluated through a complete rheological and photo-rheological characterization. Finally, release studies of curcumin were conducted on physical and photo-cured hydrogels incubated in contact with a physiological-like watery environment (i.e., phosphate buffered saline, pH 7.4, 37 °C). Finally, the general potential of such SM hydrogel systems as cutting-edge and highly engineered devices for advanced applications in regenerative medicine through the integration of drug delivery and tissue engineering strategies was discussed.

3. Materials and Methods

3.1 Materials

HHP407 was synthesized as indicated in the previous chapter *Section 3 – Chapter 3.1 – Materials and Methods – Synthesis of HHP407*. All reagents for HHP407 synthesis, TSP, gelatin (type A, from porcine skin) and methacrylic anhydride were purchased from Merck/Sigma-Aldrich (Milan, Italy). α -CDs (from now on simply indicated with the acronym “CDs”) and lithium phenyl-2,4,6-trimethylbenzoylphosphinate (LAP, a photo-initiator) were obtained from TCI Chemicals Europe (Zwijndrecht, Belgium).

3.2 Gelatin methacryloyl (GelMA) synthesis and physico-chemical characterization

3.2.1 GelMA synthesis protocol

Gelatin methacryloyl was synthesized according to the procedure reported by Buckle *et al.*²⁶ In detail, gelatin was solubilized in phosphate buffered saline (PBS, pH 7.4) at 10% w/v concentration (100 ml) and at 50 °C under stirring. Then, methacrylic anhydride was added (0.5

ml every 1 g of gelatin) dropwise and the reaction was conducted for 3 hours under vigorous stirring at 50 °C and in the dark. Subsequently, the reaction was stopped through the addition of PBS in order to dilute 1:5 v/v the starting reaction volume. The resulting diluted solution was filtered and dialyzed (cut-off 10-12 kDa, Sigma Aldrich) for 7 days at 37 °C in order to remove any traces of methacrylic anhydride and salts. Finally, the purified solution was freeze dried for 2 days (Martin Christ ALPHA 2-4 LSC, Germany) and stored at 3 °C under vacuum and in the dark.

3.2.2 Chemical characterization of GelMA

The synthesized GelMA was characterized through ¹H-NMR spectroscopy as reported in *Section 2 – Chapter 2.2 – Materials and Methods – Chemical characterization of PEUs – ¹H-NMR spectroscopy*. Native gelatin was also analyzed for comparative purposes. The degree of methacryloylation (DM) was calculated as the percentage of amino domains of native gelatin (i.e., mainly lysine and hydroxylysine) that were converted into amide groups. The quantification of DM was conducted through the implementation of the following equation 1, as reported by Zhou and colleagues.¹⁸

$$DM (\%) = \left(1 - \frac{A_{\text{lysine methylene of GelMA}}}{A_{\text{lysine methylene of Gelatin}}}\right) \times 100 \text{ Eq. 1}$$

In which $A_{\text{lysine methylene of GelMA}}$ and $A_{\text{lysine methylene of Gelatin}}$ correspond to the area related to methylene lysine protons for GelMA and gelatin, respectively.

3.3 Biosynthetic and supramolecular hydrogels preparation and characterization

3.3.1 Preparation and physical characterization of bioartificial and supramolecular hydrogels based on GelMA, HHP407 and CDs

SM hydrogels composed of GelMA, HHP407 and CDs were designed at various concentrations of the constituent components. Systems containing GelMA at 1, 3 and 5% w/v, HHP407 at 1, 3 and 5% w/v and CDs at 10% w/v were produced starting from concentrated solutions of GelMA and HHP407 containing CDs at 10% w/v. In detail, the required amounts of GelMA and HHP407 were solubilized in PBS added with LAP (0.05% w/v, PBS/LAP) at 37 °C and 3 °C, respectively. Then, a clear solution of CDs at 14% w/v concentration in PBS/LAP was produced and added to the previously prepared solutions of GelMA and HHP407 thus obtaining solution at 10% w/v CD concentration. The final hydrogel formulations were obtained through the fast mixing of equal volumes of GelMA-CD and HHP407-CD solutions. Homogenization of the obtained mixtures was performed utilizing a vortex system (40 Hz for 30 seconds). The resulting hydrogels were indicated as HHP407 X% - GelMA Y% - CD Z%, in which X, Y and Z correspond to the concentrations (% w/v) of HHP407, GelMA and CDs, respectively. Gelation time and ability were characterized at 25 °C through vial inversion and by visual inspection every 5 minutes. “Gel” state was assessed when a condition of “no-flow” was maintained for 30 seconds. Phase-separation phenomena were evaluated at 3, 25 and 37 °C. Injectability was evaluated at 25 and 37 °C using a conventional syringe system (5 mL, Carlo Erba, Milan, Italy) equipped with a G22 needle.

3.3.2 Curcumin encapsulation and release studies

Curcumin encapsulation, hydrogel mechanical characterization (i.e., rheological and photo-rheological characterizations) and release studies were conducted as indicated in *Section 3 – Chapter 3.1 – Materials and Methods – Preparation and characterization of HHP407- and CD-based SM hydrogels – Curcumin encapsulation and release studies*. The resulting hydrogels were coded as HHP407 X% - GelMA Y% - CD Z% Cur, where X, Y and Z correspond to the concentrations (% w/v) of HHP407, GelMA and CDs, respectively. Cur content was 715 $\mu\text{g ml}^{-1}$. For release studies, photo-induced crosslinking was performed on both sides of cylindrical hydrogels placed within glass vials (0.5 ml hydrogels, 10 mm inner diameter) for 1 minute (365 nm, 10 mW cm^{-2}). Photo-cured samples were indicated with the addition of “UV” at the end of the hydrogel codes. 5 samples were produced for each condition and results are indicated as average \pm standard deviation.

3.4 Statistical Analysis

Statistical analysis was conducted as indicated in *Section 2 – Chapter 2.2 – Materials and Methods – Statistical Analysis*.

4. Results

4.1 Physico-chemical characterization of GelMA – $^1\text{H-NMR}$ spectroscopy

$^1\text{H-NMR}$ characterization of GelMA indicated a successful reaction with methacrylic anhydride through the appearance of new peaks at chemical shift values of 5.7 and 5.4 ppm, which indicated the presence of acrylic protons of methacrylamide domains covalently bond to lysine and hydroxylysine, respectively. Figure 1 shows the differences between gelatin and GelMA spectra. Moreover, the additional presence of a peak at chemical shift value of 1.9 ppm in GelMA spectrum was referred to the methyl protons of methacrylamide. The quantification of DM (%) was calculated as described by Zhou and colleagues¹⁸ and resulted to be 95.3%, thus indicating an almost complete functionalization of gelatin through the addition of photo-sensitive groups on lysine domains.

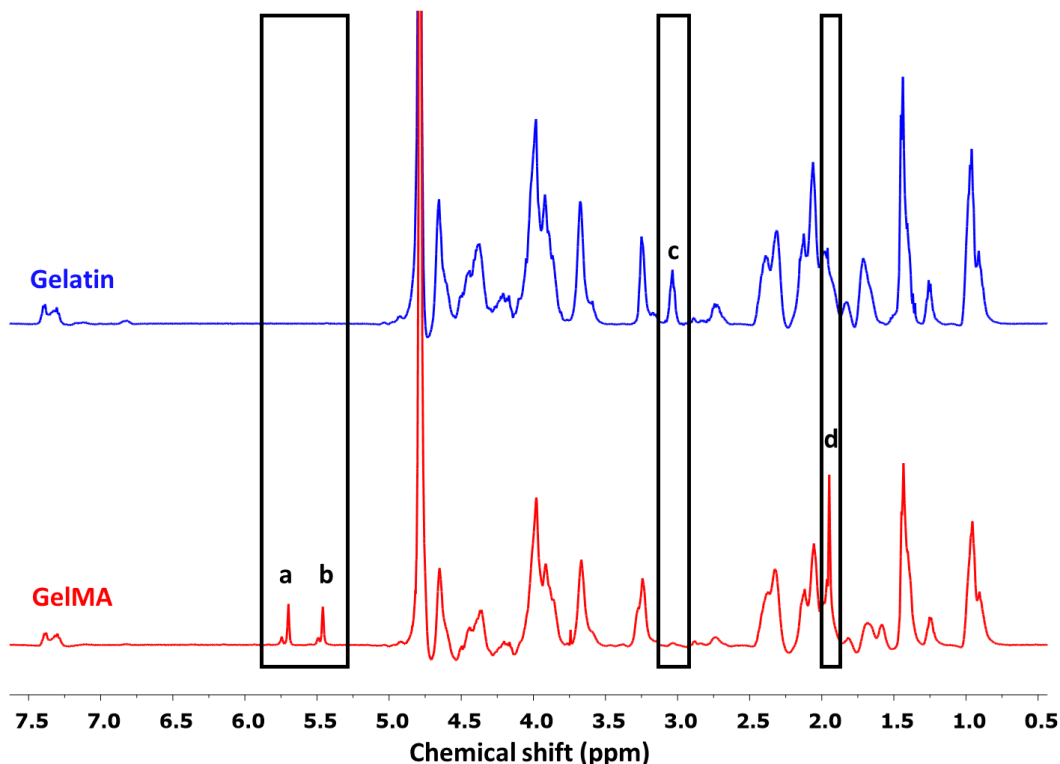


Figure 1 – $^1\text{H-NMR}$ spectra of gelatin (blue) and GelMA (red). Black rectangles highlight the differences between the two spectra. The peaks at 5.4 and 5.7 ppm indicate the acrylic protons (2H) of methacrylamide domains of (a) lysine and (b) hydroxylysine. The peak at 2.9 ppm chemical shift indicates the methylene protons (c, 2H) of unreacted lysine domains, while the one at 1.9 ppm indicates the protons of methyl group (d, 3H) of methacrylamide.

4.2 Preparation and characterization of bioartificial hydrogels based on GelMA, HHP407 and CDs

4.2.1 Hydrogel formulation and gelation kinetics

Generally, almost all the formulated hydrogels showed the ability to undergo a sol-gel transition at room temperature (25 °C) in a relatively restricted temporal window, which resulted to be within 30 minutes. The only exception was represented by the formulation HHP407 1% - GelMA 5% - CD 10%, which required an overnight incubation to complete the gelation process. Table 1 summarizes the results in terms of gelation ability. These findings were interesting, since the thermal behavior of HHP407 and GelMA are opposite. Indeed, the former is characterized by a LCST behavior, while the latter by a UCST response. It is likely that the presence of CDs could help in terms of solution mixability and overall stability. This is the reason why these hydrogels were formulated at higher CD content (10% w/v) with respect to the formulations that were evaluated in the previous Chapter (8% w/v). Indeed, the most important contribution in terms of stability could be ascribed to the fast formation of a viscous and elastic SM network based on HHP407 and CDs. No phase separation phenomena were observed at 3 and 25 °C, while HHP407 1% - GelMA 5% - CD 10% showed a gel-to-sol transition at 37 °C within 5 minutes incubation and an evident phase separation after consecutive 8 hours of incubation. This response could be attributed to the thermal responsiveness of GelMA, which in this case constituted the predominant

polymeric constituent of the system, thus inducing a gel-to-sol transition and then crystalline phase (i.e., PPRs) precipitation at 37 °C. Nonetheless, all hydrogels showed the ability to be easily injected at 25 °C, while at 37 °C syneresis effects were generally observed for samples containing GelMA at 5% w/v and HHP407 at concentrations equal or lower than 3% w/v. Even in these cases, the thermal response of GelMA could cause the induction to phase separation phenomena upon mechanical stimulus (i.e., injection through a G22 needle). Generally, the best formulations in terms of qualitative evaluation of physical properties resulted to be those containing GelMA at 3 and 5% w/v and HHP407 at 3 and 5% w/v. In order to improve the potential interaction with biological environments maintaining a good processability, the most promising formulations were selected containing HHP407 at the concentrations of 3 and 5% w/v and GelMA at 3% w/v. Thence, HHP407 3% - GelMA 3% - CD 10% and HHP407 5% - GelMA 3% - CD 10% hydrogels were selected for further characterizations and studies.

Table 1 – Gelation time at 25 °C of resulting hydrogels containing HHP407 and GelMA at various concentrations and CDs at 10% w/v. O.N.: overnight incubation. Green color indicates the absence of phase-separation phenomena at 3, 25 and 37 °C, while yellow refers to SM crystal precipitation at 37 °C.

(% w/v)	GelMA 1%	GelMA 3%	GelMA 5%
HHP407 1%	GEL (t=30')	GEL (t=30')	GEL (O.N.)
HHP407 3%	GEL (t=30')	GEL (t=25')	GEL (t=25')
HHP407 5%	GEL (t=25')	GEL (t=20')	GEL (t=20')

4.3 Curcumin encapsulation and release studies

4.3.1 Rheological characterization of pure and Curcumin-loaded SM and bioartificial hydrogels

Hydrogels containing Cur were also produced according to the same protocol for hydrogel preparation. The only difference consisted in the production of a native solution of CDs at 14% w/v containing Cur at 1 mg ml⁻¹, as showed in the previous *Chapter 3.1* of this Section. The procedure for hydrogel formulation allowed the production of systems containing Cur at 715 µg ml⁻¹, which was strictly related to the CD content in the hydrogels (10% w/v). In fact, as a consequence of the mixture between the PEU solution and the CD counterpart (14% w/v) containing Cur at 1 mg ml⁻¹, the resulting payload of such drug within the final hydrogels (CD at 10% w/v) resulted to be 715 µg ml⁻¹. Rheological and photo-rheological evaluations were essential to validate the general stability of the resulting bioartificial networks based on HHP407, GelMA, CDs and Cur.

Strain sweep tests were performed to observe the general hydrogel mechanical response to applied incremental strain at 37 °C. Interestingly, all investigated hydrogels were characterized by an evident strain range characterized by a linear behavior of both G' and G'' (i.e., linear viscoelastic region, LVE), as represented in figure 2. Although at 37 °C GelMA at 3% w/v concentration is expected to behave as a “sol” within the SM HHP407-based network, strain sweep test results indicated a clear system response typical of fully developed hydrogels. Hence, all the contribution of the resulting physical stability could be ascribed to HHP407 and its ability to form PPR-based SM crystals with CDs. The additional content of Cur induced a general decrease of critical strain

values (γ_L) with respect to control samples. Indeed, γ_L for HHP407 3% - GelMA 3% - CD 10% was quantified to be equal to 0.9%, while for HHP407 3% - GelMA 3% - CD 10% Cur it resulted to be 0.05%. The same trend was observed for HHP407 5% - GelMA 3% - CD 10% and HHP407 5% - GelMA 3% - CD 10% Cur, which showed γ_L equal to 0.2% and 0.06%, respectively. Differently, no significant contribution of Cur loading was observed in terms of G'_{LVE} and G''_{LVE} , which resulted to be around 10^4 and 10^3 Pa for all hydrogel formulations, respectively. Nonetheless, higher mechanical properties were observed for HHP407 5% - GelMA 3% - CD 10% with respect to HHP407 3% - GelMA 3% - CD 10% (i.e., approx. 40%). The presence of GelMA did not generally affect such typical behavior of mixtures composed of PEUs and CDs even in terms of reversibility. Indeed, the typical self-healing ability was maintained in these totally different formulations compared to the ones solely composed of PEUs and CDs. Accordingly, a recovery between 80 and 85% was observed for all the investigated hydrogels.

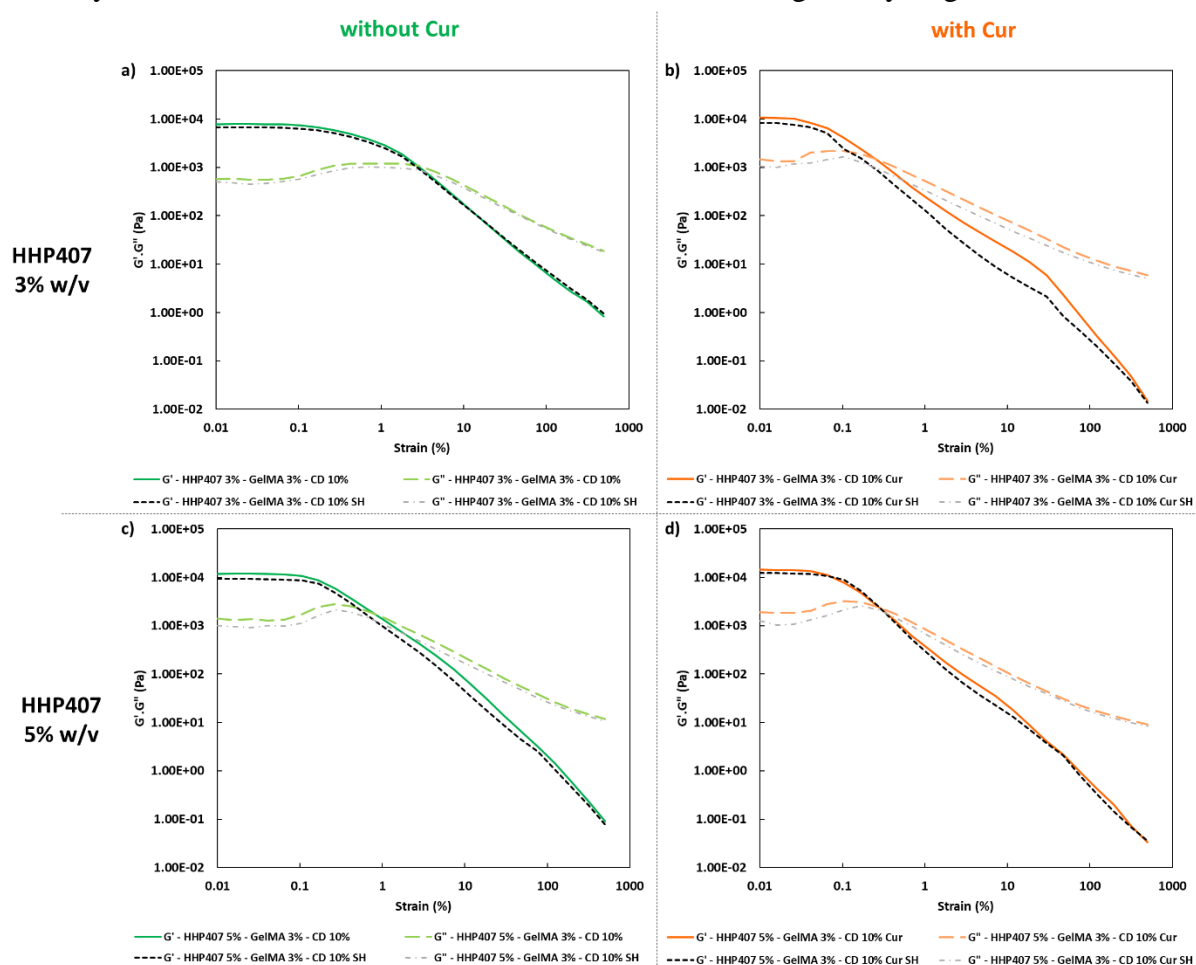


Figure 2 – Strain sweep tests showing the trends of G' (continuous lines) and G'' (long dashed lines) as a function of applied strain at 37 °C. Control samples (green) are compared to hydrogel samples containing Cur (orange). G' (black short dashed lines) and G'' (grey dash-dotted lines) trends after complete rupture and recovery in quiescent state for 15 minutes at 37 °C are also shown.

Frequency sweep tests were performed in order to evaluate the general stability of the developed biosynthetic hydrogel systems within a range of frequencies and temperatures that represent typical operative conditions (i.e., 25, 30 and 37 °C). From a general perspective, no crossover points between G' and G'' were detected within the entire range of investigated frequencies and temperatures for each sample, thus indicating well-developed hydrogel networks, as reported in

figure 3. Interestingly, no significant dependence of G' and G'' over temperature was observed for both the formulations HHP407 3% - GelMA 3% - CD 10% and HHP407 5% - GelMA 3% - CD 10%. This result was particularly noteworthy, since two thermo-sensitive contributions were characterizing the developed systems, namely HHP407 and GelMA. The fact that no relevant dependence over temperature increase was observed indicated the development of highly stable PPR-based SM networks, which turned out to be probably predominant over the thermo-induced physical crosslinking (i.e., hydrophobic interactions). In this regard, even the contribution of GelMA was negligible, although a general decrease of mechanical properties could be supposed due to a probable interference with hydrogel network development (e.g., interaction with available free CDs, steric hindrance). Interestingly, the presence of Cur did not induce significant variations in G' and G'' trends at 25 °C. As temperature increased, lower values of G' were detected. Moreover, G'' resulted to be generally higher for Cur loaded systems compared to the ones not containing the drug. In this regard, the results obtained from strain sweep tests were useful to better understand such outcomes. Indeed, strain sweep tests evidenced that Cur-loaded samples were characterized by lower critical strain values (γ_L) with respect to control hydrogels. In detail, γ_L values for Cur-loaded hydrogels were typically lower than 0.1% strain at 37 °C (1 rad s⁻¹). This indicated that frequency sweep tests were characterizing hydrogel networks containing initial cracks, since the imposed strain during the tests was set at 0.1%. In these conditions the difference between G' and G'' turned out to be reduced with respect to the samples not containing Cur. The behavior of Cur-loaded hydrogels could be attributed to the interaction of such drug with hydrogel forming domains (i.e., mainly CDs and micelles composed of HHP407), thus inducing weakening effects on the resulting networks. The fact that a lower influence was observed at 25 °C with respect to 37 °C could be related to the physical competition between the integration of Cur within hydrophobic domains of HHP407 and the formation of hydrophobic interactions upon thermal stimulus. Indeed, the presence of Cur at such high concentration (715 $\mu\text{g ml}^{-1}$) could interfere with the formation of hydrophobic interactions within the polymeric networks based on HHP407, thus inducing a detectable decrease of mechanical properties in terms of toughness. A reinforcing element for this hypothesis could be found in the fact that a less evident effect was observed for the sample formulated at the highest tested HHP407 concentration (5% w/v), thus indicating a marked Cur encapsulation ability due to the higher availability of hydrophobic domains. Additionally, although GelMA could show a potential ability in terms of Cur solubilization and encapsulation,^{27,28} no sufficient data were available to evaluate its contribution in this regard.

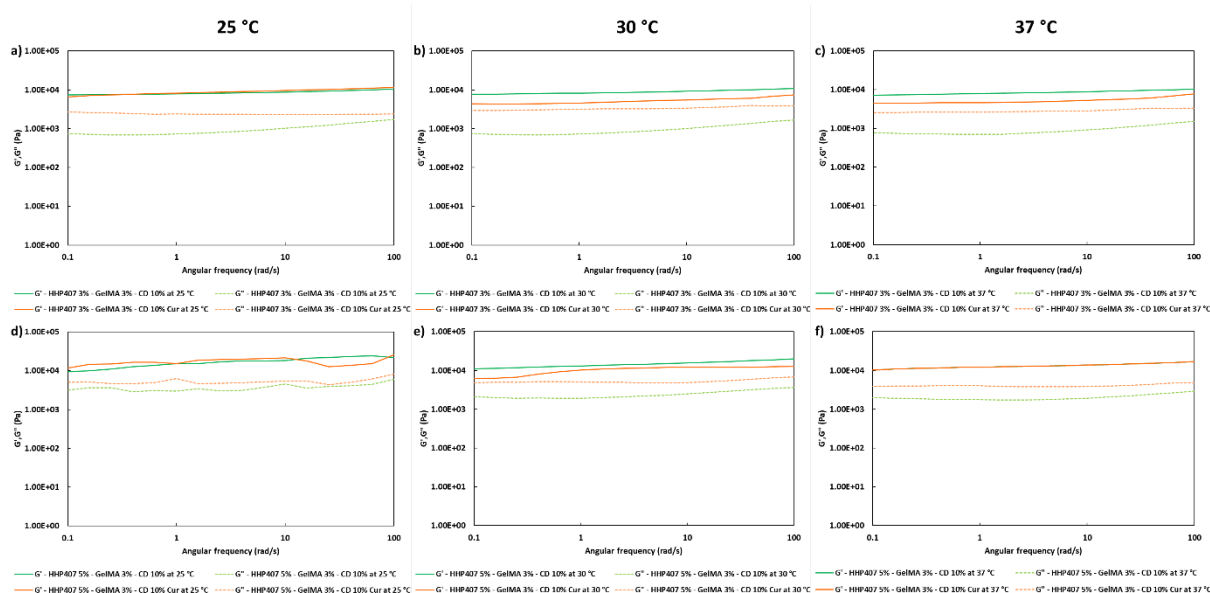


Figure 3 – G' (continuous lines) and G'' (dashed lines) trends as a function of applied angular frequency at 25, 30 and 37 °C for a,b,c) HHP407 3% - GelMA 3% - CD 10% and d,e,f) HHP407 5% - GelMA 3% - CD 10% as such (green) and containing Cur (orange) at $715 \mu\text{g ml}^{-1}$.

Self-healing tests were also conducted to evaluate hydrogel ability to recover their mechanical properties after multiple rupture cycles at high strain (100% for 60 seconds), as showed in figure 4. Interestingly, all hydrogel systems were characterized by good self-healing ability after 3 complete rupture cycles. Indeed, a G' recovery of 92% was observed for both HHP407 3% - GelMA 3% - CD 10% and HHP407 3% - GelMA 3% - CD 10% Cur, while 75% and 89% resulted for HHP407 5% - GelMA 3% - CD 10% and HHP407 5% - GelMA 3% - CD 10% Cur, respectively. No clear and straightforward explanation could be given for the lower recovery ability of HHP407 5% - GelMA 3% - CD 10%. It was hypothesized that a more fragile network was developed in this case due to the marked formation of hydrophobic interactions through HHP407 domains (i.e., PPO and HDI), thus reducing the overall reversibility of the system upon cyclic rupture.²⁹ The addition of Cur did not negatively affect the typical self-healing ability of the developed hydrogel systems, since no relevant differences were observed between Cur-loaded hydrogels and control samples. The observed, slight variability in mechanical properties between the various rheological tests was acceptable and suggested a reliable and consistent behavior of the here-developed hydrogel systems. Finally, it is important to remark the fact that GelMA did not constructively contribute to the formation of hydrogel networks at 37 °C, thus indicating that the SM network based on HHP407 and CDs showed the capability to stably integrate such “sol” phase.

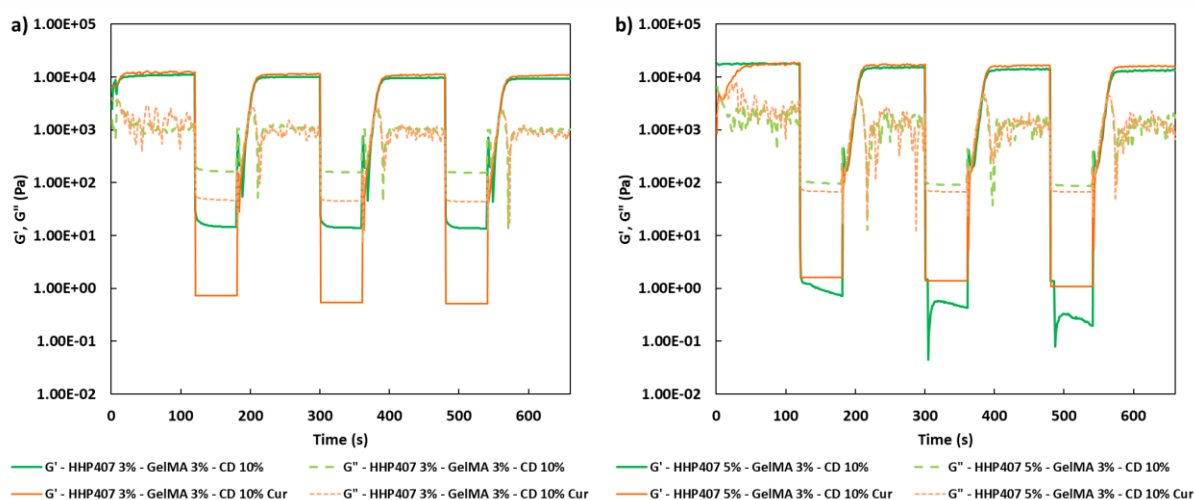


Figure 4 – Strain test curves reporting the trends of G' (continuous lines) and G'' (dashed lines) as a function of time during cyclic rupture (100% strain, 60 seconds) and recovery (0.1% strain, 120 seconds) of hydrogel networks at a) 3% and b) 5% w/v HHP407 concentrations (GelMA at 3% w/v and CDs at 10% w/v concentration) at 37 °C. Control sample hydrogels (green lines) are compared to those containing Cur (orange lines) at 715 $\mu\text{g ml}^{-1}$ concentration.

Photo-rheological characterization was also performed in order to evaluate the overall ability of the hydrogels to undergo photo-induced crosslinking. Despite the typical turbidity of these SM hydrogels based on PPRs, all the investigated systems resulted to be photo-crosslinkable, as shown in figure 5. The formulations not containing Cur generally showed a higher ability to undergo photo-induced crosslinking. Indeed, a G' increase of 69% and 56% was measured for HHP407 3% - GelMA 3% - CD 10% and HHP407 5% - GelMA 3% - CD 10%, respectively. Differently, HHP407 3% - GelMA 3% - CD 10% Cur showed a G' increase equal to 18%, while for HHP407 5% - GelMA 3% - CD 10% a G' improvement of 27% was observed. As discussed in the previous Chapter, the presence of Cur significantly affected the ability of these systems to undergo photo-crosslinking probably because of the additional UV light absorbance and dissipation provided by such drug molecule. Nonetheless, no relevant color fade was observed by visual inspection after a prolonged UV-light irradiation (for 60 seconds at 10 mW cm^{-2}).

Thence, the entire set of these rheological characterizations demonstrated a good stability of the designed hydrogels from a physical perspective. This achievement represents an important factor for the validation of the rationale underpinning the idea of designing relatively complex and highly bioartificial systems based on properly synthesized PEUs, CDs and GelMA. GelMA polymer chain integration within PEU-based SM networks resulted in still handle, reliable and processable matrices. Moreover, the further addition of Cur at high concentration (715 $\mu\text{g ml}^{-1}$) did not significantly affect the overall behavior, thus additionally highlighting the feasibility and versatility of HHP407-based SM networks. A good photo-sensitivity was also observed for the systems containing Cur, opening the way to the possibility to tune the overall hydrogel mechanical properties, responsiveness and potential release kinetics, in the end.

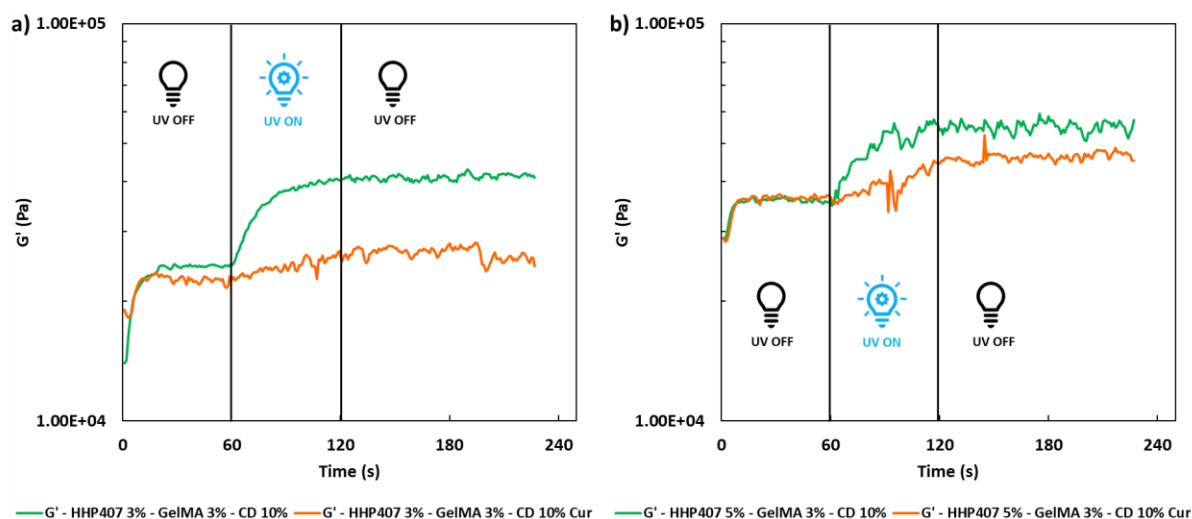


Figure 5 – G' trends as a function of time for GelMA-containing hydrogels at a) 3 and b) 5% w/v HHP407 concentration as such (green lines) and containing curcumin (orange lines) at $715 \mu\text{g ml}^{-1}$ concentration. G' trend was registered before photo-crosslinking for 60 seconds. Then, exposure to UV-light (365 nm , 10 mW cm^{-2}) was conducted for 60 seconds and resulting mechanical behavior was registered for additional 120 seconds.

4.3.2 Curcumin release profiles from bioartificial hydrogels based on GelMA, HHP407 and CD

In order to reliably quantify Cur release, it was necessary to define calibration curves that could represent proper references. HHP407 3% - GelMA 3% - CD 10% Cur and HHP407 5% - GelMA 3% - CD 10% Cur hydrogels (1 ml) were solubilized in PBS to obtain a final Cur concentration of $100 \mu\text{g ml}^{-1}$. Then, standard samples containing Cur at precise quantities were analyzed through an UV-Vis spectrometer and the resulting calibration curves are reported in figure 6. As expected, significant differences were observed between the two formulations in terms of optical properties. This observation further confirmed the central role of the PEU in terms of encapsulation and delivery of Cur, since the only variable between the two systems was given by HHP407 concentration. In this case, the combined contribution of HHP407 and CD were extremely important for Cur stabilization and release, since the concentration of such drug within the hydrogels was remarkably high ($715 \mu\text{g ml}^{-1}$). Cur release profiles in highly destabilizing conditions for hydrogel networks (i.e., 0.5 ml hydrogels having 10 mm diameter in contact with 1 ml of PBS) were characterized by a general progressive kinetics allowing the quantification of the total amount of encapsulated Cur (theoretically, approx. $358 \mu\text{g ml}^{-1}$) over time for most hydrogel systems, as reported in figure 7. Significantly slower release rates were showed by UV-cured hydrogel networks. Indeed, HHP407 3% - GelMA 3% - CD 10% Cur UV and HHP407 5% - GelMA 3% - CD 10% Cur UV samples (i.e., hydrogels crosslinked through UV light exposure) were able to sustain Cur delivery up to 18 and 21 days, respectively. A maximum temporal release of 48 and 30 hours was observed for HHP407 3% - GelMA 3% - CD 10% Cur and HHP407 5% - GelMA 3% - CD 10% Cur, respectively. However, in the case of HHP407 5% - GelMA 3% - CD 10% Cur, the total amount of encapsulated Cur was not released after complete dissolution of the hydrogel networks within the temporal window of 30 hours of incubation in contact with PBS.

This behavior could be explained by observing the extremely high release rate of Cur that was quantified at the time step of 24 hours (i.e., $> 250 \mu\text{g ml}^{-1}$). Indeed, this datum was suggesting a probable precipitation of an aliquot of Cur due to the resulting high concentration within the obtained eluates. In such conditions, it is likely that the carriers aimed at Cur encapsulation (i.e., HHP407-based micelle aggregates and CDs) were partially disassembled causing the precipitation of a portion of the total payload. This behavior was induced by the extremely destabilizing conditions of these release tests, which were also performed with the intention to evaluate the stability of both hydrogel networks and Cur carriers. Nonetheless, the simulated scenario represents a highly improbable condition compared to real biological environments, which are generally characterized by exudates rather than high amounts of pure watery solutions.³⁰

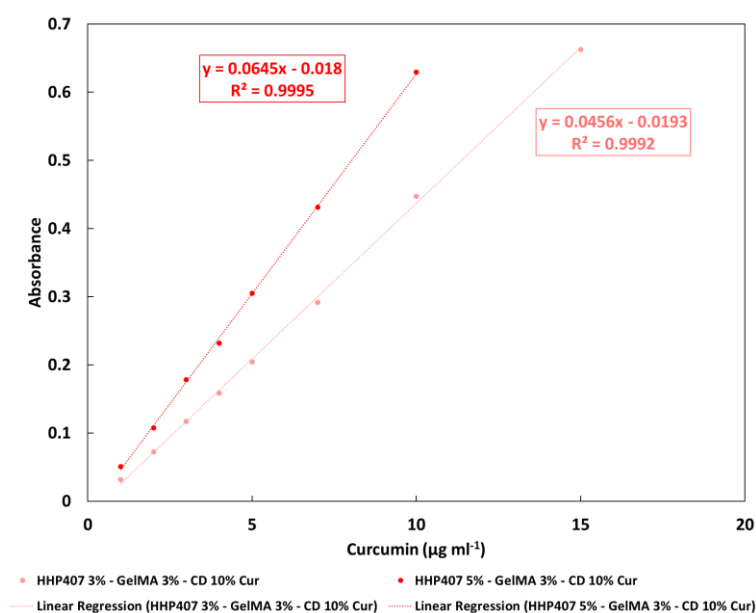


Figure 6 – Calibration curves showing the absorbances of standard samples as a function of solubilized Cur after dissolution of HHP407 3% - GelMA 3% - CD 10% Cur (light red) and HHP407 5% - GelMA 3% - CD 10% Cur (red) in order to obtain storage solutions at $100 \mu\text{g ml}^{-1}$ Cur concentration. Linear regressions are also reported with the resulting equations, which showed a good fitting.

Interestingly, a general and common behavior was observed between purely physical hydrogels and photo-cured ones. The systems characterized by a HHP407 concentration of 3% w/v showed an initial faster release rate with respect to the hydrogels containing the same PEU at 5% w/v. This behavior could be ascribed to the overall physical and morphological properties that derived from the mixing between HHP407 and GelMA solutions. Indeed, it could be likely that the presence of GelMA contributed to the formation of a more porous network within the formulations containing HHP407 at 3% w/v due to the overall lower polymeric content compared to the systems containing the same PEU at 5% w/v. Then, the behaviors of the two different systems were inverted and HHP407 3% - GelMA 3% - CD 10% Cur showed slower release kinetics with respect to HHP407 5% - GelMA 3% - CD 10% Cur in both conditions of physically and chemically crosslinked networks. Such behavior could be ascribed to the typical higher stability of SM networks deriving by lower PEU/CD ratios, which was the case of HHP407 3% - GelMA 3% - CD 10% Cur, as discussed in all the previous Chapters.

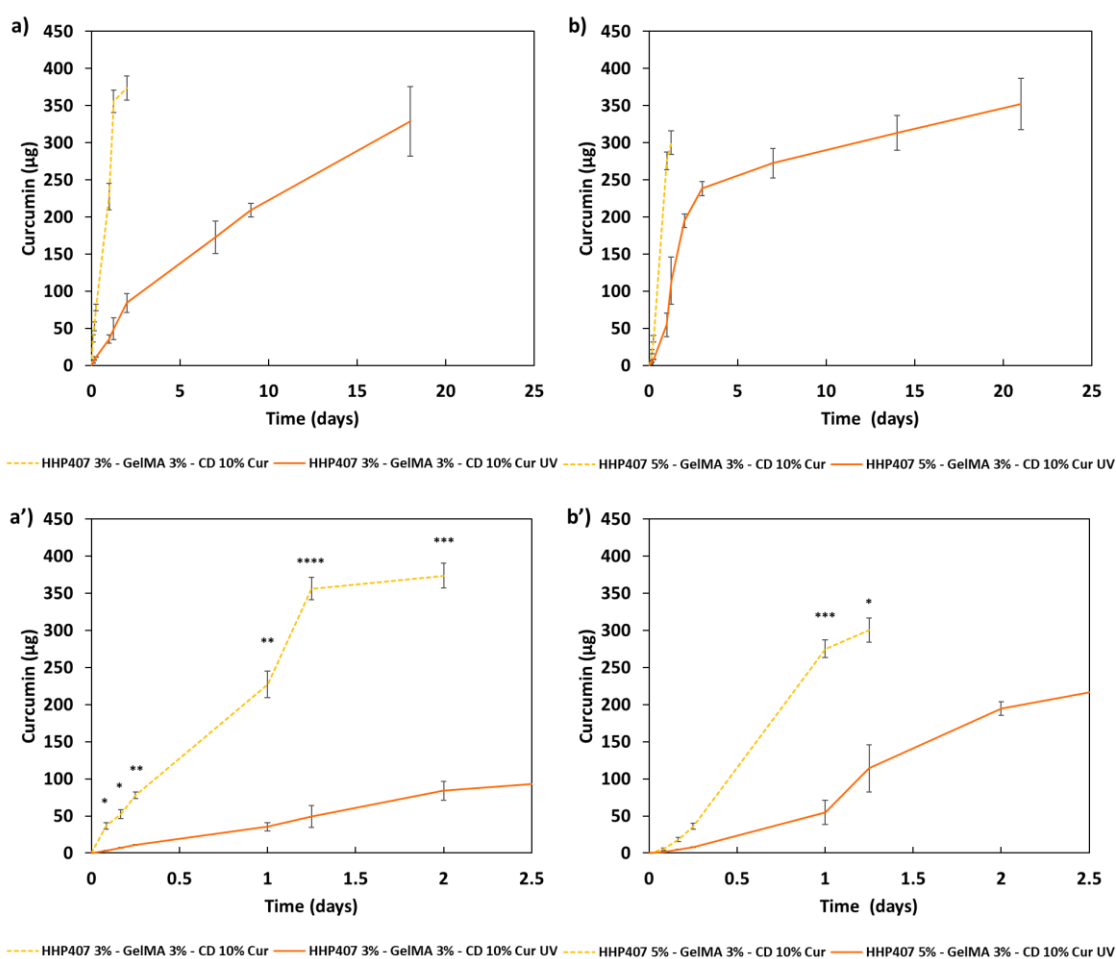


Figure 7 – Cur release profiles of hydrogel systems in contact with PBS at 37 °C for a,a') HHP407 3% - GelMA 3% - CD 10% Cur and HHP407 3% - GelMA 3% - CD 10% Cur UV, and b.b') HHP407 5% - GelMA 3% - CD 10% Cur and HHP407 5% - GelMA 3% - CD 10% Cur UV. Physical hydrogels (yellow dashed lines) are compared with photo-cured systems (orange continuous lines). a') and b') graphs represent in detail the release kinetics within 2.5 days observation.

Surely, physical hydrogels did not represent an optimal condition for prolonged drug release or even tissue engineering applications. Indeed, their stability could be negatively affected by the inclusion of GelMA, which was in “sol” condition at 37 °C and was quickly solubilized during the incubation in contact with PBS. Nonetheless, the resulting progressive release kinetics (no burst release) was attributed to the high stability of HHP407-based SM networks. The photo-induced crosslinking allowed prolonged release profiles of Cur over time, as expected from the previous photo-rheological characterization.

5. Conclusions

In this Chapter, the development of a novel biosynthetic system based on a properly synthesized and photo-sensitive PEU, GelMA and CDs was carried out. GelMA at high methacryloylation degree (i.e., 95%) was synthesized and characterized in order to contribute in the formation of bioactive hydrogels for the regeneration of biological tissues after the administration of therapeutic or stimulant agents. HHP407 turned out to be a proper PEU for the formation of stable SM

networks with CDs showing the ability to blend with completely different polymer in terms of thermal response (i.e., GelMA, which in watery environments shows a UCST behavior). A wide plethora of novel hybrid hydrogel systems was developed and the most promising formulations were selected for mechanical characterizations and curcumin encapsulation and release. Rheological tests showed a noteworthy stability of physical hydrogels composed of HHP407, GelMA and CDs, thus highlighting the applicability of this PEU for the formation of solid networks. Good mechanical properties were coupled with good self-healing behavior and photosensitivity. High dosages of curcumin were encapsulated through the exploitation of CDs and HHP407, without significantly affecting the good physical response of the resulting hydrogels, which maintained the ability to undergo photo-induced crosslinking even in the presence of such colored drug. Release studies evidenced a marked ability of the designed hydrogels to progressively deliver the total payload of encapsulated curcumin in a highly destabilizing aqueous environment. The resulting kinetics turned out to be importantly dependent over hydrogel formulation and processing (i.e., photo-induced crosslinking) and were protracted up to three weeks, thus indicating the effectiveness of the protective action of HHP407 and CDs on curcumin in aqueous environments.

Finally, it can be concluded that the physical and chemical properties of the here-investigated hydrogel networks open the way to the possibility to properly design hydrogel systems having a biosynthetic nature with tunable release kinetics and mechanical properties. These hydrogel networks could be thus elected as promising and versatile matrices for future investigations and applications as one-stage strategies for regenerative pharmacology coupled with tissue engineering.

6. References

- (1) Bao, Z.; Xian, C.; Yuan, Q.; Liu, G.; Wu, J. Natural Polymer-Based Hydrogels with Enhanced Mechanical Performances: Preparation, Structure, and Property. *Adv. Healthcare Mater.* **2019**, *8* (17), 1900670. <https://doi.org/10.1002/adhm.201900670>.
- (2) Catoira, M. C.; Fusaro, L.; Di Francesco, D.; Ramella, M.; Boccafoschi, F. Overview of Natural Hydrogels for Regenerative Medicine Applications. *J Mater Sci: Mater Med* **2019**, *30* (10), 115. <https://doi.org/10.1007/s10856-019-6318-7>.
- (3) Bhatia, S. Natural Polymers vs Synthetic Polymer. In *Natural Polymer Drug Delivery Systems*; Springer International Publishing: Cham, 2016; pp 95–118. https://doi.org/10.1007/978-3-319-41129-3_3.
- (4) Dinescu, S.; Albu Kaya, M.; Chitoiu, L.; Ignat, S.; Kaya, D. A.; Costache, M. Collagen-Based Hydrogels and Their Applications for Tissue Engineering and Regenerative Medicine. In *Cellulose-Based Superabsorbent Hydrogels*; Mondal, Md. I. H., Ed.; Polymers and Polymeric Composites: A Reference Series; Springer International Publishing: Cham, 2018; pp 1–21. https://doi.org/10.1007/978-3-319-76573-0_54-1.
- (5) Zhang, Y.; Desai, M. S.; Wang, T.; Lee, S.-W. Elastin-Based Thermoresponsive Shape-Memory Hydrogels. *Biomacromolecules* **2020**, *21* (3), 1149–1156. <https://doi.org/10.1021/acs.biomac.9b01541>.
- (6) Park, C. H.; Woo, K. M. Fibrin-Based Biomaterial Applications in Tissue Engineering and Regenerative Medicine. In *Biomimetic Medical Materials*; Noh, I., Ed.; Advances in Experimental Medicine and Biology; Springer Singapore: Singapore, 2018; Vol. 1064, pp 253–261. https://doi.org/10.1007/978-981-13-0445-3_16.
- (7) Ribeiro, V. P.; Pina, S.; Oliveira, J. M.; Reis, R. L. Silk Fibroin-Based Hydrogels and Scaffolds for Osteochondral Repair and Regeneration. In *Osteochondral Tissue Engineering*; Oliveira, J. M., Pina, S., Reis, R. L., San Roman, J., Eds.; Advances in Experimental Medicine and Biology; Springer International Publishing: Cham, 2018; Vol. 1058, pp 305–325. https://doi.org/10.1007/978-3-319-76711-6_14.
- (8) Echave, M. C.; Hernáez-Moya, R.; Iturriaga, L.; Pedraz, J. L.; Lakshminarayanan, R.; Dolatshahi-Pirouz, A.; Taebnia, N.; Orive, G. Recent Advances in Gelatin-Based Therapeutics. *Expert Opinion on Biological Therapy* **2019**, *19* (8), 773–779. <https://doi.org/10.1080/14712598.2019.1610383>.
- (9) Mohammadzadeh Pakdel, P.; Peighambaroust, S. J. Review on Recent Progress in Chitosan-Based Hydrogels for Wastewater Treatment Application. *Carbohydrate Polymers* **2018**, *201*, 264–279. <https://doi.org/10.1016/j.carbpol.2018.08.070>.
- (10) Rastogi, P.; Kandasubramanian, B. Review of Alginate-Based Hydrogel Bioprinting for Application in Tissue Engineering. *Biofabrication* **2019**, *11* (4), 042001. <https://doi.org/10.1088/1758-5090/ab331e>.
- (11) Noh, I.; Kim, N.; Tran, H. N.; Lee, J.; Lee, C. 3D Printable Hyaluronic Acid-Based Hydrogel for Its Potential Application as a Bioink in Tissue Engineering. *Biomater Res* **2019**, *23* (1), 3. <https://doi.org/10.1186/s40824-018-0152-8>.
- (12) Van Hoorick, J.; Tytgat, L.; Dobos, A.; Ottevaere, H.; Van Erps, J.; Thienpont, H.; Ovsianikov, A.; Dubruel, P.; Van Vlierberghe, S. (Photo-)Crosslinkable Gelatin Derivatives for Biofabrication Applications. *Acta Biomaterialia* **2019**, *97*, 46–73. <https://doi.org/10.1016/j.actbio.2019.07.035>.
- (13) Van Vlierberghe, S. Crosslinking Strategies for Porous Gelatin Scaffolds. *J Mater Sci* **2016**, *51* (9), 4349–4357. <https://doi.org/10.1007/s10853-016-9747-4>.

- (14) Bigi, A.; Cojazzi, G.; Panzavolta, S.; Rubini, K.; Roveri, N. Mechanical and Thermal Properties of Gelatin Films at Different Degrees of Glutaraldehyde Crosslinking. *Biomaterials* **2001**, *22* (8), 763–768. [https://doi.org/10.1016/S0142-9612\(00\)00236-2](https://doi.org/10.1016/S0142-9612(00)00236-2).
- (15) Yue, K.; Trujillo-de Santiago, G.; Alvarez, M. M.; Tamayol, A.; Annabi, N.; Khademhosseini, A. Synthesis, Properties, and Biomedical Applications of Gelatin Methacryloyl (GelMA) Hydrogels. *Biomaterials* **2015**, *73*, 254–271. <https://doi.org/10.1016/j.biomaterials.2015.08.045>.
- (16) Klotz, B. J.; Gawlitta, D.; Rosenberg, A. J. W. P.; Malda, J.; Melchels, F. P. W. Gelatin-Methacryloyl Hydrogels: Towards Biofabrication-Based Tissue Repair. *Trends in Biotechnology* **2016**, *34* (5), 394–407. <https://doi.org/10.1016/j.tibtech.2016.01.002>.
- (17) Duconseille, A.; Andueza, D.; Picard, F.; Santé-Lhoutellier, V.; Astruc, T. Variability in Pig Skin Gelatin Properties Related to Production Site: A near Infrared and Fluorescence Spectroscopy Study. *Food Hydrocolloids* **2017**, *63*, 108–119. <https://doi.org/10.1016/j.foodhyd.2016.08.001>.
- (18) Zhu, M.; Wang, Y.; Ferracci, G.; Zheng, J.; Cho, N.-J.; Lee, B. H. Gelatin Methacryloyl and Its Hydrogels with an Exceptional Degree of Controllability and Batch-to-Batch Consistency. *Sci Rep* **2019**, *9* (1), 6863. <https://doi.org/10.1038/s41598-019-42186-x>.
- (19) Lim, K. S.; Martens, P.; Poole-Warren, L. Biosynthetic Hydrogels for Cell Encapsulation. In *Functional Hydrogels as Biomaterials*; Li, J., Osada, Y., Cooper-White, J., Eds.; Springer Series in Biomaterials Science and Engineering; Springer Berlin Heidelberg: Berlin, Heidelberg, 2018; Vol. 12, pp 1–29. https://doi.org/10.1007/978-3-662-57511-6_1.
- (20) Nichol, J. W.; Koshy, S. T.; Bae, H.; Hwang, C. M.; Yamanlar, S.; Khademhosseini, A. Cell-Laden Microengineered Gelatin Methacrylate Hydrogels. *Biomaterials* **2010**, *31* (21), 5536–5544. <https://doi.org/10.1016/j.biomaterials.2010.03.064>.
- (21) Gao, G.; Schilling, A. F.; Hubbell, K.; Yonezawa, T.; Truong, D.; Hong, Y.; Dai, G.; Cui, X. Improved Properties of Bone and Cartilage Tissue from 3D Inkjet-Bioprinted Human Mesenchymal Stem Cells by Simultaneous Deposition and Photocrosslinking in PEG-GelMA. *Biotechnol Lett* **2015**, *37* (11), 2349–2355. <https://doi.org/10.1007/s10529-015-1921-2>.
- (22) Hoang Thi, T. T.; Lee, J. S.; Lee, Y.; Park, H. B.; Park, K. M.; Park, K. D. Supramolecular Cyclodextrin Supplements to Improve the Tissue Adhesion Strength of Gelatin Bioglues. *ACS Macro Lett.* **2017**, *6* (2), 83–88. <https://doi.org/10.1021/acsmacrolett.6b00841>.
- (23) Wang, Z.; An, G.; Zhu, Y.; Liu, X.; Chen, Y.; Wu, H.; Wang, Y.; Shi, X.; Mao, C. 3D-Printable Self-Healing and Mechanically Reinforced Hydrogels with Host–Guest Non-Covalent Interactions Integrated into Covalently Linked Networks. *Mater. Horiz.* **2019**, *6* (4), 733–742. <https://doi.org/10.1039/C8MH01208C>.
- (24) Hou, D.; Tong, X.; Yu, H.; Zhang, A.; Feng, Z. A Kind of Novel Biodegradable Hydrogel Made from Copolymerization of Gelatin with Polypseudorotaxanes Based on α -CDs. *Biomed. Mater.* **2007**, *2* (3), S147–S152. <https://doi.org/10.1088/1748-6041/2/3/S12>.
- (25) Lee, D. H.; Tamura, A.; Arisaka, Y.; Seo, J.-H.; Yui, N. Mechanically Reinforced Gelatin Hydrogels by Introducing Slidable Supramolecular Cross-Linkers. *Polymers* **2019**, *11* (11), 1787. <https://doi.org/10.3390/polym11111787>.
- (26) Van Den Bulcke, A. I.; Bogdanov, B.; De Rooze, N.; Schacht, E. H.; Cornelissen, M.; Berghmans, H. Structural and Rheological Properties of Methacrylamide Modified Gelatin Hydrogels. *Biomacromolecules* **2000**, *1* (1), 31–38. <https://doi.org/10.1021/bm990017d>.

- (27) Gómez-Estaca, J.; Balaguer, M. P.; López-Carballo, G.; Gavara, R.; Hernández-Muñoz, P. Improving Antioxidant and Antimicrobial Properties of Curcumin by Means of Encapsulation in Gelatin through Electrohydrodynamic Atomization. *Food Hydrocolloids* **2017**, *70*, 313–320. <https://doi.org/10.1016/j.foodhyd.2017.04.019>.
- (28) Dai, X.; Liu, J.; Zheng, H.; Wichmann, J.; Hopfner, U.; Sudhop, S.; Prein, C.; Shen, Y.; Machens, H.-G.; Schilling, A. F. Nano-Formulated Curcumin Accelerates Acute Wound Healing through Dkk-1-Mediated Fibroblast Mobilization and MCP-1-Mediated Anti-Inflammation. *NPG Asia Mater* **2017**, *9* (3), e368–e368. <https://doi.org/10.1038/am.2017.31>.
- (29) Ligoure, C.; Mora, S. Fractures in Complex Fluids: The Case of Transient Networks. *Rheol Acta* **2013**, *52* (2), 91–114. <https://doi.org/10.1007/s00397-012-0668-0>.
- (30) Cutting, K. F. Wound Exudate: Composition and Functions. *British Journal of Community Nursing* **2003**, *8* (Sup3), S4–S9. <https://doi.org/10.12968/bjcn.2003.8.Sup3.11577>.

Section 4 – Conclusion

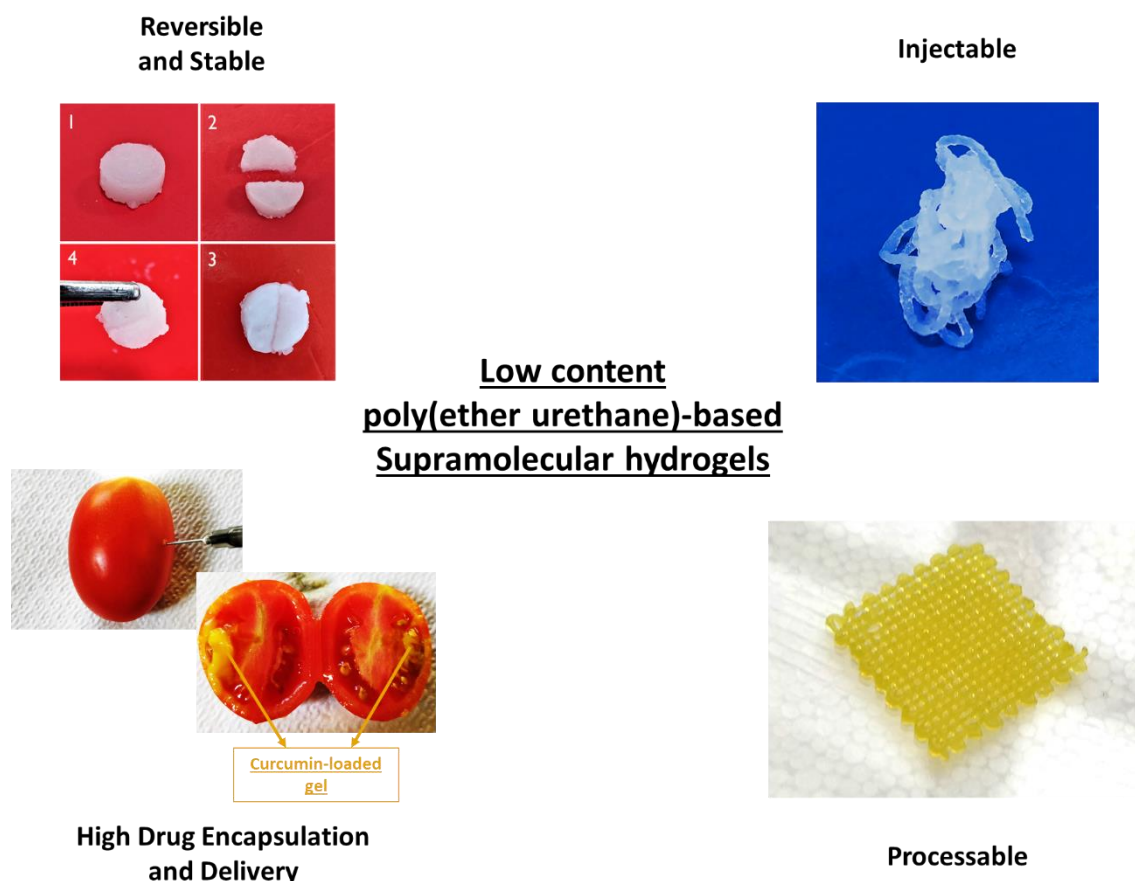
The development of effective strategies for controlled drug delivery and tissue engineering requires highly functional devices. In this regard, the design of synthetic polymers represents a powerful tool. In particular, the simplicity and versatility of poly(urethane) synthesis allows the production of multifaceted macromolecules, which can be particularly suitable for the aims of advanced therapies. In this work, a facile and reliable synthesis method was utilized to assemble a plethora of novel poly(ether urethane)s for the design of supramolecular hydrogels. The use of commercial virgin α -cyclodextrin coupled with properly synthesized thermo-sensitive poly(ether urethane)s composed of commercially available amphiphilic tri-block copolymers (i.e., P407 and F68) allowed the preparation of supramolecular hydrogel networks based on poly(pseudo)rotaxanes. Depending on the reagents selected for the synthesis of the poly(ether urethane)s, different yields in terms of supramolecular self-assembly were achieved. Generally, the utilization of cyclic and hydrophobic diols as chain extenders (i.e., 1,4-cyclohexanedimethanol) resulted in the best macromolecular features for the threading of α -cyclodextrin along the polymeric chains and the consecutive formation of poly(pseudo)rotaxanes in watery environment with respect to other diols characterized by the presence of pendant groups (i.e., N-Boc serinol). Nonetheless, the use of N-Boc serinol as chain extender opened the way to the possibility to chemically treat the resulting poly(ether urethane)s in acid environments in order to expose free primary amines as pendant groups. This additional feature makes such poly(ether urethane)s bearing free amino groups suitable for specific functionalization procedures through carbodiimide chemistry or the design of hydrogel systems with pH-responsiveness to acidic environments. The contribution of the selected macrodiol (i.e., P407 or F68) turned out to be crucial for the properties of the resulting hydrogel systems. P407 showed the best physico-chemical features for the fast formation of supramolecular hydrogels with remarkable mechanical properties, while F68 resulted in poly(ether urethane)s with weaker gelation potential. It was then observed that higher poly(ethylene oxide) contents were not representing the most influencing factor for the fast formation of poly(ether urethane)-based supramolecular hydrogel networks. These studies indicated that the final behavior of the designed hydrogel systems was strongly dependent on a specific balance between molecular mass, poly(ethylene oxide) content, and hydrophobic block (i.e., poly(propylene oxide), 1,6-hexamethylene diisocyanate) quantity and distribution along poly(ether urethane) chains, which resulted to be even strictly correlated to the thermo-responsiveness of the resulting macromolecules. The most promising hydrogel formulations were characterized by remarkably low poly(ether urethane) contents (i.e., poly(ether urethane) concentration ranging between 1 and 5% w/v) and α -cyclodextrin concentration at 10% w/v. All these formulations turned out to be cytocompatible according to ISO rules. One of the most important results of this study was represented by the design of supramolecular hydrogels with poly(ether urethane)s at low concentration (i.e., 1% w/v) in combination with α -cyclodextrin at higher content (i.e., 10% w/v), which resulted to be the best conditions for the supramolecular development of hydrogels with enhanced stability and responsiveness in aqueous environments. This result clearly evidenced that the significant reduction of polymeric content was not negatively affecting the overall functionality of hydrogel systems. Indeed, in such conditions the good mechanical properties (i.e., high values of elastic modulus) and self-healing ability of hydrogels were preserved. This peculiarity highlighted the relevant value of the developed poly(ether

urethane)s for the formation of supramolecular hydrogels with α -cyclodextrin, thus enhancing the technological potential of the engineered hydrogel platform. In fact, poly(ether urethane)-based networks showed a promising suitability for the easy injection *in situ* and the subsequent ability to solidly sustain the surrounding tissues and organs. Differently, from a biological perspective, the possibility to produce hydrogels at low polymeric content represents a noteworthy advantage to potentially optimize the therapeutic effects of a pharmacological strategy, while minimizing the risk of side-effects within host organisms. Moreover, the wide domain of chemical features of the designed polymers permitted the design of hydrogels based on blends composed of different poly(ether urethane)s to further engineer their final properties. In detail, the best poly(ether urethane) in terms of hydrogel formation (i.e., CHP407) was mixed with the one bearing the highest number of functional groups (i.e., SHF68, which exposed primary amines along its chains). The plethora of developed and thoroughly characterized purely physical hydrogels permitted the selection of the best formulations to conduct various drug delivery studies. Indeed, after a preliminary evaluation of hydrogel release potential using a hydrophilic model molecule (i.e., fluorescein isothiocyanate 4), the effective encapsulation of curcumin was conducted and release studies were performed highlighting a protective ability of poly(ether urethane)s and α -cyclodextrin against drug payload degradation. The hydrogels were able to sustain progressive release kinetics up to 4 days. Moreover, ciprofloxacin was also encapsulated within poly(ether urethane)-based hydrogels and effectively delivered with no burst release phenomena. Another study was conducted with the aim to effectively integrate a supramolecular hydrogel within solid porous scaffolds produced through the conventional salt leaching technique and release studies of a drug model molecule (i.e., fluorescein isothiocyanate 4) were successfully performed, thus indicating the suitability of such poly(ether urethane)s for the promising development of single-stage tissue engineering strategies. Moreover, through the simple modification of the synthesis process and the use of a specific reagent (i.e., 2-hydroxyethyl methacrylate) a novel photo-sensitive poly(ether urethane) was obtained through an end-capping procedure of the prepolymers rather than a chain extension reaction. The resulting polymer was characterized by the best balance in terms of physico-chemical properties (i.e., molecular mass and hydrophobic features) for the formation of supramolecular structures with α -cyclodextrins. The exploitation of this remarkable gelling ability allowed a significant improvement in terms of curcumin encapsulation and a concurrent reduction of the amount of α -cyclodextrins needed for network stabilization. Good mechanical properties of physical hydrogels (i.e., self-healing) were coupled with the possibility to perform photo-induced chemical crosslinking, further widening the available options for the tuning of hydrogel behavior. A remarkably high curcumin payload (i.e., 540 $\mu\text{g ml}^{-1}$) was encapsulated within these novel systems and release profiles were sustained up to 5 weeks in physiological-like environment. The role of the poly(ether urethane) was highly important for the effective encapsulation, delivery and chemical protection of such drug payload. Finally, an interesting bioartificial system based on the integration of this photo-sensitive poly(ether urethane) and gelatin methacryloyl was developed. The exploitation of fast gelling kinetics of such polymer with α -cyclodextrin allowed the reliable incorporation of gelatin methacryloyl as highly biomimetic component for tissue regeneration purposes. The resulting systems were easily injectable and also suitable for curcumin encapsulation (715 $\mu\text{g ml}^{-1}$) and release as therapeutic or stimulant agent up to 3 weeks.

The entire set of these investigations and studies highlighted a notable versatility of the utilized synthesis method for the development of highly functional poly(ether urethane)s. These polymers were successfully employed as constituents of injectable hydrogels for drug delivery or more sophisticated systems for single-stage tissue engineering strategies, indicating a promising and

valuable potential of such customized polymers to effectively answer a wide plethora of clinical needs in the future. With regard to the current state of the art, one of the most important achievements of this work is represented by the possibility to produce a plethora of hydrogel-forming polymers combining both good mechanical response (i.e., fast storage modulus recovery upon breakage at high strain values) and low polymeric content, in addition to notably high stability and negligible cytotoxicity in aqueous environments.¹ Indeed, to the best of our knowledge, very few examples in the literature show comparable favorable conditions and versatility for both purely physical hydrogels^{2,3} and chemically crosslinked networks⁴. More specific investigations will be required for the development of *ad-hoc* strategies, as this work mainly represents a promising starting point and a reliable reference for future applications. Nonetheless, a platform of potential devices for the treatment of cancer and severe infections has been already developed by designing supramolecular hydrogels encapsulating curcumin and ciprofloxacin, respectively. Moreover, the composition of hybrid drug-loaded systems based on the integration of different counterparts (i.e., with solid scaffolds or bioactive natural polymers) represents an additional proof of the huge potential and versatility of poly(ether urethane)-based supramolecular hydrogels towards their successful application in the wide field of regenerative medicine.

Visual summary of the overall achievements of this work



References

- (1) Zhang, Y. S.; Khademhosseini, A. Advances in Engineering Hydrogels. *Science* **2017**, *356* (6337), eaaf3627. <https://doi.org/10.1126/science.aaf3627>.
- (2) Domiński, A.; Konieczny, T.; Kurcok, P. α -Cyclodextrin-Based Polypseudorotaxane Hydrogels. *Materials* **2019**, *13* (1), 133. <https://doi.org/10.3390/ma13010133>.
- (3) Poudel, A. J.; He, F.; Huang, L.; Xiao, L.; Yang, G. Supramolecular Hydrogels Based on Poly (Ethylene Glycol)-Poly (Lactic Acid) Block Copolymer Micelles and α -Cyclodextrin for Potential Injectable Drug Delivery System. *Carbohydrate Polymers* **2018**, *194*, 69–79. <https://doi.org/10.1016/j.carbpol.2018.04.035>.
- (4) Jalalvandi, E.; Shavandi, A. Shear Thinning/Self-Healing Hydrogel Based on Natural Polymers with Secondary Photocrosslinking for Biomedical Applications. *Journal of the Mechanical Behavior of Biomedical Materials* **2019**, *90*, 191–201. <https://doi.org/10.1016/j.jmbbm.2018.10.009>.